AURK Inhibitors as Radiosensitising Agents in NSCLC

Kathryn Anne Egerton

A thesis submitted for the degree of Doctor of Philosophy

University of Sheffield

Faculty of Medicine, Dentistry and Health

Division of Clinical Medicine

2024

Acknowledgements

I would like to thank Prof Helen Bryant for her unrelenting support. She was a true mentor, and it has been a pleasure working in her research group. Her immense knowledge and scientific curiosity made solving problems together a joy.

I would like to thank Prof Munitta Muthana for her expertise and guidance for our *in vivo* work and Matthew Fisher for his invaluable expertise during the *in vivo* trials.

Thank you to Prof Claire Eyers at the University of Liverpool for hosting me in her lab and to Leonard for teaching me all things mass spec. Thank you to Dr Pat Eyers for his support and knowledge on Aurora kinases.

I thank my fellow AURKB scientist and friend Dr Timothy Mitchell for his team work on Barasertib and comradery in the lab. I also thank Dr Polly Gravells for her training and support in the Bryant lab.

I am grateful to Dr Spencer Collis and Dr Ruth Thompson for their insightful questions during lab meetings and to Aurelie, Eloise, Az, Devon, Morgan and Nikky for their friendship. I especially thank Connor and Dan for their friendship, advice and humour which got me through many a long day in the lab.

Thank you to my partner Hugh for his unwavering support and encouragement. As a PhD graduate, he was always an open ear and a source of good advice. I would like to thank my Mum and my sister Jane supporting me in every way possible. Finally, I thank my Dad for instilling in me a love of science which led me to where I am today.

Abstract

Lung cancer accounts for the most cancer deaths in the UK by any cancer type. Survival remains poor due to limited treatment strategies and high treatment resistance. Radiotherapy is commonly used in NSCLC but resistance and normal tissue toxicity limit its effectiveness. The Aurora kinases, Aurora kinase B (AURKB) and Aurora kinase A (AURKA), are attractive therapeutic targets in human cancers due to their roles in cell division and the DDR. The AURKB inhibitor Barasertib was shown to be safe and tolerable in human trials but showed limited efficacy as a monotherapy. We hypothesised that AURKB inhibition by Barasertib would radiosensitised NSCLC.

We demonstrated that Barasertib radiosensitises NSCLC *in vitro*. Radiosensitisation by Barasertib required Barasertib treatment in the 24 Hr period after radiation and further sensitised if present as a pretreatment in a time-dependant manner (max $DEF_{0.1} = 1.83$).

We also present phosphoproteomic analysis showing the early phosphorylation pathways are altered by Barasertib or the AURKA inhibitor Alisertib with IR. Analysis after IR indicated that Barasertib and Alisertib can alter phosphorylation in cell cycle and DDR pathways 1 Hr after IR.

We established that Barasertib increases mitotic aberrance after IR by 20% ($p = 0.0145$). Barasertib treatment increased the metaphase population and overall mitotic population at 24 Hr, demonstrating prolonged mitosis during the first mitosis after cell cycle restart. Barasertib enhanced post-IR death by 47 % after 72 Hr ($p = 0.01$), indicative of mitotic catastrophe.

We also demonstrated strong anti-tumour activity *in vivo* by Barasertib in a xenograft model and established a suitable dose of 10 mg/kg for combination with radiotherapy in future studies.

Overall, Barasertib is a promising clinical radiosensitiser with the potential to improve treatment outcomes in lung cancer patients.

Project Outputs

Manuscript in Preparation

Egerton, K.A., Mitchell, T.A., Gravels, P.L., Harrison, C.J., Danson, S., Hatton, M., K Sisley, K., Bryant, H.E. “Barasertib radiosensitises by mitotic catastrophe in NSCLC.”

Presentations

Oral Seminar Presentation, Institute of Cancer Research (London, July 2024).

Egerton, K.A., Mitchell, T.A., Gravels, P.L., Fisher, M., Katse, R.Y., Harrison, C.J., Muthana, M., Daly, L., Eyers, P.A., Eyers, C.E., Bryant, H.E. “The Aurora B inhibitor Barasertib as a Radiosensitising Agent in NSCLC”

Poster Presentation, University of Sheffield School of Medicine and Population Health Research Meeting (Sheffield, July 2024).

Egerton, K.A., Mitchell, T.A., Gravels, P.L., Fisher, M., Katse, R.Y., Harrison, C.J., Muthana, M., Eyers, P.A., Eyers, C.E., Bryant, H.E. “The Aurora B inhibitor Barasertib as a Radiosensitising Agent in NSCLC”

Poster Presentation, ESMO Molecular Analysis for Precision Oncology Congress (Paris, Oct 2023)

Egerton, K.A., Mitchell, Fisher, M., Katse, R.Y., Daly, L., P.A., Eyers, C.E., Bryant, H.E. “Targeting Aurora Kinase B to Improve Radiotherapy in NSCLC”.

Poster Presentation at the University of Sheffield Medical School Annual Research Meeting (Sheffield, June 2022)

Egerton, K.A., Daly, L., P.A., Eyers, C.E., Bryant, H.E. “Targeting Aurora Kinase B to Improve Radiotherapy in NSCLC”

Table of Contents

Acknowledgements……ii

Abstract……iii

Project Outputs……v

List of Figures……xiii

List of Tables ……xvi

Abbreviations……xvii

1. Introduction 1
1.1. Lung Cancer 1
1.1.1. Subtypes of Lung Cancer 1
1.1.2. Treatment Options for Lung Cancer 1
1.1.3. Use of Radiotherapy in Lung Cancer 2
1.2. The Cellular Response to Radiotherapy 3
1.2.1. DNA Damage Response Initiation 4
1.2.2. Cell Cycle Arrest 6
1.2.3. SSB Repair 8
1.2.4. DSB Repair 9
1.2.5. Mitotic Aberrance after IR 12
1.2.6. Cell Fate after IR 14
1.2.7. DDR during Mitosis 20
1.3. Aurora Kinase B 23
1.3.1. The Role of AURKB in Mitosis 23
1.3.1.1. The CPC 23
1.3.1.2. AURKB Activation during Mitosis 24
1.3.1.3. Chromosome Condensation 26
1.3.1.4. Correction of Erroneous MT-KT Attachments 26
1.3.1.5. The Spindle Assembly Checkpoint (SAC) 29
1.3.1.6. Anaphase 31
1.3.1.7. Cytokinesis 31
1.3.1.8. Abscission and the NoCut Pathway 32

1.3.2. Non-Mitotic Functions of AURKB 36
1.3.2.1. AURKB and Chromatin Organisation 37
1.3.2.2. AURKB and the DDR 37
1.3.2.3. AURKB and Replication stress 41
1.4. Aurora Kinase A 43
1.4.1. Mitotic Roles of Aurora Kinase A 43
1.4.1.1. G_2-M Transition 43
1.4.1.2. Centrosome Maturation 46
1.4.1.3. Mitotic Spindle Formation and Control 47
1.4.1.4. Kinetochore-Microtubule Attachment (KT-MT) 48
1.4.1.5. Spindle Assembly Checkpoint (SAC) 48
1.4.1.6. Anaphase and Cytokinesis 49
1.4.2. Non-Mitotic Roles of AURKA 49
1.4.2.1. AURKA Regulation of p53 49
1.4.2.2. AURKA and Cell Cycle Checkpoints 53
1.4.2.3. AURKA and the DDR 54
1.5. Aurora Kinases and Cancer 57
1.5.1. Aurora Kinase Expression in Cancer and Clinical Significance 57
1.5.2. AURKB and Oncogenesis 58
1.5.3. AURKA and Oncogenesis 59
1.5.4. AURKB Inhibitors 61
1.5.4.1. Barasertib in Clinical Trials 62
1.5.5. Alisertib (MLN8237) in Clinical Trials 65
1.6. AURK Inhibitors as Radiosensitisers 66
1.6.1. Radiosensitisation by AURKB Inhibition 66
1.6.2. Radiosensitisation by AURKA Inhibitors 68
1.7. Research Aims 70

2. Materials and Methods 72
2.1. Materials 72
2.1.1. Cell lines 72
2.1.2. Buffers 72
2.1.3. Antibodies, Drugs and Kits 72

2.2. Methods 72
2.2.1. Cell Culture 72
2.2.2. Irradiation using a Cs137 Gamma Ray Source 73
2.2.3. Survival Assays 74
2.2.3.1. Clonogenic Assays 74
2.2.3.2. Dose Modulation Factor (DMF) Calculation from Clonogenic Survival Fraction 74
2.2.3.3. Nocodazole Treatment 75
2.2.4. Western Blotting 75
2.2.4.1. Protein Extraction in RIPA Buffer 75
2.2.4.2. Protein Collection for Phosphoproteins 76
2.2.4.3. SDS-PAGE 77
2.2.4.4. Protein Transfer 77
2.2.4.5. Blocking and Probing 78
2.2.4.6. Enhanced Chemiluminescence (ECL) Detection 78
2.2.4.7. Densitometry 78
2.2.5. Mass Spectrometry (MS) 79
2.2.5.1. H460 Treatment and Cell Harvesting 79
2.2.5.2. Sample Lysis 79
2.2.5.3. Reduction and Alkylation 80
2.2.5.4. Sp3 Bead Purification and Proteolytic Digestion 80
2.2.5.5. Tandem Mass Tag (TMT) Labelling 81
2.2.5.6. HPLC Purification/Fractionation 82
2.2.5.7. Titanium Dioxide Phosphopeptide Enrichment 82
2.2.5.8. Sample Processing and Storage 83
2.2.5.9. MS/MS Analysis by Orbitrap 83
2.2.5.10. MS/MS Data Analysis 84
2.2.6. Flow Cytometry Assays 86
2.2.6.1. Cell Harvesting for Methanol Fixation 86
2.2.6.2. Cell Cycle Analysis 86
2.2.6.3. Bromodeoxyuridine (BrdU) Analysis 88
2.2.6.4. Annexin V/PI Analysis 90
2.2.7. Immunofluorescence 92

2.2.7.1. Beta-Tubulin and Pericentrin Immunofluorescence 92
2.2.7.2. Phospho-H2AX Immunofluorescence 93
2.2.7.3. 53BP1 Immunofluorescence 95
2.2.7.4. RAD51 Immunofluorescence 96
2.2.8. Live Cell Imaging 97
2.2.9. Senescence Assay 98
2.2.10. In Vivo Experiments 99
2.2.10.1. Tumour Implantation 99
2.2.10.2. HEB8 – Monotherapy Dose Optimisation 100
2.2.10.3. HEB9 – Radiotherapy and Barasertib Combination 102
2.2.11. Immunohistochemistry 103
2.2.12. Statistical Analysis 105

3. In Vitro Evaluation of AURKB inhibitors as a Radiosensitisation Strategy in NSCLC 107
3.1. Introduction, Aims and Hypothesis 107
3.2. Time Course of Phosphorylation of AURKs during the Radiation Response 109
3.3. Evaluation of the Toxicity and Effective Inhibitory Dose of Barasertib 113
3.4. Evaluation of AURKB inhibitors as Radiosensitisers 117
3.4.1. Barasertib as a Radiosensitiser 117
3.4.2. Radiosensitisation by Alternative AURKBi 122
3.5. Investigation of Apoptosis and Death after IR and Barasertib Treatment in H460 Cells 124
3.6. Investigation of Senescence after IR and Barasertib Treatment in H460 cells 128
3.7. Discussion 131

4. Phospho-Proteomic Analysis of H460 cells after AURK Inhibitors and Radiation 136
4.1. Introduction, Aims and Hypothesis 136
4.2. Proteomic analysis after IR and Barasertib Treatment in H460 Cells 139
4.2.1. MS/MS and Identification of Differentially Abundant Peptides 139

4.2.2. Identification of Differentially Abundant Phosphopeptides after IR and Barasertib 141
4.2.3. Pathway Enrichment Analysis of Phosphorylation Changes after IR and Barasertib 147
4.2.3.1. DMSO vs 50 nM Barasertib (Metascape) 149
4.2.3.2. DMSO vs IR (Metascape) 152
4.2.3.3. IR vs Combination (Barasertib + IR) (Metascape) 154
4.2.3.4. IR vs Combination (Barasertib + IR) (DAVID) 155
4.3. Pathway Enrichment Analysis of Differentially Abundant Proteins after IR and Barasertib in Non-Enriched Samples 159
4.4. Investigation of MTOR Ser 2448 after IR and Barasertib Treatment in H460 Cells 165
4.4.1. MTOR Ser2448 Phosphorylation 165
4.5. Proteomic Analysis after IR and Alisertib Treatment in H460 Cells 168
4.5.1. MS/MS and Identification of Differentially Abundant Peptides 168
4.5.2. Identification of Differentially Abundant Phosphopeptides after IR and Alisertib 169
4.5.3. Pathway Enrichment Analysis of Phosphorylation Changes after IR and Alisertib 173
4.5.4. DMSO vs 25 nM Alisertib (Metascape) 173
4.5.5. DMSO vs IR (Metascape) 175
4.5.6. IR vs Combination (Alisertib + IR) (Metascape) 178
4.6. Discussion 180

5. Mechanistic Investigation of Radiosensitisation by Barasertib and IR 188
5.1. Introduction, Hypothesis and Aims 188
5.2. Investigation of the Effects of Barasertib on Cell Cycle Progression 190
5.2.1. Barasertib Alone 190
5.2.2. IR and Barasertib 195
5.3. Investigation of the Effects of IR and Barasertib Treatment on Mitosis in H460 cells 203
5.3.1. Live Cell Analysis of Mitotic Progression 203
5.3.2. Immunofluorescence Analysis of Mitotic Phenotype 211

5.3.2.1. Mitotic Population 211
5.3.2.2. Mitotic Aberrance 214
5.3.2.3. Mitotic Phase 221
5.4. Investigation of Active Replication after IR and Barasertib Treatment in H460 Cells 225
5.4.1. Effect of Hydroxyurea (HU) Treatment on Cell Survival after Barasertib Treatment 227
5.5. Investigation of DDR Markers after IR and Barasertib Treatment 228
5.5.1. γH2AX and Micronuclei after Barasertib and IR Treatment 228
5.5.1.1. γH2AX Foci 228
5.5.1.2. Investigation of Micronuclei after IR and Barasertib 234
5.5.2. 53BP1 Foci and Nuclear Bodies after Barasertib and IR treatment 236
5.5.2.1. 53BP1 Foci 236
5.5.2.2. 53BP1 Nuclear Bodies 244
5.6. RAD51 Foci 245
5.7. P53 Stabilisation after Barasertib Treatment 251
5.8. Discussion 252

6. Radiosensitising Effects of Barasertib in a Subcutaneous Model of NSCLC .. 262
6.1. Introduction, Aims and Hypothesis 262
6.2. Evaluation of Barasertib and Radiation Monotherapies in a H460 Xenograft Model 264
6.2.1. HEB8 Study Protocol 264
6.2.2. Tumour Growth Response to Barasertib at 10-50 mg/kg/day (HEB8 Trial) 266
6.2.3. Phospho-H3 response in HEB8 Study 268
6.2.4. Optimisation of Radiation Dose 270
6.2.5. Weight Response and Toxicity in HEB8 Study 272
6.3. Evaluation of Barasertib as a Radiosensitiser in a H460 Xenograft Model (HEB9 Trial) 273
6.3.1. HEB9 Study Protocol 273
6.3.2. Tumour Volume Response to 10 mg/kg Barasertib and 15 Gy IR 274
6.3.3. Weight response and Toxicity in HEB9 Study 279

6.4. Discussion 280

7. Final Discussion 284

8. Appendices 289
8.1. Buffers 289
8.2. Tables (Appendices) 291
8.3. Figures (Appendices) 299

9. References 324

List of Figures

Figure 1. 1: Cell cycle checkpoint activation as result of DNA damage signalling following IR 7
Figure 1. 2: DSB repair pathway choice 10
Figure 1. 3: Cell fate following mitotic catastrophe 17
Figure 1. 4: Localisation and activity of AURKB during the cell cycle 25
Figure 1. 5: AURKB and p53 38
Figure 1. 6: Localisation and activation of AURKA during the cell cycle 44
Figure 1. 7: AURKA and p53 50

Figure 2. 1: Example gating for PI and pH3 staining in fixed cells 87
Figure 2. 2: Example gating for PI and BrdU staining in fixed cells 89
Figure 2. 3: Example gating for PI and Annexin V staining in live cells 91
Figure 2. 4: Irradiation shield 101

Figure 3. 1: Phosphorylation of Aurora kinases is activated by radiation in H460 cells 110
Figure 3. 2: Phosphorylation of Aurora kinases is activated by IR in H1299 cells .. 111
Figure 3. 3: Barasertib reduces clonogenic survival in H460 cells and inhibits AURKB and AURKC 115
Figure 3. 4: H460 cells are radiosensitised by 50-100 nM Barasertib 118
Figure 3. 5: Barasertib radiosensitises H460 cells *in vitro* in a time-dependent manner 120
Figure 3. 6: Fractionated delivery of IR does not enhance radiosensitisation by Barasertib 121
Figure 3. 7: AURKBi inhibitor ZM447439 reduces clonogenic survival of H460 cells and sensitises to IR 122
Figure 3. 8: Barasertib increases late apoptosis and necrosis after IR treatment in H460 cells 126
Figure 3. 9: Senescence after Barasertib and IR treatment in H460 cells 130

Figure 4. 1: Work flow of MS/MS protocol for Barasertib and IR treated cells 139

Figure 4. 2: Relative abundance of phosphopeptides between untreated, Barasertib, 4 Gy and combination conditions in H460 cells 147
Figure 4. 3: Top 20 Enriched pathway clusters generated by Metascape pathway analysis 149
Figure 4. 4: Top 20 enriched pathway clusters generated by Metascape pathway analysis 151
Figure 4. 5: KEGG pathway Charts for analysis of differentially abundant phosphopeptides between 4 Gy and 4 Gy + 50 nM Barasertib conditions 158
Figure 4. 6: Relative abundance of proteins between untreated, Barasertib, 4 Gy and 4 Gy + 50 nM Barasertib Conditions in non-enriched samples (H460 Cells)..... 162
Figure 4. 7: Top 20 enriched pathway clusters generated by Metascape pathway analysis for total protein changes after Barasertib and IR 164
Figure 4. 8: Phospho-MTOR Ser2448 expression by phosphoproteomics and western blotting 167
Figure 4. 9: Work flow of MS/MS protocol for Alisertib and IR treated cells 168
Figure 4. 10: Relative abundance of phosphopeptides between untreated, Alisertib, 4 Gy and 4 Gy + Alisertib combination conditions in H460 cells..... 172
Figure 4. 11: Top 20 Enriched Pathway Clusters generated by Metascape pathway analysis for phosphopeptide changes after IR and Alisertib 174
Figure 4. 12: Top 20 enriched pathway clusters generated by Metascape pathway analysis for phosphopeptide changes after IR and Alisertib 176

Figure 5. 1: Cell cycle analysis in H460 cells after 50-200 nM Barasertib treatment 191
Figure 5. 2: Cell cycle analysis in H460 Cells after Barasertib and IR treatment.... 199
Figure 5. 3: Live cell imaging of H460 cells after Barasertib and IR treatment 204
Figure 5. 4: Barasertib and IR increase live aberrance between 27-72 Hr post IR. 209
Figure 5. 5: Mitotic population is increased by Barasertib after 24 Hr treatment 213
Figure 5. 6: IR and Barasertib contribute to increased mitotic defects 220
Figure 5. 7: Barasertib leads to accumulation of cells in early mitosis..... 223
Figure 5. 8: Barasertib and IR contibute to decreases in replicating populations ... 226
Figure 5. 9: Barasertib sensitises to HU treatment 227
Figure 5. 10: γH2AX Foci are induced by IR but affected by Barasertib..... 229

Figure 5. 11: γH2AX micronuclei are induced by IR after 24 Hr 235
Figure 5. 12: 53BP1 foci and nuclear bodies are induced by IR but unaffected by Barasertib 243
Figure 5. 13: RAD51 foci are initiated after IR and unaffected by Barasertib 247
Figure 5. 14: Barasertib decreases p53 protein levels 251
Figure 5. 15: Mechanistic basis for Barasertib radiosensitisation 258

Figure 6. 1: HEB8 treatment schedule 264
Figure 6. 2: Barasertib reduces tumour growth in a NSCLC xenograft model 267
Figure 6. 3: Phospho-H3 (Ser10) tumour staining is not affected by 48 Hr Barasertib treatment 269
Figure 6. 4: IR reduces tumour volume in a NSCLC xenograft model 271
Figure 6. 5: Weight change during HEB8 study 272
Figure 6. 6: HEB9 treatment schedule 273
Figure 6. 7: Barasertib does not sensitise to IR in a NSCLC Xenograft model 276
Figure 6. 8: 10 mg/kg Barasertib was not reproducible between HEB8 and HEB9 studies 278
Figure 6. 9: Weight change during HEB9 study 279

Appendix Figure 1: Radiosensitation by Alisertib in NSCLC cell lines 299
Appendix Figure 2: Effect of varying Alisertib IR dosing schedule in H460 cells 300
Appendix Figure 3: Survival and AURKB inhibition after Barasertib treatment in NSCLC cell lines 301
Appendix Figure 4: Barasertib Radiosensitisation in NSCLC cell lines H1299 and SW900 304
Appendix Figure 5: Barasertib radiosensitises NSCLC cell lines H1299 and SW900 305
Appendix Figure 6: H460 cell confluency after IR + Barasertib combination in H460 cells 306
Appendix Figure 7: Additional KEGG pathway charts for analysis of differentially abundant phosphopeptides between 4 Gy and 4 Gy + 50 nM Barasertib conditions 311

Appendix Figure 8: Flow cytometry gating of cell cycle analysis after Barasertib treatment 312
Appendix Figure 9: Flow cytometry gating of cell cycle analysis after IR and Barasertib 313
Appendix Figure 10: Flow cytometry gating of BRDU staining 315
Appendix Figure 11: Representative images of 53BP1 foci after Barasertib and IR treatment 316
Appendix Figure 12: Representative images of RAD51 foci after Barasertib and IR treatment 319
Appendix Figure 13: Comparison of IR dose response in H460 xenografts between multiple studies 322

List of Tables

Table 1. 1 Clinical Trials with the AURKB Inhibitor Barasertib (AZD1152) 62
Table 1. 2 Clinical Trials with the AURKB Inhibitor Defosbarasertib (AZD2811) 64
Table 1. 3: Radiosensitisation parameters for Barasertib in H460 Cells after 1 Hr pretreatment 118

Table 4. 1: The number of (phospho)peptides discovered per MS/MS experiment and the filtering process 140
Table 4. 2: 10 Phosphopeptide isoforms most increased in the combination (Barasertib + IR) compared to IR alone 142
Table 4. 3: 10 Phosphopeptide isoforms most decreased in the combination (Barasertib + IR) compared to IR alone 143
Table 4. 4: The number of peptides discovered per Alisertib/IR MS/MS experiment and the filtering process 169

Appendix Table 1: Chemicals and materials used in laboratory protocols 291
Appendix Table 2: Primary antibodies used in laboratory protocols 293
Appendix Table 3: Secondary antibodies used in laboratory protocols 293
Appendix Table 4: Drug compounds used in laboratory protocols 294
Appendix Table 5: Reagent kits used in laboratory protocols 294
Appendix Table 6: Solutions required for resolving gels (8% acrylamide) for SDS-PAGE. 295
Appendix Table 7: Solutions required for resolving gels (10% acrylamide) for SDS-PAGE 295
Appendix Table 8: Solutions required for resolving gels (12% acrylamide) for SDS-PAGE 295
Appendix Table 9: Solutions required for stacking gels (5% acrylamide) for SDS-PAGE 296
Appendix Table 10: Lysis buffer for mass spectrometry sample preparation 296
Appendix Table 11: DMF and SF values for H460 cells 297
Appendix Table 12: DMF and SF values for H1299 and SW900 cells 298

Abbreviations

•OH	Hydroxyl radicals
53BP1	p53-binding protein 1
A-EJ	Alternative end-joining
Ab	Antibody
ABC	Avidin–biotin complex
ACN	Acetonitrile
AKI	Aurora kinase inhibitor
ALK	Anaplastic lymphoma kinase
AML	Acute myeloid leukaemia
ANOVA	Analysis of variance
APAF1	Apoptotic protease-activating factor 1
APC/C	Anaphase-promoting complex
APE1	Apurinic/apyrimidinic endonuclease 1
APLF	Aprataxin and PNK-like factor
APS	Ammonium persulfate
APTX	Aprataxin
ATM	Ataxia-telangiectasia mutated
ATP	Adenosine triphosphate
ATR	Ataxia-telangiectasia and rad3 related
ATRIP	ATR interacting protein
AURKA	Aurora kinase A
AURKAi	Aurora kinase A inhibitor
AURKB	Aurora kinase B
AURKBi	Aurora kinase B inhibitor
AURKC	Aurora kinase C
AURKi	Aurora kinase inhibitor
AURKs	Aurora kinases
BARD1	BRCA1-associated RING domain protein 1
Bcl-XL	B-cell lymphoma-extra large
BRCA1	Breast cancer type 1 susceptibility protein
BRCA2	Breast cancer type 2 susceptibility protein
BRDU	Bromodeoxyuridine
BSA	Bovine serum albumin
Bub1	Budding uninhibited by benzimidazoles 1
Bub3	Budding uninhibited by benzimidazoles 3
BubR1	Bub1-related kinase
ACN	Acetonitrile
Cdc20	Cell division cycle 20
Cdc25	Cell division cycle 25
Cdk	Cyclin-dependant kinase
CENP-A	Centromere protein A
CENP-H	Centromere protein H

CENP-I	Centromere protein I
CENP-E	Centromere protein E
Cep192	Centrosomal protein 192
Chk1	Checkpoint kinase 1
Chk2	Checkpoint kinase 2
CHMP4	Charged multivesicular body protein 4
CPC	Chromosomal passenger complex
CSFs	Common fragile sites
CXCL5	C-X-C Motif chemokine ligand 5
DAB	3,3′-Diaminobenzidine
DAPI	4′,6-Diamidino-2-phenylindole
DAVID	Database for Annotation, Visualization and Integrated Discovery
DDR	DNA damage response
DMEM	Dulbecco's modified eagle medium
DMF	Dose modulation factor
DMSO	Dimethyl sulfoxide
DNA-PK	DNA-dependant protein kinase
DNA-PKcs	DNA-dependent protein kinase catalytic subunit
DPX	Dibutylphthalate polystyrene xylene
DSB	Double strand break
DSBR	Double strand break repair
DTT	Dithiothreitol
ECL	Enhanced chemiluminescence
EDTA	Ethylenediaminetetraacetic acid
EGFR-TK	Epidermal growth factor receptor tyrosine kinase
EMT	Epithelial-mesenchymal transition
ERCC1	Excision repair 1
ESCRT	Endosomal sorting complex required for transport
FBS	Foetal bovine serum
FEN1	Polynucleotide kinase 3'-phosphatase
FITC	Fluorescein isothiocyanate
FSC	Forward scatter
G-CSF	Gonadotropin-colony stimulating factor
Gadd45α	Growth arrest and DNA damage inducible alpha
GAPDH	Glyceraldehyde-3-phosphate dehydrogenase
H2AX	H2A histone family member X
H3	Histone 3
HCD	Higher-energy collisional dissociation
HDR	Homology directed repair
HEPES	4-(2-hydroxyethyl)-1-piperazineethanesulfonic acid
hnRNPK	Heterogeneous nuclear ribonucleoprotein K
HNSCC	Head and neck squamous cell carcinoma
HP1-α	Heterochromatin protein 1α
HPLC	High-performance liquid chromatography

HQPA	Hydroxyquinazoline-pyrazol-aniline
HR	Homologous recombination
HU	Hydroxyurea
IAC	Iodoacetamide
IC50	Half-maximal inhibitory concentration
IF	Immunofluorescence
IHC	Immunohistochemistry
INCENP	Inner centromere protein
iPOND	Isolation of proteins on nascent DNA
IR	Ionising radiation
JAK2	Janus kinase 2
K3H9me3/S10ph	Double H3 modification tri-methylated K9/phosphorylated S10
KEGG	Kyoto Encyclopedia of Genes and Genomes
Kif11	Motor kinesin family member 11
KT	Kinetochore
Ku	Ku70/Ku80 heterodimer
LC-MS/MS	Liquid chromatography–tandem mass spectrometry
LD50	50% lethal dose
LogP	"-Log10 (P value)
MAD1	Mitotic arrest deficiency 1
MAPK	Mitogen-activated protein kinases
MAPK1	Mitogen-activated protein kinase 1
MCAK	Mitotic centromere-associated kinesin
MCC	Mitotic checkpoint complex
Mcl-1	Induced myeloid leukaemia cell differentiation protein
MDC1	Mediator of DNA damage checkpoint protein 1
MDM2	Mouse double minute 2 homolog
MiDAS	Mitotic DNA synthesis
MiDAS	Mitotic DNA synthesis
Mklp1	Mitotic kinesin-like protein 1
MOMP	Mitochondrial outer membrane permeabilization
Mps1	Monopolar spindle 1
MRN	Mre11-Rad50-Nbs1
mRNA	Messenger RNA
MS/MS	Tandem mass spectrometry
MT	Microtubule
MTOCs	MT organising centres
NaOH	Sodium hydroxide
NCD	Nominal collision energy
ncRNA	Non-coding RNA
NDEL1	NudE Neurodevelopment Protein 1 Like 1
NEDD-9	Neural precursor cell expressed, developmentally down-regulated 9
NFκB	Nuclear factor kappa B
NHEJ	Non-homologous end joining

NIR	Novel INHAT repressor
NSCLC	Non-Small Cell Lung Cancer
NTCP	Normal tissue complication probability
OCT	Optimal cutting temperature
P16	Protein 16
P21	Protein 21
P27	Protein 27
p53	Tumour protein 53
PAK	P21 (RAC1) activated kinase
PALB2	Partner and localizer of BRCA2
PARP1	Poly(ADP-ribose) polymerase 1
PARylation	Auto-poly(ADP)ribosylation
PARylation	Poly(ADP)ribosylation
PAXX	PAXX non-homologous end joining factor
PBS	Phosphate buffered saline
PCM	Pericentriolar material
PD-L1	Programmed death ligand 1
PDGF	Platelet-derived growth factor
PFA	Paraformaldehyde
pH3	Phospho-histone 3
PI	Propidium iodide
PIKK	Phosphatidylinositol 3-kinase-related kinase
PLK1	Polo-like kinase 1
PNKP	Polynucleotide kinase 3'-phosphatase
PP1	Protein phosphatase 1
PT	Pretreatment
PTM	Post-translational modifications
RacGAP1	Rac GTPase-activating protein 1
RAD51	RADiation sensitive protein 51
RAD52	RADiation sensitive protein 52
RASSF1	Ras association domain family member 1 isoform A
Rb	Retinoblastoma protein
RIPA	Radio-immunoprecipitation assay
RNA-seq	RNA-seq
RNF168	Ring finger protein 168
RNF8	Ring finger protein 8
ROS1	C-Ros oncogene 1
RPA	Replication protein A
RPM	Revolutions per minute
RPMI	Roswell Park Memorial Institute
SAC	Spindle assembly checkpoint
SASP	Senescence-induced secretory phenotype
SCF	Stem cell factor
SCLC	Small Cell Lung Cancer

SD	Standard deviation
SDS	Sodium dodecyl sulphate
SDS-PAGE	Sodium dodecyl-sulphate polyacrylamide gel electrophoresis
SEM	Standard error of the mean
Ser	Serine
siRNA	Small interfering RNA
Ska1	Spindle and kinetochore associated complex subunit 1
SSA	Single strand annealing
SSB	Single strand break
SSC	Side scatter
ssDNA	Single stranded DNA
STAT3	Signal transducer and activator of transcription 3
TACC	Transforming acidic coiled coil
TCP	Tumour control probability
TEMED	N,N,N,N,tetramethylethylenediamine
TFA	Trifluoroacetic acid
Thr	Threonine
TIFs	Telomere dysfunction-induced foci
TiO_2	Titanium dioxide
TMT	Tandem mass tags
TNF	Tumour necrosis factor
TOPBP1	DNA topoisomerase II binding protein 1
TPX2	Targeting protein For Xklp2
TRF2	Telomeric repeat-binding factor 2
TRITC	Tetramethylrhodamine
VPS4	Vacuolar protein sorting-associated protein 4
W/V	Weight by volume
WB	Western blot
WRN	Werner protein
XLF	XRCC4-like factor
XPF	Xeroderma pigmentosum group F-complementing protein
XRCC1	X-ray repair cross-complementing protein 1
XRCC4	X-ray repair cross-complementing protein 4
γ-TURCs	γ-Tubulin ring complexes
γH2AX	Gamma-H2AX

Chapter 1: Introduction

1. Introduction

1.1. Lung Cancer

Lung cancer is the third most common cancer in the UK after Breast and Prostate Cancer. While only accounting for 13 % of cancer cases, lung cancer was responsible for 19 % of UK cancer deaths in 2022 (Globocan 2022). One-year survival is 44.3 % (NCLA, 2022). The high mortality of lung cancer compared to more common cancers is related to the late stage of disease in patients at diagnosis. Lung cancer is most commonly diagnosed at stage IV (43 % of cases), for which survival after 1 year is 17 % (Navani et al., 2022)

1.1.1. Subtypes of Lung Cancer

Lung cancers can be divided into two main subtypes, non-small cell lung cancer (NSCLC) which accounts for 85% of cases and small cell lung cancer (SCLC) which accounts for 15% of cases. NSCLC is further classified into three distinct histopathological groups; adenocarcinoma, squamous cell carcinoma and large cell carcinoma (Zappa and Mousa, 2016).

1.1.2. Treatment Options for Lung Cancer

The current treatment options for lung cancer include surgical resection for stages I, II and IIIA with adjuvant radiotherapy, chemotherapy, or targeted biological therapies. Surgery resection is less effective in advanced NSCLC, so stage III-IV NSCLC is predominantly treated with chemotherapy/targeted therapies and radiotherapy (NDRS, 2024). Squamous cell NSCLC is treated with platinum doublet

therapy with the addition of pembrolizumab in tumours with >50% programmed death ligand 1 (PD-L1) tumour proportion score (CRUK, 2019).

For non-squamous NSCLC, combined chemotherapy of pemetrexed, pembrolizumab and platinum chemotherapy is offered. If PD-L1 tumour expression is greater than 50%, pembrolizumab monotherapy is offered. Many targeted therapies have replaced cytotoxic chemotherapy as first line treatment including therapies targeting epidermal growth factor receptor tyrosine kinase (EGFR-TK) mutations, anaplastic lymphoma kinase (ALK) gene fusions and c-Ros oncogene 1 (ROS1) mutations (Yuan et al., 2019). Platinum doublet therapy, platelet-derived growth factor (PDGF) inhibitors and taxane therapies are also offered as second and third-line therapies (CRUK, 2019).

1.1.3. Use of Radiotherapy in Lung Cancer

Radiotherapy plays a key role in the management of NSCLC and was used in over 25.4 % of NSCLC cases for curative or palliative treatment in the UK (NDRS, 2024). Radiotherapy is commonly employed across all stages of NSCLC, with the highest use in treatment of stage III tumours (37.1 %) (NDRS, 2024).

Optimal radiotherapy doses are those which maximise tumour control probability (TCP) and minimise normal tissue complication probability (NTCP) (Nuraini and Widita, 2019). The balance between these is referred to as the therapeutic index or ratio (Reda et al., 2020). The cellular effects of repopulation, repair, redistribution and re-oxygenation (the four R’s) determine TCP while NTCP is affected by the rate of repair (Nuraini and Widita, 2019). The therapeutic index is optimised using

regimens of dose and fractionation that maximise effect on the four R's and by image-guided delivery systems to reduce the volume of normal tissue irradiated.

The therapeutic ratio can also be altered by molecular radiosensitisers. These therapies can improve tumour response by targeting cancer cells specifically. Strategies including increasing tumour oxygenation, inhibiting DNA repair, or increasing local free radical production using metallic nanoparticles. However, some strategies can also affect repair in normal tissues and lead to increased NTCP (Reda et al., 2020).

For treatment of cancers in the thorax such as lung cancer, delivering radiotherapy is challenging. Firstly, the impact on radiation-sensitive tissues such as the heart, oesophagus and healthy lung tissue must be restricted to control toxicity. Secondly, delivering the correct dosage to lung tissue is complex due to the low electron density of lung tissue which can alter the dose distribution (Brown et al., 2019). Developments in delivery including stereotactic approaches and breath tracking have enhanced the accuracy and tolerability of radiotherapy for lung cancer.

1.2. The Cellular Response to Radiotherapy

Radiotherapy damages tumour cells by the delivery of ionising radiation (IR). IR affects cells in a stochastic manner, where the probability of effect depends on the dose. Damage to DNA can be caused by direct ionisation of the DNA or by indirect damage arising from by ionization products of other molecules. A major source of indirect damage is the ionisation of water molecule. This reaction leads to ejection of electrons and the formation of an ionized water molecule, which upon reaction with other water molecules, generates hydroxyl radicals (•OH) in addition to other

byproducts (Ward, 1988). DNA damage via reaction with OH radicals is considered as a major mechanism of DNA damage following IR.

Damage to DNA includes single-strand breaks (SSBs) and double strand breaks (DSBs), as well as base damage, DNA-DNA or DNA-protein crosslinks, and oxidation products such as 8-hydroxyadenine (Goodhead, 1994, Mundt et al., 2003).

SSBs are believed to be the most common form of damage. These result from hydroxyl radical attack of the deoxyribose sugar units of the sugar phosphate backbone of DNA. Direct ionisation of the π-bonds within DNA bases can also create SSBs (Ward, 1988). DSBs can result from multiple localised DNA backbone attacks. DSBs are the most serious form of DNA damage and are responsible for cell lethality after IR (Ward, 1988).

The main determinant in response to radiation is cell turnover, with highly proliferative cells being the most affected (McBride and Schaue, 2020). The phase of the cell cycle also determines sensitivity, with cells being most sensitive in mitosis and the least sensitive in G_1 or late S phase, depending on cell line (Terasima and Tolmach, 1963, Sinclair and Morton, 1965, Biade et al., 1997, Pawlik and Keyomarsi, 2004). Following activation of upstream DNA damage response (DDR) sensors and effectors, the cell undergoes cell cycle arrest and attempts DNA repair (Powell and McMillan, 1990). If the damage is left unrepaired/unrepairable, cell death may result.

1.2.1. DNA Damage Response Initiation

Following IR-induced damage, DNA damage sensors and early signal transducers are critical for timely activation of DDR pathways.

In response to IR-induced damage, the phosphatidylinositol 3-kinase-related kinase (PIKK) proteins Ataxia-telangiectasia mutated (ATM), Ataxia-telangiectasia and Rad3 related (ATR) or DNA-dependant protein kinase (DNA-PK) are recruited and activated to sites of damage. DNA-PK and ATM are activated at sites of DSBs while ATR is activated in response to SSBs and replication stress (Podhorecka et al., 2010). These three proteins are key effectors of the DDR and are required to stimulate local responses to DNA damage. The PIKKs can initiate global responses such as cell cycle checkpoint activation through the downstream activation of other kinases, including Checkpoint kinases 1 and 2 (Chk1 and Chk2), respectively (Chen and Poon, 2008, Blackford and Jackson, 2017).

The three PIKKs are recruited and activated at DNA damage sites by independent cofactors. ATR and its binding partner ATRIP are recruited to SSBs and replication stress by Replication protein A (RPA) which promotes ATRIP binding to ssDNA (Zou and Elledge, 2003). ATM is recruited and activated by the MRN complex (Mre11-Rad50-Nbs1) (Lee and Paull, 2004, Uziel et al., 2003). ATM activates Mediator of DNA damage checkpoint protein 1 (MDC1) and amplifies MRN/ATM signalling in a positive feedback loop at DSBs (Syed and Tainer, 2018, Stucki et al., 2005, Turinetto and Giachino, 2015). In addition to signalling activity, the MRN complex can interact directly with DNA to tether broken DNA ends and unwind DNA duplexes with 3’ overhangs (Lavin et al., 2015, Paull and Gellert, 1999). This activity is key for the initiation of homologous recombination (HR), also known as homology directed repair. ATM orchestrates key cellular responses to DSBs including DNA repair pathways, cell cycle arrest, apoptosis and senescence by phosphorylating hundreds of substrates (Blackford and Jackson, 2017). Tumour protein 53 (P53) is one key downstream target. ATM stabilises p53 directly and indirectly, preventing Mouse

double minute 2 homolog (MDM2)-mediated degradation (Canman et al., 1998, Shiloh and Ziv, 2013, Harris and Levine, 2005).

DNA-PKcs is recruited and activated at DSBs by Ku70 and Ku80 (Gottlieb and Jackson, 1993, Singleton et al., 1999). Ku (Ku70/Ku80 heterodimer) is a key DNA sensor which rapidly binds at DSB sites and specifically initiates the non-homologous end-joining (NHEJ) DSB repair pathway (Davis and Chen, 2013).

The DNA perturbation sensor H2AX is activated through Serine (Ser) 139 phosphorylation by ATM, ATR and DNA-PK, promoting recruitment of DDR proteins to DNA breaks (Reitsema et al., 2005, Mukherjee et al., 2006, Ward and Chen, 2001, Ward et al., 2004, Mohiuddin and Kang, 2019). γH2AX (Ser139) foci remain until the damage is repaired and are widely used as a biomarker of DNA damage (Campillo-Marcos and Lazo, 2018, Popp et al., 2016).

1.2.2. Cell Cycle Arrest

In addition to activation of DNA repair pathways, early DNA sensors initiate cell cycle arrest to prevent further damage to DNA integrity and to allow time for repair (summarised in Fig 1.1).

Cell cycle arrest is achieved by inhibition of specific cyclin-dependant kinases (Cdk) which promote cell cycle progression (Blackford and Jackson, 2017).

Specific cyclins proteins drive each stage of the cell cycle and rely on Cdk partners for activation. Chk1 and Chk2 instigate cell cycle arrest by inhibiting cyclin-Cdk complexes (Matthews et al., 2022).

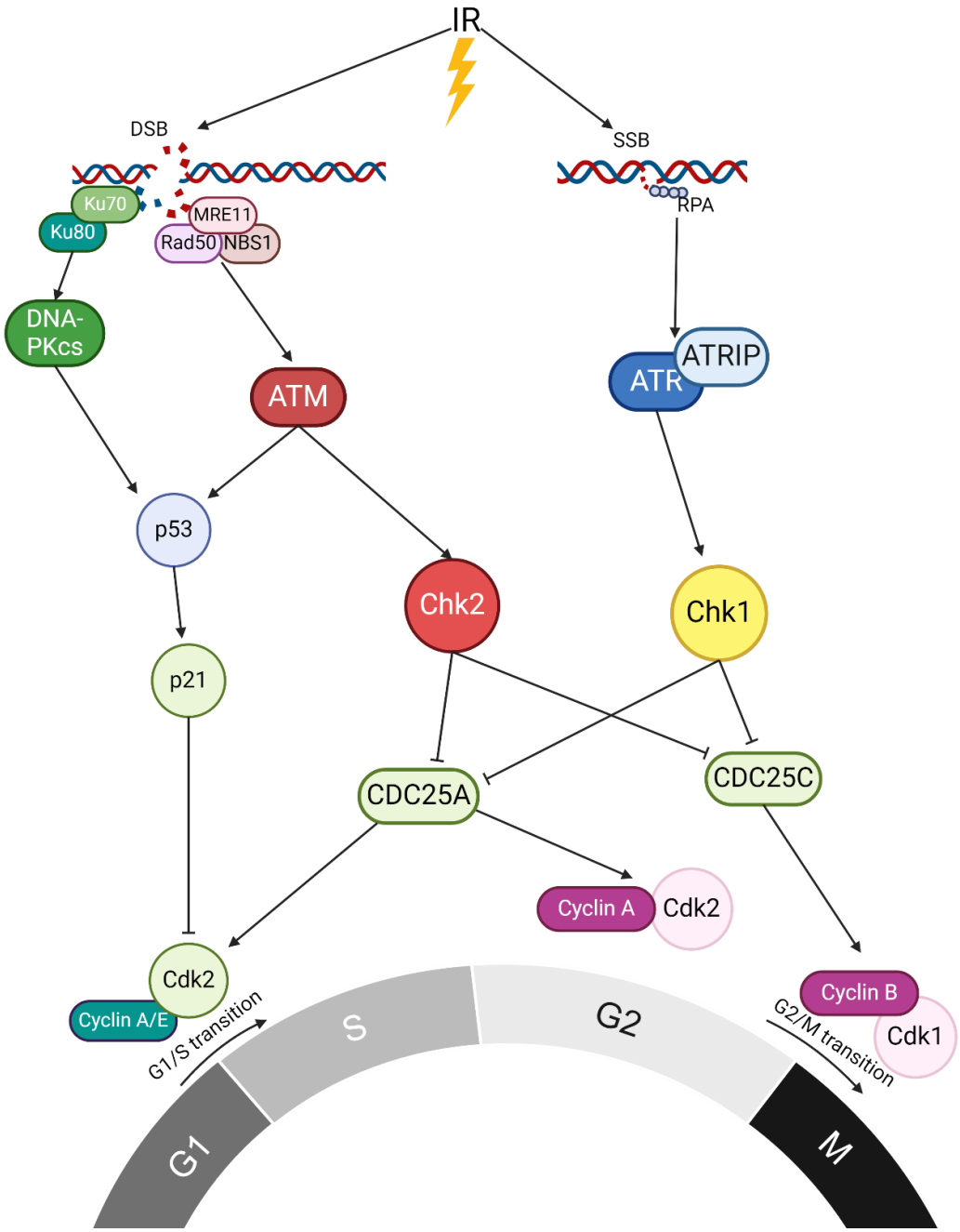

Figure 1. 1: Cell cycle checkpoint activation as result of DNA damage signalling following IR.

DSBs created by IR lead to γH2AX activation which are activated at and bind to DSBs to form foci. γH2AX starts a downstream signalling pathway involving ATM in the case of DSBs. ATM activates the downstream effectors p53 and Chk2, which G_1 or G_2 cell cycle arrest via p21 inhibition of cyclin-dependant kinases (CDKs) and cyclin inhibition, or via inhibition of Cdc25 phosphatases. ATR and Chk1 DDR pathways are the downstream effectors in the DDR to SSBs and replication forks. Similarly, they can induce cell cycle arrest. Figure produced in Biorender.

(Boutros et al., 2007). Chk1 also prevents mitotic entry via activation of Wee1 kinase, which inhibits Cyclin B-Cdk1 and Cyclin A- Cdk2 activity (Poon, 2016). Cyclin B-Cdk1 activation can also be inhibited by p21 (Smits et al., 2000). These signalling events prevent entry to mitosis which is dependent on Cyclin B-Cdk1 activity.

1.2.3. SSB Repair

SSBs and base damage are repaired through single strand break repair and base excision repair respectively (Abbotts and Wilson, 2017). SSBs and damaged bases when left unrepaired can lead to replication stress through replication fork arrest and collapse, which can create DSBs (Scully et al., 2019).

Single strand break repair (SSBR) involves detection, DNA end processing, gap filling and ligation (Caldecott, 2008). Poly(ADP-ribose) polymerase 1 (PARP1) transiently detects SSBs, inducing auto-poly(ADP)ribosylation (PARylation) which recruits DNA repair proteins to the site (Ray Chaudhuri and Nussenzweig, 2017). Increased auto-PARylation promotes dissociation from DNA thus allowing access to the DNA by repair machinery. DNA end processing is carried out by Apurinic/apyrimidinic endonuclease 1 (APE1), Polynucleotide Kinase 3'-Phosphatase (PNKP), Flap endonuclease 1 (FEN1) and Aprataxin (APTX), depending on the type of damaged terminus (Izumi et al., 2000, Wiederhold et al., 2004, Whitehouse et al., 2001, Caldecott, 2014, Clements et al., 2004). Once DNA ends have been processed to restore hydroxyl configuration, gap filling is carried out to replace missing nucleotides. The primary DNA polymerase involved is Pol β but Pol θ and Pol ε can also perform this step (Winters et al., 1999, Caldecott, 2014). Lig1 and Lig3α complete ligation (long patch and short patch mechanisms, respectively) supported by Proliferating cell nuclear antigen (PCNA) and X-ray repair cross-

complementing protein 1 (XRCC1) (Caldecott, 2014, Caldecott et al., 1994, Parsons et al., 2005, Prasad et al., 1996, Smirnova et al., 2005).

1.2.4. DSB Repair

There are two main pathways of DSB repair, NHEJ and homologous recombination (HR) (also known as homology directed repair (HDR)). DNA repair pathway choice depends on many factors such as DNA end structure, cell cycle phase, chromatin structure and speed of repair (Scully et al., 2019).

HR requires sister chromatid homology and therefore is active in S and G_2, while NHEJ is the predominant repair pathway at other stages of the cell cycle (Pannunzio et al., 2018, Scully et al., 2019).

NHEJ is initiated by Ku binding, recruitment of DNA Ligase IV, and scaffolding factors X-ray repair cross-complementing protein 4 (XRCC4), XRCC4-like factor (XLF) and Non-homologous end joining factor (PAXX). A “synaptic complex” involving DNA-PK tethers the two DNA ends (Cary et al., 1997, Weterings and van Gent, 2004). DNA end processing is then facilitated by Artemis, Werner protein (WRN) and Aprataxin and PNK-like factor (APLF) to create ligatable ends (Davis and Chen, 2013). DNA ligase IV, stabilised by XRCC4, then ligates the broken ends (Grawunder et al., 1997, Gu et al., 2007). While NHEJ is traditionally considered error-prone, it can be genetically silent, with mostly error-free repair or at least minimal divergence from the original sequence (Rodgers and McVey, 2016).

NHEJ is only active when there is minimal resection and thus DNA end resection by MRN can disrupt NHEJ in favour of HR. DNA end resection is initiated when in S-

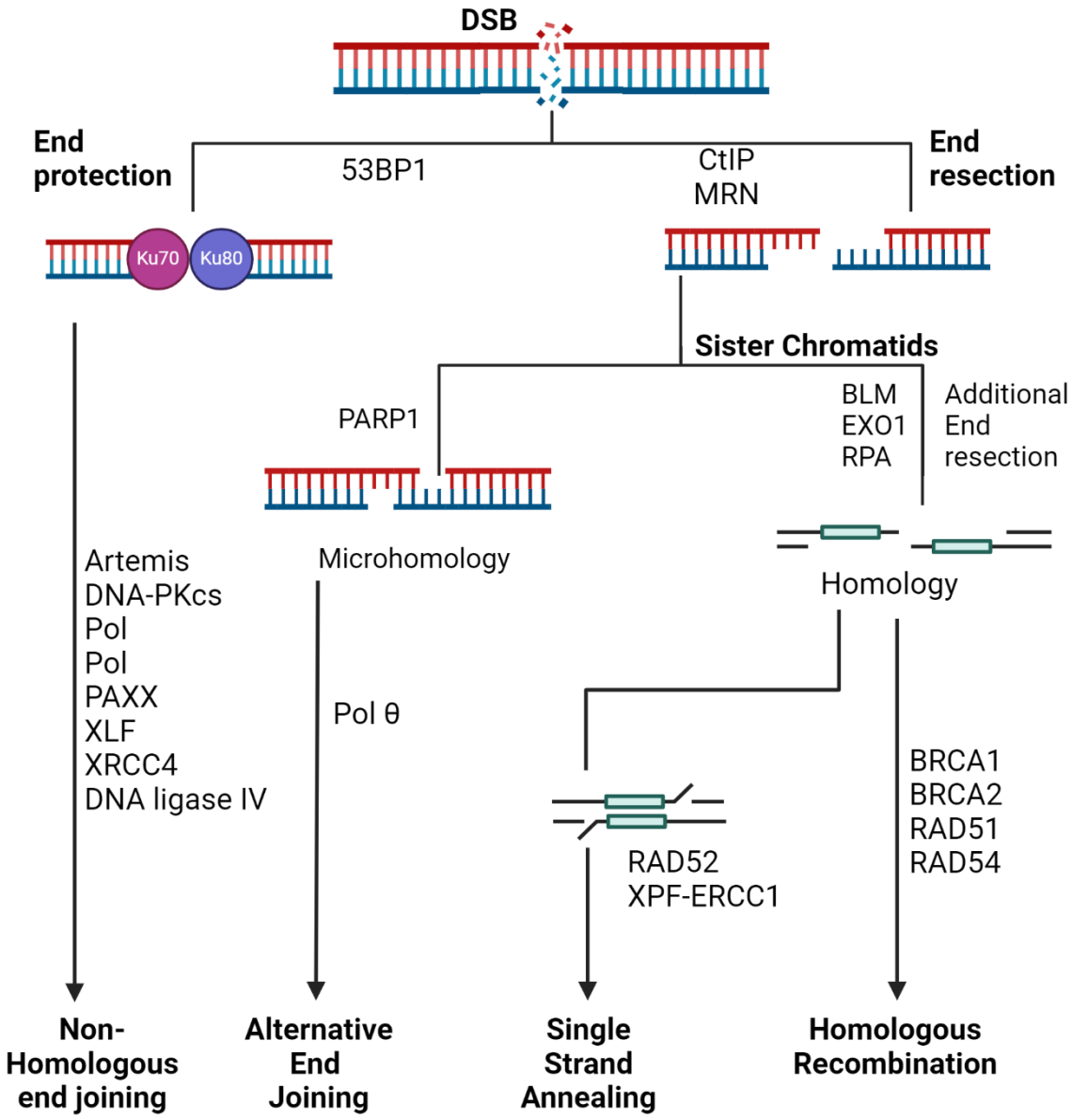

Figure 1. 2: DSB repair pathway choice

The requirement for DSB end resection is a major factor is DSB repair pathway choice. NHEJ requires minimal resection and NHEJ factors Ku70 and Ku80 protect ends from resection. End resection is carried out by MRN and CtIP, which generates single-stranded DNA required for alternative end-joining (a-EJ), SSA and HR. SSA requires >20 bp for homology whilst HR requires >50 bp. A-EJ requires <25bp for microhomology-based repair. Figure produced in Biorender.

phase Cdk1 mediated phosphorylation of C-terminal binding protein (CtIP) promotes its interaction with Breast cancer type 1 susceptibility protein (BRCA1). BRCA1 and CtIP antagonise 53BP1-Replication timing regulatory factor 1 (Rif1) binding to DNA ends. Rif1 recruitment by 53BP1 at DNA ends prevents end resection (Isono et al., 2017). Once CtIP/BRCA1 displace Rif1, the MRN complex can generate ssDNA overhangs. The single stranded DNA is quickly coated by RPA, subsequently BRCA1, BRCA1-associated RING domain protein 1 (BARD1) and Breast cancer type 2 susceptibility protein (BRCA2) promote replacement of RPA by Radiation sensitive protein 51 (RAD51) to form RAD51 filament nucleoproteins (Zhao et al., 2017). BRCA2 and Partner and localizer of BRCA2 (PALB2) then enhance RAD51 mediated strand invasion of the homologous DNA sequence to form a D-loop (Buisson et al., 2010). Following invasion, DNA synthesis occurs by extending the D-loop past the region of the DSB. Most extended D-loops are then resolved by synthesis dependent strand annealing repairing the DSB. Alternatively second end capture can occur and the DSB is then repaired after resolution/dissolution of a double holiday junction (Wright et al., 2018). The role of DNA resection in DSBR pathway choice is summarised in Figure 1.2.

Single stranded lesions produced by IR can lead to stalled replication forks in S phase and creation of a one-ended DSB. This can be repaired by HR. Alternatively stalled forks can be processed and reversed to allow lesion bypass or repair (Rickman and Smogorzewska, 2019).

HR can also lead to RAD51-independent repair mechanism known as single-strand annealing. This pathway anneals the 3’ DNA ends while deleting the single-stranded sequence overhang and therefore introduces errors (Chang et al., 2017). Radiation

sensitive protein 52 (RAD52) anneals the complementary single stranded tails (Rothenberg et al., 2008). The nucleotide excision repair complex of Xeroderma pigmentosum group F-complementing protein (XPF) and Excision Repair 1 (ERCC1) processes and removes the non-homologous ssDNA tails (Motycka et al., 2004).

Alternative end-joining (a-EJ) is a microhomology-dependant repair pathway which requires Pol θ but also involves PARP1, CtIP and MRN (Wyatt et al., 2016, Luedeman et al., 2022, Sfeir and Symington, 2015). This pathway can repair DSBs in the absence of Ku or the DNA ligase complex. Regions of microhomology near DNA ends promote alignment of ssDNA following resection. Pol θ stabilises the ssDNA overhangs to promote annealing, and can extend DNA ends by insertions > 10 nucleotides, using the annealed strand as a template (Chang et al., 2017). The intermediate can then be sealed by DNA ligase I and DNA ligase III (Masani et al., 2016, Chang et al., 2017).

1.2.5. Mitotic Aberrance after IR

DNA damage that occurs during or is carried into mitosis has serious consequences for the genomic integrity of future cells. Damage promotes mitotic aberrations which are known to accumulate in cancer cells in the days after IR (Hayashi and Karlseder, 2013). These defects are more common in cancer cells due to aberrant cell cycle control and DDR, leading to cells containing unrepaired DNA intermediates passing prematurely into mitosis.

After IR, unrepaired DNA breaks can present issues during chromosome segregation. DSBs can produce acentric chromosomes which are broken chromosomes with no centromeric region. This can result in anaphase delay, issues

in cytokinesis and post-mitotic micronuclei – small nucleic compartments separate from the main nucleus of the cell (Krupina et al., 2021).

IR has been shown to promote centrosome amplification due to prolonged G_2 arrest (Dodson et al., 2007). Centrosomal aberrations such as amplification or structural abnormalities can lead to chromosome separation defects such as lagging chromosomes or chromatin bridges, resulting in micronuclei. Multipolar spindles can also produce aneuploid daughter cells. These defects can activate the spindle assembly checkpoint (SAC) (also known as the mitotic spindle checkpoint) which has implication for cell fate (Godinho and Pellman, 2014, Wu et al., 2020).

After IR, broken chromosomes or unrepaired DNA intermediates can lead to chromosome bridges, fragments or lagging chromosomes in the cleavage plane during cytokinesis (Chow and Poon, 2010). These events activate the abscission checkpoint which delays abscission to prevent chromatin bridge breakage or aneuploidy occurring via regression of the cleavage furrow. Thus, failure of the abscission checkpoint can result in regression, where the cytoplasm of daughter cells recombines. Alternatively, if abscission occurs and cytokinesis proceeds and the chromatin bridge is cut in the final stages of mitosis, this promotes further DNA damage and can result in micronuclei.

Polyploidy (cells with >4N after mitosis) is a common result of SAC activation following mitotic catastrophe due to slippage (Adjemian et al., 2020, Brito and Rieder, 2009). This occurs due to prolonged arrest at the SAC and is further discussed in section 1.2.6.

DNA repair during mitosis is discussed in section 1.2.7.

1.2.6. Cell Fate after IR

The main mechanisms of cell death following IR are apoptosis and necrosis. IR can also induce autophagy, or an irreversible cell cycle arrest called senescence (Sia et al., 2020). Additionally, IR induces mitotic catastrophe, an onco-suppressive mechanism that promotes death during or after defective mitosis.

Apoptosis is a form of programmed cell death mediated by Caspase cleavage and activation. It results in cellular breakdown via “blebbing” of apoptotic bodies, which can be cleared by phagocytes (Taylor et al., 2008). Apoptosis can be activated by IR through the intrinsic (mitochondrial) pathway by DDR machinery and particularly by p53. P53 activates the B-cell lymphoma 2 (Bcl-2) family. BCL2 Associated X (Bax) and BCL2 Antagonist/Killer 1 (Bak), Bcl-2 proteins, dimerise into a complex which alters mitochondrial permeability via Bax-Bak holes (Eriksson and Stigbrand, 2010, Jiao et al., 2022). This is supported by other Bax-like proteins as well as BH3-only proteins (Jin and El-Deiry, 2005). The formation of Bax-Bak holes leads to mitochondrial outer membrane permeabilization (MOMP). This irreversibly releases pro-apoptotic factors such as Cytochrome C (Riedl and Shi, 2004). Cytochrome C forms the apoptosome via activation of Apoptotic protease-activating factor 1 (APAF1) and mediates Caspase-9 activation, the initiator caspase (Li et al., 1997). A chain reaction of caspase activation by effector caspases commences leading to death substrate cleavage and the phenotypic cell changes of apoptosis (Eriksson and Stigbrand, 2010).

Alternatively, IR can activate the extrinsic (death receptor) pathway through the upregulation of tumour necrosis factor (TNF) death receptors, leading to binding and activation of Caspase 8/10 (Eriksson and Stigbrand, 2010, Sia et al., 2020). This

promotes cleavage and activation of Caspase-3, Caspase-6 and Caspase-7 (Taylor et al., 2008). Apoptotic signalling can then be amplified by Caspase 8/10 by activating Bcl-2 and triggering MOMP, similar to the intrinsic pathway (Luo et al., 1998).

Senescence is a cellular state characterized by cell cycle arrest, preventing further proliferation (Huang et al., 2022). Induction of senescence leads to morphological changes, including cell flattening, vacuolisation and increased granularity (Bourdens et al., 2019, Gewirtz et al., 2008). Expansion of the lysosomal compartment leads to increased β-galactosidase activity, which is used as a marker of senescence (Gewirtz et al., 2008). Senescence is associated with ageing but can also be induced by various triggers, including DNA damage as a result of IR. P53 and Protein 21 (p21) signalling is an upstream activator of senescence, but it can also be activated by Protein 16 (p16), Retinoblastoma protein (Rb) and Protein 27 (p27) signalling (Huang et al., 2022). Many cancer therapies induce senescence which has implications for tumour development and resistance. Senescence-induced secretory phenotype (SASP) is the promotion of inflammatory signalling by senescent cells, commonly induced by the DDR. Persistent SASP can promote proliferation, migration, invasiveness, angiogenesis and Epithelial-mesenchymal transition (EMT) in tumour cells (Xiao et al., 2023).

Mitotic catastrophe is an antiproliferative pathway which regulates cell fate after aberrant mitosis (Galluzzi et al., 2007). This process is sometimes referred to as a death mechanism. Apoptotic, necrotic and autophagic processes have been identified as eventual fates of cells experiencing mitotic catastrophe, so it seems

more appropriate to refer to this as a severe effect of abnormal mitosis that can induce death by known pathways.

Mitotic catastrophe occurs when a cell encounters mitotic aberrance that cannot be resolved and undergoes a prolonged mitotic arrest. This can result in death during mitosis or slippage. Cells which undergo slippage may die in G_1, become senescence or survive as a polyploid cell. Mitotic catastrophe exists to suppress oncogenesis, which can be promoted by aneuploidy following defective mitosis (Mc Gee, 2015). Mitotic catastrophe is summarised in Fig 1.3.

Prolonged mitotic arrest occurs when the SAC is activated and cannot be resolved. DNA damage is known to trigger mitotic catastrophe via the SAC (Kim and Burke, 2008). This can result from defective G_2 checkpoints which allow mitotic entry with unrepaired damage and leads to mitotic catastrophe (Chan et al., 1999, Castedo et al., 2004c). Centrosomal amplification due to IR-induced DNA damage can also promote mitotic catastrophe (Kawamura et al., 2004). Centrosomal amplification can occur due to late S or G_2-arrest and is promoted by Cyclin E and Cyclin A and is more common in p53-deficient cells (Hanashiro et al., 2008, Eriksson and Stigbrand, 2010).

Prolonged mitotic arrest can be resolved via death in mitosis or mitotic exit. Gascoigne and Taylor (2008) proposed a dual threshold model, where the cell fate is determined by whether the mitotic exit or death threshold is met first. Mitotic exit occurs via the gradual decline of Cyclin B levels during prolonged mitosis, which eventually allows mitotic exit via slippage, producing a tetraploid cell. If Cyclin B

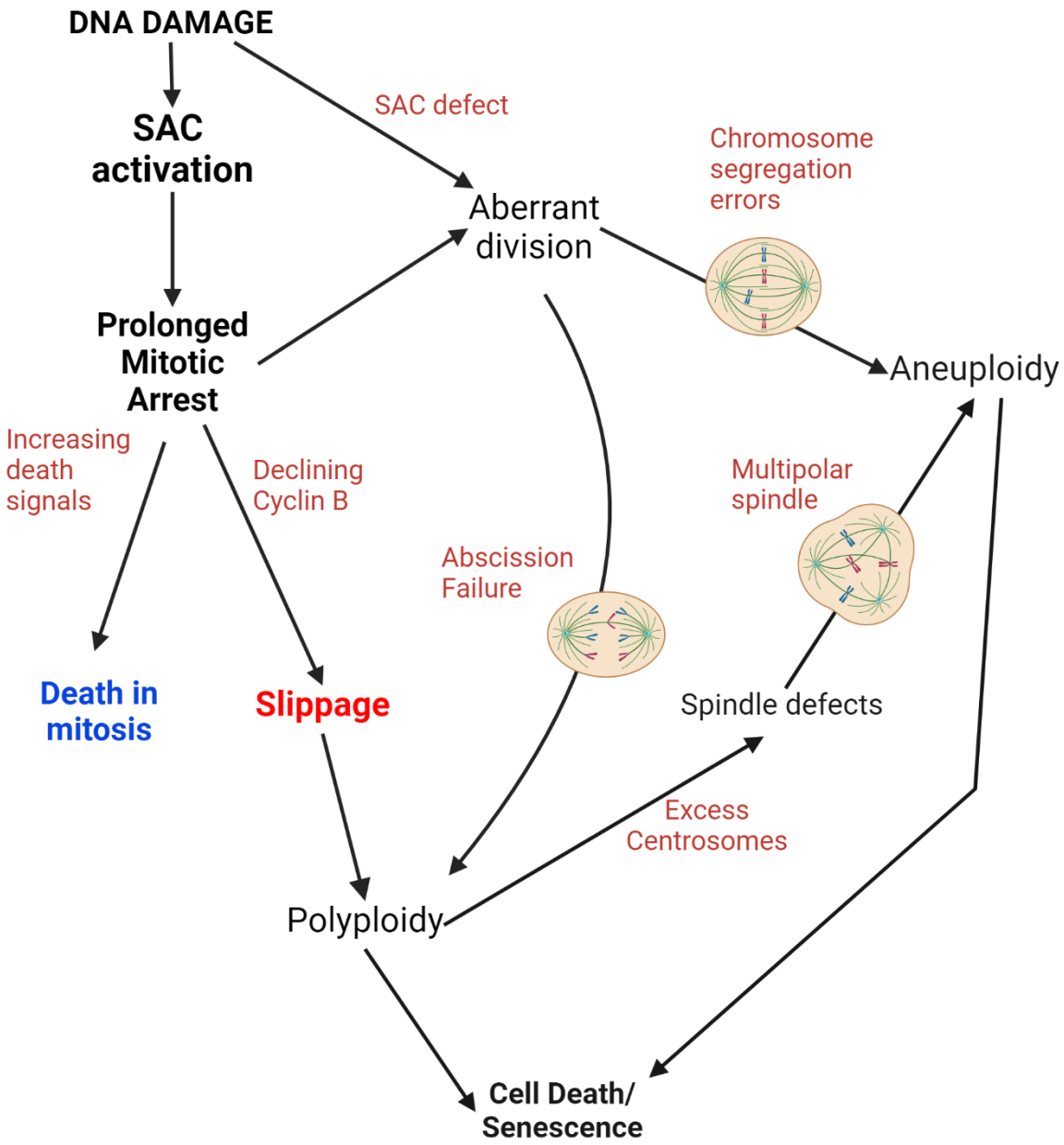

Figure 1. 3: Cell fate following mitotic catastrophe

DNA damage in mitosis activates the SAC which arrests the cell before anaphase. If the checkpoint cannot be resolved due to aberrance, mitosis is prolonged. Over time Cyclin B degrades whilst death signalling (p53, Caspase-2 activation) increases. These two processes will lead to mitotic exit or death in mitosis, respectively. If the cell does divide in the presence of severe DNA damage, it is likely to divide aberrantly and may result in unequal division or abscission failure/regression. Mitotic exit before anaphase generates one polyploid cell, which may undergo p53-dependant apoptosis, death by other mechanisms or senescence. In rare cases, polyploid cells can cycle, but this is likely to result in further aberrance. Figure produced in Biorender.

levels do not decrease below the threshold for mitotic exit, cells can die in mitosis due to accumulating death signals. Individual thresholds are proposed to vary between cell lines and individual cells, promoting the observed variability in response to mitotic catastrophe (Gascoigne and Taylor, 2008).

How cells die during mitosis is also a subject of debate. Apoptotic death is the most common mechanism proposed and mitotic catastrophe has also been described as a specialised apoptosis (Castedo et al., 2004b). Apoptosis during mitotic catastrophe is activated by Caspase-2 and P53, which promote downstream Caspase cleavage and MOMP (Castedo et al., 2004a, Castedo et al., 2004b, Imreh et al., 2011). In support of this, inhibition of pan-Caspase activity can reduce mitotic death (Gascoigne and Taylor, 2008). Caspase-2 is inhibited by mitotic kinases. During mitosis, Cdk1-Cyclin B1 and AURKB can inhibit Caspase-2 activation via phosphorylation at Ser340 and Ser384, respectively (Andersen et al., 2009, Lim et al., 2021). Dephosphorylation is thought to occur by Protein phosphatase 1 (PP1) which becomes uninhibited during prolonged mitosis.

P53 is an upstream activator of apoptosis and is regulated by mitotic kinases. P53 is negatively regulated by Aurora kinases A and B (AURKA and AURKB), Polo-like kinase 1 (Plk1) and Budding Uninhibited by Benzimidazoles 1 (Bub1) whilst Monopolar spindle 1 (Mps1) and Bub1-related kinase (BubR1) promote p53 activity. However, these interactions have been characterised in interphase and are more applicable to post-mitotic p53 signalling. Whether these kinases can regulate death during mitosis catastrophe via p53 requires further investigation (Ha and Breuer, 2012). The regulation of p53 by AURKB and AURKA are further discussed in sections 1.3.2.2 and 1.4.2.1, respectively.

Additionally, regulation of apoptotic factors by Cyclin B-Cdk1 complex have been identified that shed light on apoptotic activation. Cyclin B-Cdk1 inhibit the anti-apoptotic proteins Bcl-2, B-cell lymphoma-extra-large (Bcl-XL) and Induced myeloid leukaemia cell differentiation protein (Mcl-1) during mitosis via inhibitory phosphorylation or targeting for ubiquitin-mediated degradation (Terrano et al., 2010, Upreti et al., 2008, Harley et al., 2010, Kelly et al., 2014). Additionally, Cdk1 phosphorylation of Bim promotes Bak activation and MOMP (Abbotts and Wilson, 2017). These interactions provide a basis for cell death in the event of high Cyclin B-Cdk1 levels during mitotic arrest.

If cells survive aberrant mitosis, they may have chromosomal aberrance. They may also survive as polyploid and aneuploid cells which are generally non-proliferative. In G_1, polyploidy can trigger arrest due to supernumerary centrosomes and these cells commonly undergo apoptosis in G_1 (Ganem et al., 2014, Vitale et al., 2011, Herriage et al., 2024).

DNA damage signalling after prolonged mitosis is promoted by a telomere-dependant pathway. During prolonged mitoses, telomere ends become deprotected through Telomeric repeat-binding factor 2 (TRF2) dissociation. Deprotected ends activate ATM and promote DDR signalling and results in the formation of telomere dysfunction-induced foci (TIFs). TIFs are formed of γH2AX and 53BP1 which bind to telomeric chromatin and telomere ends, respectively. Foci formation activates DDR pathways via p53 in G_1, which promotes elimination by p53-dependant apoptosis. AURKBi by Hesperidin prevent prevents TIF formation, suggesting a role for AURKB in telomere deprotection (Hayashi et al., 2012). Polyploid cells can also survive in a senescent state.

In the absence of p53, polyploid cells are more likely to survive. For these cells, necrosis is the primary cell death mechanism following mitotic catastrophe, although autophagy has also been documented (Sazonova et al., 2021, Fragkos and Beard, 2011). Occasionally, cells can also escape a non-proliferative fate and attempt further division. Further aberrant divisions exaggerate defects and make mitotic death more probable.

1.2.7. DDR during Mitosis

During mitosis, DNA is highly condensed, and the cell has the complex task of chromosome segregation. It used to be thought that the DDR was absent from mitotic cells. However emerging evidence makes it clear that this is not the case and there is complex interplay between DDR proteins and mitotic processes.

Many DDR pathways are inhibited during mitosis. At the start of mitosis, Plk1 phosphorylates Wee1 leading to its degradation, thus attenuating CDK inhibition by upstream DDR effectors (Watanabe et al., 2004b). Plk1 also phosphorylates Claspin, an activator of ATM, resulting in Claspin degradation (Kumagai and Dunphy, 2000, Mailand et al., 2006, Peschiaroli et al., 2006). ATM-Chk2 DDR signalling is also reduced during mitosis (although some activity remains), and Chk2 activation is reduced by Plk1 phosphorylation at mitotic entry (Van Vugt et al., 2010). Transcription during mitosis is greatly limited due to the highly condensed state of chromatin. Therefore, transcriptionally activated DDR effectors such as p21 are inhibited (Blackford and Stucki, 2020). At sites of DSBs, the downstream repair proteins Ring Finger Protein 8 (RNF8), Ring Finger Protein 168 (RNF168), 53BP1 and BRCA1 are not recruited during mitosis (Nakamura et al., 2010, Nelson et al., 2009, Giunta et al., 2010).

MDC1 interactions with RNF8 are inhibited (Orthwein et al., 2014). This explains the lack of 53BP1 at mitotic DSBs; 53BP1 binding sites rely on RNF168 ubiquitination of H2A histones (Fradet-Turcotte et al., 2013, Ochs et al., 2016, Gatti et al., 2012, Mattiroli et al., 2012, Thorslund et al., 2015). Therefore, when DSBs are formed during mitosis, 53BP1 does not localise so foci do not form at these DSBs until G_1 (Lee et al., 2014). 53BP1 mitotic stress bodies, distinct from nuclear bodies or DDR-induced foci, have been reported which may have a negative regulatory role. These occur during prolonged mitosis (due to mitotic arrest agents such as Nocodazole) near centrosomes, where 53BP1 has a mitotic role. These foci do not associate with γH2AX foci and do not require the DNA-binding domain. They contain Lamin-A which inhibits 53BP1 DNA binding thus inhibiting its repair activity. Once mitotic arrest is overcome, these foci migrate away from centromeres and disappear by the end of mitosis. These foci are thought to prevent 53BP1-mediated apoptosis and NHEJ during mitotic stress (Bleiler et al., 2023).

This said, some elements of the DSB response still occur. ATM and DNA-PK activity promote the formation of γH2AX foci formation and recruitment of MDC1 (Rogakou et al., 1999). Inhibiting ATM and DNA-PK during mitosis reduces the γH2AX response and viability after IR, suggesting the mitotic response for DSBs is still important for recovery from damage.

How DSB repair might occur in mitosis is an area of ongoing debate. Most studies suggest that HR is inactive, but whether NHEJ or over-resection could take place during mitosis is unclear.

Tethering of broken ends may serve as a protection mechanism until DSBR is active in G_1. In mitosis, MDC1 recruits DNA topoisomerase II binding protein 1 (TOPBP1)

at DSBs to form bridging complexes with TOPBP1 between MDC1 foci. It is suspected that these structures tether broken chromosomes (Leimbacher et al., 2019). Acentric chromosomes are tethered by AURKB, PLK1 and BubR1. Acentric fragments are then pulled with their centric chromatid to the correct daughter cell, which prevents mis-segregation of broken chromatin or chromatin loss (Royou et al., 2010). DSB repair can then occur after mitosis to repair the chromatin breaks.

Under-replicated DNA poses an issue for cells undergoing mitosis as it could compromise genetic integrity. Increased evidence supports the existence of replication in mitosis, known as mitotic DNA synthesis (MiDAS). MiDAS occurs in prophase and prometaphase and resolves stalled replication forks that occur following replication stress (Bournaka et al., 2024). During MiDAS, stalled replication forks are processed by endonucleases such as MUS81 and DNA synthesis is facilitated by POLD3. RAD52 and FANCD2 are also required for MiDAS in cancer cells, while in non-cancerous lines, RAD52 is not essential (Graber-Feesl et al., 2019). RAD52 and FANCD2 localise to sites of replication stress in S phase where they promote MiDAS once cells progress into mitosis (Said et al., 2022). In the absence of MiDAS, the formation of 53BP1 bodies is increased after mitosis, which mark replication stress and associate with sites of stress such as common fragile sites (Bhowmick et al., 2016).

1.3. Aurora Kinase B

The three aurora kinases A, B and C (AURKA, AURKB and AURKC) are a family of serine-threonine kinases. Homologs of each are highly conserved in higher and lower eukaryotes due to the essential role they play in mitosis (Marumoto et al., 2005, Magnaghi-Jaulin et al., 2019). AURKA and AURKB are expressed in most normal cell types as they are critical for executing mitosis and ensuring genetic integrity during cell division. Both kinases phosphorylate many substrates and thus play a regulatory role in many stages of the cell cycle. The third member, AURKC, is highly expressed in reproductive cells and is required for meiotic division in mammalian oocytes and sperm (Balboula et al., 2016, Kimmins et al., 2007, Yang et al., 2010b).

AURKB is a master regulator of mitosis and is essential for chromatin condensation during mitosis, faithful segregation of DNA and the SAC. It also regulates cytokinesis and the timing of abscission via the abscission checkpoint. Whilst AURKB is mostly known for its pivotal roles in mitosis, there is growing knowledge of its other roles, such as interaction with the DDR and p53, replication stress recovery and telomere regulation. This thesis focuses on AURKB.

1.3.1. The Role of AURKB in Mitosis

1.3.1.1. The CPC

During mitosis, AURKB forms a complex with Inner centromere protein (INCENP), Borealin and Survivin called the chromosomal passenger complex (CPC). At the onset of mitosis, the CPC localises at the inner centromeres from prophase until metaphase. At the inner centromere, an AURKB diffusion gradient forms, with levels

decreasing further from the centromeres (Wang et al., 2011a). CPC localisation at the centromeres supports AURKB's roles regulating microtubule (MT) - kinetochore (KT) attachments, the SAC and chromosome congression to the metaphase plate (Kitagawa and Lee, 2015). During the metaphase to anaphase transition, the CPC relocates to the cell equator where it functions in cleavage furrow formation (Murata-Hori and Wang, 2002). During cytokinesis, it is present at the midbody and regulates abscission timing (Goldenson and Crispino, 2015, Kitagawa and Lee, 2015). The localisation and roles of AURKB in mitosis are summarised in Fig. 1.4.

1.3.1.2. AURKB Activation during Mitosis

INCENP functions as a scaffold for the CPC, and is also required for AURKB activation and targeting of the complex (Gohard et al., 2014). The N-terminus of INCENP binds Borealin and Survivin, while the C-terminus (the "IN-box" domain) binds AURKB (Jeyaprakash et al., 2007, Bishop and Schumacher, 2002). AURKB binding to the IN-box domain is essential for AURKB activation.

Following INCENP-AURKB binding, AURKB phosphorylates a transcription start site (TSS) motif on the IN-box domain which promotes autophosphorylation of AURKB at Thr232, the key activating residue (Bishop and Schumacher, 2002, Honda et al., 2003, Yasui et al., 2004, Sessa et al., 2005). The initial interaction is thought to provide some activation to initiate autophosphorylation.

AURKB activation also involves phosphorylation at Ser331 by Chk1 at centromeres. This is proposed to enhance activity and is required for AURKB functions related to the SAC (Petsalaki et al., 2011). This interaction is thought to be promoted by ATR

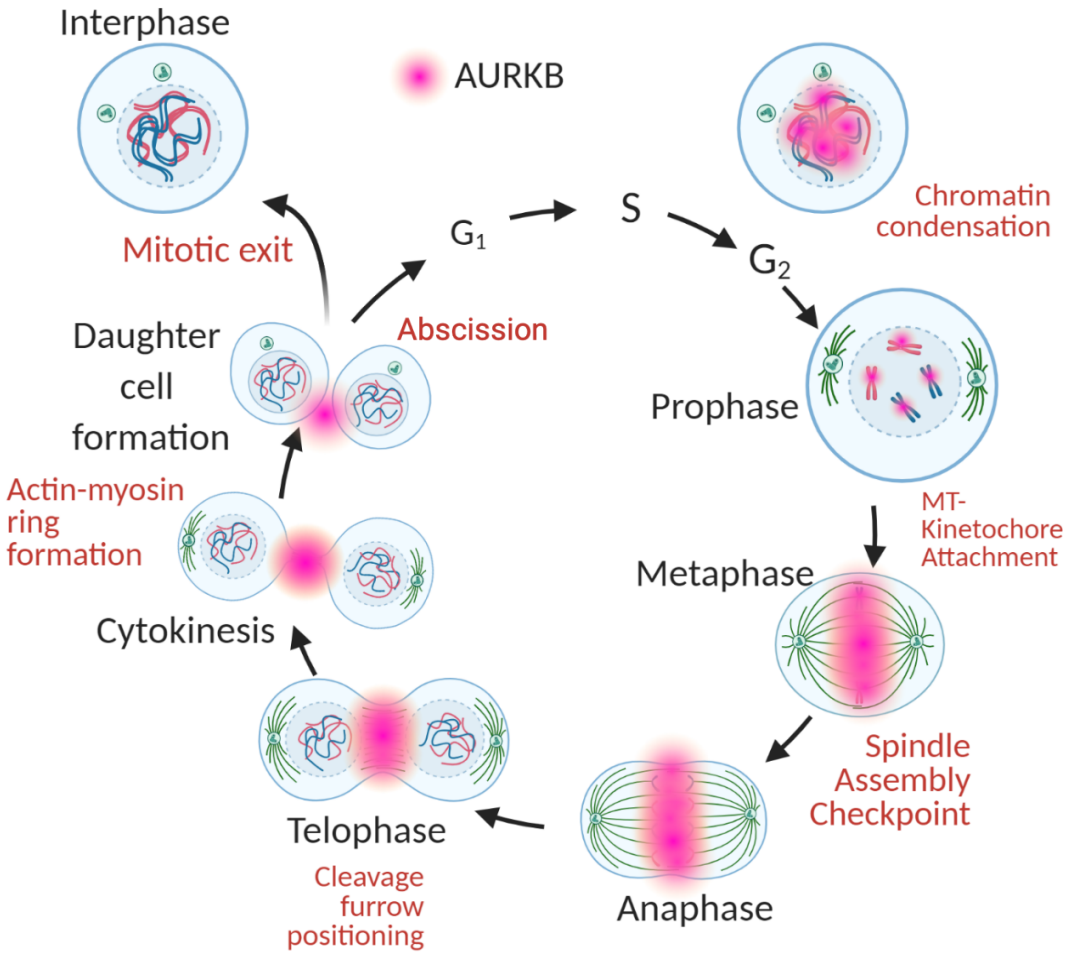

Figure 1. 4: Localisation and activity of AURKB during the cell cycle

AURKA localises in the nucleus during late G_2 and prophase where it drives chromatin condensation. From early mitosis to anaphase, AURKB is located at the centromeric regions where it regulates MT-kinetochore interactions, correcting erroneous attachments. AURKB also recruits SAC proteins to the kinetochores. In anaphase, AURKB is found at the spindle midzone and equatorial complex. It then regulates cleavage furrow positioning and formation of the actin-myosin required for daughter cell formation. AURKA is localised at the midbody and furrow during telophase and cytokinesis, and can be seen extracellularly with the midbody after cytokinesis. Here it regulated abscission and the associated checkpoint. AURKB degradation at the end of cytokinesis is required for mitotic exit. Figure produced in Biorender.

as ATR localises to centromeres during mitosis and ATRi can reduce pAURKB (Kabeche et al., 2018). *In vitro* assays demonstrated that activation by Chk1 is independent of AURKB-INCENP interaction and could increase AURKB catalytic activity beyond that generated by INCENP binding. It is proposed that peak AURKB activity requires phosphorylation at Threonine (Thr) 232 and Ser331 (Petsalaki et al., 2011).

INCENP, Survivin and Borealin form a triple-helix and their complex is required for CPC localisation to the centromere, the spindle midzone and the midbody (Vader et al., 2006, Klein et al., 2006).

1.3.1.3. Chromosome Condensation

In prophase, AURKB promotes chromosome condensation and resolution. AURKB regulates chromatin condensation via phosphorylation of Histone 3 (H3)-Ser10 and Heterochromatin Protein 1α (HP1-α) (Hsu et al., 2000, Nishibuchi et al., 2019). Along with Plk1 and Condensin I, AURKB also promotes the 'prophase pathway' of cohesin release from the chromatid arms which facilitates chromatid resolution (Losada et al., 2002, Sumara et al., 2002, Hirota et al., 2004).

1.3.1.4. Correction of Erroneous MT-KT Attachments

In early mitosis, AURKB promotes correction of erroneous KT-MT attachments. AURKB localisation to centromeres is critical for this function. Centromeric targeting of AURKB is promoted by two histone phosphorylations. Haspin phosphorylates H3 (Thr3). Haspin activation relies on phosphorylation by AURKB in a positive feedback loop (Wang et al., 2010, Yamagishi et al., 2010, Wang et al., 2011b). Secondly, Bub1 phosphorylates H2a (Thr120), which recruits Shugoshin proteins Sgo1 and

Sgo2 (Yamagishi et al., 2010, Kawashima et al., 2007). The Shugoshins target AURKB and Mitotic centromere-associated kinesin (MCAK) to the centromeres (Kawashima et al., 2007, Huang et al., 2007).

At the centromeres, AURKB regulates chromosome segregation by correcting erroneous MT-KT attachments. The tension between KT and MT is believed to act as a signal of correct or erroneous MT-KT attachment. Only correct bi-orientation and KT-MT attachment creates high tension and leads to fulfilment of the SAC and progression to anaphase (Nicklas, 1997, Lampson and Grishchuk, 2017)

The current mechanism for tension mediated correction of erroneous MT-KT attachments relies on the spatial separation model. This model proposes that phosphorylation of AURKB substrates is spatially regulated by MT-KT tension. KTs are a collection of proteins assembled around Centromere protein A (CENP-A). KTs are established on the centromere, a specific region of chromatin. A diffusion gradient of AURKB forms around the centromere, which is at its highest at the inner centromere and decreases towards the outer KT (Fuller et al., 2008, Wang et al., 2011a). Under tension, KT proteins become distanced from the centromeric region (and AURKB) because tension stretches the KTs away from the centromeres (Carmena et al., 2012). This model is supported by the importance of centromeric AURKB in higher eukaryotic cells, and the correlation between tension and phosphorylation of AURKB KT substrates (Lampson and Grishchuk, 2017, Liu et al., 2009, Welburn et al., 2010). Additional ideas stemming from this model include a combination of increased auto-activation between AURKB molecules at the centromere and increased phosphatase activity further from the centromeres,

leading to a steep non-linear gradient in AURKB activity at the KTs (Lampson and Grishchuk, 2017).

Further mechanisms for spatial regulation involve a distinct pool of AURKB located transiently at KTs allowing additional interaction with KT substrates, although how it is targeted here is a subject of debate (Broad et al., 2020). Some evidence supports the idea that centromeric accumulation of AURKB is second to KT recruitment (Krenn and Musacchio, 2015a). While spatial separation is the most accepted model, there have been multiple contradictory observations which obscure the issue (Krenn and Musacchio, 2015a, Lampson and Grishchuk, 2017).

At the centromere, AURKB function is essential for correction of erroneous MT-KT attachments. AURKB destabilises KT-MT attachments by promoting detachment and MT depolymerisation.

AURKB can promote detachment of KTs from the MTs via phosphorylation of Ndc80 in the KMN complex. This reduces KT affinity for MTs and is thought to be achieved via successive phosphorylations of Ndc80 which incrementally decrease KT affinity for MTs (Cheeseman et al., 2006, Ciferri et al., 2008, Zaytsev et al., 2015). Additionally, AURKB phosphorylation of Ndc80 inhibits its ability to stabilise MT tips and slow the rate of disassembly (Umbreit et al., 2012).

AURKB can also promote depolymerisation of MTs via phosphorylation of the Ska1 complex. The Spindle and kinetochore associated complex subunit 1 (Ska1) complex attaches to and stabilises depolymerising MTs and maintains Ndc80 at MT ends thus maintaining attachment (Gaitanos et al., 2009, Welburn et al., 2009). Phosphorylation of Ska1 by AURKB reduces Spindle And Kinetochore Associated

Complex Subunit 1 (Ska1) interaction with Ndc80, promoting detachment and allowing depolymerisation (Lampert et al., 2010, Tien et al., 2010, Chan et al., 2012).

AURKB phosphorylates MCAK, an MT depolymerase which corrects erroneous attachments by destabilising microtubules (Kline-Smith et al., 2003). This phosphorylation localises MCAK to centromeres and regulates MCAK binding to chromatin and MTs (Zhang et al., 2007, Lan et al., 2004, Ems-McClung et al., 2013).

AURKB also targets Centromere-associated protein E (CENP-E) to the KTs. CENP-E is a kinesin motor protein which attaches to kinetochores to mobilise unattached chromosomes to the metaphase equator via plus-end directed microtubule motility (Craske and Welburn, 2020, Ditchfield et al., 2003).

The DDR protein 53BP1 is recruited to the KTs by AURKB phosphorylation at Ser1342. At the kinetochores, p53BP1 (Ser1342) aids resolution of merotelic attachments in conjunction with MCAK (Wang et al., 2017). This phosphorylation by AURKB is not required for 53BP1's DDR activation.

AURKB also supports successful segregation of acentric chromosomes. These are chromatin fragments no longer attached to the centrosome-containing region. Segregation of these fragments is achieved via tethering of the acentric to the centric chromosome region. This tethering complex contains AURKB as well as PLK1 and BubR1 (Royou et al., 2010).

1.3.1.5. The Spindle Assembly Checkpoint (SAC)

The transition between metaphase and anaphase is controlled by the SAC. This checkpoint prevents anaphase until all sister chromatids are bio-orientated and aligned to the mitotic spindle (Musacchio and Salmon, 2007). The SAC relies on the

Mitotic checkpoint complex (MCC), made of Mitotic arrest deficiency 1 (MAD1), BubR1 and Budding Uninhibited By Benzimidazoles 3 (Bub3), which assembles on unattached kinetochores. The MCC binds and inhibits Cell Division Cycle 20 (Cdc20). While bound, Cdc20 cannot bind and activate the Anaphase-promoting complex (APC/C), which is required for anaphase (Lischetti and Nilsson, 2015).

AURKB is required for spindle checkpoint function and supports the checkpoint in several ways. Checkpoint signalling only occurs in the presence of unattached kinetochores (Rieder et al., 1995). By destabilising KT-MT attachments, AURKB creates unattached kinetochores which provides a platform for MCC binding (van der Waal et al., 2012). MCC signalling at kinetochores maintains SAC activation.

AURKB is required for recruitment of the SAC proteins BubR1, Mitochondrial-processing peptidase subunit alpha (Mas2), Bub1 and CENP-E to unattached KTs (Hauf et al., 2003, Ditchfield et al., 2003, Vigneron et al., 2018, Lens et al., 2003). This is attributed to AURKB activation and kinetochore targeting of the kinase Mps1 (Saurin et al., 2011). Msp1 localises MCC proteins by activating Knl1, a scaffold protein at kinetochores (Pachis and Kops, 2018, Ji et al., 2017). AURKB phosphorylation of ATM (Ser1403) is required for SAC function (Yang et al., 2011a). However, given dual roles for ATM in SAC and DDR signalling during mitosis, a role in facilitating crosstalk between the two processes should be considered (Xiao et al., 2022).

AURKB associates with p53 during mitosis. They co-localise at the centromeres in metaphase and at the spindle midzone during cleavage furrow development (anaphase-telophase) (Gully et al., 2012). It is proposed that p53 has a role in chromosomal segregation as its depletion can promote polyploidy or aneuploidy

(Cross et al., 1995). However, considering the role of p53 in promoting cell death during mitotic catastrophe, it seems more probable that p53 is required in mitosis to promote cell death over slippage, rather than a functional role in chromosome segregation.

1.3.1.6. Anaphase

During anaphase, AURKB relocalises to bridging fibre MTs, then to the spindle midzone and the equatorial cortex (Hadders and Lens, 2022). At the spindle midzone, an AURKB activity gradient forms towards the cell cortex, which co-ordinates cleave furrow positioning (Fuller et al., 2008, Wang et al., 2011a). AURKB also promotes axial shortening of chromosome arms which prevents damage in the cell furrow as chromosomes migrate toward the poles (Mora-Bermúdez et al., 2007) AURKB at the midzone is also proposed to protect lagging chromosomes from damage by preventing nuclear envelope reformation in the presence of chromatin, as well as stabilising KT-MT attachments and promoting spindle elongation (Hadders and Lens, 2022).

1.3.1.7. Cytokinesis

In cytokinesis, AURKB promotes cleavage furrow ingression during cytokinesis. AURKB phosphorylates Vimentin, an intermediate filament protein, which promotes the filament formation required during cleavage furrow ingression (Goto et al., 2003).

AURKB regulates the Centralspindlin complex during furrow ingression. The Centralspindlin complex is an essential component of the actomyosin contractile ring, which forms during cytokinesis and facilitates cleavage furrow ingression (Carmena, 2008). AURKB is required for the localisation of the complex to the

midzone and also stable association of the complex with the spindle (Piekny et al., 2005, Severson et al., 2000, Kaitna et al., 2000).

AURKB may also support cleavage furrow formation via BRCA2. BRCA2 localises to the spindle midzone and the intracellular canal during cytokinesis. BRCA2-deficient cells exhibit greater cytokinetic failure rates and in these cells, myosin II localisation is dysregulated (Daniels et al., 2004). This activity is thought to involve AURKB as BRCA2 complexes with AURKB in cytokinesis via BARD1 (Ryser et al., 2009).

1.3.1.8. Abscission and the NoCut Pathway

Abscission is the final step of cytokinesis, whereby the intracellular channel between daughter cells is cut. A second ingression leads to formation of an intercellular channel which contains the midbody. The midbody is the structure formed from the compacted spindle midzone and is formed of the Flemming body and the midbody arms. The Flemming body is the bulging central unit of the midbody containing the microtubule plus ends as well as contractile ring structures and central spindle proteins (D'Avino and Capalbo, 2016). The midbody acts as a platform for recruitment of proteins involved in abscission. The midbody is a dynamic structure which gains two constrictions at either side of the Flemming body, producing a bow-tie shape. The microtubule bundles either side gradually decrease in thickness and an abscission point develops, usually to one side of the midbody. Therefore, after abscission, the midbody is inherited by one daughter cell (D'Avino and Capalbo, 2016). At the time of abscission, often 80 - 90 minutes after furrow ingression, daughter cells have clearly formed and chromatin has decondensed (Agromayor and Martin-Serrano, 2013).

Recruitment of the Endosomal sorting complex required for transport (ESCRT) proteins is critical for abscission. ESCRT proteins carry out fission events such as vesicle budding (Hurley and Hanson, 2010). They are known to produce filaments capable of membrane scission by constrictive force and are thought to carry out the physical abscission during cytokinesis (Carlton et al., 2012). In cytokinesis, the ESCRT components ESCRT-I, ESCRT-III and Vacuolar protein sorting-associated protein 4 (VPS4) are recruited to the midbody arms (Elia et al., 2011).

Here, the ESCRT-III protein Chromatin-modifying protein/charged multivesicular body protein 4 (VPS4) is thought to carry out abscission in a formation of spiral filaments which induce a narrowing of the intracellular bridge (Elia et al., 2011). The subunits of CHMP4 are recruited to the midbody by Centrosomal protein of 55 kDa (Cep55), while ESCRT-I is recruited by Tumour susceptibility gene 101 protein (TSG101) and ALG-2-interacting protein X (ALIX) (D'Avino and Capalbo, 2016). In late cytokinesis the CHMP4B subunit and VPS4 localise to the abscission site immediately prior to cell separation, suggesting a direct role in scission (Elia et al., 2011). The ESCRT-III subunit DID2B also recruits Spastin, a MT-severing protein, which can cut microtubules. MT cleavage is required before membrane abscission by ESCRT proteins (Hurley and Hanson, 2010, Connell et al., 2009)

Abscission is regulated by the abscission checkpoint (also referred to as the NoCut pathway), a checkpoint that pauses abscission of the intercellular bridge when it contains chromatin (Agromayor and Martin-Serrano, 2013). This checkpoint is regulated by AURKB and is essential to prevent chromatin breakage and allow time for resolution of chromosome segregation issues. AURKB and the CPC localise to the midbody arms during cytokinesis and dissociate from the midbody after the

bowtie formation occurs (Capalbo et al., 2012). Once triggered, AURKB activation at the abscission checkpoint leads to actin polymerisation and thus stabilisation of the intracellular channel (Bai et al., 2020). During late abscission if the checkpoint is activated, AURKB can also be found within the Flemming body (Petsalaki and Zachos, 2016).

Without a checkpoint, abscission can result in two aberrant fates. Firstly, abscission regression can occur where the daughter cells recombine resulting in a multinucleated, polyploid cell. Secondly, the daughter cells can separate despite chromatin in the intracellular bridge, resulting in DNA damage (Petsalaki and Zachos, 2021a).

The checkpoint is activated via the MRN complex, which localises to the midbody when chromatin bridges are present in cytokinesis (Petsalaki and Zachos, 2021b). The MRN activates ATM at Ser1981, leading to mid-body localisation and phosphorylation of Chk2 (Thr68). Chk2 in turn phosphorylates INCENP at Ser91. This promotes an association between INCENP and Mklp2 and recruitment of both proteins (and the CPC containing INCENP) to the midbody (Petsalaki and Zachos, 2021b).

AURKB regulates the abscission checkpoint through regulation of ESCRT-III components. ANCHR regulates the abscission checkpoint via spatial inhibition of VPS4 in an AURKB-dependant manner. ANCHR binds VPS4 at the midbody ring and prevents it localising to the midbody arms in late abscission events. ANCHR protects against failed abscission regression; depletion increases the number of multinucleated cells. The function of ANCHR in cytokinesis requires AURKB activity, although how AURKB regulates ANCHR is unknown (Thoresen et al., 2014).

AURKB and the CPC are proposed to block abscission through surveillance of the Charged Multivesicular Body Protein 4 (CHMP4) ESCRT-III protein. Depletion of CHMP4C leads to more rapid abscission, whilst overexpression led to abscission delay. Carton et al (2010) proposed that CHMP4 Subunit C (CHMP4C) relocation to the midbody blocks abscission. AURKB phosphorylates CHMP4C and relocates it to the Flemming body during abscission delay. The function of this localisation was proposed to prevent assembly of abscission complex. They also suggested a possible role for CHMP4C in chromatin detection during the abscission checkpoint activation (Carlton et al., 2012).

Alternatively, Capalbo et al (2012) suggested that AURKB phosphorylation of CHMP4C prevents polymerisation into fibres, preventing its scission ability, and that Borealin association with CHMP4A,-B and -C prevents their membrane association (Capalbo et al., 2012). They also found two pools of CHMP4C proteins (Capalbo et al., 2016). The first was tri-phosphorylated by AURKB and localised to midbody arms. The second was not phosphorylated by AURKB and localised at the Flemming body. They proposed that the CPC binds CHMP4C prior to cytokinesis and as the CPC degrades during late cytokinesis, CHMP4C becomes dephosphorylated. This would promote localisation to the Flemming body to allow abscission.

AURKB is also proposed to promote stabilisation of the midbody and the intracellular canal by phosphorylation of Mitotic kinesin-like protein 1 (Mklp1) phosphorylation at Ser708 and phosphorylation of Rac GTPase-activating protein 1 (RacGAP1) (Guse et al., 2005, Minoshima et al., 2003). Mklp1 and RacGAP1 are subunits of the Centralspindlin complex which promotes plasma membrane tethering after furrow

ingression (Horváth and Müller-Reichert, 2020). Preventing AURKB phosphorylation of RacGAP1 leads to abscission regression.

Chromatin breakage or abscission regression can occur if lagging chromosomes or chromatin bridges are not resolved prior to completion of abscission (Hoffelder et al., 2004, Ma and Poon, 2020). Inhibition of AURKB promotes abscission regression but inhibition of Chk1 promotes chromatin breakage and premature abscission. It is proposed that this is due to the role of AURKB in early abscission before stabilisation of the midbody. Therefore, AURKB inhibition only promotes abscission regression (recombination of daughter cells). Chk1, on the other hand, is involved in the late midbody. Chk1 inhibition does not affect the checkpoint until late abscission after midbody stabilisation. After this point, Chk1 inhibition leads to complete abscission with resulting DNA damage (Steigemann et al., 2009, Petsalaki and Zachos, 2021b).

At the end of mitosis, AURKB is ubiquitinylated via the APC/C, and targeted for proteasomal degradation. BARD1 also promotes AURKB degradation by ubiquitination (Ryser et al., 2009).

1.3.2. Non-Mitotic Functions of AURKB

Knowledge of AURKB's functions outside mitosis is more limited. While most AURKB protein is degraded at the end of mitosis, AURKB remains at low levels during other cell cycle phases, during which other functions have been found (Lindon et al., 2016).

1.3.2.1. AURKB and Chromatin Organisation

AURKB plays a role in chromatin remodelling and epigenetic regulation. This was initially investigated due to the ability of AURKB inhibitors such as Reversine to reverse differentiation (Amabile et al., 2009). AURKB phosphorylates H3 at Ser10 at the onset of mitosis, but also carries out this activity in differentiated cells after mitosis with differing effects (Sabbattini et al., 2007). This phosphorylation generates double H3 modification tri-methylated K9/phosphorylated S10 (K3H9me3/S10ph). H3-Ser10 phosphorylation causes HP1 proteins to dissociate from methylated H3 (Musacchio and Salmon, 2007, Terada, 2006). These effects allow epigenetic silencing and support a role for AURKB in maintaining differentiation (Amabile et al., 2009).

AURKB is also implicated in telomerase activity and telomere maintenance. In S phase, the p-arm of chromosomes are phosphorylated by AURKB at Histone 3 (Ser10) in centromeric, telomeric and sub-telomeric regions. AURKB inhibition reduced pH3 in S phase cells, and over weeks, led to telomere shortening. This is due to the open chromatin structure maintained by pH3 on these regions, as well as positive regulation of telomerase activity by AURKB (Mallm and Rippe, 2015, Wang et al., 2023).

1.3.2.2. AURKB and the DDR

AURKB co-localises with p53 during mitosis at the centromeres and in interphase nuclei, supporting AURKB regulation of p53 outside mitosis. In interphase, AURKB can directly and indirectly regulate p53 (Fig 1.5). Wu et all (2011) found that AURKB binds to p53 and novel INHAT repressor (NIR) to form a complex. NIR binding

repressed p53 transcriptional activity. Additionally, AURKB can directly phosphorylate p53 at Ser183, Ser269 and Thr284. These phosphorylations reduced p53's transcriptional activity such as transactivation of p21 and Bax (Wu et al., 2011b).

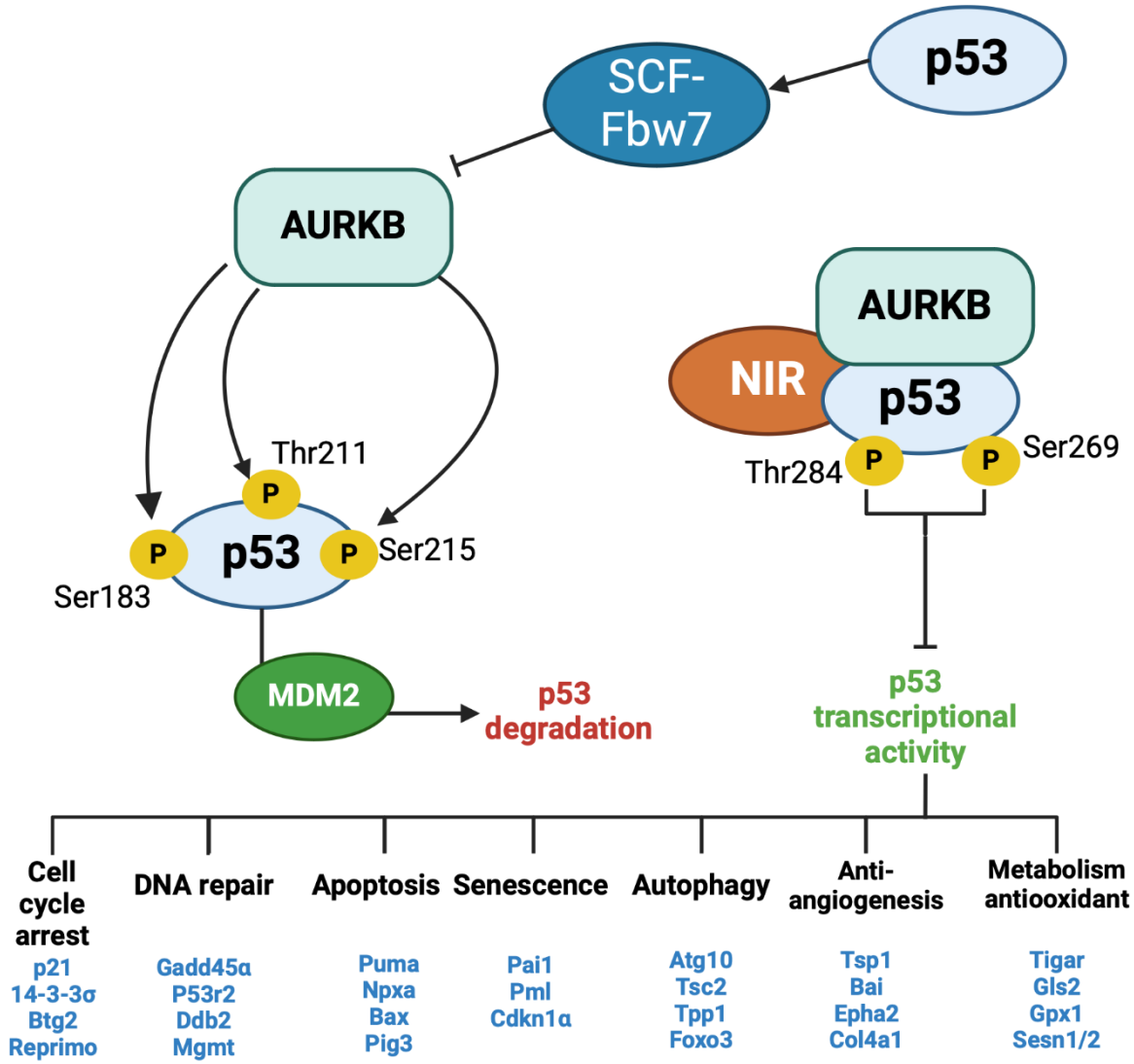

Figure 1. 5: AURKB and p53

AURKB inhibits p53 by direct phosphorylation leading to MDM2-mediated degradation. AURKB also forms a complex with NIR and p53 which facilitates phosphorylation leading to inhibition of p53 transcriptional activity. Key transcription targets and processes downstream of p53 are shown. P53 is thought to inhibit AURKB indirectly by SCF-Fbw7 phosphorylation.

Gully et al (2012) also shows that AURKB negatively regulates p53 by promoting p53 degradation. AURKB inhibition via the selective AURKB inhibitor Barasertib

(AZD1152) leads to an increase in p53 protein levels. During interphase, AURKB phosphorylates p53 at Ser183, Thr211 and Ser215. These modifications promoted p53 ubiquitination by MDM2 leading to proteasomal degradation. Interestingly, Gully et al (2012) found no *in vitro* phosphorylation of p53 at Ser269 and Thr284 by AURKB in an *in vitro* kinase assay. This contradicts the findings of Wu et al (2011), who demonstrated these phosphorylations, also in an *in vitro* kinase assay (Wu et al., 2011b).

The regulation of p53 by AURKB has consequences for cell cycle regulation and stress signalling. AURKB mediated inhibition/degradation of p53 means AURKB can promote G_1-S transition and survival. AURKB depletion by conditional knockout (*Cre/Lox*) leads to delayed replication following G_1 arrest associated with increased p21 expression (Trakala et al., 2013). AURKB depletion by inhibitors (AZD1152-hydroxyquinazoline pyrazol anilide (HQPA)) or siRNA can promote p53-dependant apoptosis (Wu et al., 2011b). In addition, a negative feedback loop between p53 and AURKB may exist via the targeting of AURKB for degradation by the Stem Cell Factor (SCF)-subunit Fbw7, a pathway regulated by p53 (Wu et al., 2011a, Teng et al., 2012).

The downstream activation of p21 after AURKB inhibition is also dependant on p38 Mitogen-activated protein kinases (MAPK) as well as p53 activation/stabilisation. P38 regulates key upstream signalling events in programmed cell death and cell cycle checkpoints (Whitaker and Cook, 2021). AURKB inhibition by ZM447439 promotes p21 expression in a P38 dependant pathway. P38 inhibition did not affect

p53 binding to the p21 promotor but prevented transcriptional elongation of p21 (Kumari et al., 2013).

Several DDR proteins can inhibit AURKB through inhibition of kinase activity or by targeting it for degradation. In response to DNA damage AURKB is inhibited by PARP1-mediated PARylation. In addition, DNA damage induces a PARP dependent block on phosphorylation of H3 (Monaco et al., 2005).

There is a bidirectional negative regulation between the AURKs (AURKB and AURKB) with BRCA1 and BRCA2. Small interfering RNA (SiRNA) depletion of BRCA1 led to increased AURKB protein expression, which was amplified when BRCA2 was also depleted. SiRNA depletion of AURKB increased BRCA1 and BRCA2 protein expression. AURKA depletion had a greater effect on BRCA1 and BRCA2 expression and depleting both AURKs led to a greater increase In BRCA1 and BRCA2 than either alone (Wang et al., 2014, Sagulenko et al., 2007). These expression changes were abrogated by proteasomal inhibition (Mg132) suggesting protein degradation underpins the expression changes. The AURK/BRCA signalling axis may influence cell cycle progression via cyclin A and p53 modulation.

Ku70 is recruited to damaged DNA and has key roles in NHEJ and DNA-PKcs recruitment. Ku70 phosphorylation at Ser155 was found to promotes the interaction between AURKB and Ku70, and inhibits AURKB kinase activity (Fell et al., 2016).

As previously discussed in section 1.2.7, AURKB activity is required for a telomere dependant DDR pathway in prolonged mitoses (Hayashi et al., 2012). This represents an alternative role for AURKB in promoting the DNA damage response which contrasts it role in negatively regulating p53.

1.3.2.3. AURKB and Replication stress

There have been preliminary investigations into the response of AURKB to replication stress. ZuaZua-Villar et al (2014) found that AURKB played a role in cell cycle regulation following replication stress. Following Thymidine treatment, cells accumulate in mitosis due to inhibition of deoxynucleotide metabolism. The authors found that when cells were depleted of Chk1 by siRNA and treated with thymidine, there was an increase in phospho-H3 positive cells at DNA contents <4N, i.e., under-replicated cells entering mitosis. This premature mitotic entry was found to be dependent on AURKB activity. AURKB activation 24 Hr after replication stress required Chk1 depletion and was enhanced by p53 knockout. These results suggest AURKB is activated following replication stress and that Chk1 and p53 inhibit this activation to prevent erroneous cell cycle progression. This could be direct or Chk1 could inhibit an upstream activator of AURKB (Zuazua-Villar et al., 2014).

Another report by Erin et al (2021) (BioRXiv – not peer reviewed) found that AURKB has a role in replication and recovery from replication stress (Erin et al., 2021). Using isolation of proteins on nascent DNA (iPOND), they demonstrated localisation of AURKB, Borealin and AURKB-dependant pH3 at unchallenged replisomes. The pH3 signalling increased following a thymidine chase, suggesting that AURKB activity increases on maturing chromatin.

AURKB activity at replisomes increased after replication stress by Hydroxyurea (HU). HU inhibits replication via inhibition of deoxynucleotide metabolism but additionally generates ROS which can cause additional DNA damage. After HU treatment, an ATRi further increased pH3 activity at replisomes. This supports the

inhibitory effect of Chk1 on AURKB shown by ZuaZua-Villar et al (2014) and suggests that this inhibition also impacts signalling at replication sites.

Erin et al (2021) provided mechanistic data supporting a role for AURKB in replication stress recovery. Inhibition of AURKB stalled replication by inhibiting fork restart after stress. Restart was found to depend on pAURKB (ser331) and downstream PLK1 activation (Erin et al., 2021). AURKB Ser331 is the phosphorylation target of Chk1 during mitosis but the upstream kinase at replication sites was not investigated. They found that AURKB activity was required to release Chk1 and its activator Claspin from replication sites after HU release. Surprisingly, AURKBi or PLK1i promoted an exaggerated increase in pChk1 after HU release, suggesting negative regulation between Chk1 and AURKB may be bi-directional (Erin et al., 2021).

These two papers also reveal that AURKB activity after replication stress is important for S phase recovery and cell cycle control. There is evidence that Chk1 negatively regulates AURKB during prolonged S phase to prevent premature cell cycle progression. Meanwhile, AURKB activity at replication sites is important for replication stress recovery.

Both papers support a role for AURKB in promoting cell cycle progression following replication stress, either in enabling fork restart thus continuing replication or in promoting mitotic entry. They also reveal a Chk1-dependant restraint on AURKB activation until replication stress is resolved.

1.4. Aurora Kinase A

AURKA is best known for its roles in mitosis co-ordinating centrosome formation and mitotic entry. It has been extensively studied in its mitotic role but is also involved in p53 regulation and DDR pathways.

1.4.1. Mitotic Roles of Aurora Kinase A

AURKA is known for its regulation in late G_2 and mitosis and is the better studied of the aurora kinases. AURKA regulates many of the initial stages of mitosis, including mitotic entry, centrosome maturation and spindle morphogenesis. Severe AURKA mutations lead to defects in centrosome separation and organisation, spindle formation and alignment as well as monopolar or multipolar spindles (Glover et al., 1995, Giet et al., 2002, Lee et al., 2006, Wang et al., 2006). AURKA localises to the centrosomes in S phase, where it becomes highly enriched during G_2. AURKA then localises to the centrosomes and spindle between prophase and metaphase (Honda et al., 2000). In late mitosis, AURKA levels decline but low levels can still be found at the midzone and centrosomes (Yan et al., 2016). AURKA is largely inactive during cytokinesis and at low levels during S and G_1 phases (Nikonova et al., 2013). The localisation and roles of AURKA through mitosis are discussed below and are summarised in Figure 1.6.

1.4.1.1. G_2-M Transition

In late G_2, AURKA activates Plk1 through Thr210 phosphorylation which drives mitotic entry (Macůrek et al., 2008). This is dependent on the AURKA cofactor Bora which enhances AURKA activation of Plk1 (Seki et al., 2008). Plk1 promotes mitotic entry by targeting Cdc25 and Cyclin B1 to the nucleus

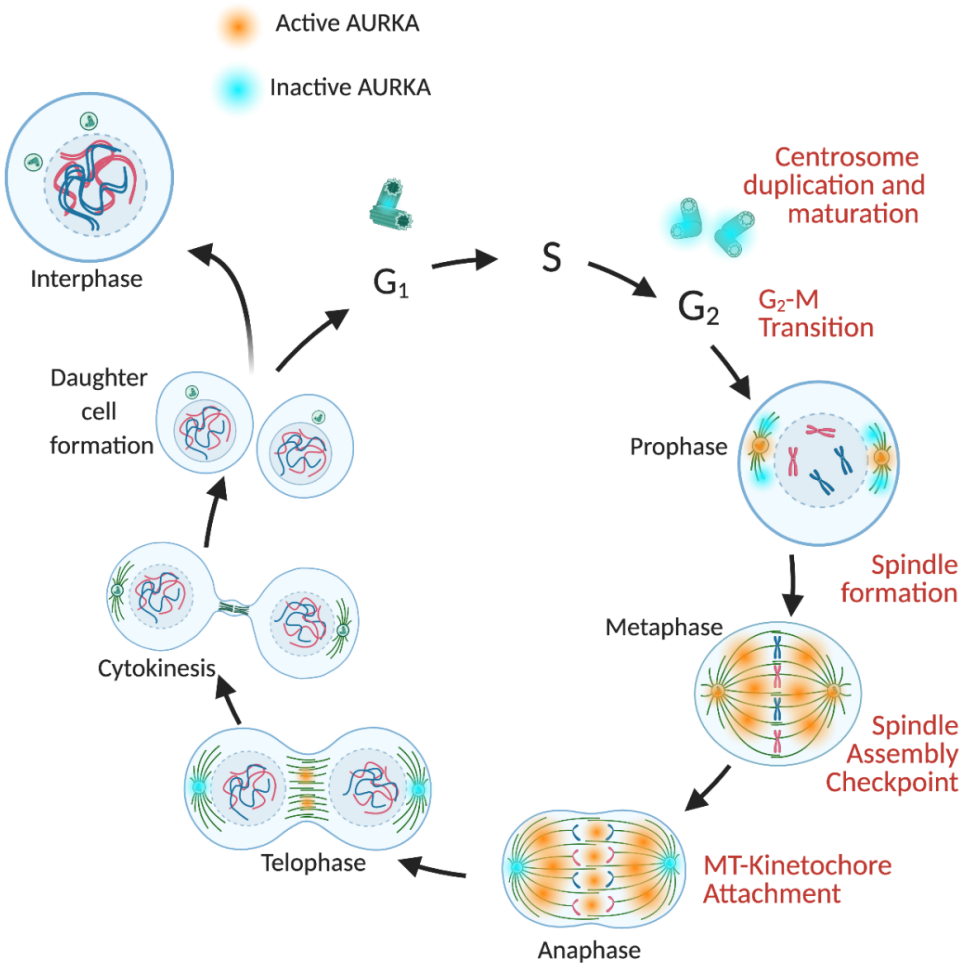

Figure 1. 6: Localisation and activation of AURKA during the cell cycle

AURKA localises to the centrosomes during G_2 and is activated between G_2 and beginning of mitosis where it contributes to centrosome maturation and duplication. Active AURKA localises to the mitotic spindle and regulates spindle formation. In anaphase, AURKA is still found at the spindle and in the midzone, but AURKA levels and activity decrease greatly by the end of anaphase. AURKA is localised at the midzone and centrosomes during telophase and cytokinesis. Figure produced in Biorender.

during the G_2-M transition (Toyoshima-Morimoto et al., 2002, Toyoshima-Morimoto et al., 2001). The G_2-M transition depends on the trigger-like activation of Cyclin B-Cdk1 by Cdc25 phosphatases. Wee1 suppresses Cdk1 activity through phosphorylation at Tyr15 (Fung and Poon, 2005, Poon, 2016). Cdc25c removes this inhibitory phosphorylation at Tyr15 of Cdk1. Plk1 also supports Cdc25 activation by triggering Wee1 degradation (Qian et al., 2001, Watanabe et al., 2004a).

The AURKA-Bora-Plk1 interaction is regulated through several mechanisms. Upon DNA damage, Bora is phosphorylated by ATR and Plk1, which targets it for degradation to prevent mitotic entry (Qin et al., 2013, Chan et al., 2008). Cdk1 phosphorylation of Bora promotes Plk1 activation, creating a positive feedback loop which can overcome the G_2/M checkpoint (Chan et al., 2008, Thomas et al., 2016).

Following checkpoint activation by DSBs, AURKA is inhibited in a Chk1-dependant manner which may involve inhibition of its interaction with and recruitment by its cofactor Bora (Bruinsma et al., 2017). The downstream effect of this inhibition is loss of Plk1 activation which prevents mitotic entry.

AURKA is also negatively regulated at the G_2/M checkpoint via ubiquitination by the Chfr, a mammalian RNF8 homolog. In response to DNA damaging stress, Chfr is activated via auto-ubiquitination (Kim et al., 2011). Activated Chfr then ubiquitinylates AURKA and Plk1 leading to degradation (Yu et al., 2005).

Downregulation of AURKA and Plk1 at the checkpoint leads to delayed mitotic entry by preventing AURKA/Plk1-dependant activation of Cdc25 and inhibition of Wee1 (Kang et al., 2002, Chaturvedi et al., 2002).

1.4.1.2. Centrosome Maturation

Aurora A localises at the centrosomes at the end of S phase, where it regulates centrosome maturation (Magnaghi-Jaulin et al., 2019). Centrosome maturation is the accumulation of γ-tubulin ring complexes (γ-TURCs) and pericentriolar material (PCM) proteins which increase the centrosome's MT-nucleating potential (Lukasiewicz and Lingle, 2009).

In late G_2, Centrosomal Protein 192 (Cep192), Plk1 and Tyr148 localise AURKA to the centrosomes (Joukov et al., 2010, Luca et al., 2006, Barretta et al., 2016). Interaction with CEP192 promotes dimerization of AURKA and autophosphorylation at Thr298 and Thr288, leading to its activation. At the centrosomes, AURKA also interacts with Ajuba, Neural Precursor Cell Expressed, Developmentally Down-Regulated 9 (NEDD-9), P21 (RAC1) Activated Kinase (PAK) and Nucleophosmin which are required for its activation (Hirota et al., 2003, Pugacheva and Golemis, 2005, Zhao et al., 2005, Joukov et al., 2010, Reboutier et al., 2012). Protein Kinase D2 (PKD2) also promotes AURKA stability at the centrosomes (Roy et al., 2018).

CEP192-AURKA complexes recruit NEDD1 and Plk1, key PCM proteins which are required for MT nucleation. AURKA activates Plk1 at the centrosomes. Plk1 subsequently phosphorylates CEP192 which promotes γ-TuRC recruitment to the centrosomes (Joukov et al., 2014). NEDD1 interacts with γ-TuRC at the centrosomes to facilitate its localisation to MT organising centres (MTOCs) and its function as a MT template (Haren et al., 2006, Kollman et al., 2011, Lüders et al., 2006).

1.4.1.3. Mitotic Spindle Formation and Control

As MT spindle growth begins, AURKA localises to the spindles. AURKA is essential for bipolar spindle formation and regulates a wide range of substrates which contribute to spindle growth and MT stabilisation. The activation of spindle-associated AURKA differs from that of centrosomal pool of AURKA and instead is dependent on Targeting Protein For Xklp2 (TPX2) (Bayliss et al., 2003, Eyers et al., 2003). Following release from importins, TPX2 targets AURKA to the spindle and activates AURKA by promoting AURKA autophosphorylation and preventing inactivation by phosphatases (Kufer et al., 2002, Eyers et al., 2003, Trieselmann et al., 2003, Nikonova et al., 2013). The nuclear scaffold SAF-A directly interacts with TPX2 and AURKA, and is also required for AURKA localisation to spindle poles and spindle MTs (Ma et al., 2011).

AURKA and TPX2 have been shown to form a complex with the microtubule-associated protein XMAP215, the plus-end directed motor Kinesin Family Member 11 (Kif11)/Eg5, and the kinetochore fibre stabilising protein HURP (Koffa et al., 2006), which is implicated in aster-to-spindle conversion in early spindle formation.

AURKA phosphorylation of Transforming acidic coiled coil (TACC) proteins stabilises centrosomal microtubules and promotes astral growth (Kinoshita et al., 2005). It also activates the complex of D-TACC and Minispindles (Msps), which promote MT assembly at the centrosomes (Barros et al., 2005, Giet et al., 2002, Kinoshita et al., 2005). Activation of spindle protein TACC3 is dependent on AURKA phosphorylation and centrosomal targeting of NudE Neurodevelopment Protein 1 Like 1 (NDEL1) (Mori et al., 2007).

AURKA negatively regulates many microtubule-associated proteins (MAPs) to regulate spindle formation. AURKA inhibits Hice1, a subunit of the Augmin complex which targets γ-tubulin to MTs and can lead to MT branching (Tsai et al., 2011). AURKA inhibits the MT binding ability of the MAPs Dynactin, WD Repeat Domain 62 (WDR62), MCAK and Ras Association Domain Family Member 1 isoform A (RASSF1a) in order to regulate MT growth (Yu et al., 2010, Wordeman and Mitchison, 1995, Venoux et al., 2008, Romé et al., 2010)

1.4.1.4. Kinetochore-Microtubule Attachment (KT-MT)

AURKA plays several roles in KT-MT attachment with overlapping function to AURKB. AURKA is recruited to the centromeres by Bub1. AURKA depletion leads to an increase in cells showing premature sister chromatid separation (Eot-Houllier et al., 2018). At the centromeres, AURKA activates CENP-A in prophase through phosphorylation at Ser7. CENP-A is a variant of H3 that forms the inner plate of the kinetochore and is required for the recruitment of other necessary kinetochore proteins, CENP-E, Centromere Protein I (CENP-I) and Centromere Protein H (CENP-H) (Goshima et al., 2003). This phosphorylation by AURKA supports the activation by AURKB later in metaphase (Kunitoku et al., 2003, Zeitlin et al., 2001). AURKA phosphorylation of CENP-E regulates its kinetochore binding by inhibiting PPI-mediated stabilisation, preventing incorrect kinetochore attachment (Kim et al., 2010).

1.4.1.5. Spindle Assembly Checkpoint (SAC)

P73 plays a key role in regulating the SAC. AURKA can phosphorylate p73 at Ser235 which results in inhibition of DNA binding and transactivation activity. This is

thought to promote SAC inactivation by promoting dissociation of p73, MAD2 and CDC20 (Katayama et al., 2012). AURKA is also thought to promote SAC function through targeting of the SAC protein MAD2 to the kinetochores (Courtheoux et al., 2018).

1.4.1.6. Anaphase and Cytokinesis

Low levels of AURKA remain at the centrosomes and spindles in early anaphase, and at the midzone and centrosomes in late anaphase and cytokinesis (Yan et al., 2016). AURKA undergoes proteasome-mediated degradation promoted by the APC/C in late mitosis (Honda et al., 2000, Castro et al., 2002). Both overexpression and Ab-mediated interference of AURKA can lead to failed cytokinesis and it is thought that cytokinesis is subject to temporal regulation through AURKA inactivation and degradation, and subsequent dephosphorylation of AURKA substrates (Marumoto et al., 2003, Meraldi et al., 2002, Anand et al., 2003, Zhang et al., 2004).

1.4.2. Non-Mitotic Roles of AURKA

While the mitotic function of AURKA is well characterised, it is emerging that AURKA plays additional functions outside mitosis.

1.4.2.1. AURKA Regulation of p53

AURKA and p53 can negatively regulate each other via several mechanisms (summarised in Fig 1.7). AURKA can directly phosphorylate p53 resulting in inhibition. AURKA phosphorylates p53 at Ser315 which destabilises p53 (Katayama et al., 2004). This destabilisation and degradation was shown to be MDM2-dependant (Katayama et al., 2004). In some gastric cancer cell lines, AURKA was

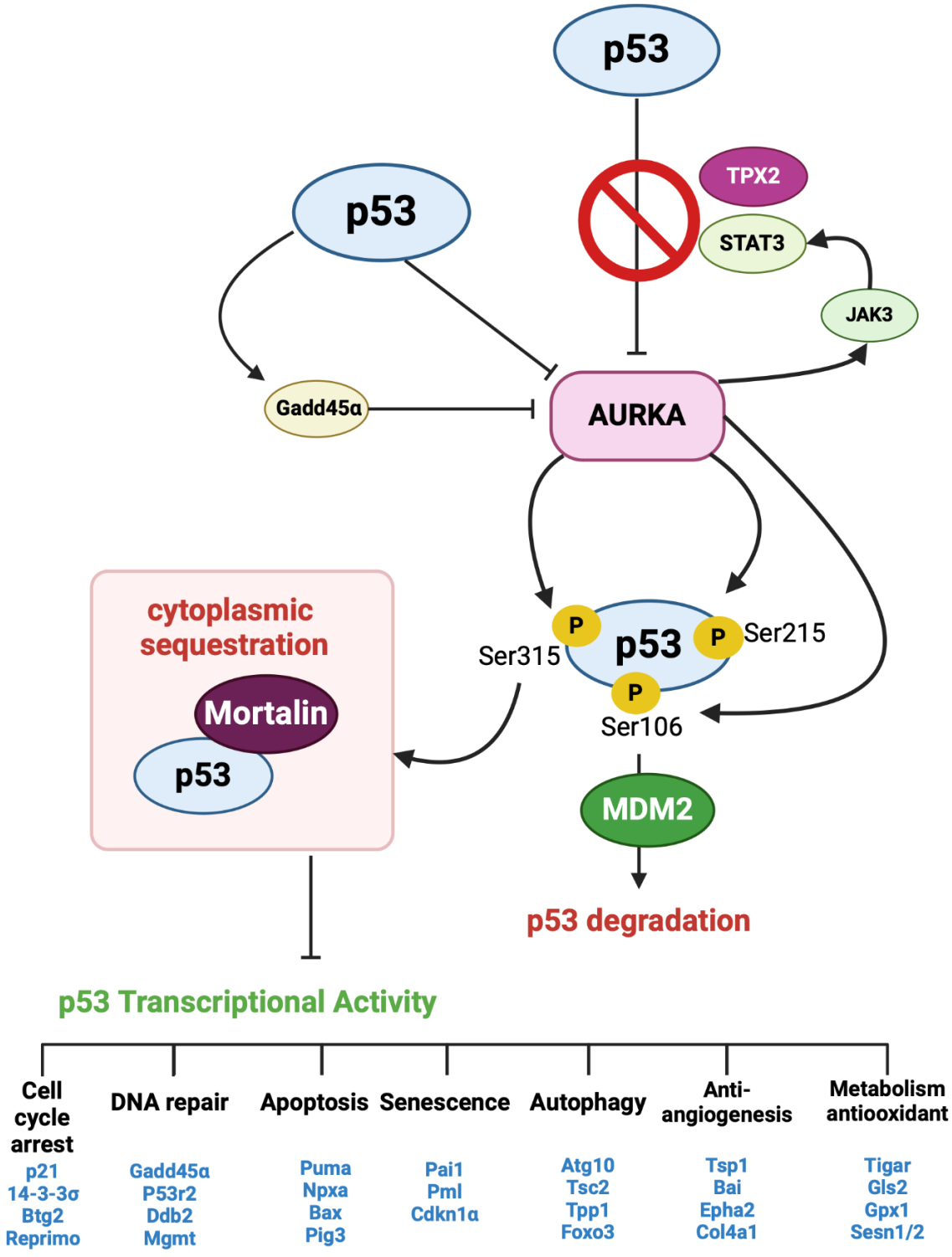

Figure 1. 7: AURKA and p53

AURKA inhibits p53 by direct phosphorylating which promote MDM2-dependant degradation oy cytoplasmic sequestration which inhibit the transcriptional activity of p53. Key transcription targets and processes downstream of p53 are shown. AURKA is directly inhibited by p53, and indirectly via Gadd45α. TPX2 and JAK3-STAT3 signalling block p53 inhibition of AURKA. Figure produced in Biorender.

found to negatively regulate p53 indirectly through MDM2 phosphorylation. AURKA overexpression led to increased MDM2 expression and phosphorylation of MDM2

Ser166, as well as decreased p53 levels which were attenuated by inhibiting MDM2 expression (Sehdev et al., 2014). The same study reported that in 94 gastric adenocarcinoma tissues samples, there was correlation in the overexpression of AURKA and MDM2. The authors suggest that the AURKA-MDM2 regulation may account for documented AURKA-mediated resistance to Taxol and cisplatin chemotherapy in gastric cancer (Sehdev et al., 2014). While this report did not assess how MDM2 expression affected survival or therapeutic response, a later publication demonstrated that MDM2 was correlated with poor response to 5-FU plus oxaliplatin in gastric cancer (Li et al., 2020).

A subsequent study demonstrated that AURKA also phosphorylates p53 at Ser215 (Liu et al., 2004). The resultant inhibition of p53-DNA binding led to reduced expression of downstream genes such as p21 and PTEN in ovarian and lung cancer cell lines. In addition, Ser215 phosphorylation inhibited p53's ability to induce apoptosis in response to cisplatin and overcame IR induced G_2/M checkpoint arrest. In this study AURKA mediated phosphorylation of Ser315 did not alter the biological function of p53, and the authors argue that Ser215 not Ser315 is responsible for the majority of AURKA mediated effects on p53 (Liu et al., 2004). Ser215 phosphorylation also contributes to cytoplasmic sequestration of p53, as a result of Mortalin tethering (Katayama et al., 2012).

A later study identified a third phosphorylation site which positively regulates p53 stability (Hsueh et al., 2013). AURKA was shown to phosphorylate p53 at Ser106,

which weakened the interaction between MDM2 and p53 and increased p53 half-life. Ser106 phosphorylation by AURKA therefore stabilises p53, which contrasts the negative regulation of Ser215 and Ser315 phosphorylation on p53 stability and activity. This directly opposes previous thinking about the regulation of p53 by AURKA. This finding also contradicts reports of inverse correlation between AURKA and p53 levels in human tumours (Ma and Poon, 2020).

AURKA was also reported to regulate p53 through interaction with its coactivator Heterogeneous Nuclear Ribonucleoprotein K (hnRNPK) (Hsueh et al., 2011). hnRNPK expression is induced by DNA damage through ATM, and is required for transcription of p53 target genes in the DDR (Moumen et al., 2005). AURKA phosphorylates hnRNPK at Ser379, reducing its affinity for p53 but not affecting hnRNPK's localisation or transcriptional regulation of p21 (Hsueh et al., 2011).

These studies have shed light on several mechanisms by which AURKA regulates p53 activity. How these different interactions fit into the one picture is unclear. In the case of the gastric cancer cell lines, Sehdev et al (2014) did not find a direct interaction between AURKA and p53, demonstrating differences between cell lines. Additionally, in cases of direct interaction, how positive and negative regulation via different phosphorylation sites on p53 is controlled is also unclear.

While being a phosphorylation target of AURKA, p53 in turn negatively regulates AURKA (Chen et al., 2002). This can occur via direct interaction with the catalytic domain resulting in AURKA inhibition which could be blocked by TPX2 (Eyers and Maller, 2004). The AURKA gene promoter region was identified as a novel binding site for p53, which could down-regulate AURKA expression in MCF-7 and HCT116 cells (Nikulenkov et al., 2012). P53 may also inhibit AURKA via upregulation of

Growth Arrest And DNA Damage Inducible Alpha (Gadd45α), which is induced by genotoxic stress. Gadd45α binds and inhibits AURKA, and is able to prevent AURKA-mediated centrosome amplification (Shao et al., 2006, Sánchez et al., 2010). AURKA can indirectly block negative regulation by p53 by activation of Janus Kinase 2 (JAK2), which promotes Signal Transducer And Activator Of Transcription 3 (STAT3) activity. STAT3 inhibits p53 from binding to the AURKA gene promoter region through binding to the promoter region itself (Katsha et al., 2014).

1.4.2.2. AURKA and Cell Cycle Checkpoints

In addition to regulation of p53, AURKA regulates the G_1 and G_2 checkpoints in other ways.

AURKA plays a key role in the G_2-M transition and its activity is reported to be similarly required to promote mitotic entry following activation of the G_2/M checkpoint. AURKA mutation or overexpression can override the G_2/M checkpoint. This can occur via constitutive activation of Cdk1, which deregulates mitotic entry and abrogation of the G_2/M Checkpoint (Stark and Taylor, 2006, Krystyniak et al., 2006).

AURKA also promotes progression through G_1. AURKA deletion, inhibition or silencing has been shown to activate the G_1/S checkpoint and increases accumulation of cells in G_0-G_1. P53 activation of P21 and pRB activate the G_1/S checkpoint so the role of AURKA in this checkpoint may be related to its regulation of p53 (Yang et al., 2010a, Wang et al., 2011c, Huck et al., 2010, Tomita and Mori, 2010).

These studies demonstrate the various regulatory pathways affecting AURKA during the cell cycle and will aid our understanding this of the radiosensitisation mechanism of AURKA inhibitors.

1.4.2.3. AURKA and the DDR

There are growing links between AURKA and DDR pathways, which have suggested both positive and negative effects on repair.

AURKA overexpression has been demonstrated to regulate expression of the HR proteins BRCA1 and BRCA2. AURKA demonstrates a mutually repressive relationship on expression with either BRCA proteins, BRCA1 and BRCA (Wang et al., 2014, Sun et al., 2014a). Sun et al (2014) also provided evidence that AURKA can dysregulate DDR pathways downstream via ATM. AURKA overexpression also increased cisplatin resistance and inhibited apoptosis, both of which could be reversed by inducing BRCA1 or BRCA2 expression (Sun et al., 2014a).

In a separate report AURKA was seen to impair RAD51 filament formation and repress HR as a result. AURKA overexpression also sensitised MCF10A cells to IR and sensitised BRCA2 competent cells to PARP inhibitors (Sourisseau et al., 2010). This directly contradicted Sun et al (2014) who found increased IR resistance with high AURKA expression, although this was attributed to apoptotic inhibition rather than DDR deficiency.

Studies of AURKA expression in ovarian tumour tissue also support downregulation of BRCA2. Significant negative correlation between BRCA2 and AURKA was found in high grade serous carcinoma samples, and the expression ratio of AURKA to BRCA2 in these samples predicted poorer overall survival. Negatively correlating

expression was also found in pancreatic, breast and gastric cancer (Yang et al., 2011b).

Several studies have contradicted the repressive role of AURKA on DDR by providing evidence that AURKA positively regulates BRCA1 and BRCA2 function. In ovarian cancer cells, AURKA inhibition by Alisertib down-regulates BRCA1 and BRCA2, and could mimic the synergistic lethality of BRCA proteins when used in combination with PARP inhibitors (Do et al., 2017, Wang et al., 2014). A later paper reported that AURKA, with its co-factor TPX2, facilitates BRCA1 localisation to DSBs after IR, which contradicts its role as negative regulator of BRCA1 (Byrum et al., 2019).

Byrum et al (2019) also demonstrated that AURKA negatively regulates the protein 53BP1 with downstream effects in promoting HR. 53BP1 protects DNA ends from end resection. TPX2 facilitates AURKA-53BP1 interaction, and when depleted, led to reduced end resection. Both AURKA and TPX2 depletion also led to Mre11 degradation of stalled replication forks following HU treatment, in a 53BP1 dependant pathway. These results suggest that AURKA-TPX2 complex represses 53BP1 and that AURKA regulation of 53BP1 promotes end resection and HR. As TPX2 and AURKA also facilitated BRCA1 localisation to DSBs, these results highlight a theme of HR promotion (Byrum et al., 2019).

These studies highlight the complexity of the role of AURKA in DDR. Many of the repressive roles of AURKA were promoted by overexpression (as seen in many human tumours). This raises the question as to whether high expression promotes non-canonical functions in DDR. As the functions of AURKA in DDR pathways at

endogenous or over-expression levels is still not well understood, this is currently unclear.

1.5. Aurora Kinases and Cancer

1.5.1. Aurora Kinase Expression in Cancer and Clinical Significance

AURKB and AURKA are frequently overexpressed in many human cancers (Du et al., 2021, Tang et al., 2017, Borah and Reddy, 2021).

AURKB

AURKB overexpression is associated with aneuploidy and enhanced cell survival. In NSCLC, AURKB commonly shows high expression (Smith et al., 2005, Vischioni et al., 2006). In general, AURKB also correlates with poor prognosis, as it correlates with tumour grade, genetic instability, reduced overall survival and reduced disease-free survival (Smith et al., 2005, Vischioni et al., 2006, Yu et al., 2018, Zhang et al., 2015). Gastric cancer was an exception as high AURKB expression was prognostically favourable (Enjoji et al., 2009).

The mechanisms behind AURKB dysregulation in tumours are multi-fold. Genetic alterations include mutation, amplification and deep deletion in some cases (Ahmed et al., 2021). AURKB overexpression has also been linked to dysregulated protein signalling via MYC and TIP60/Cdk1 (Jiang et al., 2020, Mo et al., 2016).

High AURKB activity is associated with chemoresistance. In NSCLC, AURKB promotes chemoresistance *in vitro*, including to cisplatin and paclitaxel (Yu et al., 2018, Al-Khafaji et al., 2017). Clinically, AURKB expression correlates with chemoresistance in NSCLC and breast cancer (Zhang et al., 2015, Al-Khafaji et al., 2017). AURKB was also found to promote resistance to the BRAF V600E kinase inhibitor vemurafenib in melanoma (Chang et al., 2020).

AURKA

Overexpression of AURKA has been shown to result from gene amplification, transcriptional promotion and post-transcriptional modifications (Du et al., 2021). Mis-localisation of AURKA is been reported in tumours, whereby AURKA localised to the nucleus rather than cytoplasm (Burum-Auensen et al., 2007). This is thought to promote oncogenic activity through non-canonical roles (Tatsuka et al., 2009).

Similarly to AURKB, overexpression of AURKA also correlates with poor prognosis in several cancer types (Pohl et al., 2011, Zeng et al., 2007, Nie et al., 2020, Qi et al., 2007, Pannone et al., 2011, Li et al., 2021, Huang et al., 2019, Chieffi et al., 2006). AURKA expression has also been associated with tumour grade in glioblastoma (Araki et al., 2004).

1.5.2. AURKB and Oncogenesis

AURKB is proposed to promote malignancy via genetic instability, p53 inhibition and regulation of downstream oncogenes. *In vitro* overexpression of AURKB results in aneuploidy and spontaneous tumour formation in mice models (González-Loyola et al., 2015). AURKB promotes cell cycle progression via its mitotic function but also via inhibition of p53. Suppression of p53 leads to reduced expression of p21, aberrant activation of Cdk1 and increased proliferation (González-Loyola et al., 2015).

As discussed in section 1.3.2.2, AURKB can downregulate p53 signalling. Increased cell survival associated with AURKB overexpression is thought to rely on this downregulation. P53 is an essential regulator of cellular stress response. P53 suppresses proliferation in events of cellular stress such as DNA damage or uncontrolled proliferation (Marei et al., 2021). P53 can activate senescence,

autophagy or death pathways to limit damage, so reducing the probability of malignant transformation. In tumours, suppression of p53 can allow genomic instability to go unchecked and is a key requirement for AURKB's oncogenic potential (Yu et al., 2018).

AURKB phosphorylates the oncogene MYC, which stabilises MYC by preventing FBXW7-dependant degradation (Jiang et al., 2020). MYC can also activate AURKB transcriptionally in a positive feedback loop. In NSCLC, an upstream regulator was identified; Gemin6 promotes AURKB mRNA maturation which leads to MYC stabilisation (Lin et al., 2022). AURKB inhibition blocks MYC-driven proliferation and promotes apoptosis. Additionally, increases in apoptosis after AURKBi are greater in cells overexpressing MYC (Den Hollander et al., 2010).

AURKB is also linked to EMT phenotypes and metastasis. In multiple cancer types, AURKB promotes migration and invasion (Zhang et al., 2020, Ma et al., 2023). AURKBi decreased expression of mesenchymal markers and increased epithelial marker expression. *In vivo,* AURKB silencing by short hairpin or knockout reduced the number of lung metastases while AURKB overexpression increases metastases. These effects were attributed to AURKB activation of Akt, which in turn stabilises the mesenchymal Snail1 (Zhang et al., 2020, Ma et al., 2023).

1.5.3. AURKA and Oncogenesis

AURKA contributes to oncogenesis via activation and oncogenic signalling, activation of EMT and downregulation of apoptosis.

AURKA downregulates IκBα via phosphorylation leading to its downregulation (Briassouli et al., 2007). This interaction promotes chemoresistance via activation of

Akt and Nuclear Factor Kappa B (NFκB) (Yang et al., 2006, Yao et al., 2009, Xu et al., 2011, Saiprasad et al., 2014). Akt signalling promotes cell survival, cell cycle progression and cell growth (Fresno Vara et al., 2004). Inhibition of Akt abrogates the growth inhibition of AURKA inhibitors demonstrating that Akt is critical to AURKA-driven proliferation. Additionally AURKA activation of Akt has been shown to increase migration and invasion (Guan et al., 2007). AURKA regulation of the Akt pathway can also suppress autophagy via MTOR (Zou et al., 2012). AURKA also promotes downstream NFκB activation. NFκB drives oncogenesis via proliferation, angiogenesis, EMT and suppression of apoptosis (Xia et al., 2014). AURKA also promotes transformation via Ras activation via the upstream protein Src (Kanda et al., 2005).

Additionally, AURKA activity can suppress apoptosis via inhibition of Bcl-1, MCL-1 and PUMA (Huang et al., 2008b, Yang et al., 2013, Sun et al., 2014b).

EMT processes are promoted by AURKA activity. AURKA upregulates the pro-mesenchymal factors SLUG and fibrillin 1, whilst downregulating adherence proteins E-cadherin and β-catenin (Fenouille et al., 2012, Sengle et al., 2012, Wan et al., 2008). Additionally, AURKA promotes migration and invasion by increasing expression of the metalloproteinases MMP-2, MMP-7 and MMP-10 (Wang et al., 2012, Chefetz et al., 2011, Chen et al., 2015).

In addition to these pathways, AURKA can also inhibit p53 as discussed in section 1.4.2.1. In human cancers, p53 is an important responder to DNA damage or oncogenic stress. P53 transcriptional targets activate a wide range of anti-tumour pathways including cell cycle arrest, DDR or apoptosis (Marei et al., 2021).

1.5.4. AURKB Inhibitors

Due to their oncogenicity and association with poor prognosis, a range of clinical Aurora kinase inhibitors (AKIs) have been developed and trialled over several decades (Lakkaniga et al., 2024, Galetta and Cortes-Dericks, 2020, Tang et al., 2017, Du et al., 2021). These include inhibitors of specific family members as well as many pan-AURK inhibitors which broadly inhibit Aurora kinases A, B and C.

The four specific AURKB inhibitors are ATP competitors. Hesperadin is an inhibitor specific to AURKB and based on indolinone chemistry. It is known to inhibit growth *in vitro* and induce polyploidy (Kovacs et al., 2023). GSK1070916 is an azaindole-based AURKB inhibitor which also inhibits AURKC at high doses (Adams et al., 2010). GSK1070916 induces growth inhibition and polyploidy in a range of cancer cell lines (Hardwicke et al., 2009).

ZM447439 is based on quinazoline chemistry and works as an ATP competitor at the ATP binding site (de Groot et al., 2015, Ditchfield et al., 2003, Gadea and Ruderman, 2005)

Barasertib (AZD1152) is an ATP-competitive AURKBi and is the most potent and selective inhibitor of AURKB to date. Barasertib development by AstraZeneca built on the structure of ZM447439 (de Groot et al., 2015). Barasertib is highly specific for AURKB over AURKA, with an IC50 of 0.36 nM for AURKB (vs IC50 of 1369 nM for AURKA) (Wilkinson et al., 2007). AZD1152 is a prodrug which is rapidly converted into the active form in plasma, which known as AZD1152-HQPA (Mortlock et al., 2007).

1.5.4.1. Barasertib in Clinical Trials

Barasertib (AZD1152) entered clinical trials in 2005 and reached Phase III, with most success in acute myeloid leukaemia (AML). Clinical trials of the Barasertib pro-drug (AZD1152) are shown in Table 1.1.

Table 1. 1 Clinical Trials with the AURKB Inhibitor Barasertib (AZD1152)

NCT ID	Tumour Type	Phase	Start	Status	Notes
NCT00497731	Advanced Solid Malignancies	Phase I	2005	Terminated	Efficacy seen in the solid tumour patient population was not sufficient to continue research with AZD1152 monotherapy in solid tumours at that time.
NCT00338182	Advanced Solid Malignancies	Phase I	2006	Completed	
NCT00497991	Relapsed Acute Myeloid Leukaemia	Phase I/II	2006	Completed	
NCT00497679	Advanced Solid Malignancies	Phase I	2007	Terminated	Terminated due to technical difficulties with administration of study drug in this patient population with this schedule
NCT00530699	Acute Myeloid Leukaemia (AML)	Phase I	2007	Completed	
NCT00926731	Acute Myeloid Leukaemia (AML)	Phase I	2009	Completed	Combination with low dose cytosine arabinoside (LDAC)

NCT00952588	Acute Myeloid Leukaemia (AML)	Phase II / III	2009	Completed	Combination with low dose cytosine arabinoside (LDAC)
NCT01019161	Acute Myeloid Leukaemia (AML)	Phase I	2009	Completed	Pharmacokinetics only
NCT01354392	Diffuse Large B-Cell Lymphoma	Phase II	2011	Completed	

In solid tumours, the best response was stable disease. Dose testing found that longer durations of continuous dosing by 7-day continuous infusion every 21 days produced the best clinical response in AML (Kantarjian et al., 2013). This dosing schedule required in-patient care and a central line.

Neutropenia was a common side effect and was dose limiting. Stomatitis was also experienced in <20% of patients (Löwenberg et al., 2011, Kantarjian et al., 2013). The tolerated doses produced moderate effects and performed best in haematological malignancies due to the higher relative dose in blood than within solid tumours.

To achieve higher doses in solid tumours as well as overcome the issues of neutropenia and the continuous dose schedule, a nanoparticle-encapsulated drug form known as AZD2811 (Defosbarasertib) was developed using the active AZD1152-HQPA. The aim was to greater target tumour sites and release slowly over several days (Ashton et al., 2016). AZD2811 was shown to have a prolonged inhibition of AURKB and reduced bone marrow toxicity in mouse models compared to AZD1152 (Ashton et al., 2016).

Clinical trials with AZD2811 started in 2015 and included AML and small cell lung cancer patients (see Table 1.2). The first of five trials were completed, but the next 3 phase II trials were terminated and one trial remains active but not recruiting.

The completed Phase I trial of AZD2811 found that it produced continuous but limited anti-tumour activity, although improved over AZD1152 (Johnson et al., 2023). AZD2811 maintained stable disease in 45% of patients compared to 23% by AZD1152. The treatment was well-tolerated and 3 patients remained on treatment for over a year. Neutropenia was still an associated side effect but stomatitis, induced by AZD1152, was not seen in this cohort. Neutropenia was managed by Gonadotropin-colony stimulating factor (G-CSF) addition to treatment regimes, which supported neutrophil recovery and allowed higher doses (Ashton et al., 2016). Following, the relative success in phase I with AZD2811, phase II trials were conducted in AML and SCLC.

NCT03366675 was terminated in 2018 and reported early detection of the purpose of the study. NCT04525391 was reported as terminated in February 2022, with the reason listed as a suspected unexpected serious adverse reaction (SUSAR) in another trial. NCT03217838 was terminated in July 2021 by strategic decision.

Table 1. 2 Clinical Trials with the AURKB Inhibitor Defosbarasertib (AZD2811)

NCT ID	Tumour Type	Phase	Start	Status	Notes
NCT02579226	Advanced Solid Tumours	Phase I	2015	Completed	
NCT03217838	Acute Myeloid Leukaemia (AML)	Phase I/II	2017	Terminated	Reason for termination: "strategic decision"

NCT03217838	Relapsed Small Cell Lung Cancer Patients	Phase I/II	2017	Terminated	Reason for termination: "strategic decision"
NCT03366675	Relapsed Small Cell Lung Cancer Patients	Phase II	2017	Terminated	Reason for termination: "Early detection of the purpose of the study"
NCT04525391	Relapsed Small Cell Lung Cancer	Phase II	2020	Terminated	Reason for termination: "Recommended completion of the study due to SUSAR occurring in other clinical trials conducted with the same drug"
NCT04745689	Extensive Stage Small-Cell Lung Cancer.	Phase II	2021	Active, not recruiting	Combination with Durvalumab

1.5.5. Alisertib (MLN8237) in Clinical Trials

So far, MLN8237 (Alisertib) is the only AURKA inhibitor to reach phase III clinical trials. Preclinically, Alisertib reduces tumour growth in a range of cancer types, (Görgün et al., 2010, Liu et al., 2013, Ding et al., 2015). In clinical trials, Alisertib achieved modest anti-tumour activity as a monotherapy in phase II trials in breast cancer, SCLC, liposarcoma, castration-resistant prostate cancer and T cell lymphoma (Melichar et al., 2015, Beltran et al., 2019, Dickson et al., 2016). Alisertib also achieved moderate anti-tumour activity in phase II trials in T cell lymphoma, leading to phase III trials for this cancer type (Barr et al., 2015). In contrast to the numerous pan-AKIs, Alisertib is highly selective for AURKA at nanomolar doses but

at higher doses (>100 nM *in vitro*) can also inhibit AURKB (Nair and Schwartz, 2016).

1.6. AURK Inhibitors as Radiosensitisers

Given the tolerability of AURK inhibitors but failure to control tumour growth as a monotherapy, repurposing drugs such as Barasertib and Alisertib is an attractive option. There is plentiful clinical data to support their pharmacological profile. The issues so far lie in their dose-limiting toxicity which limit their ability to control tumour growth in isolation.

If radiosensitisation could be achieved, this could utilise a lower dose than needed for single agent success and build on the progress to date with these agents.

1.6.1. Radiosensitisation by AURKB Inhibition

Radiosensitisation by Barasertib (AZD1152 or AZD1152-HQPA) has been previously studied in colon, prostate and lung cancer cell lines (Tao et al., 2008, Tao et al., 2009, Niermann et al., 2011, Sak et al., 2012).

Tao et al (2008) published the first report that Barasertib could radiosensitise cancer cells. They tested AZD1152-HQPA (active form) and found that it could radiosensitise *in vitro* and *in vivo* in HCT116 p53-/- cells. They provided some evidence that wildtype p53 prevented radiosensitisation by AZD1152-HQPA *in vitro*, although *in vivo* HCT116 xenografts were sensitised regardless of p53 status. Radiosensitisation was also tested using AURKB siRNA and an inducible kinase-dead system, which was less convincing (Tao et al., 2008). Tao et al (2009) further proposed that radiosensitisation by AZD1152-HQPA could be enhanced by pre-

treating or delaying treatment with AZD1152-HQPA by 24 Hr by increasing polyploidy (Tao et al., 2009).

In prostate cancer, the cell lines DU145 and PC3 were radiosensitised by a 48 Hr pre-treatment of 60 nM Barasertib (AZD1152) (Niermann et al., 2011). Neither DU145 nor PC3 express functional p53 (Chappell et al., 2012, Scott et al., 2003). In cell cycle analysis, Barasertib treatment let to 4N accumulation in PC3 cells. Conversely, >4N DU145 cells increased but the 4N fraction was not increased by Barasertib. In prostate cells, Barasertib was found to increase γH2AX response to IR and slow down resolution of γH2AX foci over time, indicating modulation of the DDR or enhanced DNA damage (Niermann et al., 2011). Tao et al reported no change in γH2AX foci in HCT116 cells but the data was not shown (Tao et al., 2009).

In NSCLC, the cell lines H460 (functional p53) and A549 (functional p53) were radiosensitised by AZD1152-HQPA, but not in the p53mut cell lines H661 and H520 (Sak et al., 2012). Barasertib did not radiosensitise the H661 cell line after single dose but did after fractionated IR, shown by monolayer growth studies. They found that plaque monolayer growth control probability was higher with AZD1152-HQPA in H460, and H661 (p53 mutant) cells, with increased effect using a fractionated approach. They proposed that AZD1152-HQPA reduced repopulation due to increases in polyploid, non-proliferative cells. However, they did not investigate if the combination increased polyploidy above levels induced by IR.

Overall, these results show AURKBi by Barasertib (AZD1152 or AZD1152-HQPA) radiosensitises several cancer types *in vitro*. In general, p53 status did not appear to predict radiosensitisation. The timing of treatment had different effects in different models. In HCT116 cells, radiosensitisation appeared to increase when AZD1152-

HQPA was added 24 Hr before or after IR (Tao et al., 2008). However, other studies achieved radiosensitisation with pre-treatment of 48 Hr (removed in recovery) and 2 Hr of AZD1152 (-HQPA) before IR (Sak et al., 2012, Niermann et al., 2011).

1.6.2. Radiosensitisation by AURKA Inhibitors

Previous work by the Bryant Lab provided evidence that 25nM Alisertib treatment can radiosensitise p53 proficient NSCLC cell lines *in vitro* (Appendix Fig 1). The radiosensitisation was time-dependant and required Alisertib dosing within 24 hours post IR (Appendix Fig 2).

Elsewhere, AURKAi is known to radiosensitise. Liu et al (2019) showed that lung cancer cell lines could be radiosensitised by Alisertib in p53 proficient lines only (Liu et al., 2019), which agrees with work carried out by the Bryant Lab. However, 100nM Alisertib was used in this study, higher than 25nM dose used in the Bryant Lab. Our data suggests that 100nM is lethal to NSCLC cell lines and is above the maximum tolerated dose *in vivo.* Lui et al (2019) investigated death pathways activated by Alisertib and found induced Caspase-3 cleavage but this was also seen in cells treated with IR alone.

Wang et al (2021) investigated the mechanism of radiosensitisation by AURKAi (Wang et al., 2021). Radiosensitisation of NSCLC cell lines was achieved using AURKA siRNA interference. They used RNA-seq to screen for expression changes downstream of AURKA. They identified C-X-C Motif Chemokine Ligand 5 (CXCL5), a chemokine which activates EGFR, Mitogen-Activated Protein Kinase 1 (MAPK1) and Akt/PI3K signalling pathways. AURKA was shown to transcriptionally activate CXCL5. By overexpressing CXCL5 alongside AURKA siRNA, they could rescue the

anti-tumour effects and radiosensitivity of AURKA downregulation. This paper shows compelling evidence that CXCL5 is a downstream effector of AURKA and is involved in its response to high dose IR.

Additionally, they demonstrated a link between AURKA and autophagic cell death. They found upregulation of autophagic markers when AURKA was depleted, which could be increased further with radiation or reversed with CXCL5 overexpression. The up-regulation of CXCL5 by AURKA was attributed to its activation of NFκB. Analysis of the CXCL5 structure identified a NFκB binding site. They demonstrated *in vitro* that NFκB upregulates CXCL5, and that this transcriptional binding was reduced with AURKA depletion.

1.7. Research Aims

The aims of this project are to investigate if AURKB inhibition by Barasertib can radiosensitise NSCLC and to investigate the mechanisms by which Barasertib radiosensitises. A further aim was to investigate how global phosphorylation changes after IR and after treatment with the AURK inhibitors Barasertib (AURKBi) and Alisertib (AURKAi).

Chapter 2: Materials and Methods

2. Materials and Methods

2.1. Materials

Laboratory reagents are detailed in Appendix Table 1.

2.1.1. Cell lines

The NSCLC lines H460, H1299 and SW900. H460 and H1299 cells were grown in RPMI1640 media (Lonza) with 10% Foetal Bovine Serum (FBS) (Thermo Fisher Scientific) and 1% MEM Non-essential-amino acids (Sigma). SW900 cells were grown in DMEM media (Sigma-Aldrich) with 10% FBS (Thermo Fisher Scientific), 1% MEM Non-essential-amino acids (Sigma) and 2 mM L-Glutamate (Sigma-Aldrich).

2.1.2. Buffers

The makeup of commonly used buffers is described in Appendix (Section 8.1) and other buffers are detailed within protocols.

2.1.3. Antibodies, Drugs and Kits

The primary and secondary antibodies used in experiments are detailed in Appendix Table 2 and Appendix Table 3. The drugs used in experiments are detailed in Appendix Table 4. The assay kits used in experiments are detailed in Appendix Table 5. Protocol & Usage are detailed in the methods section.

2.2. Methods

2.2.1. Cell Culture

Cell Maintenance and Passage

Cells were grown in incubators at 37 °C with 5% CO_2 and were passaged once they reached 90% confluency as follows; cells were washed twice with sterile phosphate buffered saline (PBS) and incubated for 5 minutes with 1 ml trypsin EDTA (Sigma-Aldrich) or until detached from flask. Warm RPMI media containing 10% FCS and 1% non-essential amino acids was then added and cells were transferred to a clean tube for counting.

Freezing and Thawing Cells

To prepare for storage at -80 °C, cells were trypsinised as described above and transferred to a 15 ml tube. Cells were then pelleted by centrifugation at 1500 rotations per minute (RPM) for 5 minutes and the supernatant media was removed. The cells were resuspended in culture media with 10% dimethyl sulfoxide (DMSO) added. 1 ml of cell solution was aliquoted per cryovial and frozen at -80°C in a Mr Frosty freezing containers and stored long-term at -80°C.

Cell Counting

Cells were counted using a haemocytometer. Resuspended cell solution (>7 µl) was dispensed onto the haemocytometer under the cover slip. The number of viable cells were counted and averaged. The cell concentration (cells/ml) was achieved the multiplying the average cell number per square by 10,000.

2.2.2. Irradiation using a Cs137 Gamma Ray Source

IR was delivered using a Cs137 source. Cells were placed in a metal cannister and placed in the entry point of the machine. Duration of exposure was altered to adjust

dose delivery The time per Gy was adjusted annually based on the decay rate (2023: 1.97 Gy/Min).

2.2.3. Survival Assays

2.2.3.1. Clonogenic Assays

Cells were trypsinised and counted as detailed above. Clonogenic assays for NSCLC cells were carried out in 6 well plates or 10cm dishes.

For clonogenic assays carried out in 6 well plates involved pre-treatment in flasks, before trypsinisation and counting in drugged media as required. Cells were then irradiated at plating concentration in suspension. After irradiation, treated cells in suspension were plated and allowed to grow for 8 days or until formation of clear colonies with greater than 50 cells.

For clonogenic assays in 10 cm dishes, cells were plated then allowed to settle for >4 Hr before drug treatment or irradiation. After 8 days or once clear colonies with greater than 50 cells formed, plated were fixed.

To fix and stain, plates were fixed at room temperature in methanol with 0.4 g/L methylene blue for 10 minutes before manual counting.

2.2.3.2. Dose Modulation Factor (DMF) Calculation from Clonogenic Survival Fraction

Dose modulation factor (DMF) was calculated for Barasertib and IR clonogenic survival based on the dose of IR required to produce a survival fraction of 0.1 (Citrin and Mitchell, 2014). Linear quadratic curve fit was carried out on the clonogenic

survival curves. The X value (IR dose) at Y (Survival fraction) = 0.1 was interpolated from the linear quadratic curve.

DMF was calculated as follows:

$$\mathrm{DMF} = \frac{\text{IR Dose for 0.1 Survival in DMSO condition}}{\text{IR Dose for 0.1 Survival in Drug condition}}$$

2.2.3.3. Nocodazole Treatment

To achieve G_2/M arrest, cells were treated with nocodazole. Cells were seeded at a density of $1x10^6$ per 10cm plates with 10 ml media and allowed to settle overnight. Cells were treated with 100 nM for 16 Hr. The media containing nocodazole was removed and cells were gently washed twice with warm media. Fresh media was added, and inhibitors were added for 2 Hr incubation (if applicable).

2.2.4. Western Blotting

2.2.4.1. Protein Extraction in RIPA Buffer

1x Radioimmunoprecipitation assay (RIPA) buffer (1 ml) was prepared by mixing 200 µl 5 x RIPA buffer, 10 µl PMSF, 100 µl 10x cOmplete protease inhibitor, 100 µl 10x Phosstop phosphatase inhibitor and 590ul water. Protein was collected from 10 cm plates with 0.5-1 $x10^6$ cells per plate. Media was removed and plates were washed with ice cold sterile PBS. Cells were scraped into 60- 100 µl of RIPA buffer, and transferred to a chilled Eppendorf tube on ice, then pipetted up and down 10 times. Samples were vortexed for 10 s on full, then incubated on ice. This was repeated twice more and vortexed a 4^{th} time. Samples were passed through a 25 G syringe 5 times to shear DNA, then centrifuged for 10 minutes at 13,000 RPM at 4°C. The supernatant was collected in a fresh tube and stored at -80°C or in ice for use.

To quantify protein content, bovine serum albumin (BSA) standards of 1/5/10/15/20 µg/ml were prepared and 50 µl Bradford reagent was added to 450 µl per standard. 1 µl per protein extract were diluted in 180 µl in water and 20ul Bradford reagent was added for a final dilution of 1:200. Protein concentration was measured by absorbance at 595 nM by a microplate photometer, and extract concentrations were calculated from the BSA standard master curve.

To prepare samples for sodium dodecyl-sulphate polyacrylamide gel electrophoresis (SDS-PAGE), the volume required per sample was calculated. 20-40 µg was loaded, dependant on target protein. Protein extracts were prepared with water and 20% 5 x sodium dodecyl-sulphate (SDS) sample buffer (v/v) with total volume of 20 µl. Protein samples were then boiled at 90°C for 10 minutes, briefly centrifuged to clear the lid, then moved to ice before loading.

2.2.4.2. Protein Collection for Phosphoproteins

Protein was collected from 10 cm plates with 0.5-1 x10^6 cells per plate. Media was removed and plates were washed with ice cold sterile PBS. Cells were scraped into 100 µl of sample buffer (50% 5x SDS sample buffer, 10% 1M Dithiothreitol (DTT), 10% Phosstop x1, 10% cOmplete protease inhibitor and 20% H_20) and transferred to a pre-chilled Eppendorf tube. Samples were passed through at 25G needle 5-10 times to shear DNA. Protein samples were then boiled at 90°C for 10 minutes, briefly centrifuged to clear the lid, then moved to ice. If not being used immediately, samples were stored at -80°C for future use.

2.2.4.3. SDS-PAGE

Gels for SDS-PAGE were poured fresh for each blot. Resolving gels with 8, 10 or 12% polyacrylamide and stacking gels with 5% polyacrylamide were prepared (volumes detailed in Appendix Tables 6-9).

For frozen phosphoprotein samples collected in boiling mix, samples were reboiled for 10 minutes at 90°C and 20 µl was loaded per sample.

Gels were run in 1 x SDS running buffer. Gels were run with voltage of 180V for migration through the stacking gel and 100-150 V for separation in the resolving gel.

2.2.4.4. Protein Transfer

Following SDS-PAGE, gels were removed from the electrophoresis tanks and soaked in 1x Towbin transfer buffer. Protein transfer to a Cytiva Amersham™ Protran™ Nitrocellulose blotting membrane (Fisher Scientific) was carried out in a Bio-Rad Criterion blotter tank. To facilitate transfer, the gels and transfer materials were soaked in Towbin transfer buffer and stacked as follows:

Sponge – 2xblotting paper - SDS-PAGE gel (top side down) – membrane - 2xblotting paper -sponge

Transfers were run for 1 Hr at 100 V for proteins below 100 kDa, 2 Hr at 50V for phosphoproteins and 2 Hr at 100V for proteins over 100 kDa. Towbin transfer buffer was pre-chilled, an ice pack was included in the tank and the tank was stored on ice while running to prevent overheating.

2.2.4.5. Blocking and Probing

Blots were blocked at room temperature for 1 Hr in 5 ml 5 % milk in TBST. All antibodies were diluted in 5 % milk in TBST. Primary antibody probing was carried out over night at 4-8 °C. Blots were washed 3 times in 5 ml TBST for 10 Mins before probing with a secondary antibody. Blots were incubated in secondary antibody for 1 Hr at room temperature. Blots were washed 3 times in 5 ml TBST for 10 minutes before detection.

2.2.4.6. Enhanced Chemiluminescence (ECL) Detection

Amersham™ ECL™ Western Blotting Detection Reagents were mixed in equal volumes and 1 ml was added to each blot to incubation at room temperature for 1 minute. Blots were visualised using X Ray film processed using a SRX101A developer machine.

2.2.4.7. Densitometry

X-Ray films were scanned at minimum 1600 DPI. Densitometry was performed on film scans using the ImageJ Gels in-built macro.

2.2.5. Mass Spectrometry (MS)

Mass spectrometry was carried out at the Centre for Proteome Research, Institute of Systems, Molecular and Integrative Biology, University of Liverpool, Crown Street, Liverpool, L69 7BE.

High performance liquid chromatography (HPLC) grade solvents and high purity reagents were used. Lo-bind samples tubes were used for sample preparation to reduce sample-surface binding.

2.2.5.1. H460 Treatment and Cell Harvesting

750,000 H460 cells were seeded in T25 flasks and left to settle overnight. Cells were treated with DMSO, 50 nM Barasertib or 25 nM Alisertib for 1 Hr. Cells were then sham irradiated or irradiated with 4 Gy IR. After 1 Hr incubation, cells were harvested. The flasks were washed twice with PBS, and trypsinised. Once detached cells were washed with media and collected in a 15 ml tube. Cells were pelleted by centrifugation for 5 minutes at 1500 RPM. The supernatant media was removed and the cells were resuspended in ice cold PBS with 1x Phosstop phosphatase inhibitor. Cells were transferred to cold sample tubes and recentrifuged for 5 minutes at 1500 RPM. Supernatant PBS was removed and the pellets were snap frozen using an ethanol-dry ice bath. The pellets were stored at -80C until lysis.

2.2.5.2. Sample Lysis

Frozen pellets were transported to Liverpool on dry ice. 10 ml lysis buffer was prepared per experiment as shown in Appendix Table 10. Pellets were thawed and 500 µl lysis buffer was added to each sample. Samples were incubated at 80 °C for 10 minutes, then probe sonicated on ice for DNA shearing. Sonication was

performed for 10 s with 20 s pause five times (with 30% amplitude). Samples were incubated at 80 °C for 2 minutes, then stored on ice. BSA quantification was carried out using a Pierce Protein BCA Assay kit.

2.2.5.3. Reduction and Alkylation

15 µl of DTT (100mg/ml in HPLC water) was added per sample (working concentration of 3.5 mM). Samples were incubated at 60 °C for 10 minutes. 15 µl of 46.6 mg/ml Iodoacetamide (IAC) was added per sample (working concentration of 11 mM). Samples were incubated at room temperature in the dark for 30 minutes. 7.5 µl of DTT (100mg/ml) was added to quench excess IAC.

2.2.5.4. Sp3 Bead Purification and Proteolytic Digestion

Sp3 magnetic beads were warmed to room temperature on a shaker for 5 minutes. 100 µl of each bead type were mixed in a sample tube. The Sp3 beads washes were carried out by attaching to a magnetic rack and removing supernatant, then adding 500 µl HPLC water and resuspending by pipetting (off the magnetic rack). The beads were washed three times with 500 µl HPLC water.

In fresh sample tubes, 250 µg protein was added to 15 µl Sp3 beads. Acetonitrile (ACN) was added to reach 80 % concentration. The samples were shaken at 25°C for 30 minutes at 1500 RPM.

Sample tubes were placed on the magnetic rack and washed with 200 µl ACN three times. Samples were then dried using vacuum centrifugation for 10 minutes to remove ACN.

The Sp3 beads (protein-bound) were resuspended in 215 µl 50 mM HEPES buffer pH8. 5 µg Trypsin was added per sample to achieve a 1:50 ratio (Trypsin: protein). Sample were incubated on a shaker at 37 °C overnight (16 Hr) at 1400 RPM. The protein is digested off the beads by the trypsin.

The bead:protein sample was placed on a magnetic rack and the supernatant (containing peptides) was transferred to a clean sample tube and stored on ice. 30 µl 8M Urea in 50 mM HEPES buffer pH 8 was added to the beads and mixed. The Urea:bead mixture was incubated on a shaker at 37 °C for 30 minutes to remove any remaining peptides. The bead sample was placed on the magnetic rack, and the urea supernatant was removed and added to the Eppendorf containing the peptide sample. The peptide sample was placed on the magnetic rack for 3 minutes then the supernatant was transferred to another clean Eppendorf to ensure no Sp3 beads in the sample and stored on ice until TMT-tagging.

2.2.5.5. Tandem Mass Tag (TMT) Labelling

The 16 TMT labels were defrosted at room temperature. 12.5 µl ACN was added per tube (0.5mg TMT). The TMT tags were vortexed for 20 s incubated at room temperature for 5 minutes three times.

Per peptide sample, 100 µl was transferred to a new tube for TMT tagging. 0.5 mg TMT was added per tube and vortexed. Peptide-TMT samples were incubated on a shaker at 25 °C for 1 Hr (900 RPM). 11 µl of 5% Hydroxyalanine in HPLC water (10% volume) was added to quench unbound TMT. Peptide samples were incubated on a shaker at 25 °C for 15 minutes (900 RPM).

All 16 TMT-tagged peptide samples were then combined into one tube per experiment (i.e. all Alisertib samples combined and all Barasertib samples combined).

2.2.5.6. HPLC Purification/Fractionation

Peptide samples were purified using HPLC to remove excess TMT and urea. The combined TMT-peptide sample was loaded and run at 150 µl/minute flow rate. The unbound sample was collected in two fractions. 50 µl formic acid (50%) was added per fraction. The sample bound in the C18 column was released by ACN gradient and collected in 56 fractions. 5 µl formic acid (50%) was added per fraction. Fractions were combined into 7 larger fractions, by combining every 8^{th} fraction (i.e. fractions 1, 9 17, 25, 33, 41 and 49 were combined). As peptides were released from the C18 in order of increasing hydrophobicity, combining the fractions this way ensured a range of hydrophobicity in the combined fractions. The fractions were dried in the speed vacuum over 2 days. 10% of each fraction was removed, dried separately and was not subjected to phosphopeptide enrichment.

2.2.5.7. Titanium Dioxide Phosphopeptide Enrichment

Peptides fractions were dissolved in 1 mg/ml loading buffer (80% ACN, 5% Trifluoroacetic acid (TFA), 1 M Glycolic acid in HPLC-grade water) and sonicated for 10 minutes (full power). TiO_2 beads were prepared at 0.1mg/ml in loading buffer and added to reach a ratio of 10:1 beads:protein (w/w), then mixed at 1500 RPM for 30 minutes on a shaker at 25 °C. Samples were centrifuged for 1 minutes at 2000 g and supernatant was removed.

The samples were sequentially washed with buffers of increasing pH to enhance specificity for phosphopeptides. Samples were first washed with 150ul of 80% and ACN 1% TFA in HPLC-grade water. Samples were agitated on a shaker at 1500 RPM for 10 minutes at 25 °C, before centrifuging at 2000g for 1 minutes and removing the supernatant. The second wash used 10% ACN, 0.2% TFA in HPLC-grade water. The fractions were then dried by vacuum centrifugation for 15 minutes.

To elute the phosphopeptides, 200 µl 5% ammonium hydroxide was added per sample, agitated on a shaker at 1500 RPM for 10 minutes at 25 °C, before centrifuging at 2000 g for 1 minute. The supernatant was collected and dried by vacuum centrifugation (1 Hr)

2.2.5.8. Sample Processing and Storage

Dried peptides were stored at -80 °C until MS analysis. For analysis, dried peptides (phosphopeptide enriched and unenriched) were resuspended in 20 µl of 97% H_20 with 3% Methanol and 1% TFA. Samples were centrifuged at 13,000 g for 15 minutes at 4 °C to precipitate aggregate and 18 µl was taken for LC-MS/MS analysis (liquid chromatography tandem mass spectrometry).

2.2.5.9. MS/MS Analysis by Orbitrap

Peptide samples were separated by reverse phase HPLC using an Ultimate 3000 Nano System (Dionex) coupled with an Orbitrap Fusion Mass Spectrometer (Thermo Scientific). A PepMap 100 C18 column was used. Samples were loaded in 2% ACN, 0.1% TFA in water at a flow rate of 9 µl/min for 7 minutes total. Peptide resolution was carried out on an Easy-Spray C18 column at a 0.3 µl/min with a 60 minute gradient from 96.2:3.8 ratio to a 50:50 ratio of 0.1% Formic acid (in water):80% ACN

with 0.1% Formic acid (in water), with a final wash in 80% ACN with 0.1% Formic acid (in water).

MS1 spectra were obtained within a m/z range of 350-2000 (60K resolution at a m/z of 200). MS2 data was carried out in DDA with a top speed method with a 3s cycle time. Higher-energy collisional dissociation (HCD) fragmentation was set to 32% nominal collision energy (NCD) in the ion trap. Orbitrap MS2 was set to 30K resolution at m/z 200 with a maximum injection of 250 ms.

2.2.5.10. MS/MS Data Analysis

Proteome Discoverer (PD)

LC-MS/MS data was processed by Proteome Discoverer v2.4 to identify phosphopeptide sequence and PTM localisation. Mascot was used for sequence searches against the Uniprot Human database. PTM localisation was identified using the ptmRS node in PD. TMT tags, methionine oxidation and phosphorylation of S/T/Y were allowed as peptide modifications. Maximum of two missed trypsin cleavages were allowed per peptide isoforms. Mass tolerances for MS1 were 10 ppm and for MS2 were 0.01 Da. Peptide spectral matches were filtered for a 1 % false discovery rate.

A One-way Analysis of Variance (ANOVA) was carried out for each peptide isoform with comparisons of all treatment groups vs DMSO control, plus 4Gy vs 4 Gy + 50 nM Barasertib. P-values were only calculated for peptide isoforms detected in $\geqslant 3$ repeats per condition.

MaxQuant Perseus and R

Using Perseus, peptide isoform datasets were filtered to remove peptide isoforms with Contamination = True and peptide isoforms with no p-values (due to presence of this peptide isoform in <3 biological repeat). Abundance ratio values (i.e. fold change) by Log2, and p-values by -Log10 for use in Volcano plotting. Volcano plots were generated in R using a custom R script.

Metascape Analysis

Metascape analysis (Metascape.com) was performed using the master protein (Uniprot accession) of each peptide isoform with p-value <0.05 for each comparison (Zhou et al., 2019). A custom analysis was performed for enrichment using the pathway databases GO Biological processes, canonical pathways, Hallmark Gene sets, Reactome Gene sets, Kyoto Encyclopedia of Genes and Genomes (KEGG) pathways, Wikipathways and Biocarta Gene sets (2024). We performed one joint analysis for phosphopeptides with increased and decreased abundance as phosphorylation may indicate positive or negative regulation of a protein. Therefore, abundance change in one direction cannot be attributed to an up or down-regulation of a pathway.

Further Pathway Enrichment analysis

Database for Annotation, Visualization and Integrated Discovery (DAVID) functional clustering analysis using KEGG pathways was carried out for the master proteins with p<0.05 between 4 Gy and 4Gy + Barasertib conditions (Huang da et al., 2009, Sherman et al., 2022).

2.2.6. Flow Cytometry Assays

2.2.6.1. Cell Harvesting for Methanol Fixation

Cells were plated in 10 cm dishes and allowed to settle overnight. Cells were then treated and incubated until the appropriate timepoint. At collection, cells were washed with PBS twice, collecting the PBS and incubated media. 1 ml Trypsin was added per plate and incubated for 3-5 minutes. Collected PBS/media was added to the plate to collect the cells and was pipetted gently over the plate to wash all cells off. Cells in the wash solution were pelleted by centrifugation at 1500 RPM for 5 minutes. Supernatant was removed and the cells were resuspended in PBS and then recentrifuged. PBS was poured off and cells were resuspended in residual liquid by agitation. While gently agitating the cells on a vortex, 1 ml ice cold methanol was added to fix the cells. Samples were then stored at -20°C for up to 1 week (minimum overnight).

2.2.6.2. Cell Cycle Analysis

Cell cycle phase was analysed by prodium iodide (PI) and phospho-H3 (pH3) (Ser10) staining. Following fixation, cells were pelleted by centrifugation at 2000 RPM for 5 minutes. Methanol was removed. Cells were washed in 1 ml PBS twice (PBS added, gently pipetted, pelleted and supernatant removed by pouring off). Cells were then resuspended in 100 µl of 1:500 dilution of pSer10 pH3 primary antibody (in 0.5% BSA and 0.25% Triton-X100 in PBS). Cells were incubated for 1 Hr at room temperature. Cells were then washed twice with 0.25% Triton-X100 in PBS. Cells were then resuspended in 100 µl of 1:200 dilution of Anti-rabbit Alexa 488 secondary antibody (in 1% BSA in PBS). Cells were incubated for 30 minutes at

room temperature in the dark. Cells were then washed with PBS. Cells were then resuspended in 18 µg/ml PI and 8 µg/ml RNAse A in PBS.

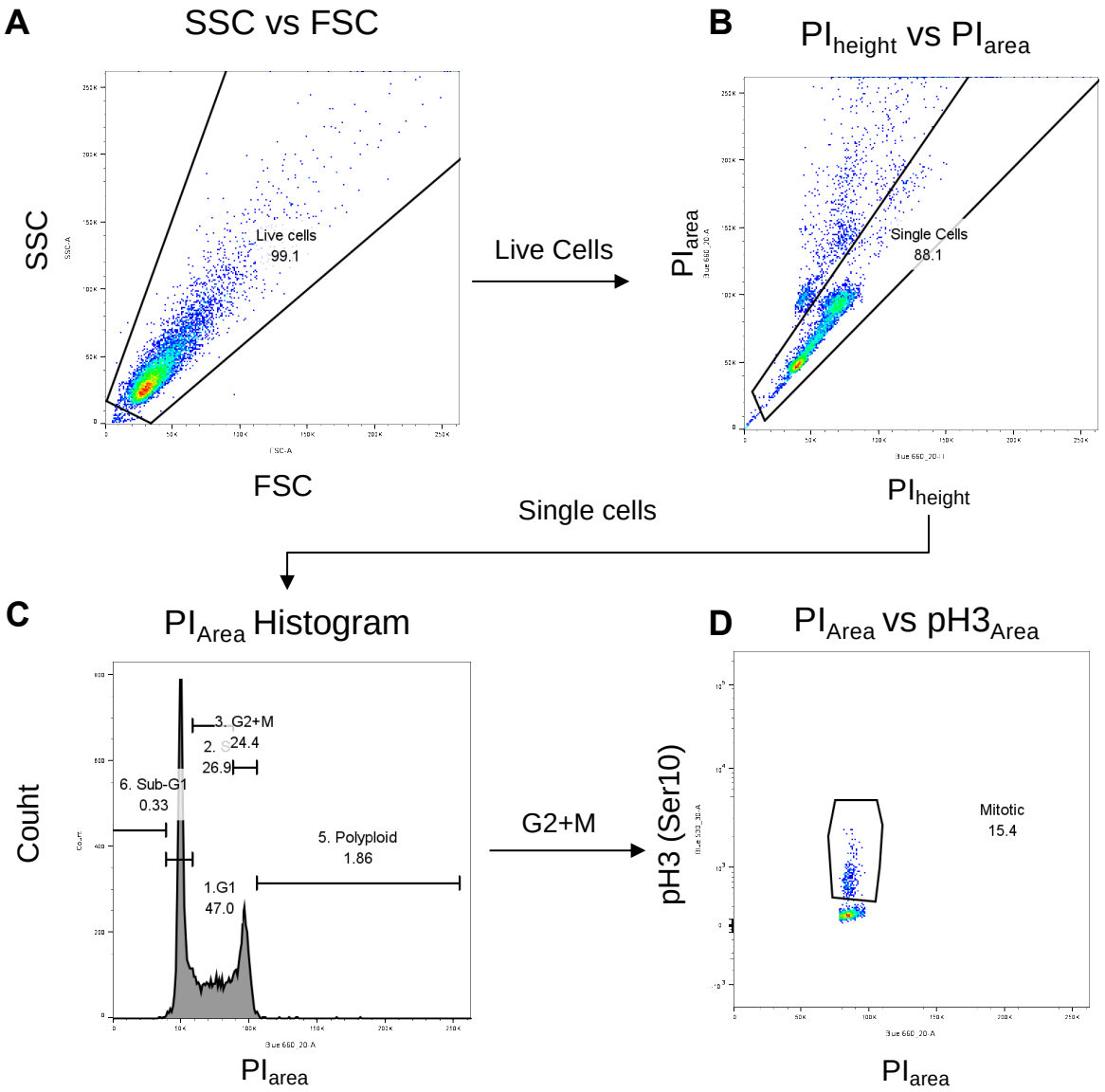

Figure 2. 1: Example gating for PI and pH3 staining in fixed cells

A Gating was applied to the forward scatter (FSC) vs side scatter (SSC) scatter plot to filter for cells and avoid cell debris. **B** PI (height vs area) fluorescence were plotted for cells gated in A. Gates were applied to select for single cells and avoid doublet cells. **C** Single cells were plotted on a PI Area Histogram. Gates were applied to the G1 Peak (at 100 AU), G2+M peak (peak at 200 AU), S phase (between the peaks), Sub-G1 (below G1 peak) and polyploid (above G2 peak). **D** PI was plotted against pH3 for G2+M cells and the pH3 positive cells were gated (Mitotic population). Gating performed on FlowJo.

Samples were incubated overnight at 4-8 °C before analysis. Stained samples were analysed on an LRSII flow cytometer using the blue 660/20 laser for PI and Blue 530/30 for Alexa 488 analysis. Per sample, 10,000 cells were recorded. Density/Histogram plots were gated on FlowJo as shown in Figure 1.1.

2.2.6.3. Bromodeoxyuridine (BrdU) Analysis

Cells were plated in 10 cm dishes at appropriate cell densities (100-750 K depending on timepoint and treatment effect) and allowed to settle overnight. After treatment with IR/inhibitors, cells were incubated with 1 μM BrdU for 15 minutes at the appropriate timepoint. Cells were then immediately fixed as described in section 3.3.6.1.

Following fixation, cells were pelleted by centrifugation at 2000 RPM for 5 minutes. Methanol was removed. Cells were washed in 1 ml PBS twice (PBS added, gently pipetted, pelleted and supernatant removed by pouring off). Cells were resuspended in 50 μl 2M HCL and incubated for 30 minutes at room temperature. Cells were washed 3 times with PBS and once with PBS-T (PBS + 0.1% BSA + 0.2% Tween20, pH 7.4). Cells were then incubated in 10 μl of 50 % primary anti-BrdU Ab in PBS for 30 minutes at room temperature.

Cells were washed twice with PBS-T, then incubated in 50 μl of 1:10 anti-mouse Fluorescein isothiocyanate (FITC) secondary antibody for 20 minutes at room temperature in the dark. Cells were then washed once with PBS, and treated with 50ul of RNAse A (100 μg/ml) for 15 minutes at room temperature in the dark. 200 μl PI (50 μg/ml) was added to cells and incubated for 10-15 minutes before analysis on

the LRSII analyser. Density/Histogram plots were gated on FlowJo as shown in Figure 2.2.

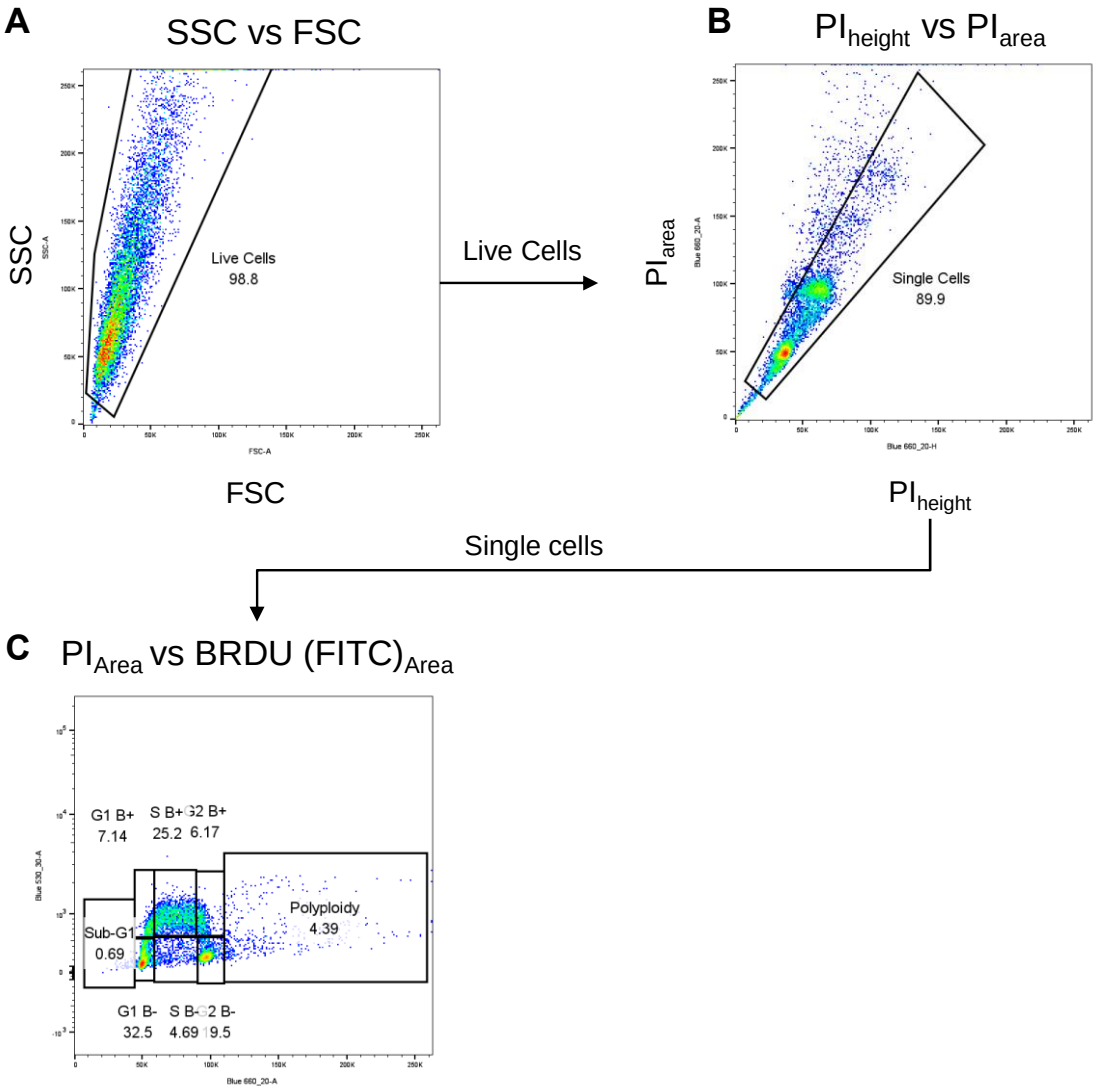

Figure 2. 2: Example gating for PI and BrdU staining in fixed cells

A Gating was applied to the FSC vs SSC scatter plot to filter for cells and avoid cell debris. **B** PI (height vs area) fluorescence were plotted for cells gated in A. Gates were applied to select for single cells and avoid doublet cells. **C** BrdU-positive and BrdU-negative G1, S and G2 positive populations were gated for. BrdU+ cells were calculated by the sum of all BrdU+ gates. Gating performed on FlowJo.

2.2.6.4. Annexin V/PI Analysis

Live cell staining for PI and Annexin V was carried out to assess the proportion of dead (PI+/Annexin V+), early apoptotic (PI-/Annexin+) and healthy (PI-/Annexin V-) cells. Cells treated with 2 µM Campothecin for 24 Hr were used as a positive control for apoptosis and death.

At the appropriate timepoint, cells were washed with PBS twice, collecting the PBS and incubated media. PBS and media were stored on ice. 1 ml Trypsin was added per plate and incubated for 3-5 minutes. Collected PBS/media was added to the plate to collect the cells and was pipetted gently over the plate to wash all cells off. Cells were stored on ice during the processing. Cells in the wash solution were pelleted by centrifugation at 4°C at 1500 RPM for 5 minutes, and the supernatant media was removed. Cells were resuspended in 5 ml cold PBS to wash, then centrifuged and PBS removed. Cells were resuspended in 1 ml cold PBS, and cell concentration was determined using a haemocytometer. Cells were re-pelleted and PBS was removed. Cells were then suspended in 1x binding buffer in PBS at $1x10^6$ cells/ml.

100 µl (100K cells) were transferred to a clean tube. 5 µl of PI and 5 µl of Annexin V-FITC stain (both included in kit) were added to each sample. Cells were mixed by vortexing gently and incubated for 15 minutes at room temperature. 400 µl of 1x Binding buffer in PBS was added per sample and cells were immediately analysed on the LRSII analyser. Density plots were gated on FlowJo as shown in Figure 2. 3.

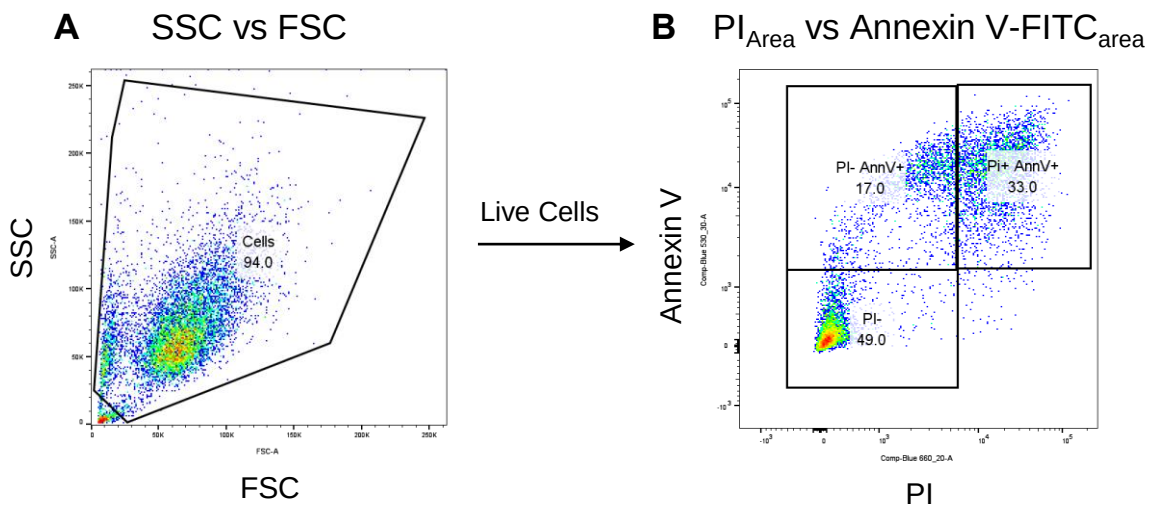

Figure 2. 3: Example gating for PI and Annexin V staining in live cells

A Gating was applied to the FSC vs SSC scatter plot to filter for cells and avoid cell debris. **B** PI and Annexin V-FITC fluorescence were plotted for cells gated in A. Gates were applied to select for PI-negative/Annexin V negative population (lower left), PI-negative/Annexin V positive population (top left) and PI positive/Annexin V positive population (top right). Gating performed on FlowJo.

2.2.7. Immunofluorescence

2.2.7.1. Beta-Tubulin and Pericentrin Immunofluorescence

Cells were plated at 200,000 per well in 6 well plates onto sterile coverslips and allowed to settle overnight. Cells were treated for 1 Hr with DMSO or 50 nM Barasertib, then irradiated with 4Gy IR. After 24 Hr, the media was removed and cells were gently washed with PBS. Cells were fixed with 4% formaldehyde for 15 minutes at room temperature. After briefly washing, cells were permeabilised by incubating with 0.5% Triton-X in PBS for 5 minutes on a rocker. After gently washing 3 times with PBS, cells were blocked with 3% BSA in PBS for 1 Hr at room temperature on a rocker. 1 ml of primary antibodies for Beta-Tubulin (1:500) and Pericentrin (1:2000) in 0.5% BSA in PBS was added per well and incubated overnight at 2-8°C in a humidified chamber.

Cells were washed 3 times with PBS, rocking for 10 minutes per wash. 1 ml of Secondary anti-mouse 488 and anti-rabbit 594 fluorophore antibodies (both at 1:1000) in 0.5% BSA in PBS was added to each well and incubated for 1 Hr at room temperature on a rocker. Cells were washed 3 times with PBS. Cells were incubated with 1 µg/ml DAPI in water for 5 minutes at room temperature on a rocker. Cells were then washed 3 times with PBS.

To mount slides, coverslips were placed cell side down onto the slide on a drop of immuno-mount, after dipping in water and removing excess liquid from the coverslips. The slides were left to set at room temperature for 3 Hr then edges were sealed with nail vanish. Slides were then stored at 2-8°C.

Slides were imaged on the Nikon AR Elements. FITC and TRITC filters were used to capture Beta-tubulin/488 fluorophore and Pericentrin/594 fluorophores respectively. Per condition, >200 cells were imaged at x20 and the number of mitotic cells were counted. At x60, >50 mitotic cells were captured per condition and scored manually for mitotic stage and defects.

2.2.7.2. Phospho-H2AX Immunofluorescence

H460 cells were plated on square coverslips in 6 well plates and left to settle overnight. Cells were treated with DMSO or 50 nM Barasertib for 1 Hr followed by 4Gy.

At each timepoint, the media was removed and cells were gently washed with TBS. Cells were fixed with 4% paraformaldehyde in PBS for 10 minutes at room temperature. After washing with TBS for 5 minutes, cells were permeabilised by incubating with 0.2% Tween-20 in TBS for 5 minutes on a rocker. Cells were washed for 5 minutes 3 times with TBS. Cells were blocked with 3% BSA in TBS for 1 Hr at room temperature on a rocker. The blocking solution was removed. Cells were washed twice with TBS, rocking for 10 minutes per wash.

100 µl of (Phospho-H2AX (Ser139) (Millipore)(1:500) primary antibody in TBS2 was pipetted onto the underside of the 6-well plate lid and the coverslip was inverted to lie cell-side down in the antibody solution. The cells were then incubated at 2-8 °C overnight in a humidified chamber.

Cells were removed from the lid section, blotted dry and placed into TBS in fresh 6-well plates. The cells were then washed 4 times with TBS, rocking for 10 minutes per

wash. Secondary anti-mouse fluorophore 488 antibodies (1:500) was diluted in 1% BSA, 0.25% Triton X-100 in TBS.

100 µl of secondary antibody (anti-mouse 594, 1:500) in TBS2 was pipetted onto the underside of the 6-well plate lid and the coverslip was inverted to lie cell-side down in the antibody solution. The cells were then incubated in the dark for 1 Hr at room temperature. Cells were removed from the lid section, blotted dry and placed into TBS to wash for 5 minutes. 1 ml of 1 µg/ml DAPI was added per well and incubated for 40 minutes at room temperature in the dark. The cells were then washed 2 times with TBS in the dark, rocking for 5 minutes per wash.

To mount slides, coverslips were placed cell side down onto the slide on a drop of immuno-mount, after dipping in water and removing excess liquid from the coverslips. The slides were left to set at room temperature for 3 Hr then edges were sealed with nail vanish. Slides were then stored at 2-8°C.

Slides were imaged on the Nikon AR Elements software. TRITC filter was used to capture Alexa 594 fluorophore immunofluorescence at x60. All images per repeat were captured with the same TRITC exposure. >100 cells were imaged per condition.

Cell Profiler was used to quantify foci. This pipeline is based on the foci counter pipeline available from www.cellprofiler.com (Stirling et al., 2021). For x60 images, foci between 7 and 30 pixels diameter were counted. Image background was filtered using Otsu three-class thresholding.

2.2.7.3. 53BP1 Immunofluorescence

H460 cells were plated on square coverslips in 6 well plates and left to settle overnight. Seeding density was tailored to incubation time. Cells were treated with DMSO or 50 nM Barasertib for 1 Hr followed by 4 Gy.

At each timepoint, the media was removed and cells were gently washed with PBS twice for 5 minutes. Cells were fixed with 4% paraformaldehyde in PBS for 20 minutes at room temperature. Cells were washed 3 times with PBSt. 1 ml PBS2+ buffer was added per well and incubated on a rocker at room temperature for an Hr to blocking and permeabilise. 100 µl of 1:1000 primary antibody (53BP1-abcam (AB36823)) in PBS2+ was pipetted onto the underside of the 6-well plate lid and the coverslip was inverted to lie cell-side down in the antibody solution. The cells were then incubated at 2-8°C over night in a humidified chamber.

Cells were washed 3 times with PBSt. 100 µl of secondary antibody (Alexa-fluor Anti-rabbit 594 at 1:1000) in PBS2+ was pipetted onto the underside of the 6-well plate lid and the coverslip was inverted to lie cell-side down in the antibody solution. The cells were then incubated at room temperature for 1 Hr in a humidified chamber. Cells were washed 2 times with PBS.

To mount slides, coverslips were placed cell side down onto the slide on a drop of immuno-mount, after dipping in water and removing excess liquid from the coverslips. The slides were left to set at room temperature for 3 Hr then edges were sealed with nail vanish. Slides were then stored at 2-8°C.

Slides were imaged using Nikon AR Elements software. TRITC filter was used to capture Alexa 594 fluorophore immunofluorescence at x60. All images per repeat

were captured with the same TRITC exposure. Foci/cell were counted for >100 cells per condition manually using a counter tool on NIS Elements Analysis. Cellprofiler was not used due to high background.

2.2.7.4. RAD51 Immunofluorescence

Cells were plated in 6 well plates onto sterile coverslips and allowed to settle overnight.

Cells were treated pre-treated for 1 Hr with DMSO or 50 nM Barasertib, then irradiated with 4 Gy IR. At the timepoint, the media was removed and cells were gently washed with PBS twice. Cells were fixed with 4% formaldehyde with 0.1% Triton-X 100 for 20 minutes at room temperature. Cells were then washed in PBS Btx (0.1% Triton X and 0.15% BSA in PBS) for 15 minutes 4 times.

100 µl of 1:500 primary antibody (in 3% BSA in PBS) was pipetted onto the underside of the 6-well plate lid and the coverslip was inverted to lie cell-side down in the antibody solution. The cells were then incubated at 2-8 °C overnight in a humidified chamber.

Slides were placed back into the well, cell side up and washed with PBS with 0.3% Triton-X 100 for 10 minutes, before washing with PBS-Btx for 15 minutes 4 times. 100 µl of 1:500 secondary antibody anti-rabbit Alexa 488 and 1 µg/ml DAPI (in 3% BSA in PBS) was pipetted onto the underside of the 6-well plate lid and the coverslip was inverted to lie cell-side down in the antibody solution. The cells were then incubated at room temperature in a humidified chamber for 1 Hr.

Slides were placed back into the well, cell side up and washed with PBS with 0.3% Triton-X 100 for 10 minutes, before washing in PBS Btx for 15 minutes twice. Cells

were washed in PBS for 10 minutes before mounting. To mount slides, coverslips were placed cell side down onto the slide on a drop of immuno-mount, after dipping in water and removing excess liquid from the coverslips. The slides were left to set at room temperature then edges were sealed with nail vanish. Slides were stored at 2-8 °C.

Slides were imaged on the Nikon AR Elements software. FITC filter was used to capture Alexa 488 fluorophore (RAD51) immunofluorescence at x 60. All images per repeat were captured with the same FITC exposure. >100 cells were imaged per condition. Foci/cell were counted for >100 cells per condition manually using a counter tool on NIS Elements Analysis. Cellprofiler was not used due to high background.

2.2.8. Live Cell Imaging

500,000 H460 cells/dish were plated into two 10 cm dishes and left to settle overnight. The next day, the cells were treated with DMSO or 50 nM Barasertib for 1 Hr. The cells were then trypsinised and resuspended in drugged media at 10 K/ml concentration. Two suspensions of each drug condition were prepared and one tube per condition was irradiated with 4 Gy IR (sham IR for the remaining suspension). The cells were then plated into 24 well plates with ranging seeding densities of 1K to 20K per condition. After 27 Hr, cells were taken for live cell imaging in an incubator environment (37 °C, 5% CO_2) on a Leica brightfield microscope.

There was a range of confluencies per condition due to the seeding density range. One well with 30-50% confluency was chosen per condition, and 6 imaging non-

overlapping fields of view were set up in each well. Imaging was scheduled every 10 minutes until 72 Hr post IR.

Analysis was carried out by manual scoring. >60 mitotic cells per condition were tracked for mitotic entry and exit by timeframe. Defects were tracked with timeframe of occurrence noted. Each timeframe was 10 minutes apart so the time frame was multiplied by 10 to give time in mitosis (minutes) or the time from start of recording that an event occurred.

2.2.9. Senescence Assay

A Senescence β-Galactosidase Staining Kit was used to measure senescent populations. H460 cells were plated in 6 well dishes in 3 ml media on sterile square coverslips and allowed to settle overnight.

Timepoints were treated in reverse order to allow fixing of all timepoints at the same time. Cells were pre-treated for 1 Hr with DMSO or 50 nM Barasertib, then irradiated with 4Gy IR. After the appropriate time, wells were washed twice gently with PBS then incubated with 4% PFA in PBS for 15 minutes. Wells were washed gently with PBS again. A staining solution was prepared using the kit reagents as specified in the kit protocol. 1 ml staining solution was added to each well and incubated at 37 °C in a dry incubator overnight. The wells were washed with PBS twice. Coverslips were dipped in water, dried and mounted cell-side down on glass slides using Immuno-mount.

Slides were imaged on a brightfield Nikon Optiphot-2 microscope at x40. 300-400 cells were imaged per condition. Cells were manually counted and cored. Blue-stained cells were recorded as positives and % positive cells was calculated.

2.2.10. *In Vivo* Experiments

All animal work was carried out under Project License PP1099883. Procedures for establishment and monitoring of tumour growth, metastasis and animal welfare followed best practice e.g. NCRI Guidelines for the welfare and home office guidelines and as outlined in PPL1099883.

Group size was calculated using the sample size calculation tool available within the NC3Rs Experimental Design Assistant (eda.nc3r.org.uk).

2.2.10.1. Tumour Implantation

H460 cells were implanted subcutaneously in Balb/c mice on the dorsal flank to establish tumours xenografts. 1 x 10^6 cells were injected per mouse in a 1:1 mixture of PBS:Matrigel (50ul per injection). Mice were anaesthetised using Isoflurane in O_2 and kept under anaesthesia using an Isoflurane nose mask while on a heated mat.

Tumours were measured daily for each mouse using callipers until the endpoint. The endpoint was met when tumours reached an average diameter of 12 mm (calculated from weight and length) or a maximum diameter of 15mm in any direction, or 30 days from the start of treatment.

Length, width and height (mm) were measured to calculate volume. Length was defined as the longest diameter of the tumour, and width was measured perpendicularly. Volume (mm^3) was calculated as follows:

$$\text{Tumour volume} = (\text{Height} \times \text{Width} \times \text{Length}) \times 0.52$$

Treatment was started when tumours reached 100 mm^3.

2.2.10.2. HEB8 – Monotherapy Dose Optimisation

HEB8 Trial aimed to assess 3 doses of Barasertib and vehicle response for tumour growth inhibition and pH3 inhibition. Power calculations indicated need for 4 mice per group. Given an 80% tumour uptake in previous Bryant Lab trials, 5 mice were assigned per group to assess tumour growth inhibition up to 30 days. An additional group of 5 mice per treatment was planned to allow *ex vivo* tumour analysis 48 Hr after first treatment. Therefore, 4 groups of 10 mice were assigned to the following treatments: Vehicle, 10 mg/kg Barasertib, 25 mg/kg Barasertib and 50 mg/kg Barasertib.. There was an additional treatment group of 5 mice to assess IR dose which did not require tissue analysis.

Tumour implantation was carried out by Matthew Fisher and Kathryn Egerton. Barasertib (AZD1152) was prepared in DMSO at 25mg/ml and diluted to 1 mg/ml, 2.5 mg/ml and 5 mg/ml in TBS pH 9. Mice were injected peritoneally with 10 ml/kg to achieve 10, 25 and 50 mg/kg doses. Vehicle control was 20% DMSO in TBS pH9. Drug delivery was performed by Kathryn Egerton and Matthew Fisher.

4 Gy was delivered to mice using an ADO X-ray irradiator. 2 Gy was delivered to each side of the tumour to reach 4 Gy total dose at a rate of 1 Gy/Min (delivered as sheet irradiation). During irradiation, mice were restrained in a lead shield which allowed protrusion of the tumour, but shielded their head, abdomen and legs from the irradiation (Fig 2.4).

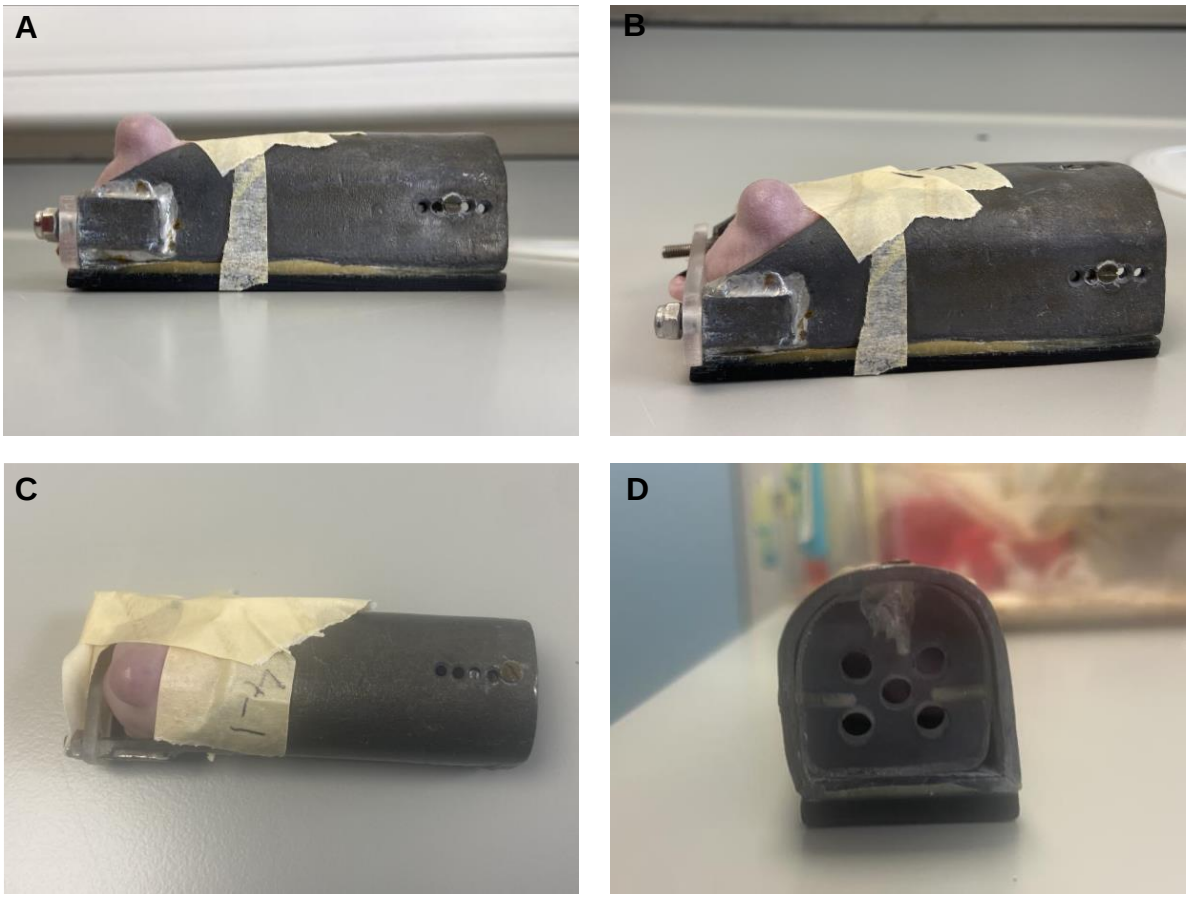

Figure 2. 4: Irradiation shield

Mice were shielded from irradiation in a lead restraint which protects the head, abdomen, and legs whilst the tumour on the dorsal flank is exposed. **A and B** Side view **C** Top down view **D** View from front (facing head).

Tumour volume was measured regularly once tumours were over 100 mm^3. Mice were weighed at least once weekly while on treatment. Tumour diameter and weight measurements in HEB8 were performed by Matthew Fisher.

2.2.10.3. HEB9 – Radiotherapy and Barasertib Combination

Study HEB9 included 4 treatments groups of 8 mice per group (32 total). A power calculation was performed based on results from HEB8 given suggested group size of 6. Considering loss of numbers in HEB8 from blistering and fighting, a group size of 8 was chosen. Once tumours reached 100 mm^3, treatment was started with vehicle (4% DMSO in TBS pH9) or 10 mg/kg Barasertib. Mice were treated with Barasertib or vehicle for 10 days. Mice received sham IR or 3 Gy per day for 5 consecutive days starting on day 2. Irradiation was delivered in 2 x 1.5 Gy doses, one to each side of the tumour.

Tumour volume was measured every day from the start of treated (measured by Kathryn Egerton). Weight was measured at least twice a week during the trial.

2.2.11. Immunohistochemistry

H460 xenograft tumour samples were frozen in Optimal cutting temperature (OCT) Compound (Scigen) on dry ice after excision. Tumours were paraffin-embedded and cryosectioned (performed by Maggie Glover), then stored at -80 °C.

Before staining, slides were air-dried for 30 minutes at room. Slides were then incubated in in ice cold methanol:acetone (1:1) at -20 °C for 10 minutes for fixation. The slides were then rehydrated in PBS by washing for 5 minutes twice.

Slides were then incubated in 10% H_2O_2 in methanol for 30 minutes on a rocker at room temperature to, before washing slides under running tap water.

To perform antigen retrieval, slides were submerged in 10% DAKO retrieval solution in PBS and pressured heated for 2 Hr. Slides were then rinsed in PBS twice (shaken for 5 minutes).

A hydrophobic barrier was made around each tissue section using an Immedge barrier pen. 10% goat serum in PBST was then added to each tissue section as a blocking agent and incubated for 1 Hr in a humidified chamber. Serum block was removed and the anti-pH3 primary antibody (Rabbit) at 1:1000 (diluted in 2% goat serum in PBST) was added to each sample. A negative control sample was incubated in 2% goat serum in PBST with no Ab. Slides were incubated overnight at 4 °C in a humidified chamber.

Primary antibody was discarded and slides were rinsed in PBST twice for 5 minutes. Goat ani-rabbit biotinylated secondary was diluted to 1:200 (diluted in 2% goat serum in PBST) and added to each section for 1 Hr incubation at room temperature

in a humidified chamber. Secondary antibody was discarded and slides were rinsed in PBST twice for 5 minutes.

Avidin–Biotin Complex (ABC) solution was then added to each section and slides were incubated for 30 minutes at room temperature in a humidified chamber. Slides were rinsed in PBST twice for 5 minutes. DAB solution was prepared in water, and added to each slide for 1 minutes before washing all slides under running tap water.

Light haematoxylin staining was performed by submerging slides in haematoxylin for 5 seconds. Slides were then washed under running tap water. Sample dehydration was carried out by submerging slides in increasing concentrations of ethanol. Slides were submerged for 3 minutes in the following ethanol concentrations: 70%, 90%, 95%, 100%, 100%. Slides were then submerged in xylene before mounting in Dibutylphthalate Polystyrene Xylene (DPX) Mounting Medium (Sigma-Aldrich).

2.2.12. Statistical Analysis

Results were determined to be normally distributed or not using Shapiro-Wilk test for normality, prior to analysis with a paired Student's t-test/Anova, Mann–Whitney or a Kruskal Wallis test as relevant and indicated. Clonogenic survival curves were compared by an extra sum of squares F test on non-linear regression of survival curves. Tumour volume over time was analysed by two-way mixed methods analysis when possible. P-values below 0.05 were considered representative of data that were significantly different.

GraphPad Prism software was used for analysis of all data except for MS data (statistical testing carried out in Proteome Discoverer).

Chapter 3: *In Vitro* Evaluation of AURKB Inhibitors as a Radiosensitisation Strategy in NSCLC

3. *In Vitro* Evaluation of AURKB inhibitors as a Radiosensitisation Strategy in NSCLC

3.1. Introduction, Aims and Hypothesis

AURKB is an attractive therapeutic target in human cancers due to its role in cell division, and links to DDR and tumorigenesis. As a result, several inhibitors have been developed and trialled clinically. The AURKB inhibitor Barasertib has been shown to be well tolerated in phase I-II trials as a monotherapy. However, dose-limiting toxicities, primarily neutropenia, hindered the trials from achieving outcomes beyond partial responses (Schwartz et al., 2013, Löwenberg et al., 2011, Kantarjian et al., 2013). Barasertib development moved towards nanoparticle encapsulation (AZD2811) to increase tumour targeting and reduce systemic effects, but clinical development has slowed down.

Clinical trials established doses of Barasertib which could achieve mild to moderate effect and were tolerable for long treatment durations. The safety and tolerability of these doses opens up potential for combination treatment, such as using Barasertib as a radiosensitiser.

The effect of Barasertib on the radiation response has been tested previously *in vitro* and shown successful radiosensitisation in a range of tumour types, including colon cancer, prostate cancer and lung cancer (Tao et al., 2008, Niermann et al., 2011, Sak et al., 2012). In NSCLC lines, Barasertib is reported to radiosensitise *in vitro*. Greater sensitivity and radiosensitisation by Barasertib was reported in p53-NULL cells lines than p53 wildtype cell lines (Sak et al., 2012). The p53 status was also

implicated in whether Barasertib could radiosensitise colorectal cancer cells (Tao et al., 2008)

This Chapter will address the toxicity and radiosensitisation of AURKBi in NSCLC *in vitro.*

The hypothesis is that due to role of AURKB in mitotic regulation and DDR, inhibition of AURKB will sensitise NSCLC cells to IR *in vitro.*

The aims of this chapter are:

1. To examine AURKA/B/C activity by phosphorylation after ionising radiation.
2. To determine how inhibition of AURKB alone effects clonogenic survival of NSCLC cells.
3. To assess whether inhibition of AURKB by Barasertib and other methods can radiosensitise NSCLC cells.

3.2. Time Course of Phosphorylation of AURKs during the Radiation Response

To understand the role of AURKB in the radiation response, the phosphorylation of AURKA and AURKB at their activating residues was investigated in the 24 Hr following irradiation, when most DNA damage repair and cell cycle restart after IR are known to take place (Frankenberg-Schwager, 1989, Sturgeon and Roberge, 2007). This was carried out in both the p53-wildtype cell line H460 and the p53-null cell line H1299.

H460 cells were exposed to 4 Gy IR and protein expression examined at 1, 4, 8, 10, 12, 14, 16 and 24 Hr post-irradiation. Western blotting for Phospho-AURKA (Thr288) and Phospho-AURKB (Thr232) revealed similar trends for both kinases (Fig 3.1 A-C): by 1 Hr, both phospho-proteins showed a reduction of signal which continued until 4 Hr. Phospho-protein levels then increased above the endogenous levels to a peak around 12 Hr post-IR and remained highly activated until 16 Hr. At 24 Hr, the trend was more variable; some experimental repeats showed AURK activity reduced back to endogenous levels while in other repeats activation remained high. Phospho-AURKB (Thr232) showed low activity at 1hr in 1 repeat while Phospho-AURKA (Thr288) was always absent at 1hr.

In H460 cells, total protein levels were also examined (Fig 3.1 A, D and E). Total AURKA and AURKB shows lower variability across the time points with ranges of 0.51-2.13 and 0.21-1.59, while phosphorylated counterparts exceeded 4-fold and 3-fold increase compared to controls, respectively.

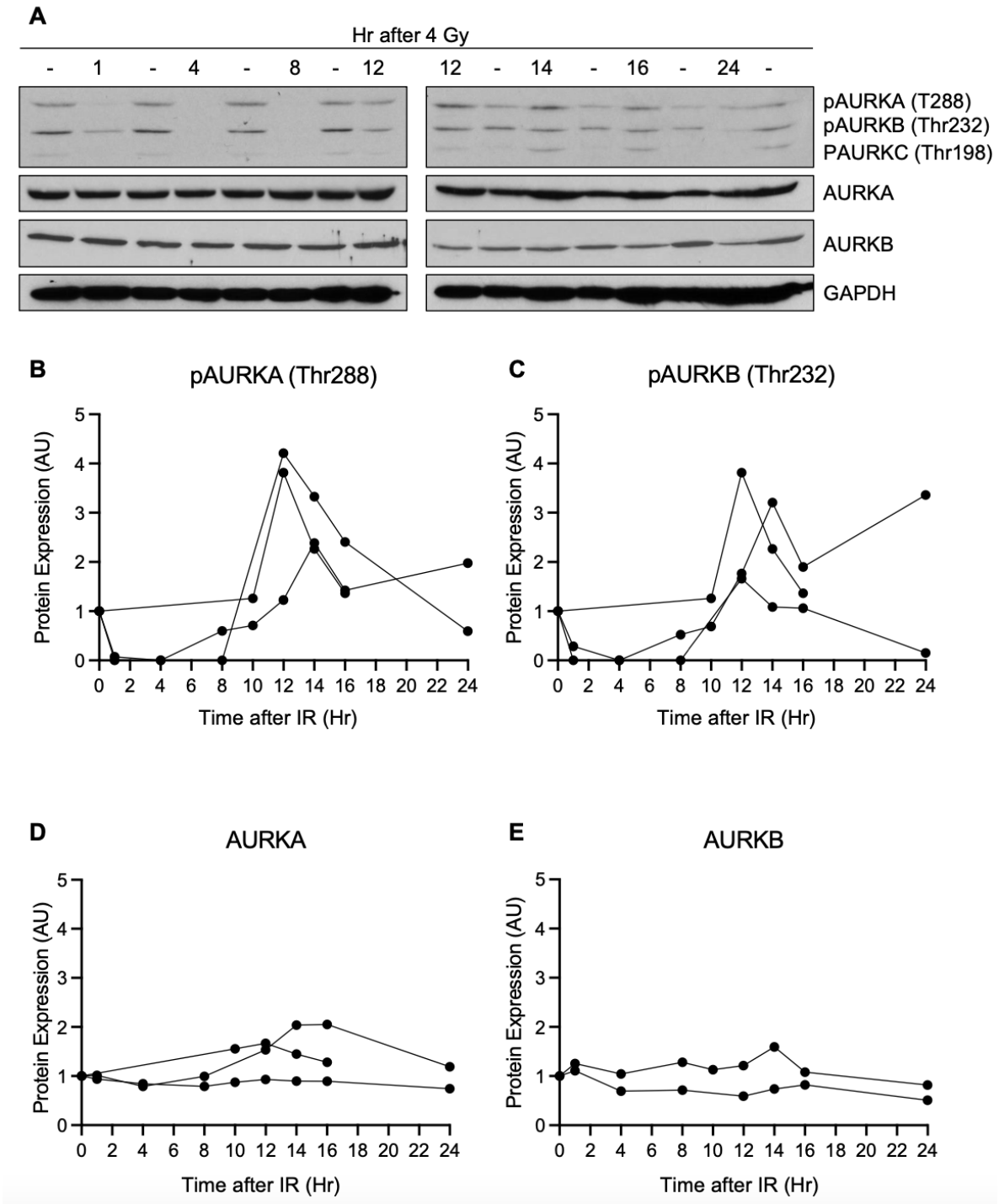

Figure 3. 1: Phosphorylation of Aurora kinases is activated by radiation in H460 cells

Protein expression of p-AURKA/B/C, AURKA, AURKB and GAPDH in H460 cells 0-24 hours after 4 Gy IR. **A** Representative western blot. '-' indicates DMSO control collected at time of IR. Individual repeats of quantification of **B** pAURKA, **C** pAURKB, **D** AURKA and **E** AURKB, showing 3 independent repeats (pAURK and AURKA) and 2 independent repeats (AURKB). For quantification protein levels were normalised to GAPDH and are shown relative to DMSO control.

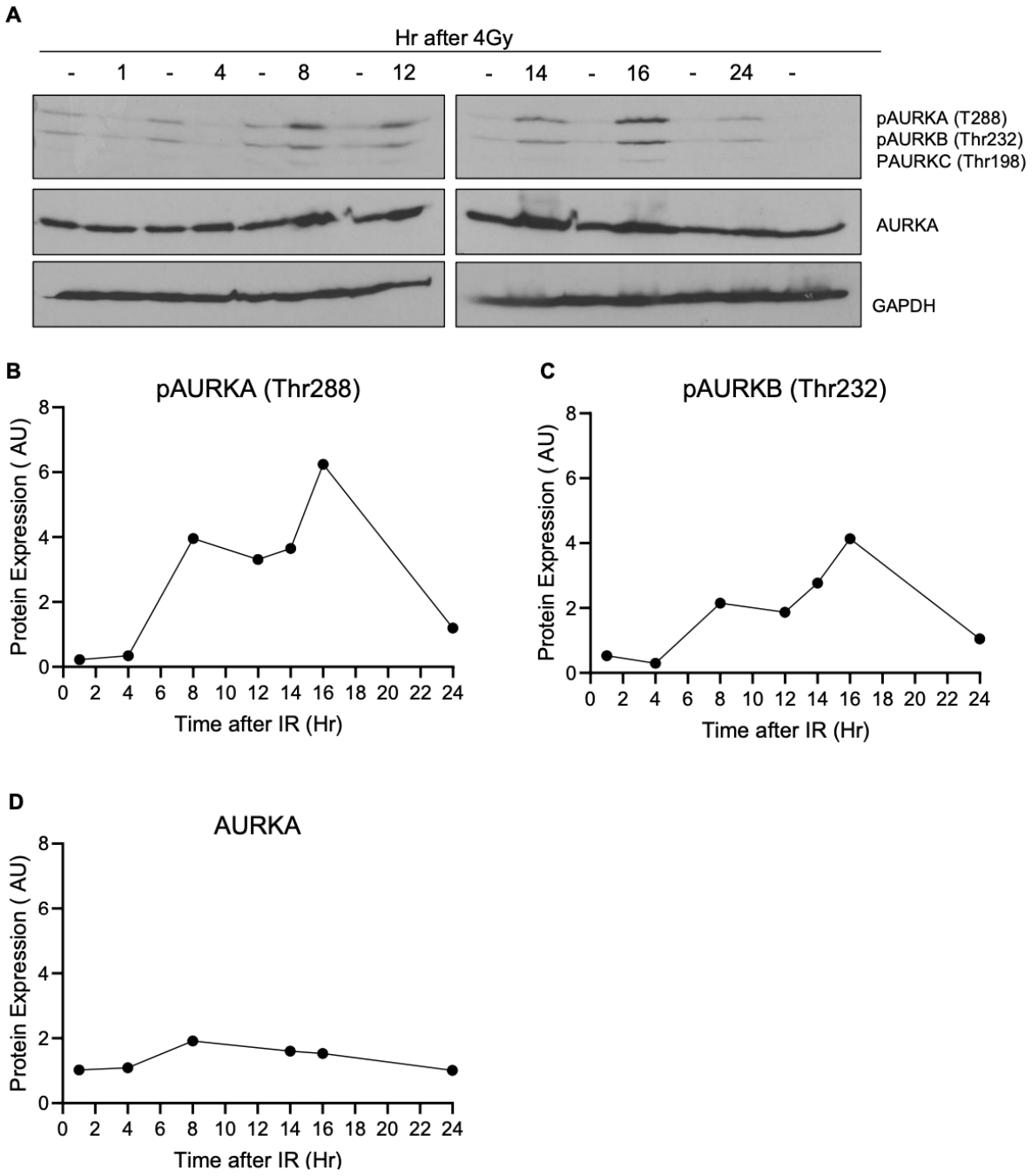

Figure 3. 2: Phosphorylation of Aurora kinases is activated by IR in H1299 cells

Protein expression of p-AURKA/B/C, AURKA, AURKB and GAPDH in H1299 cells 0-24 hours after 4 Gy IR. **A** Representative western blot. '-' indicates DMSO control collected at time of IR. Individual repeats of quantification of **B** pAURKA, **C** pAURKB and **D** AURKA, showing 1 repeat. For quantification protein levels were normalised to GAPDH and are shown relative to DMSO control.

In the p53-deficient cell line, H1299, phosphorylated AURKA/B and total AURKA were also investigated (Fig 3.2). Note, this experiment was only conducted once limiting interpretation. However, it appeared that both Phospho-AURKA (Thr288) and Phospho-AURKB (Thr232) levels peaked later following radiation in this cell line compared to H460 (Fig 3.2 B and C). Interestingly, there was a greater increase in Phospho-AURKA (Thr288) level in H1299 cells than seen in H460 cells but there was no difference in the level of Phospho-AURKB (Thr232).

Total AURKA shows stable levels across timepoints (Fig 3.1 D). Unfortunately, total AURKB was not investigated in these samples.

In summary, we see a decrease in phospho-AURKA/B levels in response to radiation followed by an increase after 12-16 Hr. These results suggest that regulation of AURKA/B following radiation is via phosphorylation rather than protein degradation. The small reduction in phospho-AURK levels immediately after IR is perhaps indicative of the cell cycle arrest induced by proteins of the DDR pathway including p53 which has been shown previously to inhibit AURKA directly (Katayama et al., 2004). The later peak in phosphorylation at 12-16 Hr may be coincident with or essential to cell cycle restart and progression following DNA damage resolution.

If activation of AURKA/B after radiation is required for survival to radiation, this suggests that inhibition of these kinases could be used to radiosensitise. Previous work in the Bryant lab demonstrated that AURKA inhibition can radiosensitise so work here focused on AURKB.

3.3. Evaluation of the Toxicity and Effective Inhibitory Dose of Barasertib

Before investigating the potential radiosensitisation effects of Barasertib, we needed to establish its single agent toxicity and effective inhibitory dose. To investigate the toxicity of Barasertib, clonogenic survival assays were carried out. Barasertib concentrations between 25 nM to 200 nM were tested and survival relative to DMSO control determined. In H460 cells, Barasertib led to significant inhibition of colony formation at all doses tested and an LD50 of 69.7 nM (Fig 3.3 A).

The responses to Barasertib in additional NSCLC cell lines (H1299, SW900, H520, H322, A549) were also assessed by clonogenic assays (Appendix Fig. 3 A – work carried out by Timothy Mitchell). The IC_{50} values were 24.8 nM, 21.4 nM, 13.9 nM, 16.6 nM, and 15.2 nM, respectively (Appendix Fig 3 B).

To confirm the AURKB inhibitory effect and specificity of Barasertib, the inhibition of AURKA/B/C activity was investigated by western blot (Fig 3.3 B - F). H460 cells were treated with DMSO or Barasertib for 24 Hr before protein extraction. Both phospho-AURKB (Thr232) and total AURKB protein levels reduced in response to 200 nM Barasertib (Fig 3.3 B-D). Surprisingly, phospho-AURKC (Thr198) show similar inhibition to phospho-AURKB. The decrease in AURKB levels could be due to protein degradation or a cell death response. AURKA was not inhibited but showed increasing phosphorylation from 50 nM to 200 nM (Fig 3.3 E).

We also examined phospho-H3 (Ser10) expression, a direct substrate of AURKB (de Groot et al., 2015) (Fig 3.3 G). Similarly to pAURKB, we only saw inhibition at 200 nM in H460 cells.

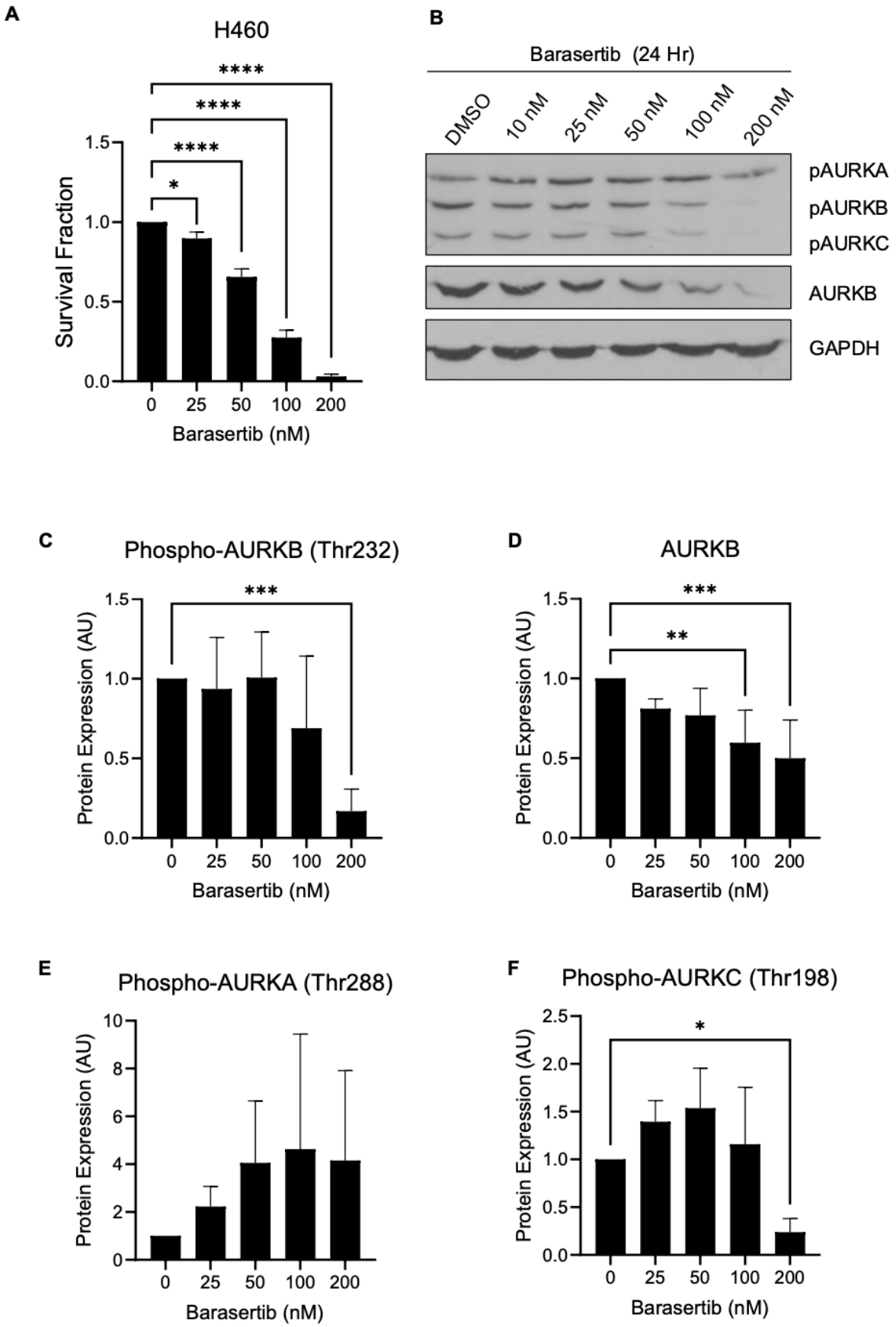

Figure 3. 3: Barasertib reduces clonogenic survival in H460 cells and inhibits AURKB and AURKC

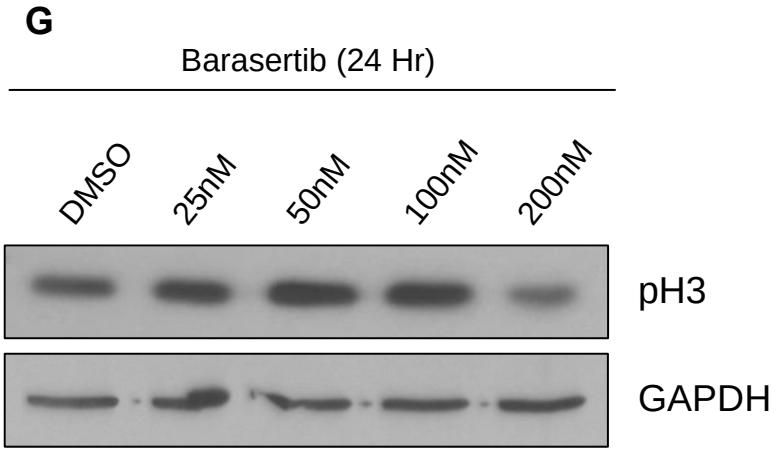

Figure 3. 3: Barasertib reduces clonogenic survival in H460 cells and inhibits AURKB and AURKC

A. Clonogenic survival of H460 cells following 8-day treatment with Barasertib. Survival fraction was calculated relative to DMSO control. Statistical significance was calculated using one-way ANOVA. In each case mean and standard deviation of three independent repeats are shown. * = $p < 0.05$, ** = $p < 0.01$, *** = $p<0.001$. **** = $p<0.0001$. **B – F** Protein expression of p-AURKA/B/C, AURKB and GAPDH in H460 cells treated with Barasertib for 24 hours. **B** Representative western blot and mean and standard deviation of quantification of >3 independent repeats for **C** pAURKB, **D** AURKB, **E** pAURKA and **F** pAURKC. For quantification protein levels were normalised to GAPDH and are shown relative to DMSO control. **G** (Overleaf) Protein expression of phospho-H3 (Ser10) and GAPDH control in H460 cells treated with Barasertib for 24 hours.

Given the IC_{50} of Barasertib is 69.7 nM in H460 cells, we were surprised not to see reduced phosphorylation at 50 nM. This suggests that the strong inhibition of AURKB is not required for radiosensitisation.

We also examined the inhibitory effect of Barasertib in H1299 and SW900 cells (Appendix Fig 3 C-M). This experiment was only performed twice for H1299 and once for SW900, which limits interpretation. In H1299 cells, inhibition of pAURKB

(Thr232) was achieved at lower doses with <30% signal after 50 nM Barasertib treatment (Appendix Fig 3 E).

In SW900 cells endogenous AURKB activity is exceptionally low and so Nocodazole was used to cause a mitotic block and then cells released into Barasertib for 2 Hr. Only a dose of 200 nM Barasertib inhibited pAURKB (Thr232) in SW900 cells (Appendix Fig 3 J). Interestingly, in this cell line the total AURKB levels increased with Barasertib (Appendix Fig 3 K). The lack of inhibition by Barasertib in SW900 cells may be due to the short Barasertib treatment time, which was chosen to maintain the high mitotic population and increase overall AURKB levels in SW900 cells. Similar to H460 cells, Barasertib did not decrease Phospho-AURKA (Thr288) levels in H1299 or SW900 cells, while pAURKC (Thr198) levels were reduced in both cell lines at the high doses of Barasertib (Appendix Fig 3 G-H & L-M).

3.4. Evaluation of AURKB inhibitors as Radiosensitisers

3.4.1. Barasertib as a Radiosensitiser

To investigate if Barasertib could radiosensitise H460 cells, clonogenic survival assays were performed. H460 cells were pretreated for 1 Hr with 50 nM and100 nM Barasertib or DMSO before treatment with 1-5 Gy IR or sham IR.

Barasertib doses of 50 nM and 100 nM radiosensitised H460 cells similarly ($p<0.0001$ and $p=0.0012$, respectively) (Fig 3.4 A-C). The $DMF_{0.1}$ (dose enhancement factor at 0.1 survival fraction) was 1.15 and 1.20 for 50 nM and 100 nM Barasertib (Table 1.3). A dose of 50 nM Barasertib was chosen for further use because this dose conferred similar radiosensitisation to 100 nM but had a more moderate effect on clonogenic survival.

Using 50 nM Barasertib, clonogenic survival assays were performed with various schedules of Barasertib treatment relative to radiation (Fig 3.5). When cells were treated just prior to treatment with 0-5 Gy IR, Barasertib radiosensitised H460 cells ($DMF_{0.1}$ =1.19) ($p=0.01$) (Fig 3.5 A). When cells were pre-treated with Barasertib for 1hr or 24 Hr and the drug remained on the cells post- irradiation, the radiosensitisation effect of 50 nM Barasertib was further enhanced ($p=<0.0001$ and $p=0.0222$, respectively) (Fig 3.4 B and C). 1 Hr and 24 Hr treatments with 50 nM Barasertib led to $DMF_{0.1}$ of 1.24 and 1.83, respectively. Further radiosensitisation assessments are shown in Appendix table 11.

However, when Barasertib was present for 24 Hr before IR, but removed immediately before IR, there was no difference in survival between DMSO

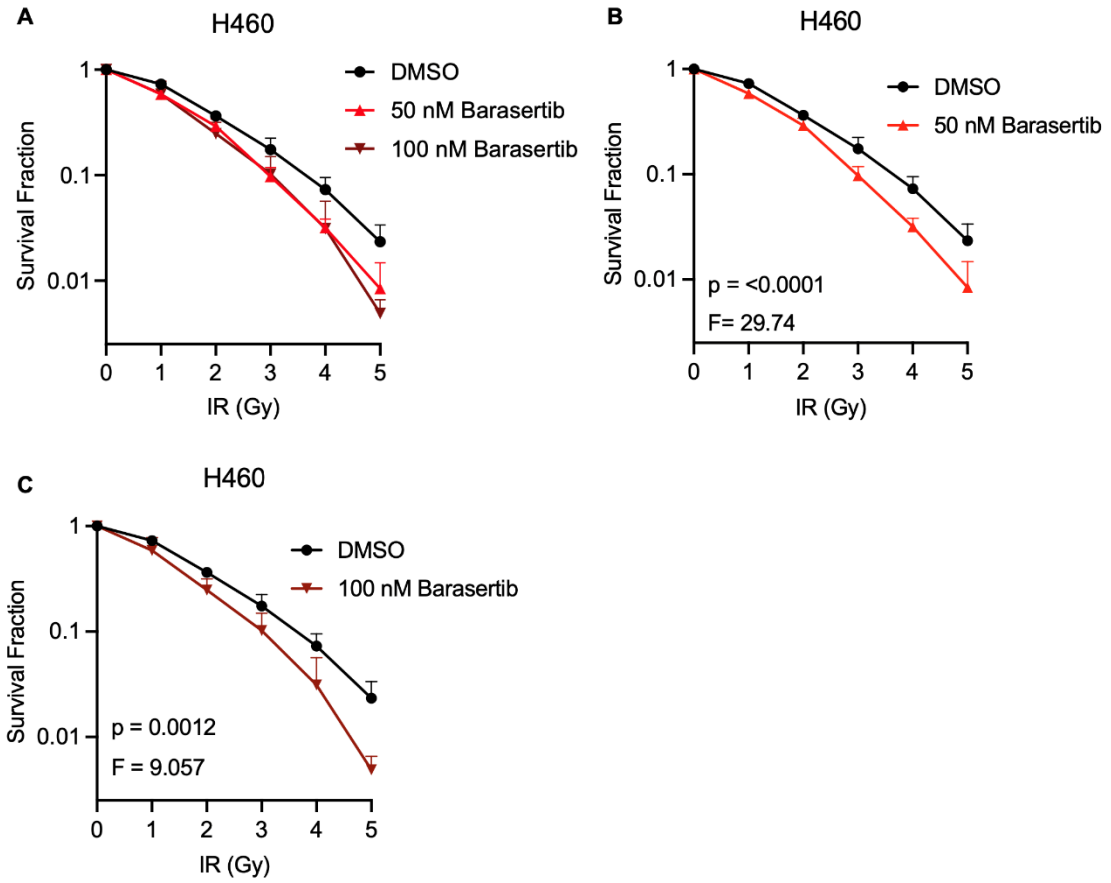

Figure 3. 4: H460 cells are radiosensitised by 50-100 nM Barasertib

Clonogenic survival of H460 cells after 8 day treatment with 50-100 nM Barasertib and 0– 5Gy IR. Cells were pretreated with Barasertib (or DMSO) for 1 Hr before irradiation. **A** All conditions **B** DMSO vs 50 nM Barasertib **C** DMSO vs 100 nM Barasertib. Statistical significance between curves was calculated by fitting to a linear quadratic model and comparison by an extra sum-of-squares F test. P and F values are displayed for each graph. In each case, mean and standard deviation of ≥3 independent repeats are shown.

Table 1. 3: Radiosensitisation parameters for Barasertib in H460 cells after 1 Hr pretreatment

DEF and SF (±SD) values are shown for H460 cells after Barasertib treatment. Radiobiological alpha and beta parameters are also shown (linear quadratic model).

	50 nM	**100 nM**	
$DEF_{0.1}$	1.15	1.2	
$DEF_{0.37}$	1.25	1.29	
	DMSO (± SD)	**50 nM (± SD)**	**100 nM (± SD)**
SF_2	0.39 ± 0.10	0.28 ± 0.05	0.26 ± 0.22
SF_4	0.06 ± 0.04	0.03 ± 0.03	0.02 ± 0.11
α	0.2198	0.4188	0.4204
β	0.125	0.1094	0.1246

DEF= dose enhancement Factor, SF = Surviving Fraction, SD = Standard deviation

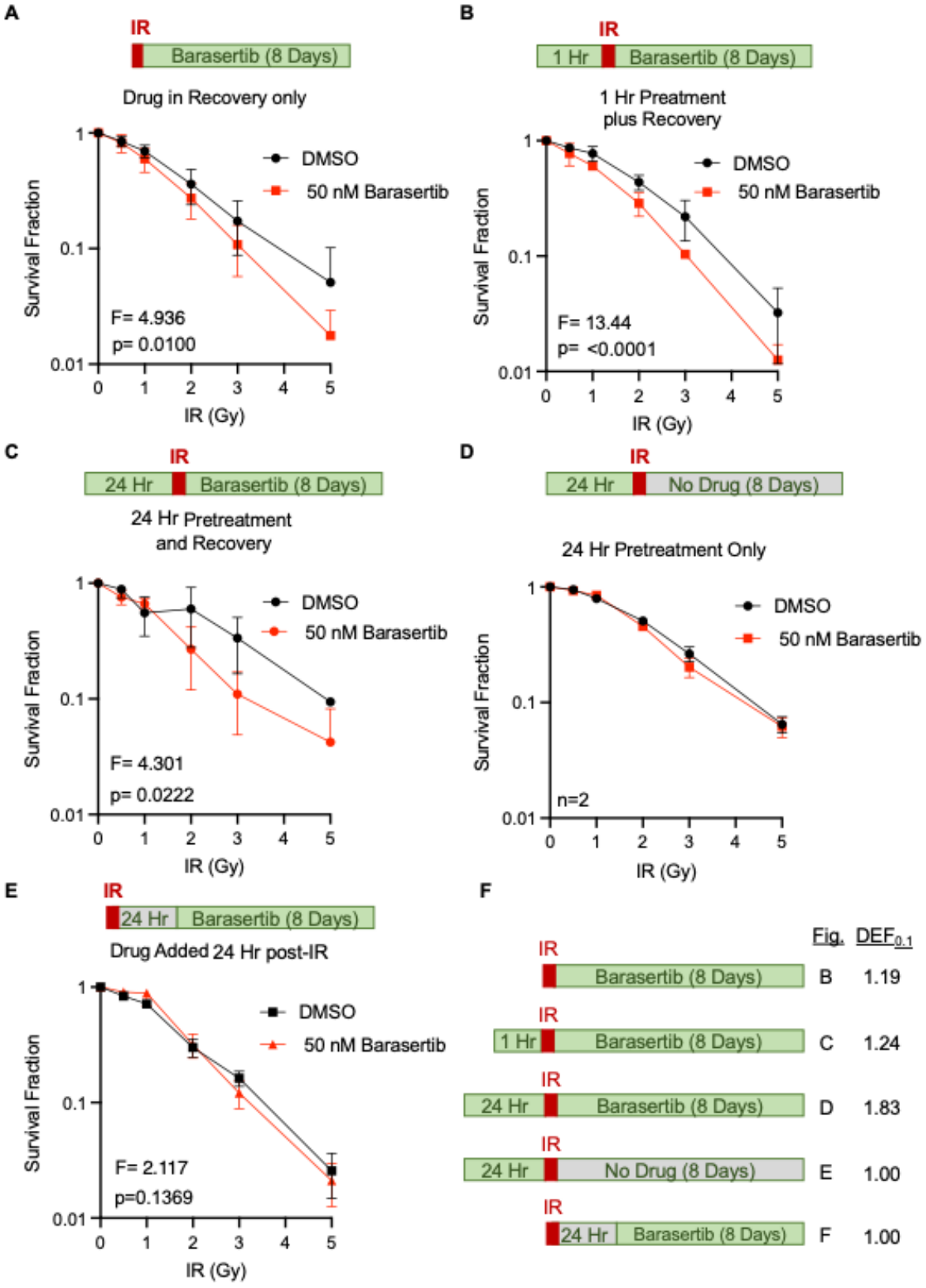

Figure 3.5: Barasertib radiosensitises H460 cells *in vitro* in a time-dependent manner

Figure 3. 5: Barasertib radiosensitises H460 cells *in vitro* in a time-dependent manner

Clonogenic survival of H460 cells after 8 day treatment with 50 nM Barasertib and 0– 5Gy IR with the following schedules: **A** Barasertib added just prior to IR through recovery, **B** 1hr Barasertib pretreatment plus recovery **C** 24 Hr Barasertib pretreatment plus recovery, **D** Barasertib pretreatment of 24 Hr and removed just prior to IR and **E** Barasertib added 24 Hr after IR. Survival fraction was calculated relative to 0 Gy control. **F** Summary of treatment schedules and DMF (for a survival fraction of 0.1). Statistical significance was calculated by fitting to a linear quadratic model and comparison by an extra sum-of-squares F test P and F values are displayed for each graph. In each case, mean and standard deviation of ≥3 independent repeats are shown (unless otherwise stated).

and 50 nM Barasertib-treated cells (Fig 3.5 D) (n=2). Additionally, a delay in Barasertib treatment until 24 Hr after IR also abrogated the radiosensitisation effect (Fig 3.5 E). These results indicate that Barasertib is required to be present in the initial 24 Hr after IR to radiosensitise.

In the clinic fractionated IR is used; therefore, we examined what effect Barasertib had on fractionated radiation treatment (Fig 3.6 A and B) (n=2). At 6 Gy, H460 cells showed resistance to fractionation as survival was lower at single doses than fractionated doses regardless of co-treatment with Barasertib. However, the radiosensitisation effect was preserved, and survival at each dose decreased with increasing Barasertib treatment, compared to DMSO (Fig 3.6 B).

The Barasertib-IR combination treatment was also investigated in the H1299 and SW900 cells (Appendix Fig 4 - data collected by Timothy Mitchell). Cells were pre-treated with 25 nM and 50 nM Barasertib for 2 Hr before IR (0-4 Gy). In both cell lines, Barasertib treatment also significantly radiosensitised ($p= 0.0069$ and $p= 0.0006$, respectively) (Appendix Figure 4 A and B). $DEF_{0.37}$ was 2.07 and 1.24 for H1299 and SW900 at 25 nM Barasertib (Appendix Table 12). Radiosensitisation was not tested in other cell lines due to single agent Barasertib toxicity.

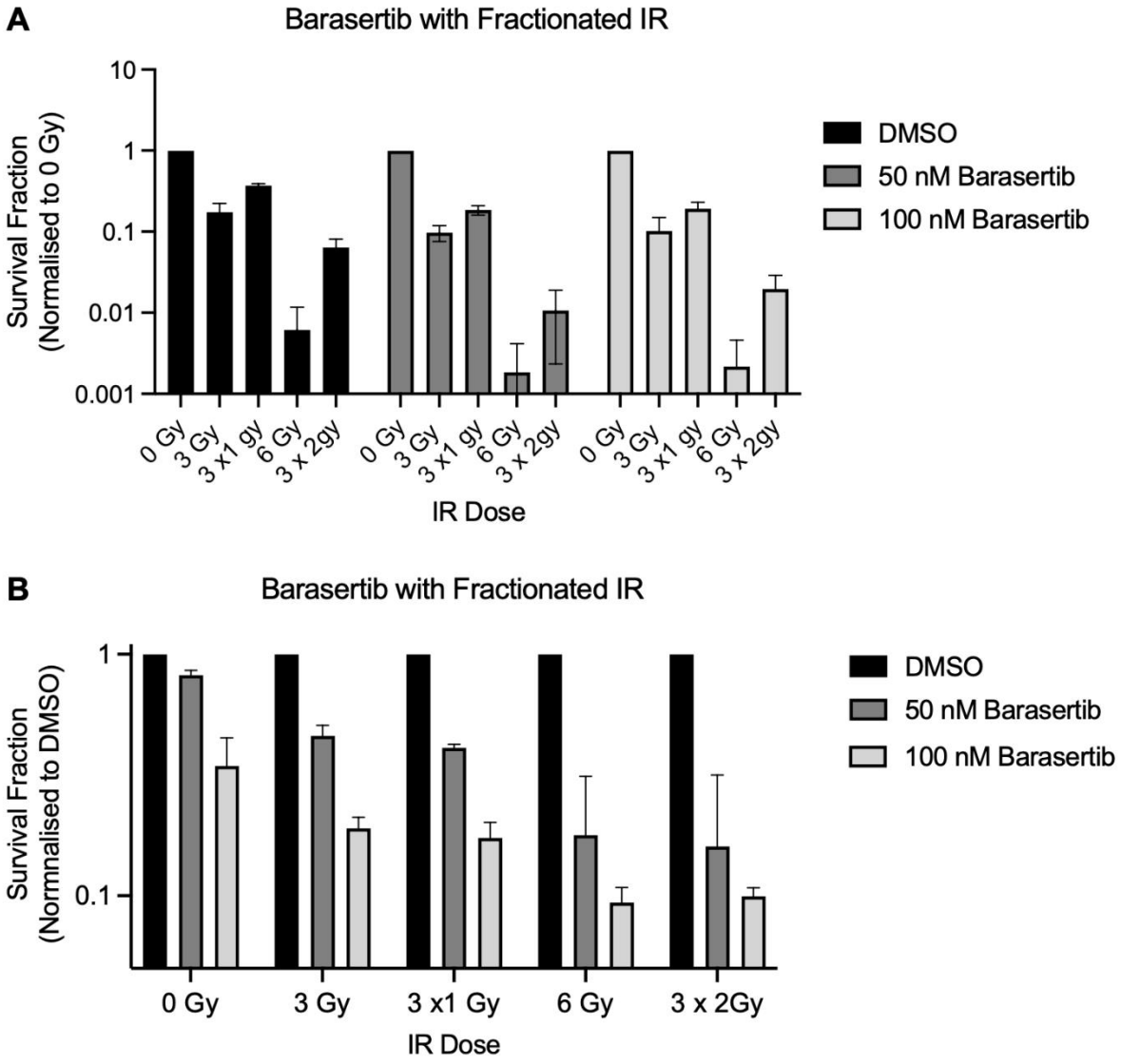

Figure 3. 6: Fractionated delivery of IR does not enhance radiosensitisation by Barasertib

Clonogenic survival of H460 cells after 8 day treatment with 50 nM Barasertib and 3 Gy IR given in a single dose or in 3 fractions. **A** Survival fraction normalised to 0 Gy control (n=2) **B** Survival fraction normalised to DMSO control per IR dose (n=2). In each case, mean and standard deviation are shown (unless otherwise stated).

3.4.2. Radiosensitisation by Alternative AURKBi

To further validify AURKB inhibition as radiosensitisation strategy, the AURKBi inhibitor ZM447439 was investigated as a radiosensitiser in NSCLC using a clonogenic survival assay. H460 cells were treated with ZM447439 between 0 – 2 µM to establish an appropriate dose for use in combination with IR. A dose of 500 nM ZM447439 (survival fraction = 0.74) was chosen as this achieved moderate killing effect (Fig 3.7 A).

To test radiosensitisation, cells were pre-treated with 500 nM ZM447439 for 1 Hr and then irradiated with 0-5 Gy IR with ZM447439 present throughout recovery and allowed to grow out into colonies in drug. ZM447439 radiosensitised H460 cells (p= 0.0367, $DEF_{0.1}$=1.1) (Fig 3.7 B).

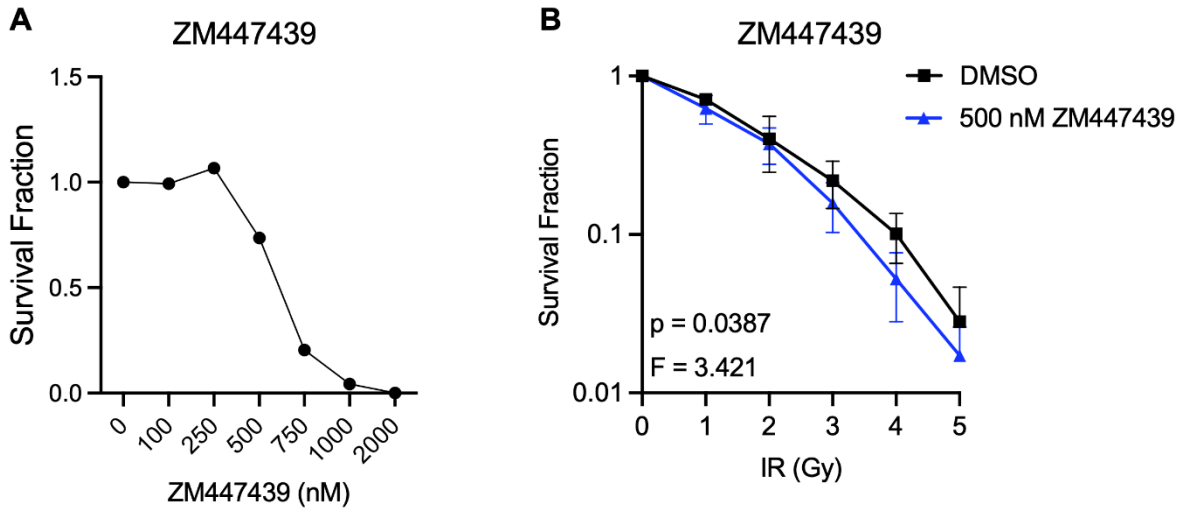

Figure 3. 7: AURKBi inhibitor ZM447439 reduces clonogenic survival of H460 cells and sensitises to IR

A Survival after ZM447439 (0-2000 nM) (1 repeat). Survival fraction normalised to DMSO control. **B** Survival after 1 Hr pretreatment of 500 nM ZM447439 before 0-5 Gy IR. Survival fraction normalized to 0 Gy control. Statistical significance between curves was calculated by fitting to a linear quadratic model and comparison by an extra sum-of-squares F test. P and F values are displayed for each graph. In B, mean and standard deviation of ≥4 independent repeats are shown (unless otherwise stated).

To further validate radiosensitisation in NSCLC by AURKBi, H460 cells were treated with siRNA against AURKB (Appendix Figure 5) (data produced by Timothy Mitchell). H460 cells were treated with control siRNA (scramble) or AURKB siRNA, each with and without 25 nM Barasertib, then exposed to IR. AURKB protein expression was investigated after 24 Hr siRNA treatment for each repeat (Appendix Fig 5 A)

As expected, 25 nM Barasertib radiosensitised in control siRNA treated cells ($p = 0.0278$) (Appendix Fig 45C). The AURKB depleted cells also showed a trend for increased sensitivity to IR compared to control siRNA treated cells (Appendix Fig 5 B), although this was not statistically significant ($p = 0.0501$), perhaps due to incomplete protein depletion. AURKB depletion abrogated the effect of 25 nM Barasertib demonstrating that the radiosensitising effect of Barasertib is due to its effects on AURKB.

3.5. Investigation of Apoptosis and Death after IR and Barasertib Treatment in H460 Cells

We established that Barasertib decreases the colonies formed after radiation, which can be a result of increased cell death and/or decreased proliferation. To investigate if cell death was increased by Barasertib, and whether apoptotic cell death is involved, flow cytometry was used to analyse live cells, staining with PI and Annexin V. H460 cells were pre-treated for 1 Hr with 50 nM Barasertib prior to 4Gy IR treatment. Barasertib treatment continued throughout recovery and cells were stained at 24, 48 and 72 Hr post-IR (Fig 3.8 A – E).

At 24 Hr and regardless of treatment, >80% of cells were negative for PI or Annexin V staining, which indicates live, non-apoptotic population (“Normal”) (Fig 3.8 C). Small increases in the percentage of early apoptotic population (PI- Annexin V+) and late apoptotic/necrotic cells (PI+ Annexin V+) were detected in IR alone and combination treated samples but these are not significant (Fig 3.8 D & E).

By 48 Hr, induction of apoptosis can be seen in the Barasertib, IR and combination conditions compared to the untreated control. This increase was small in the 50 nM Barasertib condition compared to the DMSO control and was not statistically significant. In the 4 Gy and combination groups, apoptosis was further increased, which was significant in the combination group compared to DMSO control ($p = 0.016$) (Fig 3.8 D). However, no difference between IR alone and IR + Barasertib was detected. The percentage of dead cells at 48 Hr was significantly increased in both the 4 Gy and combination groups compared to the DMSO control ($p < 0.0001$), However, there was no difference between IR alone and the combination.

The populations of apoptotic and dead cells remained high at 72 Hr. However, at this time point, there were significantly increased levels of death in the combination treatment compared to 4 Gy alone (p = 0.0100) (Fig 3.8 E). Consistent with this the percentage of live, non-apoptotic cells was lower in the combination treatment compared to IR alone (p = 0.016) (Fig 3.8 C).

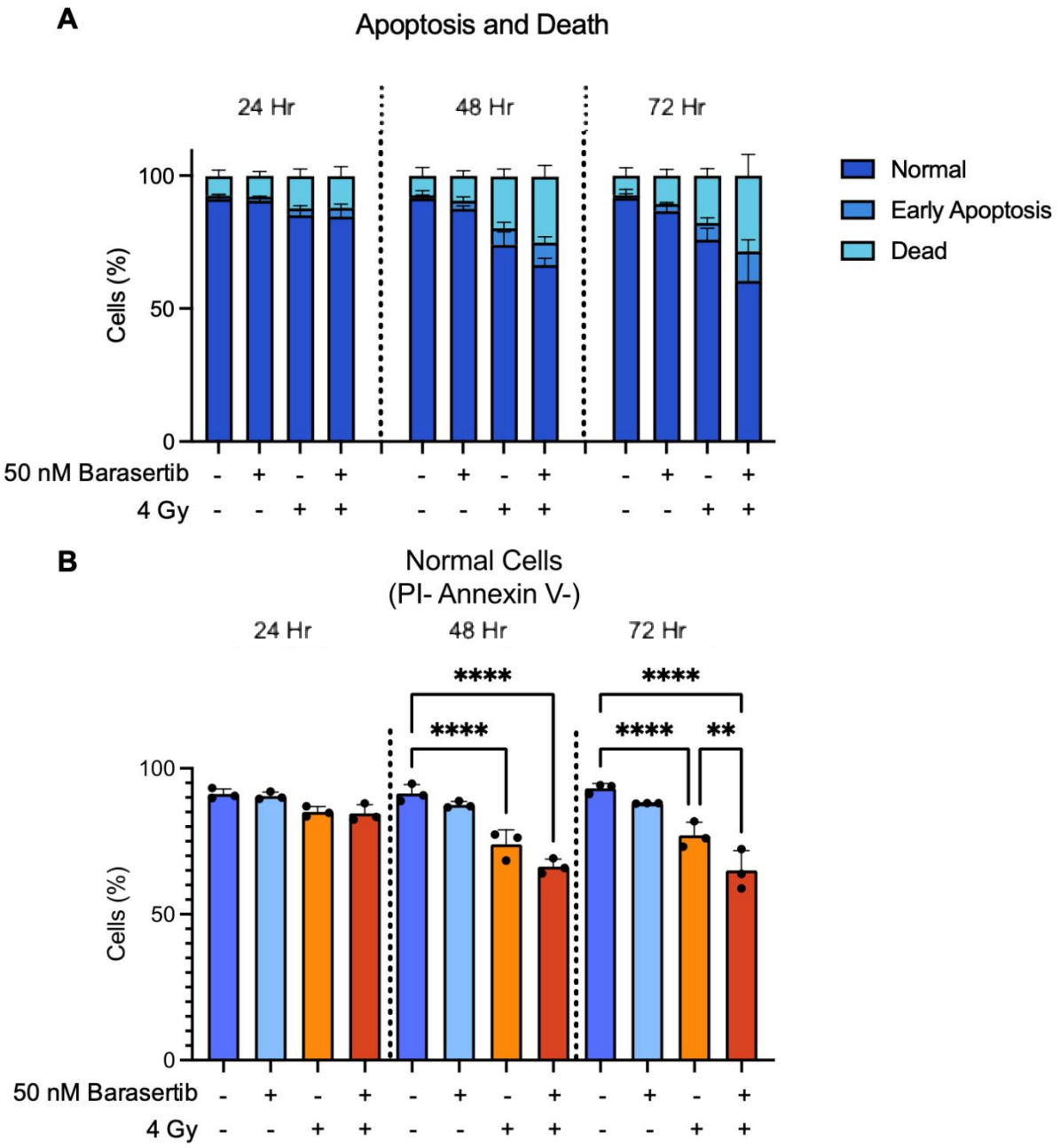

Figure 3.8: Barasertib increases late apoptosis and necrosis after IR treatment in H460 cells

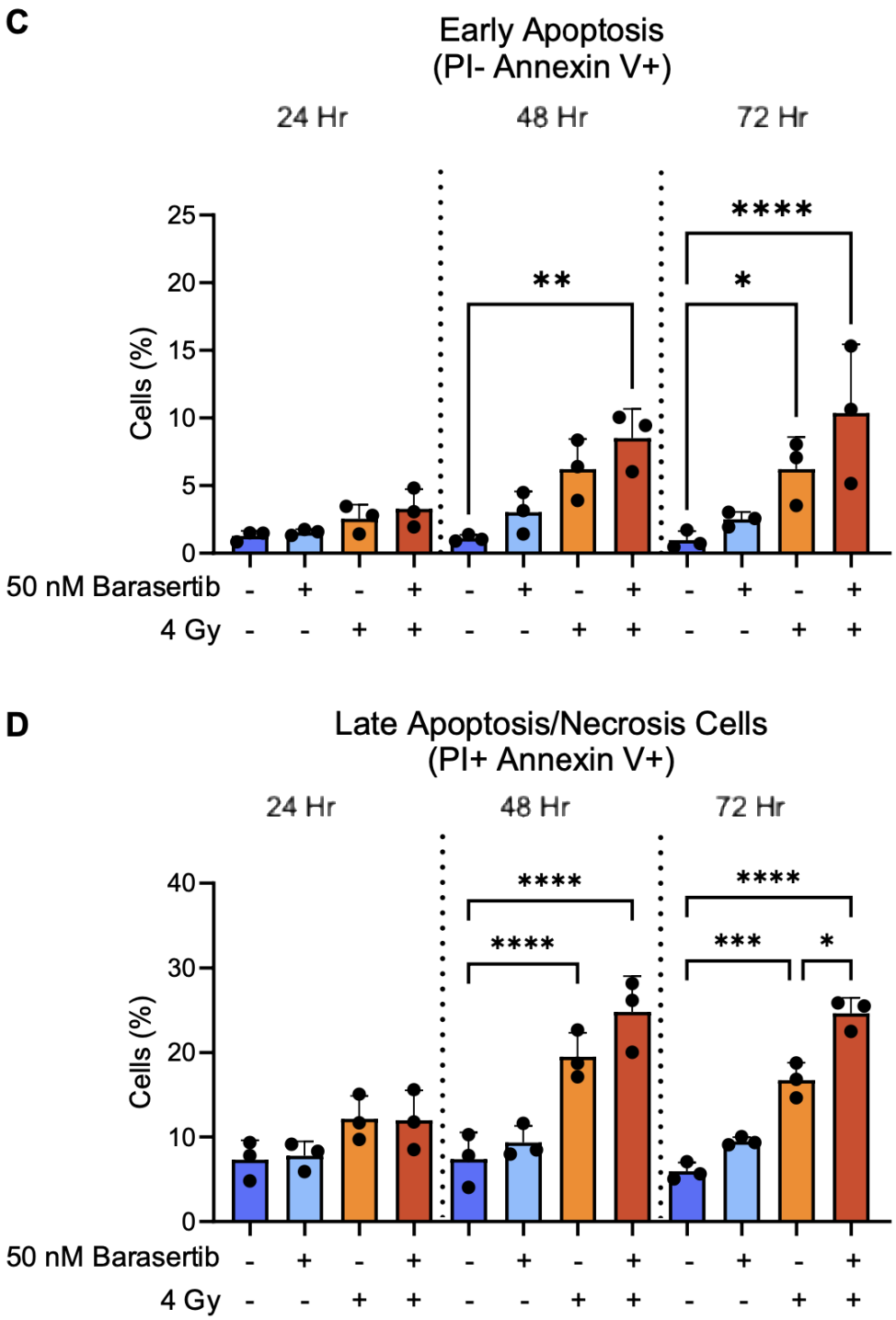

Figure 3. 8: Barasertib increases late apoptosis and necrosis after IR treatment in H460 cells

H460 cells were pretreated with 50nM Barasertib for 1 Hr before 4 Gy and during recovery. Cells were stained live for PI and Annexin V at 24, 48 and 72 Hr. **A** Quantification of normal (healthy) cells (PI-/Annexin V-), early apoptotic cells (PI-/Annexin V+) and dead cells (PI+/Annexin V+) (Overleaf) **B-D** each gate individually. Mean and standard deviation are shown (and individual repeats for C-E). P-values were calculated using an ordinary one-way ANOVA (* = $p < 0.05$, ** = $p < 0.01$, *** = $p<0.001$. **** = $p<0.0001$).

In conclusion, IR promotes apoptosis and death after 48-72 Hr, and by 72 Hr cell death is significantly increased following co-treatment with Barasertib compared to IR alone. There was also a small increase in apoptosis in the combination condition compared to IR alone but this was not statistically significant. Therefore, increased apoptosis appears to contribute to the increased death after IR in the presence of Barasertib, but other death mechanisms may be involved.

3.6. Investigation of Senescence after IR and Barasertib Treatment in H460 cells

AURKBi has previously been linked to replicative senescence, whereby cells exit the cell cycle and no longer proliferate (Sadaie et al., 2015). To investigate whether the IR + Barasertib treatment induced senescence, we stained cells with Beta-galactosidase, a marker of senescence in human cells (Dimri et al., 1995).

H460 cells were pre-treated with 50 nM Barasertib 1 Hr prior to exposure to 4Gy IR, they were then left to recover in Barasertib before fixing at 24, 48, 72 and 96 Hr post-IR and staining for Beta-galactosidase (blue) (Fig 3.9 A). By 24 Hr approximately 30% of cells in either IR or combination conditions were positive for Beta-galactosidase. Both IR treated groups showing increasing senescent populations over time (Fig 3.9 B). By 48 Hr, senescent cells made up roughly 50% of the population with both IR and combination treatments showing significant increases compared to the control ($p < 0.0001$ (both)). At 72 Hr, the senescent population in the IR and combination groups made up 53% and 57% of the population, again significantly increased compared to the DMSO control ($p < 0.0001$ (both).

However, the trend changed at 96 Hr with senescence in the IR condition decreasing to 29% while the combination treatment stayed high at 53% ($p=0.0111$) (Fig 3.9 B). The decrease of the senescent population in the IR alone condition could be explained by death of senescent cells and/or increased replication in the remaining non-senescent population. In the 4Gy condition, there are clear colonies of non-senescent cells, showing successful repopulation. In contrast in the combination condition, there appear to be fewer colonies; most cells are spaced out. To quantify

this phenotype, we calculated the cells/frame and normalised this to the seeding density to give a measure of confluency (Appendix Figure 6). Confluency is lower in the combination treatment compared to IR alone (ns). The overall trend supports the observation that cells are sparser in the combination treated population and that there is less repopulation occurring after Barasertib and IR treatment than IR alone.

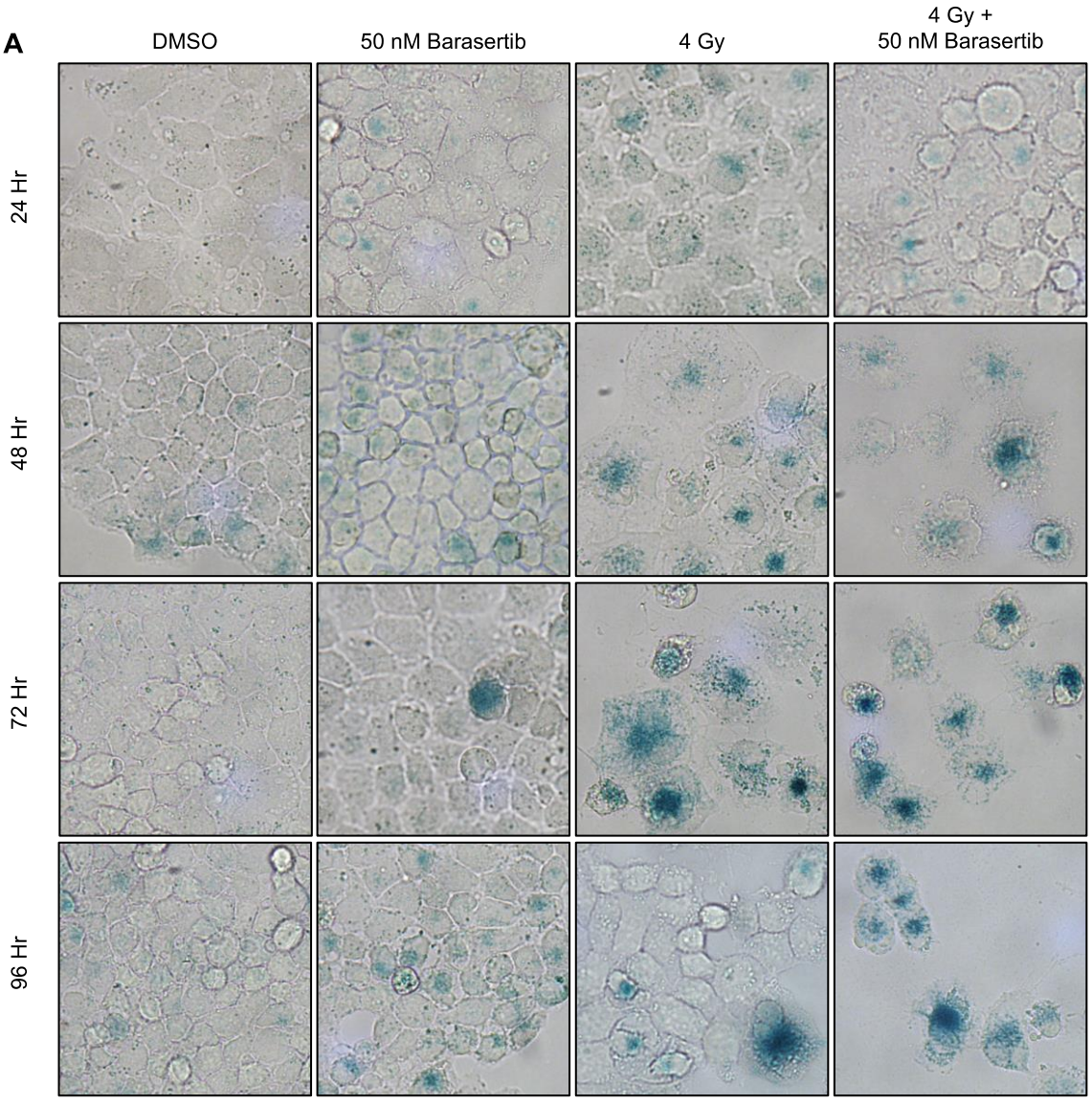

Figure 3.9: Senescence after Barasertib and IR treatment in H460 cells

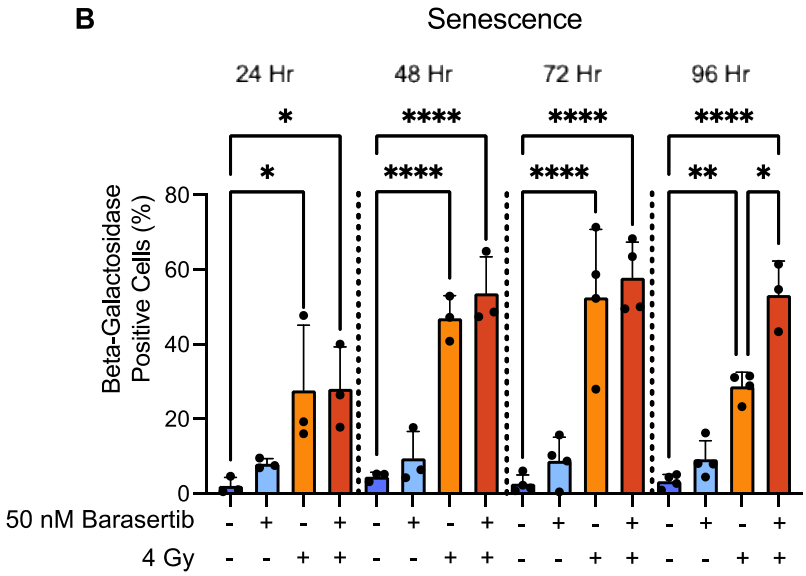

Figure 3. 9: Senescence after Barasertib and IR treatment in H460 cells

H460 cells were pretreated with 50nM Barasertib for 1 Hr before 4 Gy, then fixed at 24, 48m, 72 and 96 Hr, and stained for Beta-Galactosidase (blue). **A** Representative images **B** Quantification of positive cells as a percentage of total cells. Mean, standard deviation and individual values are shown for ≥ 3 independent repeats. P-values were calculated using an ordinary one-way anova (* = $p < 0.05$, ** = $p < 0.01$, *** = $p<0.001$. **** = $p<0.0001$).

3.7. Discussion

Here, we used three *in vitro* cell culture models to study the relationship between AURKA/B and IR, and asked whether we could radiosensitise NSCLC by AURKBi.

We showed that Barasertib was cytotoxic in a range of NSCLC cell lines. Sak et al (2012) demonstrated correlation between p53 and IC50 of AZD1152-HQPA (Barasertib is the pro-drug form of AZD1152-HQPA). In their study, p53 WT cell lines H460 and A549 were less sensitive than the two p53-deficient cell lines, H520 and H661. In contrast to this study, we found no correlation between p53 functionality and Barasertib sensitivity. We investigated Barasertib toxicity in a greater number of cell lines (6 in total). Comparing our results to theirs where the same cells were used, in our hands H520 were more sensitive than H460 but A549 cells were the most sensitive cells we tested. We did not test H661. It is not obvious why we would get differing effects by using the pro-drug form.

P53 status has been linked to the radiosensitisation effect of Barasertib (Tao et al., 2008). In HCT116 cells, *TP53* knockout was reported to enhance the radiosensitisation *in vitro* and *in vivo* by AZD1152-HQPA (active form of Barasertib) (Tao et al., 2008). We found that Barasertib treatment caused radiosensitisation regardless of p53 status. Our results indicates that p53 loss is not required for radiosensitisation in NSCLC. However, our approach was limited as we did not use p53 knockout line to test this in a uniform background.

We only tested radiosensitisation in H460, H1299 and SW900 cells. Studies of the radiosensitisation effect in the other NSCLC cell lines available was limited by the high sensitivity of H520, A549 and H322 to Barasertib alone. Why these cell lines

were so sensitive is not clear. The doubling time of these cell lines is 61 Hr, 36 Hr and 50.6 Hr, respectively (Brower et al., 1986, McMillan et al., 2018). H460 and H1299 both have doubling times of 19 and 30 Hr, so there is a weak correlation in sensitivity with short cycling time (Baguley et al., 1995, Cowley et al., 2014). It is also possible that a specific pathway is compromised in these cell lines that increases their sensitivity to AURKBi but we could not identify one from publicly available data.

We used scheduling to further investigate radiosensitisation and found that unless Barasertib was present during the 24 Hr after IR, the radiosensitisation effect was lost. This provides insight for further study into the mechanism (Chapter 5). For example, the majority of IR induced DNA damage is repaired in the first 24 Hr after IR, so perhaps AURKB is involved in DNA repair. In addition, G_2-M arrest and subsequent cell cycle restart/progression after IR also occurs before 24 Hr, suggesting that AURKB may be involved (Martinez-Pastor et al., 2021, Lonati et al., 2021). The mechanistic implications of the requirement for Barasertib in the first 24 Hr after IR are further discussed in chapter 5. The fact that no radiosensitising effect is seen with only 24 Hr pre-treatment and no drug during recovery argues against the effect being due to Barasertib putting cells into a more radiosensitive state (e.g. cell cycle stage) prior to irradiation.

We found there was a significant increase in the percentage of dead cells at 72 Hr in the combination condition compared to IR alone, supporting the radiosensitising effects of Barasertib and arguing for increased death rather than loss of growth. Our findings are similar to that of Sak et al (2011), who also found non-significant increases in apoptosis in H460s cells 72 Hr after IR (20 Gy) with 47.7 nM Barasertib.

We found elevated levels of senescence in IR-treated cells. AURKB inhibition and depletion have been shown to induce senescence, potentially through polyploidy (Sadaie et al., 2015). This may represent repopulation by non-senescent cells or by cells that had escaped senescence. Senescence was traditionally thought to be an irreversible exit from the cell cycle but escape from senescence is now considered possible, especially in cases of therapy-induced senescence. This occurs in response to cellular stress such as DNA damage and is distinct from senescence due to telomeric attrition (Evangelou et al., 2023). H460 cells specifically have been shown to recover from a DDR-induced senescent phenotype (etoposide or doxorubicin), so this is a possibility after IR (Saleh et al., 2019).

The data presented in this chapter provides convincing evidence for testing of AURKB inhibitors with radiotherapy *in vivo*. The reduced clonogenic survival, enhanced cell death and prolonged senescent phenotype demonstrates that Barasertib can modulate the response to IR. In terms of clinical application, the radiosensitisation observed with single dose IR was preserved when using fractionated IR, which aids transfer to clinical settings.

Western blots showing the phosphorylation status of the AURKs were used to investigate the inhibitory action of Barasertib. However, at the radiosensitising dose of 50 nM, a reduction in pAURKB (Thr232) was not observed in H460 or SW900 cells. A decrease in AURKB Thr232 phosphorylation was expected as the inhibitory mechanism of Barasertib is via ATP competition within the substrate binding pocket, and 50 nM Barasertib is reported to decrease Thr232 auto-phosphorylation, the key activating PTM (Sessa and Villa, 2014, Alexandre et al., 2023, Yasui et al., 2004, Zuazua-Villar et al., 2014). The downstream target pH3 Ser10, was also investigated

and showed similar inhibition to the pAURK blots. However, other groups have shown that Barasertib does not reduce AURKB or H3 phosphorylation at 50 nM, and proposed a lack of access to active sites for phosphatases (Kettenbach et al., 2011).

Technical issues could affect the quantification of the phospho-AURK signal. AURK phosphorylation groups are especially labile and we used densitometry normalisation as our method prevented protein quantification. Additionally, the low signal from the pAURK antibody extended exposure times, increasing background. However, the fact that pH3 phosphorylation was also not inhibited at doses under 200 nM in H460 cells suggests that the issue is not purely technical. H460 cells are highly proliferative and may have higher expression of pAURKB and pH3 than other cell lines. This could explain why the LD50 was higher and why inhibition of AURKB is less detectable in H460 cells than other cell lines such as H1299. The increased phosphorylation of AURKA and inhibitory effect on AURKC could also play a role in Barasertib‘s mechanism of action.

Chapter 4: Phospho-Proteomic Analysis of H460 cells after AURK Inhibitors and Radiation

4. Phospho-Proteomic Analysis of H460 cells after AURK Inhibitors and Radiation

4.1. Introduction, Aims and Hypothesis

To assess global protein levels, mass-spectrometry proteomics have been developed to detect and quantify peptides in a high-throughput manner. The optimisation of post-translational modification (PTM) localisation techniques and methods of selective enrichment for phosphopeptides have created a form of proteomics that gives greater insight into kinase signalling.

We were interested in how phosphorylation signalling after IR changes with and without Barasertib treatment. We were also interested in the effect of the AURKA inhibitor Alisertib on phosphorylation signalling after IR. Alisertib was investigated as a radiosensitiser by a previous lab member, and found to successfully radiosensitise *in vitro* and *in vivo.* The mechanistic basis of AURKAi as a radiosensitiser was still unsolved. As MS/MS analysis of Alisertib with IR has never been investigated to our knowledge, we included this in our experimental plan to shed light on Alisertib's effect on the radiation response.

As AURKB and AURKA modulate their substrates via phosphorylation, we were interested in how Barasertib and Alisertib alter downstream phosphorylation. Additionally, many of the relevant pathways to IR and AURKs, such as DNA repair, cell cycle checkpoints and mitotic processes are regulated by phosphorylation.

This chapter will cover a phospho-proteomic analysis of Barasertib, Alisertib and IR treatments alone, as well as the effect of each AURK Inhibitor with IR in H460 cells. The two inhibitors were assessed in independent experiments with independent

DMSO and IR controls for either inhibitor. Sample processing and mass spectrometry was also carried out independently.

The aims of the chapter are:

1. To carry out MS/MS of phosphopeptide-enriched and total protein extracts from H460 cells in the following conditions: DMSO, 50 nM Barasertib, 4 Gy and Combination (4Gy + 50 nM Barasertib)
2. To carry out MS/MS of phosphopeptide-enriched and total protein extracts from H460 cells in the following conditions: DMSO, 25 nM Alisertib, 4 Gy and Combination (4Gy + 25 nM Alisertib)
3. To investigate which peptides significantly change in relative abundance between conditions
4. To determine which pathways are affected by peptides with altered abundance using pathway enrichment analysis.

Our hypothesis is that both AURK inhibitors and 4 Gy IR will induce significant changes to phosphorylation signalling in H460 cells and that this might provide insight into the mechanism of radiosensitisation by Barasertib and Alisertib.

The cost of the experiment limited it to one cell line and one timepoint. Per experiment, we carried out 4 conditions with 4 biological repeats per condition. H460 cells were used as a model cell line. An early timepoint of 1 Hr after IR with a 1 Hr pretreatment of Barasertib or Alisertib was chosen to prioritise changes in phosphorylation immediately downstream of AURK inhibition, rather than indirect secondary effects.

We also carried out MS/MS of the protein samples without enrichment to analyse relative abundance of total proteins.

4.2. Proteomic analysis after IR and Barasertib Treatment in H460 Cells

4.2.1. MS/MS and Identification of Differentially Abundant Peptides

To investigate phosphorylation signalling after Barasertib and IR, mass spectrometry analysis of H460 cells was carried out. Cells were pretreated with DMSO or 50 nM Barasertib for 1hr then treated with 4 Gy IR. Cells were then harvested with trypsin, then flash frozen to preserve phosphorylated peptides.

An overview of the subsequent MS/MS workflow is shown in Figure 4.1. In collaboration with Prof Claire Eyers' lab (University of Liverpool), samples were prepared for peptide analysis. TMT-multiplex labelling was used to reduce technical

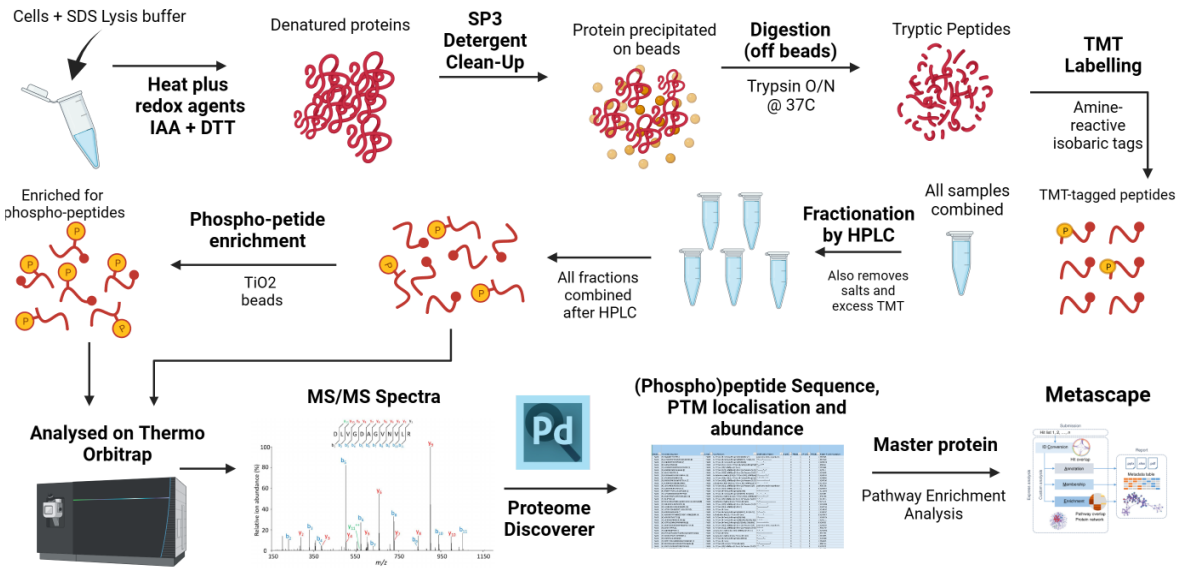

Figure 4. 1: Work flow of MS/MS protocol for Barasertib and IR treated cells

Cells were lysed in SDS lysis buffer then heated with IAA and DTT to aid denaturation. To remove salts, the sample underwent SP3 bead clean up after which protein was digested with trypsin into peptides. TMT labelling was carried out and all samples were combined. HPLC fractionation was performed to desalt and remove unbound TMTs. 10% of the sample was reserved and the rest underwent phosphopeptide enrichment using TiO2 beads. Peptide analysis was performed by LC-MS/MS on a Thermo Orbitrap. The MS/MS spectra was analysed using Proteome Discoverer (2.4) to determine peptide sequence (MASCOT was used for master protein determination).

Table 4. 1: The number of (phospho)peptides discovered per MS/MS experiment and the filtering process

	Barasertib Samples (No enrichment)	Barasertib Phospho-Enriched Samples
All isoforms	6,077	25,661
Phosphopeptides	ND	14,851
No Contaminant	6,061	14,847
Quantified peptides	5,651	13,025
Altered Abundance (FC >20%, p-value < 0.05)		
Barasertib vs DMSO	10	135
4 Gy vs DMSO	21	1131
Combined vs DMSO	12	1058
Combination vs 4 Gy	350	714

ND = not determined

variation during sample preparation and provide relative peptide quantification. Enrichment for phosphopeptides was carried out using TiO_2 beads Phospho-enriched and total samples were analysed by LC-MS/MS. LC-MS/MS data was processed using Proteome Discover v2.4 for peptide identification and PTM localisation (Orsburn, 2021).

In the phosphopeptide enriched samples, 25,661 peptides were identified. Of these, 14,851 were phosphopeptides. After filtering to remove peptides with contaminants and unquantified peptides (i.e. without p-values), 13,025 phosphopeptides were taken forward for further analysis (Table 4.1).

In the non-enriched samples, 6,077 proteins were detected. After filtering for contamination and quantified peptides, there were 5,651 proteins remaining.

4.2.2. Identification of Differentially Abundant Phosphopeptides after IR and Barasertib

Using TMT tags, phosphopeptide isoforms were quantified by relative abundance (relative to the same peptide isoform in other samples in the same run).. The relative abundance of phosphopeptides were filtered for fold change > 20% (abundance ratio <0.8 or >1.2) and p-value of < 0.05 (calculated by one-way ANOVA). The fold change threshold of 20% is lower than other large-scale analyses such as RNA-seq but are appropriate in phospho-proteomics due to the amplification of phosphorylation signalling through kinase cascades, and are commonly used in phosphopeptide analysis (Luo et al., 2022, Zhang et al., 2023).

Phosphopeptides with altered abundance were identified between DMSO vs Barasertib (135 peptides), DMSO vs 4Gy (1131 peptides), and IR vs IR + 50 nM Barasertib (714 peptides) (Table 4.1).

The same significance thresholds and fold change thresholds were applied to the peptide isoforms in the non-enriched samples ($p<0.05$, >20% fold change). Fewer differentially abundant proteins were found compared to the phosphopeptide results. This is likely due to the smaller size of the data set but also highlight the difference in speed and scale of phosphorylation changes compared with protein expression changes (Table 4.1).

Master Protein Accessions	Gene Name	Master Protein Descriptions	Annotated Peptide Sequence	Modification Pattern	Modifications in Master Proteins	Abundance Ratio: Barasertib/ Untreated	Abundance Ratio: IR / Untreated	Abundance Ratio: IR + Barasertib / Untreated	Abundance Ratio: IR + Barasertib / IR	Abundance Ratio P-Value: (IR + Barasertib/IR)
A3KN83	SBNO1	Protein strawberry notch homolog 1	[K].SIDPDSIQSALLASGLGSK.[R]	*————-*	A3KN83 1xPhospho [S794(100)]	0.897	1.108	0.448	0.483	0.04827
Q96LD4	TRIM47	E3 ubiquitin-protein ligase TRIM47	[R].RGGIPASPIDPFQSR.[L]	*—*——	Q96LD4 1xPhospho [S588(100)]	1.242	1.294	0.608	0.524	0.03852
Q12888	TP53BP1	TP53-binding protein 1	[R].ETAVPGPLGIEDISPNLSPDDKSFSR.[V]	*————*—*—	Q12888 1xPhospho [S1430(100)]	1.548	1.647	0.876	0.532	0.00846
O60271	SPAG9	C-Jun-amino-terminal kinase-interacting protein 4	[K].ATTPASTANSDVATIPTDTPLKEENEGFVK.[V]	*————-—-*—*——-*	O60271 1xPhospho [T292(99.6)]	1.374	1.036	0.576	0.556	0.03063
Q8TDD1	DDX54	ATP-dependent RNA helicase DDX54	[R].KLGPGRPLPTFPTSECTSDVEPDTR.[E]	*————*-*——	Q8TDD1 1xPhospho [S75(99.6)]	1.005	1.408	0.760	0.561	0.01446
P49454	CENPF	Centromere protein F	[R].GSPLLGPVVPGPSPIPSVTEK.[R]	**—————*——*	P49454 2xPhospho [S2900(100); S2911(100)]	0.949	0.441	0.220	0.568	0.02236
P46013	MKI67	Proliferation marker protein Ki-67	[R].ASQPDLVDTPTSSKPQPK.[R]	*———*—*—*	P46013 1xPhospho [T1747(100)]	1.023	0.824	0.509	0.570	0.02082
Q86YS7	C2CD5	C2 domain-containing protein 5	[K].NKELYEINPPEISEEIIGSPIPEPR.[Q]	**———————*——	Q86YS7 1xPhospho [S643(100)]	1.190	1.023	0.604	0.591	0.03049
Q86YZ3	HRNR	Hornerin	[QR].QGSGSGQSPSR.[G]	*——*—	Q86YZ3 1xPhospho [S659(100)]; 1xPhospho [S1712(100)]; 1xPhospho [S1829(100)]; 1xPhospho [S2299(100)]; 1xPhospho [S2652(100)]	1.238	1.367	0.916	0.591	0.00508
Q8IZT6	ASPM	Abnormal spindle-like microcephaly-associated protein =2	[K].ILSPDSFIK.[D]	*-*——	Q8IZT6 1xPhospho [S367(100)]	0.914	0.818	0.480	0.596	0.02762

Table 4. 2: 10 Phosphopeptide isoforms most increased in the combination (Barasertib + IR) compared to IR alone

Master Protein Accessions	Gene Name	Master Protein Descriptions	Annotated Sequence	Modification Pattern	Modifications in Master Proteins	Abundance Ratio: Barasertib/ Untreated	Abundance Ratio: IR / Untreated	Abundance Ratio: IR + Barasertib / Untreated	Abundance Ratio: IR + Barasertib / IR	Abundance Ratio P-Value: (IR + Barasertib/IR)
Q9NPI1	BRD7	Bromodomain-containing protein 7	[K].VGGNEVTELSTGSSGHDSSLFEDK.[N]	positions not distinguish	Q9NPI1 5xPhospho [S38(99.6); T39(99.6); S41(99.6); S42(99.6); S/T]	1.070	0.647	1.347	2.353	0.0154
P46937	YAP1	Transcriptional coactivator YAP1	[R].GDSETDLEALFNAVMNPK.[T]	*-*———*–*	P46937 1xPhospho [S61(100)]	1.010	0.751	1.365	2.079	0.0322
Q9H3Q1	CDC42EP4	Cdc42 effector protein 4	[K].NAMSLPQLNEK.[E]	*–*——*	Q9H3Q1 1xPhospho [S118(100)]	0.839	0.748	1.460	1.957	0.0093
P78559	MAP1A	Microtubule-associated protein 1A	[K].MASPPPSGPPSATHTPFHQSPVEEK.[S]	positions not distinguish	P78559 4xPhospho [S996(100); S1000(99.7); S1013(100); S/T]	0.977	0.621	1.348	1.862	0.0075
Q09666	AHNAK	Neuroblast differentiation-associated protein AHNAK	[K].GGVTGSPEASISGSKGDLK.[S]	*–—*—*–-**—*	Q09666 3xPhospho [S5731(100); S5735(100); S5739(99.6)]	0.961	0.774	1.446	1.818	0.0042
Q9NWB6	ARGLU1	Arginine and glutamate-rich protein 1	[R].SRSTNTAVSR.[R]	*-*——	Q9NWB6 2xPhospho [S58(100); S60(100)]	1.231	0.730	1.536	1.815	0.0144
P30622	CLIP1	CAP-Gly domain-containing linker protein 1	[K].TASESISNLSEAGSIK.[K]	*–-*—*–-*-*	P30622 3xPhospho [S195(100); S200(100); S204(100)]	0.912	0.720	1.236	1.770	0.0066
Q09666	AHNAK	Neuroblast differentiation-associated protein AHNAK	[K].SKGHYEVTGSDDETGK.[L]	**-——*–—*	Q09666 2xPhospho [S5832(100); S5841(100)]	0.917	0.740	1.198	1.751	0.0088
P11137	MAP2	Microtubule-associated protein 2	[R].LASVSADAEVAR.[R]	*-*———–	P11137 1xPhospho [S821(100)]	0.940	0.759	1.177	1.745	0.0287
Q09666	AHNAK	Neuroblast differentiation-associated protein AHNAK	[R].ISAPNVDFNLEGPK.[V]	**-———*	Q09666 1xPhospho [S5448(100)]	0.874	0.840	1.360	1.730	0.0209

Table 4. 3: 10 Phosphopeptide isoforms most decreased in the combination (Barasertib + IR) compared to IR alone

Filtering by p-value and fold change resulted in a list of differentially-abundant peptides for each comparison. As examples of the information gathered per peptide, the 10 phosphopeptides with highest or lowest relative abundance, i.e. the most increased and decreased phosphopeptides in the combination treatment compared to IR alone (Barasertib + IR vs 4Gy) are displayed in Table 4.2 and 4.3 respectively. Site localisation of the phosphorylation on the peptides is shown as modification within the master peptides, where confidently identified. This presents the phosphorylation site at its amino acid position in the whole protein sequence and allows easy identification of phosphorylation residues.

The IR vs DMSO comparison revealed the highest number of differentially abundant phosphopeptides(Fig 4.2 A-D). The highest fold-changes between IR and DMSO were also greater than between IR + Barasertib vs IR or Barasertib vs DMSO. This indicates a stronger biological effect by IR than 50 nM Barasertib alone.

Several phosphorylation sites were identified as upregulated in the 4 Gy condition compared to DMSO which are known to occur within the DDR. These included ATM Ser1981 (x2.65↑), BRCA1 Ser1524 (x2.23↑), BRCA1 Ser1542(x2.82↑), 53BP1 Ser302 (x4.356↑) and DNA-PKcs Ser3205 (x2.39↑)

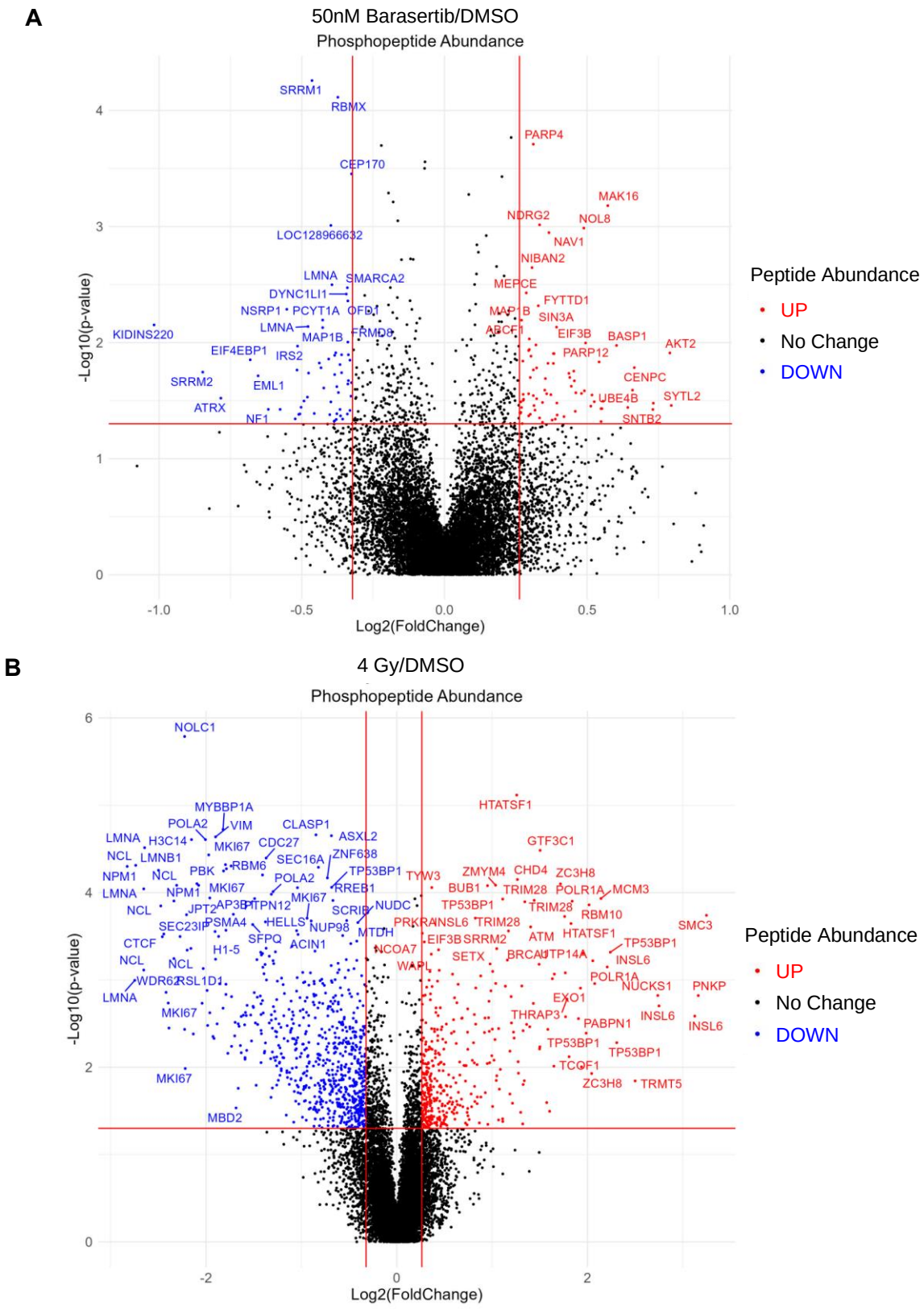

Figure 4.2: Relative abundance of phosphopeptides between untreated, Barasertib, 4 Gy and combination conditions in H460 cells

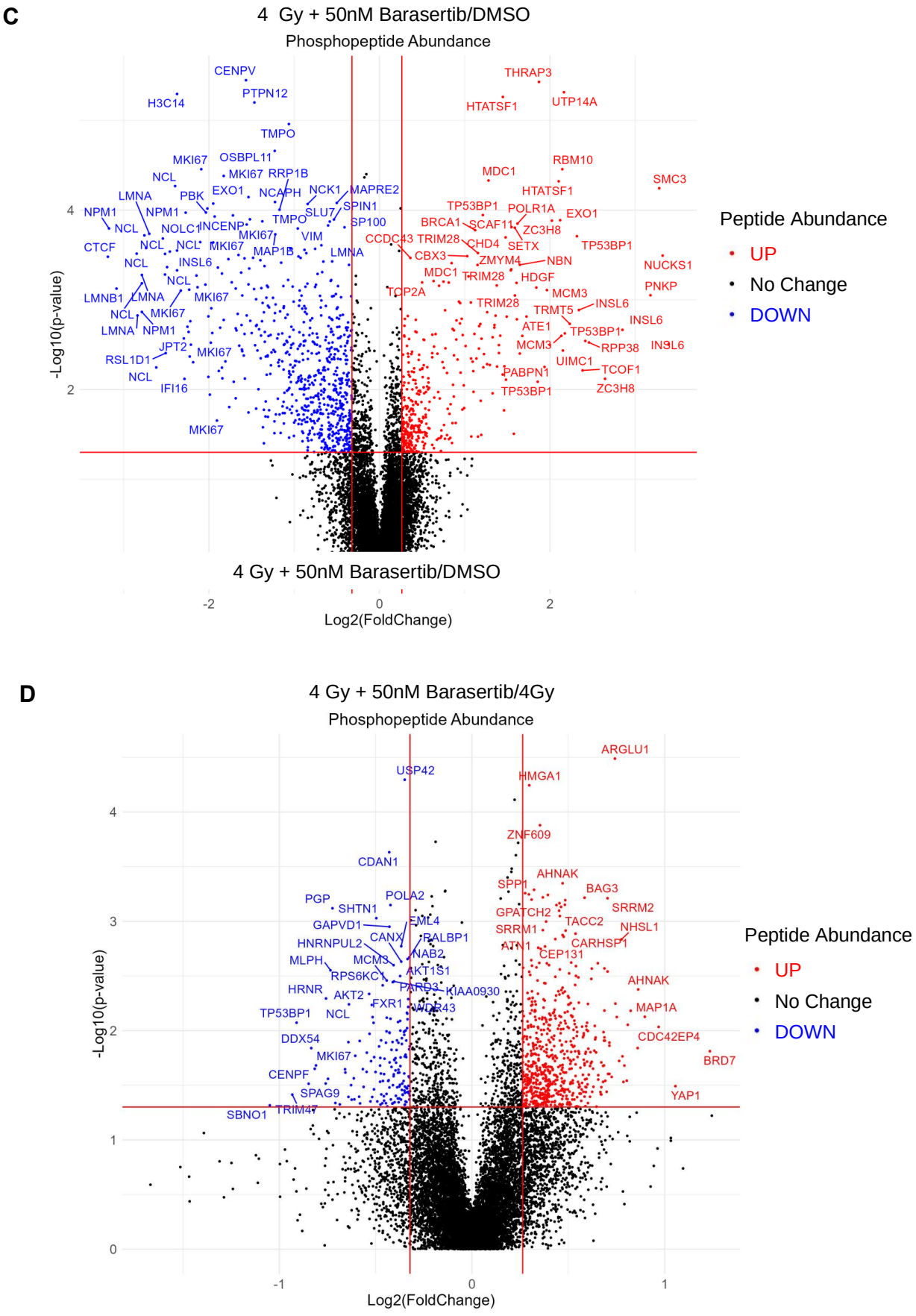

Figure 4.2: Relative abundance of phosphopeptides between untreated, Barasertib, 4 Gy and combination conditions in H460 cells

Figure 4. 2: Relative abundance of phosphopeptides between untreated, Barasertib, 4 Gy and combination conditions in H460 cells

Volcano plots of Log(2)(Fold change) vs –Log(10)(p-value) for relative abundance. Phosphopeptides were labelled as UP or DOWN to signify direction of change in relative abundance, and labelled with the official gene symbol to replace master protein accession **A** 50 nM Barasertib compared to Untreated, **B** 4 Gy IR compared to Untreated, **C** 4Gy + 50 nM Barasertib compared to Untreated **D** 4Gy + 50 nM Barasertib compared to 4 Gy. Red lines indicate upper and lower thresholds for fold change (0.8 and 1.2) and p-value threshold (0.05). Red and blue points indicate peptide with significant increase or decrease in relative abundance between conditions respectively (labelled as UP or DOWN). P-values calculated by one-way ANOVA (only calculated for peptides quantified in ≥3 repeats). Plots produced in R. Gene Symbols displayed for the master protein of the depicted phosphopeptide. Labels arranged using the GGRepel function.

(So et al., 2009, Cortez et al., 1999, Bunch et al., 2021, Jowsey et al., 2007, Neal et al., 2020). We also identified a 27.64 fold increase in Chk2 Ser260 abundance, a key autophosphorylation after DNA damage (Zannini et al., 2014). This peptide isoform was not included in the analysis as it was only detected in 1 DMSO repeat.

4.2.3. Pathway Enrichment Analysis of Phosphorylation Changes after IR and Barasertib

To understand which biological pathways showed changes in phosphorylation, we used pathway enrichment analysis. Pathway enrichment analysis by Metascape was undertaken to identify pathways enriched for the master proteins (Uniprot accession) of the differentially abundant phosphopeptides (Zhou et al., 2019). As multiple peptides from the same master protein could be detected in one sample, there may be fewer master proteins than the number of differentially abundant phosphopeptides. Metascape combines gene ontology from multiple sources and then groups similar terms in clusters to reduce redundancy. Each term and cluster are given a p-value representing significant presence (i.e. enrichment) in the gene list of that term. Metascape analysis was performed for all comparisons except the

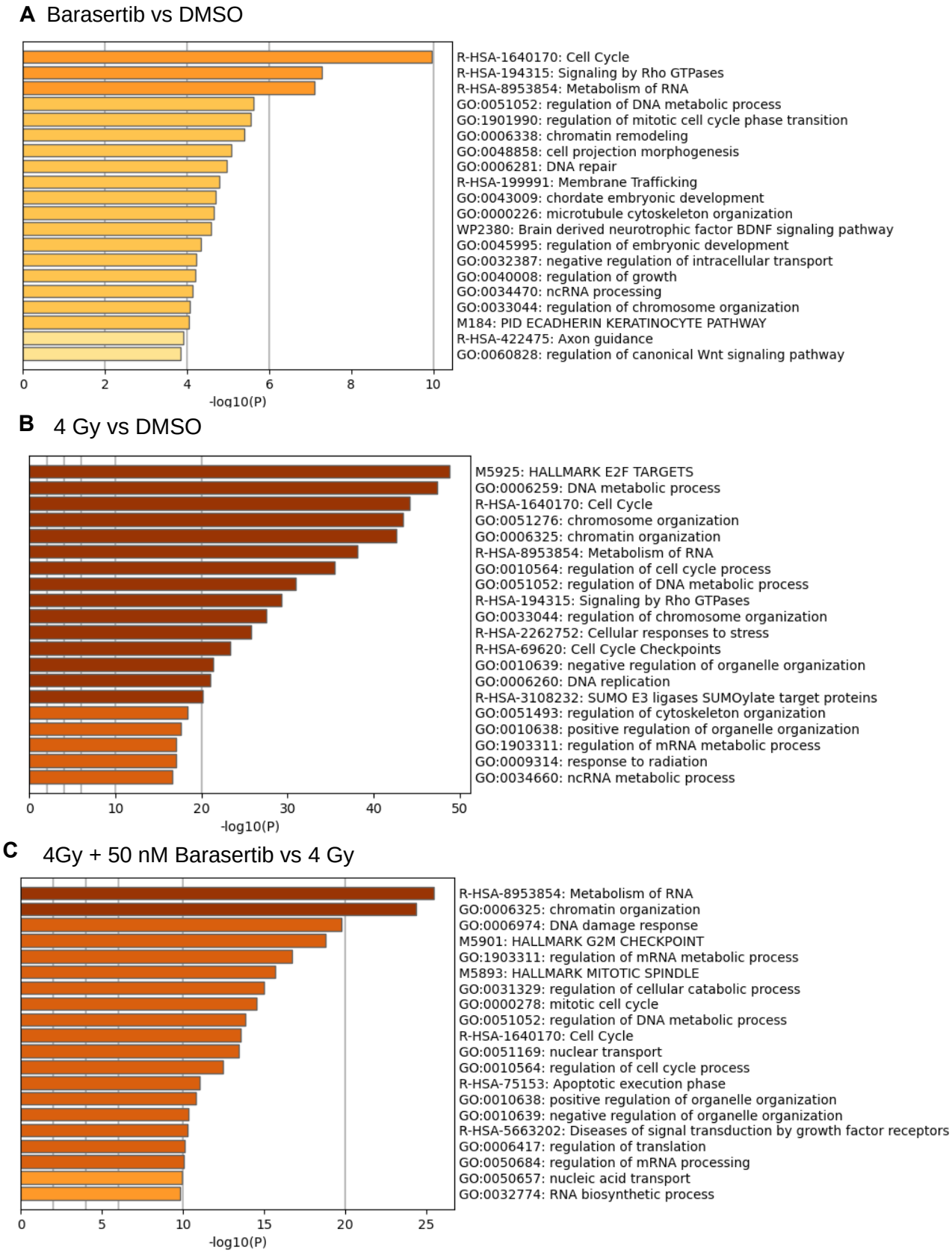

Figure 4.3: Top 20 enriched pathway clusters generated by Metascape pathway analysis

Figure 4. 3: Top 20 Enriched pathway clusters generated by Metascape pathway analysis

Pathway & Process Enrichment Analysis was carried out on Metascape.com using the list of differentially abundant phosphopeptides per comparison. Enrichment was analysed for all available pathway gene lists using the Custom Analysis mode. Enrichment is calculated as terms with a p-value< 0.01, count of 3 or more and enrichment factor >1.5. Cumulative hypergeometric distribution was used for p-value calculation and q-values were calculated via Benjamini-Hochberg procedure. To perform hierarchical clustering in terms, enriched terms with Kappa similarity scores > 3 are clustered and are represented by the most significant term as a Cluster summary term. Cluster summary terms are displayed with – Log(10)(p-value) for the following comparisons **A** 50 nM Barasertib vs Untreated, **B** 4 Gy vs Untreated, and **C** 4Gy + 50 nM Barasertib vs 4 Gy.

Barasertib + IR vs DMSO comparison. Full Metascape enrichment analysis results for the Barasertib experiment can be accessed here.

4.2.3.1. DMSO vs 50 nM Barasertib (Metascape)

For the 136 differentially abundant phosphopeptides between DMSO and 50 nM Barasertib conditions, there were 128 unique master proteins. The top 20 most-significant clusters in the enrichment analysis were ranked by Log(p-value) (Fig 4.3 A) and displayed in network format (Fig 4.4 A).

The most significantly enriched cluster was Cell Cycle (-Log10 (P value) (LogP) = -9.967), one of two clusters related to cell cycle and mitosis in the top 20 (regulation of mitotic cell cycle phase transition (LogP=-5.542)). Within the cell cycle cluster, the majority of subterms relate to mitotic phase events (M Phase, prometaphase, metaphase, anaphase), except the term Cell cycle checkpoint. Specific processes such as Amplification of signal from the kinetochores and separation of Sister Chromatids are enriched. Additional cell cycle-related terms including microtubule cytoskeleton

A Barasertib vs DMSO

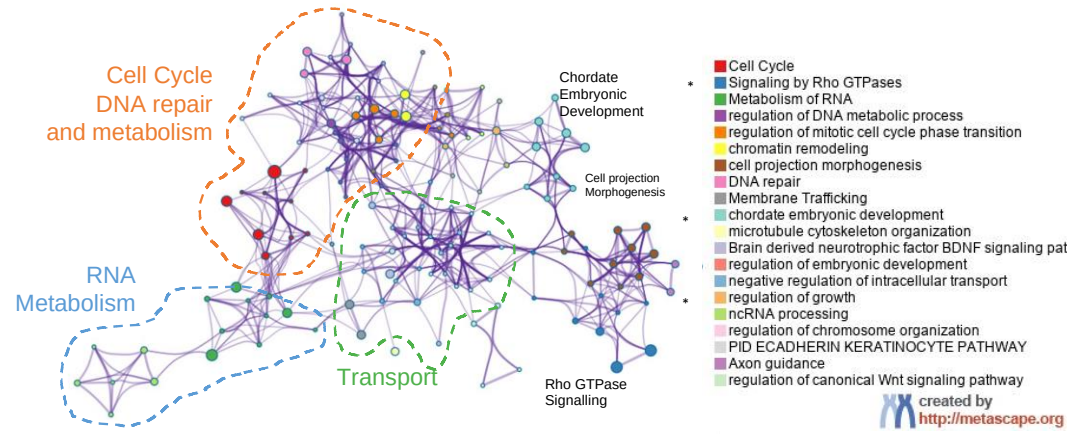

B 4 Gy vs DMSO

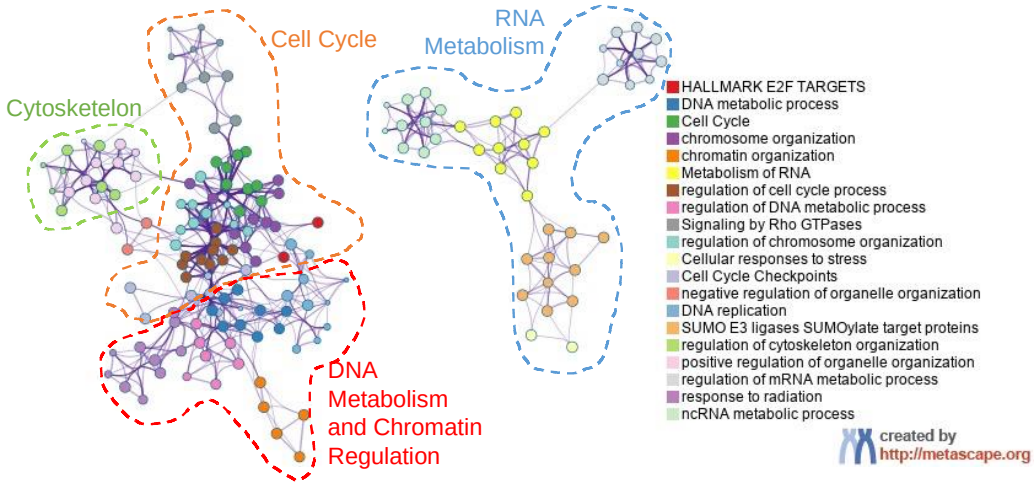

C 4Gy + 50 nM Barasertib vs 4 Gy

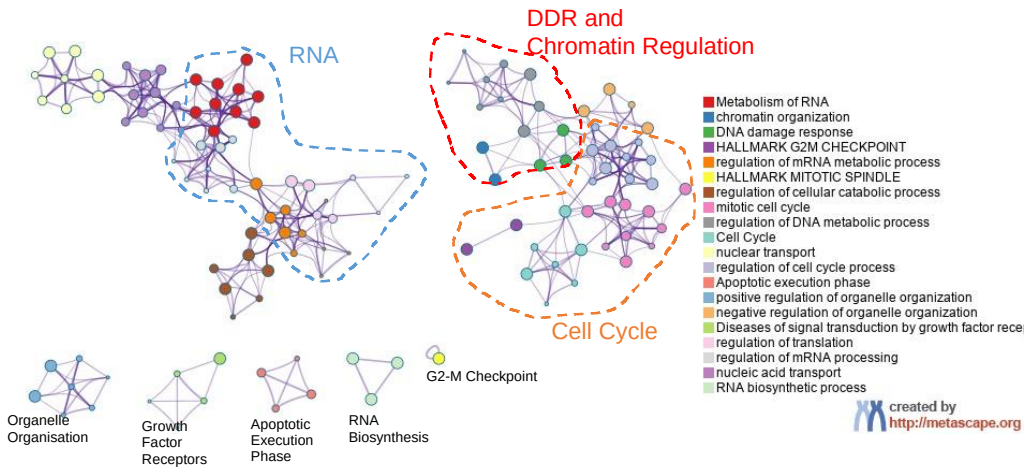

Figure 4.4: Top 20 enriched pathway clusters generated by Metascape pathway analysis

Figure 4. 4: Top 20 enriched pathway clusters generated by Metascape pathway analysis
Further visualization of Pathway & Process Enrichment Analysis was carried out on Metascape.com using the list of differentially abundant phosphopeptides per comparison. Enrichment was analysed and terms clustered as described in Figure 4.3. Network visualisations were generated for the a subset of terms within the top 20 clusters per comparison. **A** 50 nM Barasertib vs Untreated, **B** 4 Gy vs Untreated, and **C** 4 Gy 50 nM Barasertib vs 4 Gy. Each circular node represents a specific term, coloured according to cluster and labelled by its cluster summary term. The size of the circular node is proportional to the number of input genes within that term. The edges link terms with similarity score > 0.3 (thickness proportional to score). Dotted lines were drawn around clusters with overlapping biological function (drawn in PowerPoint).

organization were enriched. Regulation of chromosome organization (LogP=-4.068) and chromatin remodelling (LogP=-5.403) were also enriched.

These processes reflect the canonical functions of AURKB as discussed in Chapter 1. AURKB is a key regulator of kinetochore-MT attachments, and is involved in correction of incorrect attachment and the spindle assembly checkpoint, which controls metaphase-anaphase transition (Krenn and Musacchio, 2015b). AURKB is involved in chromatin regulation via Histone 3 and HP1 (Fischle et al., 2005, Hirota et al., 2005) so alteration of chromatin regulation signalling after Barasertib is consistent with known AURKB functions. Chromatin regulation pathways could also include DNA-binding proteins involved in DNA repair. The inclusion of microtubule cytoskeleton organization is more surprising. Whilst AURKB is not closely linked to spindle formation, AURKB does alter MT depolymerisation such as via KifA to detach MTs from KTs during metaphase (Borah and Reddy, 2021).

Signalling by Rho GTPases was the second most significant cluster (LogP=-7.274). This protein family affect a range of cellular processes by regulating cytoskeletal and cell adhesion (Hodge and Ridley, 2016). AURKB is known to phosphorylate the Rho

protein including Racgap1 (MgcRacGAP) which has roles in cytokinesis and has been identified as a potential kinase to additional Rho GTPase substrates through phosphoproteomic analyses (Rouillard, 2016, Minoshima et al., 2003). Therefore, this finding aligns with existing literature supporting AURKB as a key regulator of Rho proteins.

DNA repair (LogP=-4.957) and regulation of DNA metabolic process (LogP=-5.612) were in the top 20 clusters. There were general DNA repair terms within the clusters as well as specific processes such as G_2/M transition, G_1/S transition and positive regulation of double-strand break repair. AURKBi by Barasertib was shown to increase H2AX foci and to slow resolution of foci after IR (Fell et al., 2016, Niermann et al., 2011), but there is little knowledge of how AURKB inhibition affects DNA repair. AURKB can affect the G_1/S transition by negative regulation of p53. Additional interactions with cell cycle arrest effectors such as Chk1 in other contexts (replication) the G_1/S and G_2/M pathways are also known.

Additional clusters in RNA metabolism (LogP= -7.109) and ncRNA processing (LogP=-4.142) suggest Barasertib may affect transcription and translation. AURKB is known to alter the activity of several transcription factors so this is likely due to that activity.

4.2.3.2. DMSO vs IR (Metascape)

For the 1131 differentially-abundant phosphopeptides between DMSO and IR conditions, there were 662 unique master proteins. The top 20 most-significant clusters from the enrichment analysis were ranked by Log (p-value) (Fig 4.3 B) and displayed in network format (Fig 4.4 B)

Pathway enrichment analysis of DMSO vs IR conditions yielded enrichment pathways with more significant p-value range than Unt vs Barasertib, likely due to the increased number of differentially abundant peptides in this comparison.

The top 20 clusters contain many terms related to the DDR such as cell cycle response (Hallmark E2F targets (LogP=-48.840), cell cycle (LogP= -44.153), regulation of cell cycle process (LogP=-35.449), cell cycle checkpoint (LogP=-23.292)), mitotic regulation (chromosome organization (LogP=-43.364) and regulation of chromosome organisation (LogP=-27.564)) and DNA repair (DNA metabolic process (LogP=-47.321), regulation of DNA metabolic process (LogP=-30.917), DNA replication (LogP=-20.967)), as well as general stress pathways (cellular responses to stress (LogP=-25.801), response to radiation (LogP=-17.006)). Within the DNA metabolic process cluster, the terms DNA Repair, double-strand break repair, DNA recombination, and double-strand break repair via homologous recombination were enriched. These enrichment terms represent expected changes after 4 Gy i.e. phosphorylation in cell cycle, DDR and DNA repair pathways is altered to respond to IR-induced damage.

The enrichment in several RNA processing terms suggests translational or transcriptional changes in response to IR. These include metabolism of RNA (LogP=-38.056), mRNA splice site recognition (LogP=-35.449), SUMO E3 ligases SUMOylate target proteins (LogP=-20.082), regulation of mRNA metabolic process (LogP= -17.0871), and ncRNA metabolic process (LogP= -16.5752).

4.2.3.3. IR vs Combination (Barasertib + IR) (Metascape)

For the 714 differentially abundant phosphopeptides between IR and Barasertib + IR conditions, there were 438 unique master proteins. The top 20 most-significant clusters from the enrichment analysis were ranked by Log(p-value) (Fig 4.3 C) and displayed in network format (Fig 4.4 C).

The most significantly enriched cluster was metabolism of RNA (LogP=-25.499). Other clusters related to transcription and translation such as regulation of mRNA metabolic process (LogP=-16.709), regulation of translation (LogP=-10.105), and regulation of mRNA processing were enriched (LogP=-10.024). This

DNA damage related terms were significantly enriched including DNA damage response (LogP=-19.791) and regulation of DNA metabolic process (LogP=-13.850). The latter cluster contained specific enriched terms which provide more information on specific DDR pathways. These included DSBR, and DSBR via non-homologous end-joining (NHEJ).

The cluster regulation of cell cycle process (LogP = -12.453) covers a broader range of cell cycle response pathways which overlap with DDR pathways. ATM and ATR signalling pathways were enriched. NHEJ, homology-directed repair and G_2/M checkpoint regulation-related pathways are also enriched. These results show that Barasertib may alter signalling in key DNA damage signal transduction and repair pathways. An effect on G_2/M arrest could have implications for survival after IR.

Other cell cycle pathways were also enriched; Cell cycle (LogP=-13.561) and mitotic cell cycle (LogP=-14.543) were present as clusters. The subterms under cell cycle mainly related to mitosis and include prometaphase, metaphase and anaphase

specifically. Cell cycle checkpoints and cellular responses to stress were also included as sub-terms.

These results indicate that Barasertib alters mitotic phosphorylation signalling. While these experiment was conducted 1 Hr after IR when cell cycle arrest in underway, the altered mitotic signalling by Barasertib here and vs DMSO are likely to transfer to mitotic processes later in the response. For example, this may increase aberrance when the G_2/M checkpoint is released and cells enter mitosis.

Within the mitotic cell cycle cluster, there is further specificity. Chromosome segregation, organelle fission, spindle organisation and nuclear division pathways were enriched. AURKB is a key player in regulating chromosome segregation and is essential for metaphase-anaphase transition so these pathways reflect known roles. AURKA, rather than AURKB, is involved in mitotic spindle regulation so it is interesting to see several mitotic spindle pathways altered Barasertib + IR and IR alone (Galetta and Cortes-Dericks, 2020).

Looking beyond DDR and cell cycle, the apoptotic execution phase pathway was enriched (LogP=-11.056). Another cluster, the regulation of cellular catabolic process (LogP=-15.021) was enriched and included several terms related to autophagy. These pathways suggests that Barasertib may affect death signalling in the immediate IR response.

4.2.3.4. IR vs Combination (Barasertib + IR) (DAVID)

To further investigate the pathways represented by the differentially abundant phosphopeptides between IR and Barasertib + IR conditions, DAVID Bioinformatics Functional Annotation was used, specifically by KEGG pathways (Table 4.4) This in-

depth analysis was carried out for the Barasertib + IR vs IR as this was the most important comparison for insights into how Barasertib promotes radiosensitisation. KEGG pathways provides pathway enrichment analysis with signalling pathway visualisation. This allowed us to identify signalling cascades with multiple hits in a row, and provided more insight than Metascape into the relationship between proteins in one pathway.

The same master proteins list was analysed by DAVID which found 15 KEGG charts with significant pathway enrichment. 5 of the pathways were overlapping: longevity regulating pathway (Fig 4.5), longevity regulating pathway - multiple species, cellular senescence, MTOR signalling pathway, and autophagy - animal (Appendix Figure 7 A-D). These pathway charts show similar signalling pathways with 4/5 pathways containing the following proteins from our master protein list: Akt2, MTOR, TSC2, AKT1S1 and EIF4EBP1. This pathway is linked to autophagy, senescence and longevity.

The phosphopeptide from MTOR contained one phosphorylation at Ser2448. This is a well-documented PTM known to positively regulate MTOR activity (Rosner et al., 2010, Phosphosite, 2023). Barasertib treatment after IR led to a decrease in pMTOR (s2448) abundance relative to IR alone, which could indicate decreased MTOR activity. This phosphorylation is targetable by rapamycin. Due to the biological importance and targetability of this PTM, MTOR was chosen as protein of interest within the longevity pathway and will be investigated later in this chapter.

Category	Term	Count	%	PValue	List Total	Pop Hits	Pop Total	Fold Enrichment	Bonferroni	Benjamini	FDR
KEGG_PATHWAY	hsa04211:Longevity regulating pathway	10	2.22	1.08E-04	185	89	8644	5.2499	0.0239	0.0241	0.0239
KEGG_PATHWAY	hsa03250:Viral life cycle - HIV-1	8	1.78	3.57E-04	185	63	8644	5.9332	0.0766	0.0398	0.0395
KEGG_PATHWAY	hsa04213:Longevity regulating pathway - multiple species	7	1.56	0.00180265	185	61	8644	5.3618	0.3313	0.1225	0.1214
KEGG_PATHWAY	hsa03040:Spliceosome	13	2.89	0.002198	185	216	8644	2.8121	0.3878	0.1225	0.1214
KEGG_PATHWAY	hsa03013:Nucleocytoplasmic transport	8	1.78	0.0080963	185	108	8644	3.4611	0.8368	0.3611	0.3579
KEGG_PATHWAY	remodeling	8	1.78	0.01228914	185	117	8644	3.1948	0.9365	0.4501	0.4461
KEGG_PATHWAY	hsa05211:Renal cell carcinoma	6	1.33	0.0155125	185	69	8644	4.0630	0.9694	0.4501	0.4461
KEGG_PATHWAY	hsa04150:mTOR signaling pathway	9	2.00	0.0181672	185	156	8644	2.6956	0.9832	0.4501	0.4461
KEGG_PATHWAY	hsa04218:Cellular senescence	9	2.00	0.0181672	185	156	8644	2.6956	0.9832	0.4501	0.4461
KEGG_PATHWAY	hsa04140:Autophagy - animal	9	2.00	0.02450535	185	165	8644	2.5486	0.9960	0.5441	0.5393
KEGG_PATHWAY	hsa04910:Insulin signaling pathway	8	1.78	0.02684087	185	137	8644	2.7284	0.9977	0.5441	0.5393
KEGG_PATHWAY	hsa05131:Shigellosis	11	2.44	0.03799676	185	247	8644	2.0808	0.9998	0.7061	0.6998
KEGG_PATHWAY	hsa04152:AMPK signaling pathway	7	1.56	0.04419026	185	121	8644	2.7031	1.0000	0.7580	0.7512
KEGG_PATHWAY	hsa05165:Human papillomavirus infection	13	2.89	0.04998533	185	331	8644	1.8351	1.0000	0.7962	0.7891
KEGG_PATHWAY	hsa03015:mRNA surveillance pathway	6	1.33	0.05564567	185	97	8644	2.8902	1.0000	0.8273	0.8198

Table 4. 4: KEGG pathway (on DAVID Bioinformatics Functional Annotation) analysis of differentially abundant phosphopeptides (master proteins) between 4 Gy and combination conditions

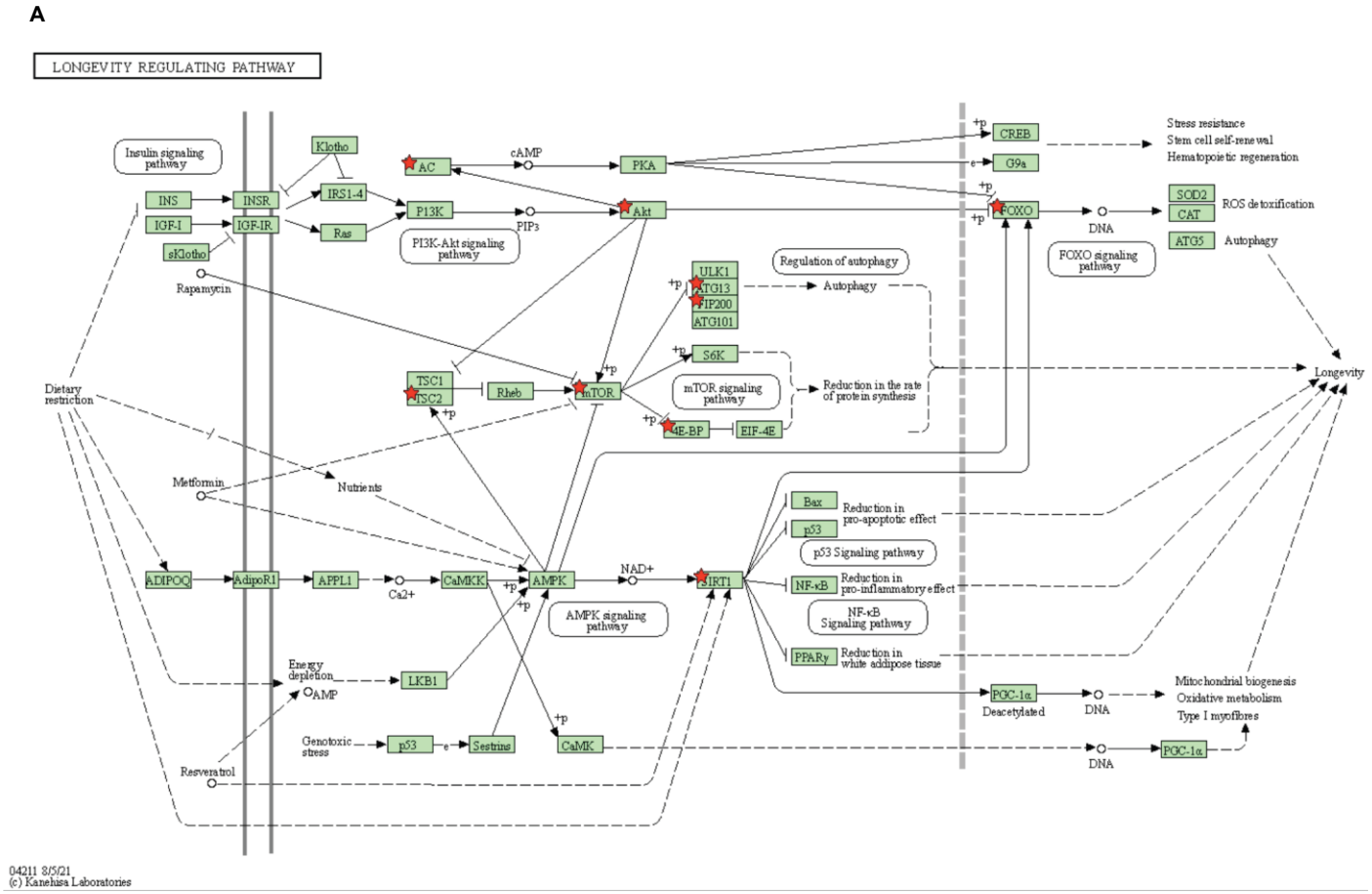

Figure 4. 5: KEGG pathway Charts for analysis of differentially abundant phosphopeptides between 4 Gy and 4 Gy + 50 nM Barasertib conditions

Pathway Analysis was carried out on DAVID Bioinformatics Functional Annotation. The following pathways were generated by KEGG pathway chart function: **A** Longevity regulating pathway. This gene enrichment uses Fisher's Exact test to calculate p-value with a threshold of $p<0.01$. Benjamini-Hochberyu analysis used the linear step-up method. The threshold of minimum gene counts for enrichment is 2.

4.3. Pathway Enrichment Analysis of Differentially Abundant Proteins after IR and Barasertib in Non-Enriched Samples

We also used MS/MS to analyse total protein samples that were not enriched for phosphopeptides. For each sample, a small fraction was removed prior to TiO_2 phosphopeptide enrichment, but was prepared identically to the phospho-enriched sample otherwise. Due to the smaller volume of these samples, the sample complexity was reduced. We used the relative abundance of master protein in these samples rather than peptide isoform, as PTM analysis was not carried out for this MS/MS analysis.

The differentially abundant proteins were identified by fold change of >20% and p-value <0.05, and $\log_2$(Fold change) and $-\log_{10}$(p-value) were plotted for each comparison (Fig 4.6 A-D). There were fewer differentially abundant peptides in this dataset for all conditions (Table 4.1). The number was especially low for comparisons with the DMSO condition. In contrast there were 350 differentially abundant peptides between IR and IR + Barasertib conditions.

To explain why there are more differentially abundant proteins in the IR vs IR + Barasertib comparison than any other comparison, we must consider the skewed ness of the data sets. The volcano plot for IR vs DMSO shows a skewing towards negative fold change (Fig 4.6 B). The opposite is true in the volcano plot for IR + Barasertib vs DMSO (Fig 4.6 C), whereby, there is more of a skewing towards a positive fold change. Most of these abundance changes aren't significant compared to the DMSO sample, but because of the skewedness in opposite directions, when compared to each other, a larger fold change will result. Interestingly comparing IR +

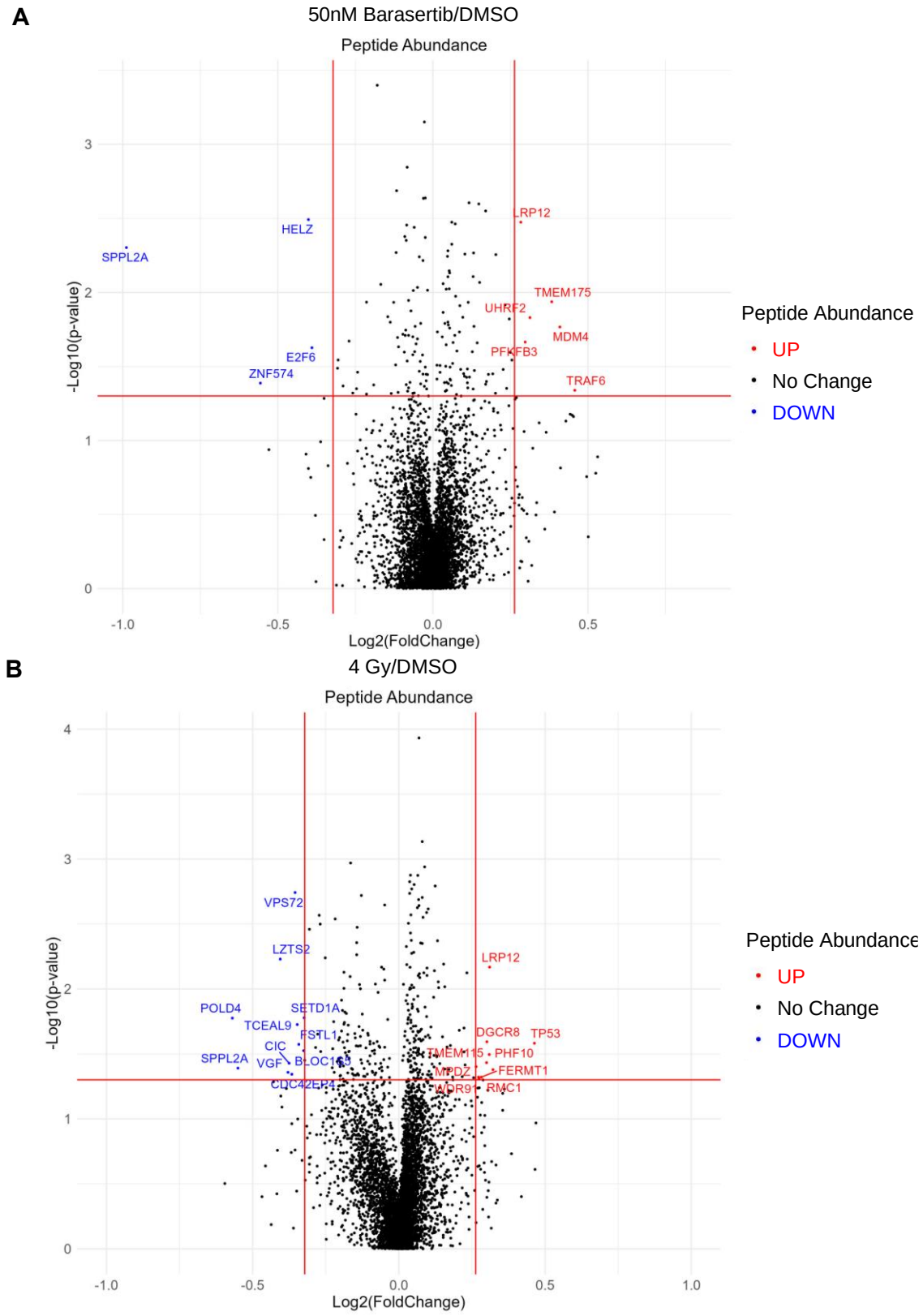

Figure 4.6: Relative abundance of proteins between untreated, Barasertib, 4 Gy and 4 Gy + 50 nM Barasertib Conditions in non-enriched samples (H460 Cells)

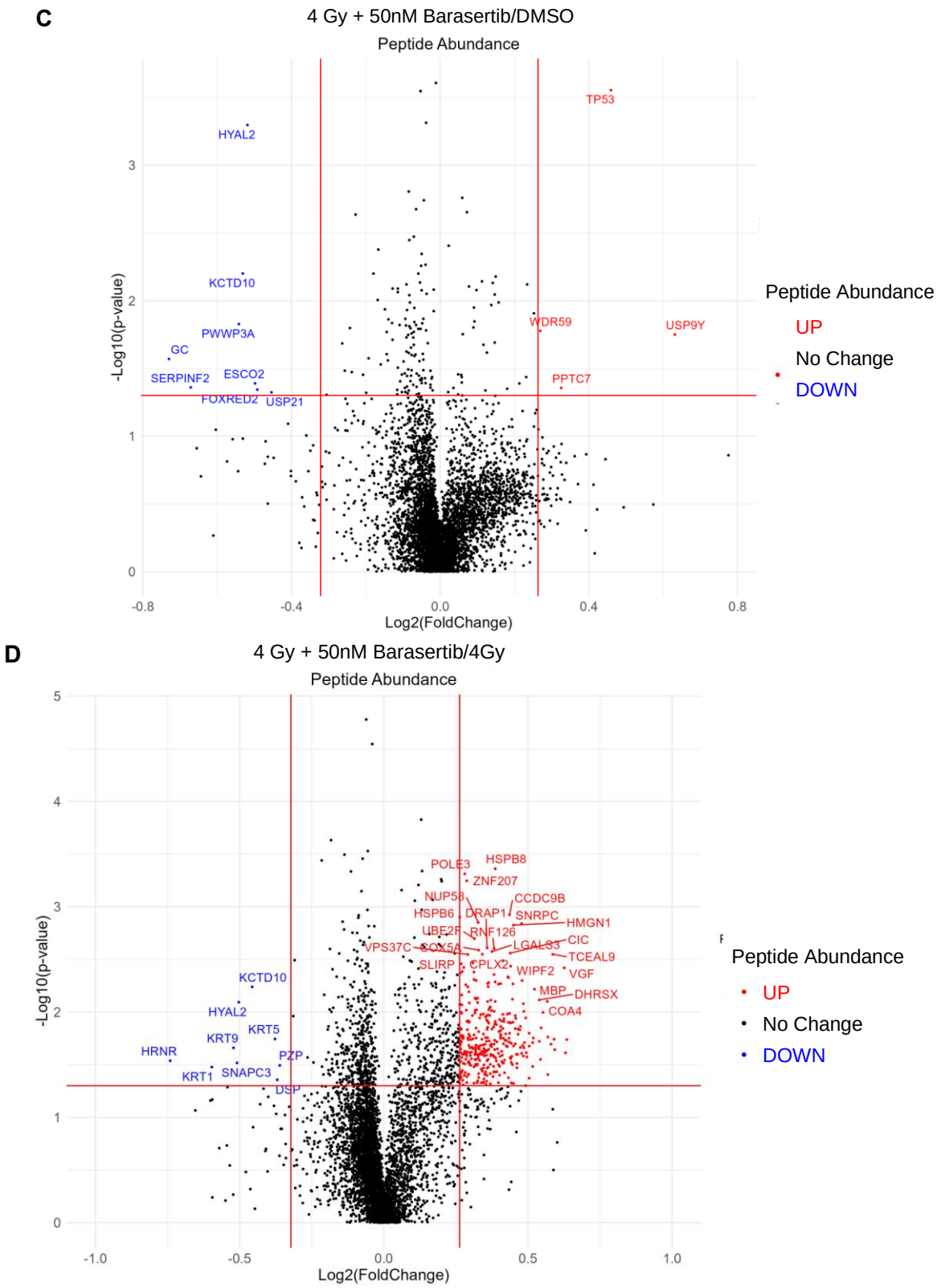

Figure 4.6: Relative abundance of proteins between Untreated, Barasertib, 4 Gy and 4 Gy + 50 nM Barasertib Conditions in non-enriched samples (H460 Cells)

Figure 4. 6: Relative abundance of proteins between untreated, Barasertib, 4 Gy and 4 Gy + 50 nM Barasertib conditions in non-enriched samples (H460 Cells)

Volcano plots of Log(2)(Fold change) vs –Log(10)(p-value) for relative abundance. **A** 50 nM Barasertib/Untreated, **B** 4 Gy IR/Untreated, **C** Combination/Untreated, **D** Combination/4 Gy (overleaf). Red lines indicate upper and lower thresholds for fold change (0.8 and 1.2) and p-value threshold (0.05). Red and blue points indicate peptide with significant increase or decrease in relative abundance between conditions, respectively (labelled as UP or DOWN). P-values calculated by one-way ANOVA (only calculated for peptides quantified in ≥3 repeats). Plots produced in R. Gene Symbols displayed for the master protein of the relevant peptide. Labels arranged using the GGRepel function.

Pathway enrichment analysis (Metascape) was only performed for IR + Barasertib to IR due to the low number of differentially abundant peptides in the other comparisons

Barasertib to IR most changes were increases in relative abundance, suggesting Barasertib suppresses IR induced changes in protein abundance (Fig 4.7 A and B). Increased and decreased changes were grouped due to the low number of changes. Full Metascape enrichment analysis results for the Barasertib experiment can be accessed here.

The most significantly enriched cluster was metabolism of RNA (LogP= -22.725). Additional clusters in regulation of RNA splicing (LogP= -6.605) and mRNA processing (LogP= -6.596) were also enriched (Appendix Table 4). This echoes what we saw in the phosphopeptide results, as several RNA processes were also enriched.

Mitotic regulation was also altered, shown by the clusters mitotic cell cycle process (LogP= -11.835) and cell cycle, mitotic (LogP=-6.142). The subterms of these

clusters mostly covered chromosome segregation and the metaphase-anaphase transition.

Regulation of DNA metabolic process was enriched and included subterms related to DNA repair and chromatin organisation.

There were enriched pathways here that weren't present in the corresponding phosphopeptide pathway analysis. These include HALLMARK MYC TARGETS V1 (LogP=-9.689) and VEGFA VEGFR2 signalling (LogP=-7.408).

Overall, the pathway enrichment shows some similarity to the phosphopeptide analysis. RNA regulation, mitotic regulation and DNA metabolism were enriched. Given the small size of the dataset, the enrichment of other pathways not seen in the phosphopeptide analysis may not be reliable.

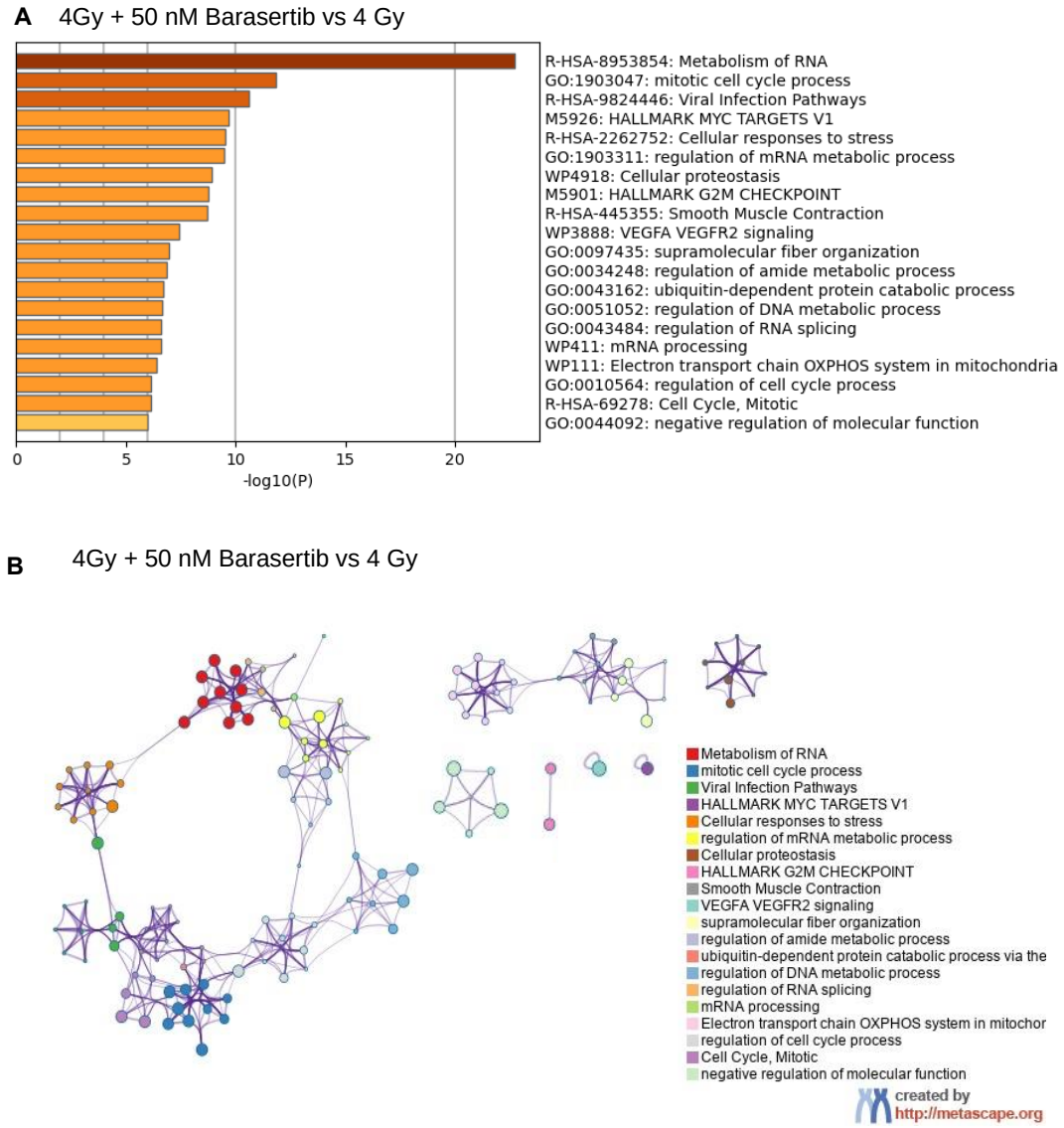

Figure 4. 7: Top 20 enriched pathway clusters generated by Metascape pathway analysis for total protein changes after Barasertib and IR

Pathway & Process Enrichment Analysis was carried out on Metascape.com using differentially abundant proteins between Barasertib + 4Gy and 4 Gy conditions. Enrichment was analysed for all available pathway genelists using the Custom Analysis mode. Enrichment is calculated as terms with a p-value< 0.01, count of 3 or more and enrichment factor >1.5. Cumulative hypergeometric distribution was used for p-value calculation and q-values were calculated via Benjamini-Hochberg procedure. To perform hierarchial clustering in terms, enriched terms with Kappa similarity scores > 3 are clustered and are represented by the most significant term as a Cluster summary term. **A** Top 20 enriched cluster summary terms are displayed with – Log(10)(p-value). **B** Network visualisations were generated for a subset of terms within the top 20 clusters for the same comparison as A. Each circular node represents a specific term, coloured according to cluster and labelled by its cluster summary term. The size of the circular node is proportional to the number of input genes within that term. The edges link terms with similarity score > 0.3 (thickness proportional to score).

4.4. Investigation of MTOR Ser 2448 after IR and Barasertib Treatment in H460 Cells

In our phospho-proteomic analysis after Barasertib and IR, we found that the longevity pathway encompassing Akt/MTOR signalling was significantly altered, with multiple hits in interactors of MTOR, up- and downstream. MTOR has been extensively studied due to its roles in proliferation, senescence, autophagy and apoptosis. Due to these roles and its activation in many tumours, it has attracted attention as a therapeutic target in cancer (Zou et al., 2020, Cayo et al., 2021). Given the change in cell death and senescence shown in Chapter 3, we wondered if MTOR signalling was involved.

4.4.1. MTOR Ser2448 Phosphorylation

An MTOR peptide with phosphorylation at Ser 2448 was detected in the phospho-MS/MS analysis. The relative abundance was found to be significantly decreased in the Barasertib + IR condition compared to 4 Gy at 1 Hr post-IR ($p=0.02$) (Fig 4.8 A). The abundance of the total protein was similar across conditions, with no significant change between IR alone and the Barasertib + IR treatment (Fig 4.8 B).

To validate the change in phosphorylation, western blotting of pMTOR (Ser2448) and total MTOR was carried out. H460 cells were treated with DMSO or 50 nM Barasertib plus sham IR or 6 Gy. In addition, a 10 Gy control was included. Lysates were collected 6 Hr after IR. An additional control with the MTOR inhibitor 100 nM Rapamycin was collected 7 Hr after treatment. The proteomics samples were collected 1 Hr after IR treatment. A later timepoint and increased radiation dose was chosen to allow time for an increased response that could be detected by western

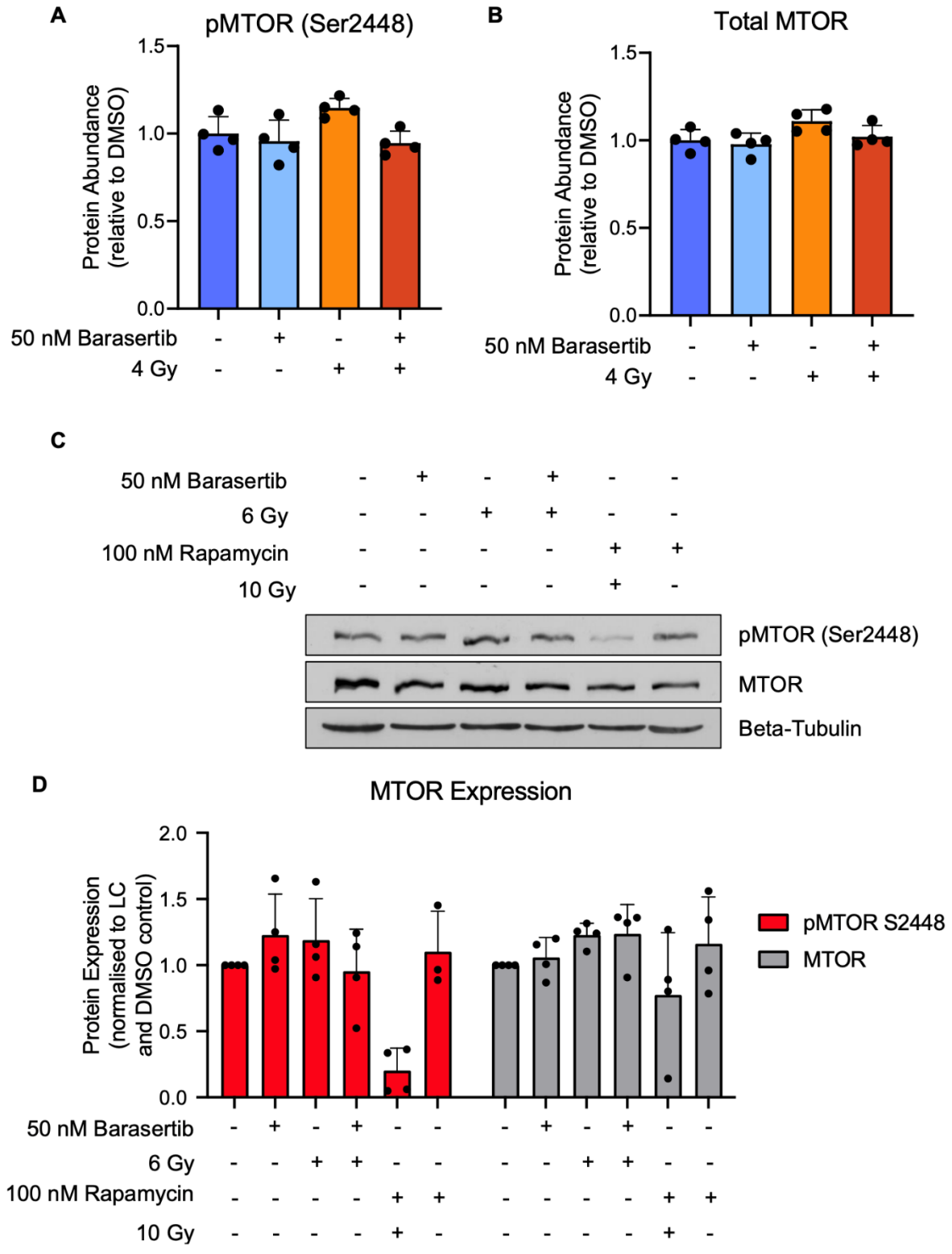

Figure 4.8: Phospho-MTOR Ser2448 expression by phosphoproteomics and western blotting

Figure 4. 8: Phospho-MTOR Ser2448 expression by phosphoproteomics and western blotting

A Relative abundance (to DMSO control) of a phosphopeptide isoform of MTOR with a phosphorylation at Ser2448 detected by phospho-MS in phospho-enriched samples treated with Barasertib and IR. **B** Relative abundance (to DMSO control) of MTOR protein in non-enriched samples by MS/MS. **C and D** Western blot and corresponding densitometry of pMTOR Ser2448 and total MTOR (plus Beta-tubulin loading control) in H460 cells treated with 1 Hr treated treatment of Barasertib or DMSO before IR, then collected after 6 Hr. H40 cells were also collected after 7 Hr Rapamycin treatment and 6 Hr after 10 Gy IR. Mean and standard deviation are shown for 4 independent repeats.

blotting as separate studies performed by a masters student had failed to detect any changes at 1 Hr post-IR.

100 nM Rapamycin inhibited pMTOR (Ser2448) and inhibited total MTOR levels in one out of four repeats, demonstrating that the phospho-antibody was reporting pMTOR (ser2448) and that in H460 cells there is endogenous mTOR activity (Fig 4.8 C). 50 nM Barasertib induced little change in pMTOR or MTOR levels, similar to the mass-spec results. However, despite widely reported activation of MTOR's downstream substrates by IR, we failed to detect any activation of pMTOR with either 6 Gy or 10 Gy IR. Attempts to detect this activation at other time points also failed (studies by a Masters student in Bryant lab). Similarly, in the Barasertib + IR treatment, there was no consistent change in pMTOR or total MTOR levels, compared to DMSO or the IR control (Fig 4.8 B).

The reduction in pMTOR Ser2448 detected in the mass spectrometry was a small change. While small changes in phosphorylation can have significant effects on signalling, such changes are difficult to confirm by western blot and ultimately this was not detected in the western blot. The error rates inherent in densitometry analysis further complicated this issue.

4.5. Proteomic Analysis after IR and Alisertib Treatment in H460 Cells

4.5.1. MS/MS and Identification of Differentially Abundant Peptides

To investigate phosphorylation signalling after 25 nM Alisertib and IR, mass spectrometry analysis of H460 cells was carried out similarly to the Barasertib experiment. Cells were pretreated with DMSO or 25 nM Alisertib for 1hr then treated with 4 Gy IR. Cells were then harvested with trypsin, then flash frozen to preserve phosphorylated peptides. The MS/MS workflow was identical for the Barasertib and Alisertib experiment, except that erroneously none of the peptide sample was saved before phosphopeptide enrichment (Figure 4.9). This meant that total protein abundance could not be analysed for the Alisertib and IR samples.

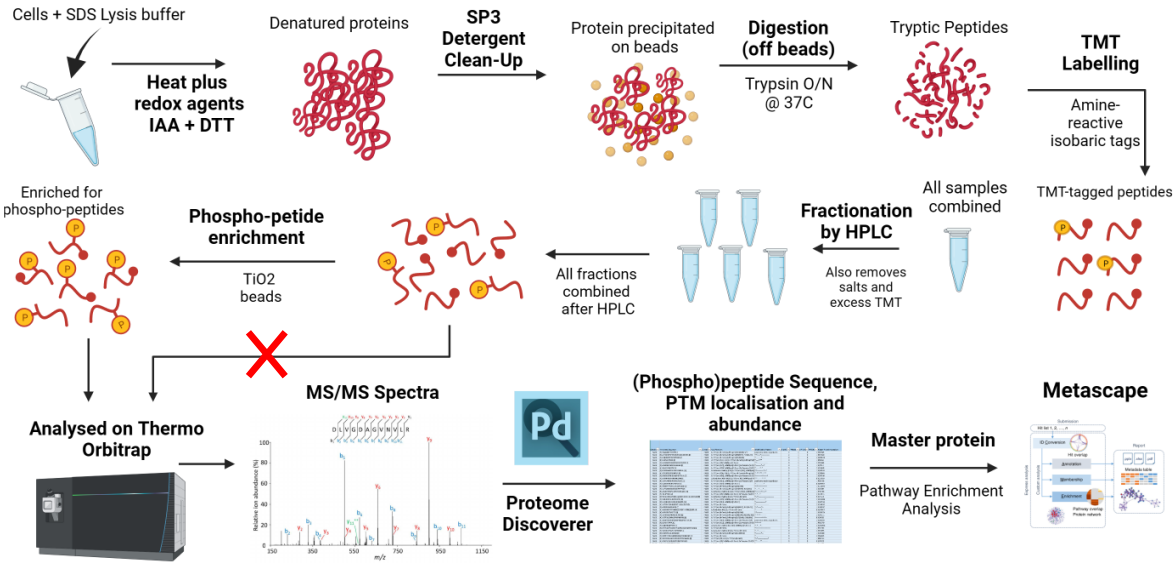

Figure 4. 9: Work flow of MS/MS protocol for Alisertib and IR treated cells

Cells were lysed in SDS lysis buffer then heated with IAA and DTT to aid denaturation. To remove salts, the sample underwent SP3 bead clean up after which protein was digested with trypsin into peptides. TMT labelling was carried out and all samples were combined. HPLC fractionation was performed to desalt and remove unbound TMTs. The peptide sample underwent phosphopeptide enrichment using TiO2 beads (Erroneously, 10% sample was not removed before phospho-peptide enrichment). Peptide analysis was performed by LC-MS/MS on a thermo orbitrap. The MS/MS spectra was analysed using Proteome Discoverer (2.4) to determine peptide sequence (MASCOT was used for master protein determination).

Table 4. 5: The number of peptides discovered per Alisertib/IR MS/MS experiment and the filtering process

	Alisertib Phospho-Enriched Samples
All isoforms	25,099
Phosphopeptides	15,360
No Contaminant	15,336
Quantified peptides	12,617
Altered Abundance (FC >20%, p-value < 0.05)	
DMSO vs Alisertib	197
DMSO vs 4 Gy	1440
DMSO vs 4 Gy + 25 nM Alisertib	1607
4 Gy vs 4 Gy + 25 nM Alisertib	229

In the phosphopeptide enriched sample, 25,099 peptides were identified. Within these, there were 15,360 phosphopeptides. Peptides with contaminants and unquantified peptides were filtered out and 12,617 remaining phosphopeptides were retained for analysis (Table 4.5).

4.5.2. Identification of Differentially Abundant Phosphopeptides after IR and Alisertib

Similar to the Barasertib experiment, the phosphopeptides were filtered by p-value (<0.05) and fold change thresholds (Fold change >20%). Phosphopeptides with altered abundance were identified between DMSO vs Alisertib (197 peptides), DMSO vs 4Gy (1440 peptides), DMSO vs IR + 25 nM Alisertib and IR vs IR + 25 nM Alisertib (229 peptides) (Table 4.5).

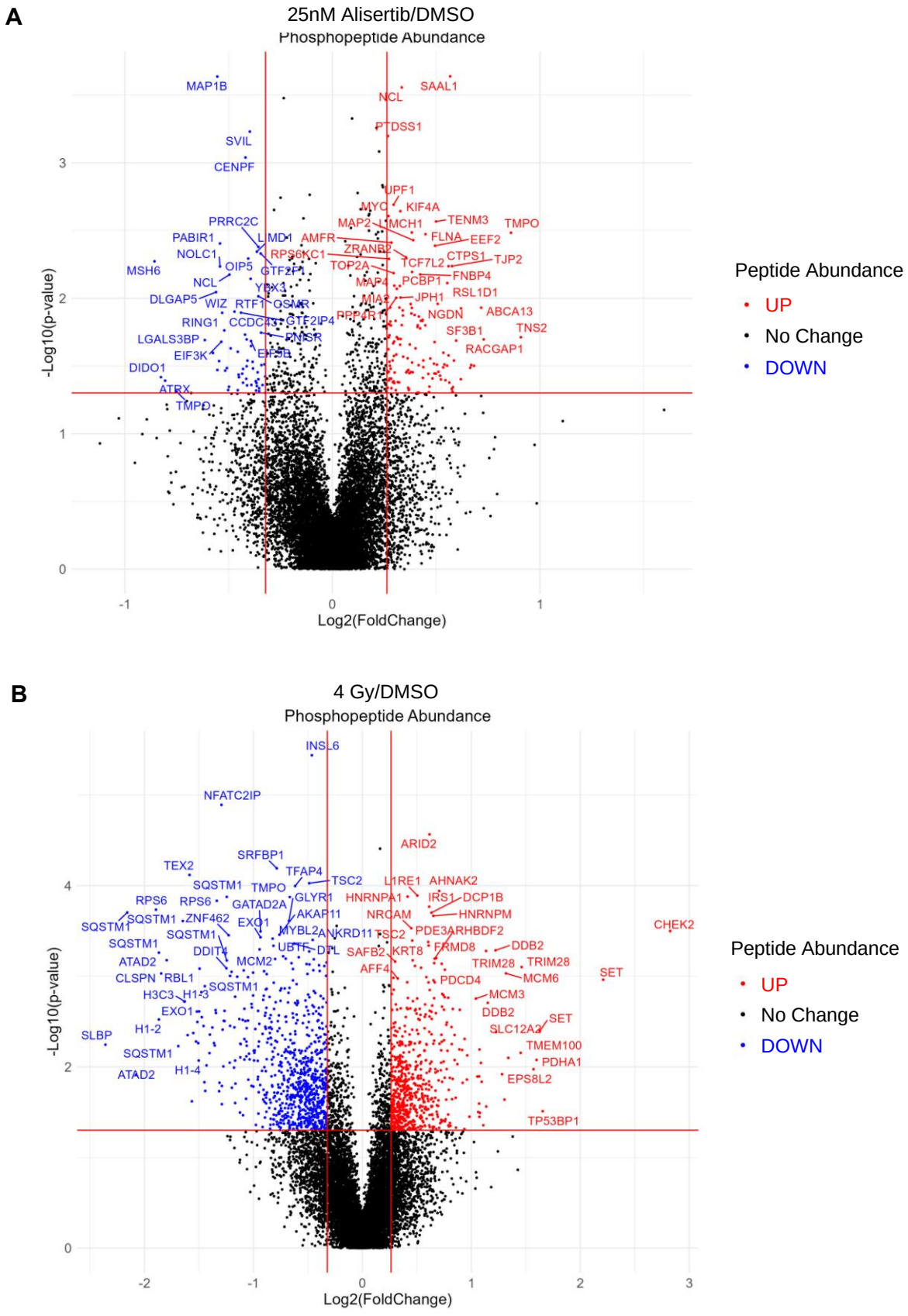

Figure 4.10: Relative abundance of phosphopeptides between untreated, Alisertib, 4 Gy and 4 Gy + Alisertib combination conditions in H460 cells

C

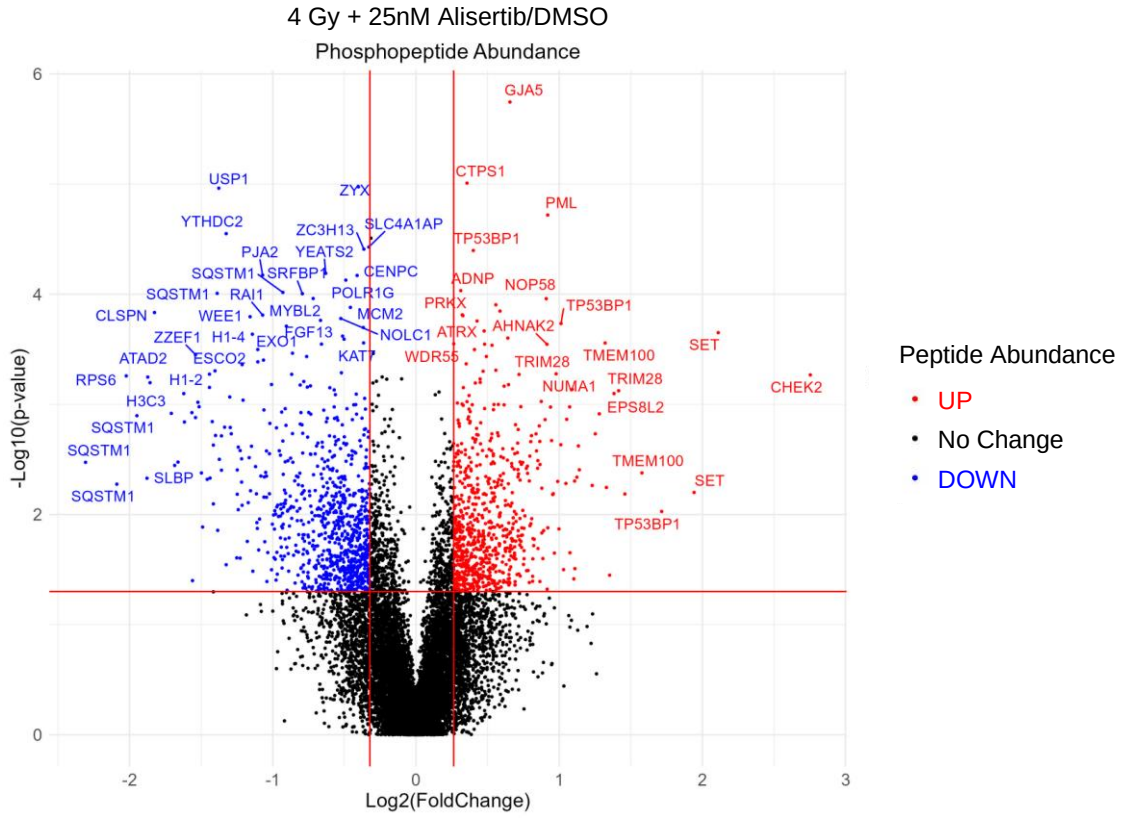

D

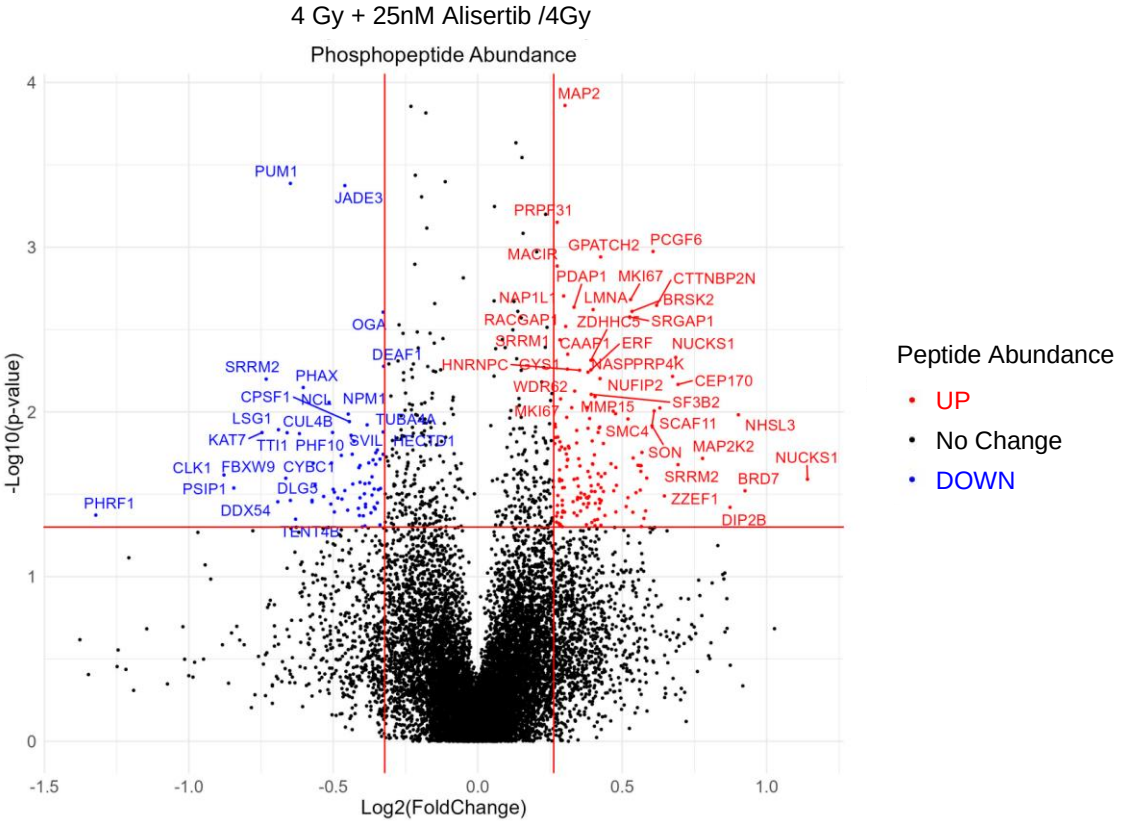

Figure 4.10: Relative abundance of phosphopeptides between untreated, Alisertib, 4 Gy and 4 Gy + Alisertib combination conditions in H460 cells

Figure 4. 10: Relative abundance of phosphopeptides between untreated, Alisertib, 4 Gy and 4 Gy + Alisertib combination conditions in H460 cells

Volcano plots of Log(2)(Fold change) vs –Log(10)(p-value) for relative abundance. **A** 25 nM Alisertib compared to Untreated, **B** 4 Gy IR compared to Untreated, **C** 4 Gy + 25 nM Alisertib compared to Untreated and **D** 4 Gy + 25 nM Alisertib compared to 4 Gy. Red lines indicate upper and lower thresholds for fold change (0.8 and 1.2) and p-value threshold (0.05). Red and blue points indicate peptide with significant increase or decrease in relative abundance between conditions respectively (labelled as UP or DOWN). P-values calculated by one-way ANOVA (only calculated for peptides quantified in ≥3 repeats). Plots produced in R. Gene Symbols displayed for the master protein of the depicted phosphopeptide. Labels arranged using the GGRepel function.

The $\log_2$(Fold change) and -$\log_{10}$(p-value) were plotted for each comparison (Figure 4.10 A-D). Again, the IR vs DMSO comparison yielded the most differentially abundant peptides of the 4 comparisons.

4.5.3. Pathway Enrichment Analysis of Phosphorylation Changes after IR and Alisertib

Similarly to the Barasertib and IR analysis, Metascape pathway enrichment analysis was used to identify which biological pathways were enriched in the differentially abundant peptides. Pathway enrichment analysis was carried out for the following comparisons: DMSO vs Alisertib (197 peptides), DMSO vs 4Gy (1440 peptides), and IR vs IR + 25 nM Alisertib (229 peptides). Full Metascape enrichment results for the Alisertib experiment can be accessed here.

4.5.4. DMSO vs 25 nM Alisertib (Metascape)

For the 197 differentially abundant phosphopeptides between DMSO and 25 nM Alisertib samples, there were 176 unique master proteins. The 20 top clusters from the enrichment analysis are displayed in Figure 4.11 A and as a network diagram in Figure 4.12 A. The most significantly enriched cluster was Hallmark G2M checkpoint pathway (LogP= -14.487). Within this cluster, HALLMARK MYC TARGETS V1 was enriched and the Myc master protein was included in this list, suggesting that Alisertib treatment augments phosphorylation in the Myc pathway from upstream of Myc. Given the known links with Myc and AURKA provide validity for this. The phosphosite on the Myc phosphopeptide could not be identified but sat between 157-166 in the amino acid sequence. There are 5 known phosphorylations in this region, although none are known to occur downstream of AURKA (Phosphosite, 2024).

Additional cell cycle related clusters were also enriched including regulation of cell cycle process (LogP=-9.301) and cell cycle (LogP =-6.883). A chromosome organisation cluster was enriched (LogP= -7.553) with enriched subterms relating to

A 25 nM Alisertib vs DMSO

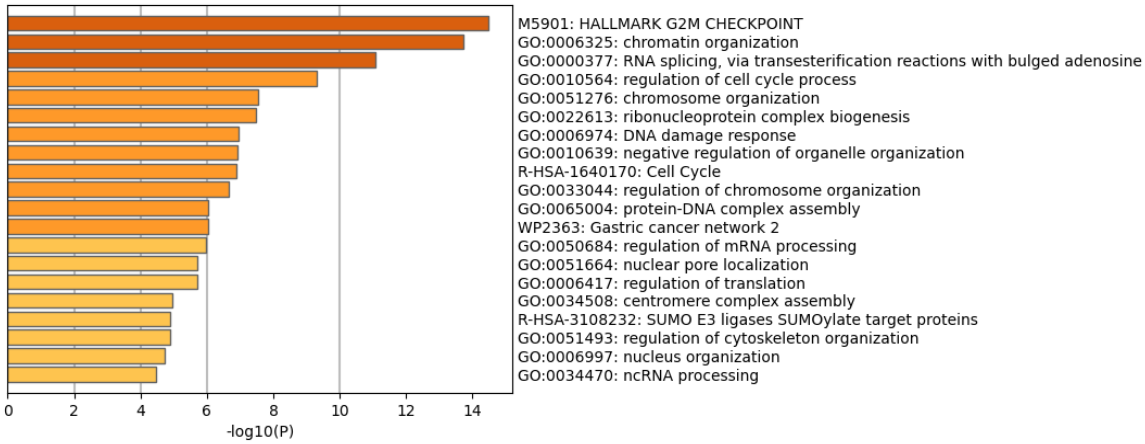

B 4 Gy vs DMSO

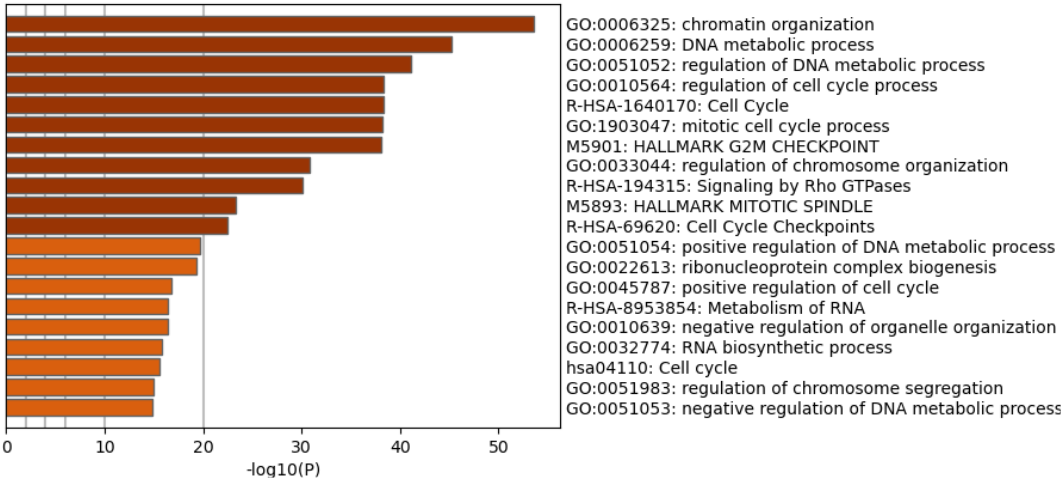

C 25 nM Alisertib + 4 Gy vs 4 Gy

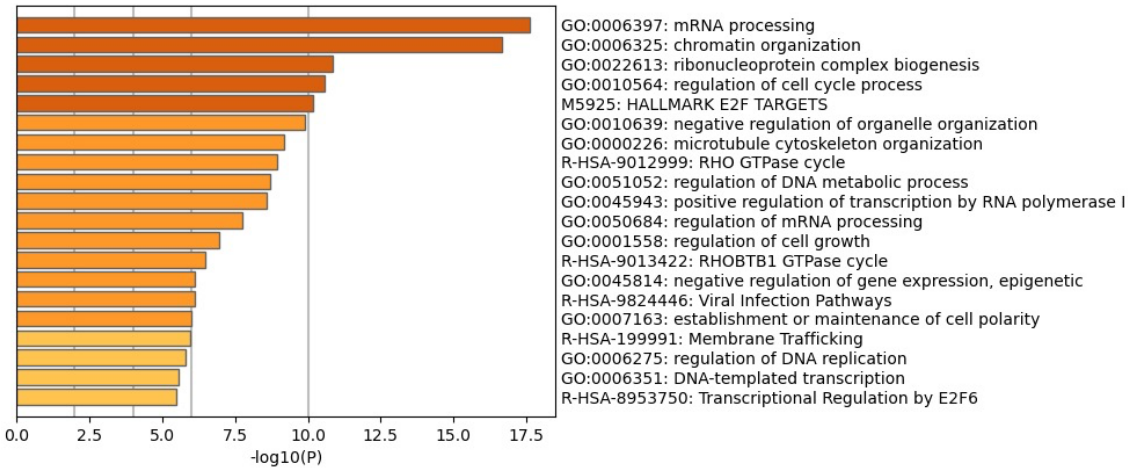

Figure 4. 11: Top 20 Enriched Pathway Clusters generated by Metascape pathway analysis for phosphopeptide changes after IR and Alisertib

Figure 4.11 : Top 20 Enriched Pathway Clusters generated by Metascape pathway analysis for phosphopeptide changes after IR and Alisertib

Pathway & Process Enrichment Analysis was carried out on Metascape.com using the list of differentially abundant phosphopeptides per comparison. Enrichment was analysed for all available pathway genelists using the Custom Analysis mode. Enrichment is calculated as terms with a p-value< 0.01, count of 3 or more and enrichment factor >1.5. Cumulative hypergeometric distribution was used for p-value calculation and q-values were calculated via Benjamini-Hochberg procedure. To perform hierarchial clustering in terms, enriched terms with Kappa similarity scores > 3 are clustered and are represented by the most significant term as a Cluster summary term. Cluster summary terms are displayed with – Log(10)(p-value) for the following comparisons **A** 25 nM Alisertib vs Untreated, **B** 4 Gy vs Untreated, and **C** 4 Gy + 25 nM Alisertib vs 4 Gy.

mitotic cell cycle, chromosome separation and organelle organisation. These clusters cover the known functions of AURKA, namely G_2/M transition and mitotic spindle organisation and KT-MT Attachment.

Several clusters related to RNA processing, ribonucleoprotein complex biogenesis (LogP=-7.467), regulation of mRNA processing (LogP=-5.957) and ncRNA processing (LogP=-4.460) were also enriched.

A DNA damage response cluster was enriched (LogP=-6.955) and included subterms related to DNA metabolic process and DNA repair (DSB and HR). AURKA has been reported to negatively regulate DNA repair proteins BRCA1, BRCA2, 53BP1 and RAD51, so there are existing links to DSBR.

4.5.5. DMSO vs IR (Metascape)

For the 1440 differentially abundant phosphopeptides between DMSO and 25 nM Alisertib samples, there were 887 unique master proteins. The 20 top clusters from

A 25 nM Alisertib vs DMSO

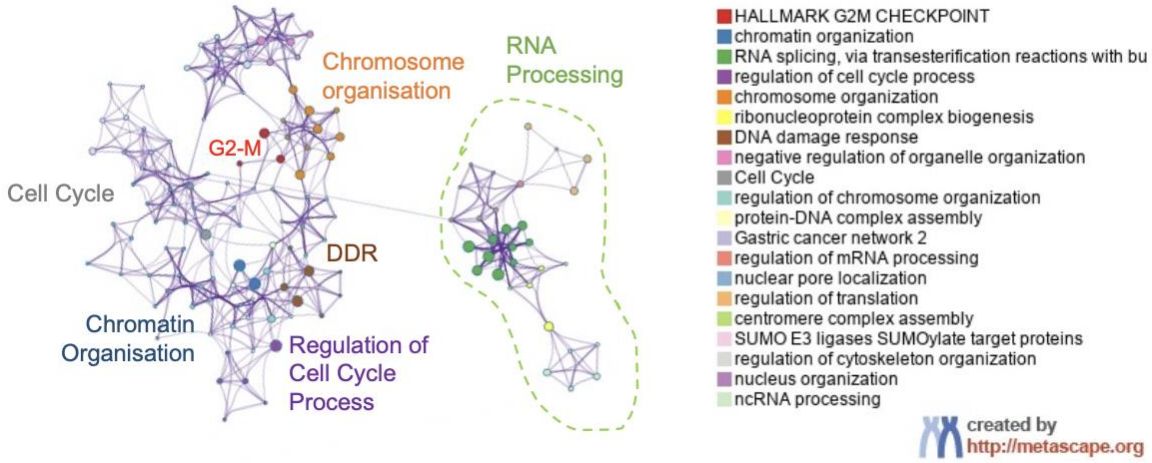

B 4 Gy vs DMSO

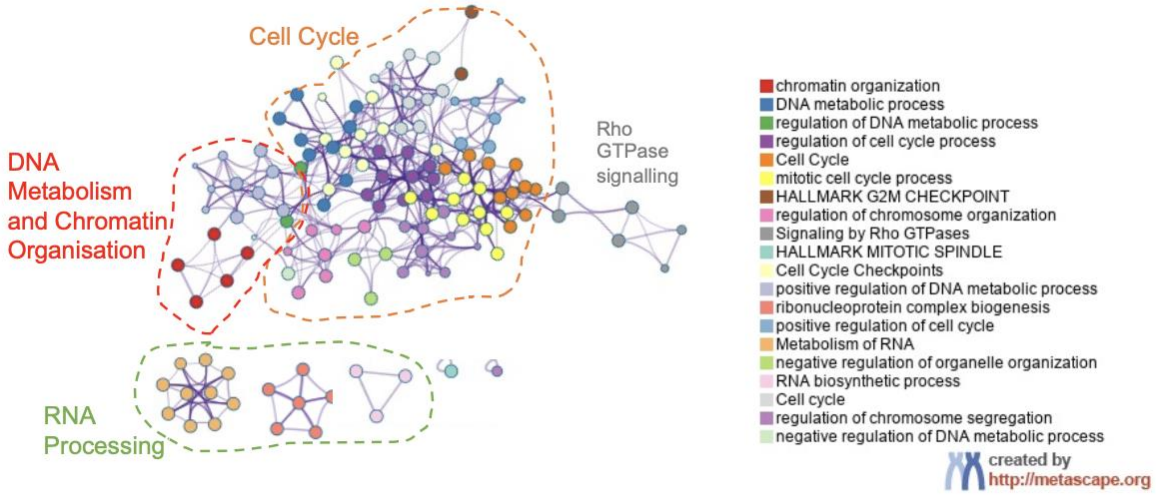

C 25 nM Alisertib + 4 Gy vs 4 Gy

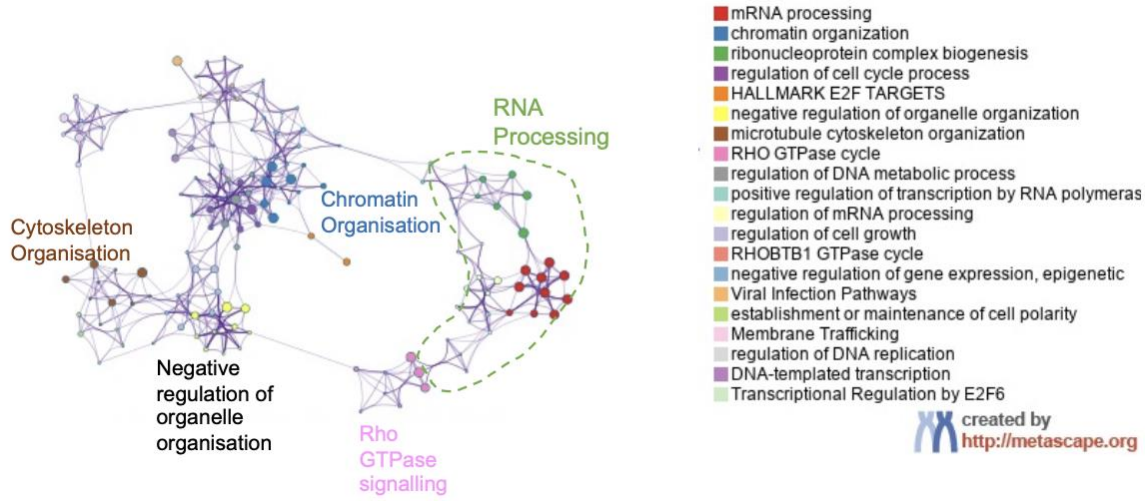

Figure 4. 12: Top 20 enriched pathway clusters generated by Metascape pathway analysis for phosphopeptide changes after IR and Alisertib

Figure 4.12: Top 20 enriched pathway clusters generated by Metascape pathway analysis for phosphopeptide changes after IR and Alisertib

Further visualization of Pathway & Process Enrichment Analysis was carried out on Metascape.com using the list of differentially abundant phosphopeptides per comparison. Enrichment was analysed and terms clustered as described in Figure 4.3. Network visualisations were generated for the a subset of terms within the top 20 clusters per comparison. A 25 nM Alisertib vs Untreated, B 4 Gy vs Untreated, and C 25 nM Alisertib + 4 Gy vs 4 Gy. Each circular node represents a specific term, coloured according to cluster and labelled by its cluster summary term. The size of the circular node is proportional to the number of input genes within that term. The edges link terms with similarity score > 0.3 (thickness proportional to score). Dotted lines were drawn around clusters with overlapping biological function (drawn in powerpoint). Further visualization of Pathway & Process Enrichment Analysis was carried out on Metascape.com using the list of differentially abundant phosphopeptides per comparison. Enrichment was analysed and terms clustered as described in Figure 4.3. Network visualisations were generated for the a subset of terms within the top 20 clusters per comparison. **A** 25 nM Alisertib vs Untreated, **B** 4 Gy vs Untreated, and **C** 25 nM Alisertib + 4 Gy vs 4 Gy. Each circular node represents a specific term, coloured according to cluster and labelled by its cluster summary term. The size of the circular node is proportional to the number of input genes within that term. The edges link terms with similarity score > 0.3 (thickness proportional to score). Dotted lines were drawn around clusters with overlapping biological function (drawn in powerpoint).

the enrichment analysis is displayed in Figure 4.11 B and as a network diagram in Figure 4.12 B.

The clusters shown represent pathways expected to be altered by radiation. Chromatin organisation (LogP=-53.621), DNA metabolic process (LogP=-45.202), regulation of DNA metabolic process (LogP=-41.079), positive regulation of metabolic process (LogP=-19.644) and negative regulation of DNA metabolic process (LogP=-14.787) were altered. These represent DNA regulation most likely related to DNA repair.

Additionally, many cell cycle related pathways were enriched. This included regulation of cell cycle process (LogP=-38.383), Cell cycle (R-HAS-1640170) (LogP=-38.2784), G_2M checkpoint (LogP=-38.034), Cell cycle checkpoints (LogP=-

22.455), positive regulation of cell cycle (LogP==16.764), Cell cycle (hsa04110) (LogP=-15.577).

Additionally, many mitotic process pathways were altered. Mitotic cell cycle process (LogP=-38.242), regulation of chromosome organisation (LogP=-30.872), Hallmark mitotic spindle (LogP=-23.329) and regulation of chromosome segregation (LogP=-14.947) pathways were altered. Mitosis is a DNA damage sensitise phase and DNA damage can activate mitotic DDR signalling and the SAC after chromosomal damage.

4.5.6. IR vs Combination (Alisertib + IR) (Metascape)

There were 229 differentially abundant phosphopeptides between the IR alone condition and the combination condition of 4Gy and 25 nM Alisertib. Of these, there were 198 unique master proteins. The 20 top clusters of the enrichment analysis are displayed in Figure 4.11 C and as a network diagram in Figure 4.12 C.

Enrichment analysis showed that pathways involved in DNA regulation following IR were altered by the addition of Alisertib. Chromatin organisation was enriched (LogP=-16.672), as was regulation of DNA metabolic process (LogP=-8.695). These pathways contained subterms related to DDR, DNA repair and DSBR. There was also enrichment in regulation of DNA replication (LogP=-5.805). These pathways warrant investigation into AURKA's role in the DDR.

There was also enrichment in ribonucleoprotein complex biogenesis (LogP=-10.868), regulation of mRNA processing (LogP=-7.752), regulation of mRNA processing (LogP=-7.75174) and DNA-templated transcription (LogP=-5.567), suggesting augmentation of RNA processing and transcription.

There was enrichment in cell cycle related pathways including regulation of cell cycle process (LogP=-10.576) and hallmark E2F targets (LogP=-10.176), transcriptional Regulation by E2F6 (LogP=-5.503), RHO GTPase cycle (LogP=-8.94432). This suggests that Alisertib can alter cell cycle signalling after IR. While these clusters contained some mitosis-related subterms, but there were no mitosis-related clusters.

Pathways involved in organisation of the cell were enriched, including as negative regulation of organelle organization (LogP=-9.894) and microtubule cytoskeleton organization (LogP=-9.179). These pathways may be related to AURKA's spindle regulatory functions (Du et al., 2021). The regulation of cytoskeleton organisation was also enriched in the DMSO vs Alisertib alone comparison so this process appears to be reliably altered by Alisertib.

4.6. Discussion

In this chapter, we analysed the phosphoproteomic changes in H460 cells after IR and AURK inhibition by the AURKB inhibitor Barasertib and the AURKA inhibitor Alisertib. We performed Metascape pathway enrichment analysis on the differentially abundant peptides between DMSO and IR, DMSO and AURK inhibitors and between IR and combination treatments for each inhibitor.

After IR, the presence of Barasertib led to altered phosphorylation of proteins in the DDR, chromatin regulation and cell cycle pathways whilst the presence of Alisertib led to altered phosphorylation of proteins in cytoskeletal organisation, RNA processing, organelle organisation, DNA metabolism and chromatin organisation.

Proteomic Analysis of Barasertib and IR Treatment

The DMSO vs Barasertib comparison allowed us to examine what pathways Barasertib affected in non-irradiated cells. This highlighted expected biological functions as well as areas of potential interest. DNA repair and the cell cycle checkpoint pathways. AURKB has been linked to DNA repair but it is interesting to see these pathways implicated after Barasertib alone with no DNA damaging agent and a short treatment duration of 2 Hr (Ma and Poon, 2020). Many DDR proteins have functions in mitosis regulating spindle formation, the SAC, chromosome segregation and cytokinesis, and AURKB is known to phosphorylate ATM (Ser1403) during mitosis (Petsalaki and Zachos, 2020). Additionally, AURKB negatively regulates the DDR proteins p53 and BRCA2 (Wang et al., 2014, Sagulenko et al., 2007). Therefore, that DDR pathways may be enriched due to altered signalling in a mitotic context. Our results also suggest possible changes to checkpoint regulation.

AURKB's regulation of p53 could affect downstream checkpoint regulation (Wu et al., 2011a, Wu et al., 2011b, Harris and Levine, 2005).

When we analysed the changes between DMSO and IR, most of the enriched pathways were characteristic DDR processes. This included DNA repair, cell cycle regulation and chromatin regulation. 1 Hr after IR, the cell cycle checkpoint will be activated and many DDR response proteins will be highly active in response to DNA breaks (Maréchal and Zou, 2013, Poon, 2016, Podhorecka et al., 2010). Therefore, altered phosphorylation in these pathways at our timepoint concurs with current understanding of the DDR.

Overall, when we analysed the effect of Barasertib or IR alone the expected biologicals pathways were shown, increasing our confidence in pathway enrichment analysis.

The pathway enrichment analysis for changes between 4Gy and the Barasertib + IR conditions was the most important for our investigation of radiosensitisation by Barasertib. Many of the pathways shown covered the cell cycle. Cell cycle control is a key process that allows cells to prevent further damage in replication or mitosis, and allows time for repair. If and how they are affected by Barasertib needs to be determined to fully understand the biological significance. Also, at 1 Hr, AURKB is partially inhibited by IR (shown in Chapter 3). Therefore, Barasertib's effect on the cell cycle, for example checkpoint release or mitotic progression, may be more pertinent at later timepoints when the cell cycle is not arrested.

We did find enrichment in DDR pathways related to DNA repair. At 1 Hr after IR, changes to DNA repair regulation could lead to increases DNA damage-related

toxicity. The appearance of HR and NHEJ pathways appeared within this cluster provides further specificity. NHEJ recruitment (Ku70) is rapid while RAD51 starts between 30 minutes - 1hr and peaks at 3 Hr after DNA damage (Kim et al., 2005). Our results indicate altered regulation of NHEJ pathways at 1 Hr, at which point the pathway should be highly active (Marková et al., 2007). Therefore, this pathway is of interest. Homologous recombination repairs DNA more slowly but this pathway could also be affected by Barasertib (Gravells et al., 2018). Any effects of Barasertib on HR are likely to persist as DDR by HR becomes more active. The enrichment of these pathways warrants investigation of DSBR kinetics after IR.

We also investigated the Akt/Mtor pathway which regulates longevity as activation can inhibit autophagy and promote senescence (Heras-Sandoval et al., 2014, El Maï et al., 2020). This pathway peaked our interest as it has the potential to influence post-IR survival. However, we could not confirm these changes by western blotting of pMTOR.

We also analysed pathway enrichment in the non-enriched samples (i.e. total protein). This was a smaller dataset and there were fewer differentially abundant peptides in DMSO vs IR and DMSO vs Barasertib comparisons. The range of fold changes was also smaller than that of the phosphopeptide relative abundances. This may be due to differing speed of regulation; phosphorylation can happen more rapidly than upregulation of protein expression (refs).

There were over 300 differentially abundant peptides between IR and Barasertib + IR conditions. Why there were so many seems to be due to the direction of change in peptide level in the IR and Barasertib + IR samples. These trends could be result of technical error, such as the IR sample being more dilute than the Barasertib + IR

sample but this is unlikely across 4 repeats. If it is a biological effect, it could represent downregulation of expression or upregulation of degradation in IR alone condition, which is reversed when Barasertib is present. The specificity of the enriched terms in the pathway analysis suggests that effect is potentially biological.

We consistently found RNA processing pathways in our analyses. The enrichment of such terms indicates a change to pathways regulating transcription or translation. RNA-seq analysis would be required to investigate this fully. However, given the wide scope of RNA processing and the fact that transcriptional regulation is a critical regulatory mechanism, RNA processing is likely to appear in most pathway enrichment analyses.

Proteomic Analysis of Alisertib and IR Treatment

The effect of Alisertib in a non-irradiated and irradiated background on phosphorylation signalling was also studied. This follows on from work in the Bryant Lab by Thomas Jones. Due to time restraints exploration of the data and follow up experiments for the Alisertib analysis was limited. We found that Alisertib alone leads to altered phosphorylation signalling in cell cycle checkpoint, DNA damage and DNA metabolism pathways.

Analysis of altered pathways after IR vs DMSO in the Alisertib analysis revealed similar results to the IR vs DMSO analysis in the Barasertib cohort. Most of the top 20 enriched clusters included cell cycle, DDR, chromatin organisation and DNA metabolism. Comparing IR alone with IR and Alisertib, the enriched pathways were surprising. There were clusters relating to the cell cycle and DNA repair related terms but many cytoskeletal related and cellular organisation pathways, as well as

DNA metabolism and chromatin organisation pathways. Further exploration of this data would yield further insight into how Alisertib affects the immediate IR response.

Comparison with existing phosphoproteomic analysis

Kettenbach et al (2011) examined phosphoproteomic changes after Alisertib and Barasertib treatment in Hela cells (Kettenbach et al., 2011). Their analyses focused mainly on identifying direct substrates by phosphorylation motif and large decrease in phosphopeptide abundance under inhibitory conditions. They completed STRING analysis on a selection of high confidence predicted substates, which showed both AURKA and AURKB substrates in cell cycle regulation, RNA processing and splicing, and DNA damage repair, supporting our observations in similar pathways.

A key difference in their approach was the decision to use high concentration of Alisertib (5 µM) and Barasertib (1 µM) which provided stronger inhibition. Whilst Using a stronger dose in our study would have led to higher fold change in abundance, and we could have performed more rigorous analyses.

Strengths and limitations of proteomic analysis by mass spectrometry

Phospho-MS/MS is a valuable technique for understanding global signalling in biological samples due to the high output. Sample complexity, variation in ionisation efficiency and low abundance peptides limit full detection within samples (Liu et al., 2021). We addressed this by enriching the samples for phosphopeptides using a TiO_2 method (Thingholm and Larsen, 2016). Ionisation efficiency is determined by the chemical composition of a peptide but is improved by phosphorylation (Jalili et al., 2007). We employed a TMT (tandem mass tag) labelling system which increases

throughout, reduce technical variation and improves ionisation efficiency (Liu et al., 2021, Westbrook et al., 2015).

In the context of experimental design, another advantage of this technique is the unbiased approach. We chose the timepoint of 1 hour after IR and 2 hours after AURK inhibition (1 Hr pretreatment) for two reasons. Firstly, to increase kinase specificity and secondly, given the results from our drug-scheduling clonogenic experiment, we hypothesised that DDR may be involved in the mechanism. Many DDR phosphorylation events happen rapidly after IR, (Blackford and Jackson, 2017). Multiple timepoints would have provided more information about the later IR response but the experimental cost limited us to one timepoint.

We generated a large dataset of peptide isoforms for each MS/MS experiment. Due to the low threshold for phosphorylation changes to have biological significance, we decided to use standard p-value to prevent the more stringent adjusted p-value analysis from discarding phosphopeptides with small changes that we would consider biologically relevant. This decision means we couldn’t interpret biological events based on individual peptide isoforms but instead any concrete analysis must be based on multiple peptides.

The aim of pathway enrichment analysis was to aid selection pathways for further investigation. A limitation of pathway enrichment analysis is that such tools are built with whole protein or gene expression in mind, so some complexity is lost.. These phosphoproteomic experiments were planned to take place early in the PhD process (2020) to allow time for the follow-up of individual pathways. Due to Covid-19, the collaboration was delayed until 2 years into the project, which limited the time for follow-up.

Another limitation of pathway enrichment analysis is that proteins with multiple functions will promote enrichment of multiple pathways. This is pertinent given the enrichment of many cell cycle and DDR pathways. Therefore, there will be some unavoidable redundancy across pathways.

The strength of this data lies in the isolation of phosphorylated peptides. Phosphorylation plays a pivotal role in cell signalling and can change rapidly as cells undergo stress. Whole protein analysis is important for understanding signalling changes at an expression level but the function of many proteins in these pathways is linked to their phosphorylation. As phosphorylation is so intrinsic to the cell cycle and DDR pathways, the changes we see in phosphorylation site abundance and in whole pathway enrichment are indicative of real time signalling changes.

In conclusion, our phospho-proteomic analysis and pathway enrichment has highlighted several key pathways for further investigation in the effects of Barasertib and Alisertib after IR.

Chapter 5: Mechanistic Investigation of Radiosensitisation by Barasertib and IR

5. Mechanistic Investigation of Radiosensitisation by Barasertib and IR

5.1. Introduction, Hypothesis and Aims

AURKB is well known for its mitotic role, but emerging evidence in other cell cycle phases and pathways reveal many ways that AURKB could affect the radiation response. NSCLC lines H661 (p53 mut) and H460 (p53 wt) could be radiosensitised by Barasertib (AZD1152-HQPA). A mechanism based on abrogation of the spindle checkpoint resulting formation of polyploid cells was proposed (Sak et al., 2012). In colorectal cancer, HCT116 cells could be radiosensitised by Barasertib, but when p53 was knocked out (Tao et al., 2008). A mechanism dependant on G_2 checkpoint arrest or due to the role of p53 in preventing accumulation of damage by arresting cells with mitotic aberrance was proposed. Radiosensitisation by Barasertib was also studied in prostate cancer cell lines PC3 and DU145, where a polyploidy phenotype was also seen (Niermann et al., 2011). In addition, a reduction in the DDR after radiation was seen (as indicated by lack of resolution of via H2AX foci positive cells following IR).

Our phospho-proteomic analysis also gave a snapshot into phosphorylation signalling 1 Hr after IR. In our pathway enrichment analysis, many key processes known to be involved in radiation recovery were altered by Barasertib, such as the DDR, DSB repair mechanisms, cell cycle checkpoints and mitotic cell cycle pathways.

Considering these findings and known roles of AURKB, there were several areas of interest to us when considering mechanism of radiosensitisation by Barasertib. Firstly, does the cell cycle response change after IR when treated with Barasertib

i.e., are IR-induced checkpoints altered, and is polyploidy induced after IR. Secondly, how does Barasertib change mitotic processes after IR? Finally, are DDR signalling and DNA repair impeded after IR?

Our hypothesis is that Barasertib alters DNA damage response signalling after IR and/or impedes the cell cycle or mitosis to prevent repopulation after IR.

The aims of this chapter were as follows:

1. To investigate if Barasertib disrupts cell cycle progression after IR.
2. To investigate if Barasertib disrupts mitosis after IR.
3. To investigate if DNA repair after IR is affected by Barasertib.

5.2. Investigation of the Effects of Barasertib on Cell Cycle Progression

Due to the intrinsic regulation of the cell cycle within the DDR and the role of AURKB in mitosis, the cell cycle was of key interest while investigating the mechanism of radiosensitisation by Barasertib. To understand how Barasertib impacted cell cycle progression, we first investigated whether Barasertib treatment alone impacted progression, then investigated how the cell cycle response to IR was affected by Barasertib.

5.2.1. Barasertib Alone

To investigate the effect of Barasertib on cell cycle progression and polyploidy, flow cytometry analysis was performed to quantify G_1, S, G_2 phase, polyploid and Sub-G_1 cells as well as pH3+ (mitotic) cells (n=3 independent repeats) (Appendix Figure 8).

In the DMSO condition, the majority of H460 cells were in G_1 at all timepoints (Fig 29 A-C). There were small populations of polyploid and sub-G_1 cells in the DMSO condition which remained low in number (Fig 5.1 H and I).

After 50 nM Barasertib, there was no difference in cell cycle phase populations compared to the DMSO control (Fig 5.1 A-C), although 2/3 repeats had higher levels of mitotic cells at 24 and 48 Hr compared to DMSO control (Fig 5.1 G).

At 100 nM Barasertib, most phases showed similar population percentages as the DMSO control (Fig 5.1 A-C), except for a small increase in mitotic populations at 24 and 48 Hr ($p= 0.0605$ (ns) at 24 Hr) (Fig 5.1 G) and increased polyploidy at 48 Hr ($p = 0.0313$) (Fig 5.1 H).

At 200 nM Barasertib, no changes were seen at 2 Hr but there was a significant increase in polyploid cells at 24 Hr and 48 Hr compared to the DMSO control ($p<0.0001$ (both)) (Fig 5.1 H), characteristic of AURKB inhibition. There were corresponding decreases in G_1 populations at 24 and 48 Hr ($p=0.0007$ and $p=0.0015$, respectively) (Fig 5.1 D) and in S phase populations at 24 Hr ($p=0.0077$) (all compared to the DMSO control) (Fig 5.1 E) There was an increase in G_2 cells at 24 hours compared to the DMSO control ($p=0.0260$) (Fig 5.1 F), which could represent cells stalled in G_2 or tetraploid G_1 cells (4N).

Overall, there was little change in cell cycle phase distribution and polyploidy after treatment with Barasertib at 50nM and 100 nM. At 200 nM, Barasertib treatment caused an increase in polyploid cells after 24 Hr.

At lower Barasertib doses, there were increases in mitotic populations. Although these were not significant, there was a weak trend of increasing mitotic population with Barasertib concentration at 24 Hr. This effect continued to 48 Hr in 2/3 repeats.

Figure 5. 1: Cell cycle analysis in H460 cells after 50-200 nM Barasertib treatment

H460 cells were treated with DMSO or 5—200 nM Barasertib for 2 – 48 Hr, then fixed and stained for DNA content (PI) and phospho-Histone 3 (ser10) and analysed by Flow cytometry. **A** 2 Hr treatment **B** 24 Hr Treatment **C** 48 Hr Treatment and phases are shown independently **D** G1, **E** S phase, **F** G2, **G** Mitotic cells, **H** Polyploid cells, and **I** Sub-G1 cells. Mean and standard error of the mean are shown (plus individual repeats for F-K). P-values were calculated using an ordinary one-way ANOVA per timepoint (* = $p < 0.05$, ** = $p < 0.01$, *** = $p<0.001$. **** = $p<0.0001$).

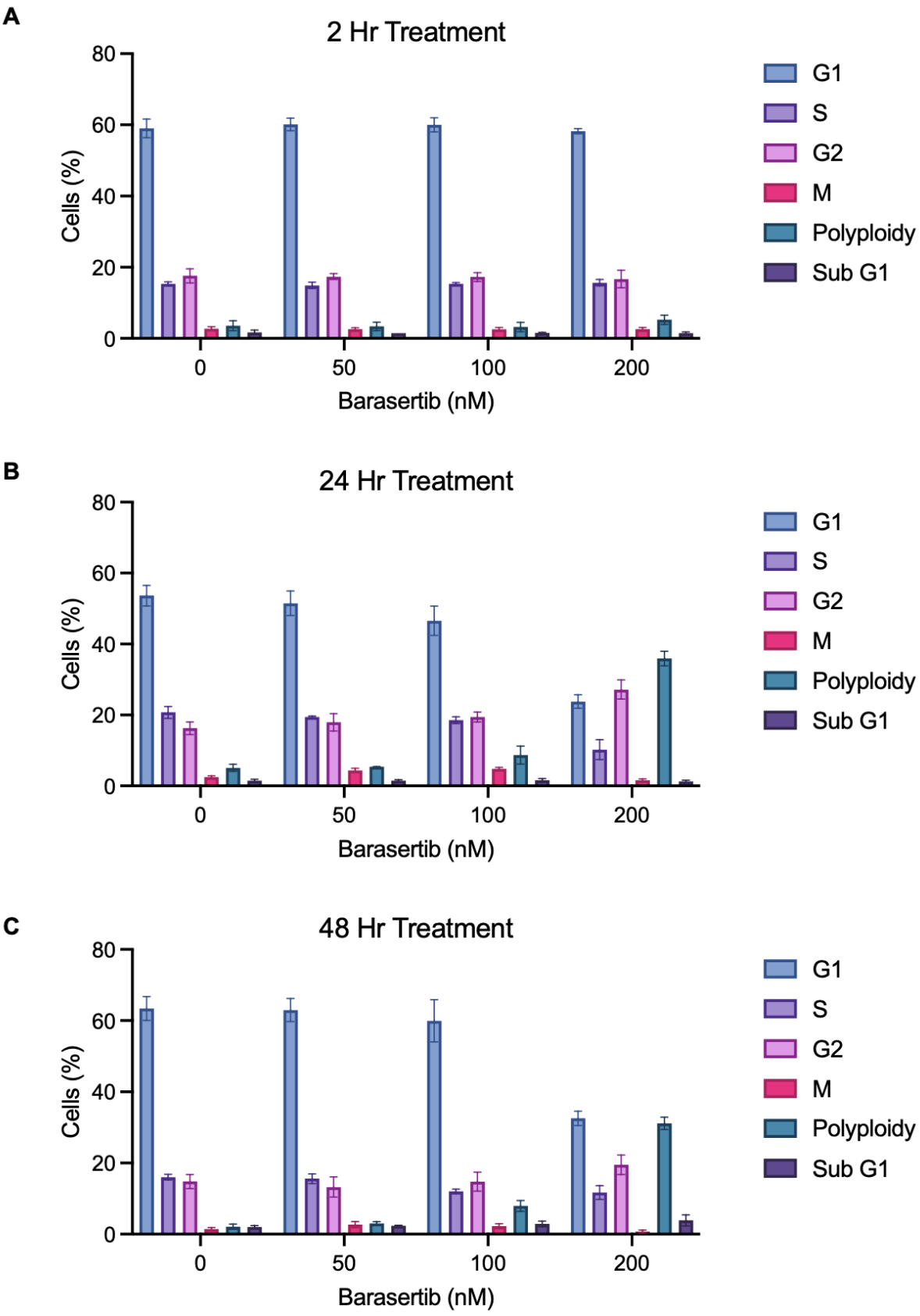

Figure 5.1: Cell cycle analysis in H460 cells after 50-200 nM Barasertib treatment

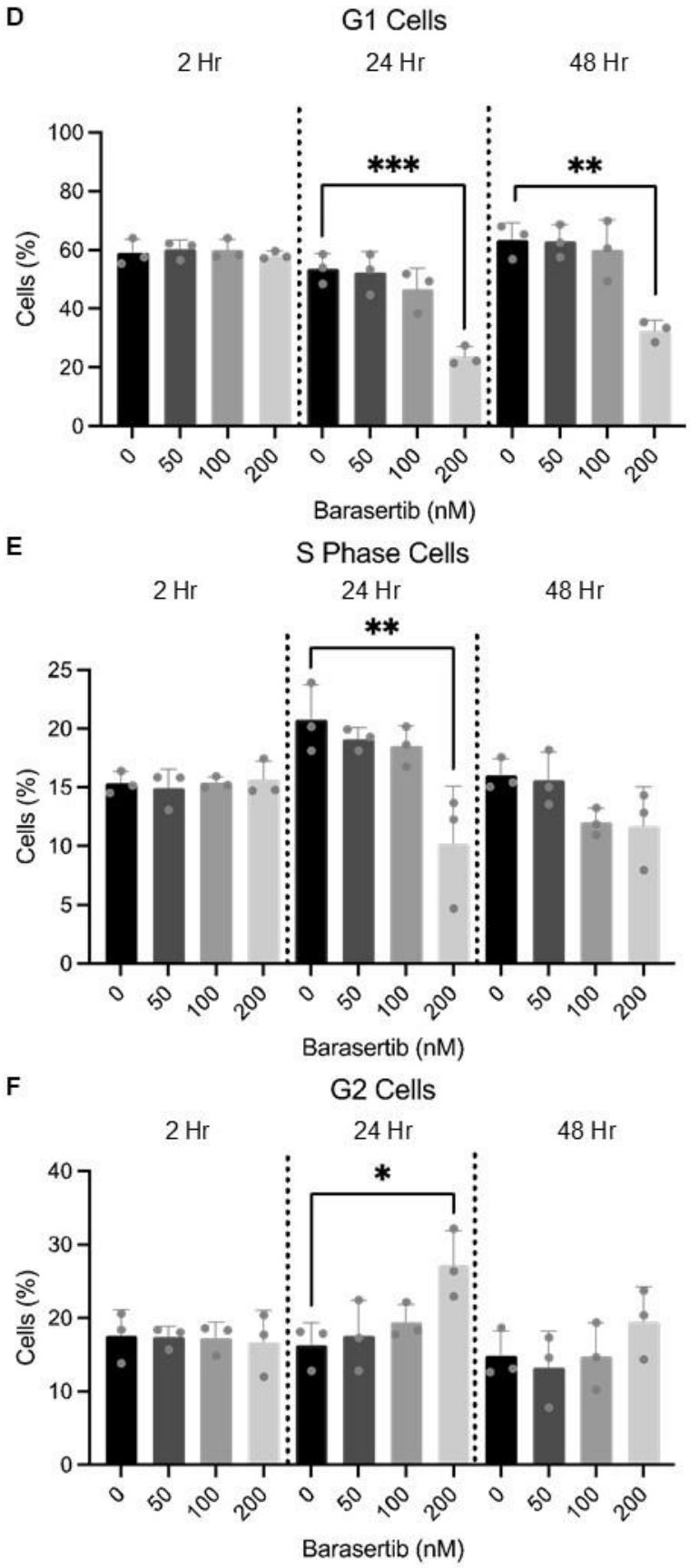

Figure 5.1: Cell cycle analysis in H460 cells after 50-200 nM Barasertib treatment

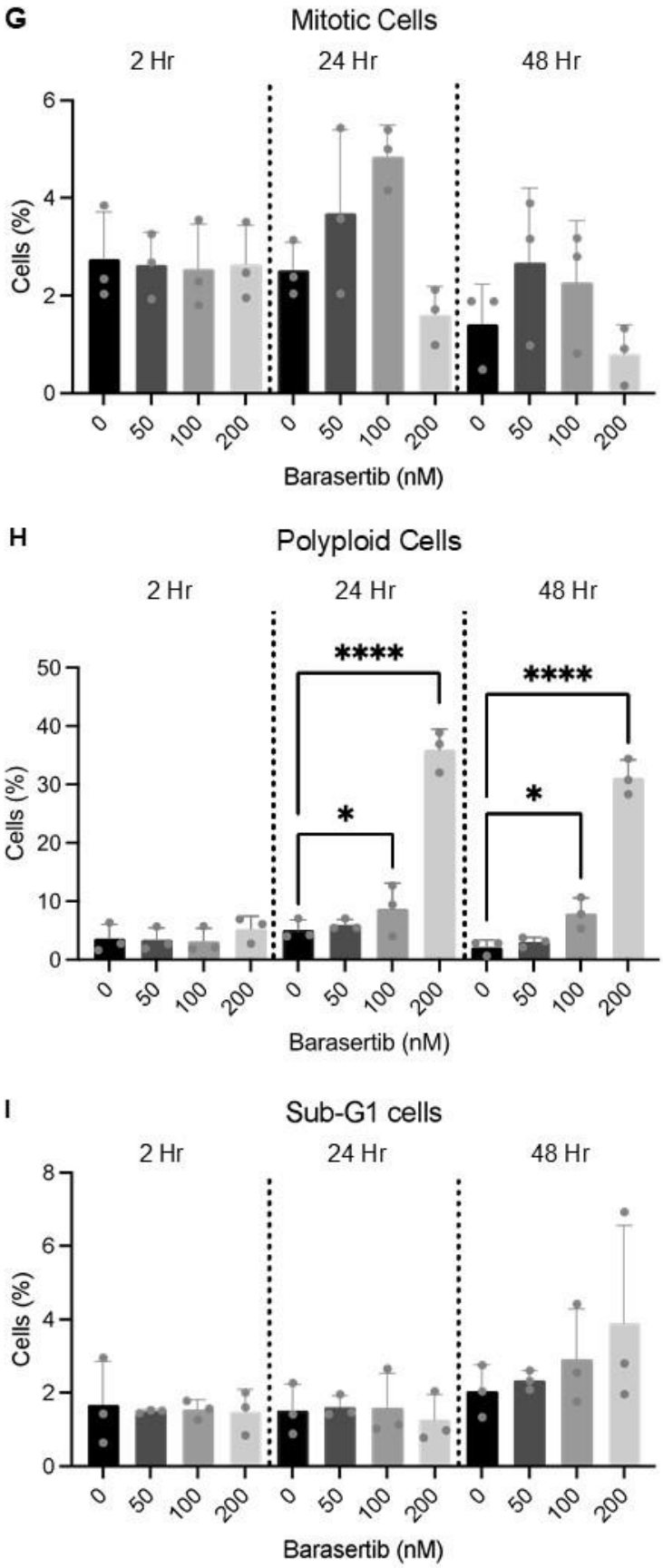

Figure 5.1: Cell cycle analysis in H460 cells after 50-200 nM Barasertib treatment

5.2.2. IR and Barasertib

The cell cycle arrest in response to IR-induced damage is an essential part of the DDR. This arrest allows time for DNA repair and prevents escalation of the severity of damage by blocking entry to sensitive cell cycle phases. To investigate whether Barasertib treatment alters the cell cycle response to IR, H460 cells were treated with DMSO or 50 nM Barasertib 1 Hr prior to 4 Gy or Sham IR and investigated at 8, 24, 48 and 72 Hr after IR to capture the initial checkpoint activation, the release from checkpoint, and the return to normal cell cycle distribution (n=3 independent repeats) (Fig). Density plots are shown in Appendix Figure 9.

In the DMSO condition, as expected, the distribution across the cell cycle phases was consistent across all timepoints (Fig 5.2 A-D). After 50 nM Barasertib, the cell cycle distribution was similar to the DMSO control, demonstrating little effect by Barasertib alone (Fig 5.2 A-D). This mirrored the results from Section 5.2.1. The exception to this was an increase in mitotic cells at 8 Hr compared to the DMSO control ($p=0.0200$) as well as a consistent yet statistically non-significant increase at 24 Hr (increased in all 3 independent repeats - Fig 5.2 H). There was a slight increase in mitotic population after 50 nM Barasertib at 72 Hr compared to DMSO, but this was not consistent across repeats. This adds weight to the trend of increased mitosis at 24 Hr at 50nM and 100 nM Barasertib in Fig 5.1. There was also increased polyploidy 24 Hr after 50 nM Barasertib compared to the DMSO control ($p=0.0200$) (Fig 5.2 I), although this was not seen with 50 nM Barasertib in Fig 5.1, raising questions about its significance.

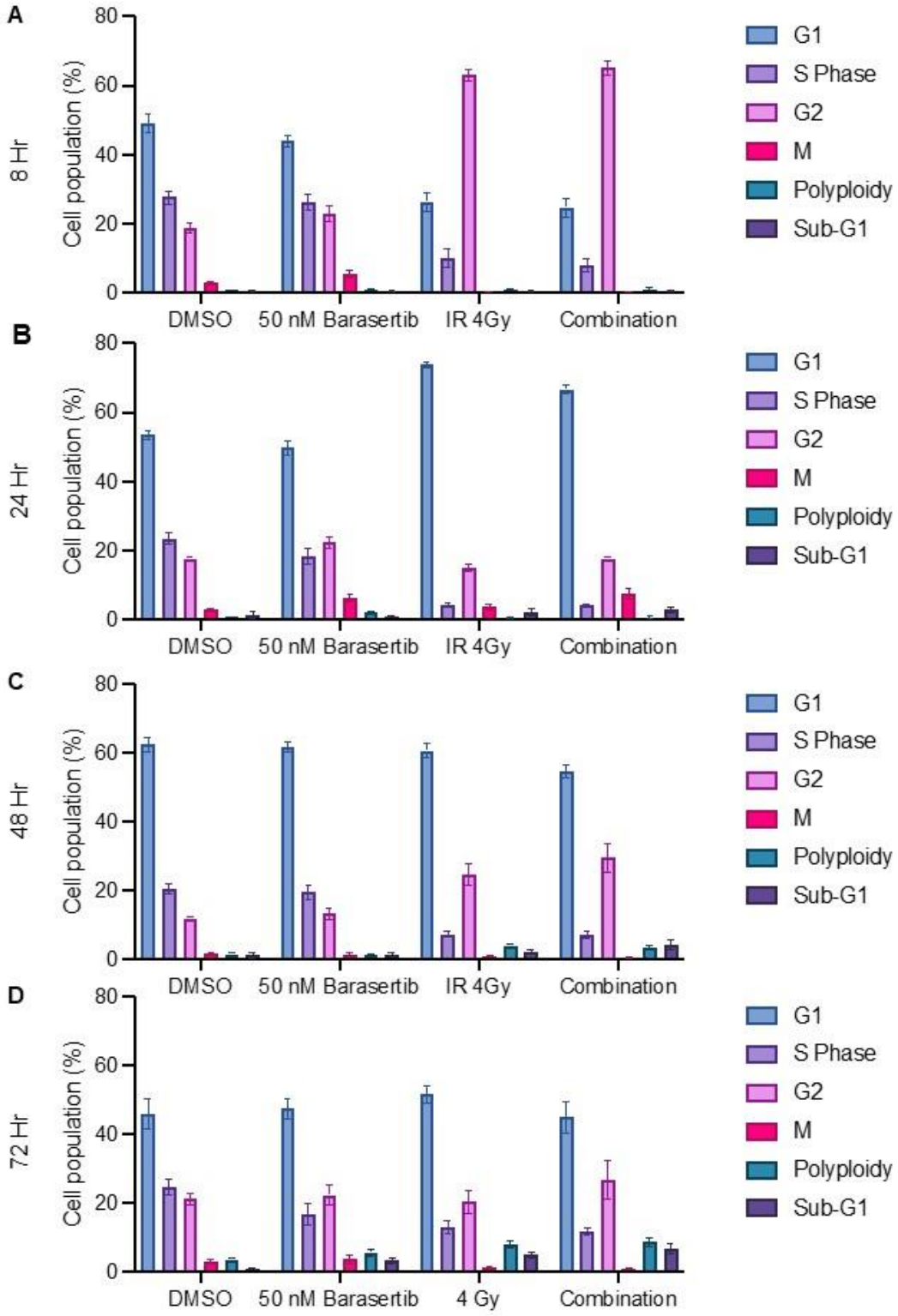

Figure 5.2: Cell cycle analysis in H460 cells after Barasertib and IR treatment

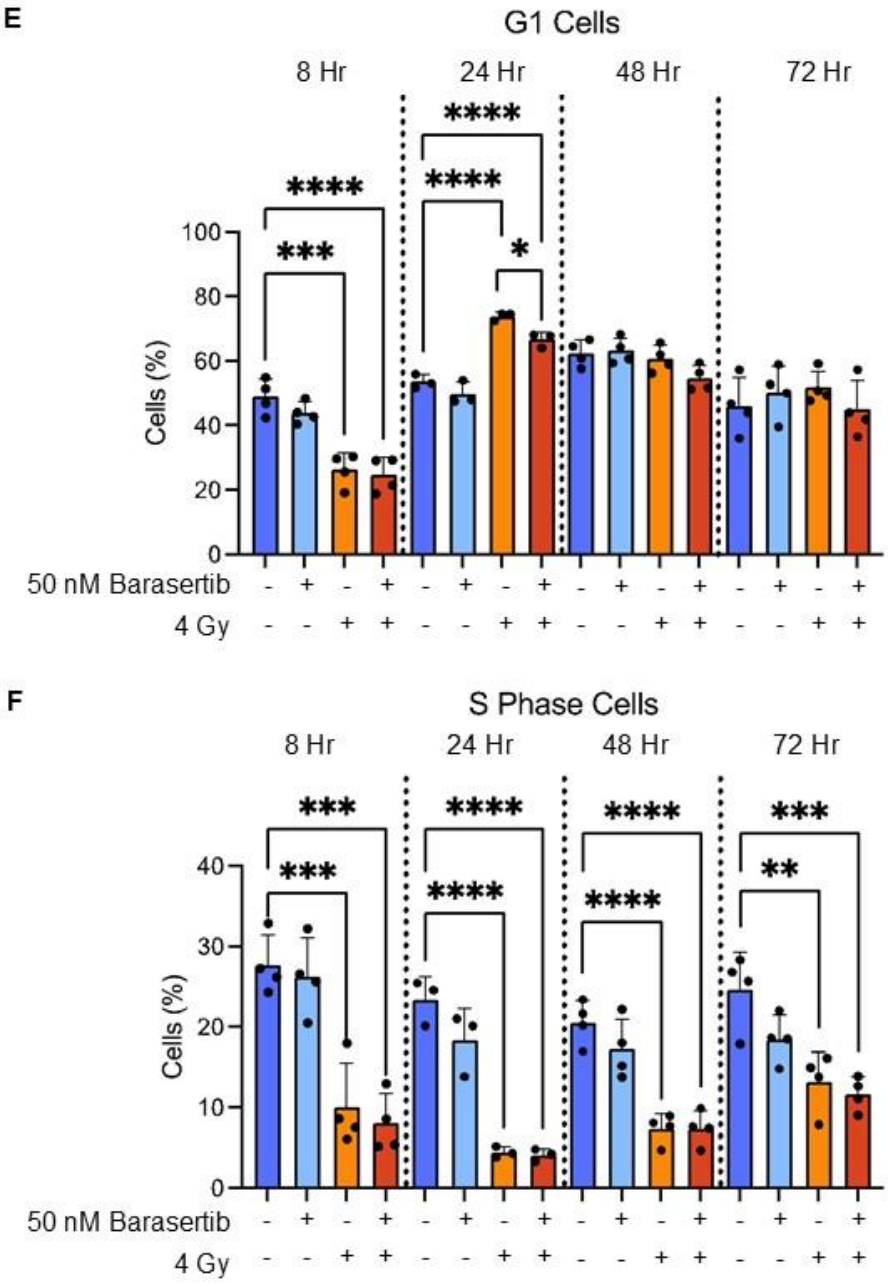

Figure 5.2: Cell cycle analysis in H460 cells after Barasertib and IR treatment

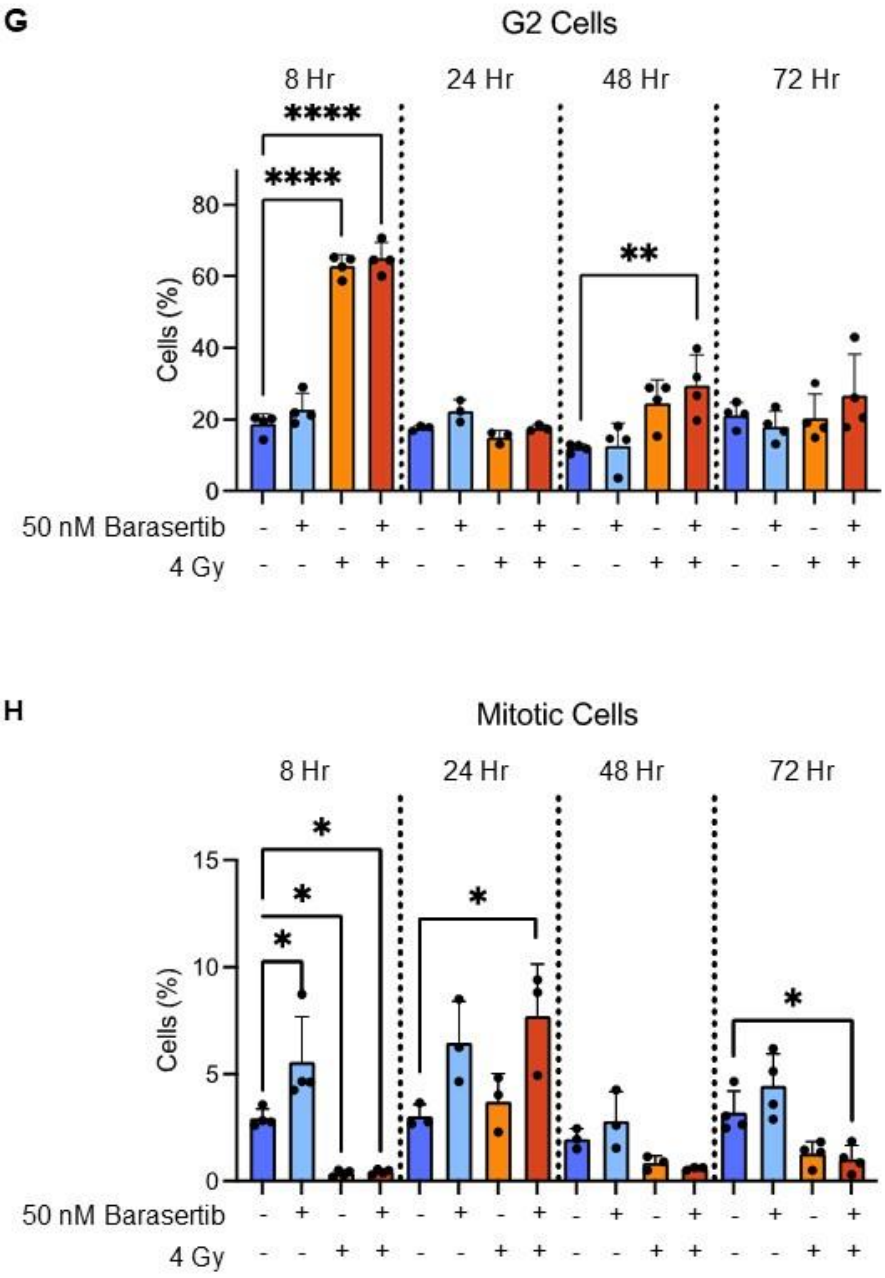

Figure 5.2: Cell cycle analysis in H460 cells after Barasertib and IR treatment

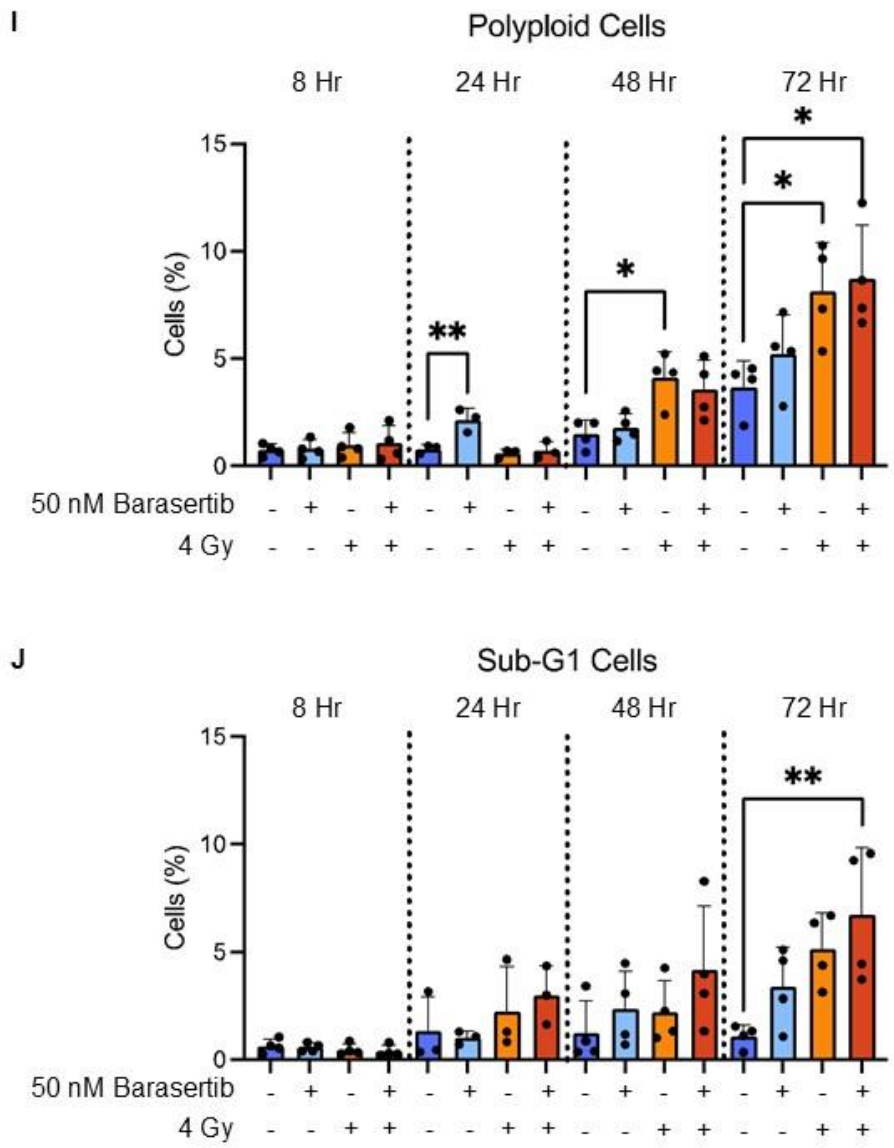

Figure 5. 2: Cell cycle analysis in H460 Cells after Barasertib and IR treatment

H460 cells were pretreated with DMSO or 50 nM Barasertib for 1 Hr before 4 Gy (or sham) IR. Cells were fixed and stained for DNA content (PI) and phospho-Histone 3 (ser10) and analysed by Flow cytometry. Quantification of cells per phase as a percentage of all live, singlet cells at the following timepoints after IR: **A** 8 Hr treatment **B** 24 Hr Treatment **C** 48 Hr **D** 72 Hr. Cell (%) per phases are shown independently **E** G1 **F** S phase **G** G2 **H** Mitotic cells **I** Polyploid cells and **J** Sub-G1 cells. Mean and standard error of the mean are shown (plus individual repeats for F-K). P-values were calculated using an ordinary one-way ANOVA per timepoint (* = $p < 0.05$, ** = $p < 0.01$, *** = $p<0.001$. **** = $p<0.0001$).

As expected, in the 4 Gy IR condition at 8 Hr, there was a strong G_2 arrest and accompanying reduced G_1, S and mitotic populations compared to the DMSO control ($p<0.0001$, $p<0.0001$, $p=0.0005$, and $p=0.0222$, respectively) (Fig 5.2 E, F and H). At 24 Hr, the 4 Gy-treated population returned to a G_1-dominant distribution (Fig 5.2 G) but the S phase population was still decreased compared to the DMSO control ($p<0.0001$) (Fig 5.2 F). The reversion to a large G_1 fraction indicates a release from the G_2 checkpoint. From 48 to 72 Hr after 4 Gy IR, the cell cycle distribution was largely stable, showing similar phase distribution as at 24 Hr (Fig 5.2 C and D). The S phase population increased between 48 and 72 Hr but was still decreased compared to the DMSO control at both timepoints ($p<0.0001$ and $p=0.0021$, respectively) (Fig 5.2 F). There was an increase in polyploid cells at 48 Hr and 72 Hr, compared to the DMSO control ($p=0.0131$ and $p=0.0330$, respectively) (Fig 5.2 I). There was also reduced mitotic population at 48 and 72 Hr.

The response to IR was similar in the presence of Barasertib. At 8 Hr, after IR and Barasertib treatment, there were decreased G_1, S and mitotic populations compared to the DMSO control ($p<0.0001$, $p=0.0002$ and $p=0.0265$, respectively) (Fig 5.2 E, F and H) and increased G_2 population ($p<0.0001$) (Fig 5.2 G), demonstrating a clear G_2 arrest.

At 24 Hr, similarly to IR alone, there was a recovery from the IR-induced G_2 arrest leading to a greater G_1 population, which was increased compared to DMSO ($p<0.0001$). However, there was a smaller proportion of cells in G_1 in the combination treatment compared to radiation alone ($p=0.0314$) (Fig 5.2 E). In addition, following combination treatment there was an increase in the mitotic population at 24 Hr compared to the DMSO control ($p=0.0387$). This was not seen

with radiation alone (Fig 5.2 H). The S phase population in the combination-treated condition at 24 Hr was smaller than the DMSO control ($p<0.0001$) (Fig 5.2 F), showing a similar trend to 4 Gy alone. Neither the polyploid nor sub-G_1 populations were increased at 24 Hr compared to DMSO control, again showing the same trend as radiation alone. Also, at 48-72 Hr, the mitotic population was low, with significant decrease compared to DMSO at 72 Hr ($p=0.00362$).

In the combination condition at 48 Hr, there was also a significant increase in the G_2 population compared to DMSO alone ($p=0.0070$) similar in size to the 4 Gy alone G_2 population (Fig 5.2 G). By 72 Hr, there were significant increases in the polyploid and Sub-G1 populations in the combination treatment compared to the DMSO control ($p=0.0153$ and $p=0.0070$, respectively) (Fig 5.2 I and J), but these were similar to those seen with IR alone.

Overall, the cell cycle checkpoint response to IR and subsequent checkpoint was largely not affected by 50 nM Barasertib, although additional timepoints at 12-16 Hr would provide more detail into the speed of exit from the G_2 checkpoint. As expected, radiation induced a dramatic change in the cell cycle profile, most apparent as a strong G_2 arrest at 8 Hr post IR. This arrest also occurred in the combination condition. Our phospho-proteomic data revealed phosphorylation changes in proteins involved in the G_2/M checkpoint, but this data shows that the checkpoint function is normal after Barasertib treatment (both analyses used 50 nM Barasertib). There was also a reduction in mitotic populations at later timepoints in IR and combination conditions.

However, there were some variations in the recovery from the G_2 arrest. At 24 Hr, the IR alone treated cells had recovered from G_2 arrest and transited to G_1. In the

combination, the G_2 arrest was also lost but there was a small but significant decrease in G_1 population at 24 Hr in the combination condition compared to IR. In addition, at 24 h there was an increased percentage of cells in mitosis in the combination not seen with IR alone. Together these suggest that in the presence of Barasertib, IR-treated cells pass more slowly through mitosis after recovering from G_2 arrest.

5.3. Investigation of the Effects of IR and Barasertib Treatment on Mitosis in H460 cells

Having seen a trend of increased mitotic cells in the Barasertib conditions, and in the combination treatment, we aimed to investigate in more detail how mitosis was affected. Firstly, we used live cell imaging to track mitotic cells over time and secondly, we used immunofluorescent staining to visualise mitotic structures and defects.

5.3.1. Live Cell Analysis of Mitotic Progression

Live cell analysis of H460 cells was carried out between 27 - 72 hours post 4 Gy IR or sham IR, with DMSO or Barasertib added 1 Hr prior to IR and present throughout the experiment. Mitotic cells were tracked to quantify mitotic duration and the rate of defects including division into >2 cells, slippage (exits mitosis as one cell), abscission regression (daughter cells recombine in interphase), death in mitosis, one cell dead after mitosis or both cells dead after mitosis. Representative images of each event are shown in Fig 5.3 A. At least 60 mitotic cells were manually tracked per condition (Fig 5.3 B).

Mitotic duration was calculated for each mitotic cell and no significant difference in the mean duration was found between the treatment conditions. However, there was a trend of increasing duration following Barasertib or IR alone, with further increase with the combination treatment (Fig 5.4 A). To further examine the effect of

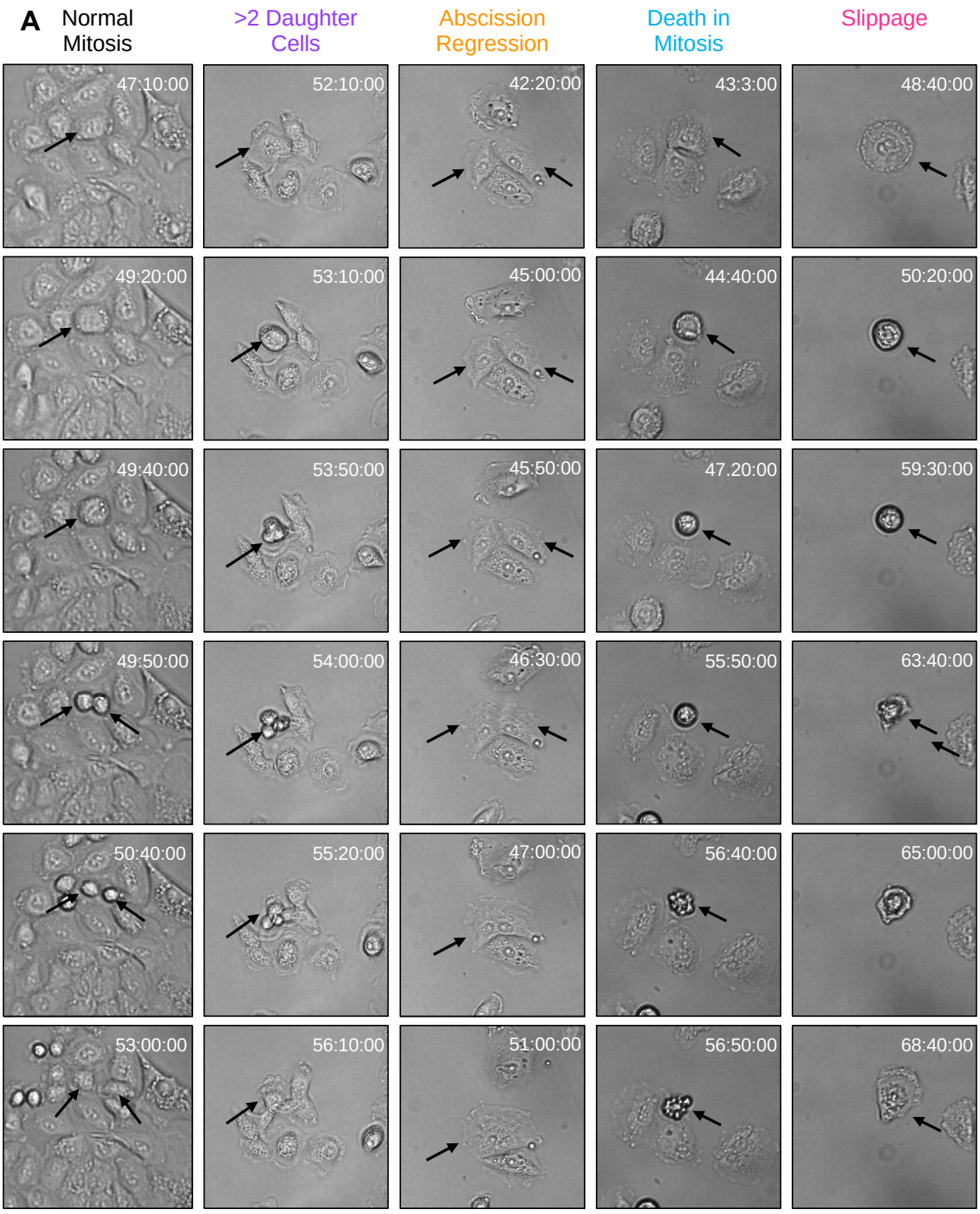

Figure 5. 3: Live cell imaging of H460 cells after Barasertib and IR treatment

H460 cells were pretreated with DMSO or 50 nM Barasertib for 1 Hr before 4 Gy (or sham) IR. Cells were imaged with time-laspe live microscopy every 10 minutes from 27 Hr post IR to 72 Hr post IR. **A** Representative brightfield images of H460 cells undergoing normal mitosis, Mitosis with >3 daughter cells, abscission regression, death in mitosis and slippage. Timestamps indicates time after start of treatment (Hr:Mins:Seconds).
B Time graphs of showing mitoses and fate (defect or normal interphase) per condition. Each line represents 1 cell. Each row represents one independent repeat.

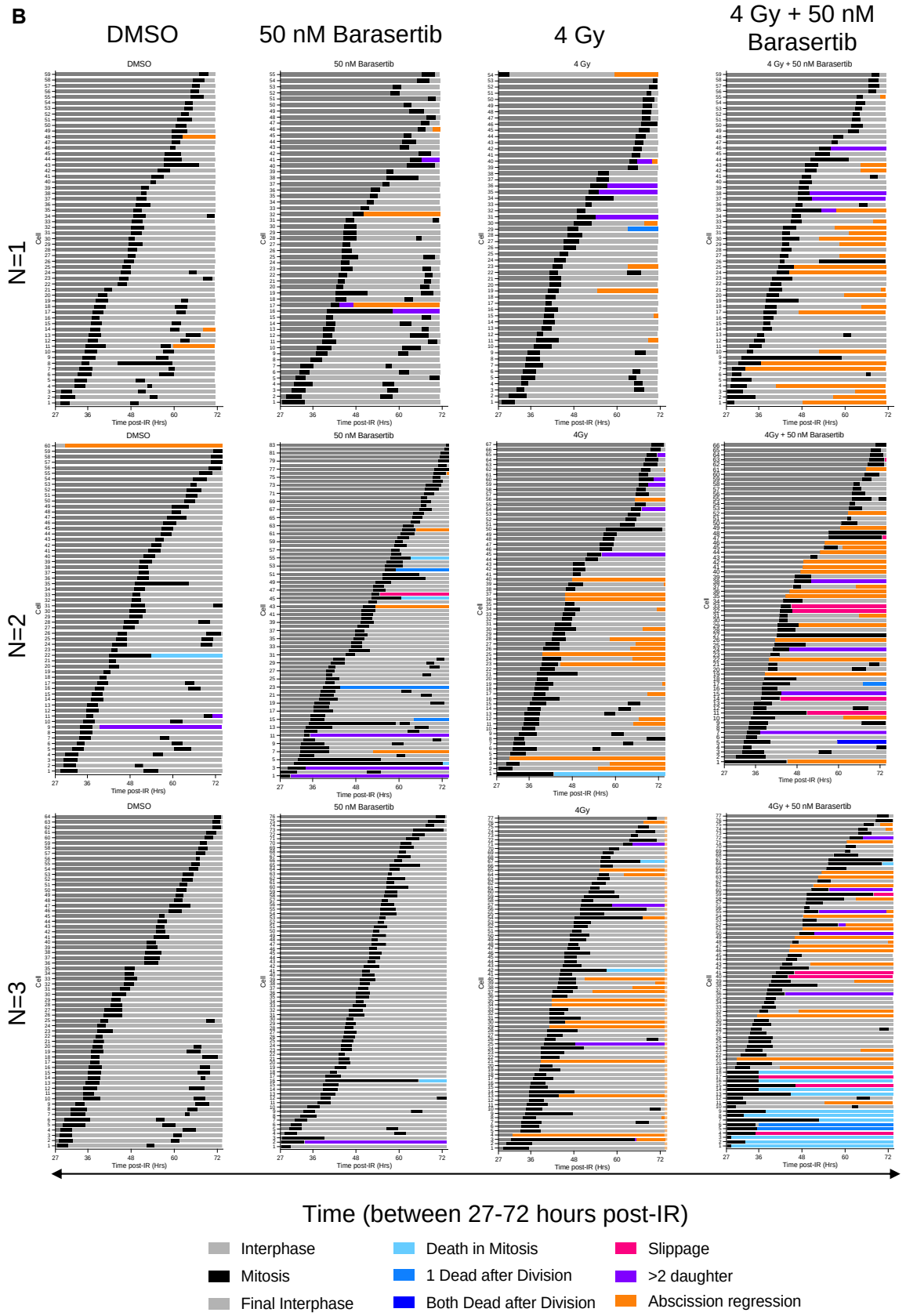

Figure 5.3: Live cell imaging of H460 cells after Barasertib and IR treatment

Barasertib and IR on mitotic duration, mitotic duration was plotted against time after treatment (Fig 5.4 B-E). Severely arrested mitoses (>1000) were most common in the Barasertib and Combination conditions. In 50 nM Barasertib-treated cells, all mitosis >1000 minutes occurred before 48 Hr post-IR. The strongest trend for increased mitotic population in flow cytometry analysis after Barasertib was seen at 8 - 24 Hr (section 5.1 and 5.2), and was mostly lost after this. The trend in mitotic duration provides some evidence that the increased mitotic population seen by flow cytometry is due to increased mitotic duration. This live cell data represents cells from 27 -l 72 Hr. Live cell analysis between 0 - 24 Hr would be preferable to examine this further.

Normal and aberrant mitoses were also quantified (Fig 5.4 E and F). 50 nM Barasertib had no significant effect on the percentage of aberrant mitoses (Fig 5.4 E). There were also no significant increases in any of the specific defects we could detect after 50 nM Barasertib treatment compared to the DMSO control (Fig 5.4 F-J).

4 Gy IR led to a significant increase in aberrant mitoses compared to the DMSO control ($p=0.0016$) (Fig 5.4 E). The most common defects after IR were abscission regression and division into >2 daughter cells, which were both significantly increased in the IR alone condition ($p=0.0083$ and $p =0.0156$, respectively) (Fig 5.4 G and H). This agrees with current evidence that DNA damage promotes mitotic aberrance such as centrosome amplification and cytokinesis failure (Hayashi and Karlseder, 2013).

In the combination treatment, there was also an increase in the incidence of aberrant mitosis compared to DMSO control ($p<0.001$) (Fig 5.4 E). Incidence of aberrance was also significantly higher in the combination treatment than in IR alone

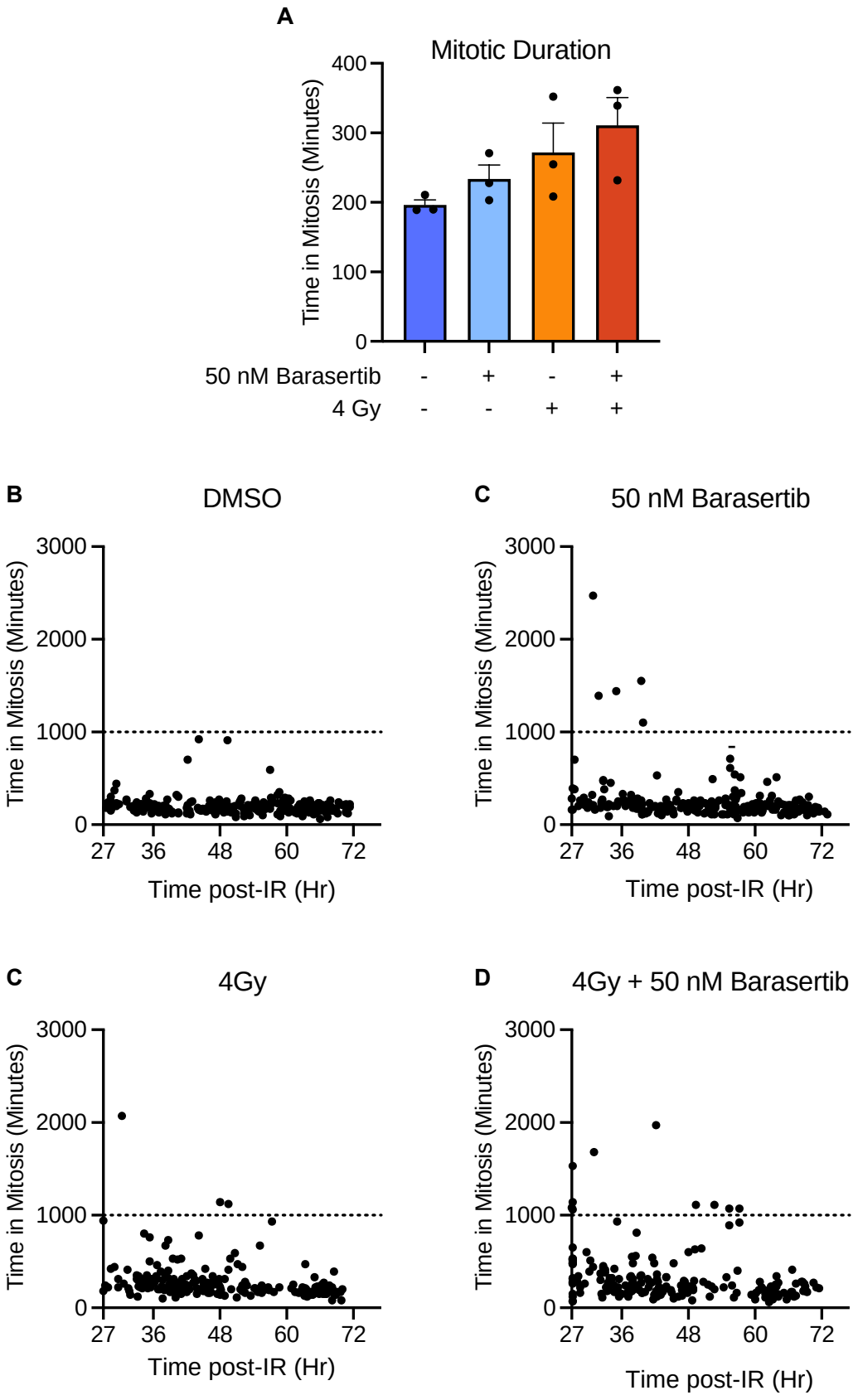

Figure 5.4: Barasertib and IR increase live aberrance between 27-72 Hr post IR

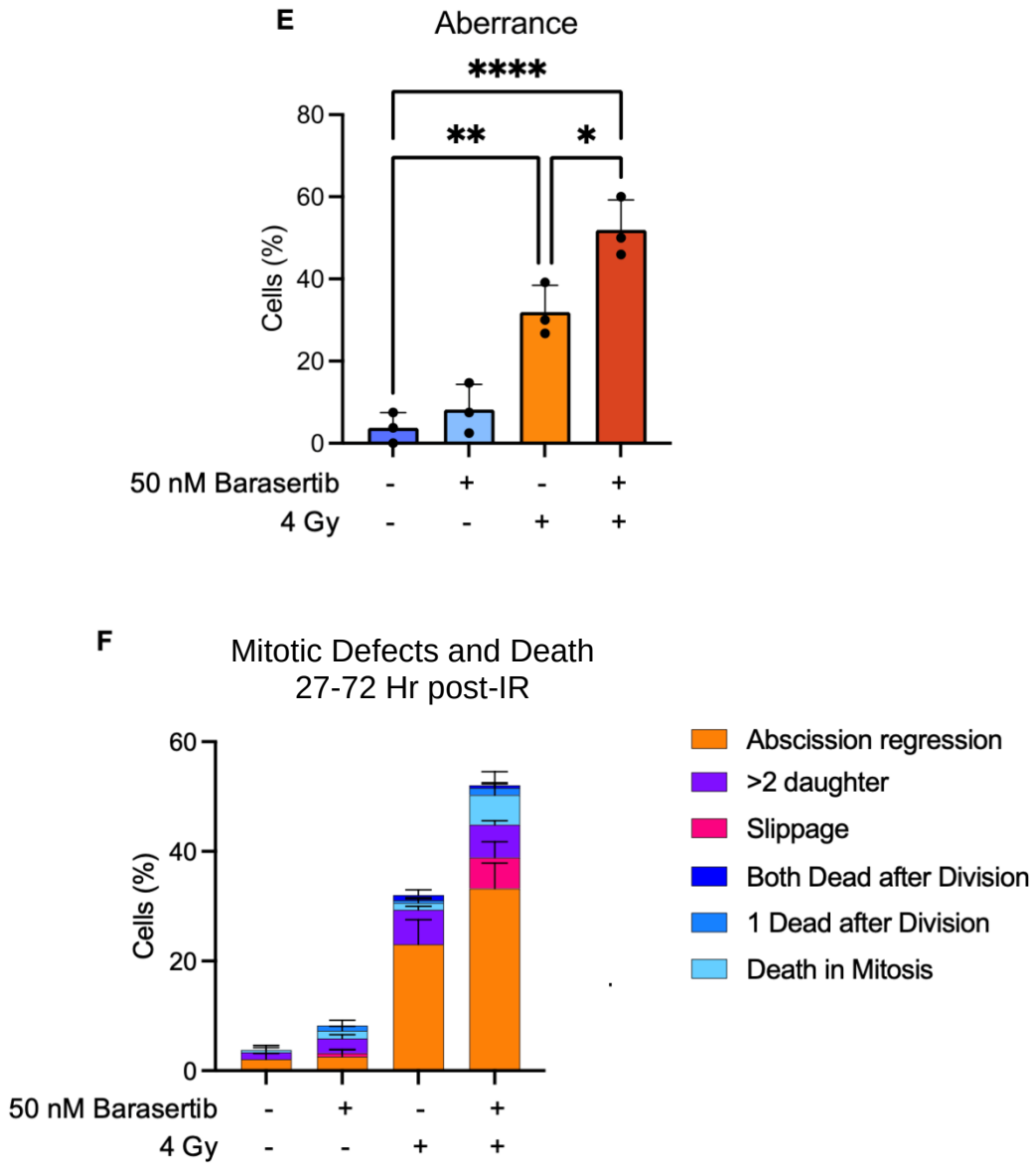

Figure 5.4: Barasertib and IR increase live aberrance between 27-72 Hr post IR

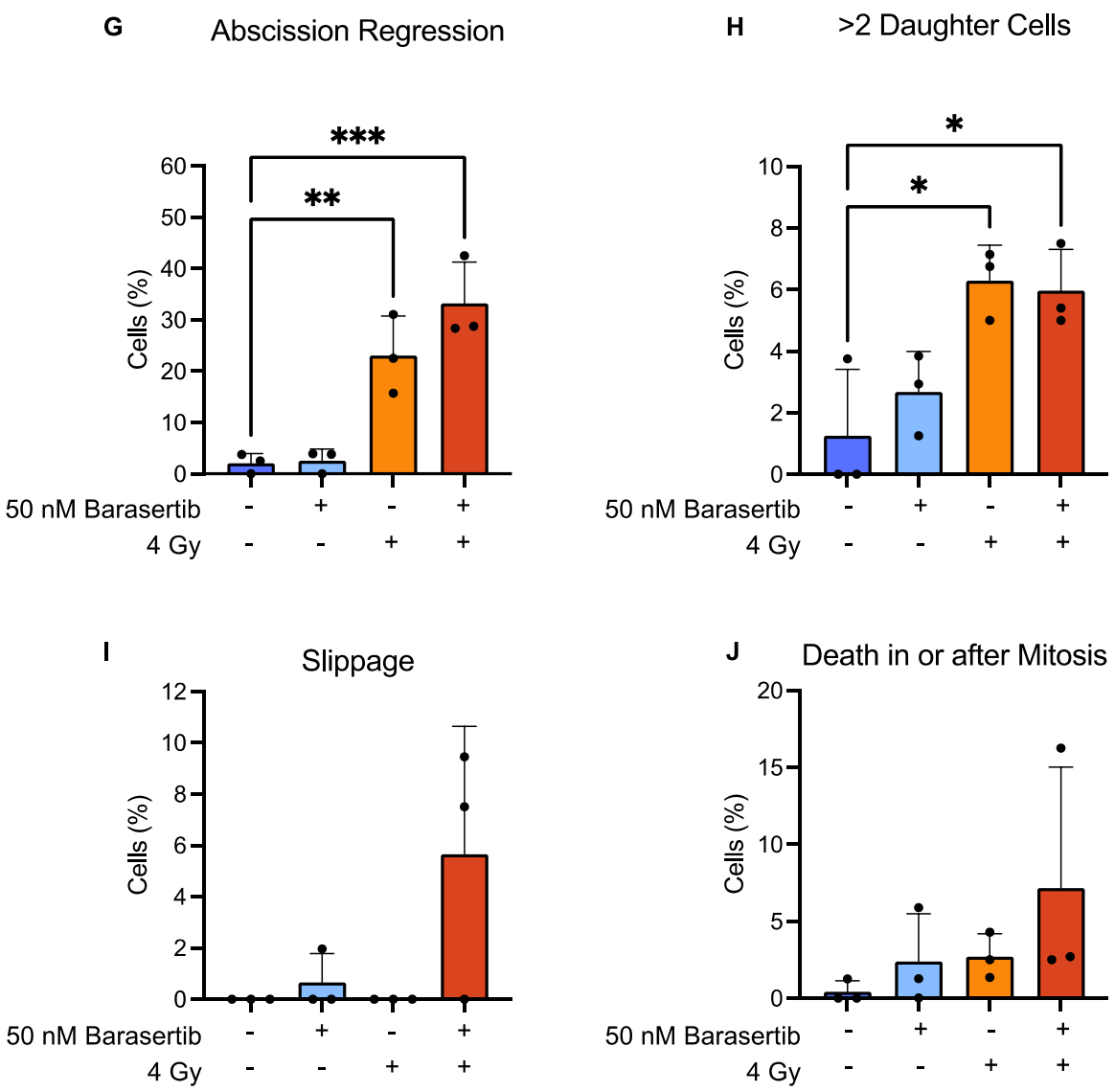

Figure 5. 4: Barasertib and IR increase live aberrance between 27-72 Hr post IR

H460 cells were pretreated with DMSO or 50 nM Barasertib for 1 Hr before 4 Gy (or sham) IR. Cells were imaged with time lapse live microscopy every 10 minutes from 27 Hr post IR to 72 Hr post IR. Mitotic duration to the nearest 10 minutes was calculated by scoring for mitotic entry and exit by timeframe. **A** Mitotic duration per condition. Mean, SEM and individual values are shown for 3 independent repeat. **B-D** Mitotic duration per cell plotted against time after IR (>190 cells pooled from 3 repeats).
Quantification of mitotic aberrance per condition as a percentage of all cells scored: **E** Aberrant cells **F** Mitotic aberrance by type of defect **G** Abscission regression **H** >2 Daughter cells **I** Death in mitotic cells in or after mitosis **J** Slippage. Mean, SD and individual values are shown for 3 independent repeats. P-values were calculated using an ordinary one-way ANOVA (* = $p < 0.05$, ** = $p < 0.01$, *** = $p<0.001$. **** = $p<0.0001$).

(p=0.0145) (Fig 5.4 E). The type of defects was similar to the IR condition i.e. increased mitoses with > 2 daughter cells and abscission regression (p=0.0225 and p=0.0007, compared to DMSO respectively) (Fig 5.4 G and H). In two repeats, there was an increase in slippage after the combination treatment (ns), and slippage was only observed in conditions with Barasertib treatment (Fig 5.4 I). However, slippage was a rare event and other defects were much more common. There was also increased abscission regression in the combination compared to IR alone conditions but again this was not statistically significant. Finally, there was increased death on average in the combination treatment, but this was due to one high repeat. There wasn't a significant change in mitosis-associated death between any treatment conditions (Fig 5.4 J).

There was increased polyploidy in IR and combination conditions (Flow cytometry analysis, Section 5.2.2). This live cell analysis suggests that polyploidy is predominantly due to abscission regression rather than slippage. Polyploidy occurred in IR and Combination conditions, as does abscission regression. Slippage was a rare event (5 cells in >880) and was not observed in the IR condition.

This analysis also shows that death in mitosis is uncommon in these cell populations. There were similarly low levels of mitotic death in Barasertib alone, IR alone and combination conditions. Likewise, death after mitosis appears rare.

5.3.2. Immunofluorescence Analysis of Mitotic Phenotype

To further investigate the defects caused by IR and Barasertib treatment, H460 cells were fixed 24 and 72 Hr after 4 Gy IR or sham IR, with DMSO or Barasertib added 1 Hr prior to IR. Immunofluorescent staining for Beta-Tubulin and Pericentrin as well as DAPI staining were carried out (n=3 independent repeats).

5.3.2.1. Mitotic Population

Over 400 cells per condition were imaged at x20 magnification and the percentage of mitotic cells in the population was quantified (Fig 5.5). This method reproduced the trend seen in the Flow cytometry data at 24 Hr, whereby mitotic population (%) was elevated after Barasertib and combination treatments at 24 hours (p=0.0015 and p-0.0051, respectively) (Fig 5.5 B). Similarly to flow cytometry data, this phenotype was mostly absent at 72 Hr but with a slight increase in the Barasertib alone condition compared to DMSO (ns).

This data differed from the flow cytometry analysis in that we did not see a reduction in mitotic populations at 72 Hr in the IR treated populations.

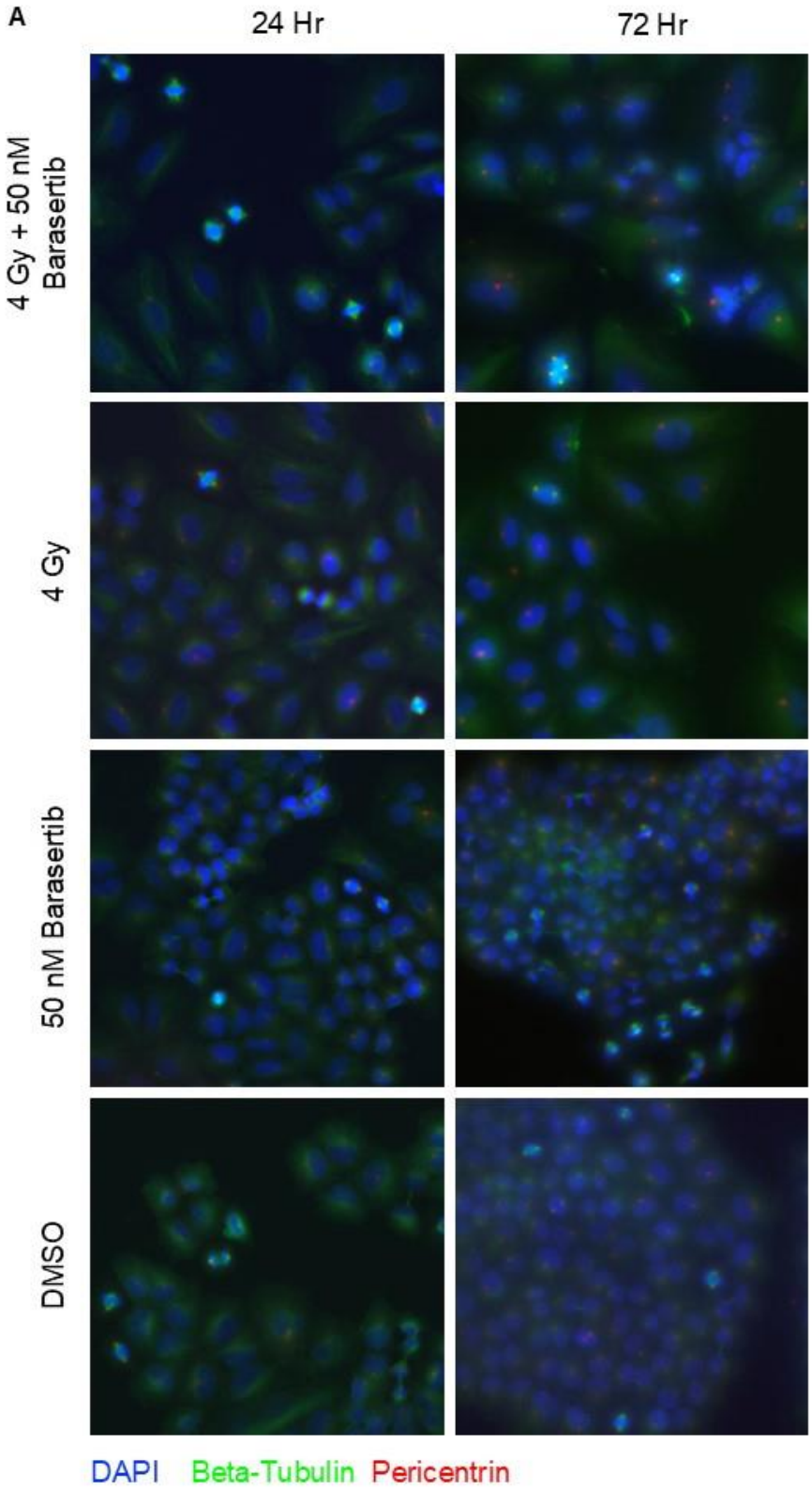

Figure 5.5: Mitotic Population is increased by Barasertib after 24 Hr treatment

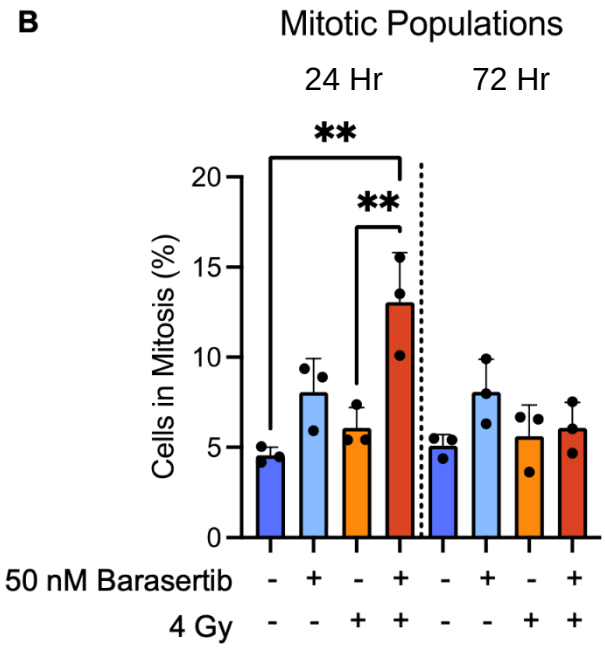

Figure 5. 5: Mitotic population is increased by Barasertib after 24 Hr treatment

H460 cells were pretreated with DMSO or 50 nM Barasertib for 1 Hr before 4 Gy (or sham) IR. Cells were fixed after 24 or 72 Hr and stained DAPI, Beta-Tubulin and Pericentrin. Mitotic populations were quantified by scoring >200 cells per repeat at x20.
A Representative images of H460 cells at x20 (white arrow indicates mitotic cell.
B Percentage of cells in mitosis at 24 Hr and 72 Hr. Mean, SD and individual values are shown for 3 independent repeats.

5.3.2.2. Mitotic Aberrance

Over 50 mitotic cells per condition were imaged at x60 magnification and scored for mitotic phenotypes (Fig 34). Mitotic cells were classed as normal or defective (Figure 34 C) and defective phenotypes were scored (Figure 34 D and E). Multinucleation was also quantified as percentage multinucleated in >200 interphase cells per condition (Figure 34 B and H).

In the DMSO condition, most mitoses at 24 and 72 Hr were normal - less than 10% of mitoses were classed as aberrant (Fig 5.6 C).

In the 50 nM Barasertib condition, most mitoses at 24 Hr were normal (Fig 5.6 C). By 72 Hr, there was an increase in aberrant mitoses at (3 fold increase) (ns) (Fig 5.6 B), which can be attributed to increased chromosome separation defects ($p=0.0236$) (Fig 5.6 D and G). Multinucleation after 50 nM Barasertib treatment was slightly elevated above the DMSO control at 24 and 72 Hr but not significantly (Fig 5.6 H).

In both the 4 Gy IR and combination conditions, there were increased defects in mitosis compared to the DMSO control at 24 and 72 Hr ($p<0.0001$ at 24 Hr (both conditions), $p=0.179$ and $p=0.0009$ at 72 Hr, respectively) (Fig 5.6 C). These were mainly centrosome and chromosome separation defects (5.6 D). Both defects significantly increased in the 4 Gy alone group at 24 Hr ($p= 0.0238$ and $p=0.0447$, respectively) (Fig 5.6 F and G). At 72 Hr, chromosome separation defects were still increased compared to DMSO control ($p=0.0335$) (Fig 5.6 G).

In the combination condition, centrosome and chromosome separation defects were increased in the combination condition at 72 Hr ($p=0.0258$ and 0.0037, respectively) - these defects were also high at 24 Hr but showed high variation (Fig 5.6 F and G).

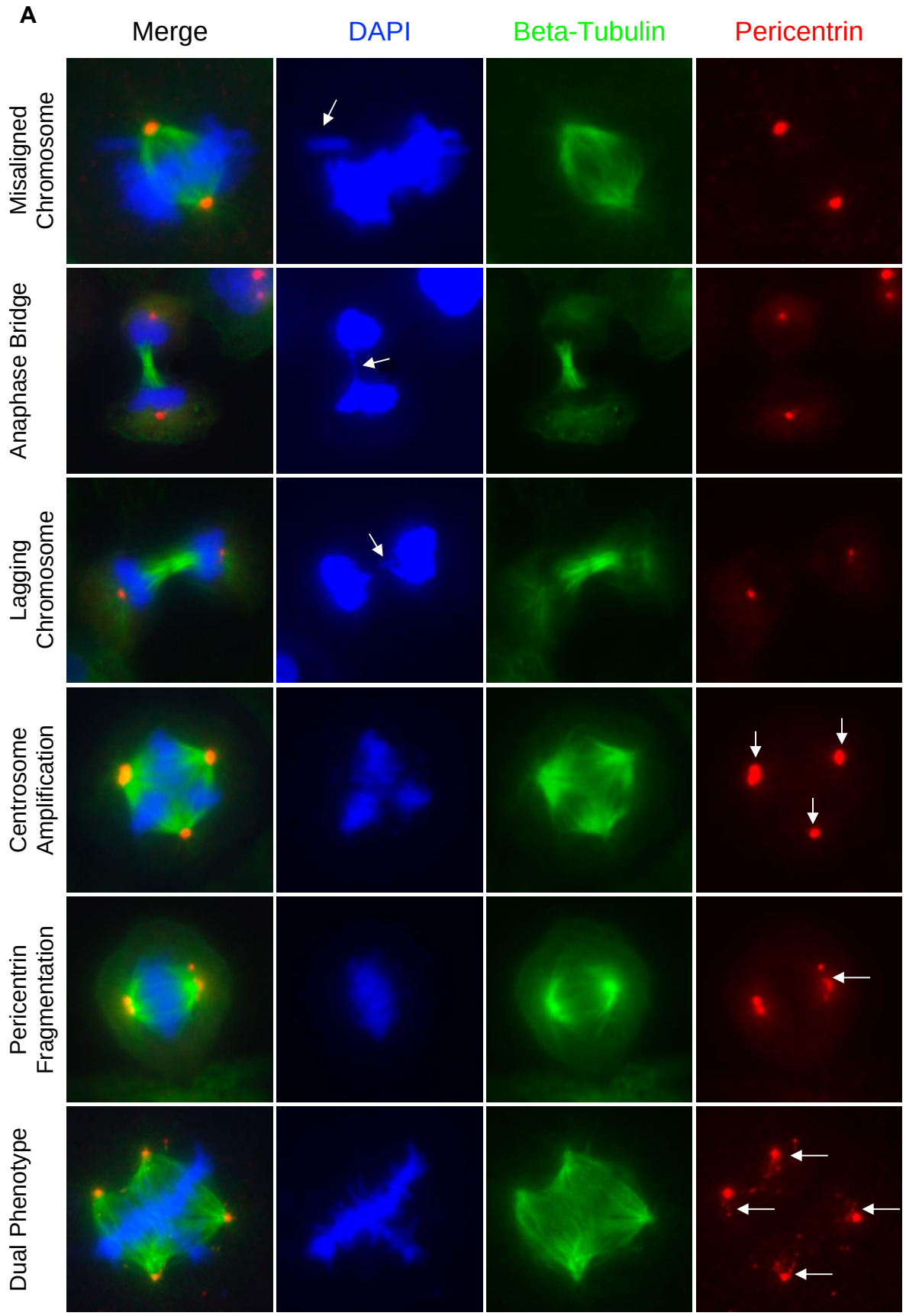

Figure 5.6: IR and Barasertib contribute to increased mitotic defects

A (Continued)

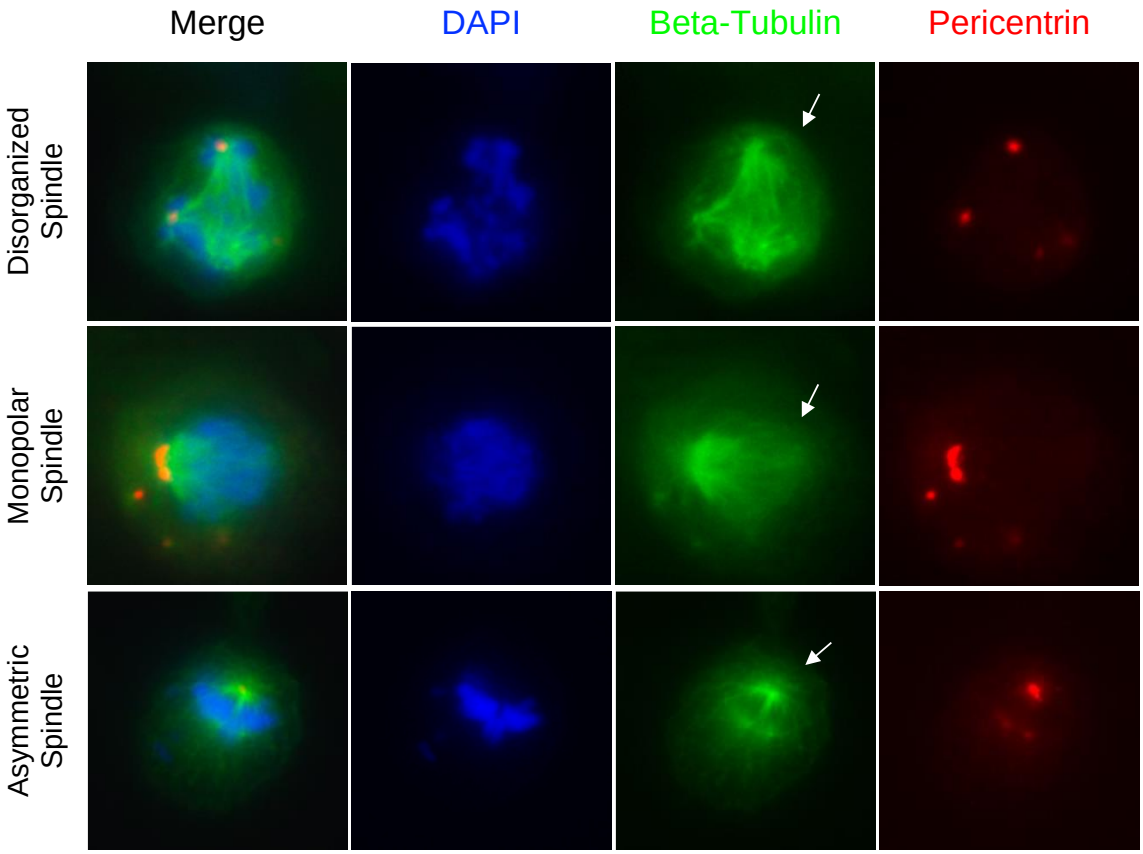

Figure 5.6: IR and Barasertib contribute to increased mitotic defects

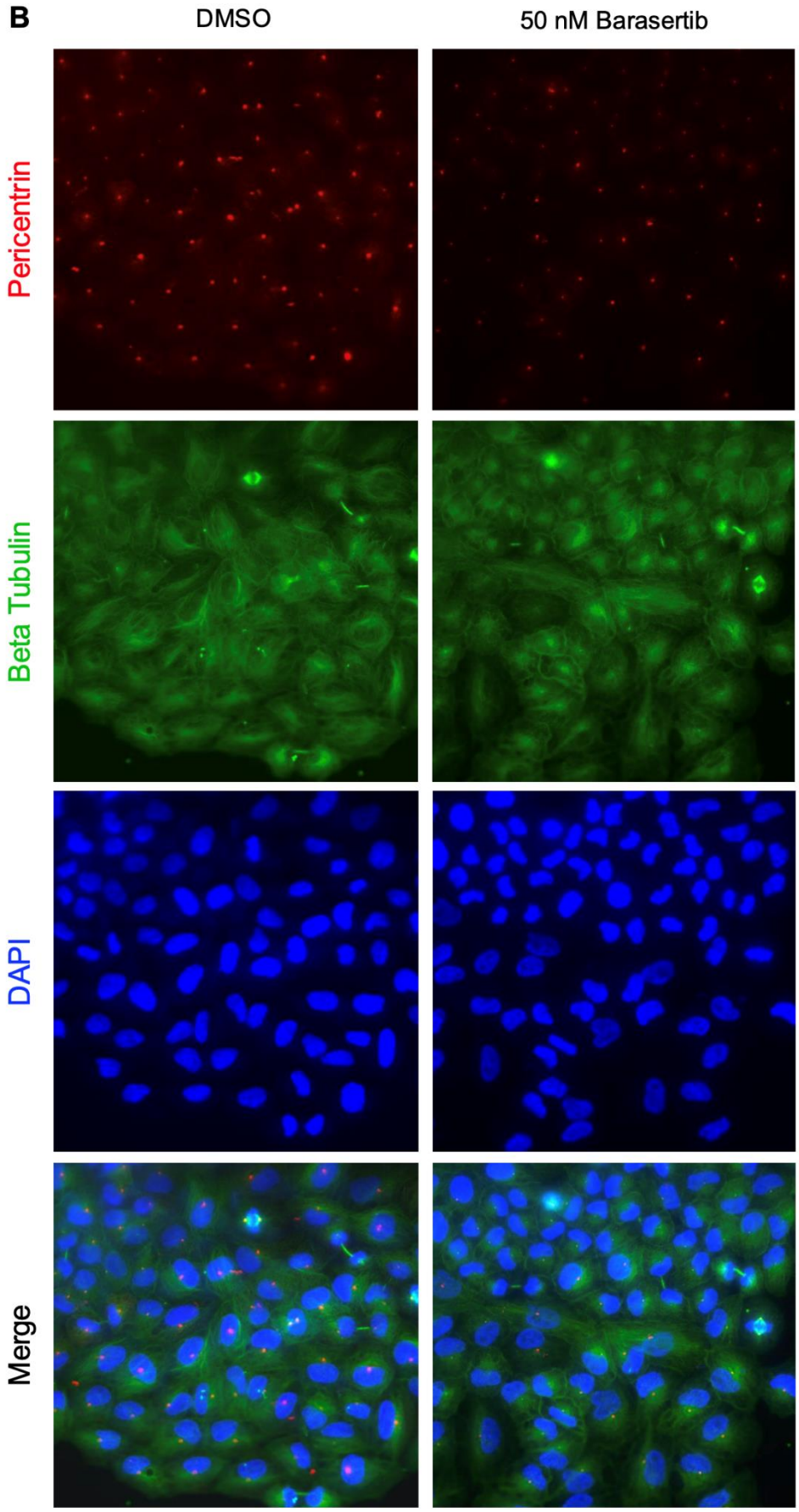

Figure 5.6: IR and Barasertib contribute to increased mitotic defects

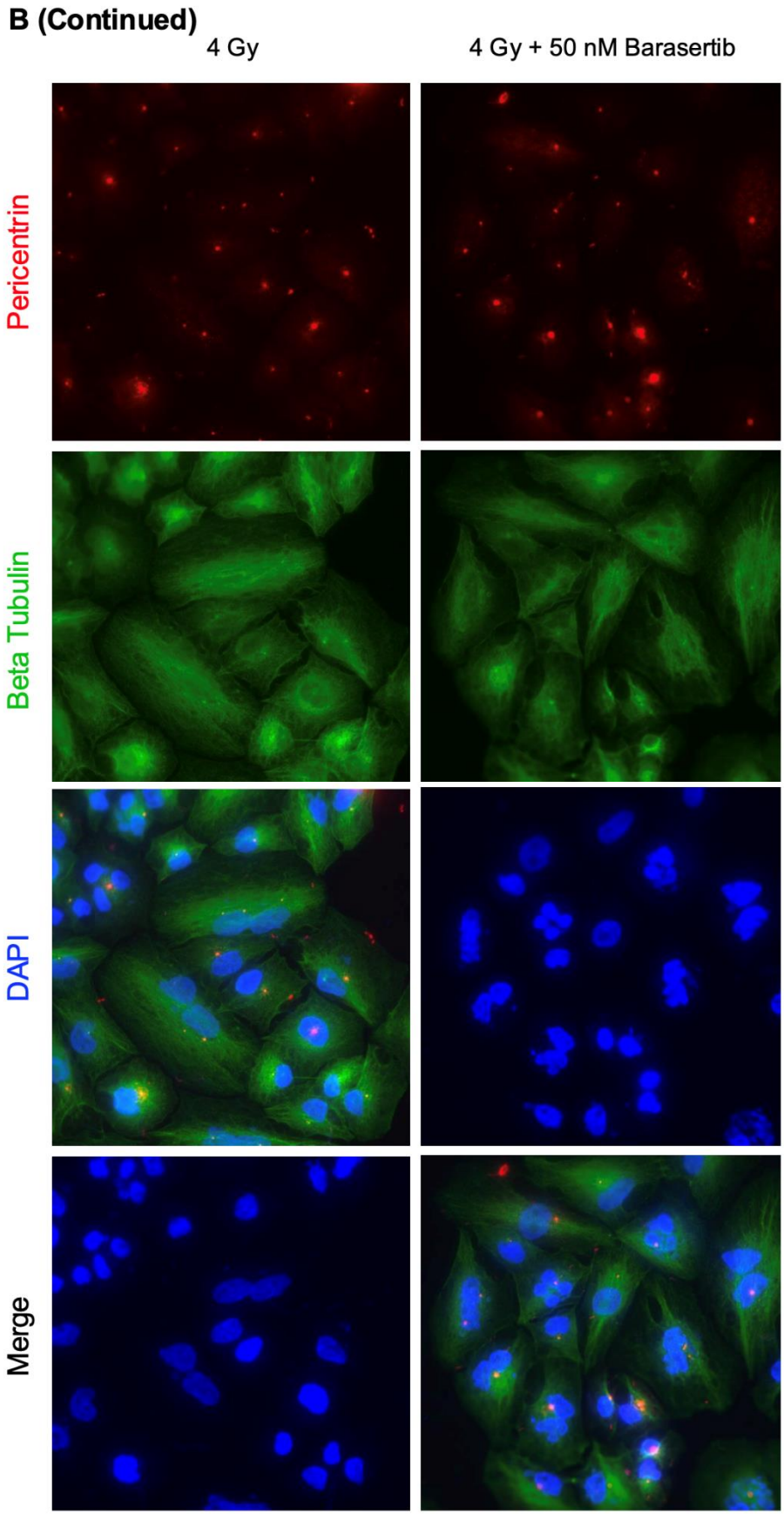

Figure 5.6: IR and Barasertib contribute to increased mitotic defects

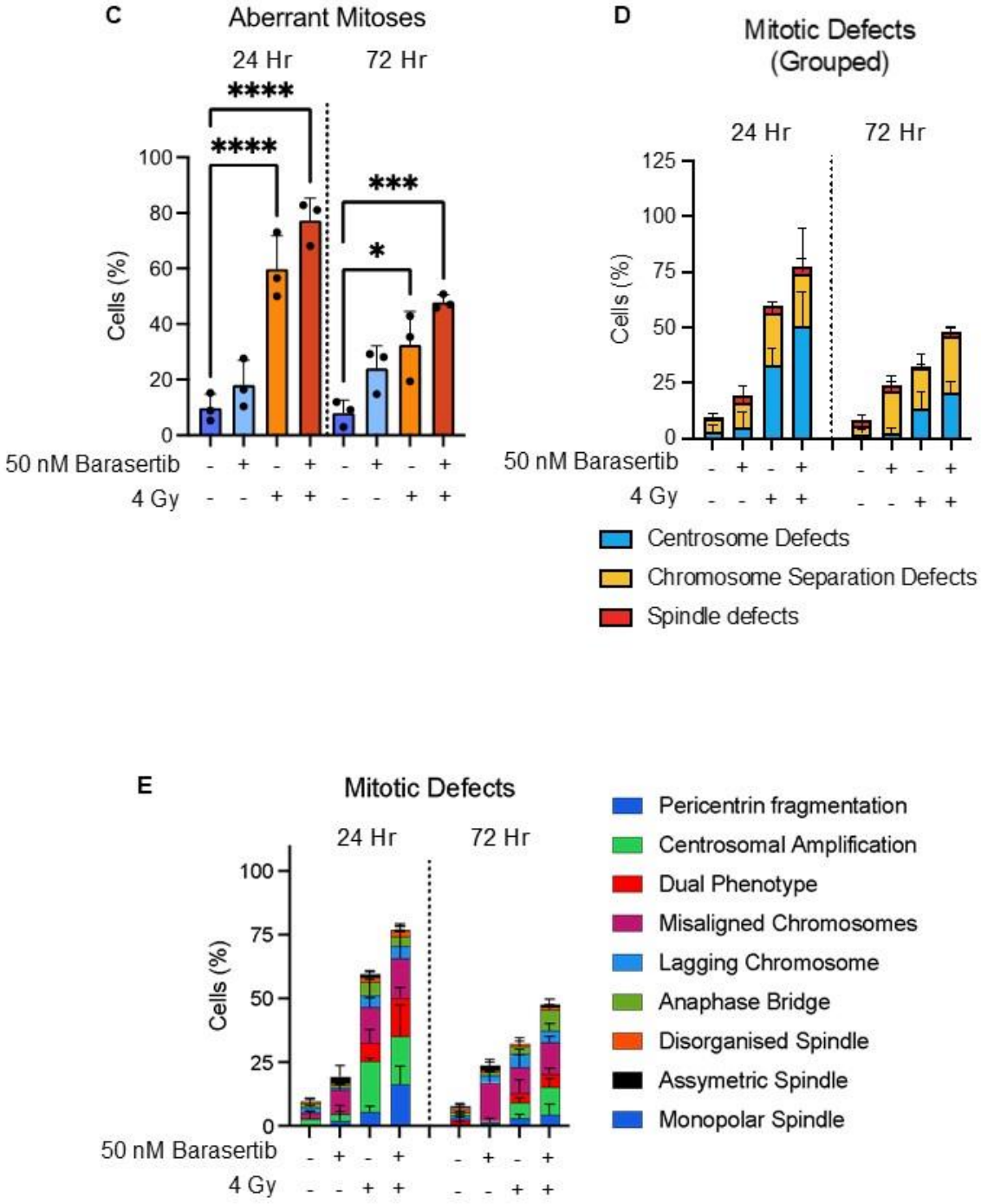

Figure 5.6: IR and Barasertib contribute to increased mitotic defects

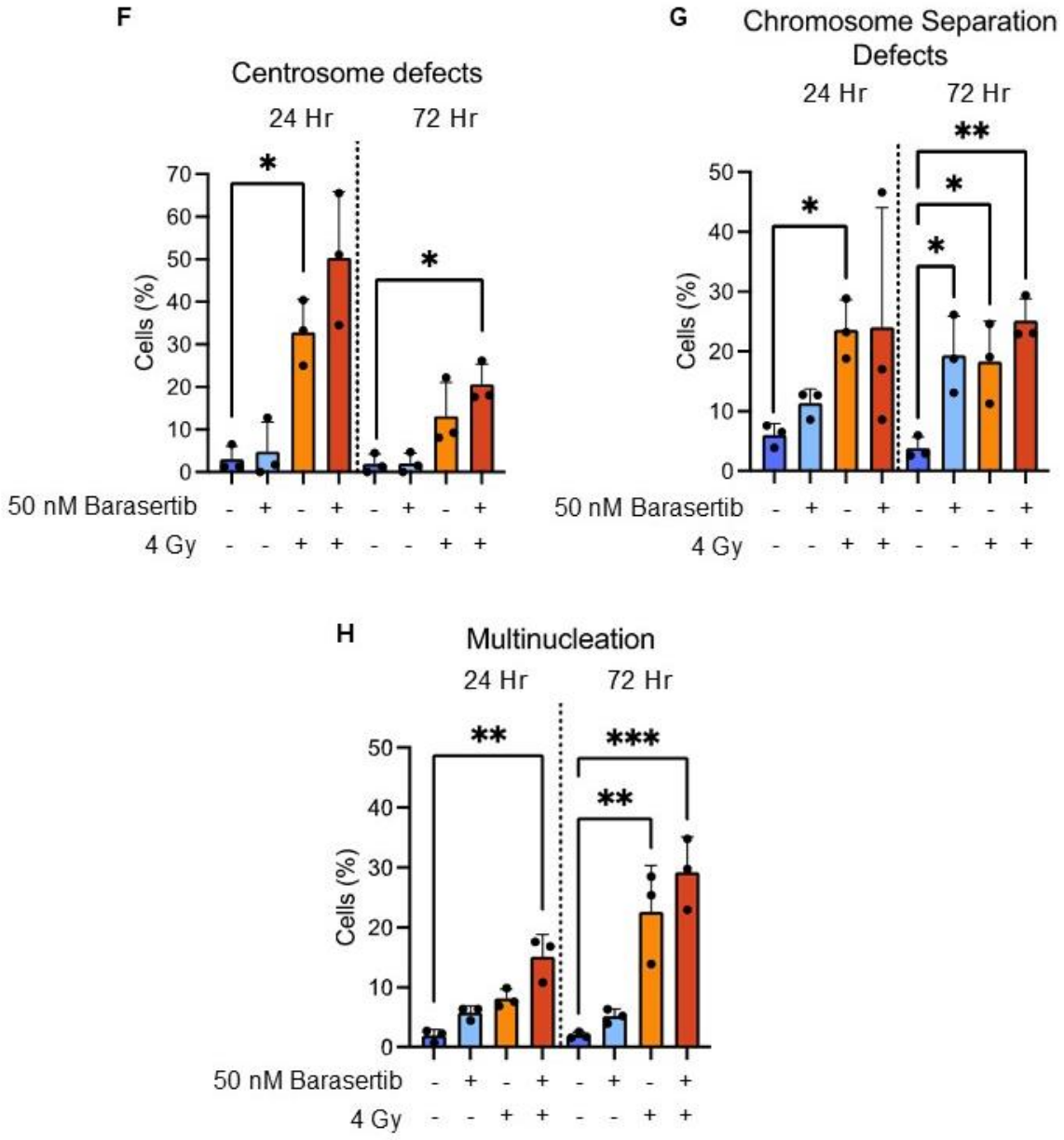

Figure 5. 6: IR and Barasertib contribute to increased mitotic defects

H460 cells were pretreated with DMSO or 50 nM Barasertib for 1 Hr before 4 Gy (or sham) IR. Cells were fixed after 24 or 72 Hr and stained DAPI, Beta-Tubulin and Pericentrin. >50 per condition per repeat were imaged and scored for mitotic aberrance. **A** Representative images of Mitotic defects (white arrows indicate cell or defect of interest). **B** Representative images of cells showing multinucleation in each condition at 24 and 72 Hr. Quantification of aberrance: **C** Aberrant Mitoses **D** Aberrant mitoses (grouped defect type) **E** Individual defect **F** Chromosome Separation Defects **G** Centrosome Defects **H** Multinucleation. Values shown are the percentage of mitotic cells. Mean, SD and individual values are shown for 3 independent repeats. P-values were calculated using an ordinary one-way ANOVA (* = $p < 0.05$, ** = $p < 0.01$, *** = $p<0.001$. **** = $p<0.0001$).

There was a small increase in multinucleation at 24 Hr with Barasertib or IR alone (ns vs DMSO) (Fig 5.6 H). In comparison, the combination treatment had higher levels, which were significantly higher than DMSO control (p=0.0025). By 72 Hr, IR-induced multinucleation was high with >20% of interphase cells being multinucleated (p=0.0035). Likewise, multinucleation in the combination treatment was high (P=0.0006), with levels being higher than that of IR alone on each of 3 independent repeats (ns).

5.3.2.3. Mitotic Phase

Mitotic cells were also scored for mitotic phase (Fig 5.7 A). Prometaphase and metaphase cells were grouped for analysis as chromosomal segregation defects can lead to accumulation in both phases. At 24 Hr post-IR, there were increased proportion of cells in prometaphase and metaphase in 50 nM Barasertib (p=0.0437) and IR, with a further increase in the combination condition (p=0.0003) (compared to DMSO control) (Fig 5.7 C). By 72 Hr, the IR alone cells show a lower prometaphase and metaphase population than the two Barasertib conditions, closer to the DMSO control. However, in 50 nM Barasertib and combination conditions metaphase cells were still increased at 72 Hr (p=0.0023 and p=0.0219), respectively, compared to DMSO control) (Fig 5.7 C). This supports an issue with chromosome segregation or extended SAC activation.

The proportion of cells in cytokinesis decreased similarly in the 50 nM Barasertib alone and 4 Gy IR alone conditions (p=0.0084 and p=0.0161, respectively, compared to the DMSO control) (Fig 5.7 D). There were fewer cells again in cytokinesis in the combination condition at 24 Hr. This decrease was significant

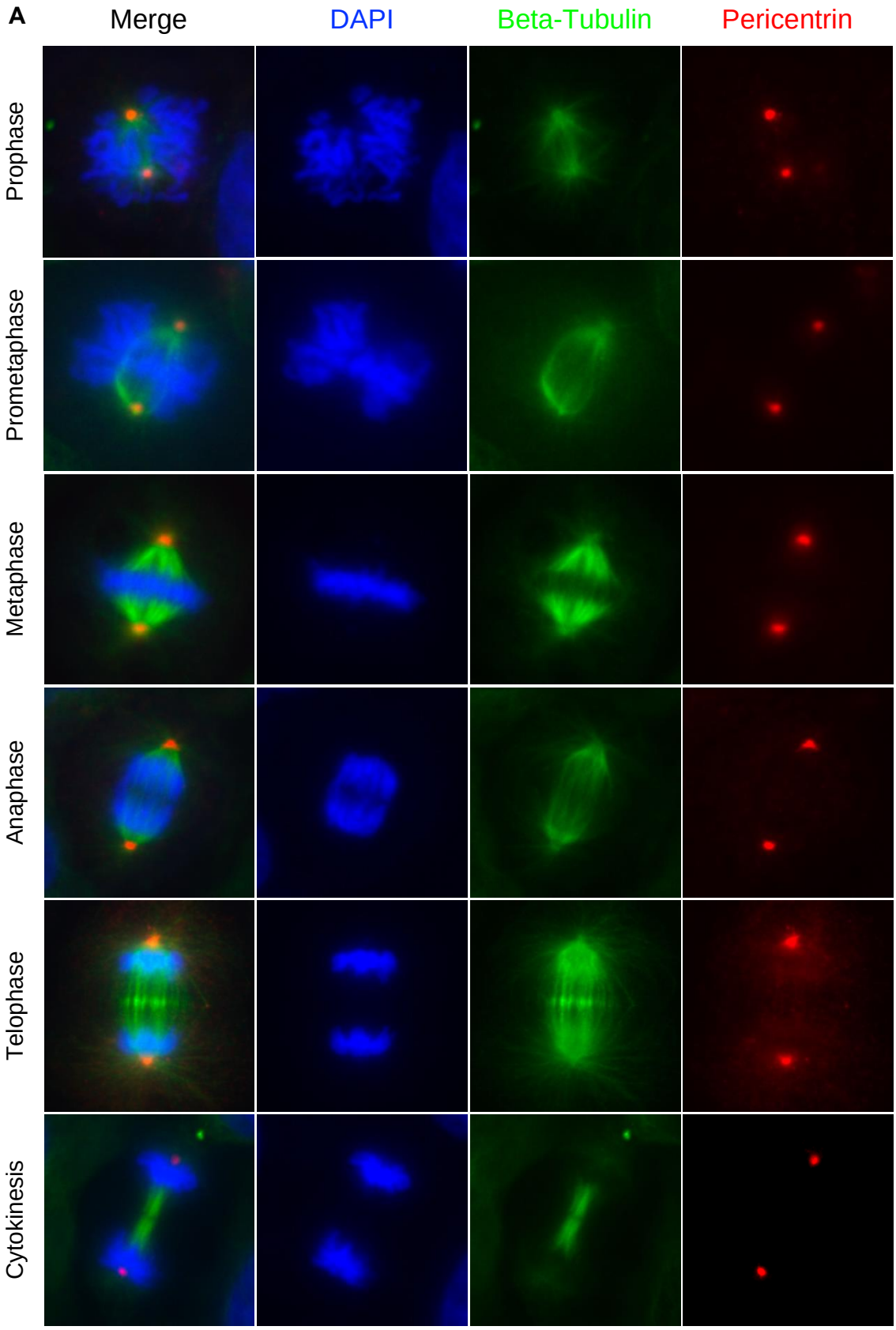

Figure 5.7: Barasertib leads to accumulation of cells in early mitosis

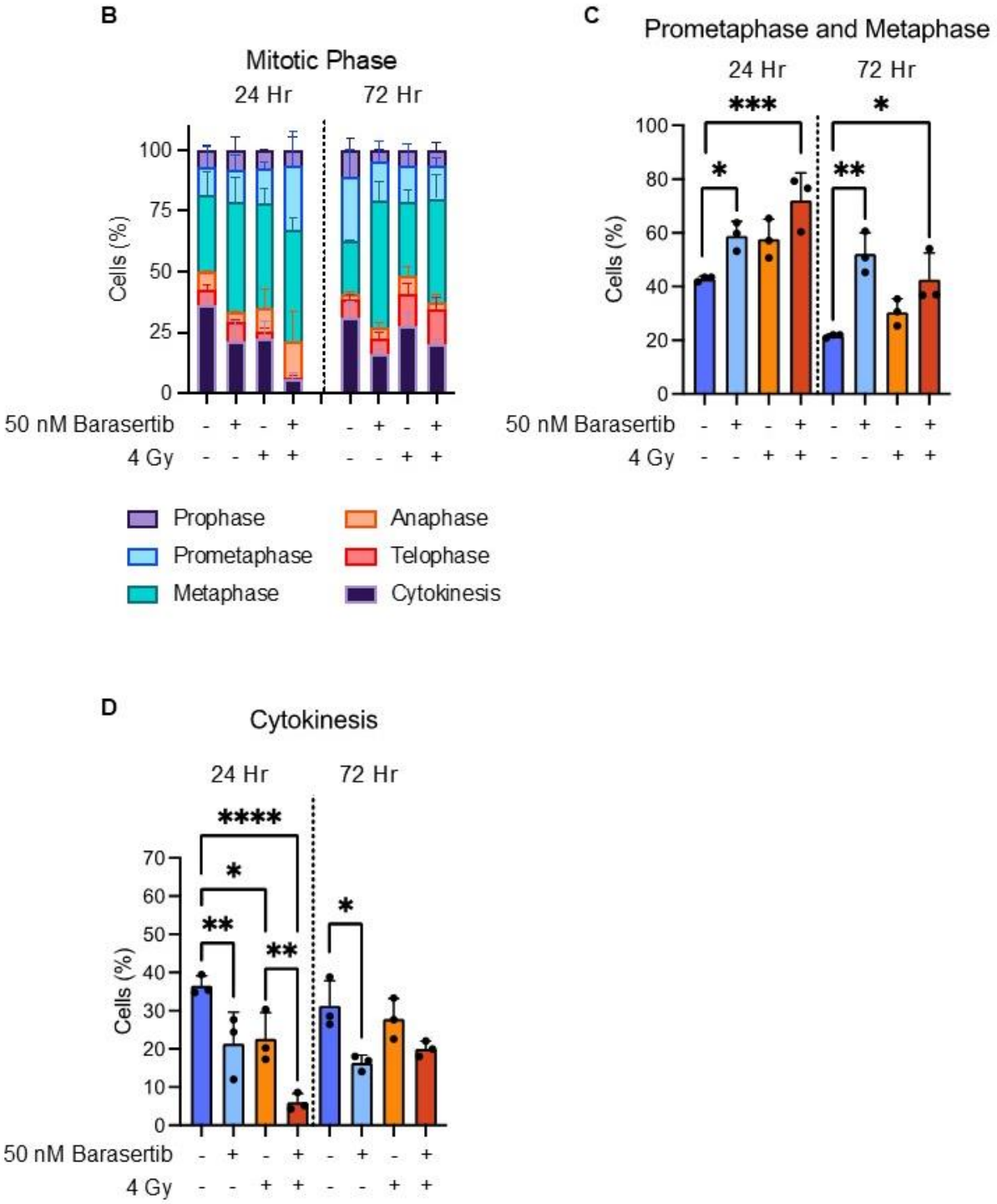

Figure 5. 7: Barasertib leads to accumulation of cells in early mitosis

H460 cells were pretreated with DMSO or 50 nM Barasertib for 1 Hr before 4 Gy (or sham) IR. Cells were fixed after 24 or 72 Hr and stained DAPI, Beta-Tubulin and Pericentrin. >50 per condition per repeat were imaged and scored for mitotic phase. **A** Representative images of Mitotic phases. Quantification of Mitotic phase: **B** All phases **C** Cells in metaphase **D** Cells in cytokinesis**.** Values shown are the percentage of mitotic cells. Mean, SD and individual values are shown for 3 independent repeats. P-values were calculated using an ordinary one-way ANOVA (* = $p < 0.05$, ** = $p < 0.01$, *** = $p<0.001$. **** = $p<0.0001$).

compared to DMSO and 4 Gy alone ($p<0.0001$ and $p=0.0041$, respectively)(Fig 5.7 D). At 72 Hr, there were still reduced proportions of cells in cytokinesis in 50 nM Barasertib ($p=0.0142$) and combination conditions (ns), whilst the IR condition showed similar cytokinesis populations to the DMSO control.

At 72 Hr, there are inverse trends in the pre-metaphase and cytokinesis populations. Longer time in metaphase could be due to chromosome segregation defects. This kind of defect was increased by all three treatments, but IR-treated cells may overcome these issues faster than cells in the combination condition as AURKB activity, required for resolution of erroneous MT-KT connections, is not inhibited.

Given that the overall trend in increasing mitotic duration (Combination > 4 Gy > 50 nM at 72 Hr Barasertib) (Section 5.3.1), it is more likely that the metaphase duration is increased by Barasertib and/or IR, than that cytokinetic duration is decreased.

5.4. Investigation of Active Replication after IR and Barasertib Treatment in H460 Cells

In section 5.2, we explored the cell cycle and found decreased S phase populations after IR up to 72 hours. While PI staining can be used to gate for S phase cells based on relative DNA content, BRDU staining is a more accurate method of identifying S phase populations. Therefore, we used BRDU incorporation, anti-BRDU staining and flow cytometry to investigate the actively replicating populations after IR and Barasertib treatment. Representative gating examples are shown in Appendix Figure 10.

H460 cells were treated with DMSO or 50 nM Barasertib 1 Hr before 4 Gy IR. Barasertib was then left in the culture during recovery from IR in the combination treatment. At 24 (n=3), 48 (n≥2) and 72 Hr (n≥1) after IR, cells were incubated with BRDU for 15 min before fixing and staining for BRDU and PI.

In the DMSO conditions, there were similar levels of BRDU+ cells over all timepoints. After 50 nM Barasertib, there was a decrease in BRDU+ cells at each timepoint. This occurred in each repeat but was not statistically significant due to the variation in data and lack of repeats.

After 4 Gy alone, there was a decrease in BRDU+ cells at 24 Hr ($p=0.0004$) (Fig 5.8). At 48 and 72 Hr, the BRDU+ population was observably lower than the DMSO control, but variation was high. The combination condition showed similar trends to the IR condition, but consistently showed slightly lower BRDU+ population than IR alone. There was a decrease in BRDU+ cells after combination treatment at 24 Hr compared to the DMSO control ($p<0.0001$) (Fig 5.8), but this was not significantly

lower than 4 Gy alone. There was also a decrease in the combination condition at 48 Hr (ns) and 72 Hr (p=0.0335) (Fig 5.8).

Overall, there was a trend of reduced levels of actively replicating cells after IR which remain low up to 72 Hr. These results support the S phase quantification from section 5.2 and show that fewer H460 cells are in S phase after IR for at least 72 Hr.

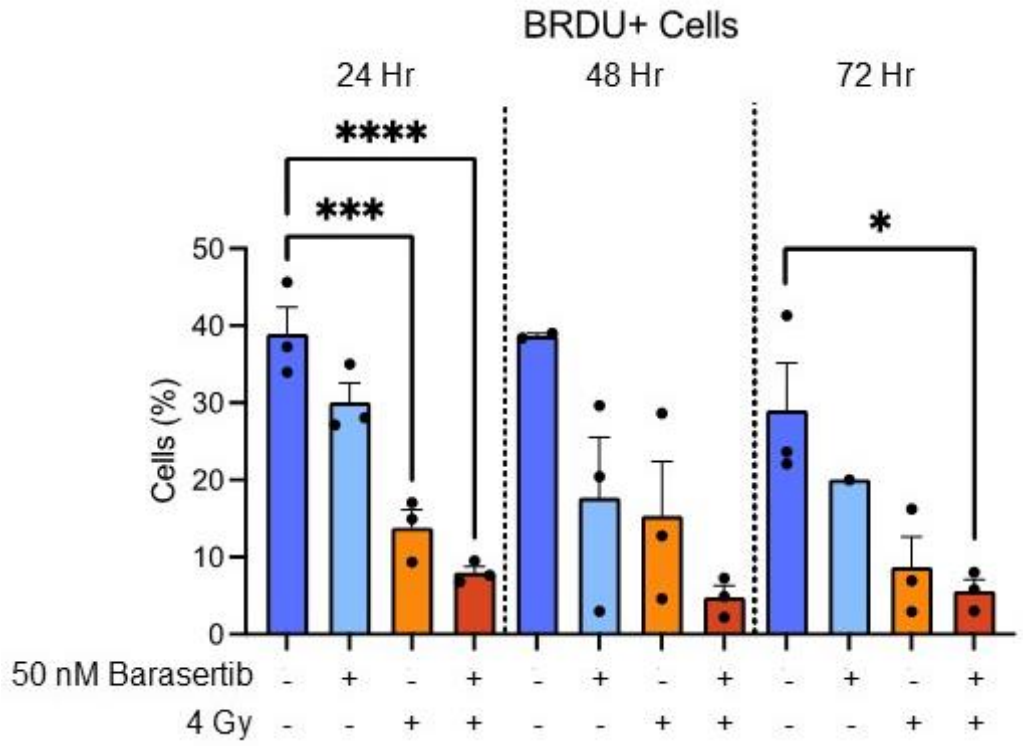

Figure 5. 8: Barasertib and IR contibute to decreases in replicating populations

H460 cells were pretreated with DMSO or 50 nM Barasertib for 1 Hr before 4 Gy (or sham) IR. Cells were treated with 10 μM BRDU then fixed and stained for DNA content (PI) and BRDU. Percentage of BRDU+ gated cells in G1, S and G2. Mean, SD and individual values are shown for 1-3 independent repeats. P-values were calculated using an ordinary one-way ANOVA (* = $p < 0.05$, ** = $p < 0.01$, *** = $p<0.001$. **** = $p<0.0001$).

.

5.4.1. Effect of Hydroxyurea (HU) Treatment on Cell Survival after Barasertib Treatment

To further explore the effect of Barasertib on replication, the effect of Barasertib on survival after HU treatment (an inducer of replication stress) was investigated by clonogenic assay. Cells were co-treated with Barasertib (DMSO or 25-100 nM) plus HU (media control or 0.1-0.2 mM), with drugs added at the same time.

Barasertib treated at 25nM, 50 nM and 100 nM significantly decreased survival after HU in a dose-dependent manner ($p=0.0004$, $p<0.0001$ and $p<0.0001$, respectively) (Fig 5.9). This corroborates published results in Hela that Barasertib sensitises to HU, and supports a role for AURKB in cell survival/proliferation after replication stress.

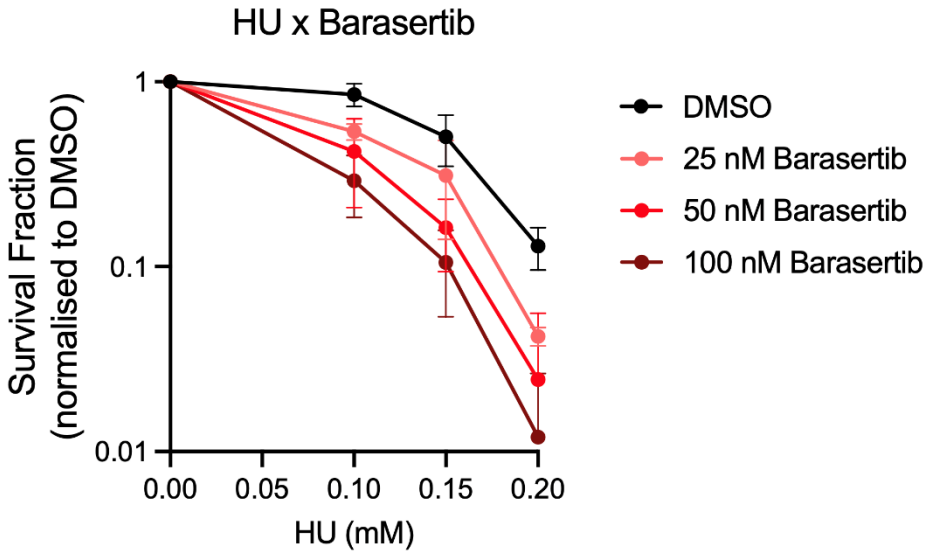

Figure 5. 9: Barasertib sensitises to HU treatment

H460 cells were cotreated with Hydroxyurea (HU) between 1-2 mM and Barasertib Between 25 – 100 mM for 8 days before staining counting colonies formed. Survival fraction normalised to DMSO survival at 0 mM HU (media control).

5.5. Investigation of DDR Markers after IR and Barasertib Treatment

Given the importance of repairing DNA damage after IR for cell survival, we wanted to investigate whether Barasertib altered DDR and repair following

To investigate the DDR after Barasertib, foci of the DDR markers γH2AX, 53BP1 and RAD51 were investigated.

5.5.1. γH2AX and Micronuclei after Barasertib and IR Treatment

5.5.1.1. γH2AX Foci

H2AX is rapidly phosphorylated at Ser139 (known as γH2AX) in response to DNA damage, which promotes recruitment of repair factors to sites of damage (Podhorecka et al., 2010). γH2AX foci at sites of damage are resolved once the damage is repaired. Therefore, γH2AX foci are commonly employed as a biomarker for DNA damage (Huang and Zhou, 2020).

H460 cells were treated as detailed above and fixed at 30 minutes, 6 and 24 Hr after IR before staining for γH2AX plus DAPI nuclear staining (Fig 5.10 A-C).

In the DMSO condition, there was a consistent low level of γH2AX foci/nuclei across all timepoints (Fig 5.10 D-F). Some cells with foci are expected as cancer cells often harbour endogenous DNA damage due to metabolic or replicative stress.

50nM Barasertib alone did not affect levels of γH2AX foci (Fig 5.10 D-F). This contradicts reports that Barasertib can induce foci, albeit after 48 Hr (Fell et al., 2016).

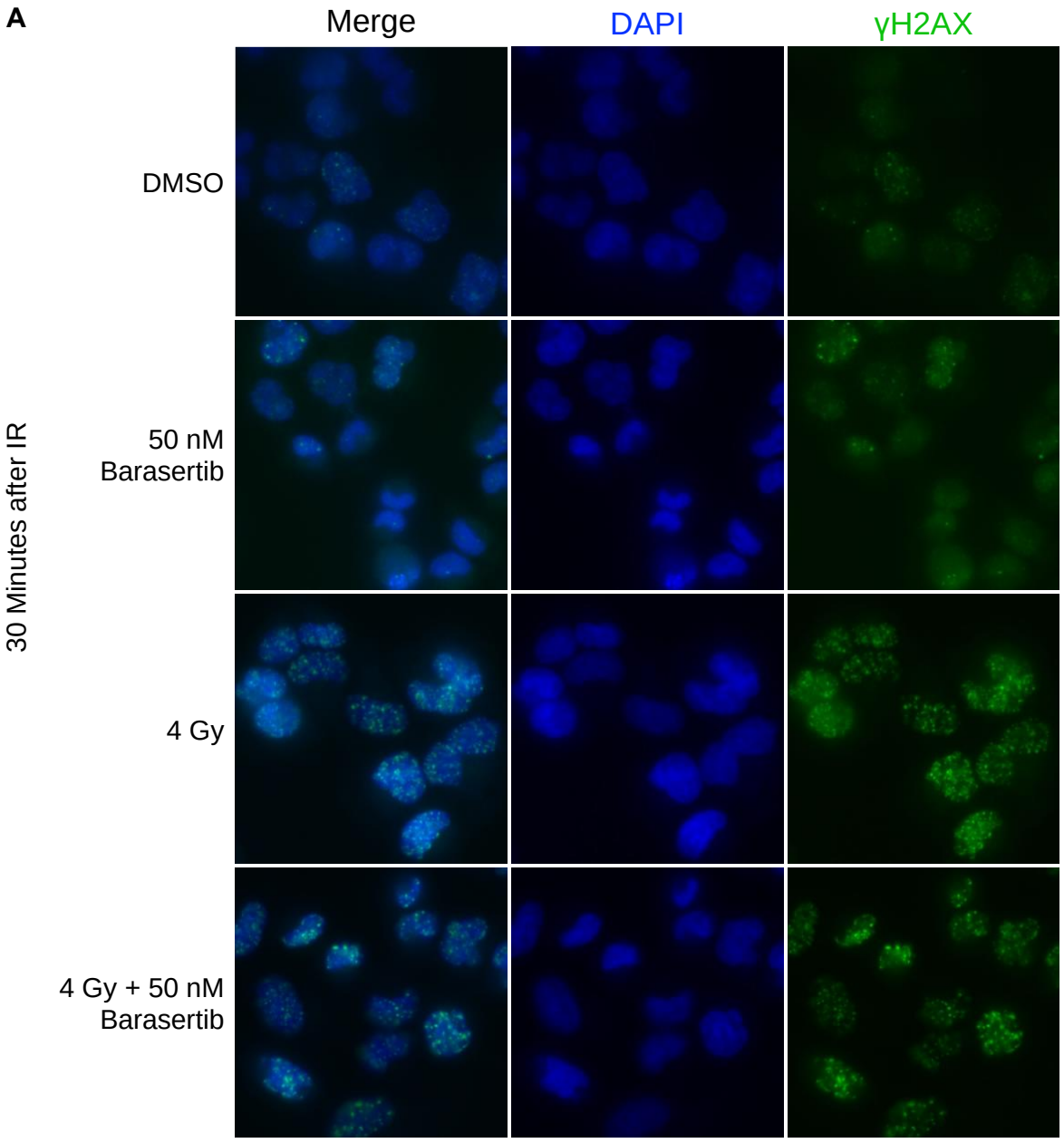

Figure 5. 10: γH2AX Foci are induced by IR but affected by Barasertib

H460 cells were pretreated with DMSO or 50 nM Barasertib for 1 Hr before 4 Gy (or sham) IR, then fixed immediately or after 30 Mins, 6 Hr or 24 Hr. Cells were stained for γH2AX (ser139) and DAPI. Foci were quantified by cell profiler pipeline for foci counting. Representative images of γH2AX Foci **A** 30 Minutes after IR **B** 6 Hr after IR and **C** 24 Hr after IR. **D** Mean γH2AX Foci per nuclei **E** Median γH2AX Foci per nuclei overtime Mean or Median, SEM and individual values are shown for ≥ 3 independent repeats. P-values were calculated using an ordinary one-way ANOVA per timepoint (* = $p < 0.05$, ** = $p < 0.01$, *** = $p<0.001$. **** = $p<0.0001$).

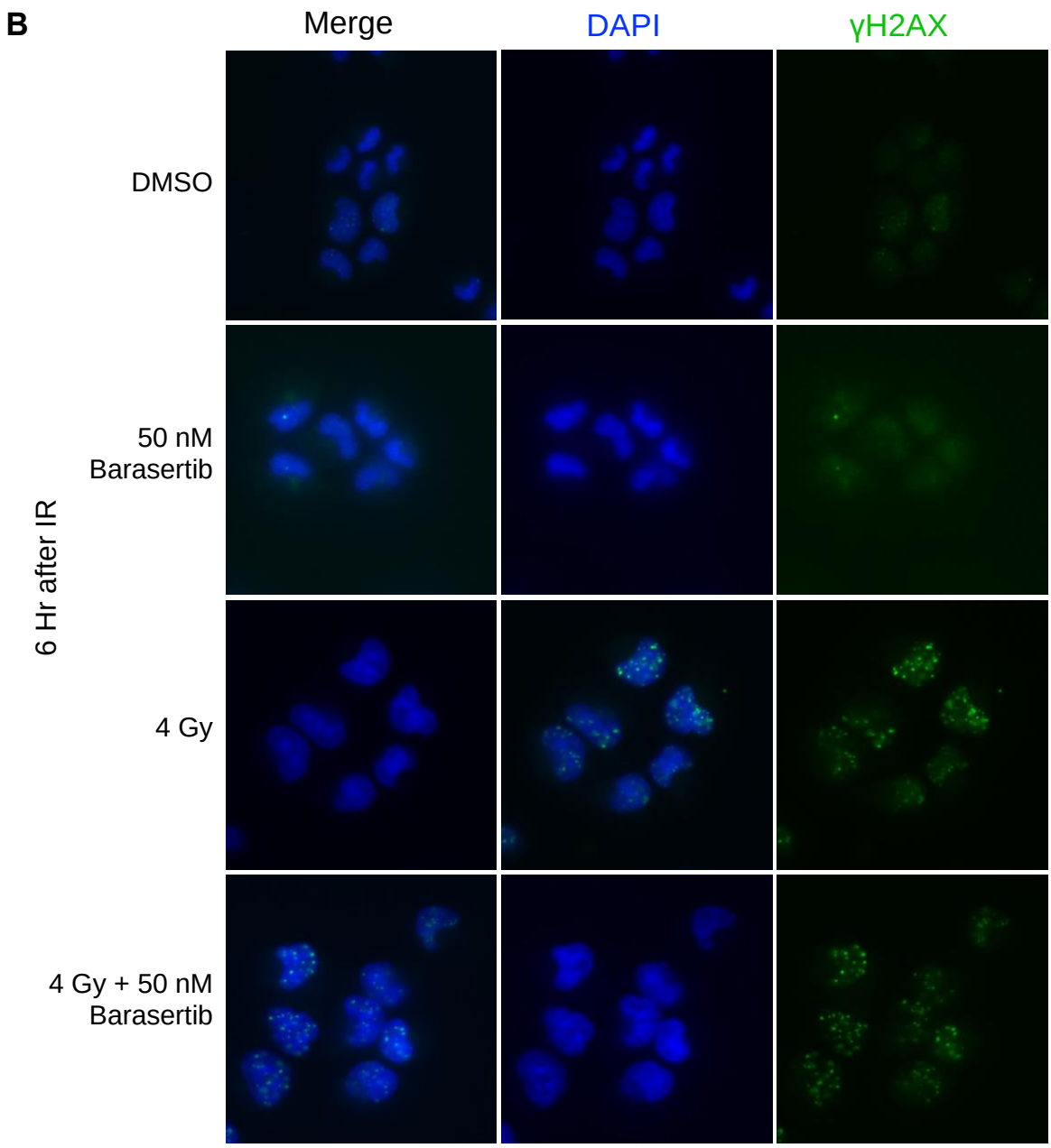

Figure 5.10: γH2AX Foci are induced by IR but affected by Barasertib

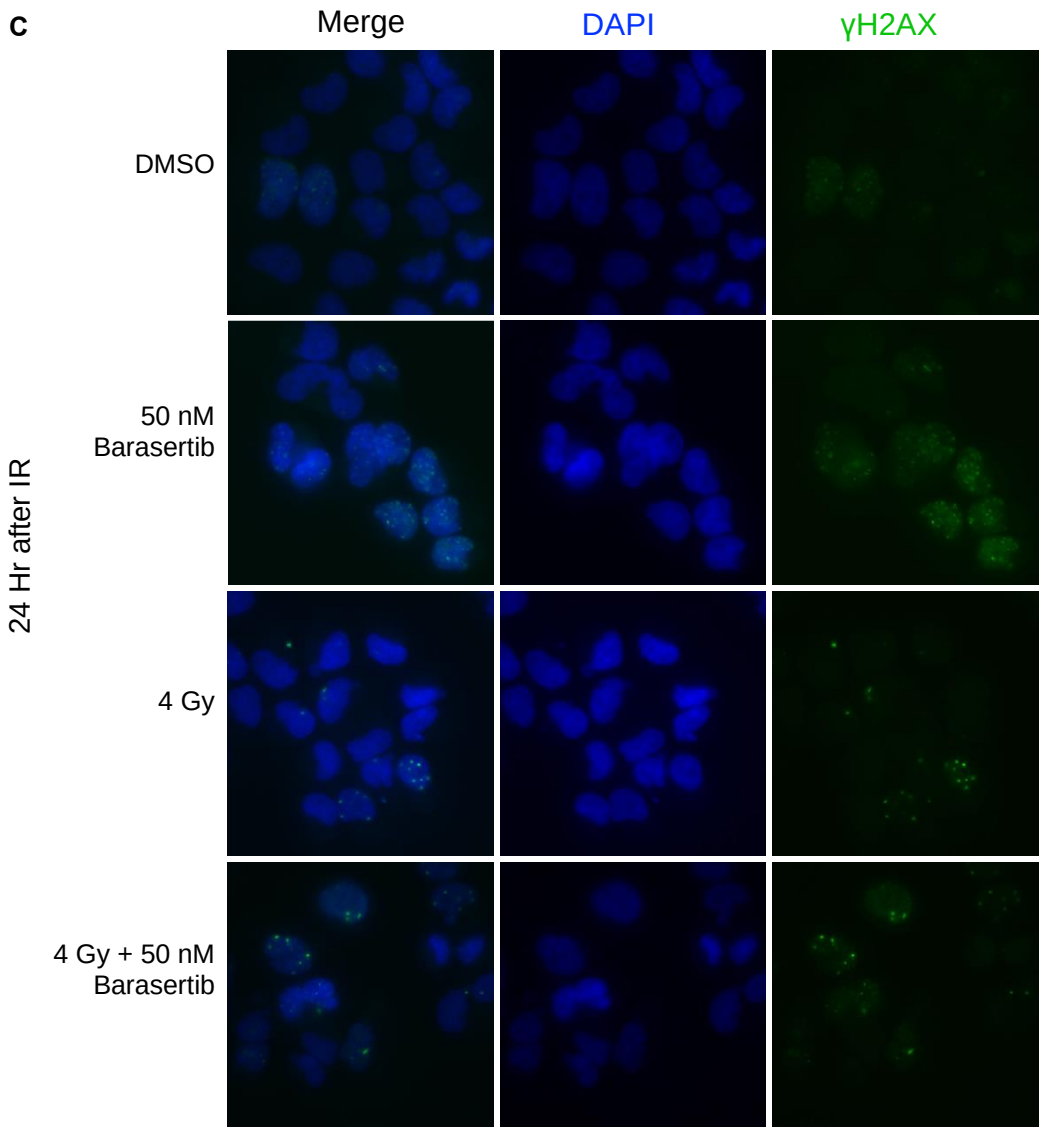

Figure 5.10: γH2AX Foci are induced by IR but affected by Barasertib

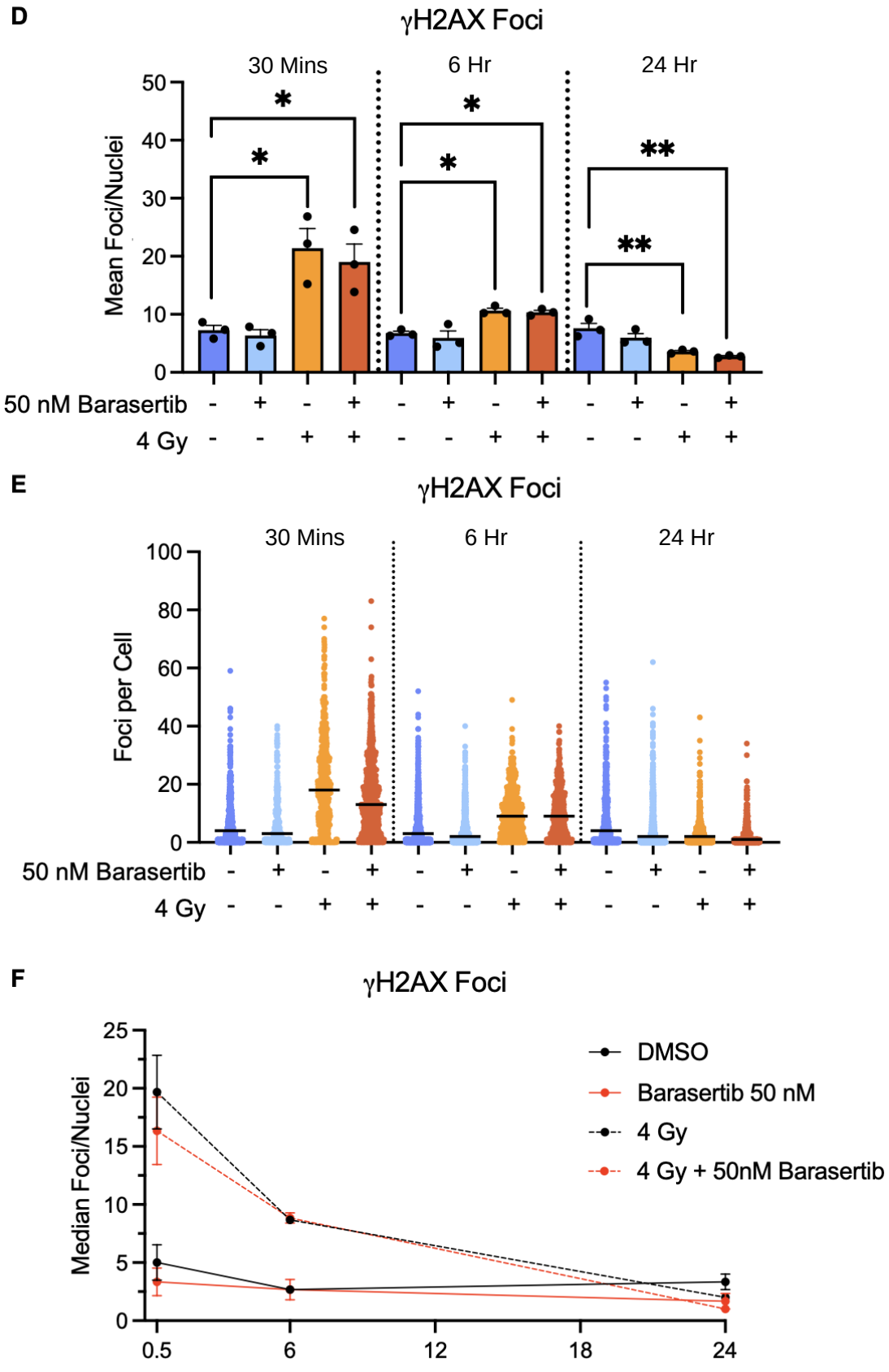

Figure 5.10: γH2AX Foci are induced by IR but unaffected by Barasertib

After 4Gy IR, there were increased γH2AX foci/nuclei after 30 minutes compared to the DMSO control (Fig 5.10 D-F). This demonstrates a normal DDR to damage induced by IR. By 6 Hr, γH2AX foci/nuclei were reduced but not to level of DMSO (Fig 5.10 D-F), which indicates partial resolution of damage. At 24 Hr, there were significantly fewer γH2AX foci in the IR condition compared to DMSO (Fig 5.10 D-F).

In the combination condition, the trend mirrored that of IR alone. There was a non-significant peak in γH2AX foci/nuclei at 30 minutes (Fig 5.10 B and C), with similar kinetics of repair over time to 4 Gy alone. At 6 Hr, γH2AX levels decreased, but were still higher than the DMSO control (Fig 5.10 D-F). At 24 Hr, γH2AX foci/nuclei were significantly lower than the DMSO control, similar to IR alone (Fig 5.10 D-F).

Overall, a normal γH2AX response was observed in H460 cells after IR which was not altered by 50 nM Barasertib. The low foci/cell number at 24 Hr in the 4 Gy and Combination conditions is unusual. This may be due to repair of endogenous damage after activation of DNA repair signalling, although we didn't see this effect reproduced in other DDR markers in later sections.

5.5.1.2. Investigation of Micronuclei after IR and Barasertib

The staining of cells with DAPI and anti-γH2AX Ab also allowed for analysis of γH2AX positive and negative micronuclei after IR and Barasertib treatment.

Micronuclei per nuclei were quantified at 30 Mins, 6 and 24 Hr after IR, and classified as γH2AX negative or positive (Fig 5.11 A). γH2AX+ scoring in micronuclei indicates persistent DNA damage and may indicate the presence of fragmented DNA. In the DMSO condition, there was a low level of micronuclei across all timepoints. The presence of Barasertib did not increase micronuclei incidence, compared to the DMSO control at any timepoint. After 4 Gy IR, there was a small increase in micronuclei formation by 6 Hr and a large increase by 24 Hr compared to the DMSO control ($p=0.0006$) (Fig 5.11 B).

In the presence of Barasertib, there was also a small increase (ns) 6 Hr after IR, and a significant increase in total micronuclei 24 Hr after IR compared to the DMSO control ($p=0.0003$) (Fig 5.11 B). The combined treatment showed similar levels of micronuclei to 4 Gy alone at each timepoint.

In summary, micronuclei formed in H460 cells after 4 Gy by 24 Hr, but micronuclei levels were unaffected by Barasertib treatment. There were no clear trends in the prevalence of γH2AX+ or γH2AX- foci across treatments with an equal number in most conditions.

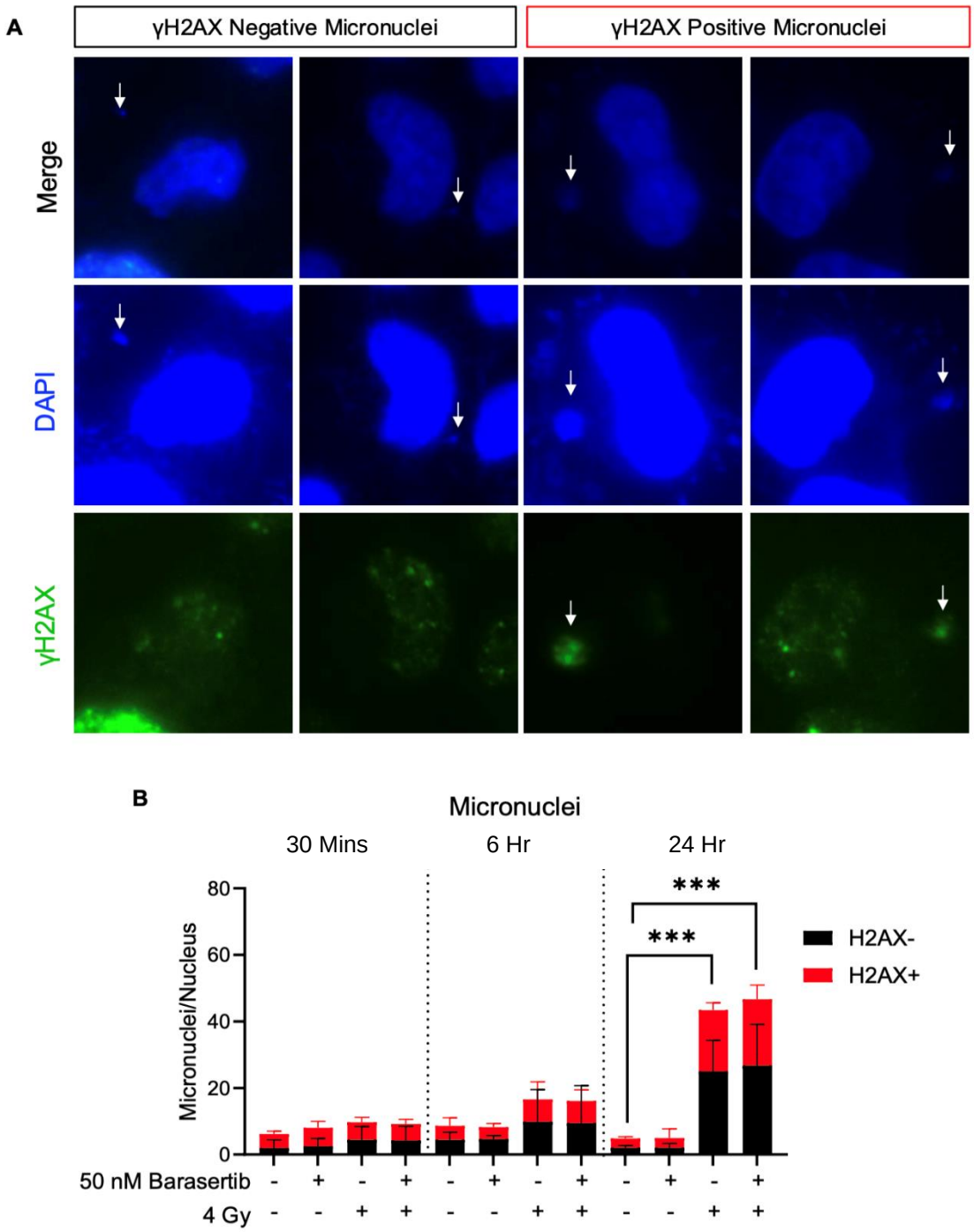

Figure 5. 11: γH2AX micronuclei are induced by IR after 24 Hr

H460 cells were pretreated with DMSO or 50 nM Barasertib for 1 Hr before 4 Gy (or sham) IR, then fixed immediately or after 30 Mins, 6 Hr or 24 Hr. Cells were stained for γH2AX (ser139) and DAPI. Micronuclei per nuclei were counted manually and scored as γH2AX positive or negative. **A** Representative images of γH2AX micronuclei – intensity was increased in single channel images to aid visualisation **C** Mean γH2AX micronuclei per nuclei. Mean or Median, SEM and individual values are shown for ≥ 3 independent repeats. P-values were calculated using an ordinary one-way ANOVA per timepoint (* = $p < 0.05$, ** = $p < 0.01$, *** = $p<0.001$. **** = $p<0.0001$).

5.5.2. 53BP1 Foci and Nuclear Bodies after Barasertib and IR treatment

53BP1 is a DDR mediator which responds rapidly to sites of DSBs to form distinct foci and recruits other DDR proteins to sites of damage. Several 53BP1 phosphopeptides were also more abundant in the combination compared to 4 Gy alone in the phosphoproteomic analysis.

5.5.2.1. 53BP1 Foci

The formation of 53BP1 foci after IR and their resolution over time was examined in H460 cells. Representative staining at 0 - 1 Hr timepoints are shown in Figure 40 A-D and representative images for later timepoints are shown in Appendix Figure 11.

In DMSO and 50 nM Barasertib conditions, there was a low number of foci/nuclei across all timepoints (Fig 5.12 E-G).

After 4 Gy, there was a large increase in foci/nuclei by 10 mins post-IR which increases further until a peak at 1 Hr. This represents recruitment of 53BP1 to sites of IR-induced DSBs. This response is known to be rapid and can be seen here after only 10 minutes. The foci/nuclei at 10 Mins, 30 Mins and 1 Hr after 4 Gy were significantly higher than the DMSO control (Fig 5. 12 E-G). Foci/nuclei decreased after 1 Hr with the majority of foci resolved by 6 Hr and an average of less than 3 foci/nuclei remaining at 24 Hr. This indicates that resolution of most DSBs was successful. Compared to the DMSO control, the 4 Gy condition was significantly increased above the control for the remaining timepoints, 3 Hr, 6 Hr and 24 Hr (Fig 5.12 E-G).

After IR and Barasertib combination treatment, there was a similar trend to the 4 Gy alone condition in initial 53BP1 foci formation up to 10 minutes (Fig 5.12 E-G).

However, the peak in 53BP1 foci after IR with Barasertib was at 30 Mins rather than 1 Hr as seen in the 4 Gy condition. By 1 Hr post-IR, 53BP1 foci/nuclei had decreased and resolution of foci was shown by further decrease until less than 3 foci/nuclei remained at 24 Hr.

After 1 Hr, the 4 Gy alone and combination conditions showed very similar kinetics for 53BP1 foci resolution. In the combination condition, foci/nuclei were increased above the DMSO control at 10 and 30 Mins, as well as 1, 3, 6 and 24 Hr post-IR (Fig 5.12 E-G). The small increase in foci/nuclei in the combination treatment above the 4 Gy condition at 30 Mins was not significant.

Overall, in both the 4 Gy and combination treatment, 53BP1 is successfully recruited to DNA after IR, and foci are resolved successfully by 24 Hr. There is some evidence of a small change in the time of the peak 53BP1 signalling, with the combination condition showing a higher and earlier peak, but the overall kinetics of DSB resolution do not appear to be affected. The change in 53BP1 peak between 30-1 Hr after IR aligns with the phosphoproteomic data which suggested altered phosphorylation of 53BP1 1 Hr after IR.

However, this change does not affect 53BP1 foci resolution. By 24 Hr, IR induced 53BP1 foci are resolved regardless of Barasertib, indicating successful DSB repair.

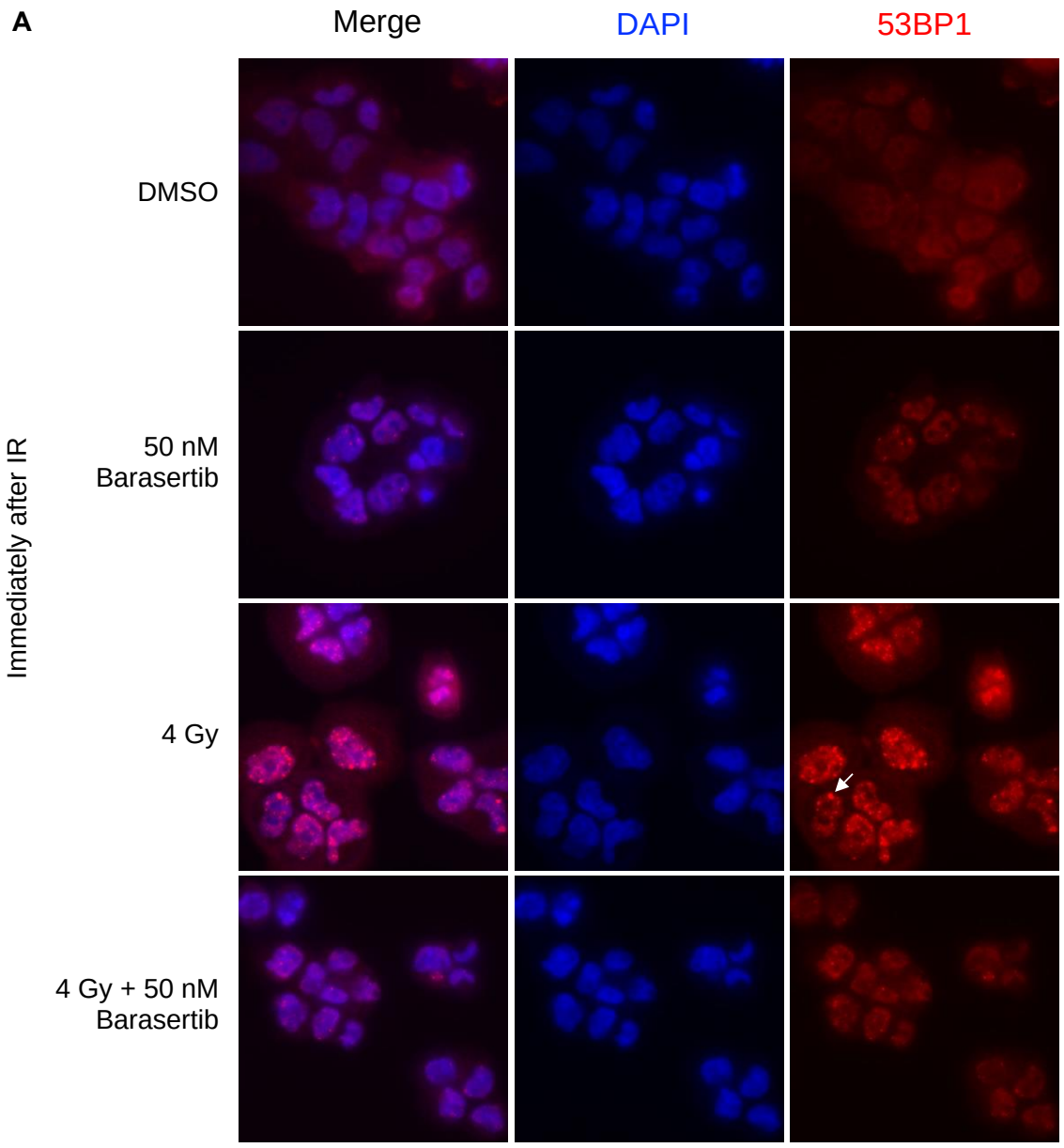

Figure 5.12: 53BP1 foci and nuclear bodies are induced by IR but unaffected by Barasertib

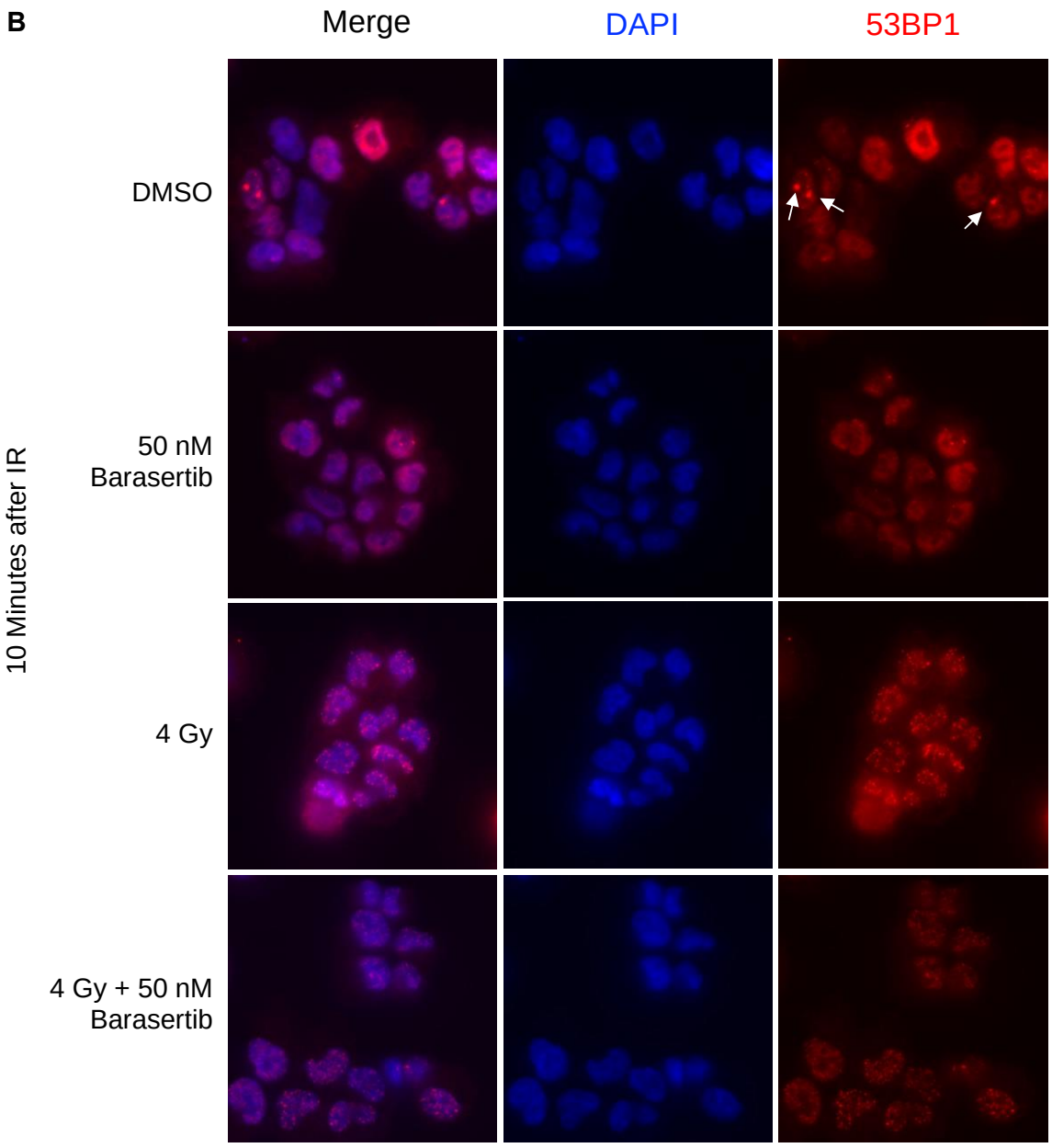

Figure 5.12: 53BP1 foci and nuclear bodies are induced by IR but unaffected by Barasertib

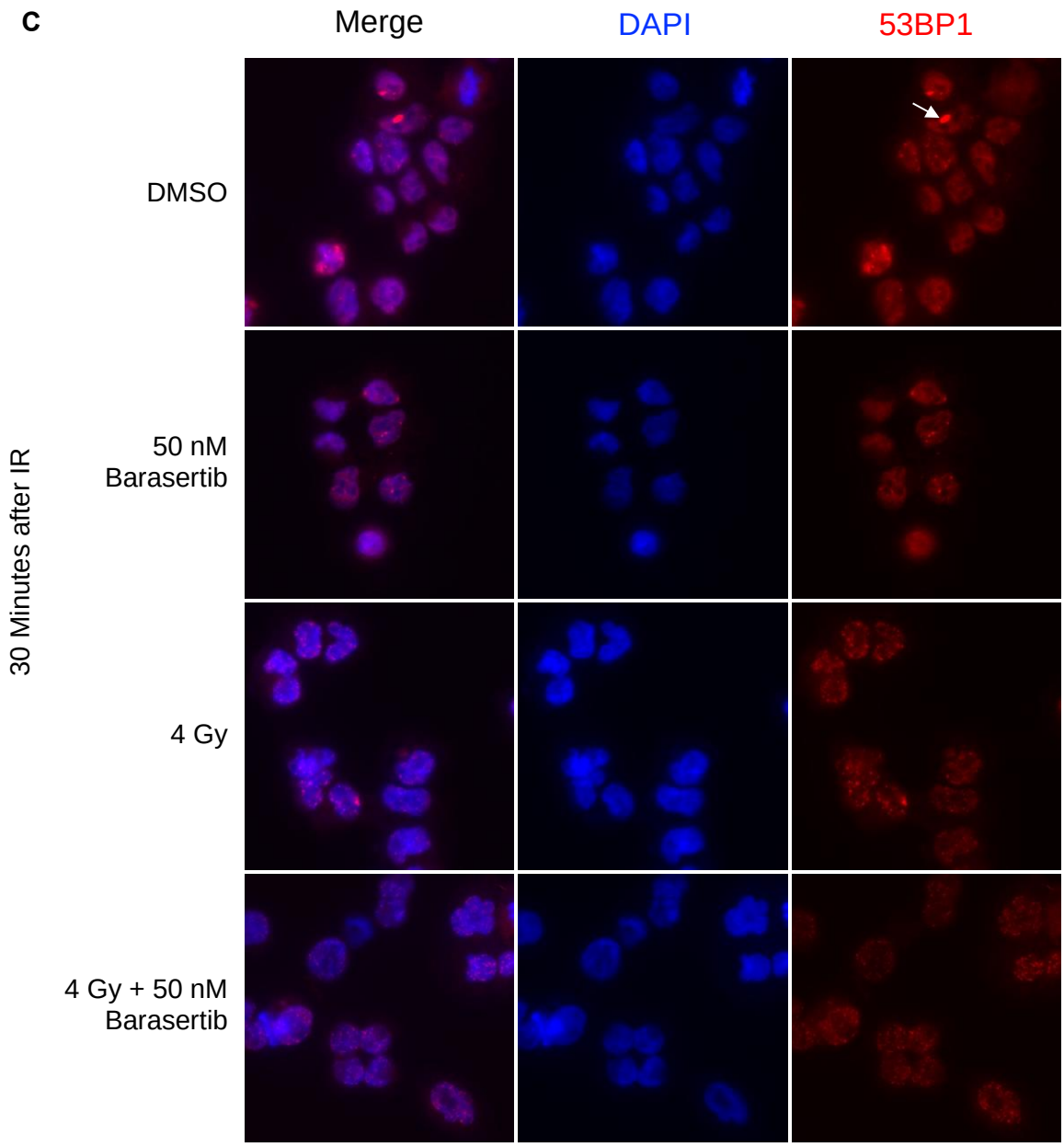

Figure 5.12: 53BP1 foci and nuclear bodies are induced by IR but unaffected by Barasertib

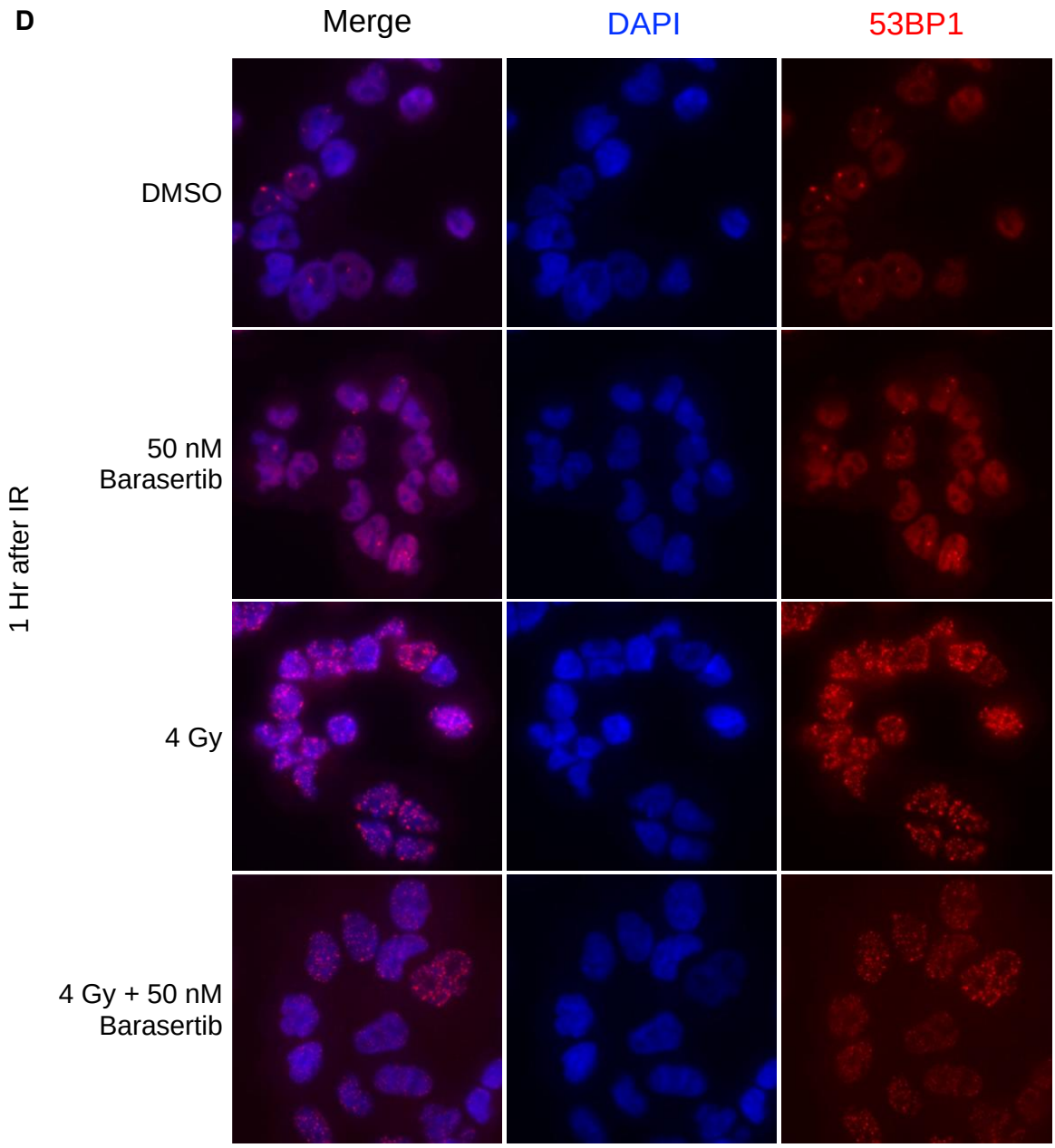

Figure 5.12: 53BP1 foci and nuclear bodies are induced by IR but unaffected by Barasertib

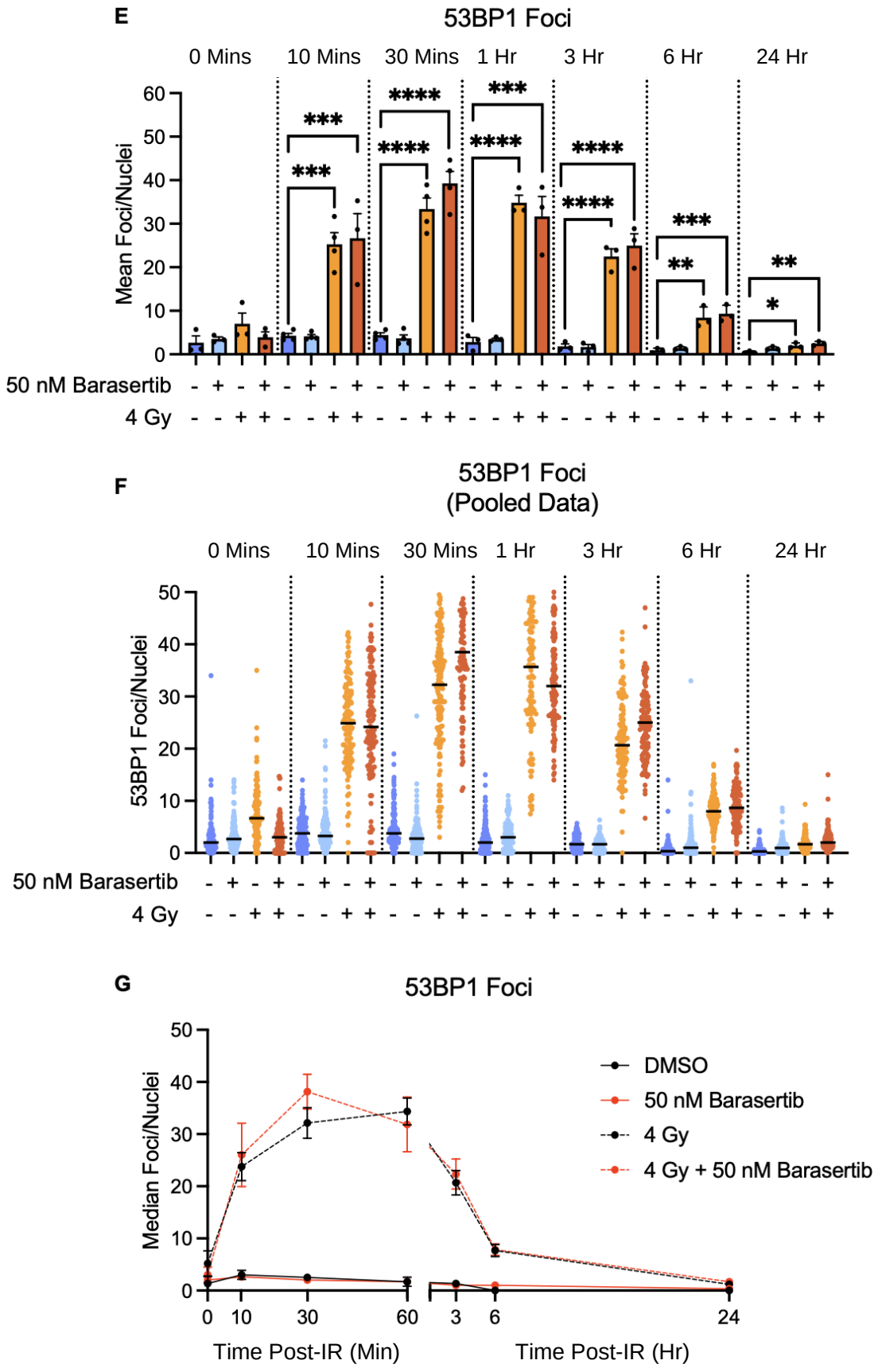

Figure 5.12: 53BP1 foci and nuclear bodies are induced by IR but unaffected by Barasertib

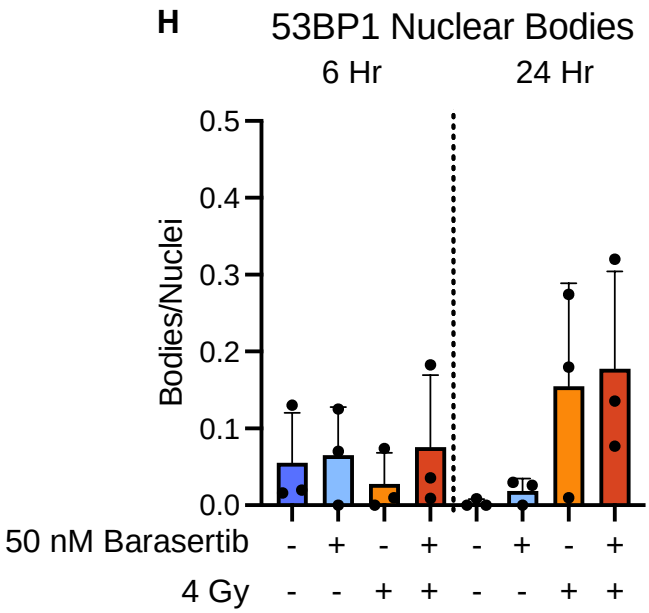

Figure 5. 12: 53BP1 foci and nuclear bodies are induced by IR but unaffected by Barasertib

H460 cells were pretreated with DMSO or 50 nM Barasertib for 1 Hr before 4 Gy (or sham) IR, then fixed immediately or 10 or 30 Mins, or 1,3,6, or 24 Hr after IR. Cells were stained for 53BP1 and DAPI. Representative images of 53BP1 foci and nuclei in H460 cells **A** immediately after IR (0 minutes)
B 10 minutes after IR **C** 30 minutes after IR and **D** 1 Hr after IR. Nuclear bodies indicated by white arrows. Foci and bodies were quantified by manual counting. **E** 53BP1 Foci/nuclei (mean and SEM) **F** Foci per nuclei (pooled data from all repeats with median indicated by black bar) **G** Median Foci/Nuclei and SEM over time **H** 53BP1 Nuclear bodies/nuclei at 6 and 24 Hr. Mean (or Median), SEM and individual values are shown for ≥ 3 independent repeats. P-values were calculated using an ordinary one-way ANOVA per timepoint (* = $p < 0.05$, ** = $p < 0.01$, *** = $p<0.001$. **** = $p<0.0001$). Data for 6 Hr and 24 Hr timepoints was collected by Refiloe Katse.

5.5.2.2. 53BP1 Nuclear Bodies

53BP1 nuclear bodies were also quantified. Examples of 53BP1 bodies are highlighted by white arrows in Figure 5.12 A-D. 53BP1 nuclear bodies are markers of replication stress and often form in G_1 after cell division (Fernandez-Vidal et al., 2017).

53BP1 nuclear bodies were quantified at 6 Hr and 24 Hr after IR, with or without a Barasertib pre-treatment (Fig 5.12 H). There were low levels of 53BP1 bodies across all conditions at 6 Hr. At 24 Hr, there was an increased in nuclear bodies in the IR and Combination conditions, but variation was high. Overall, there was a low prevalence of 53BP1 nuclear bodies in all treatment conditions at the timepoints tested. Later timepoints after multiple mitoses would have been advantageous to test if replication stress increases over time.

5.6. RAD51 Foci

RAD51 is a DNA repair protein essential for DSB repair by HR. RAD51 promotes HR by blocking MRE11-degradation of DNA strands at DSBs and catalyses key events during HR (Bhattacharya et al., 2017). It is also required for replication fork progression and restart (Hashimoto et al., 2010, Krishna et al., 2007). RAD51 form foci at DSB sites and resolution of these foci represent repair of DSBs by homologous recombination (Godthelp et al., 2002).

H460 cells were treated as detailed above and fixed at 30 minutes, 1 Hr, 3 Hr, 6 Hr and 24 Hr after IR before staining for RAD51 plus DAPI nuclear staining. Representative images for 1 – 6 Hr timepoints are shown in Figure 5.13 A – C and remaining timepoints are shown in Appendix Figure 12. Three independent repeats were carried out except the 30 minute timepoint (n=2).

In the DMSO condition, there were on average less than 3 foci/cell at all timepoints (Fig 5.13 D-F). In the 50 nM Barasertib condition, the number of RAD51 foci/cell were also very low, and mirror the DMSO condition (Fig 5.13 D-F).

After 4 Gy IR, there was initially no increase at 30 mins but foci/cell increased significantly by 1 Hr (Fig 5.13 D-F). Rad51 foci levels remained high until 3 Hr post-IR. By 6 Hr post-IR, there was a decrease in foci but numbers were still significantly increased above the DMSO control, representing partial resolution of breaks by HR. By 24 Hr, foci had returned to a low level similar to the DMSO control. The peak at 1 – 3 Hr is characteristic of RAD51 response, and is slower than the 53BP1 response (Mao et al., 2008). The resolution of foci by 24 Hr indicates successful resolution of DSBs.

After IR and Barasertib combination treatment, there was also a peak between 1 – 3 Hr post-IR. RAD51 foci/nuclei were significantly increased compared to the DMSO control at 3 Hr and 6 Hr (Fig 5.13 D-F). At 6 Hr there was a decrease in foci, which had decreased further by 24 Hr, at which point there were similar RAD51 foci numbers to the DMSO control.

The RAD51 response to IR was comparable between 4 Gy alone and combination conditions. The peak appears later in the combination condition, but given the variation between repeats at 1 and 3 Hr, this is of questionable significance. Importantly, the speed of RAD51 foci resolution is similar across 24 Hr with similarly low numbers of foci remaining by 24 Hr in either condition. In conclusion, 50 nM Barasertib does not impact RAD51 localisation to DSBs, the speed of HR or resolution of RAD51 foci.

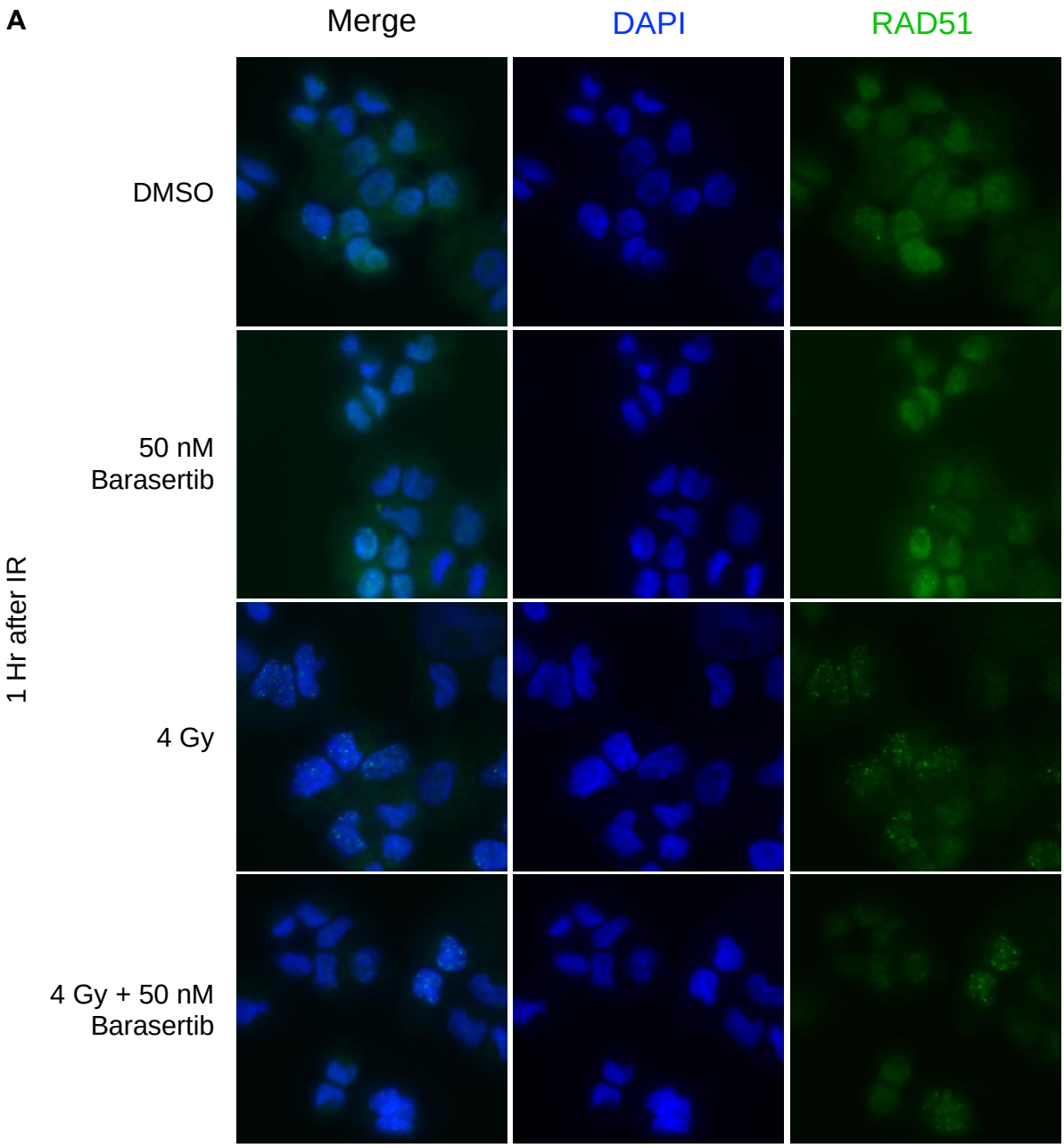

Figure 5. 13: RAD51 foci are initiated after IR and unaffected by Barasertib

H460 cells were pretreated with DMSO or 50 nM Barasertib for 1 Hr before 4 Gy (or sham) IR, then fixed immediately or 10 or 30 Mins, or 1,3,6, or 24 Hr after IR. Cells were stained for RAD51 and DAPI. Foci were quantified by manual counting. . Representative images of RAD51 foci in H460 cells at **A** 1 Hr **B** 3 Hr and **C** 6 Hr after IR. **D** Mean Foci per nuclei **C F** Foci per nuclei (pooled data from all repeats with median indicated by black bar) **F** Median Foci per nuclei over time. Mean or Median, SEM and individual values are shown for ≥ 3 independent repeats. P-values were calculated using an ordinary one-way ANOVA per timepoint (* = $p < 0.05$, ** = $p < 0.01$, *** = $p<0.001$. **** = $p<0.0001$).

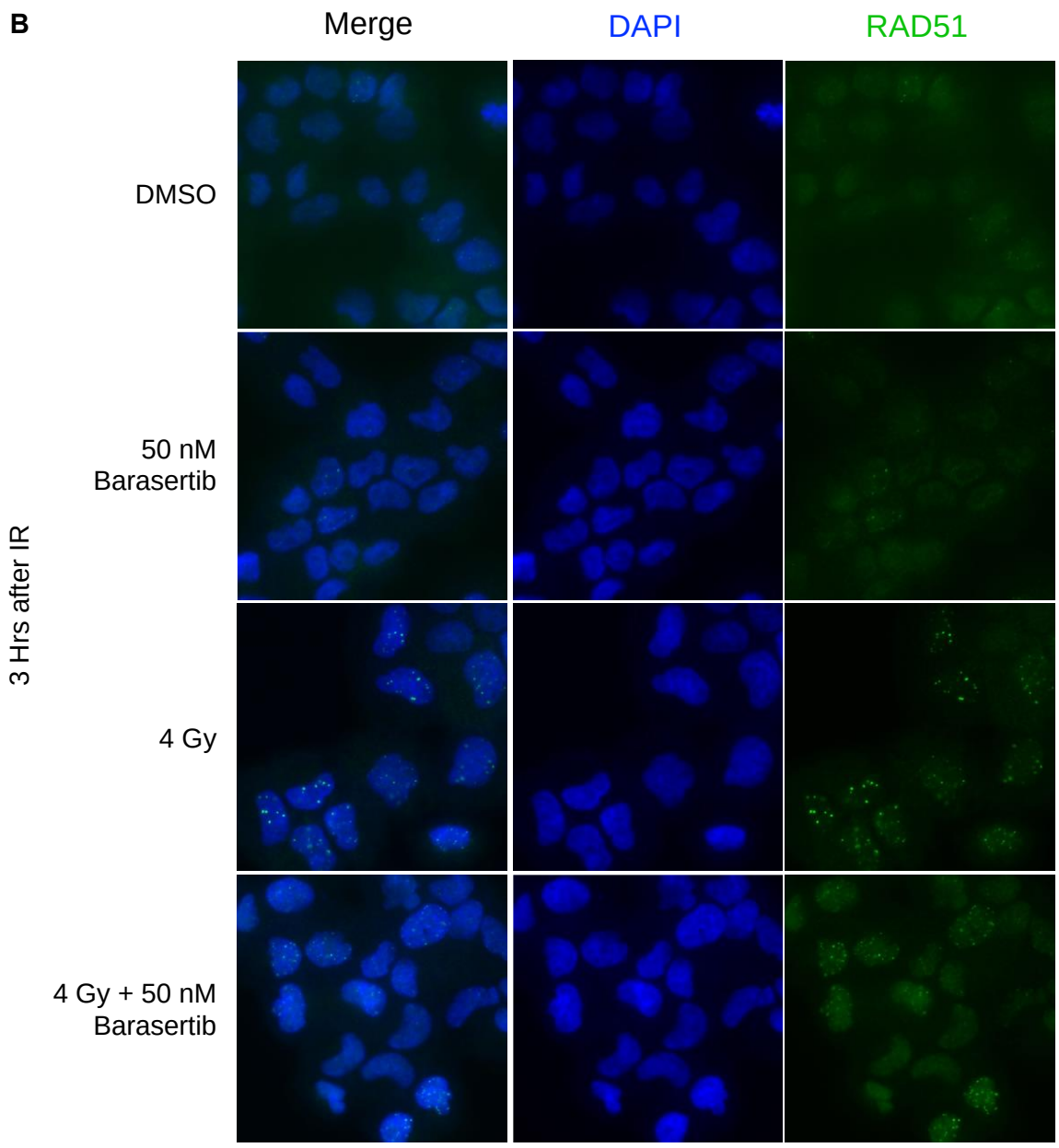

Figure 5.13: RAD51 foci are initiated after IR and unaffected by Barasertib

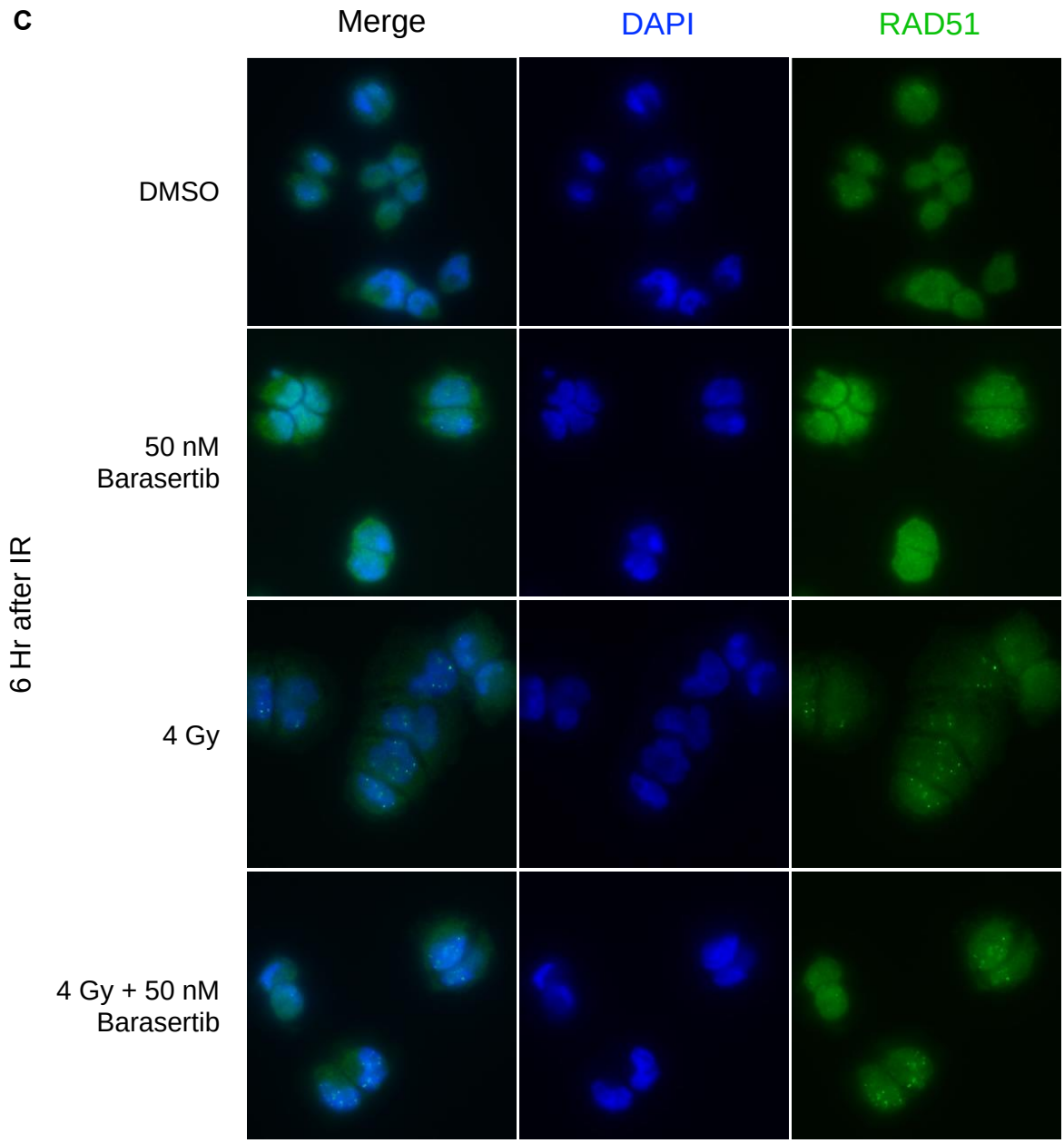

Figure 5.13: RAD51 foci are initiated after IR and unaffected by Barasertib

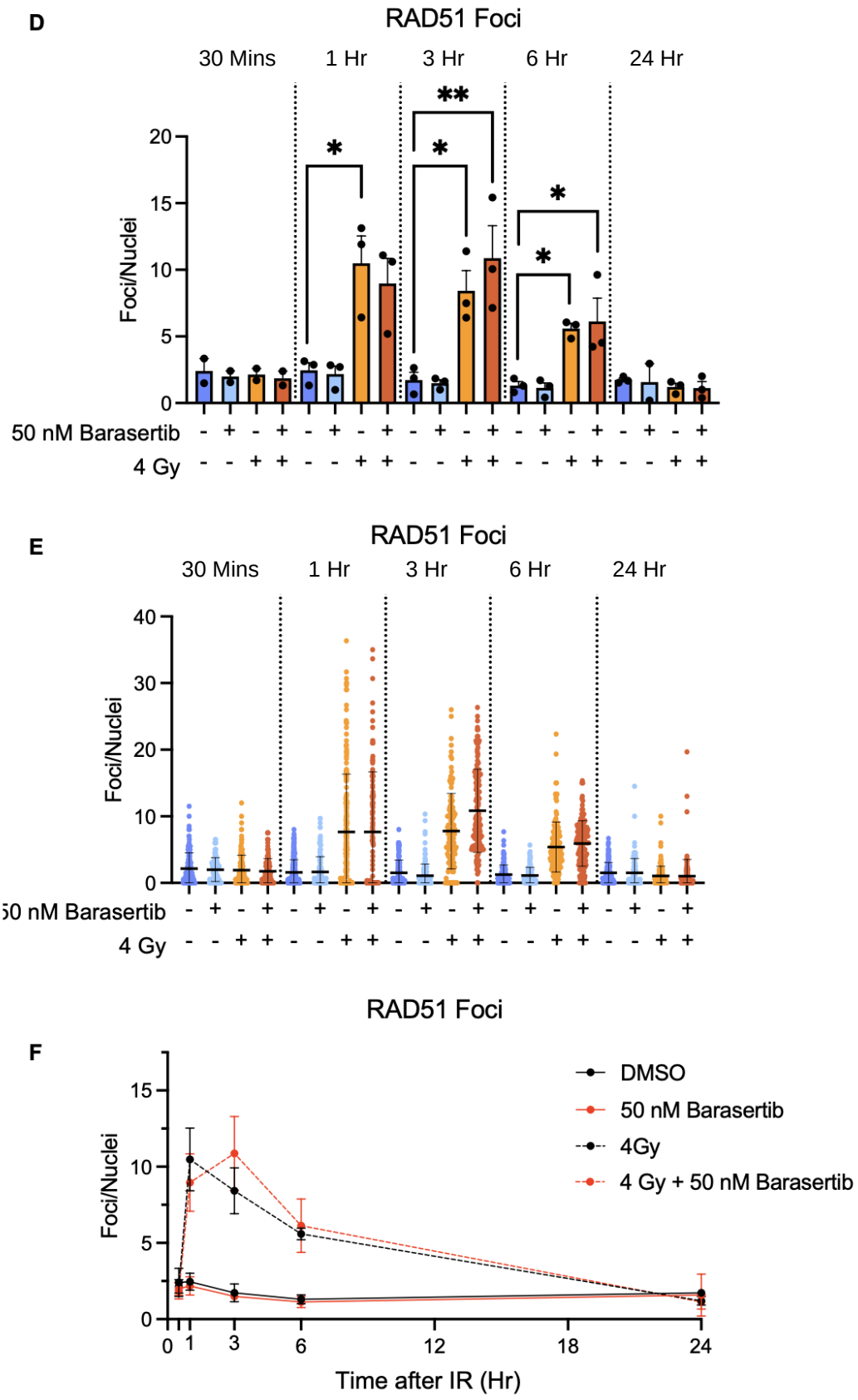

Figure 5.13: RAD51 foci are initiated after IR and unaffected by Barasertib

5.7. P53 Stabilisation after Barasertib Treatment

To investigate the effect of Barasertib on p53, H460 cells were treated with 25 – 200 nM Barasertib for 24 Hr before protein collection (Fig 5.14). Lysates were probed or p53 and GAPDH as a loading control.

There was increasing p53 protein expression with increasing Barasertib dose starting from the lowest dose tested (25 nM) (n=1). P53 stabilisation is a key regulatory mechanism upstream of death, senescence and cell cycle control after IR. This result, although only one repeat, indicates that Barasertib may promote p53 expression in H460 cells, potentially by stabilisation. This could be due to abrogation of negative regulation by AURKB but could also be due to the stress response following Barasertib treatment due to polyploidy or mitotic aberrance. Investigating the p53 response after Barasertib and IR would be advantageous to understand the role of p53 in the context of radiosensitisation by Barasertib.

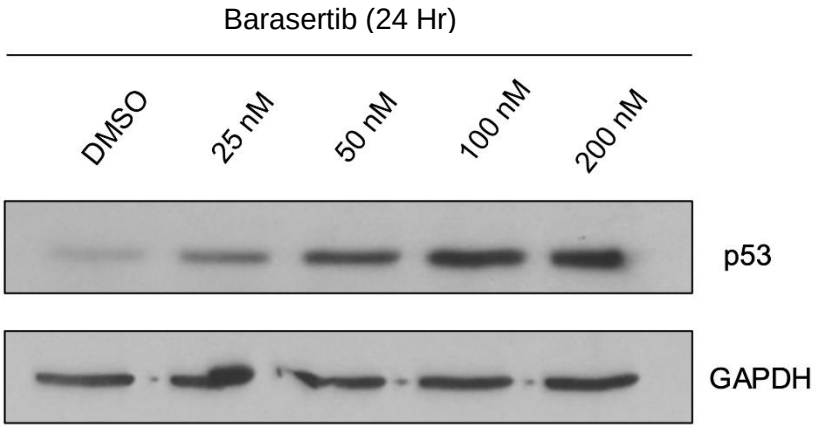

Figure 5. 14: Barasertib decreases p53 protein levels

Protein expression of p53 in H460 cells after 24 Hr of 25 – 200 nM Barasertib. Total p53 and GAPDH loading control shown.

5.8. Discussion

Here we explored the mechanism of radiosensitisation by Barasertib. We examined multiple facets of the cell cycle and DDR to investigate how Barasertib sensitises cells to IR.

Firstly, we explored the effects of Barasertib alone on the cell cycle at 50 – 200 nM up to 48 Hr. Polyploidy, a characteristic phenotype of AURKB inhibition, was induced in a dose-dependent manner, and was the most significant change across phases. This aligns with published data that AURKB inhibitors including Barasertib induce polyploidy (Nguyen et al., 2009, Wilkinson et al., 2007, Tao et al., 2009, Niermann et al., 2011, Hardwicke et al., 2009).

However, at 50 nM Barasertib, the effect on H460 cells was mild. Sak et al (2012) found similarly that high levels of polyploidy in H460 cells were induced with high dose Barasertib but not with 48 nM Barasertib (Sak et al., 2012). In contrast, low doses of Barasertib (20 nM) induces polyploidy in prostate cancer cell lines (Niermann et al., 2011). These trends highlight variability in the sensitivity to Barasertib across cell and cancer types.

Cell cycle phase was also explored after Barasertib, IR or combination treatment to examine checkpoint effects. Following checkpoint release, combination treated cells appeared to accumulate in mitosis (or pass through more slowly) then they did after radiation alone, shown by increased mitotic population after Barasertib treatment. Consistent with this, less cells appeared to have transited to G_1 after release from G_2 arrest following combination treatment than IR alone. Despite being significant the

changes to the G_1 population were small and investigating time points between 8 and 24 Hr would be helpful to determine when post-IR the largest difference occurs.

Increased mitotic population after Barasertib treatment

The most likely reason for greater mitotic population we saw is prolonged mitoses. We assessed mitotic duration between 27 – 72 Hours after treatment started by live cell analysis. This revealed that mitotic duration was slightly increased (non-significantly) by 50 nM Barasertib, IR and the combination (Combination > 4Gy > 50 nM Barasertib). Further examining how mitotic duration related to mitotic start time provided some support for the theory that prolonged mitoses occurred around 24 Hr in Barasertib and IR-treated cells. To full confirm this theory, the live cell experiment would need to be repeated from the point of irradiation onwards to capture mitosis in the 1st 24 Hr after IR (i.e. the cells entering mitosis after G_2 arrest).

Prolonged mitosis occurs as a result of SAC activation and the mitotic phase distribution supports this in our cells. We saw increased proportion of cells in the pre-SAC phases (prometaphase and metaphase) in Barasertib treated conditions compared to controls. Interestingly Barasertib alone consistently increased cells in prometaphase/metaphase, suggesting that AURKB inhibition can activate the SAC whether DNA damage is present or not. AURKB has multiple functions related to the SAC, most in support of its activation but it is also required to correct erroneous MT-KT that otherwise maintain SAC activation. We also saw peak levels of mitotic defects by IF at 24 Hr which would trigger SAC activation and mitotic arrest that we think is happening at this timepoint.

Our results disagree with reports that AURKB inhibition promotes SAC override rather than activating it (Yamauchi et al., 2013, Sak et al., 2012, Tsuda et al., 2017). However, there are reports of Barasertib prolonging mitosis; in RPE-1 cells, 50 nM Barasertib prolonged mitosis (Farrell et al., 2022). Dose-specific effects on metaphase could explain these two phenotypes; low doses may interfere with error correction (chromosome alignment and attachment) enough to trigger the SAC without inhibiting AURKB enough to cause SAC override, whilst high dose promotes SAC override and polyploidy.

Mitotic aberrance after IR and Barasertib

We investigated mitotic aberrance following IR by live cell analysis and IF staining of fixed cells. Both methods revealed that IR induces high levels of aberrance with increased levels in the presence of Barasertib. By IF, centrosome defects were the most common defects in IR treated cells (30-50% at 24 Hr) but chromosome separation defects were also common (~20% in IR conditions). Multinucleation was also induced by IR and was increased by co-treatment with Barasertib, with accumulating levels over time.

Centrosomal amplification can occur during G_2 arrest, which could explain why it is highest in timepoints closest to IR and G_2 release (Dodson et al., 2007). Another cause could be increased AURKA activity. We saw increased pAURKA (Thr288) with increased Barasertib inhibition and AURKA overexpression promotes centrosomal amplification (Guan et al., 2007).

By live cell, the most common defect was abscission regression which occurred in around 23% and 33% of mitoses in the IR and combination conditions respectively.

In H460 cells, IR alone induced abscission regression. This is expected as IR damage leads to DNA in the intracellular channel which triggers the abscission checkpoint (Huang et al., 2008a). Irradiated Hela cells undergoing abscission regression survived with a cytoplasmic bridge or recombined to a multinucleated cell, and some continued to divide without cycling delay. In our live cell imaging, thin tethers connecting daughter cells was observed semi-frequently. On occasion one daughter cell would migrate away from the other but was limited to an area close to the other cell, indicating restriction by the tether.

The high occurrence of abscission regression can be linked specifically to the chromosome separation defects and centrosomal defects induced by IR and seen by IF. Lagging chromosomes, unattached chromosomes or anaphase bridges in the intracellular channel in late mitosis can activate the NoCut pathway which stalls completion of abscission, whilst centrosomal defects can contribute to chromosome segregation issues.

H460 cells seem especially prone to abscission regression after IR and it would be interesting to explore if this happens in other cell lines after IR. Abscission regression was increased (non-significantly) by Barasertib treatment. This concurs with AURKB's role in promoting stabilisation of the intracellular channel which prevents daughter cells recombining (Minoshima et al., 2003).

Abscission regression and centrosomal amplification result in multinucleated cells, which was captured by our immunofluorescence analysis (Mason and Bessler, 2011). By 72 Hr, the levels of multinucleated cells were around 3x higher than polyploid cells at 72 Hr. This shows a trend of aneuploidy over polyploidy which could be investigated by metaphase spreads.

There was still some induction of polyploidy after IR regardless of Barasertib, but this was less than 10% of the population. Abscission regression could contribute to this by producing tetraploid cells, and octoploid cells if repeated.

Replication

We also assessed S phase populations by BRDU incorporation from 24 – 72 Hr. There was some evidence of reduced replicating populations which could be a result of fewer cycling cells. Published reports support a role for AURKB in facilitating recovery from replication stress. AURKB is proposed to facilitate replication fork restart after fork collapse and promote mitotic entry after replication stress (Erin et al., 2021, Zuazua-Villar et al., 2014). Our finding that Barasertib sensitises to HU supports a role of replication stress recovery but we did not explore this issue enough to uncover if AURKB's activity in S phase contributes to radiosensitisation.

Death after IR

In this chapter, we assessed death by PI and Annexin V by flow cytometry. We saw that IR increased levels of dead cells up to 72 Hr, with greater death in the combination condition compared to IR alone at 72 Hr. In the live cell analysis, we saw low levels of mitotic death in all conditions, though we did not follow these cells for long enough to conclusively rule out death in G_1 after mitosis. Overall, our results suggest that the most death seen in IR-treated or Combination treated H460 cells is interphase death.

Sak et al (2012) showed that H460 underwent apoptosis 72 Hr after IR (25 Gy) which was increased in the presence of 96 nM Barasertib but not 50 nM (determined by Hoechst 33342 and PI live staining) (Sak et al., 2012) – this disagrees with our

findings in H460 cells. They also investigated apoptosis after IR and Barasertib treatment in A549, H520 and H661 cell lines. The effect of Barasertib on IR-induced apoptosis varied across NSCLC cell lines, with a decrease in apoptosis in H520 cells with Barasertib but an increase in H661 cells. In their hands, A549 cells showed almost no apoptotic death after IR despite having wildtype p53. In colorectal cancer, Tao et al (2008) proposed that HCT116 cells were likely to die by mitotic catastrophe but did not investigate death pathways (Tao et al., 2008). Given the mitotic aberrance we detected in H460 cells, mitotic catastrophe is a likely cause of death in H460 cells, leading to eventual death in G_1.

DNA repair after Barasertib

Given the phospho-proteomic analysis presented in chapter 4, and published results showing links to DDR, we wondered if Barasertib would enhance or impede DDR signalling and DNA repair. We investigated if the response of key DDR proteins in the 24 Hr after IR was altered by Barasertib. H2AX, 53BP1 and RAD51 foci were assessed. There were small changes in the peak time of 53BP1 and RAD51 but induction and resolution of foci after IR were not altered by 50 nM Barasertib.

Low dose Barasertib (20 nM) and ZM447437 (50 nM) have been shown to promote H2AX and 53BP1 foci independently of DNA damage source (MEF cells) (Fell et al., 2016). Additionally, Niermann et al (2011) found increased γH2AX positive cells after IR with Barasertib (PC3 and DU145 cells) (Niermann et al., 2011). Both papers used 48 Hr treatments. Our results agree in some respects with the effect on 53BP1, as there was a significant increase albeit in a shorter timeframe. The published literature suggest AURKB plays some role in suppression pf 53BP1 or H2AX, but we did not find evidence that this effects repair of DNA as shown by markers.

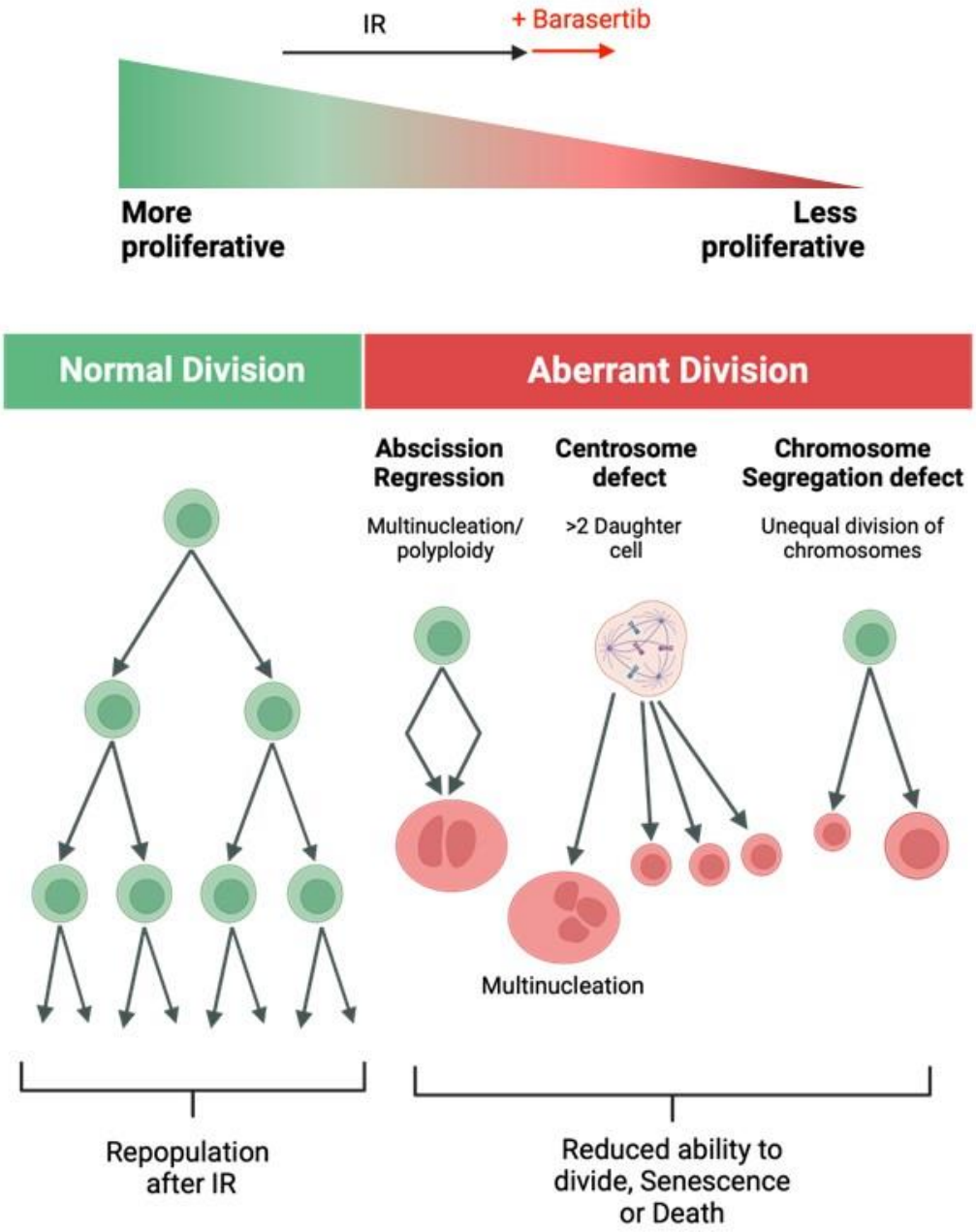

Figure 5. 15: Mechanistic basis for Barasertib radiosensitisation

After IR, mitotic aberrance including centrosomal defects, abscission regression and chromosomal defects lead to multinucleation and aneuploidy. These defects reduce the ability to proliferate or lead to death or senescence. This aberrance and its effects on proliferation and survival are increased by co-treating with Barasertib.

Mechanistic Conclusions

Overall, the effect of Barasertib on mitotic aberrance after IR is the most likely mechanism for radiosensitisation based on our data so far. After Barasertib and IR combined treatment, fewer cells are able to have a normal mitosis and therefore the proliferative potential is decreased; these cell struggle during mitosis, some leave mitosis with chromosome damage, aneuploidy or polyploidy, either they do not replicate again or replicate with increased aberrance. Eventually many die in G_1 due to mitotic catastrophe days after IR. This mechanism is summarised in Figure 5.15.

Our scheduling experiment in Section 3.4.1 revealed that Barasertib needed to be present in the first 24 Hours after IR to radiosensitise H460 cells. We hypothesised that this was due to an effect on DNA damage repair but as we see do not change in DDR foci resolution, this is not the case. Instead, the pretreatment effect is likely related to the effect on mitotic aberrance in the first mitosis after IR. Adding Barasertib 24 Hr after IR does not have the same effect, so disrupting the first mitosis may be important in the mechanism of radiosensitisation. Given the increased mitotic population at 24 Hr and mitotic difficulties at this timepoint, it is surprising that fractionated treatment did not have a greater effect on clonogenic survival in Barasertib treated cells.

More cells die after IR in the presence of Barasertib by 72 Hr. Mitotic catastrophe followed by apoptosis due to mitotic and genomic defects is the most likely cause here (Eriksson and Stigbrand, 2010). This is a slow process, occurring many days after IR, which matches our data showing a slow increase in death over 3 days. We found that p53 expression increased after Barasertib treatment (no IR treatment) so it is possible that Barasertib treatment lifts p53 negative regulation by AURKB after

IR. This could increase p53 signalling after mitotic aberrance leading to increased death over time. We found that p53-deficient cell lines were also radiosensitised and therefore, radiosensitisation is not dependant on p53 mediated apoptosis. Apoptosis could be initiated by other pathways or cells may die by necrosis or autophagic death in p53 deficient cells.

Chapter 6: Radiosensitising Effects of Barasertib in a Subcutaneous Model of NSCLC

6. Radiosensitising Effects of Barasertib in a Subcutaneous Model of NSCLC

6.1. Introduction, Aims and Hypothesis

In Chapter 3, we demonstrated that Barasertib could sensitise several NSCLC cell lines to IR *in vitro* and produced greater cell death and prolonged senescent population in H460 cells.

Barasertib has been tested extensively *in vivo*, primarily as a single agent treatment. Initial studies in colorectal cancer, NSCLC, AML and leukaemia xenograft models used osmotic mini-pumps to deliver doses between 10 – 150 mg/kg over 48 Hr by continuous infusion, either once or weekly (Wilkinson et al., 2007, Oke et al., 2009). Later *in vivo* studies employed intraperitoneal injection with doses between 25 – 100 mg/kg, with alternate day or cyclical dosing schedules (Aihara et al., 2010, Mori et al., 2011, Nie et al., 2020). High single doses of Barasertib above 100 mg/kg exhibited very strong anti-tumour effect, whilst lower doses (25 mg/kg) required repeated treatment to achieve similar control of tumour growth. At doses showing anti-tumour efficacy, a maximum of 5 % body weight lost was observed, which was regained after treatment. Transient myelosuppression was reported, mainly affecting leukocytes (Wilkinson et al., 2007).

Our hypothesis is that Barasertib will increase the tumour response to IR *in vivo*. We chose fractionated IR delivery over single dose delivery to reflect clinical delivery of radiotherapy.

We aimed to test if Barasertib could radiosensitise NSCLC in a subcutaneous xenograft model using Balb/c mice.

The aims of this chapter are:

1. To characterise the tumour response of Barasertib in H460 xenograft model to allow dose selection for combination trials.
2. To investigate the tumour response to the combination of Barasertib and IR in a H460 xenograft model.

6.2. Evaluation of Barasertib and Radiation Monotherapies in a H460 Xenograft Model

6.2.1. HEB8 Study Protocol

Before trialling the effect of Barasertib and radiotherapy combination, the doses of Barasertib and radiation to be used needed to be determined. 25 mg/kg Barasertib produced a mild inhibition of tumour growth in A549 xenografts (Wilkinson et al., 2007), providing a benchmark for initial dosing. By clonogenic, H460 cells showed a higher LD50 than A549 cells (>3 fold) indicating that a higher dose than 25 mg/kg could be required. We chose to treat for 10 days to allow for radiation treatment and recovery in the presence of Barasertib (Fig 6.1).

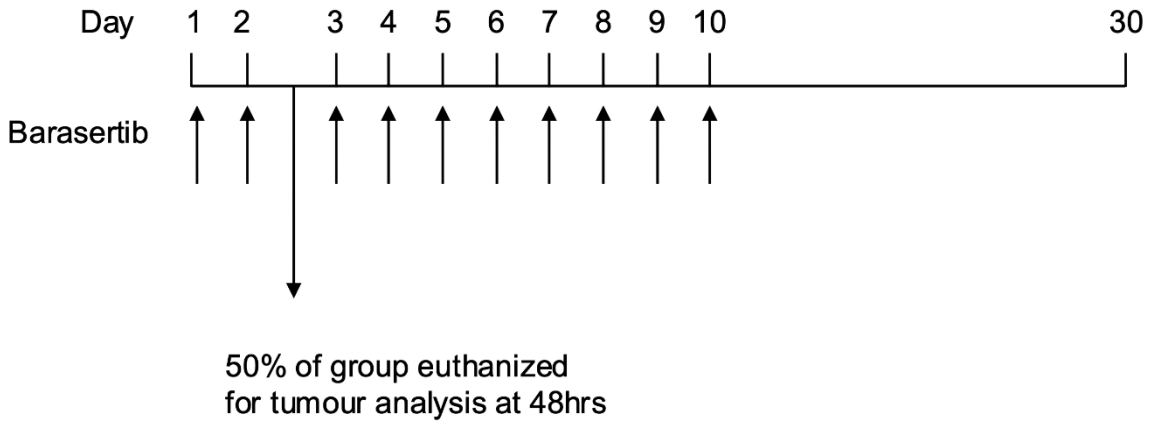

Figure 6. 1: HEB8 treatment schedule

Mice were implanted subcutaneously with H460 cells to establish tumours. Once tumours reached 100 mm^3, mice were treated intraperitoneal injection of 10, 25 or 50 mg/kg AZD1152 or Vehicle once daily for 10 days. 50 % of each tumour group were euthanised 48 Hr after the first treatment for tumour analysis of drug response. The remaining mice remained on the study until tumour size reached 12mm average or until 30 day after treatment start.

This was informed by previous radiosensitisation trial by the Bryant lab using Alisertib. Given the reduced sensitivity to Barasertib of H460 cells, doses of 10, 25 and 50 mg/kg/day were chosen to test the tolerability and efficacy of Barasertib alone.

Previously in the Bryant lab it had been observed that 5x 4 Gy fractions resulted in moderate tumour growth inhibition in H460 xenograft models, therefore this regime was tested to ensure the stocks of cells used were behaving similarly. Fractionated treatment was used to reflect clinical radiation delivery.

Group size of 4 was determined by power calculation based on expected effect of 30% change, 12.5% variability in a one-tailed t-test with 0.05% significance and 90% power. Variability and effect size was based on previous studies in this model. An extra mouse was included per group to account for 80% tumour uptake rate (established in previous studies with this model). Each dose group included 10 mice, i.e. 2 groups of 5 mice, to allow for ex vivo analysis of 1 group at 48 Hr (Fig 6.1).

6.2.2. Tumour Growth Response to Barasertib at 10-50 mg/kg/day (HEB8 Trial)

One million H460 cells were implanted subcutaneously on the dorsal flank of 40 Balb/c mice and tumour formation was monitored. Once tumour volume reached 100 mm^3, treatment was started. The schedule of treatment was 10 days of Barasertib or vehicle treatment (Fig 6.1). 48 Hr after the first treatment, half of each treatment group were euthanised to allow for pH3 analysis. The remaining mice remained on the study until day 30 from the start of treatment or until a humane endpoint (12mm average or 15 mm max diameter) was reached, whichever occurred first. Mice were treated daily with 10, 25 or 50 mg/kg, or vehicle (5 % DMSO in TBS pH 9) by intraperitoneal injection for 10 days. A clear tumour response was observed with all Barasertib doses (Fig 6.2 A). There was growth suppression in all Barasertib-treated mice until at least day 7 at all doses. Tumour volume at day 7/8 was significantly lower in the 10, 25 and 50 mg/kg treatment groups compared to the vehicle group ($p= 0.0161$, $p=0.0017$ and $p=0.0031$, respectively) (Fig 6.2 B).

After this point tumour growth was observed in some mice the 10 mg/kg treatment group but was slower than the vehicle group (Fig 6.2 A). At day 11/12, tumour volume in the 10mg/kg group was still lower than the vehicle group ($p=0.0339$) (Fig 6.2 C). The higher doses produced more consistent tumour responses, with the growth inhibition persisting after the last treatment in all animals. At day 11/12, tumour volume was also significantly lower in the 25 mg/kg and 50 mg/kg groups compared to the vehicle group ($p= 0.0016$ and $p=0.0026$, respectively) (Fig 6.2 C).

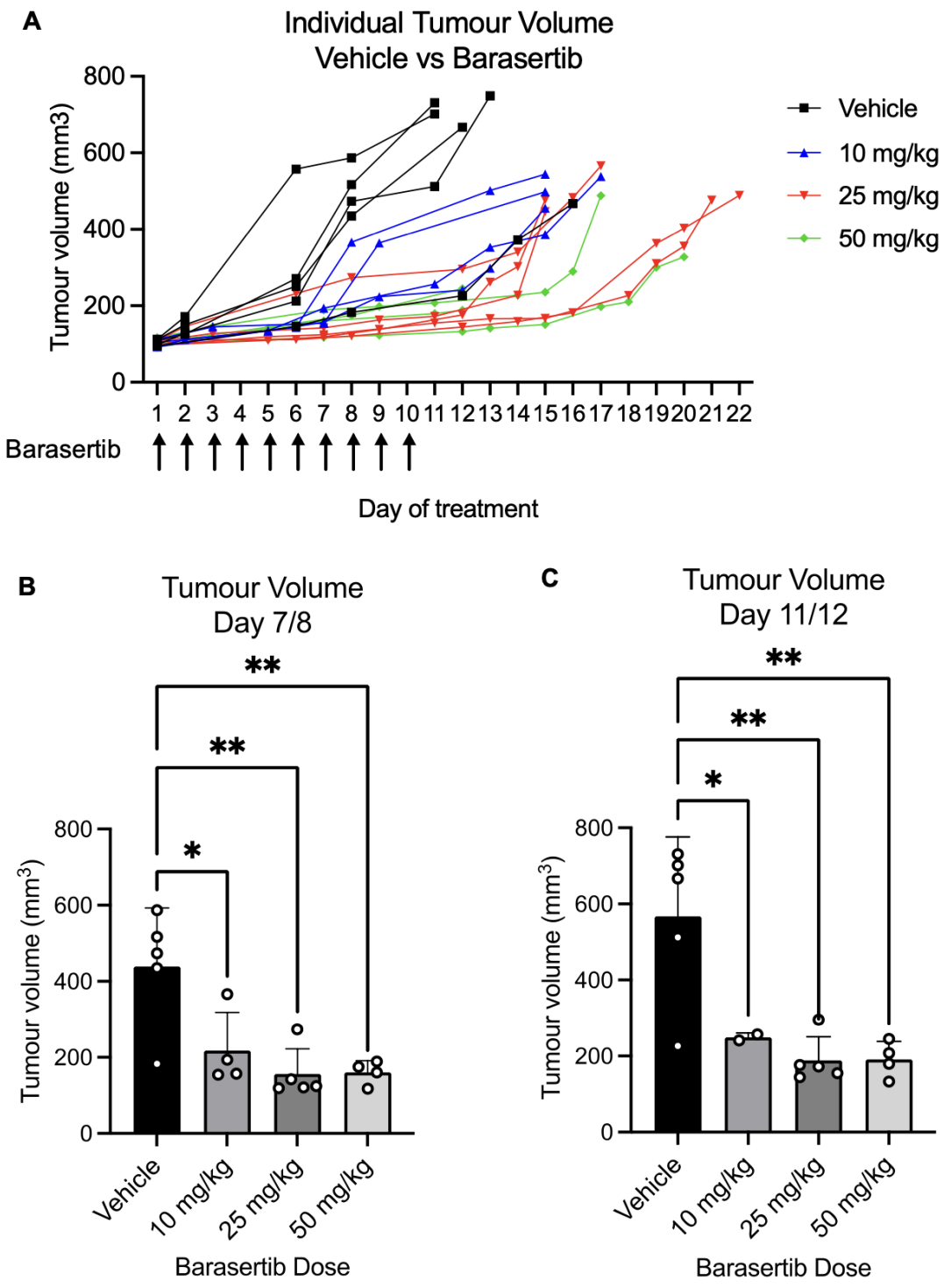

Figure 6. 2: Barasertib reduces tumour growth in a NSCLC xenograft model

H460 Xenografts were established in Balb/c mice.10/25/50 mg/kg Barasertib (AZD1152) or vehicle was administered daily for 10 days by IP injection **A** Tumour volume per mouse from Day 1 of treatment. **B** Tumour Volume at Day 7 or 8. **C** Tumour volume at Day 11/12 (if data was not available at day 7/11, day 8/12 data was used). Statistical significance was calculated using an ordinary one-way ANOVA. In B-D, mean and standard deviation are shown. * = $p < 0.05$, ** = $p < 0.01$, *** = $p<0.001$. **** = $p<0.0001$.

6.2.3. Phospho-H3 response in HEB8 Study

We analysed pH3 tissue expression in vehicle and Barasertib-treated mice 48 Hr after the start of treatment. H460 xenograft tumours from mice in vehicle and Barasertib-treated groups were snap frozen before paraffin embedment and cryosectioning. pH3 and haematoxylin staining was carried out by IHC (Fig 6.3 A). There was no significant change in pH3 positivity score between any of the groups (Fig 6.3 B).

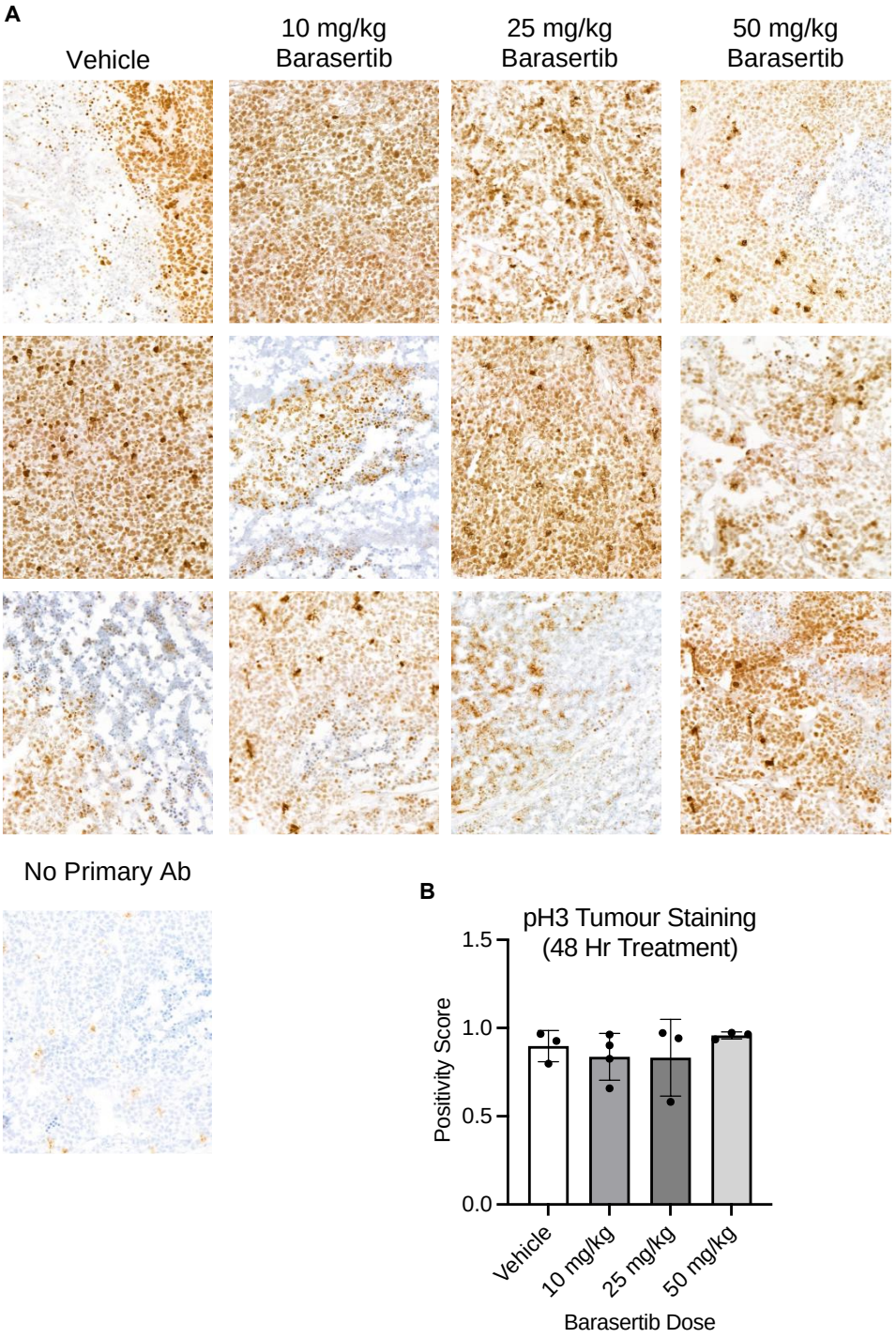

Figure 6. 3: Phospho-H3 (Ser10) tumour staining is not affected by 48 Hr Barasertib treatment

Mice were treated with 10, 25 or 50 mg/kg Barasertib for 2 days then euthanized 48 Hr after the 1st treatment. Tumours were snap frozen, paraffin-embedded and analysed by IHC for pH3. **A** pH3 (brown) and Haematoxylin (blue) in HEB8 Tumour samples **B** Positivity score for pH3 staining per tumour section where Positivity = (Total Positive Cells)/(Total Cells). Statistical significance was calculated using an ordinary one-way ANOVA. Mean and standard deviation are shown.

6.2.4. Optimisation of Radiation Dose

Alongside optimisation of Barasertib dose, IR dose was also tested. Five mice were implanted with H460 cells as described above to establish subcutaneous tumours. Once tumours reached 100 mm^3, mice were treated with 4 Gy IR daily for 5 days (Fig 6.4 A).

There was a strong growth inhibition after 20 Gy in H460 xenografts (Fig 6.4 B). At day 7.8 and day 11, tumour volume was significantly lower in the IR treated mice ($p=0.0054$ and $p=0.0064$, respectively) (Fig 6.4 C and D). Note, the IR group was compared with the same vehicle control group as shown in Figure 45 A as we ran the Barasertib alone and IR alone arms in parallel to reduce the number of animals needed.

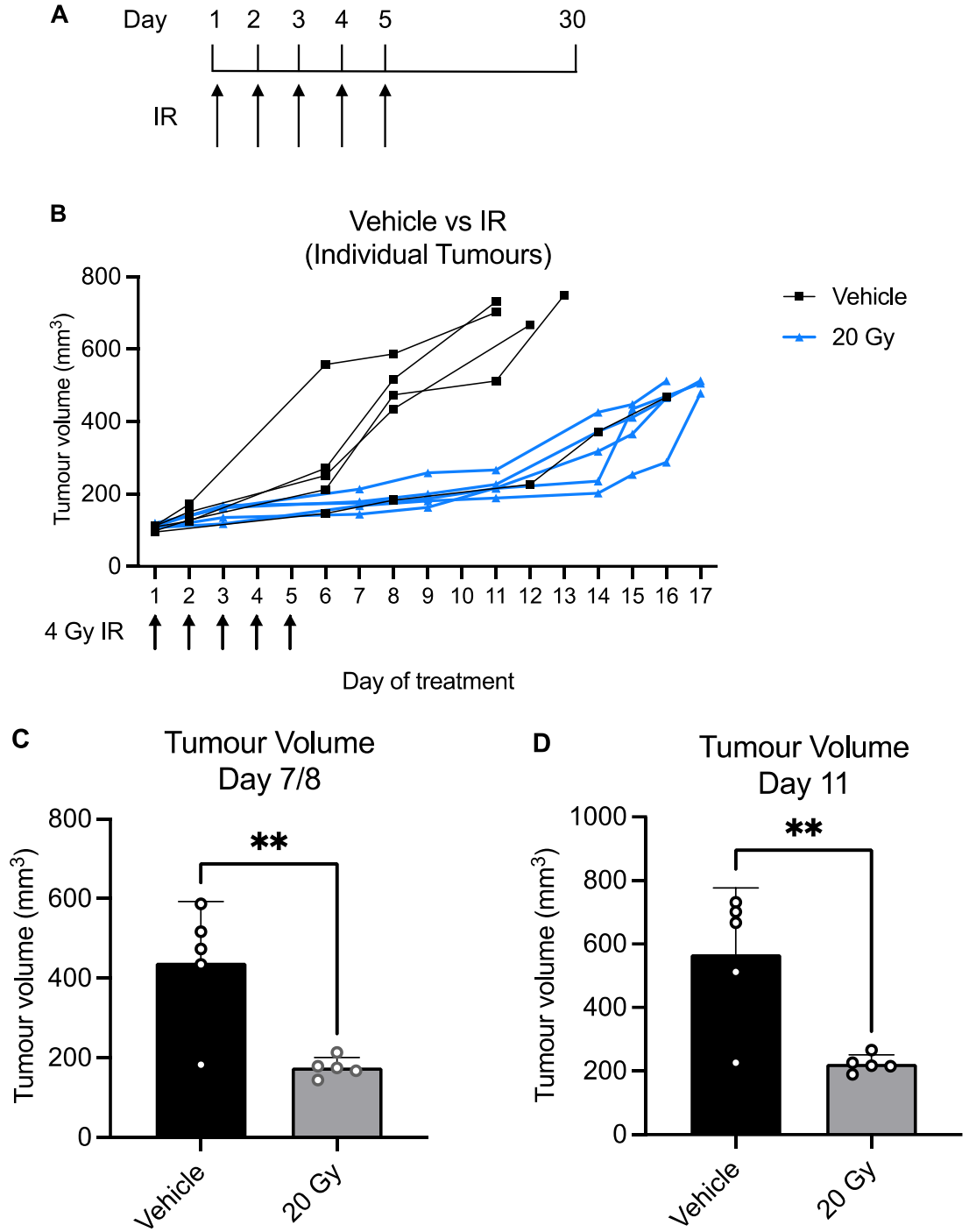

Figure 6. 4: IR reduces tumour volume in a NSCLC xenograft model

Mice were implanted subcutaneously with H460 cells to establish tumours. Once tumours reached 100 mm3, treatment commenced. **A** HEB8 IR treatment schedule: Mice were treated with 4 Gy daily for 5 days **B** Tumour volume per mouse from Day 1 of treatment (compared to Vehicle once daily for 10 days from Barasertib arm). **C** Tumour Volume at Day 7/8 (if tumour volume was not available at day 7, day 8 data was used) **D** Tumour volume at Day 11. Statistical significance was calculated using an unpaired t-test. In each case mean and standard deviation are shown. * = $p < 0.05$, ** = $p < 0.01$, *** = $p<0.001$. **** = $p<0.0001$.

6.2.5. Weight Response and Toxicity in HEB8 Study

Doses of 10 and 25 mg/kg were well tolerated. 2 mice in the 50 mg/kg Barasertib group were euthanised due to weight loss issues; one due to weight loss of >20 % and one due to low starting weight which did not improve. Overall, mice showed consistent weight across groups (Fig 6.5). Two mice were euthanised due to weeping blisters (one in vehicle group and one in 10 mg/kg group). Blistering was a common event and started before treatment, so this was deemed to be a result of subcutaneous tumour growth. No additional side effects were observed.

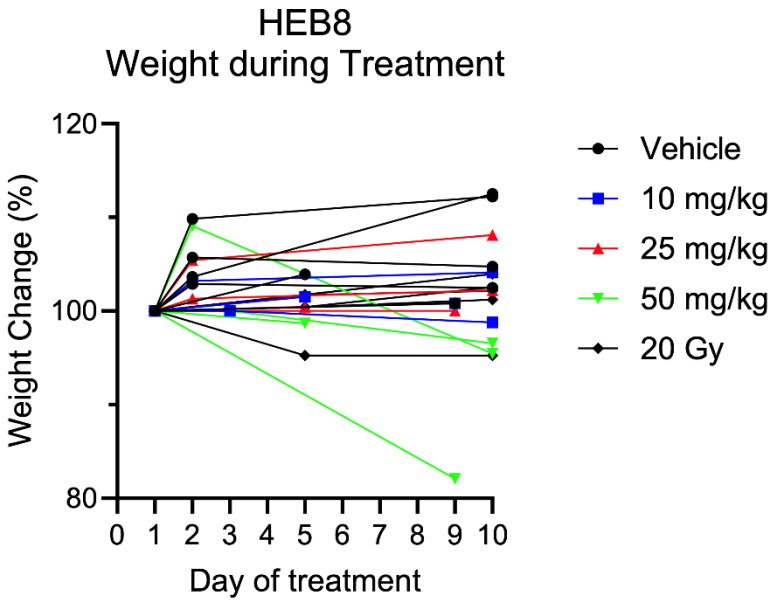

Figure 6. 5: Weight change during HEB8 study

During the HEB8 trial, mice were treated with Vehicle or 10/25/50 mg/kg Barasertib (AZD1152) daily for 10 days, or with 4 Gy daily for 5 days. All treatments started on Day 1. Mice were weighed every day from the start of treatment. Weight per mouse during treatment (% of starting weight).

6.3. Evaluation of Barasertib as a Radiosensitiser in a H460 Xenograft Model (HEB9 Trial)

6.3.1. HEB9 Study Protocol

A combination trial was planned to follow on from the results of HEB8. The Barasertib dosing schedule involved 10 days of daily treatments with 10mg/kg of Barasertib injected peritoneally. The IR dose of 20 Gy tested in HEB8 gave a stronger tumour response than desired. Therefore a 15 Gy dose delivered in five daily doses of 3 Gy was chosen for HEB9 (Fig 6.6).

Based on our clonogenic scheduling experiments, a pretreatment was opted for to enhance radiosensitisation. Barasertib treatment would be given for 10 days, and IR would commence on day 2 of treatment, 24 Hr after the first Barasertib dose (Fig 6.6).

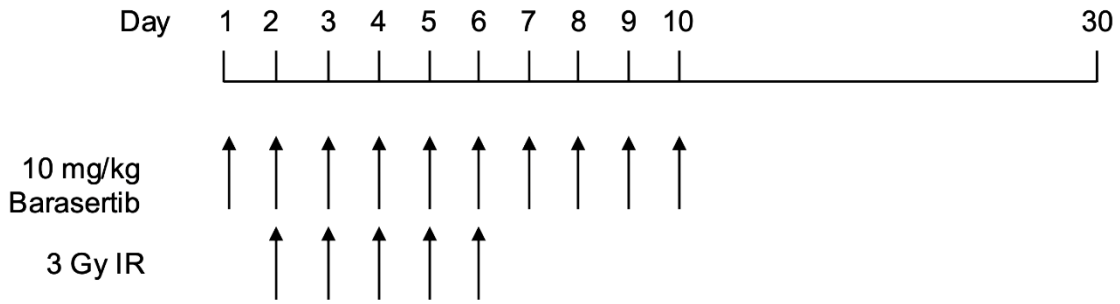

Figure 6. 6: HEB9 treatment schedule

Mice will be implanted subcutaneously with H460 cells to establish tumours. Once tumours reached 100 mm3, Mice will be treated intraperitoneal injection of 10 mg/kg AZD1152 or Vehicle once daily for 10 days, plus 3 Gy IR or Sham IR for 5 days (day 2 - day 6). Mice will remain on the study until defined humane endpoint or until 30 days after treatment start.

6.3.2. Tumour Volume Response to 10 mg/kg Barasertib and 15 Gy IR

We investigated Barasertib (10 mg/kg/day) and IR (15 Gy) alone and in combination. 32 Balb/c mice were injected with 1 x 10^6 H460 cells subcutaneously on the dorsal flank and tumour formation was monitored. Once tumours reached 100 mm^3, treatment was started. Eight mice were assigned to each treatment group. Group size was calculated by power calculation (one-sided test, effect size of 30%, variability of 15%, significance of 5%, power of 90% = 6 per group) plus 2 extra mice to account for loss to fighting or blistering which occurred in HEB8. Effect size and variability based on HEB8.

Tumour volume was measured daily from the start of treatment (Fig 6.7 A and B). The effect of treatment by day of treatment is shown in Fig 6.7 C. The 15 Gy response was comparable to 20 Gy despite the decrease in dose (Appendix Figure 13).

In HEB9, we noticed minimal effect by Barasertib alone or in the IR arm. 15 Gy IR significantly decreased tumour volume compared to the Vehicle control group ($p<0.0001$) whilst there was no significant difference between 10 mg/kg Barasertib and vehicle group, or between 15 Gy and the combination groups (Fig 6.7 A-C). Tumour volume at day 9 was significantly lower in the 15 Gy group compared to Vehicle ($p=0.0008$), but similarly 10 mg/kg Barasertib did not influence tumour volume (Fig 6.7 D).

A

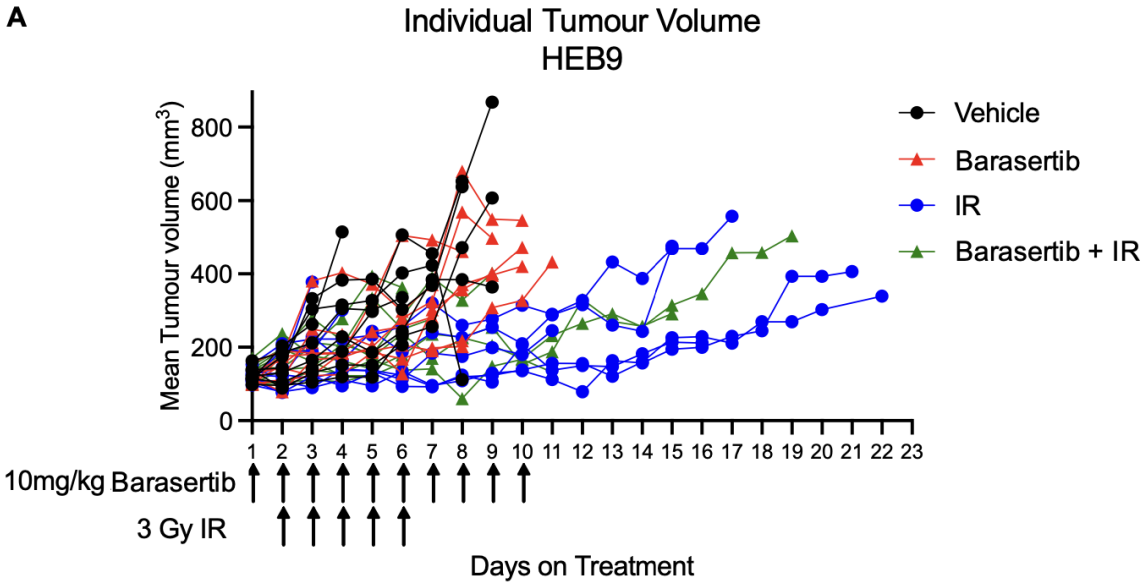

B

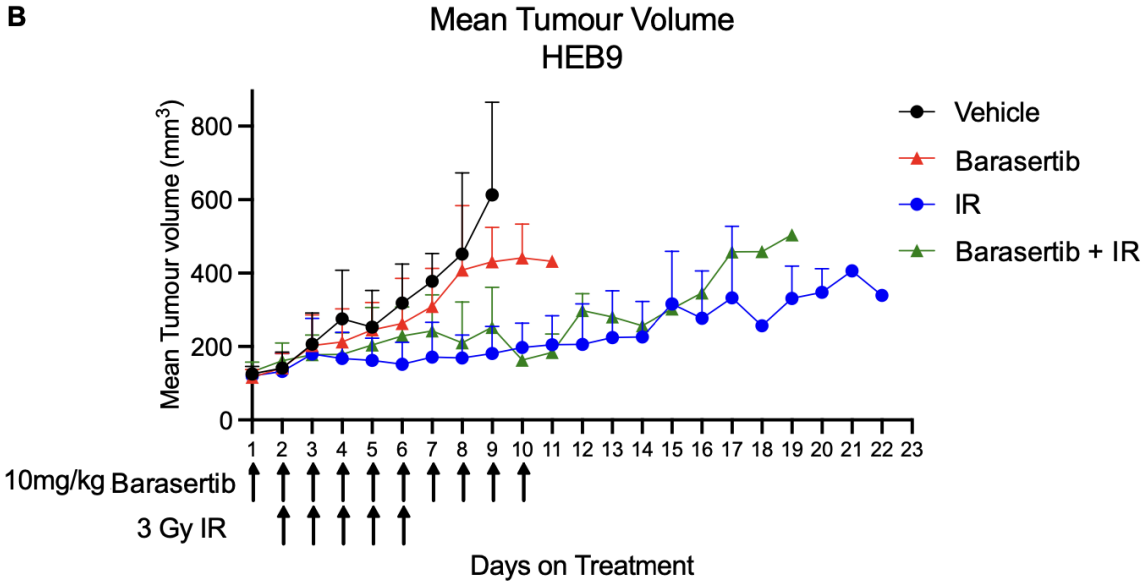

C

	Vehicle vs Barasertib	Vehicle vs IR	IR vs Barasertib + IR
Fixed effects (type III)	**p-value**		
Day	<0.0001	<0.0001	0.0062
Treatment group	0.1595	0.0007	0.2942
Day x Treatment group	**0.3402**	**<0.0001**	**0.7579**

Figure 6.7: Barasertib does not sensitise to IR in a NSCLC Xenograft model

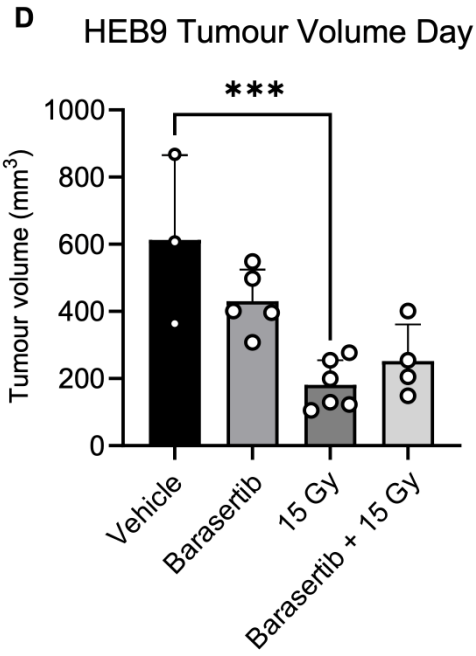

Figure 6. 7: Barasertib does not sensitise to IR in a NSCLC xenograft model

Mice were implanted subcutaneously with H460 cells to establish tumours. Once tumours reached 100 mm3, treatment commenced. Mice were treated with vehicle + Sham IR, 10mg/kg Barasertib + Sham IR, 15 Gy (3x 5Gy) + vehicle or 15 Gy (3x 5Gy) + 10 mg/kg Barasertib. Barasertib or vehicle was administered day 1-10 and IR was administered day 2-6. Tumour volume per mouse from Day 1 of treatment: **A** Individual Tumour volume per mouse **B** Grouped by Treatment (Mean and SD shown). **C** Two-way Anova (mixed methods) comparison of Vehicle vs AZD1152, Vehicle vs IR and IR vs AZD1152 + IR **D** Tumour volume at day 9 of treatment. Mean and SD shown, statistical significance was calculated using an ordinary one-way ANOVA. * = $p < 0.05$, ** = $p < 0.01$, *** = $p<0.001$. **** = $p<0.0001$.

The tumour response to 10 mg/kg Barasertib was weak given we had achieved moderate tumour growth inhibition with this dose in the HEB8 trial. Comparing the tumour response to 10mg/kg Barasertib between HEB8 and HEB9, the response to the drug was very different between trials (Fig 6.8 A). The tumour growth rate in the vehicle control group was similar between both trials so this could not account for the change in the Barasertib group (Fig 6.8 A).

The drug stock used for HEB9 was tested in an *in vitro* clonogenic assay alongside alternative Barasertib stocks. The HEB9 drug stock did not affect *in vitro* survival at 50 – 100 nM, while the alternative lab stock demonstrated the expected dose-dependent decrease in survival fraction (n=1) (Fig 6.8 C). It was concluded that the Barasertib stock had expired after incorrect storage at -20C instead of – 80 C. This explained the lack of effect by Barasertib in HEB9.

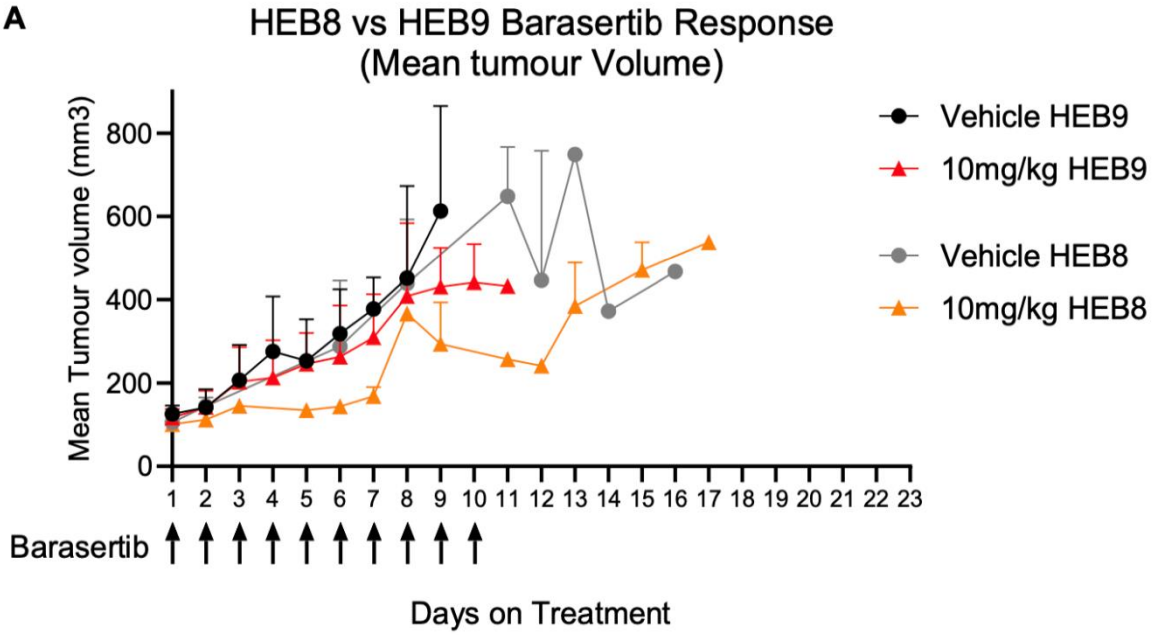

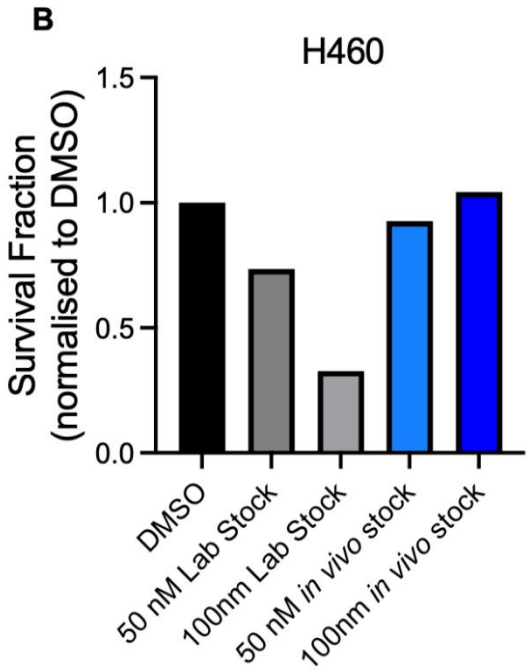

Figure 6. 8: 10 mg/kg Barasertib was not reproducible between HEB8 and HEB9 studies

A Tumour Volume after Vehicle and 10 mg/kg Barasertib in HEB8 and HEB9 (Mean and SD per group shown) **B** Clonogenic survival fraction of H460 cells *in vitro* after treatment with laboratory stock and *in vivo* stock of Barasertib (n=1).

6.3.3. Weight response and Toxicity in HEB9 Study

Mouse weight was monitored throughout the trial. There was a small weight decrease of <10% in IR-treated groups (Fig 6.9 A). One mouse in the 15 Gy group lost weight to 11% lower than the starting weight during IR treatment but regained weight once IR treatments finished. Blistering of subcutaneous tumour sites was still observed in mice across treatment groups. No other side effects were observed.

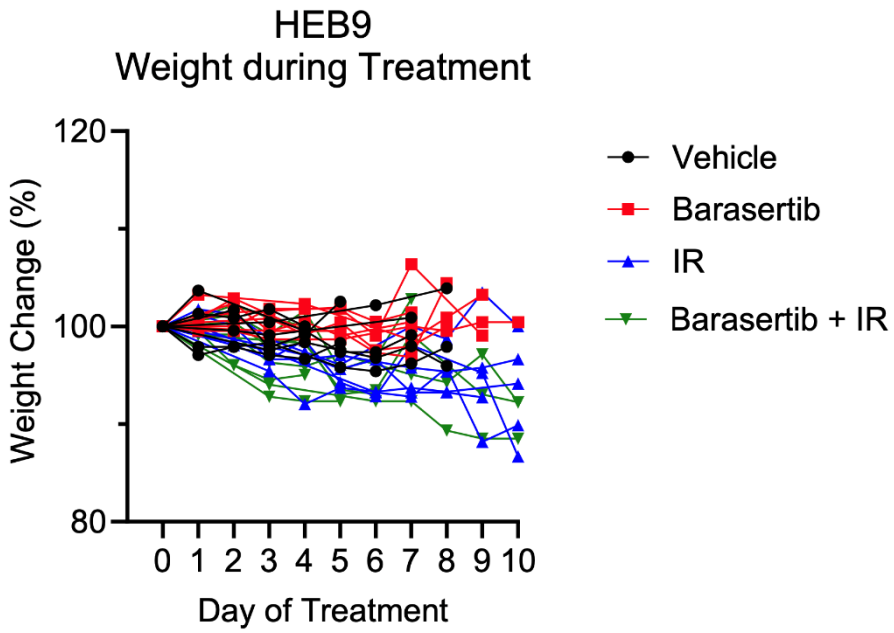

Figure 6. 9: Weight change during HEB9 study

During the HEB9 trial, mice were treated with Vehicle + Sham IR, 10mg/kg Barasertib (AZD1152) + Sham IR, 15 Gy (3x 5Gy) + vehicle or 15 Gy (3x 5Gy) + 10 mg/kg Barasertib (AZD1152). AZD1152 treatment started on day 1 and IR started on Day 2. Mice were weighed every day from the start of treatment. Weight per mouse during 10 day treatment (% of starting weight).

6.4. Discussion

Barasertib has been only trialled in combination with radiotherapy in vivo in xenograft models of colorectal cancer (Tao et al., 2008, Tao et al., 2009). Tao et al (2008) investigated radiosensitisation in HCT116 xenografts (p53wt and p53-/-) and in a HT29 xenograft model using nude mice. They used stronger IR (4-6 Gy) for shorter duration, and treated with Barasertib for 4 days total (10-=40 mg/kg depending on cell line). They observed that Barasertib could sensitise all three models to radiotherapy with the greater sensitisation in the p53 -/- HCT116 model (Tao et al., 2008).

The same group published again in 2009, and further investigated whether radiosensitisation *in vivo* is impacted by adjuvant, neoadjuvant or concurrent scheduling of Barasertib. They concluded that optimal sensitisation to one dose of radiotherapy (8 Gy) was achieved by treating with Barasertib before or after IR, not concurrently. However, when radiation was fractionated (3 Gy x 4 days) concomitant treatment was successful in radiosensitisation (Tao et al., 2009).

We trialled Barasertib alone and with radiotherapy in a NSCLC xenograft model. Barasertib demonstrated good tumour growth inhibition *in vivo* in agreement with published work across several cancer types. We tested three doses of Barasertib in a H460 xenograft model of NSCLC. Using a novel schedule of Barasertib whereby daily doses were delivered for 10 days, we established that 10 mg/kg was a suitable dose for a combination trial as it exhibited moderate inhibition of tumour growth.

We employed an adjuvant fractionated approach for the combination study and trialled 10 mg/kg Barasertib in combination with 15 Gy IR, with the 10-day schedule

for Barasertib. We chose a fractionated approach to maximise the cellular effects of IR via the radiobiological R's (repopulation, repair, redistribution and re-oxygenation). Fractionation of 24 Hr gaps allows sufficient time for cell cycle entry (redistribution) and reoxygenation of the tumour before the next fraction. Unfortunately, DNA repair can still be achieved by cancer cells in this time frame as shown by our IF experiments, but shorter timeframes would prevent repair also in normal tissue and so would increase normal tissue complication probability. Importantly, this interval is sufficiently short to prevent repopulation of the tumour during the 5 days of treatment, although repopulation then occurred after IR ceased. The speed of tumour repopulation measured by tumour volume was a key output in determining the effect of Barasertib on tumour control. In our study, IR was started 24 Hr after the first Barasertib treatment to improve radiosensitisation as we saw maximum radiosensitisation *in vitro* with 24 Hr pretreatment.

However, the effects of Barasertib in HEB10 were not reproducible. This was investigated and found to be due to drug stock stability. With new stocks of Barasertib, we plan to conduct another trial of Barasertib and IR combination in the H460 xenograft model. The IR dose of 15 Gy produced similarly strong effects to 20 Gy. Therefore, in a future trial, a lower dose of 10 Gy (5 x 2 Gy) will be used.

A subcutaneous xenograft model provides valuable information about tumour response and is easily employed for a range of human tumour types using immunocompromised mice strains. However, there are several limitations to this model. There are local adaptive and innate immune response to radiotherapy which play a key role in cancer cell survival (Wang et al., 2024). The need for

immunocompromised mice for human xenografts means these mice lack T cells so the model lacks an adaptive immune system and full tumour microenvironment.

As the tumour does not occur in the tissue of origin, local signalling will differ. The xenograft is easier to access for radiotherapy than in patients. This is relevant to radiotherapy for thoracic cancer, where delivery to lung tumours is especially challenging. The radiotherapy delivery system employed in these studies delivered radiation in an untargeted field so mice were rotated 180° to direct radiation to either side. This was a key limitation, and could be overcome by employing a small animal image-guided radiotherapy platform. These systems use stereotactic delivery of beam radiation, and can incorporate movement tracking to target thoracic areas. This platform improves precision and accuracy of dose delivery plus greater uniformity of dose across the tumour (Butterworth et al., 2017).

Chapter 7: Final Discussion

7. Final Discussion

In this thesis, we asked whether the AURKB inhibitor Barasertib would radiosensitise NSCLC and explored the mechanism by which this occurred. To our knowledge, this thesis is the first study examining how Barasertib affects mitotic progression after IR by microscopy and the first study exploring how AURKi affects phosphoproteomic signalling after IR.

Our results indicate that the biggest effect by Barasertib is promotion of mitotic aberrance and catastrophe after IR, and we propose that this leads to greater interphase death after IR.

A limitation of this study was the dependence on one cell line, H460. This is a large cell carcinoma cell line, a tumour type which accounts for only 9% of NSCLC cases (Tai et al., 2020). Squamous cell carcinoma and adenocarcinoma are more common subtypes. While we chose a less common subtype of NSCLC, it is an aggressive subtype with rapidly proliferating cells. Therefore, our study demonstrates how mechanistically radiosensitisation can be achieved with Barasertib in an aggressive NSCLC setting.

We did extend our study of Barasertib as a radiosensitiser to other subtypes of NSCLC. This work was carried out by Dr Timothy Mitchell. We took a team-based approach, whereby Tim studied the effect of Barasertib in a wider range of cell lines with less mechanistic work, whilst I focused mechanistically on one cell line. Some of the microscopy-based experiments shown in this thesis were time-intensive, which limited roll out to additional cell lines. Mass spectrometry was limited to one cell line by cost.

We only studied Barasertib in NSCLC. Use as a radiosensitiser could be applied to other cancer types. There is published evidence of radiosensitisation in prostate and colorectal cancer. Across models, Barasertib disrupts proliferation by causing mitosis defects or inducing polyploidy. The specificity to the cell cycle provides rationale for its use in highly proliferative tumours.

There are considerations for clinical translation of radiosensitisers. Many radiosensitisers are used in the clinic for NSCLC. Pemetrexed, paclitaxel, cisplatin, gemcitabine and doxorubicin are all shown to radiosensitise and are used alongside radiotherapy (Hu et al., 2024). However, these therapies were not approved specifically as radiosensitisers. So far, there is FDA approval for three drugs specifically as a radiosensitisers; Cetuximab (EGFR inhibitor), NBTXR3 (Hafnium oxide nanoparticles) and Debio 1143 (inhibitor of apoptosis proteins (IAP) antagonist) (Citrin and Camphausen, 2020).

However, there have been clinical issues with Cetuximab in multi-agent treatment regimens. Whilst cetuximab radiosensitised HNSCC in initial trials, the addition of chemotherapy (cisplatin) to the regime abrogated the benefit of cetuximab. The combination of cetuximab and cisplatin with radiotherapy increased acute toxicity and increased the need for radiotherapy treatment breaks, and overall did not improve survival or local tumour control (Citrin and Camphausen, 2020). This highlights the difficulty in adding to treatment regimens already close to the limits of acceptable toxicity.

The use of nanoparticle-based therapies could abrogate this issue for Barasertib. Nanoparticle delivery increases localisation to tumours by enhanced retention and permeability in tumour sites, and decreases systemic exposure (Subhan et al.,

2021). Nanoparticle delivery of Barasertib in nanoparticles (AZD2811) was shown to prolong Barasertib half-life in patients and reduce toxicity (neutropenia and stomatitis) (Ashton et al., 2016, Johnson et al., 2023).

Neutropenia often develops in cancer patients in response to chemotherapies such as taxanes and alkylating agents, combinations of which are routinely used in the clinic (Lustberg, 2012, Moore, 2016). This side effect of Barasertib could be a barrier to integration into chemoradiotherapy regimes. Radiotherapy can also induce neutropenia if targeted to bone marrow sites so is less applicable in treatment of primary NSCLC. Bone marrow toxicity could be examined in preclinical models with Barasertib and chemotherapies to investigate the effect on neutrophils.

In H460 cells, after IR and Barasertib we saw induction of polyploidy, multinucleation and mitotic defects which promote genomic instability. Many cancer treatments induce genomic instability for effective targeting of tumours. However, genomic instability in normal tissues is cause for concern. Patients who survive their cancer live with the risk of secondary tumours arising from the effects of their cancer therapy (Rheingold, 2003). Whilst Barasertib is not unique in its induction of genomic instability or senescence, consideration of the long-term effects on patients' health and quality of life after Barasertib treatment is also important. This is potentially more applicable in treatment of early stage tumours. Induction of senescence is also cause for concern both at the tumour site and systemically – inflammatory signalling due to SASP can promote tumorigenesis so could contribute to recurrence or to tumour promotion in non-malignant tissue (Schmitt et al., 2022).

In conclusion, we present novel data characterising the radiosensitisation of NSCLC by Barasertib and a mechanistic model. This therapy holds promise for improving the efficacy of radiotherapy in NSCLC.

Chapter 8: Appendices

8. Appendices

8.1. Buffers

PBS

To make 1x PBS, 1 Ocoid PBS tablet was added per 100 ml of ddH_2O and autoclaved for sterilisation.

TBS(T)

To make 10X TBS, 24.2g Tris Base (200mM), 80g NaCl (1.4M) were dissolved in 700 ml water, then made up to 1L. To make 1x TBST, 10X stock is diluted in water and 1 ml of Tween-20 is added per 1L TBS.

1M Tris pH 6.8

121.14g Tris Base was dissolved in 700 ml water then adjusted to pH 6.8 using HCL or NaOH. Water was then added to make up to 1L volume.

1.5M Tris pH 8.0

181.71g Tris Base was dissolved in 700 ml water then adjusted to pH8.8 using HCL or NaOH. Water was then added to make up to 1L volume.

5x SDS sample buffer

To prepare 5x SDS sample buffer, 25 ml 1 M Tris pH 6.8 (250 mM), 10 g SDS (10%), 50 ml glycerol (50%), 5 ml β-mercaptoethanol (5%) and 20 mg bromophenol blue (0.02%). Enough water was added to dissolve solutes and then the solution was made up to 100 ml final volume.

SDS-PAGE Running buffer

To make 10x SDS-PAGE Running buffer, 30.3g Tris Base (250 mM), 144g Glycine (1.9 M) and 100 ml of 10% SDS were added to 600 ml water until dissolved. The solution was then made up to 1L and diluted 1 in 10 in water for 1x working concentration.

5 x RIPA Buffer

RIPA buffer was prepared with 15 ml 5M NaCL (final conc.: 0.75 M), 5 ml 100 % NP40 (5%), 2.5 g DOC (2.5% w/v), 5ml 10% SDS (0.5%), 25 ml 1M Tris pH8 (0.25M) and 50 ml water.

Towbin transfer buffer

To prepare 10x Towbin Transfer buffer, 30.3 g Tris Base (250 mM) and 144 g Glycine (1.9 M) were dissolved in water and then made up to 1L final volume. To prepare 1x Towbin Transfer buffer, 100 ml 10x Towbin Transfer buffer, 700 ml water, 1 ml 10% SDS and 200 ml methanol were combined.

TBS2 buffer

0.2 g BSA (1%) and 50 µl Triton X-100 (0.25%) were dissolved in 20 ml TBS.

PBSt buffer

100 µl Tween-20 (0.2%) was dissolved in 50 ml PBS.

PBS2+ buffer

1 g BSA (0.5%) and 500 µl Triton X-100 (0.25%) was dissolved in 200 ml PBS.

8.2. Tables (Appendices)

Appendix Table 1: Chemicals and materials used in laboratory protocols

Reagent	Supplier	Use
Acetic Acid glacial	Fisher	MS
CAN (LC-MS Grade)	FisherMS	MS
Amersham™ ECL™ Western Blotting Detection Reagents	GE	WB
Amersham™ Protran nitrocellulose blotting membrane	GE	WB
Ammonia Solution (25%) (Suprapur)	SupelCo	MS
Ammonia persulfate (APS)	Sigma	WB
ABC reagent	Vector Labs	IHC
β-mercaptoethanol	Sigma Aldrich	WB
Bolt™ 12% Bis-Tris Plus Gels, 12-well	Fisher Scientific	WB
Bovine serum albumin	Sigma	WB/IF
Bradford reagent	Bio-Rad	WB
BrdU		FC
Bromophenol blue	Sigma Aldrich	WB
CL-Xposure Film	Thermo Scientific	WB
cOmplete Mini Protease Inhibitor tablets (EDTA Free)	Roche	WB
DAB Solution	Vector Laboratories	IHC
DAKO TRS, Citrate pH6	Agilent	IHC
DAPI	Thermo Fisher	IF
DTT	Sigma	WB
DTT	Melford	MS
DMSO	Fisher Scientific	TC
EDTA	BDH	MS
Formic Acid	Biosolve	MS
Glycerol	Sigma Aldrich	WB
Glycine	Fisher Scientific	Buffers
Glycolic Acid	Sigma Aldrich	MS
Gill's Haematoxylin	TCS Biosciences	IHC
HCL	Fisher Scientific	Buffers
HEPES Molecular Biology Grade	Promega	MS
Immuno-mount	Thermo Scientific	IF
Invitrogen™ Bolt™ MES SDS Running Buffer (20X)	Fisher Scientific	WB
IAA	Sigma	MS
Matrigel matrix	Sigma-Aldrich	IV

Marvel	Premier Foods	WB
Methanol	Fisher Scientific	CA/FC
Methanol	Honeywell	MS
Methylene Blue	Fisher Scientific	CA
NaOH	Fisher Scientific	Buffers
Paraformaldehyde	Boster	IF
Phosstop Phosphatase Inhibitor	Roche	WB/MS
Pierce BCA Protein Assay Kit	Thermo Scientific	MS
Propidium Iodide	Sigma	FC
Protogel (30% acrylamide, 0.8% bis-acrylamide)	Geneflow	WB
RNase A		FC
SDS (20% w/v)	Fisher Scientific	WB
SDS Powder	Sigma Aldrich	WB
Sera-Mag SpeedBeads A and B	GE Healthcare	MS
Sodium Chloride	G Biosciences	Buffers
Sodium Deocycholate	Sigma	MS
Sodium Dodecyl Suphate		MS
Super Premium Microscope Slides	VWR	IF
TEMED (N,N,N,N,tetramethylethylenediamine)	VWR	WB
TFA MC-MS Grade	Biosolve	MS
TiO2 Beads (TitanSphere)	GL Sciences Inc	MS
Tris	Fisher	MS
Tris base	Chem Cruz	Buffers
Triton X-100	Sigma	IF
Tween20	Fisher Scientific	IF/WB
X-Ray Developer	RG Universal	WB
X-Ray Fixer	RG Universal	WB

CA = Clonogenic Assays, FC = Flow cytometry, IF= Immunofluorescence, IHC = Immunohistochemistry, IV = In vivo work, , LCM = live cell microscopy, MS= Mass spectrometry, TC = tissue culture, WB= Western blotting

Appendix Table 2: Primary antibodies used in laboratory protocols

Primary Antibodies (Target)	Supplier	Application (dilution)
53BP1	Abcam	IF (1:1000)
AURKA	Sigma Aldrich	WB (1:500)
AURKB	Abcam	WB/IF (1:1K)
Beta-Tubulin (T8328)	Sigma	WB (1:5000)
Beta-tubulin antibody (clone TUB 2.1) (T4026)	Sigma Aldrich	IF (1:100)
BRDU	BD Biosciences	Flow cytometry (1:2)
Histone 3	Cell Signalling Technology	WB (1:1K)
MTOR (7C10)	Cell Signalling Technology	WB (1:1K)
Pericentrin antibody	Sigma Aldrich	IF (1:100)
Phospho-Histone 3 S10 (Mitosis Marker)	Millipore	Flow cytometry (1:500)
Phospho-Histone 3 serine 10	Cell Signalling Technology	WB (1:1K)
Phospho-Histone H2A.X (Ser139) Antibody	Sigma Aldrich	IF (1:500)
Phospho-MTOR S2448 (D9C2)	Cell Signalling Technology	WB (1:500)
Phospho-Aurora A (Thr288)/Aurora B (Thr232)/Aurora C (Thr198) (D13A11)	Cell Signalling Technology	WB (1:500)
RAD51	Abcam	IF (1:500)

Appendix Table 3: Secondary antibodies used in laboratory protocols

Secondary Antibodies	Supplier	Application (dilution)
F(ab')2-Goat anti-Mouse IgG (H+L) Cross-Adsorbed Secondary Antibody, Alexa Fluor 594	Thermo Scientific	IF (1:500-1:1K)
F(ab')2-Goat anti-Mouse IgG (H+L) Secondary Antibody, Alexa Fluor 488	Sigma Aldrich	IF (1:500-1:1K)
GAPDH Mouse Ab	ProteinTech	WB (1:20K)
Goat anti-Rabbit IgG (H+L) Secondary Antibody, Alexa Fluor 488	Sigma Aldrich	IF (1:500-1:1K)
Goat anti-Rabbit IgG (H+L) Secondary Antibody, Alexa Fluor 594	Thermo Scientific	IF (1:500-1:1K)

Anti-mouse FITC	DAKO	Flow cytometry (1:10)
Anti-mouse IgG, HRP-Linked Antibody	Cell Signalling Technology	WB (1:2000)
Anti-rabbit IgG, HRP-Linked Antibody	Cell Signalling Technology	WB (1:2000)

Appendix Table 4: Drug compounds used in laboratory protocols

Drug	**Supplier**	**Stock Concentration (solvent)**	**Working concentration**	**Storage**
Alisertib (MLN8237)	ApexBio	10 mM (DMSO)	10 μM	-80 °C (Long term), -20 °C (Short term)
Barasertib (AZD1152) In vitro work	MedChem Express	10 mM (DMSO)	100 μM	-80 °C (Long term), -20 °C (Short term)
Barasertib (AZD1152) *In vivo work*	GLP Bio	25 mg/ml	1-5 mg/ml	-20 – -80 °C (Long term), -20 °C (Short term)
GSK1070916	LKT Laboratories	2 mM (DMSO)	20 μM	-20 °C
ZM447439	MedChem Express	10mM	1 mM	-20 °C
Nocodazole	Sigma Aldrich	1 mg/ml (DMSO)	100 μg/μl	-20 °C
Rapamycin	Apex Bio	10 mM (DMSO)	200 μM	-20 °C
Hydroxyurea	Sigma	20 mM (media)	20 mM	4 °C

Appendix Table 5: Reagent kits used in laboratory protocols

Kits	**Supplier**	**Catalog Number**
CellEvent™ Caspase-3/7 Detection Reagent	Thermo Fisher	C10423
Senescence β-Galactosidase Staining Kit	Cell Signalling Technology	9860
Annexin V	BD Pharminogen	556547

Appendix Table 6: Solutions required for resolving gels (8% acrylamide) for SDS-PAGE.

	Volume per reagent (ml)					
	5 ml	**10 ml**	**15 ml**	**20 ml**	**25 ml**	**30 ml**
H_2O	2.3	4.6	6.9	9.3	11.5	13.9
30% Acrylamide mix	1.3	2.7	4.0	5.3	6.7	8.0
1.5 M Tris pH 8.8	1.3	2.5	3.8	5.0	6.3	7.5
10% SDS	0.05	0.1	0.15	0.2	0.25	0.3
10% Ammonium persulfate	0.05	0.1	0.15	0.2	0.25	0.3
TEMED	0.003	0.006	0.009	0.0012	0.015	0.018

Appendix Table 7: Solutions required for resolving gels (10% acrylamide) for SDS-PAGE

	Volume per reagent (ml)					
	5 ml	**10 ml**	**15 ml**	**20 ml**	**25 ml**	**30 ml**
H_2O	1.9	4.0	5.9	7.9	9.9	11.9
30% Acrylamide mix	1.7	3.3	5.0	6.7	8.3	10.
1.5 M Tris pH 8.8	1.3	2.5	3.8	5.0	6.3	7.5
10% SDS	0.05	0.1	0.15	0.2	0.25	0.3
10% Ammonium persulfate	0.05	0.1	0.15	0.2	0.25	0.3
TEMED	0.002	0.004	0.006	0.008	0.01	0.012

Appendix Table 8: Solutions required for resolving gels (12% acrylamide) for SDS-PAGE

	Volume per reagent (ml)					
	5 ml	**10 ml**	**15 ml**	**20 ml**	**25 ml**	**30 ml**
H_2O	1.6	3.3	4.9	6.6	8.2	9.9
30% Acrylamide mix	2.0	4.0	6.0	8.0	10.0	12.0
1 M Tris pH 6.8	1.3	2.5	3.8	5.0	6.3	7.5
10% SDS	0.05	0.1	0.15	0.2	0.25	0.3
10% Ammonium persulfate	0.05	0.1	0.15	0.2	0.25	0.3
TEMED	0.002	0.004	0.006	0.008	0.010	0.012

Appendix Table 9: Solutions required for stacking gels (5% acrylamide) for SDS-PAGE

	Volume per reagent (ml)							
	1 ml	**2 ml**	**3 ml**	**4 ml**	**5 ml**	**6 ml**	**8 ml**	**10 ml**
H_2O	0.69	1.40	2.10	2.70	3.40	4.10	5.50	6.80
30% Acrylamide mix	0.17	0.33	0.50	0.67	0.83	1.00	1.30	1.70
1.5 M Tris pH 8.8	0.13	0.25	0.38	0.50	0.63	0.75	1.00	1.25
10% SDS	0.01	0.02	0.03	0.04	0.05	0.06	0.08	0.10
10% Ammonium persulfate	0.01	0.02	0.03	0.04	0.05	0.06	0.08	0.10
TEMED	0.001	0.002	0.003	0.004	0.005	0.006	0.008	0.010

Appendix Table 10: **Lysis buffer for mass spectrometry sample preparation**

Reagent	**(stock conc.)**	**Working conc. in buffer**	**Volume per 10 ml**
SDS	(10%)	1%	1 ml
NP40	10%)	1%	1 ml
Sodium deoxycholate	(10%)	1%	1 ml
Tris pH8	(1 M)	100 mM	1 ml
EDTA	(0.5 M)	5 mM	100 µl
NaCl (1 M)	(1 M)	250 mM	2.5 ml
Phosstop	(10x)	1x	1 ml (or 1 tablet)
Complete Protease I	(10x)	1x	1 ml (or 1 tablet)
H_2O (HPLC grade) to 1 ml	-	-	1.4 ml (3.4 ml)

Appendix Table 11: DMF and SF values for H460 cells

DEF values for 0.1 and 0.37 survival fraction and SF(±SD) at 2Gy and 4 Gy. Radiobiological alpha and beta parameters derived by fitting to a linear quadratic model are also shown.

Schedule	**1Hr PT and Recovery**		**24 Hr PT and Recovery**		**No PT and Recovery**		**24 Hr Pretreatment**		**Started 24 Hr after IR**	
$DEF_{0.1}$	1.24		1.83		1.19		1		1	
$DEF_{0.37}$	1.37		1.57		1.21		1		1	
Schedule	**1Hr PT and Recovery**		**24 Hr PT and Recovery**		**Only Recovery**		**24 Hr Pretreatment**		**Started 24 Hr after IR**	
	DMSO	**50 nM Barasertib**	**DMSO**	**50 nM Barasertib**	**DMSO**	**50 nM Barasertib**	**DMSO**	**50 nM Barasertib**	**DMSO**	**50 nM Barasertib**
SF_2	0.451 ± 0.07	0.285 ± 0.06	0.498 ± 0.21	0.498 ± 0.07	0.379 ± 0.05	0.28 ± 0.17	0.498 ± 0.06	0.498 ± 0.06	0.355 ± 0.04	0.355 ± 0.35
SF_4	0.083 ± 0.03	0.035 ± 0.02	0.084 ± 0.17	0.084 ± 0.06	0.064 ± 0.03	0.027 ± 0.02	0.084 ± 0.05	0.084 ± 0.05	0.021 ±	0.021 ± 0.06
α	0.2273	0.4367	0.3353	0.3732	0.2827	0.3694	0.1423	0.1423	0.0683	0.0683
β	0.1136	0.1048	0.01241	0.1199	0.1012	0.1336	0.1265	0.1265	0.2249	0.2249

PT = pretreatment, DEF= dose enhancement factor, SF = surviving fraction, SD = standard deviation

Appendix Table 12: DMF and SF values for H1299 and SW900 cells

DEF values for 0.37 survival fraction and Surviving fraction (SF) at 2 Gy and 4 Gy. Radiobiological alpha and beta parameters derived by fitting to a linear quadratic model are also shown. Calculated from Data collected by Timothy Mitchell.

	$DEF_{0.37}$	
Cell Line	**25 nM**	**50 nM**
H1299	2.07	1.18
SW900	1.24	1.28

	H1299			**SW900**		
	DMSO	**25 nM**	**50 nM**	**DMSO**	**25 nM**	**50 nM**
SF_2	0.768 ± 0.07	0.548 ± 0.08	0.506 ± 0.33	0.648 ± 0.14	0.507 ± 0.16	0.494 ± 0.13
SF_4	0.368 ± 0.18	0.263 ± 0.05	0.222 ± 0.10	0.267 ± 0.08	0.196 ± 0.06	0.181 ± 0.07
α	0.01385	0.268	0.3043	0.1036	0.2716	0.2772
β	0.05897	0.0165	0.01805	0.05666	0.03394	0.03752

DEF= dose enhancement factor, SF = surviving fraction, SD = standard deviation

8.3. Figures (Appendices)

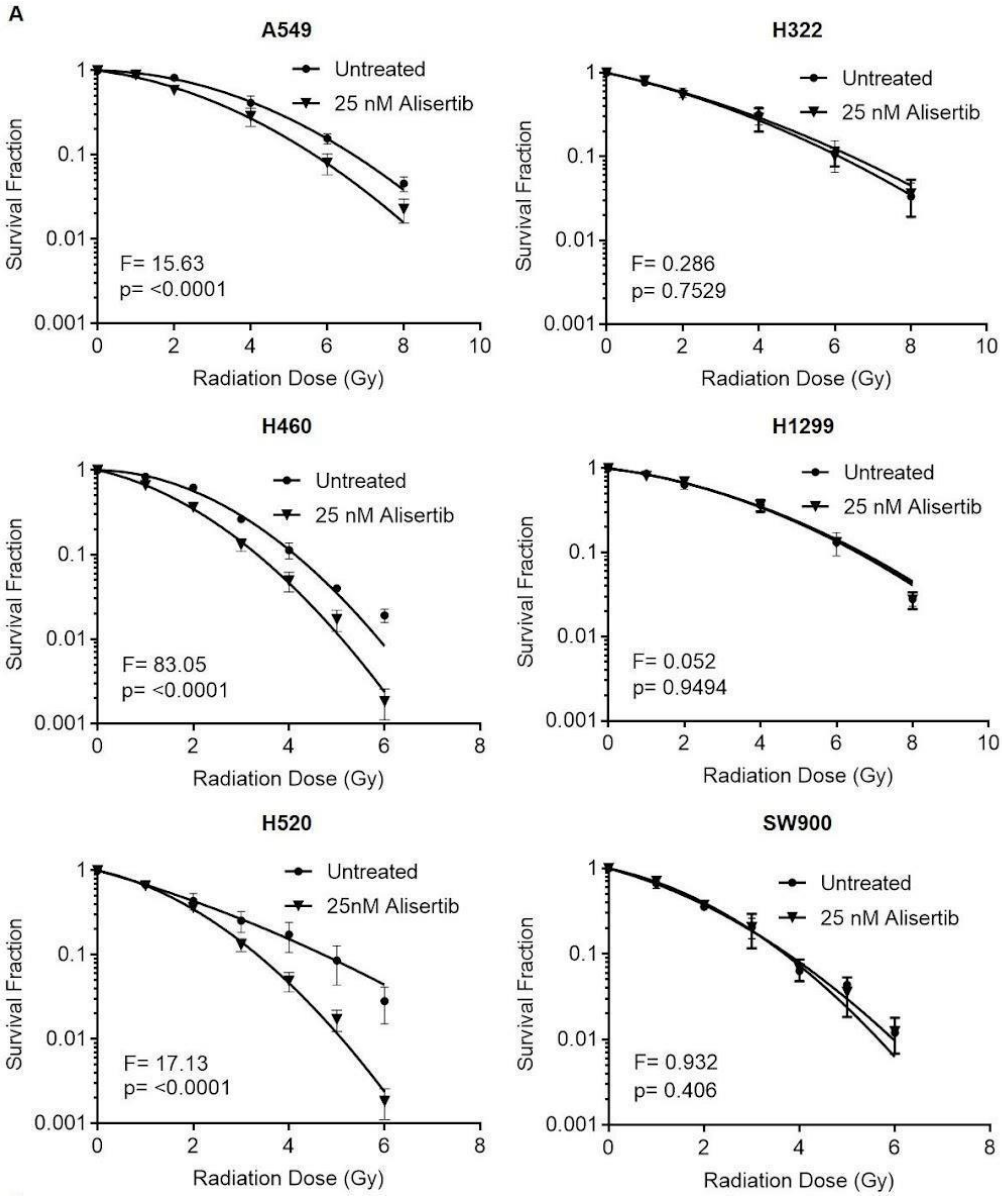

Appendix Figure 1: Radiosensitation by Alisertib in NSCLC cell lines

A Survival fraction of NSCLC cell lines after treatment with 0 - 5 Gy IR with DMSO or 25 nM Alisertib. Data points represent survival fraction normalised to 0 Gy control (Mean and SD, n≥3). F-value and p-value were calculated by an extra sum of squares test. Data produced by Thomas Jones.

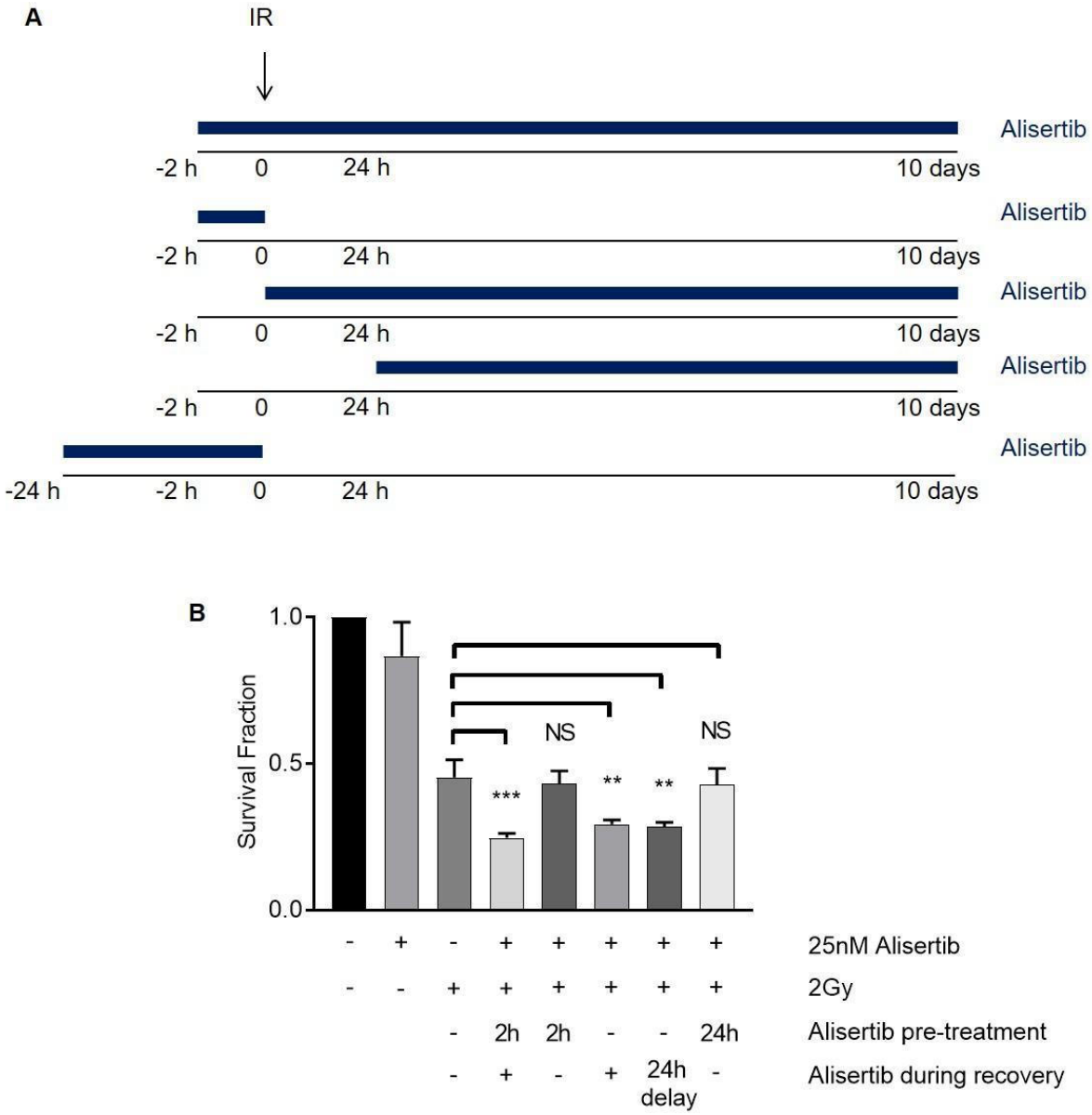

Appendix Figure 2: Effect of varying Alisertib IR dosing schedule in H460 cells

A Alisertib dosing regimen changes relative to the point of irradiation. Blue line represents presence of 25 nM Alisertib in the culture media. **B** Survival fractions of H460 cells after 2 Gy treated with or without 25 nM Alisertib (N=3). Data points represent survival fraction normalised to unirradiated control (Mean and SD, n≥3).NS (non-statistically significant) denotes p= >0.05, * denotes p= ≤0.05, ** denotes p= ≤0.01, *** denotes p=≤0.001 (One-way ANOVA with Dunnett correction for multiple comparisons). Data produced by Thomas Jones.

A

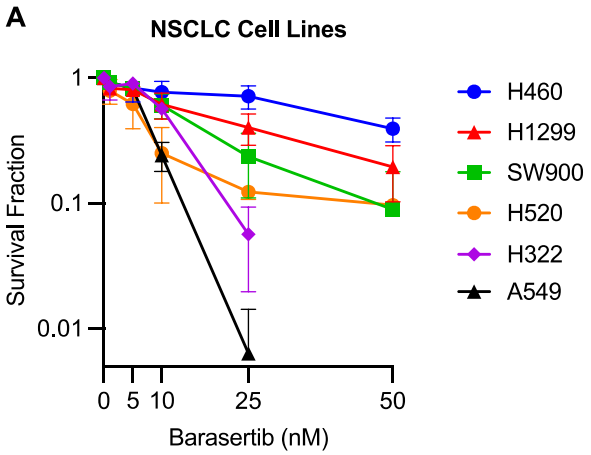

B

Cell line	p53 Status	NSCLC Subtype	Barasertib LD50 (nM)
H460	WT	Large cell carcinoma	69.7
H1299	Null	Large cell carcinoma	24.8
SW900	Mutant (c.499C>T)	Squamous cell carcinoma	21.4
H520	Mutant (c.438G>A)	Squamous cell carcinoma	13.9
H322	Mutant (c.743G>T)	Adenocarcinoma	16.6
A549	WT	Adenocarcinoma	15.2

Appendix Figure 3: Survival and AURKB inhibition after Barasertib treatment in NSCLC cell lines

A Clonogenic Survival of NSCLC lines H460, H1299, SW900, H520, H322 and A549 following Barasertib treatment (0-50 nM). Survival Fraction was calculated relative to DMSO control. **B** Table of TP53 status, NSCLC subtype and Barasertib LD50 (nM) for each cell line in A. Data in A and B produced by Timothy Mitchell
Protein expression of p-AURKA/B/C, AURKB and GAPDH in H1299 cells treated with Barasertib for 24 hours. **D** Representative western blot and mean and standard deviation of quantification of two independent repeats (DMSO, 50-200 nM) and quantification of one repeat (25 nM) are shown for **E** pAURKB, **F** AURKB, **G** pAURKA and **H** pAURKC. For quantification protein levels were normalised to GAPDH and are shown relative to DMSO control.
Protein expression of p-AURKA/B/C, AURKB and GAPDH in SW900 cells treated with Nocodazole for 16 Hr then released into Barasertib for 2 hours.**I** Representative western blot, and mean and standard deviation of quantification of one independent repeat is shown for **J** pAURKB, **K** AURKB, **L** pAURKA and **M** pAURKC. For quantification protein levels were normalised to GAPDH and are shown relative to DMSO control.

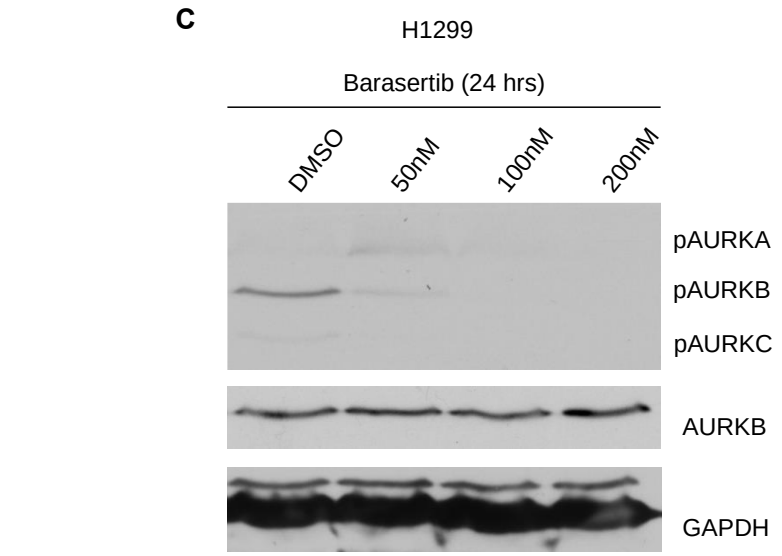

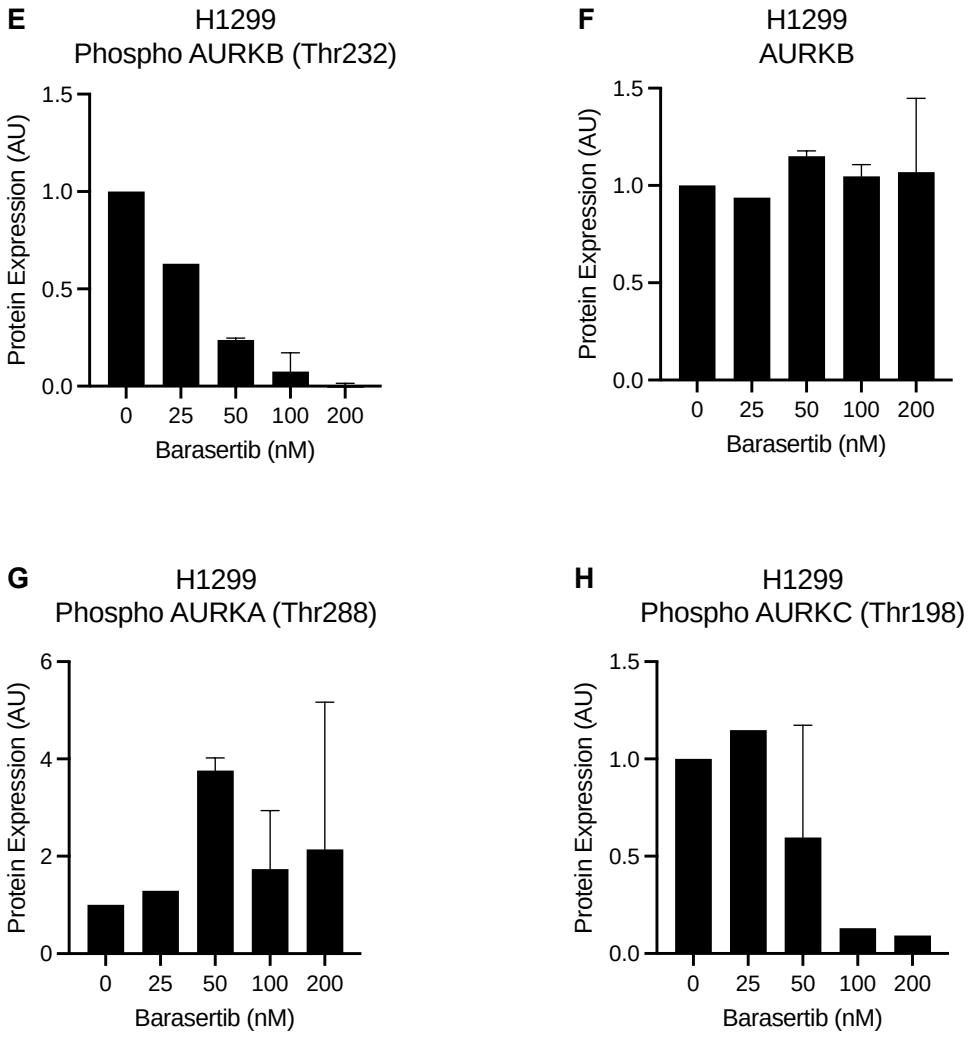

Appendix Figure 3: Survival and AURKB inhibition after Barasertib treatment in NSCLC cell lines

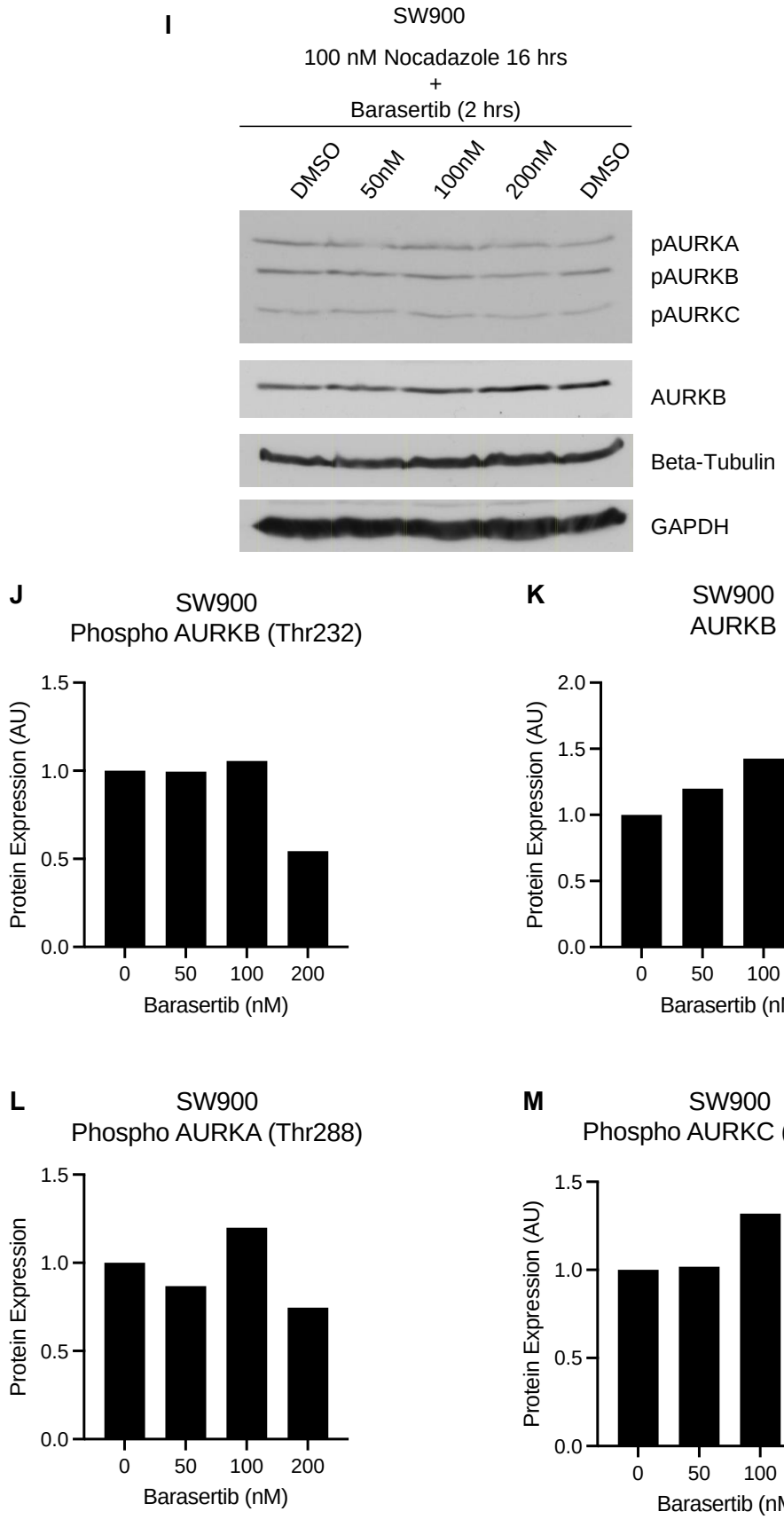

Appendix Figure 3: Survival and AURKB inhibition after Barasertib treatment in NSCLC cell lines

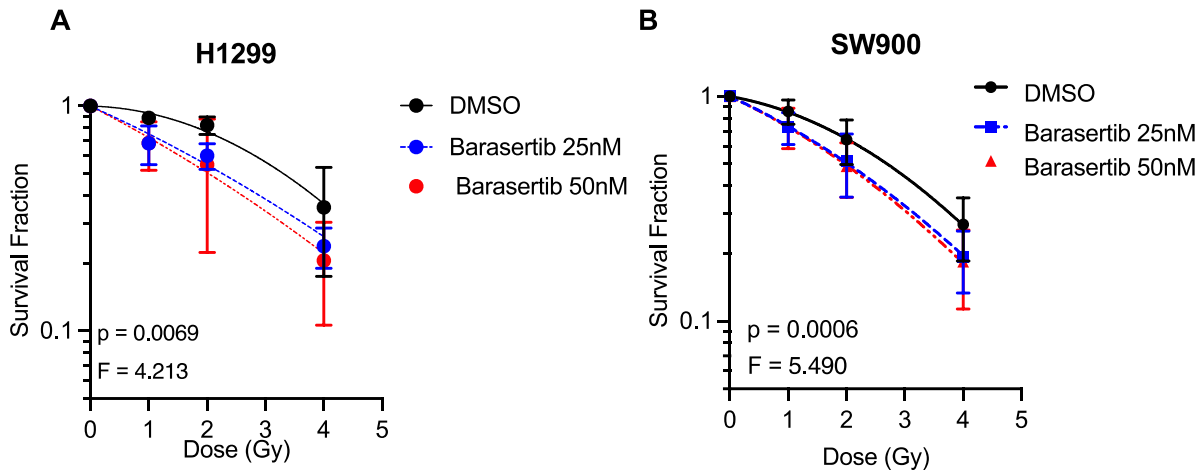

Appendix Figure 4: Barasertib Radiosensitisation in NSCLC cell lines H1299 and SW900

Clonogenic survival of **A** H1299 and **B** SW900 cells after treatment with 25-50 nM Barasertib and 0– 5 Gy IR. Survival fraction was calculated relative to 0 Gy control. Statistical significance between curves was calculated by an extra sum-of-squares F test. P and F values are displayed for each graph. In each case, mean and standard deviation of ≥3 independent repeats are shown. Data produced by Timothy Mitchell.

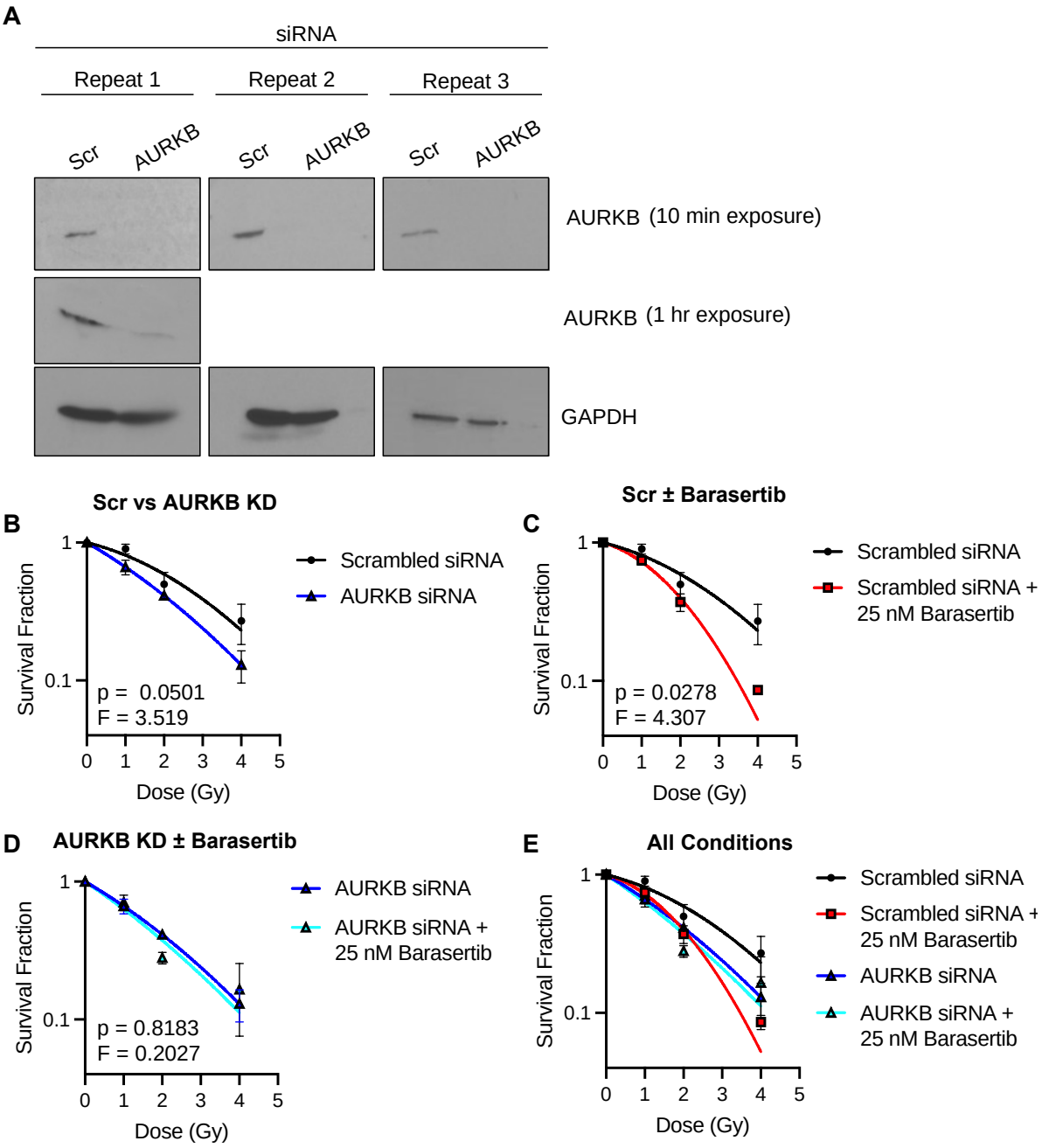

Appendix Figure 5: Barasertib radiosensitises NSCLC cell lines H1299 and SW900

A Protein expression of AURKB and GAPDH in H460 cells after treatment with siRNA or AURKB (24 Hr), showing 10 mins/1 Hr exposure for AURKB.
B-E Clonogenic survival of H460 cells after treatment with Scr or AURKB siRNA (24 Hr) before 25 nM Barasertib (2 Hr pretreatment) and 0–4 Gy IR. Survival fraction was calculated relative to 0 Gy control. Each siRNA repeat was carried out in tandem for all 3 conditions and displayed separately for clarity in **B-D**. Statistical significance between curves was calculated by an extra sum-of-squares F test. P and F values are displayed for each graph. In each case, mean and standard deviation of ≥3 independent repeats are shown. Data produced by Timothy Mitchell.

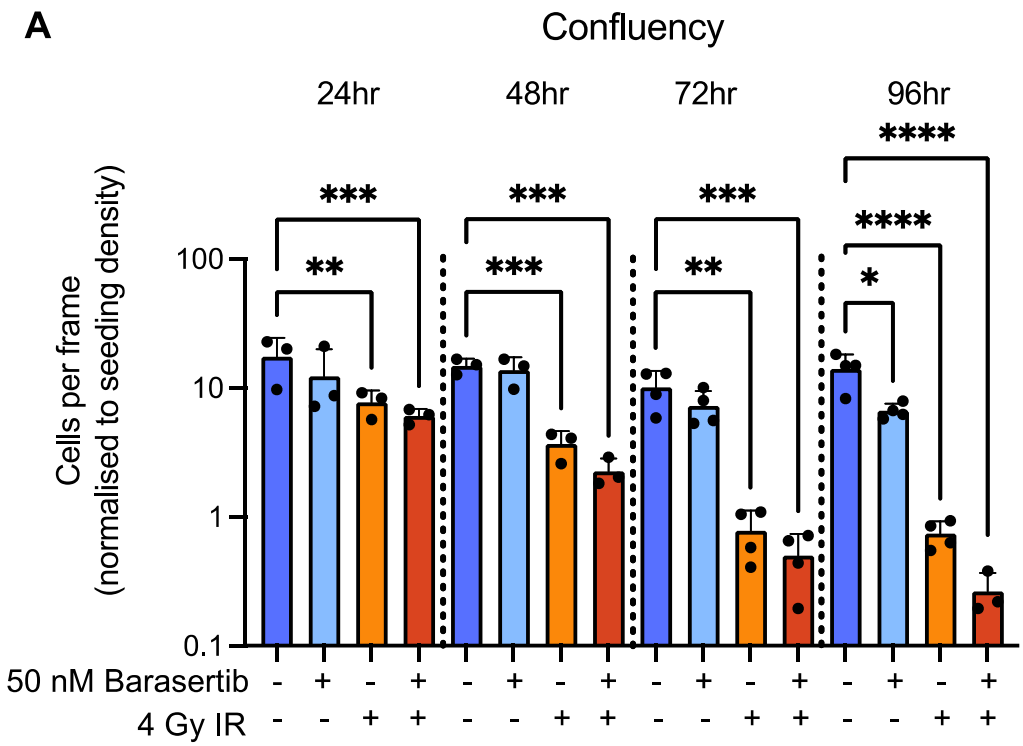

Appendix Figure 6: H460 cell confluency after IR + Barasertib combination in H460 cells

H460 cells were pretreated with 50 nM Barasertib for 1 Hr before 4 Gy, then fixed at 24, 48, 72 and 96 Hr, and stained for Beta-Galactosidase (blue). **A** Confluency was calculated as cells per frame normalized to seeding density. Mean, standard deviation and individual values are shown for ≥ 3 independent repeats. P-values were calculated using a one-way anova (* = $p < 0.05$, ** = $p < 0.01$, *** = $p<0.001$. **** = $p<0.0001$).

A

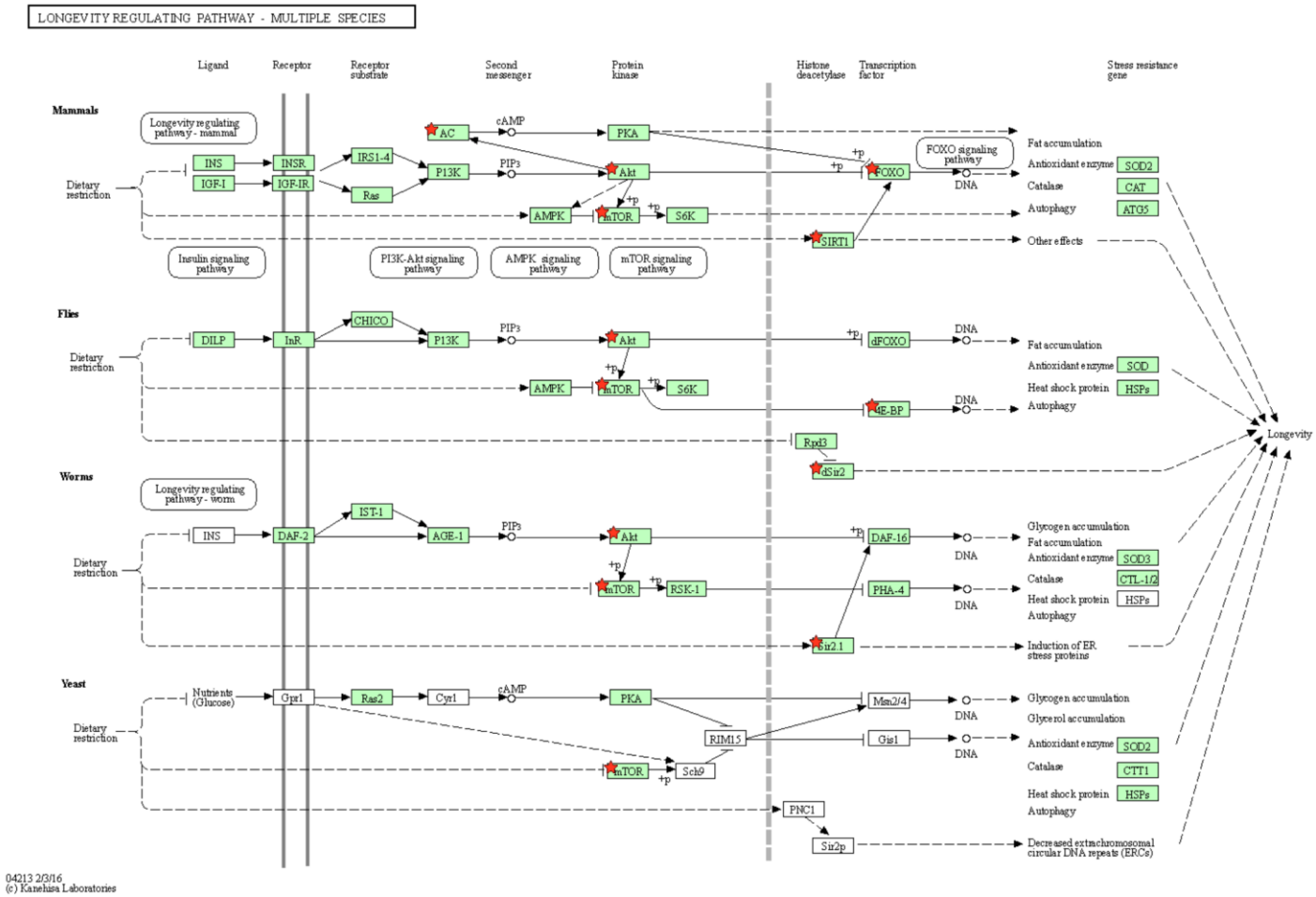

Appendix Figure 7 (over 5 pages): Additional KEGG pathway Charts for analysis of differentially abundant phosphopeptides between 4 Gy and 4 Gy + 50 nM Barasertib conditions (Legend on Pg 316)

B

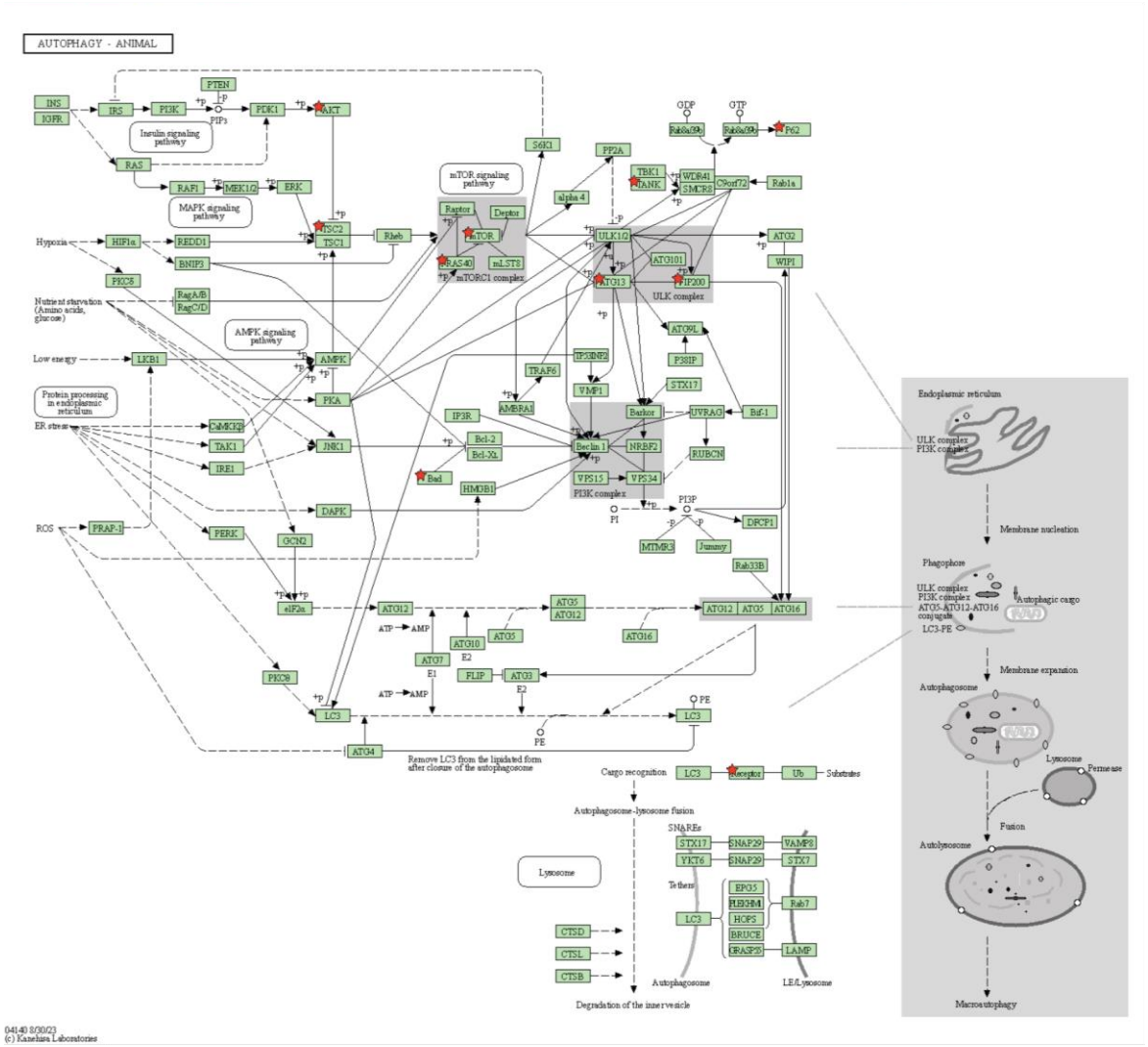

Appendix Figure 7 (over 5 pages): Additional KEGG pathway charts for analysis of differentially abundant phosphopeptides between 4 Gy and 4 Gy + 50 nM Barasertib conditions

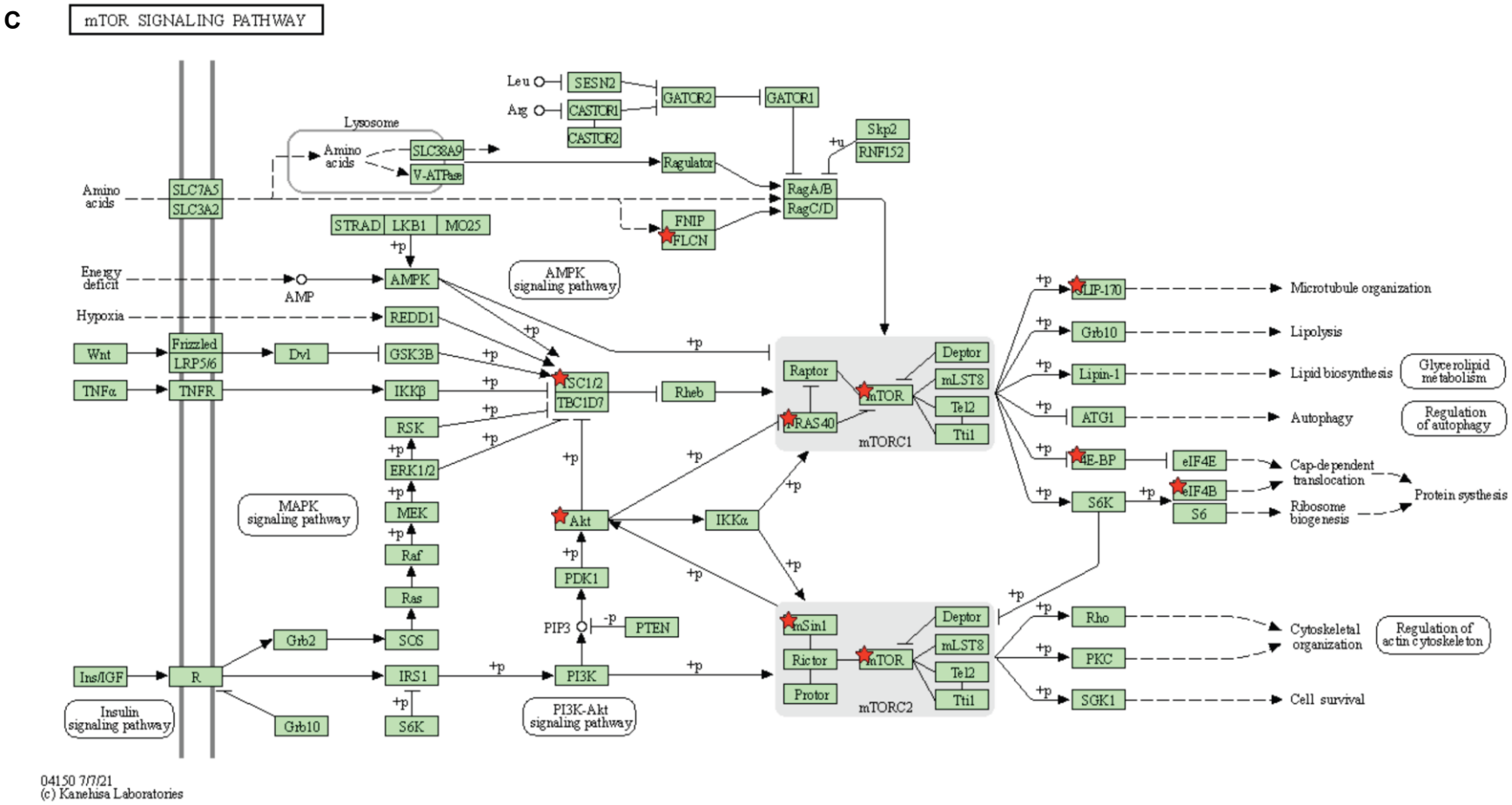

Appendix Figure 7 (over 5 pages): Additional KEGG pathway charts for analysis of differentially abundant phosphopeptides between 4 Gy and 4 Gy + 50 nM Barasertib conditions

D

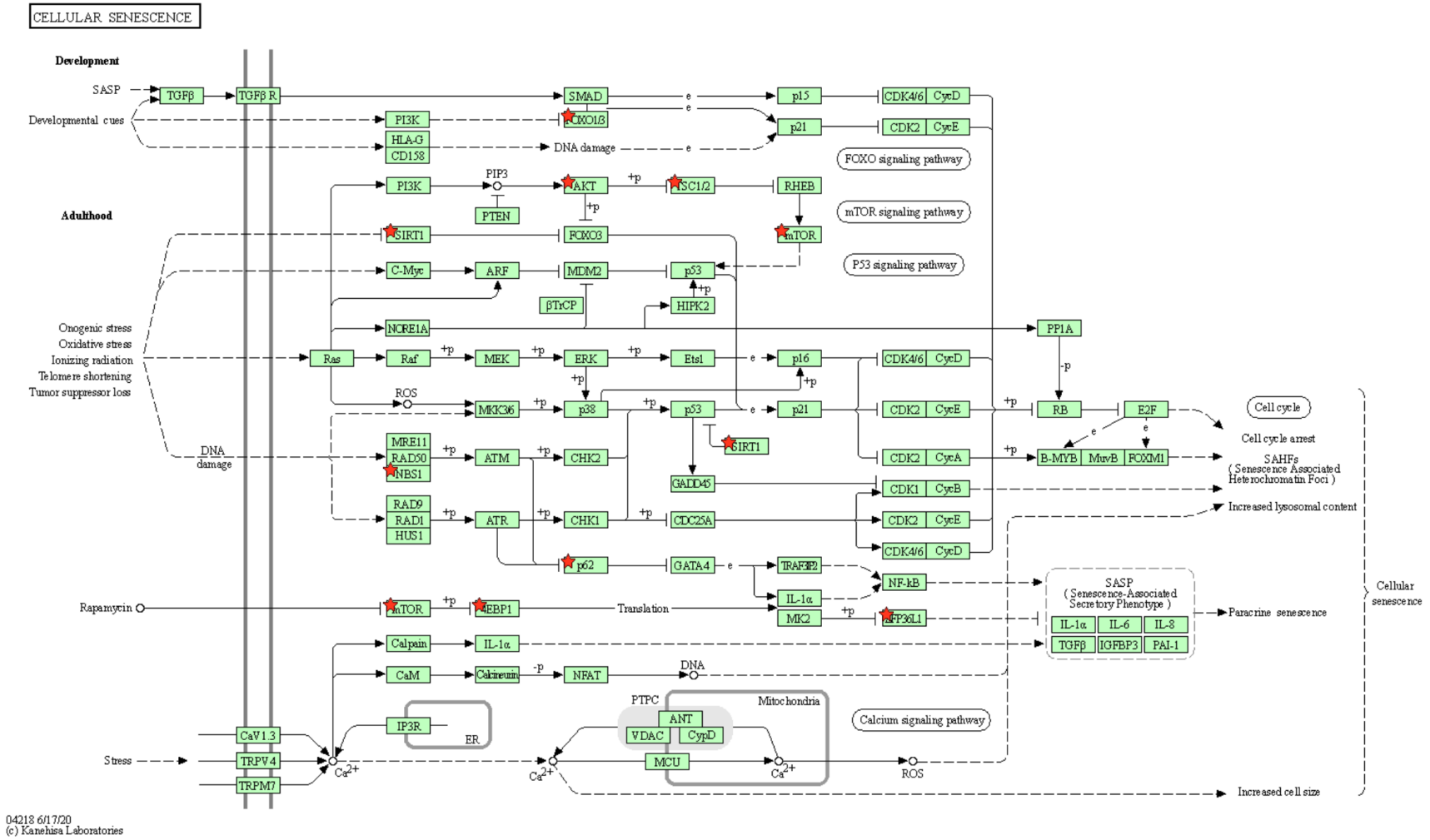

Appendix Figure 7 (over 5 pages): Additional KEGG pathway charts for analysis of differentially abundant phosphopeptides between 4 Gy and 4 Gy + 50 nM Barasertib conditions

Appendix Figure 7: Additional KEGG pathway charts for analysis of differentially abundant phosphopeptides between 4 Gy and 4 Gy + 50 nM Barasertib conditions

Pathway Analysis was carried out on DAVID Bioinformatics Functional Annotation. The following pathways were generated by KEGG pathway chart function: **A** Longevity regulating pathway - multiple specie**s B** Autophagy – Animal, **C** MTOR signalling pathway, **D** Cellular senescence. Red stars indicate proteins represented in our list of master proteins for the differentially abundant phosphopeptides.

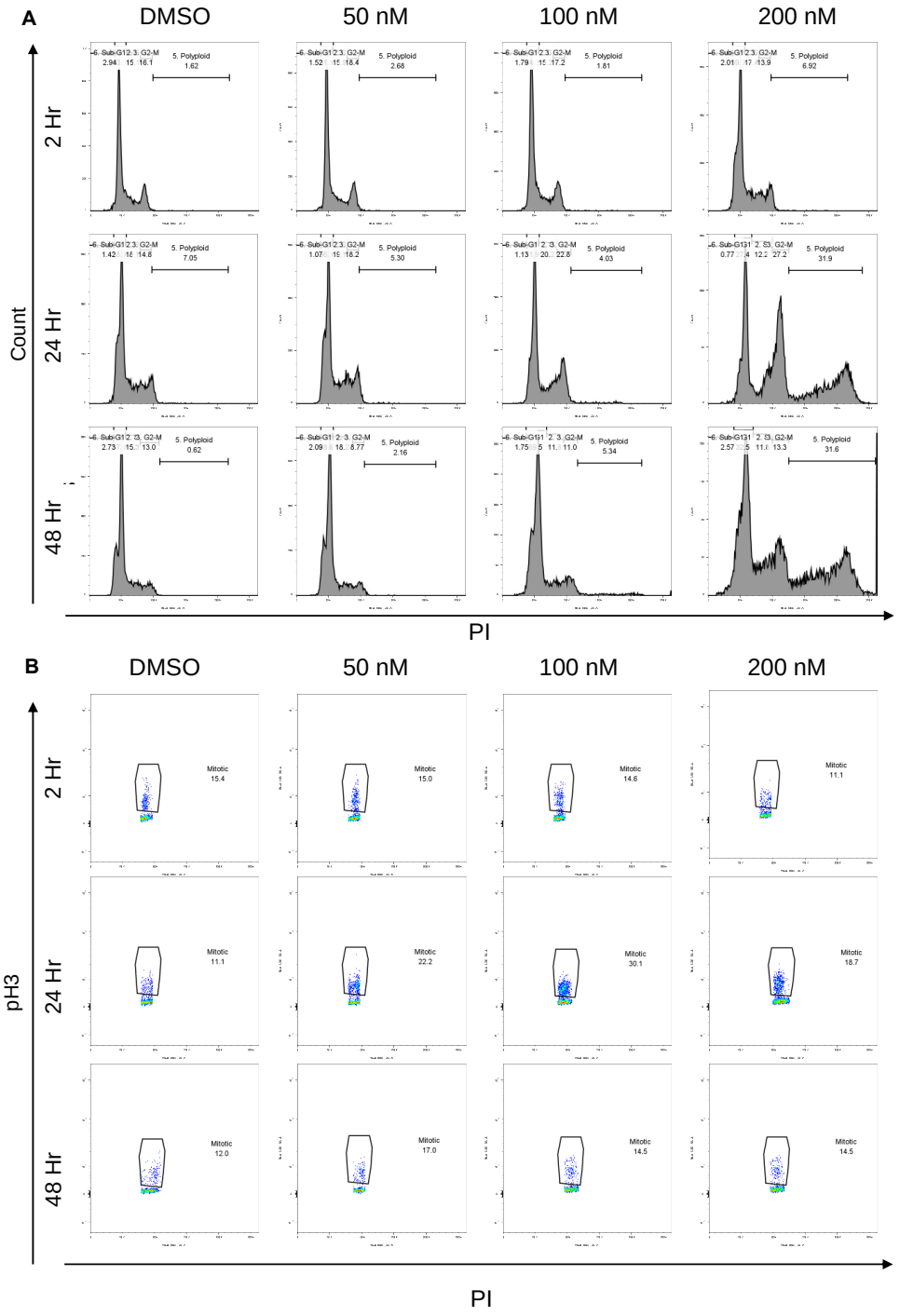

Appendix Figure 8: Flow cytometry gating of cell cycle analysis after Barasertib treatment

H460 cells were treated with DMSO or 5—200 nM Barasertib for 2 – 48 Hr, then fixed and stained for DNA content (PI) and phospho-Histone 3 (ser10) and analysed by Flow cytometry. **A** Representative PI Histograms with linear scale for PI with G1, S, G2+M, Polyploid and Sub-G1 Fractions gated **B** Flow cytometry density plots of Mitotic (pH3+) cells gating within G2+M gate - PI (660/20) (Y axis) vs phospho-H3 (Ser10) (Blue 530/30)(X axis), with Log(10) scale. Plots represent plots from one independent repeat.

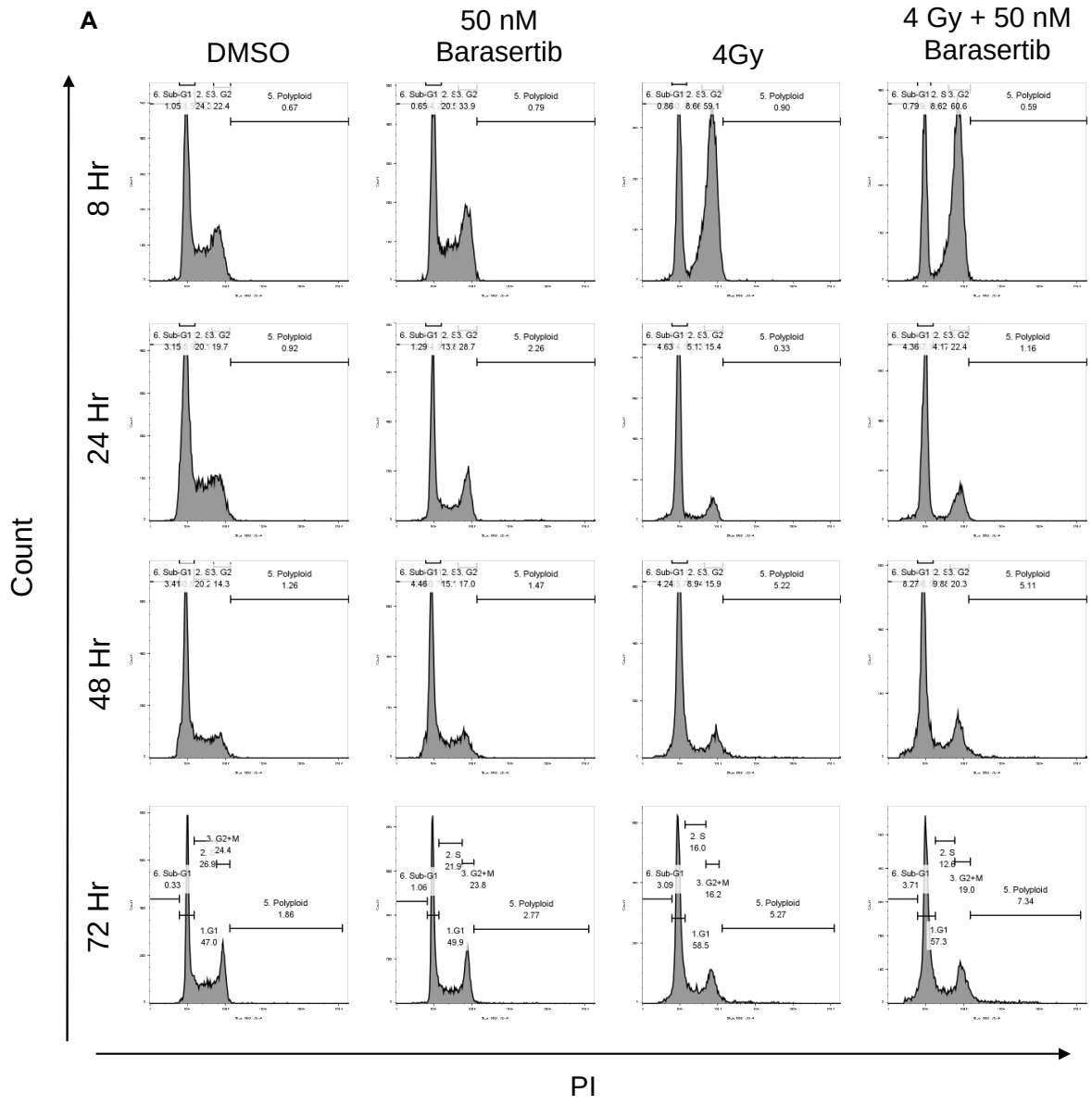

Appendix Figure 9: Flow cytometry gating of cell cycle analysis after IR and Barasertib

H460 cells were pretreated with DMSO or 50 nM Barasertib for 1 Hr before 4 Gy (or sham) IR. Cells were fixed and stained for DNA content (PI) and phospho-Histone 3 (Ser10) and analysed by Flow cytometry. **A** Representative PI Histograms with linear scale for PI with G1, S, G2+M, Polyploid and Sub-G1 Fractions gated.
B Flow cytometry density plots of Mitotic (pH3+) cells gating within G2+M gate - phospho-H3 (Ser10) (Blue 530/30)(Y axis) vs PI (660/20) (X axis), with Log(10) scale. Plots represent plots from one independent repeat.

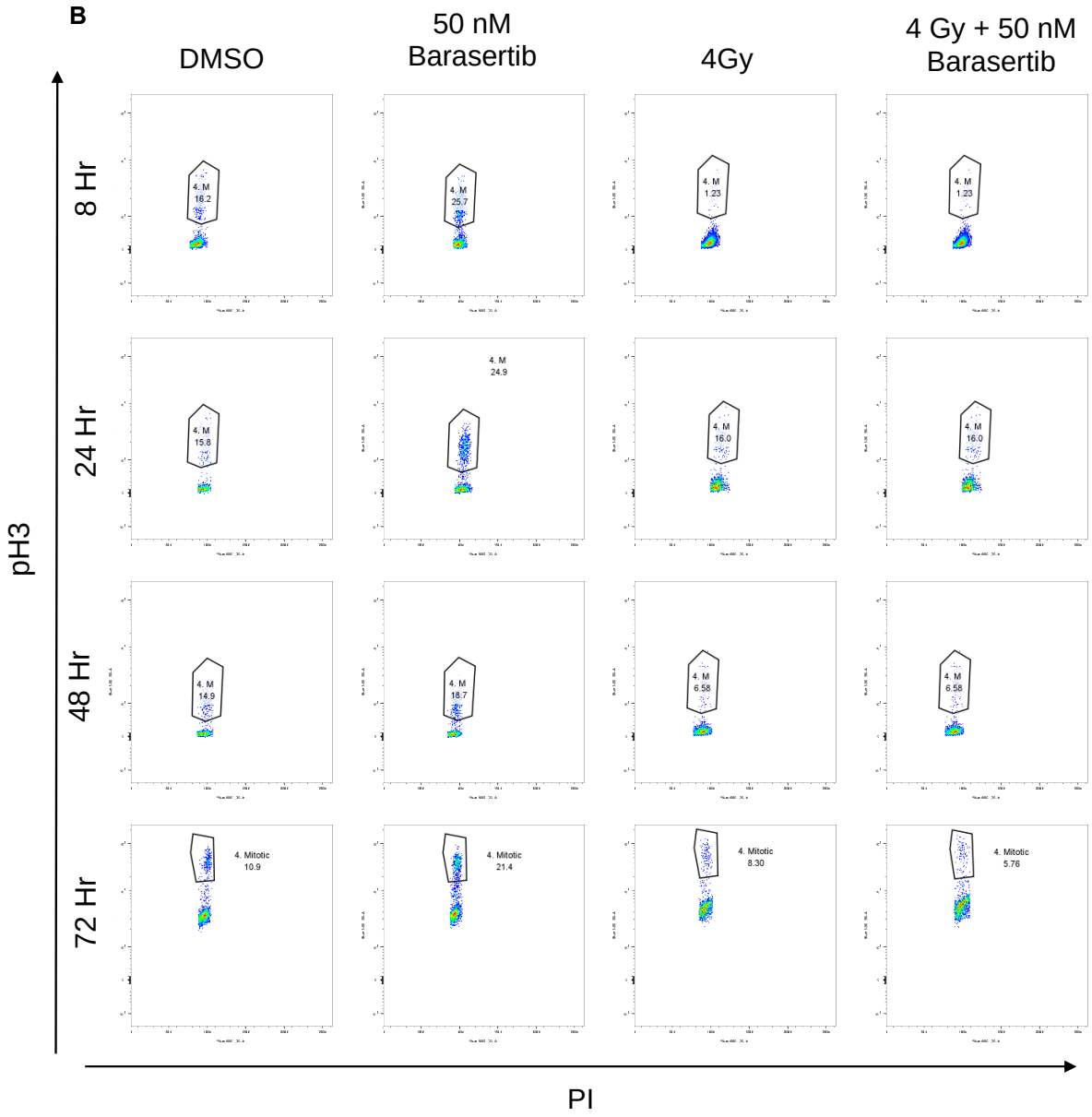

Appendix Figure 9: Flow cytometry gating of cell cycle analysis after IR and Barasertib

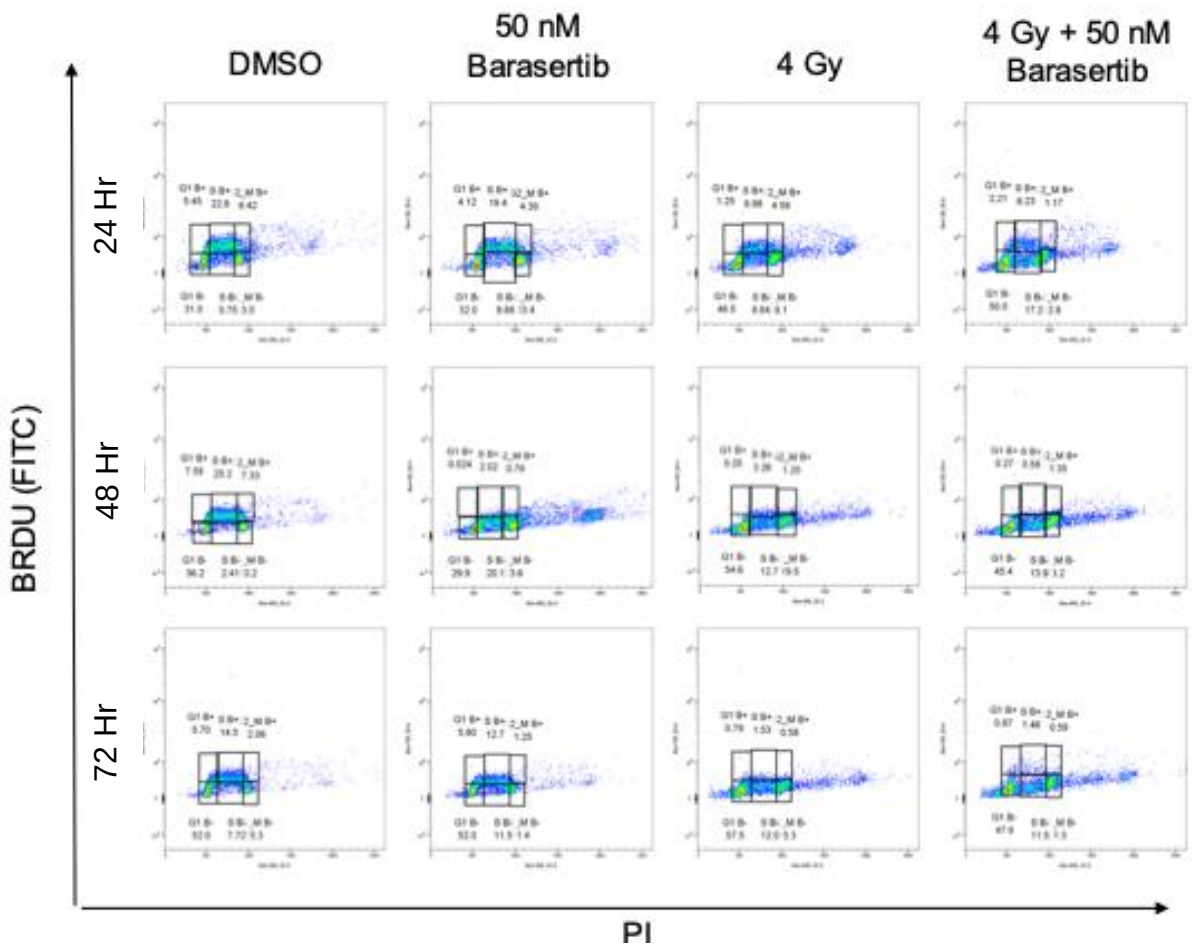

Appendix Figure 10: Flow cytometry gating of BRDU staining

Representative density plots showing vs BRDU (Blue (530/30)(Y axis) vs PI (660/20) (X axis) with Log(10) scale. H460 cells were pretreated with DMSO or 50 nM Barasertib for 1 Hr before 4 Gy (or sham) IR. Cells were treated with 10 μM BRDU then fixed and stained for DNA content (PI) and BRDU.

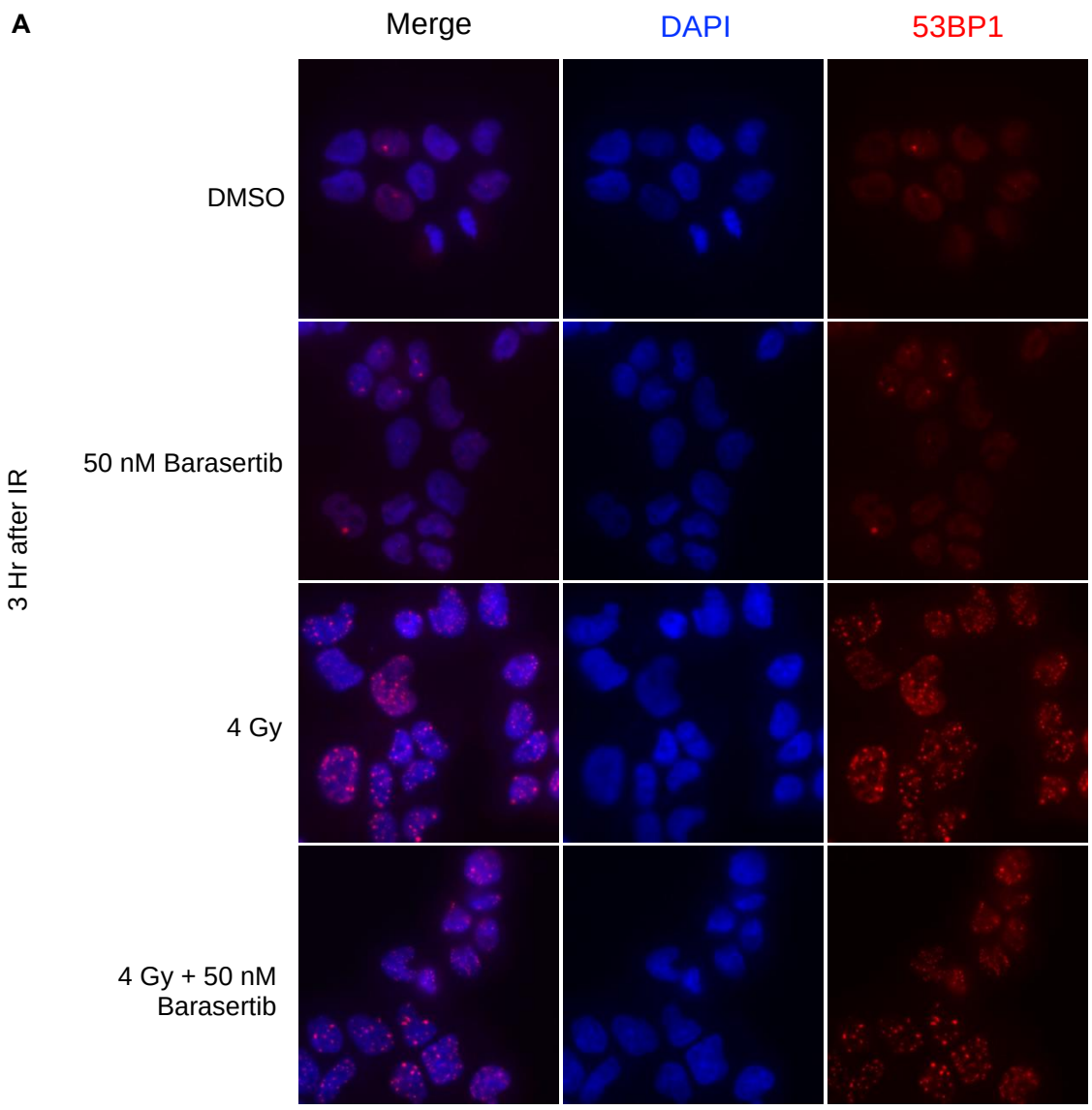

Appendix Figure 11: Representative images of 53BP1 foci after Barasertib and IR treatment

H460 cells were pretreated with DMSO or 50 nM Barasertib for 1 Hr before 4 Gy (or sham) IR, then fixed immediately or 10 or 30 Mins, or 1,3,6,or 24 Hr after IR. Cells were stained for 53BP1 and DAPI. Representative images of 53BP1 foci and nuclei in H460 cells **A** 10 minutes after IR **B** 30 minutes after IR and **C** 24 Hr after IR.

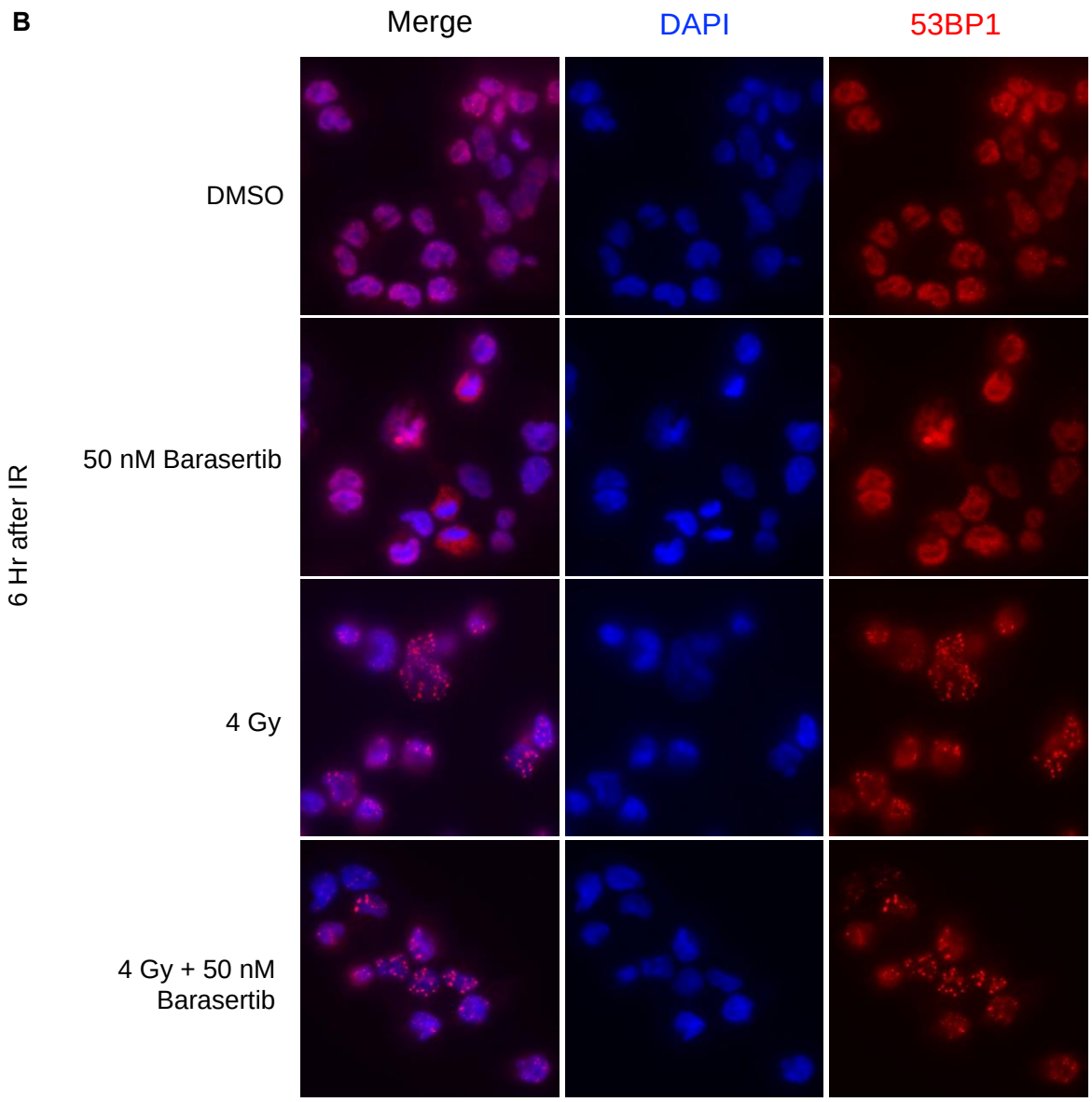

Appendix Figure 11: Representative images of 53BP1 foci after Barasertib and IR treatment

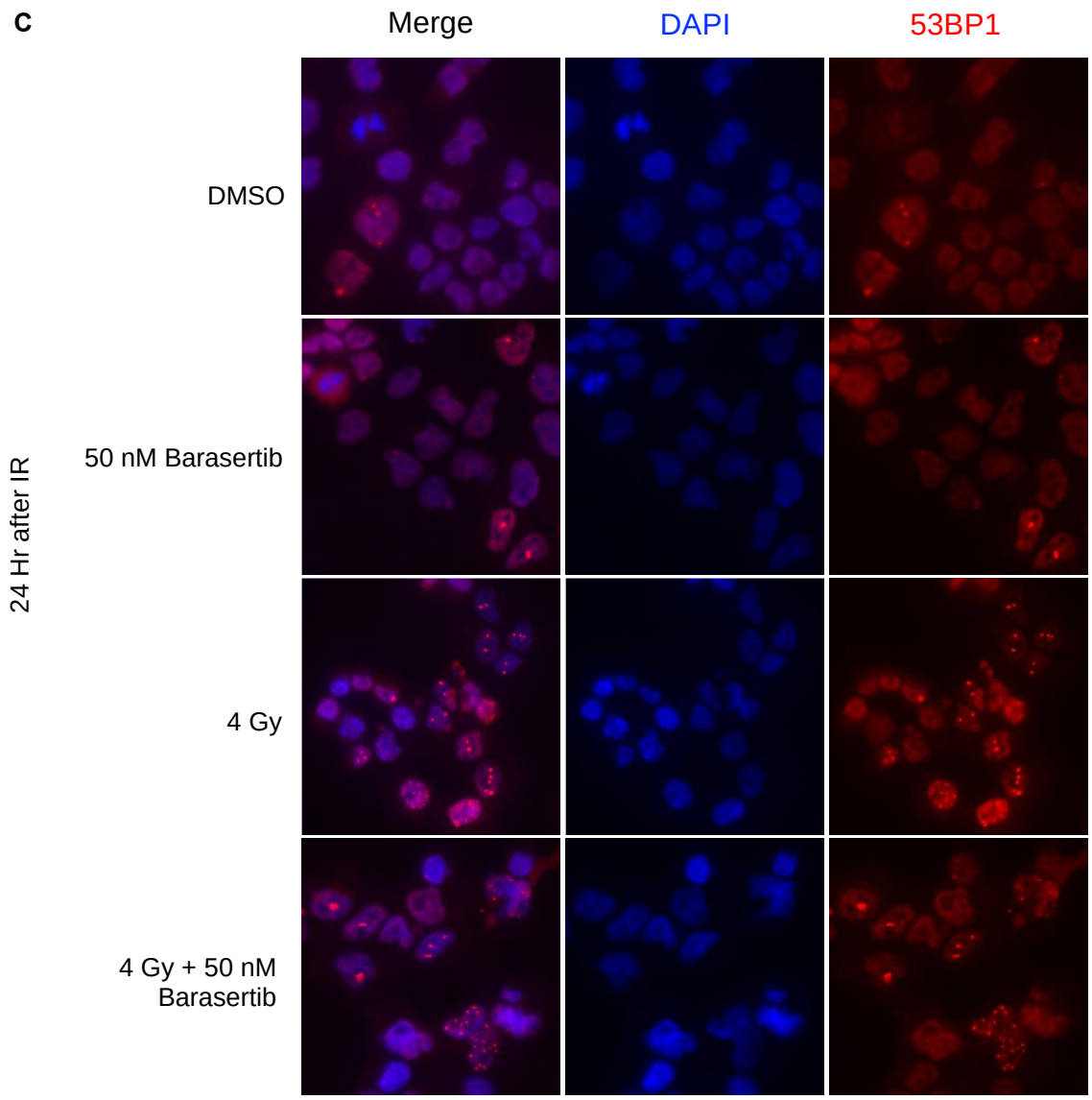

Appendix Figure 11: Representative images of 53BP1 foci after Barasertib and IR treatment

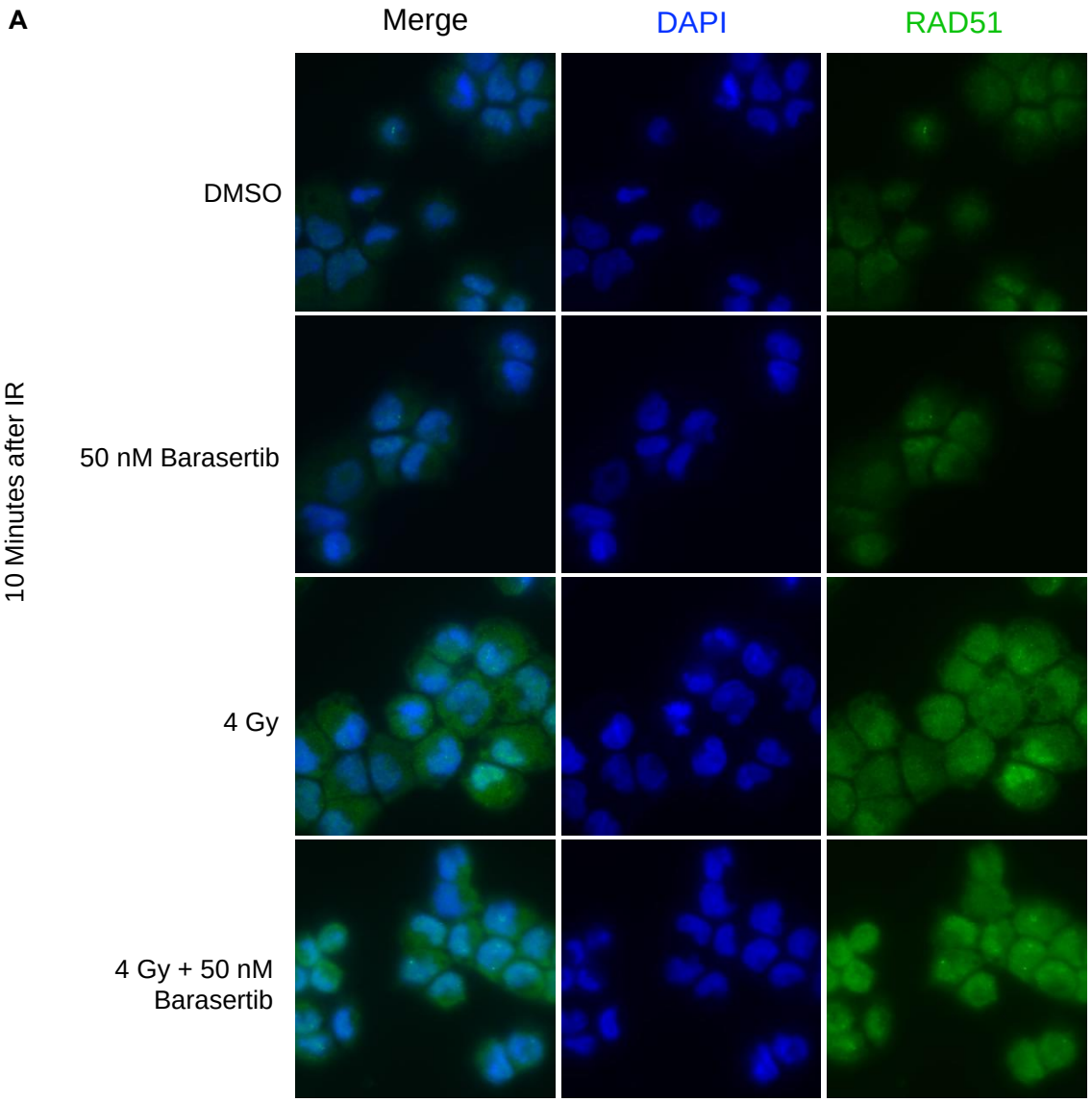

Appendix Figure 12: Representative images of RAD51 foci after Barasertib and IR treatment

H460 cells were pretreated with DMSO or 50 nM Barasertib for 1 Hr before 4 Gy (or sham) IR, then fixed immediately or 10 or 30 Mins, or 1, 3, 6, or 24 Hr after IR. Cells were stained for RAD51 and DAPI. Representative images of 53BP1 foci and nuclei in H460 cells **A** 10 minutes after IR **B** 30 minutes after IR and **C** 24 Hr after IR.

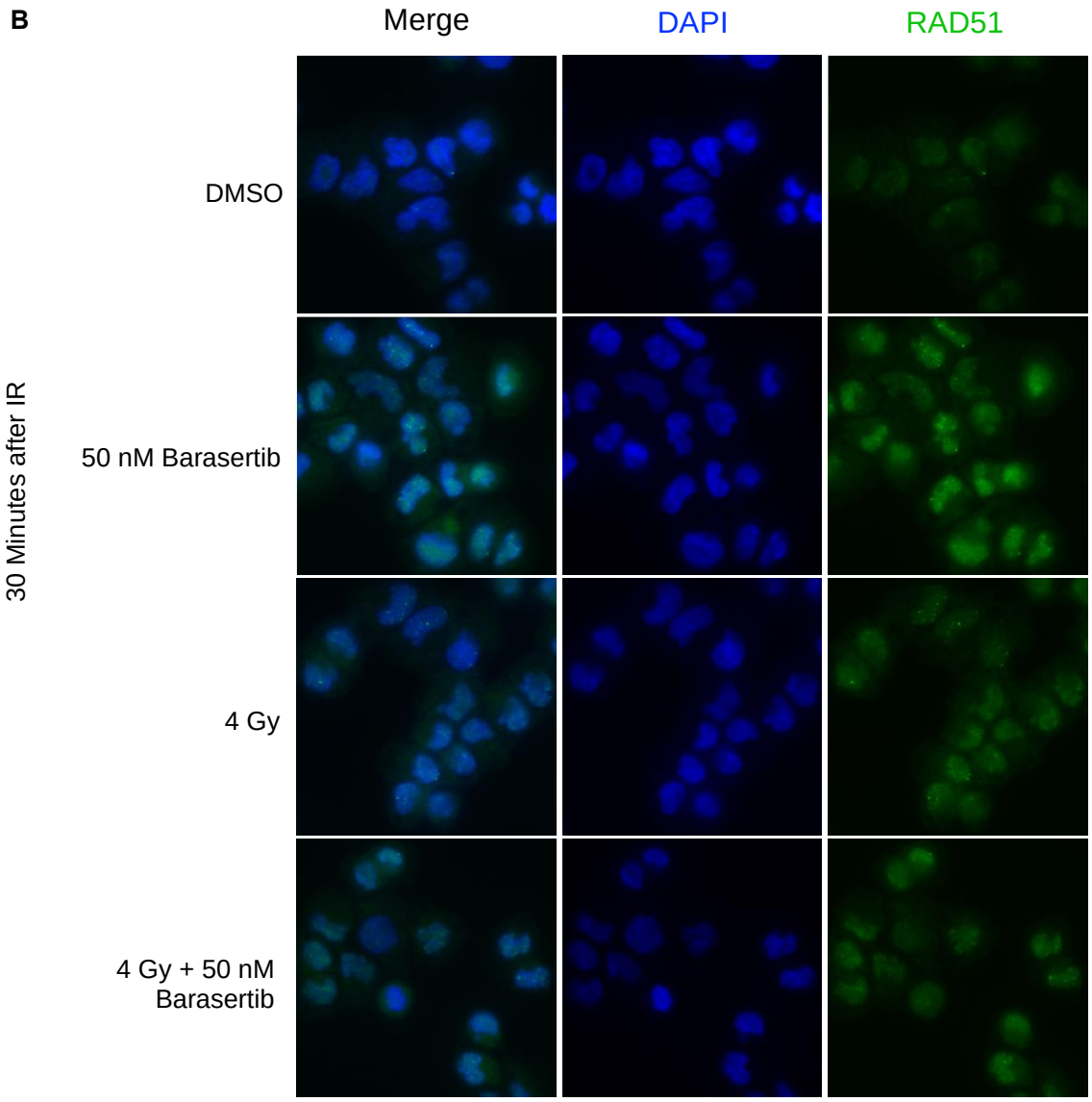

Appendix Figure 12: Representative images of RAD51 foci after Barasertib and IR treatment

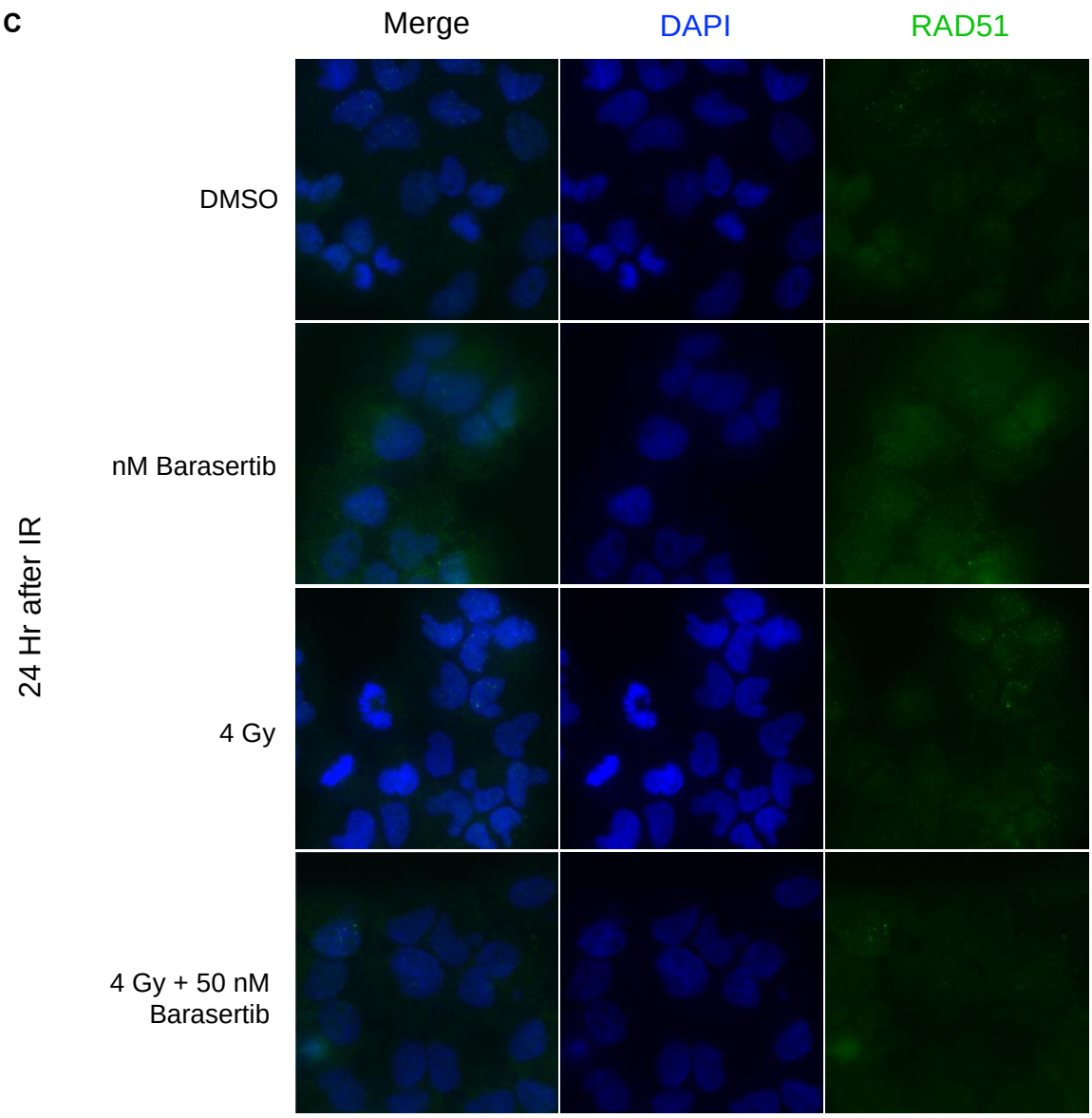

Appendix Figure 12: Representative images of RAD51 foci after Barasertib and IR treatment

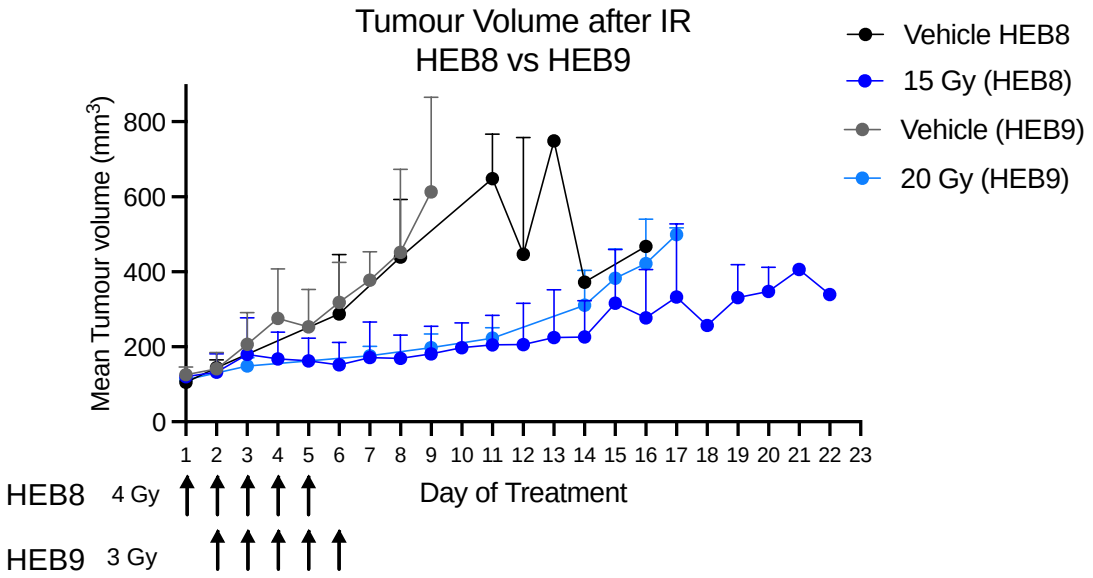

Appendix Figure 13: Comparison of IR dose response in H460 xenografts between multiple studies

Mice were implanted subcutaneously with H460 cells to establish tumours. Once tumours reached 100 mm3, treatment commenced. In HEB8 mice were treated with Vehicle or with 20 Gy (5 x 4 Gy). In HEB9, mice were treated with vehicle or 15 Gy (3 x 5Gy) + vehicle. Grouped tumour volume for Vehicle and IR groups in HEB8 and HEB9.

Chapter 9: References

9. References

ABBOTTS, R. & WILSON, D. M., 3RD 2017. Coordination of DNA single strand break repair. *Free Radic Biol Med,* 107**,** 228-244.

ADAMS, N. D., ADAMS, J. L., BURGESS, J. L., CHAUDHARI, A. M., COPELAND, R. A., DONATELLI, C. A., DREWRY, D. H., FISHER, K. E., HAMAJIMA, T., HARDWICKE, M. A., HUFFMAN, W. F., KORETKE-BROWN, K. K., LAI, Z. V., MCDONALD, O. B., NAKAMURA, H., NEWLANDER, K. A., OLEYKOWSKI, C. A., PARRISH, C. A., PATRICK, D. R., PLANT, R., SARPONG, M. A., SASAKI, K., SCHMIDT, S. J., SILVA, D. J., SUTTON, D., TANG, J., THOMPSON, C. S., TUMMINO, P. J., WANG, J. C., XIANG, H., YANG, J. & DHANAK, D. 2010. Discovery of GSK1070916, a Potent and Selective Inhibitor of Aurora B/C Kinase. *Journal of Medicinal Chemistry,* 53**,** 3973-4001.

ADJEMIAN, S., OLTEAN, T., MARTENS, S., WIERNICKI, B., GOOSSENS, V., VANDEN BERGHE, T., CAPPE, B., LADIK, M., RIQUET, F. B., HEYNDRICKX, L., BRIDELANCE, J., VUYLSTEKE, M., VANDECASTEELE, K. & VANDENABEELE, P. 2020. Ionizing radiation results in a mixture of cellular outcomes including mitotic catastrophe, senescence, methuosis, and iron-dependent cell death. *Cell Death & Disease,* 11**,** 1003.

AGROMAYOR, M. & MARTIN-SERRANO, J. 2013. Knowing when to cut and run: mechanisms that control cytokinetic abscission. *Trends in Cell Biology,* 23**,** 433-441.

AHMED, A., SHAMSI, A., MOHAMMAD, T., HASAN, G. M., ISLAM, A. & HASSAN, M. I. 2021. Aurora B kinase: a potential drug target for cancer therapy. *Journal of Cancer Research and Clinical Oncology,* 147**,** 2187-2198.

AIHARA, A., TANAKA, S., YASEN, M., MATSUMURA, S., MITSUNORI, Y., MURAKATA, A., NOGUCHI, N., KUDO, A., NAKAMURA, N., ITO, K. & ARII, S. 2010. The selective Aurora B kinase inhibitor AZD1152 as a novel treatment for hepatocellular carcinoma. *J Hepatol,* 52**,** 63-71.

AL-KHAFAJI, A. S. K., DAVIES, M. P. A., RISK, J. M., MARCUS, M. W., KOFFA, M., GOSNEY, J. R., SHAW, R. J., FIELD, J. K. & LILOGLOU, T. 2017. Aurora B expression modulates paclitaxel response in non-small cell lung cancer. *British Journal of Cancer,* 116**,** 592-599.

ALEXANDRE, G., KARTHIGA SANTHANA, K., FABIEN, K., MICHAEL, A. G. & MARTIN, B. 2023. Repression of Aurora kinase B prevents growth and tissue invasion in medulloblastoma. *bioRxiv***,** 2023.06.23.545872.

AMABILE, G., D'ALISE, A. M., IOVINO, M., JONES, P., SANTAGUIDA, S., MUSACCHIO, A., TAYLOR, S. & CORTESE, R. 2009. The Aurora B kinase activity is required for the maintenance of the differentiated state of murine myoblasts. *Cell Death and Differentiation,* 16**,** 321-330.

ANAND, S., PENRHYN-LOWE, S. & VENKITARAMAN, A. R. 2003. AURORA-A amplification overrides the mitotic spindle assembly checkpoint, inducing resistance to Taxol. *Cancer Cell,* 3**,** 51-62.

ANDERSEN, J. L., JOHNSON, C. E., FREEL, C. D., PARRISH, A. B., DAY, J. L., BUCHAKJIAN, M. R., NUTT, L. K., THOMPSON, J. W., MOSELEY, M. A. & KORNBLUTH, S. 2009. Restraint of apoptosis during mitosis through interdomain phosphorylation of caspase-2. *Embo j,* 28**,** 3216-27.

ARAKI, K., NOZAKI, K., UEBA, T., TATSUKA, M. & HASHIMOTO, N. 2004. High expression of Aurora-B/Aurora and Ipll-like midbody-associated protein (AIM-1) in astrocytomas. *J Neurooncol,* 67**,** 53-64.

ASHTON, S., SONG, Y. H., NOLAN, J., CADOGAN, E., MURRAY, J., ODEDRA, R., FOSTER, J., HALL, P. A., LOW, S., TAYLOR, P., ELLSTON, R., POLANSKA, U. M., WILSON, J., HOWES, C., SMITH, A., GOODWIN, R. J. A., SWALES, J. G., STRITTMATTER, N., TAKÁTS, Z., NILSSON, A., ANDREN, P., TRUEMAN, D., WALKER, M., REIMER, C. L., TROIANO, G., PARSONS, D., DE WITT, D., ASHFORD, M., HRKACH, J., ZALE, S., JEWSBURY, P. J. & BARRY, S. T. 2016. Aurora kinase inhibitor nanoparticles target tumors with favorable therapeutic index in vivo. *Science Translational Medicine,* 8**,** 325ra17-325ra17.

BAGULEY, B. C., MARSHALL, E. S., WHITTAKER, J. R., DOTCHIN, M. C., NIXON, J., MCCRYSTAL, M. R., FINLAY, G. J., MATTHEWS, J. H. L., HOLDAWAY, K. M. & VAN ZIJL, P. 1995. Resistance mechanisms determining the in vitro sensitivity to paclitaxel of tumour cells cultured from patients with ovarian cancer. *European Journal of Cancer,* 31**,** 230-237.

BAI, J., WIOLAND, H., ADVEDISSIAN, T., CUVELIER, F., ROMET-LEMONNE, G. & ECHARD, A. 2020. Actin reduction by MsrB2 is a key component of the cytokinetic abscission checkpoint and prevents tetraploidy. *Proc Natl Acad Sci U S A,* 117**,** 4169-4179.

BALBOULA, A. Z., NGUYEN, A. L., GENTILELLO, A. S., QUARTUCCIO, S. M., DRUTOVIC, D., SOLC, P. & SCHINDLER, K. 2016. Haspin kinase regulates microtubule-organizing center clustering and stability through Aurora kinase C in mouse oocytes. *Journal of Cell Science,* 129**,** 3648.

BARRETTA, M. L., SPANO, D., D'AMBROSIO, C., CERVIGNI, R. I., SCALONI, A., CORDA, D. & COLANZI, A. 2016. Aurora-A recruitment and centrosomal maturation are regulated by a Golgi-activated pool of Src during G2. *Nature Communications,* 7**,** 11727.

BARROS, T. P., KINOSHITA, K., HYMAN, A. A. & RAFF, J. W. 2005. Aurora A activates D-TACC–Msps complexes exclusively at centrosomes to stabilize centrosomal microtubules. *Journal of Cell Biology,* 170**,** 1039-1046.

BAYLISS, R., SARDON, T., VERNOS, I. & CONTI, E. 2003. Structural Basis of Aurora-A Activation by TPX2 at the Mitotic Spindle. *Molecular Cell,* 12**,** 851-862.

BELTRAN, H., OROMENDIA, C., DANILA, D. C., MONTGOMERY, B., HOIMES, C., SZMULEWITZ, R. Z., VAISHAMPAYAN, U., ARMSTRONG, A. J., STEIN, M., PINSKI, J., MOSQUERA, J. M., SAILER, V., BAREJA, R., ROMANEL, A., GUMPENI, N., SBONER, A., DARDENNE, E., PUCA, L., PRANDI, D., RUBIN, M. A., SCHER, H. I., RICKMAN, D. S., DEMICHELIS, F., NANUS, D. M., BALLMAN, K. V. & TAGAWA, S. T. 2019. A phase II trial of the aurora kinase a inhibitor alisertib for patients with castration-resistant and neuroendocrine prostate cancer: Efficacy and biomarkers. *Clinical Cancer Research,* 25**,** 43-51.

BHOWMICK, R., MINOCHERHOMJI, S. & HICKSON, I. D. 2016. RAD52 Facilitates Mitotic DNA Synthesis Following Replication Stress. *Molecular Cell,* 64**,** 1117-1126.

BIADE, S., STOBBE, C. C. & CHAPMAN, J. D. 1997. The Intrinsic Radiosensitivity of Some Human Tumor Cells Throughout Their Cell Cycles. *Radiation Research,* 147**,** 416-421.

BISHOP, J. D. & SCHUMACHER, J. M. 2002. Phosphorylation of the Carboxyl Terminus of Inner Centromere Protein (INCENP) by the Aurora B Kinase Stimulates Aurora B Kinase Activity*. *Journal of Biological Chemistry,* 277**,** 27577-27580.

BLACKFORD, A. N. & JACKSON, S. P. 2017. ATM, ATR, and DNA-PK: The Trinity at the Heart of the DNA Damage Response. *Molecular Cell,* 66**,** 801-817.

BLACKFORD, A. N. & STUCKI, M. 2020. How Cells Respond to DNA Breaks in Mitosis. *Trends in Biochemical Sciences,* 45**,** 321-331.

BLEILER, M., CYR, A., WRIGHT, D. L. & GIARDINA, C. 2023. Incorporation of 53BP1 into phase-separated bodies in cancer cells during aberrant mitosis. *J Cell Sci,* 136.

BORAH, N. A. & REDDY, M. M. 2021. Aurora kinase B inhibition: A potential therapeutic strategy for cancer. *Molecules,* 26.

BOURDENS, M., JEANSON, Y., TAURAND, M., JUIN, N., CARRIÈRE, A., CLÉMENT, F., CASTEILLA, L., BULTEAU, A. L. & PLANAT-BÉNARD, V. 2019. Short exposure to cold atmospheric plasma induces senescence in human skin fibroblasts and adipose mesenchymal stromal cells. *Sci Rep,* 9**,** 8671.

BOURNAKA, S., BADRA-FAJARDO, N., ARBI, M., TARAVIRAS, S. & LYGEROU, Z. 2024. The cell cycle revisited: DNA replication past S phase preserves genome integrity. *Seminars in Cancer Biology,* 99**,** 45-55.

BOUTROS, R., LOBJOIS, V. & DUCOMMUN, B. 2007. CDC25 phosphatases in cancer cells: key players? Good targets? *Nature Reviews Cancer,* 7**,** 495-507.

BRIASSOULI, P., CHAN, F., SAVAGE, K., REIS-FILHO, J. S. & LINARDOPOULOS, S. 2007. Aurora-A regulation of nuclear factor-κB signaling by phosphorylation of IκBα. *Cancer Research,* 67**,** 1689-1695.

BRITO, D. A. & RIEDER, C. L. 2009. The ability to survive mitosis in the presence of microtubule poisons differs significantly between human nontransformed (RPE-1) and cancer (U2OS, HeLa) cells. *Cell Motil Cytoskeleton,* 66**,** 437-47.

BROAD, A. J., DELUCA, K. F. & DELUCA, J. G. 2020. Aurora B kinase is recruited to multiple discrete kinetochore and centromere regions in human cells. *Journal of Cell Biology,* 219.

BROWER, M., CARNEY, D. N., OIE, H. K., GAZDAR, A. F. & MINNA, J. D. 1986. Growth of Cell Lines and Clinical Specimens of Human Non-Small Cell Lung Cancer in a Serum-free Defined Medium. *Cancer Research,* 46**,** 798-806.

BRUINSMA, W., APRELIA, M., GARCIÁ-SANTISTEBAN, I., KOOL, J., XU, Y. J. & MEDEMA, R. H. 2017. Inhibition of Polo-like kinase 1 during the DNA damage response is mediated through loss of Aurora A recruitment by Bora. *Oncogene,* 36**,** 1840-1848.

BUISSON, R., DION-CÔTÉ, A.-M., COULOMBE, Y., LAUNAY, H., CAI, H., STASIAK, A. Z., STASIAK, A., XIA, B. & MASSON, J.-Y. 2010. Cooperation of breast cancer proteins PALB2 and piccolo BRCA2 in stimulating homologous recombination. *Nature Structural & Molecular Biology,* 17**,** 1247-1254.

BUNCH, H., JEONG, J., KANG, K., JO, D. S., CONG, A. T. Q., KIM, D., KIM, D., CHO, D.-H., LEE, Y. M., CHEN, B. P. C., SCHELLENBERG, M. J. & CALDERWOOD, S. K. 2021. BRCA1-BARD1 regulates transcription through modulating topoisomerase IIβ. *Open Biology,* 11.

BURUM-AUENSEN, E., ANGELIS, P. M. D., SCHJØLBERG, A. R., KRAVIK, K. L., AURE, M. & CLAUSEN, O. P. F. 2007. Subcellular Localization of the Spindle Proteins Aurora A, Mad2, and BUBR1 Assessed by Immunohistochemistry. *Journal of Histochemistry & Cytochemistry,* 55**,** 477-486.

BUTTERWORTH, K. T., GHITA, M., MCMAHON, S. J., MCGARRY, C. K., GRIFFIN, R. J., HOUNSELL, A. R. & PRISE, K. M. 2017. Modelling responses to spatially fractionated radiation fields using preclinical image-guided radiotherapy. *British Journal of Radiology,* 90**,** 20160485.

BYRUM, A. K., CARVAJAL-MALDONADO, D., MUDGE, M. C., VALLE-GARCIA, D., MAJID, M. C., PATEL, R., SOWA, M. E., GYGI, S. P., HARPER, J. W., SHI, Y., VINDIGNI, A. & MOSAMMAPARAST, N. 2019. Mitotic regulators TPX2 and Aurora A protect DNA forks during replication stress by counteracting 53BP1 function. *Journal of Cell Biology,* 218**,** 422-432.

CALDECOTT, K. W. 2008. Single-strand break repair and genetic disease. *Nature Reviews Genetics,* 9**,** 619-631.

CALDECOTT, K. W. 2014. DNA single-strand break repair. *Experimental Cell Research,* 329**,** 2-8.

CALDECOTT, K. W., MCKEOWN, C. K., TUCKER, J. D., LJUNGQUIST, S. & THOMPSON, L. H. 1994. An interaction between the mammalian DNA repair protein XRCC1 and DNA ligase III. *Molecular and Cellular Biology,* 14**,** 68-76.

CAMPILLO-MARCOS, I. & LAZO, P. A. 2018. Implication of the VRK1 chromatin kinase in the signaling responses to DNA damage: a therapeutic target? *Cellular and Molecular Life Sciences,* 75**,** 2375-2388.

CANMAN, C. E., LIM, D.-S., CIMPRICH, K. A., TAYA, Y., TAMAI, K., SAKAGUCHI, K., APPELLA, E., KASTAN, M. B. & SILICIANO, J. D. 1998. Activation of the ATM Kinase by Ionizing Radiation and Phosphorylation of p53. *Science,* 281**,** 1677.

CAPALBO, L., MELA, I., ABAD, M. A., JEYAPRAKASH, A. A., EDWARDSON, J. M. & D'AVINO, P. P. 2016. Coordinated regulation of the ESCRT-III component CHMP4C by the chromosomal passenger complex and centralspindlin during cytokinesis. *Open Biology,* 6**,** 160248.

CAPALBO, L., MONTEMBAULT, E., TAKEDA, T., BASSI, Z. I., GLOVER, D. M. & D'AVINO, P. P. 2012. The chromosomal passenger complex controls the function of endosomal sorting complex required for transport-III Snf7 proteins during cytokinesis. *Open Biology,* 2**,** 120070.

CARLTON, J. G., CABALLE, A., AGROMAYOR, M., KLOC, M. & MARTIN-SERRANO, J. 2012. ESCRT-III Governs the Aurora B–Mediated Abscission Checkpoint Through CHMP4C. *Science,* 336**,** 220.

CARMENA, M. 2008. Cytokinesis: The final stop for the chromosomal passengers. *Biochemical Society Transactions,* 36**,** 367-370.

CARMENA, M., WHEELOCK, M., FUNABIKI, H. & EARNSHAW, W. C. 2012. The chromosomal passenger complex (CPC): from easy rider to the godfather of mitosis. *Nature Reviews Molecular Cell Biology,* 13**,** 789-803.

CARY, R. B., PETERSON, S. R., WANG, J., BEAR, D. G., BRADBURY, E. M. & CHEN, D. J. 1997. DNA looping by Ku and the DNA-dependent protein kinase. *Proceedings of the National Academy of Sciences,* 94**,** 4267.

CASTEDO, M., PERFETTINI, J.-L., ROUMIER, T., ANDREAU, K., MEDEMA, R. & KROEMER, G. 2004a. Cell death by mitotic catastrophe: a molecular definition. *Oncogene,* 23**,** 2825-2837.

CASTEDO, M., PERFETTINI, J.-L., ROUMIER, T., VALENT, A., RASLOVA, H., YAKUSHIJIN, K., HORNE, D., FEUNTEUN, J., LENOIR, G., MEDEMA, R., VAINCHENKER, W. & KROEMER, G. 2004b. Mitotic catastrophe constitutes a special case of apoptosis whose suppression entails aneuploidy. *Oncogene,* 23**,** 4362-4370.

CASTEDO, M., PERFETTINI, J. L., ROUMIER, T., YAKUSHIJIN, K., HORNE, D., MEDEMA, R. & KROEMER, G. 2004c. The cell cycle checkpoint kinase Chk2 is a negative regulator of mitotic catastrophe. *Oncogene,* 23**,** 4353-61.

CASTRO, A., VIGNERON, S., BERNIS, C., LABBÉ, J. C., PRIGENT, C. & LORCA, T. 2002. The D-Box-activating domain (DAD) is a new proteolysis signal that stimulates the silent D-Box sequence of Aurora-A. *EMBO Reports,* 3**,** 1209-1214.

CAYO, A., SEGOVIA, R., VENTURINI, W., MOORE-CARRASCO, R., VALENZUELA, C. & BROWN, N. 2021. mTOR Activity and Autophagy in Senescent Cells, a Complex Partnership. *Int J Mol Sci,* 22.

CHAN, E. H. Y., SANTAMARIA, A., SILLJÉ, H. H. W. & NIGG, E. A. 2008. Plk1 regulates mitotic Aurora A function through βTrCP-dependent degradation of hBora. *Chromosoma,* 117**,** 457-469.

CHAN, T. A., HERMEKING, H., LENGAUER, C., KINZLER, K. W. & VOGELSTEIN, B. 1999. 14-3-3σ is required to prevent mitotic catastrophe after DNA damage. *Nature,* 401**,** 616-620.

CHAN, Y. W., JEYAPRAKASH, A. A., NIGG, E. A. & SANTAMARIA, A. 2012. Aurora B controls kinetochore–microtubule attachments by inhibiting Ska complex–KMN network interaction. *Journal of Cell Biology,* 196**,** 563-571.

CHANG, H. H. Y., PANNUNZIO, N. R., ADACHI, N. & LIEBER, M. R. 2017. Non-homologous DNA end joining and alternative pathways to double-strand break repair. *Nature Reviews Molecular Cell Biology,* 18**,** 495-506.

CHANG, X., ZHANG, T., WANG, Q., RATHORE, M. G., REDDY, K., CHEN, H., SHIN, S. H., MA, W. Y., BODE, A. M. & DONG, Z. 2020. HI-511 overcomes melanoma drug resistance via targeting AURKB and BRAF V600E. *Theranostics,* 10**,** 9721-9740.

CHAPPELL, W. H., LEHMANN, B. D., TERRIAN, D. M., ABRAMS, S. L., STEELMAN, L. S. & MCCUBREY, J. A. 2012. p53 expression controls prostate cancer sensitivity to chemotherapy and the MDM2 inhibitor Nutlin-3. *Cell Cycle,* 11**,** 4579-88.

CHATURVEDI, P., SUDAKIN, V., BOBIAK, M. L., FISHER, P. W., MATTERN, M. R., JABLONSKI, S. A., HURLE, M. R., ZHU, Y., YEN, T. J. & ZHOU, B.-B. S. 2002. Chfr Regulates a Mitotic Stress Pathway through its RING-Finger Domain with Ubiquitin Ligase Activity. *Cancer Research,* 62**,** 1797.

CHEESEMAN, I. M., CHAPPIE, J. S., WILSON-KUBALEK, E. M. & DESAI, A. 2006. The Conserved KMN Network Constitutes the Core Microtubule-Binding Site of the Kinetochore. *Cell,* 127**,** 983-997.

CHEFETZ, I., HOLMBERG, J. C., ALVERO, A. B., VISINTIN, I. & MOR, G. 2011. Inhibition of Aurora-A kinase induces cell cycle arrest in epithelial ovarian cancer stem cells by affecting NFκB pathway. *Cell Cycle,* 10**,** 2206-2214.

CHEN, C.-H., CHANG, A. Y. W., LI, S.-H., TSAI, H.-T., SHIU, L.-Y., SU, L.-J., WANG, W.-L., CHIU, T.-J., LUO, S.-D., HUANG, T.-L. & CHIEN, C.-Y. 2015. Suppression of Aurora-A-FLJ10540 signaling axis prohibits the malignant state of head and neck cancer. *Molecular Cancer,* 14**,** 83.

CHEN, S.-S., CHANG, P.-C., CHENG, Y.-W., TANG, F.-M. & LIN, Y.-S. 2002. Suppression of the STK15 oncogenic activity requires a transactivation-independent p53 function. *The EMBO Journal,* 21**,** 4491-4499.

CHEN, Y. & POON, R. Y. 2008. The multiple checkpoint functions of CHK1 and CHK2 in maintenance of genome stability. *Frontiers in Bioscience,* 13.

CHIEFFI, P., COZZOLINO, L., KISSLINGER, A., LIBERTINI, S., STAIBANO, S., MANSUETO, G., DE ROSA, G., VILLACCI, A., VITALE, M., LINARDOPOULOS, S., PORTELLA, G. & TRAMONTANO, D. 2006. Aurora B expression directly correlates with prostate cancer malignancy and influence prostate cell proliferation. *Prostate,* 66**,** 326-333.

CHOW, J. & POON, R. Y. 2010. DNA damage and polyploidization. *Adv Exp Med Biol,* 676**,** 57-71.

CIFERRI, C., PASQUALATO, S., SCREPANTI, E., VARETTI, G., SANTAGUIDA, S., DOS REIS, G., MAIOLICA, A., POLKA, J., DE LUCA, J. G., DE WULF, P., SALEK, M., RAPPSILBER, J., MOORES, C. A., SALMON, E. D. & MUSACCHIO, A. 2008. Implications for Kinetochore-Microtubule Attachment from the Structure of an Engineered Ndc80 Complex. *Cell,* 133**,** 427-439.

CITRIN, D. E. & CAMPHAUSEN, K. A. 2020. Translating Targeted Radiosensitizers into the Clinic. *In:* WILLERS, H. & EKE, I. (eds.) *Molecular Targeted Radiosensitizers: Opportunities and Challenges.* Cham: Springer International Publishing.

CITRIN, D. E. & MITCHELL, J. B. 2014. Altering the response to radiation: sensitizers and protectors. *Semin Oncol,* 41**,** 848-59.

CLEMENTS, P. M., BRESLIN, C., DEEKS, E. D., BYRD, P. J., JU, L., BIEGANOWSKI, P., BRENNER, C., MOREIRA, M.-C., TAYLOR, A. M. R. & CALDECOTT, K. W. 2004. The ataxia–oculomotor apraxia 1 gene product has a role distinct from ATM and interacts with the DNA strand break repair proteins XRCC1 and XRCC4. *DNA Repair,* 3**,** 1493-1502.

CONNELL, J. W., LINDON, C., LUZIO, J. P. & REID, E. 2009. Spastin couples microtubule severing to membrane traffic in completion of cytokinesis and secretion. *Traffic,* 10**,** 42-56.

CORTEZ, D., WANG, Y., QIN, J. & ELLEDGE, S. J. 1999. Requirement of ATM-Dependent Phosphorylation of Brca1 in the DNA Damage Response to Double-Strand Breaks. *Science,* 286.

COURTHEOUX, T., DIALLO, A., DAMODARAN, A. P., REBOUTIER, D., WATRIN, E. & PRIGENT, C. 2018. Aurora A kinase activity is required to maintain an

active spindle assembly checkpoint during prometaphase. *Journal of Cell Science,* 131**,** jcs191353.

COWLEY, G. S., WEIR, B. A., VAZQUEZ, F., TAMAYO, P., SCOTT, J. A., RUSIN, S., EAST-SELETSKY, A., ALI, L. D., GERATH, W. F. J., PANTEL, S. E., LIZOTTE, P. H., JIANG, G., HSIAO, J., TSHERNIAK, A., DWINELL, E., AOYAMA, S., OKAMOTO, M., HARRINGTON, W., GELFAND, E., GREEN, T. M., TOMKO, M. J., GOPAL, S., WONG, T. C., LI, H., HOWELL, S., STRANSKY, N., LIEFELD, T., JANG, D., BISTLINE, J., HILL MEYERS, B., ARMSTRONG, S. A., ANDERSON, K. C., STEGMAIER, K., REICH, M., PELLMAN, D., BOEHM, J. S., MESIROV, J. P., GOLUB, T. R., ROOT, D. E. & HAHN, W. C. 2014. Parallel genome-scale loss of function screens in 216 cancer cell lines for the identification of context-specific genetic dependencies. *Scientific Data,* 1**,** 140035.

CRASKE, B. & WELBURN, J. P. I. 2020. Leaving no-one behind: how CENP-E facilitates chromosome alignment. *Essays Biochem,* 64**,** 313-324.

CROSS, S. M., SANCHEZ, C. A., MORGAN, C. A., SCHIMKE, M. K., RAMEL, S., IDZERDA, R. L., RASKIND, W. H. & REID, B. J. 1995. A p53-Dependent Mouse Spindle Checkpoint. *Science,* 267**,** 1353-1356.

D'AVINO, P. P. & CAPALBO, L. 2016. Regulation of midbody formation and function by mitotic kinases. *Seminars in Cell & Developmental Biology,* 53**,** 57-63.

DANIELS, M. J., WANG, Y., LEE, M. & VENKITARAMAN, A. R. 2004. Abnormal Cytokinesis in Cells Deficient in the Breast Cancer Susceptibility Protein BRCA2. *Science,* 306**,** 876-879.

DAVIS, A. J. & CHEN, D. J. 2013. DNA double strand break repair via non-homologous end-joining. *Translational Cancer Research; Vol 2, No 3 (June 2013): Translational Cancer Research (DNA Damage and Repair)*.

DE GROOT, C. O., HSIA, J. E., ANZOLA, J. V., MOTAMEDI, A., YOON, M., WONG, Y. L., JENKINS, D., LEE, H. J., MARTINEZ, M. B., DAVIS, R. L., GAHMAN, T. C., DESAI, A. & SHIAU, A. K. 2015. A Cell Biologist's Field Guide to Aurora Kinase Inhibitors. *Frontiers in Oncology,* 5.

DEN HOLLANDER, J., RIMPI, S., DOHERTY, J. R., RUDELIUS, M., BUCK, A., HOELLEIN, A., KREMER, M., GRAF, N., SCHEERER, M., HALL, M. A., GOGA, A., VON BUBNOFF, N., DUYSTER, J., PESCHEL, C., CLEVELAND, J. L., NILSSON, J. A. & KELLER, U. 2010. Aurora kinases A and B are up-regulated by Myc and are essential for maintenance of the malignant state. *Blood,* 116**,** 1498-1505.

DICKSON, M. A., MAHONEY, M. R., TAP, W. D., D'ANGELO, S. P., KEOHAN, M. L., VAN TINE, B. A., AGULNIK, M., HORVATH, L. E., NAIR, J. S. & SCHWARTZ, G. K. 2016. Phase II study of MLN8237 (Alisertib) in advanced/ metastatic sarcoma. *Annals of Oncology,* 27**,** 1855-1860.

DIMRI, G. P., LEE, X., BASILE, G., ACOSTA, M., SCOTT, G., ROSKELLEY, C., MEDRANO, E. E., LINSKENS, M., RUBELJ, I. & PEREIRA-SMITH, O. 1995. A biomarker that identifies senescent human cells in culture and in aging skin in vivo. *Proceedings of the National Academy of Sciences,* 92**,** 9363-9367.

DITCHFIELD, C., JOHNSON, V. L., TIGHE, A., ELLSTON, R., HAWORTH, C., JOHNSON, T., MORTLOCK, A., KEEN, N. & TAYLOR, S. S. 2003. Aurora B couples chromosome alignment with anaphase by targeting BubR1, Mad2, and Cenp-E to kinetochores. *Journal of Cell Biology,* 161**,** 267-280.

DO, T. V., HIRST, J., HYTER, S., ROBY, K. F. & GODWIN, A. K. 2017. Aurora A kinase regulates non-homologous end-joining and poly(ADP-ribose) polymerase function in ovarian carcinoma cells. *Oncotarget,* 8**,** 50376-50392.

DODSON, H., WHEATLEY, S. P. & MORRISON, C. G. 2007. Involvement of Centrosome Amplification in Radiation-Induced Mitotic Catastrophe. *Cell Cycle,* 6**,** 364-370.

DU, R., HUANG, C., LIU, K., LI, X. & DONG, Z. 2021. Targeting AURKA in Cancer: molecular mechanisms and opportunities for Cancer therapy. *Molecular Cancer,* 20.

EL MAÏ, M., MARZULLO, M., DE CASTRO, I. P. & FERREIRA, M. G. 2020. Opposing p53 and mTOR/AKT promote an in vivo switch from apoptosis to senescence upon telomere shortening in zebrafish. *eLife,* 9**,** e54935.

ELIA, N., SOUGRAT, R., SPURLIN, T. A., HURLEY, J. H. & LIPPINCOTT-SCHWARTZ, J. 2011. Dynamics of endosomal sorting complex required for transport (ESCRT) machinery during cytokinesis and its role in abscission. *Proceedings of the National Academy of Sciences,* 108**,** 4846-4851.

EMS-MCCLUNG, STEPHANIE C., HAINLINE, SARAH G., DEVARE, J., ZONG, H., CAI, S., CARNES, STEPHANIE K., SHAW, SIDNEY L. & WALCZAK, CLAIRE E. 2013. Aurora B Inhibits MCAK Activity through a Phosphoconformational Switch that Reduces Microtubule Association. *Current Biology,* 23**,** 2491-2499.

ENJOJI, M., IIDA, S., SUGITA, H., ISHIKAWA, T., UETAKE, H., INOKUCHI, M., YAMADA, H., KOJIMA, K. & SUGIHARA, K. 2009. BubR1 and AURKB overexpression are associated with a favorable prognosis in gastric cancer. *Mol Med Rep,* 2**,** 589-596.

EOT-HOULLIER, G., MAGNAGHI-JAULIN, L., FULCRAND, G., MOYROUD, F.-X., MONIER, S. & JAULIN, C. 2018. Aurora A-dependent CENP-A phosphorylation at inner centromeres protects bioriented chromosomes against cohesion fatigue. *Nature Communications,* 9**,** 1888.

ERIKSSON, D. & STIGBRAND, T. 2010. Radiation-induced cell death mechanisms. *Tumor Biology,* 31**,** 363-372.

ERIN, M., KATHERINE, P., KIZHAKKE MATTADA, S., BRIANNE, V., DANIEL, J. B. & STUKENBERG, P. T. 2021. AURKB/Ipl1 restarts replication forks to recover from replication stress. *bioRxiv***,** 2021.05.27.446025.

EVANGELOU, K., BELOGIANNIS, K., PAPASPYROPOULOS, A., PETTY, R. & GORGOULIS, V. G. 2023. Escape from senescence: molecular basis and therapeutic ramifications. *Journal of Pathology,* 260**,** 649-665.

EYERS, P. A., ERIKSON, E., CHEN, L. G. & MALLER, J. L. 2003. A Novel Mechanism for Activation of the Protein Kinase Aurora A. *Current Biology,* 13**,** 691-697.

EYERS, P. A. & MALLER, J. L. 2004. Regulation of Xenopus Aurora A Activation by TPX2*. *Journal of Biological Chemistry,* 279**,** 9008-9015.

FARRELL, K. C., WANG, J. T. & STEARNS, T. 2022. Spindle assembly checkpoint-dependent mitotic delay is required for cell division in absence of centrosomes. Cold Spring Harbor Laboratory.

FELL, V. L., WALDEN, E. A., HOFFER, S. M., ROGERS, S. R., AITKEN, A. S., SALEMI, L. M. & SCHILD-POULTER, C. 2016. Ku70 Serine 155 mediates Aurora B inhibition and activation of the DNA damage response. *Scientific Reports,* 6.

FENOUILLE, N., TICHET, M., DUFIES, M., POTTIER, A., MOGHA, A., SOO, J. K., ROCCHI, S., MALLAVIALLE, A., GALIBERT, M. D., KHAMMARI, A., LACOUR, J. P., BALLOTTI, R., DECKERT, M. & TARTARE-DECKERT, S. 2012. The epithelial-mesenchymal transition (EMT) regulatory factor SLUG (SNAI2) is a downstream target of SPARC and AKT in promoting melanoma cell invasion. *PLoS ONE,* 7.

FERNANDEZ-VIDAL, A., VIGNARD, J. & MIREY, G. 2017. Around and beyond 53BP1 Nuclear Bodies. *Int J Mol Sci,* 18.

FISCHLE, W., TSENG, B. S., DORMANN, H. L., UEBERHEIDE, B. M., GARCIA, B. A., SHABANOWITZ, J., HUNT, D. F., FUNABIKI, H. & ALLIS, C. D. 2005. Regulation of HP1–chromatin binding by histone H3 methylation and phosphorylation. *Nature,* 438**,** 1116-1122.

FRADET-TURCOTTE, A., CANNY, M. D., ESCRIBANO-DÍAZ, C., ORTHWEIN, A., LEUNG, C. C. Y., HUANG, H., LANDRY, M. C., KITEVSKI-LEBLANC, J., NOORDERMEER, S. M., SICHERI, F. & DUROCHER, D. 2013. 53BP1 is a reader of the DNA-damage-induced H2A Lys 15 ubiquitin mark. *Nature,* 499**,** 50-54.

FRAGKOS, M. & BEARD, P. 2011. Mitotic Catastrophe Occurs in the Absence of Apoptosis in p53-Null Cells with a Defective G1 Checkpoint. *PLOS ONE,* 6**,** e22946.

FRANKENBERG-SCHWAGER, M. 1989. Review of repair kinetics for DNA damage induced in eukaryotic cells in vitro by ionizing radiation. *Radiotherapy and Oncology,* 14**,** 307-320.

FRESNO VARA, J. A., CASADO, E., DE CASTRO, J., CEJAS, P., BELDA-INIESTA, C. & GONZÁLEZ-BARÓN, M. 2004. PI3K/Akt signalling pathway and cancer. *Cancer Treat Rev,* 30**,** 193-204.

FULLER, B. G., LAMPSON, M. A., FOLEY, E. A., ROSASCO-NITCHER, S., LE, K. V., TOBELMANN, P., BRAUTIGAN, D. L., STUKENBERG, P. T. & KAPOOR, T. M. 2008. Midzone activation of aurora B in anaphase produces an intracellular phosphorylation gradient. *Nature,* 453**,** 1132-1136.

FUNG, T. K. & POON, R. Y. C. 2005. A roller coaster ride with the mitotic cyclins. *Seminars in Cell & Developmental Biology,* 16**,** 335-342.

GADEA, B. B. & RUDERMAN, J. V. 2005. Aurora kinase inhibitor ZM447439 blocks chromosome-induced spindle assembly, the completion of chromosome condensation, and the establishment of the spindle integrity checkpoint in Xenopus egg extracts. *Mol Biol Cell,* 16**,** 1305-18.

GAITANOS, T. N., SANTAMARIA, A., JEYAPRAKASH, A. A., WANG, B., CONTI, E. & NIGG, E. A. 2009. Stable kinetochore–microtubule interactions depend on the Ska complex and its new component Ska3/C13Orf3. *The EMBO Journal,* 28**,** 1442-1452-1452.

GALETTA, D. & CORTES-DERICKS, L. 2020. Promising therapy in lung cancer: Spotlight on aurora kinases. *Cancers,* 12**,** 1-15.

GALLUZZI, L., MAIURI, M. C., VITALE, I., ZISCHKA, H., CASTEDO, M., ZITVOGEL, L. & KROEMER, G. 2007. Cell death modalities: classification and pathophysiological implications. *Cell Death & Differentiation,* 14**,** 1237-1243.

GANEM, NEIL J., CORNILS, H., CHIU, S.-Y., O'ROURKE, KEVIN P., ARNAUD, J., YIMLAMAI, D., THÉRY, M., CAMARGO, FERNANDO D. & PELLMAN, D. 2014. Cytokinesis Failure Triggers Hippo Tumor Suppressor Pathway Activation. *Cell,* 158**,** 833-848.

GASCOIGNE, K. E. & TAYLOR, S. S. 2008. Cancer Cells Display Profound Intra- and Interline Variation following Prolonged Exposure to Antimitotic Drugs. *Cancer Cell,* 14**,** 111-122.

GATTI, M., PINATO, S., MASPERO, E., SOFFIENTINI, P., POLO, S. & PENENGO, L. 2012. A novel ubiquitin mark at the N-terminal tail of histone H2As targeted by RNF168 ubiquitin ligase. *Cell Cycle,* 11**,** 2538-2544.

GEWIRTZ, D. A., HOLT, S. E. & ELMORE, L. W. 2008. Accelerated senescence: an emerging role in tumor cell response to chemotherapy and radiation. *Biochem Pharmacol,* 76**,** 947-57.

GIET, R. G., MCLEAN, D., DESCAMPS, S., LEE, M. J., RAFF, J. W., PRIGENT, C. & GLOVER, D. M. 2002. Drosophila Aurora A kinase is required to localize D-TACC to centrosomes and to regulate astral microtubules. *Journal of Cell Biology,* 156**,** 437-451.

GIUNTA, S., BELOTSERKOVSKAYA, R. & JACKSON, S. P. 2010. DNA damage signaling in response to double-strand breaks during mitosis. *Journal of Cell Biology,* 190**,** 197-207.

GLOVER, D. M., LEIBOWITZ, M. H., MCLEAN, D. A. & PARRY, H. 1995. Mutations in aurora prevent centrosome separation leading to the formation of monopolar spindles. *Cell,* 81**,** 95-105.

GODINHO, S. A. & PELLMAN, D. 2014. Causes and consequences of centrosome abnormalities in cancer. *Philos Trans R Soc Lond B Biol Sci,* 369.

GODTHELP, B. C., ARTWERT, F., JOENJE, H. & ZDZIENICKA, M. Z. 2002. Impaired DNA damage-induced nuclear Rad51 foci formation uniquely characterizes Fanconi anemia group D1. *Oncogene,* 21**,** 5002-5.

GOHARD, F. H., ST-CYR, D. J., TYERS, M. & EARNSHAW, W. C. 2014. Targeting the INCENP IN-box–Aurora B interaction to inhibit CPC activity in vivo. *Open Biology,* 4**,** 140163.

GOLDENSON, B. & CRISPINO, J. D. 2015. The aurora kinases in cell cycle and leukemia. *Oncogene,* 34**,** 537-545.

GONZÁLEZ-LOYOLA, A., FERNÁNDEZ-MIRANDA, G., TRAKALA, M., PARTIDA, D., SAMEJIMA, K., OGAWA, H., CAÑAMERO, M., DE MARTINO, A., MARTÍNEZ-RAMÍREZ, A., DE CÁRCER, G., DE CASTRO, I. P., EARNSHAW, W. C. & MALUMBRES, M. 2015. Aurora B Overexpression Causes Aneuploidy and p21Cip1 Repression during Tumor Development. *Molecular and Cellular Biology,* 35**,** 3566-3578.

GOODHEAD, D. T. 1994. Initial Events in the Cellular Effects of Ionizing Radiations: Clustered Damage in DNA. *International Journal of Radiation Biology,* 65**,** 7-17.

GOSHIMA, G., KIYOMITSU, T., YODA, K. & YANAGIDA, M. 2003. Human centromere chromatin protein hMis12, essential for equal segregation, is independent of CENP-A loading pathway. *Journal of Cell Biology,* 160**,** 25-39.

GOTO, H., YASUI, Y., KAWAJIRI, A., NIGG, E. A., TERADA, Y., TATSUKA, M., NAGATA, K.-I. & INAGAKI, M. 2003. Aurora-B Regulates the Cleavage Furrow-specific Vimentin Phosphorylation in the Cytokinetic Process *. *Journal of Biological Chemistry,* 278**,** 8526-8530.

GOTTLIEB, T. M. & JACKSON, S. P. 1993. The DNA-dependent protein kinase: Requirement for DNA ends and association with Ku antigen. *Cell,* 72**,** 131-142.

GRABER-FEESL, C. L., PEDERSON, K. D., ANEY, K. J. & SHIMA, N. 2019. Mitotic DNA Synthesis Is Differentially Regulated between Cancer and Noncancerous Cells. *Molecular Cancer Research,* 17**,** 1687-1698.

GRAVELLS, P., NEALE, J., GRANT, E., NATHUBHAI, A., SMITH, K. M., JAMES, D. I. & BRYANT, H. E. 2018. Radiosensitization with an inhibitor of poly(ADP-ribose) glycohydrolase: A comparison with the PARP1/2/3 inhibitor olaparib. *DNA Repair (Amst),* 61**,** 25-36.

GRAWUNDER, U., WILM, M., WU, X., KULESZA, P., WILSON, T. E., MANN, M. & LIEBER, M. R. 1997. Activity of DNA ligase IV stimulated by complex formation with XRCC4 protein in mammalian cells. *Nature,* 388**,** 492-5.

GU, J., LU, H., TIPPIN, B., SHIMAZAKI, N., GOODMAN, M. F. & LIEBER, M. R. 2007. XRCC4:DNA ligase IV can ligate incompatible DNA ends and can ligate across gaps. *The EMBO Journal,* 26**,** 3506-3507.

GUAN, Z., WANG, X.-R., ZHU, X.-F., HUANG, X.-F., XU, J., WANG, L.-H., WAN, X.-B., LONG, Z.-J., LIU, J.-N., FENG, G.-K., HUANG, W., ZENG, Y.-X., CHEN, F.-J. & LIU, Q. 2007. Aurora-A, a Negative Prognostic Marker, Increases Migration and Decreases Radiosensitivity in Cancer Cells. *Cancer Research,* 67**,** 10436.

GULLY, C. P., VELAZQUEZ-TORRES, G., SHIN, J. H., FUENTES-MATTEI, E., WANG, E., CARLOCK, C., CHEN, J., ROTHENBERG, D., ADAMS, H. P., CHOI, H. H., GUMA, S., PHAN, L., CHOU, P. C., SU, C. H., ZHANG, F., CHEN, J. S., YANG, T. Y., YEUNG, S. C. J. & LEE, M. H. 2012. Aurora B kinase phosphorylates and instigates degradation of p53. *Proceedings of the National Academy of Sciences of the United States of America,* 109**,** E1513-E1522.

GUSE, A., MISHIMA, M. & GLOTZER, M. 2005. Phosphorylation of ZEN-4/MKLP1 by aurora B regulates completion of cytokinesis. *Current Biology,* 15**,** 778-786.

HA, G. H. & BREUER, E. K. 2012. Mitotic Kinases and p53 Signaling. *Biochem Res Int,* 2012**,** 195903.

HADDERS, M. A. & LENS, S. M. A. 2022. Changing places: Chromosomal Passenger Complex relocation in early anaphase. *Trends in Cell Biology,* 32**,** 165-176.

HANASHIRO, K., KANAI, M., GENG, Y., SICINSKI, P. & FUKASAWA, K. 2008. Roles of cyclins A and E in induction of centrosome amplification in p53-compromised cells. *Oncogene,* 27**,** 5288-5302.

HARDWICKE, M. A., OLEYKOWSKI, C. A., PLANT, R., WANG, J., LIAO, Q., MOSS, K., NEWLANDER, K., ADAMS, J. L., DHANAK, D., YANG, J., LAI, Z., SUTTON, D. & PATRICK, D. 2009. GSK1070916, a potent Aurora B/C kinase inhibitor with broad antitumor activity in tissue culture cells and human tumor xenograft models. *Mol Cancer Ther,* 8**,** 1808-17.

HAREN, L., REMY, M.-H. L. N., BAZIN, I., CALLEBAUT, I., WRIGHT, M. & MERDES, A. 2006. NEDD1-dependent recruitment of the γ-tubulin ring complex to the centrosome is necessary for centriole duplication and spindle assembly. *Journal of Cell Biology,* 172**,** 505-515.

HARLEY, M. E., ALLAN, L. A., SANDERSON, H. S. & CLARKE, P. R. 2010. Phosphorylation of Mcl-1 by CDK1–cyclin B1 initiates its Cdc20-dependent destruction during mitotic arrest. *The EMBO Journal,* 29**,** 2407-2420-2420.

HARRIS, S. L. & LEVINE, A. J. 2005. The p53 pathway: positive and negative feedback loops. *Oncogene,* 24**,** 2899-2908.

HAUF, S., COLE, R. W., LATERRA, S., ZIMMER, C., SCHNAPP, G., WALTER, R., HECKEL, A., VAN MEEL, J., RIEDER, C. L. & PETERS, J.-M. 2003. The small molecule Hesperadin reveals a role for Aurora B in correcting kinetochore–microtubule attachment and in maintaining the spindle assembly checkpoint. *Journal of Cell Biology,* 161**,** 281-294.

HAYASHI, M. T., CESARE, A. J., FITZPATRICK, J. A. J., LAZZERINI-DENCHI, E. & KARLSEDER, J. 2012. A telomere-dependent DNA damage checkpoint induced by prolonged mitotic arrest. *Nature Structural and Molecular Biology,* 19**,** 387-394.

HAYASHI, M. T. & KARLSEDER, J. 2013. DNA damage associated with mitosis and cytokinesis failure. *Oncogene,* 32**,** 4593-601.

HERAS-SANDOVAL, D., PÉREZ-ROJAS, J. M., HERNÁNDEZ-DAMIÁN, J. & PEDRAZA-CHAVERRI, J. 2014. The role of PI3K/AKT/mTOR pathway in the modulation of autophagy and the clearance of protein aggregates in neurodegeneration. *Cellular Signalling,* 26**,** 2694-2701.

HERRIAGE, H. C., HUANG, Y.-T. & CALVI, B. R. 2024. The antagonistic relationship between apoptosis and polyploidy in development and cancer. *Seminars in Cell & Developmental Biology,* 156**,** 35-43.

HIROTA, T., GERLICH, D., KOCH, B., ELLENBERG, J. & PETERS, J.-M. 2004. Distinct functions of condensin I and II in mitotic chromosome assembly. *Journal of Cell Science,* 117**,** 6435-6445.

HIROTA, T., KUNITOKU, N., SASAYAMA, T., MARUMOTO, T., ZHANG, D., NITTA, M., HATAKEYAMA, K. & SAYA, H. 2003. Aurora-A and an Interacting Activator, the LIM Protein Ajuba, Are Required for Mitotic Commitment in Human Cells. *Cell,* 114**,** 585-598.

HIROTA, T., LIPP, J. J., TOH, B.-H. & PETERS, J.-M. 2005. Histone H3 serine 10 phosphorylation by Aurora B causes HP1 dissociation from heterochromatin. *Nature,* 438**,** 1176-1180.

HODGE, R. G. & RIDLEY, A. J. 2016. Regulating Rho GTPases and their regulators. *Nature Reviews Molecular Cell Biology,* 17**,** 496-510.

HOFFELDER, D. R., LUO, L., BURKE, N. A., WATKINS, S. C., GOLLIN, S. M. & SAUNDERS, W. S. 2004. Resolution of anaphase bridges in cancer cells. *Chromosoma,* 112**,** 389-397.

HONDA, K., MIHARA, H., KATO, Y., YAMAGUCHI, A., TANAKA, H., YASUDA, H., FURUKAWA, K. & URANO, T. 2000. Degradation of human Aurora2 protein kinase by the anaphase-promoting complex-ubiquitin-proteasome pathway. *Oncogene,* 19**,** 2812-2819.

HONDA, R., KÖRNER, R. & NIGG, E. A. 2003. Exploring the Functional Interactions between Aurora B, INCENP, and Survivin in Mitosis. *Molecular Biology of the Cell,* 14**,** 3325-3341.

HORVÁTH, P. & MÜLLER-REICHERT, T. 2020. A Structural View on ESCRT-Mediated Abscission. *Front Cell Dev Biol,* 8**,** 586880.

HSU, J.-Y., SUN, Z.-W., LI, X., REUBEN, M., TATCHELL, K., BISHOP, D. K., GRUSHCOW, J. M., BRAME, C. J., CALDWELL, J. A., HUNT, D. F., LIN, R., SMITH, M. M. & ALLIS, C. D. 2000. Mitotic Phosphorylation of Histone H3 Is Governed by Ipl1/aurora Kinase and Glc7/PP1 Phosphatase in Budding Yeast and Nematodes. *Cell,* 102**,** 279-291.

HSUEH, K.-W., FU, S.-L., CHANG, C.-B., CHANG, Y.-L. & LIN, C.-H. 2013. A novel Aurora-A-mediated phosphorylation of p53 inhibits its interaction with MDM2. *Biochimica et Biophysica Acta (BBA) - Proteins and Proteomics,* 1834**,** 508-515.

HSUEH, K. W., FU, S. L., HUANG, C. Y. F. & LIN, C. H. 2011. Aurora-A phosphorylates hnRNPK and disrupts its interaction with p53. *FEBS Letters,* 585**,** 2671-2675.

HU, X., HU, J., PANG, Y., WANG, M., ZHOU, W., XIE, X., ZHU, C., WANG, X. & SUN, X. 2024. Application of nano-radiosensitizers in non-small cell lung cancer. *Frontiers in Oncology,* 14.

HUANG, D., HUANG, Y., HUANG, Z., WENG, J., ZHANG, S. & GU, W. 2019. Relation of AURKB over-expression to low survival rate in BCRA and reversine-modulated aurora B kinase in breast cancer cell lines. *Cancer Cell International,* 19.

HUANG DA, W., SHERMAN, B. T. & LEMPICKI, R. A. 2009. Systematic and integrative analysis of large gene lists using DAVID bioinformatics resources. *Nat Protoc,* 4**,** 44-57.

HUANG, H., FENG, J., FAMULSKI, J., RATTNER, J. B., SONG, T. L., KAO, G. D., MUSCHEL, R., CHAN, G. K. T. & YEN, T. J. 2007. Tripin/hSgo2 recruits MCAK to the inner centromere to correct defective kinetochore attachments. *Journal of Cell Biology,* 177**,** 413-424.

HUANG, H., FLETCHER, L., BEEHARRY, N., DANIEL, R., KAO, G., YEN, T. J. & MUSCHEL, R. J. 2008a. Abnormal Cytokinesis after X-Irradiation in Tumor

Cells that Override the G2 DNA Damage Checkpoint. *Cancer Research,* 68**,** 3724-3732.

HUANG, W., HICKSON, L. J., EIRIN, A., KIRKLAND, J. L. & LERMAN, L. O. 2022. Cellular senescence: the good, the bad and the unknown. *Nature Reviews Nephrology,* 18**,** 611-627.

HUANG, X.-F., LUO, S.-K., XU, J., LI, J., XU, D.-R., WANG, L.-H., YAN, M., WANG, X.-R., WAN, X.-B., ZHENG, F.-M., ZENG, Y.-X. & LIU, Q. 2008b. Aurora kinase inhibitory VX-680 increases Bax/Bcl-2 ratio and induces apoptosis in Aurora-A-high acute myeloid leukemia. *Blood,* 111**,** 2854-2865.

HUCK, J. J., ZHANG, M., MCDONALD, A., BOWMAN, D., HOAR, K. M., STRINGER, B., ECSEDY, J., MANFREDI, M. G. & HYER, M. L. 2010. MLN8054, an Inhibitor of Aurora A Kinase, Induces Senescence in Human Tumor Cells Both In vitro and In vivo</em&gt. *Molecular Cancer Research,* 8**,** 373.

HURLEY, J. H. & HANSON, P. I. 2010. Membrane budding and scission by the ESCRT machinery: it's all in the neck. *Nature Reviews Molecular Cell Biology,* 11**,** 556-566.

IMREH, G., NORBERG, H. V., IMREH, S. & ZHIVOTOVSKY, B. 2011. Chromosomal breaks during mitotic catastrophe trigger γH2AX–ATM–p53-mediated apoptosis. *Journal of Cell Science,* 124**,** 2951-2963.

ISONO, M., NIIMI, A., OIKE, T., HAGIWARA, Y., SATO, H., SEKINE, R., YOSHIDA, Y., ISOBE, S.-Y., OBUSE, C., NISHI, R., PETRICCI, E., NAKADA, S., NAKANO, T. & SHIBATA, A. 2017. BRCA1 Directs the Repair Pathway to Homologous Recombination by Promoting 53BP1 Dephosphorylation. *Cell Reports,* 18**,** 520-532.

IZUMI, T., HAZRA, T. K., BOLDOGH, I., TOMKINSON, A. E., PARK, M. S., IKEDA, S. & MITRA, S. 2000. Requirement for human AP endonuclease 1 for repair of 3′-blocking damage at DNA single-strand breaks induced by reactive oxygen species. *Carcinogenesis,* 21**,** 1329-1334.

JALILI, P. R., SHARMA, D. & BALL, H. L. 2007. Enhancement of Ionization Efficiency and Selective Enrichment of Phosphorylated Peptides from Complex Protein Mixtures Using a Reversible Poly-Histidine Tag. *Journal of the American Society for Mass Spectrometry,* 18**,** 1007-1017.

JEYAPRAKASH, A. A., KLEIN, U. R., LINDNER, D., EBERT, J., NIGG, E. A. & CONTI, E. 2007. Structure of a Survivin–Borealin–INCENP Core Complex Reveals How Chromosomal Passengers Travel Together. *Cell,* 131**,** 271-285.

JI, Z., GAO, H., JIA, L., LI, B. & YU, H. 2017. A sequential multi-target Mps1 phosphorylation cascade promotes spindle checkpoint signaling. *eLife,* 6**,** e22513.

JIANG, J., WANG, J., YUE, M., CAI, X., WANG, T., WU, C., SU, H., WANG, Y., HAN, M., ZHANG, Y., ZHU, X., JIANG, P., LI, P., SUN, Y., XIAO, W., FENG, H., QING, G. & LIU, H. 2020. Direct Phosphorylation and Stabilization of MYC by Aurora B Kinase Promote T-cell Leukemogenesis. *Cancer Cell,* 37**,** 200-215.e5.

JIAO, Y., CAO, F. & LIU, H. 2022. Radiation-induced Cell Death and Its Mechanisms. *Health Phys,* 123**,** 376-386.

JIN, Z. & EL-DEIRY, W. S. 2005. Overview of cell death signaling pathways. *Cancer Biology & Therapy,* 4**,** 147-171.

JOHNSON, M. L., WANG, J. S., FALCHOOK, G., GREENLEES, C., JONES, S., STRICKLAND, D., FABBRI, G., KENNEDY, C., ELIZABETH PEASE, J., SAINSBURY, L., MACDONALD, A., SCHALKWIJK, S., SZEKERES, P., COSAERT, J. & BURRIS, H. 2023. Safety, tolerability, and pharmacokinetics of Aurora kinase B inhibitor AZD2811: a phase 1 dose-finding study in patients with advanced solid tumours. *British Journal of Cancer,* 128**,** 1906-1915.

JOUKOV, V., DE NICOLO, A., RODRIGUEZ, A., WALTER, J. C. & LIVINGSTON, D. M. 2010. Centrosomal protein of 192 kDa (Cep192) promotes centrosome-driven spindle assembly by engaging in organelle-specific Aurora A activation. *Proceedings of the National Academy of Sciences,* 107**,** 21022.

JOUKOV, V., WALTER, JOHANNES C. & DE NICOLO, A. 2014. The Cep192-Organized Aurora A-Plk1 Cascade Is Essential for Centrosome Cycle and Bipolar Spindle Assembly. *Molecular Cell,* 55**,** 578-591.

JOWSEY, P., MORRICE, N. A., HASTIE, C. J., MCLAUCHLAN, H., TOTH, R. & ROUSE, J. 2007. Characterisation of the sites of DNA damage-induced 53BP1 phosphorylation catalysed by ATM and ATR. *DNA Repair,* 6**,** 1536-1544.

KABECHE, L., NGUYEN, H. D., BUISSON, R. & ZOU, L. 2018. A mitosis-specific and R loop–driven ATR pathway promotes faithful chromosome segregation. *Science,* 359**,** 108-114.

KAITNA, S., MENDOZA, M., JANTSCH-PLUNGER, V. & GLOTZER, M. 2000. Incenp and an Aurora-like kinase form a complex essential for chromosome segregation and efficient completion of cytokinesis. *Current Biology,* 10**,** 1172-1181.

KANDA, A., KAWAI, H., SUTO, S., KITAJIMA, S., SATO, S., TAKATA, T. & TATSUKA, M. 2005. Aurora-B/AIM-1 kinase activity is involved in Ras-mediated cell transformation. *Oncogene,* 24**,** 7266-7272.

KANG, D., CHEN, J., WONG, J. & FANG, G. 2002. The checkpoint protein Chfr is a ligase that ubiquitinates Plk1 and inhibits Cdc2 at the G2 to M transition. *Journal of Cell Biology,* 156**,** 249-260.

KANTARJIAN, H. M., SEKERES, M. A., RIBRAG, V., ROUSSELOT, P., GARCIA-MANERO, G., JABBOUR, E. J., OWEN, K., STOCKMAN, P. K. & OLIVER, S. D. 2013. Phase I study assessing the safety and tolerability of barasertib (AZD1152) with low-dose cytosine arabinoside in elderly patients with AML. *Clin Lymphoma Myeloma Leuk,* 13**,** 559-67.

KATAYAMA, H., SASAI, K., KAWAI, H., YUAN, Z. M., BONDARUK, J., SUZUKI, F., FUJII, S., ARLINGHAUS, R. B., CZERNIAK, B. A. & SEN, S. 2004. Phosphorylation by aurora kinase A induces Mdm2-mediated destabilization and inhibition of p53. *Nature Genetics,* 36**,** 55-62.

KATAYAMA, H., WANG, J., TREEKITKARNMONGKOL, W., KAWAI, H., SASAI, K., ZHANG, H., WANG, H., ADAMS, H. P., JIANG, S., CHAKRABORTY, S. N., SUZUKI, F., ARLINGHAUS, R. B., LIU, J., MOBLEY, J. A., GRIZZLE, W. E., WANG, H. & SEN, S. 2012. Aurora Kinase-A Inactivates DNA Damage-Induced Apoptosis and Spindle Assembly Checkpoint Response Functions of p73. *Cancer Cell,* 21**,** 196-211.

KATSHA, A., ARRAS, J., SOUTTO, M., BELKHIRI, A. & EL-RIFAI, W. 2014. AURKA regulates JAK2–STAT3 activity in human gastric and esophageal cancers. *Molecular Oncology,* 8**,** 1419-1428.

KAWAMURA, K., FUJIKAWA-YAMAMOTO, K., OZAKI, M., IWABUCHI, K., NAKASHIMA, H., DOMIKI, C., MORITA, N., INOUE, M., TOKUNAGA, K., SHIBA, N., IKEDA, R. & SUZUKI, K. 2004. Centrosome hyperamplification and chromosomal damage after exposure to radiation. *Oncology,* 67**,** 460-70.

KAWASHIMA, S. A., TSUKAHARA, T., LANGEGGER, M., HAUF, S., KITAJIMA, T. S. & WATANABE, Y. 2007. Shugoshin enables tension-generating attachment of kinetochores by loading Aurora to centromeres. *Genes and Development,* 21**,** 420-435.

KELLY, K. R., SHEA, T. C., GOY, A., BERDEJA, J. G., REEDER, C. B., MCDONAGH, K. T., ZHOU, X., DANAEE, H., LIU, H., ECSEDY, J. A., NIU, H., BENAIM, E. & PADMANABHAN IYER, S. 2014. Phase I study of MLN8237 - Investigational Aurora A kinase inhibitor - In relapsed/refractory multiple myeloma, non-Hodgkin lymphoma and chronic lymphocytic leukemia. *Investigational New Drugs,* 32**,** 489-499.

KETTENBACH, A. N., SCHWEPPE, D. K., FAHERTY, B. K., PECHENICK, D., PLETNEV, A. A. & GERBER, S. A. 2011. Quantitative phosphoproteomics identifies substrates and functional modules of Aurora and Polo-like kinase activities in mitotic cells. *Sci Signal,* 4**,** rs5.

KIM, E. M. & BURKE, D. J. 2008. DNA damage activates the SAC in an ATM/ATR-dependent manner, independently of the kinetochore. *PLoS Genet,* 4**,** e1000015.

KIM, J.-S., KRASIEVA, T. B., KURUMIZAKA, H., CHEN, D. J., TAYLOR, A. M. R. & YOKOMORI, K. 2005. Independent and sequential recruitment of NHEJ and

HR factors to DNA damage sites in mammalian cells. *Journal of Cell Biology,* 170**,** 341-347.

KIM, J.-S., PARK, Y.-Y., PARK, S.-Y., CHO, H., KANG, D. & CHO, H. 2011. The Auto-ubiquitylation of E3 Ubiquitin-protein Ligase Chfr at G₂ Phase Is Required for Accumulation of Polo-like Kinase 1 and Mitotic Entry in Mammalian Cells *. *Journal of Biological Chemistry,* 286**,** 30615-30623.

KIM, Y., HOLLAND, A. J., LAN, W. & CLEVELAND, D. W. 2010. Aurora Kinases and Protein Phosphatase 1 Mediate Chromosome Congression through Regulation of CENP-E. *Cell,* 142**,** 444-455.

KIMMINS, S., CROSIO, C., KOTAJA, N., HIRAYAMA, J., MONACO, L., HÖÖG, C., VAN DUIN, M., GOSSEN, J. A. & SASSONE-CORSI, P. 2007. Differential functions of the Aurora-B and Aurora-C kinases in mammalian spermatogenesis. *Molecular Endocrinology,* 21**,** 726-739.

KINOSHITA, K., NOETZEL, T. L., PELLETIER, L., MECHTLER, K., DRECHSEL, D. N., SCHWAGER, A., LEE, M., RAFF, J. W. & HYMAN, A. A. 2005. Aurora A phosphorylation of TACC3/maskin is required for centrosome-dependent microtubule assembly in mitosis. *Journal of Cell Biology,* 170**,** 1047-1055.

KITAGAWA, M. & LEE, S. H. 2015. The chromosomal passenger complex (CPC) as a key orchestrator of orderly mitotic exit and cytokinesis. *Frontiers in Cell and Developmental Biology,* 3.

KLEIN, U. R., NIGG, E. A. & GRUNEBERG, U. 2006. Centromere targeting of the chromosomal passenger complex requires a ternary subcomplex of borealin, survivin, and the N-terminal domain of INCENP. *Molecular Biology of the Cell,* 17**,** 2547-2558.

KLINE-SMITH, S. L., KHODJAKOV, A., HERGERT, P. & WALCZAK, C. E. 2003. Depletion of Centromeric MCAK Leads to Chromosome Congression and Segregation Defects Due to Improper Kinetochore Attachments. *Molecular Biology of the Cell,* 15**,** 1146-1159.

KOFFA, M. D., CASANOVA, C. M., SANTARELLA, R., KÖCHER, T., WILM, M. & MATTAJ, I. W. 2006. HURP Is Part of a Ran-Dependent Complex Involved in Spindle Formation. *Current Biology,* 16**,** 743-754.

KOLLMAN, J. M., MERDES, A., MOUREY, L. & AGARD, D. A. 2011. Microtubule nucleation by γ-tubulin complexes. *Nature Reviews Molecular Cell Biology,* 12**,** 709-721.

KOVACS, A. H., ZHAO, D. & HOU, J. 2023. Aurora B Inhibitors as Cancer Therapeutics. *Molecules* [Online], 28.

KRENN, V. & MUSACCHIO, A. 2015a. The Aurora B kinase in chromosome bi-orientation and spindle checkpoint signaling. *Frontiers in Oncology,* 5.

KRENN, V. & MUSACCHIO, A. 2015b. The Aurora B Kinase in Chromosome Bi-Orientation and Spindle Checkpoint Signaling. *Frontiers in Oncology,* 5.

KRUPINA, K., GOGINASHVILI, A. & CLEVELAND, D. W. 2021. Causes and consequences of micronuclei. *Curr Opin Cell Biol,* 70**,** 91-99.

KRYSTYNIAK, A., GARCIA-ECHEVERRIA, C., PRIGENT, C. & FERRARI, S. 2006. Inhibition of Aurora A in response to DNA damage. *Oncogene,* 25**,** 338-348.

KUFER, T. A., SILLJÉ, H. H. W., KÖRNER, R., GRUSS, O. J., MERALDI, P. & NIGG, E. A. 2002. Human TPX2 is required for targeting Aurora-A kinase to the spindle. *The Journal of cell biology,* 158**,** 617-623.

KUMAGAI, A. & DUNPHY, W. G. 2000. Claspin, a novel protein required for the activation of Chk1 during a DNA replication checkpoint response in Xenopus egg extracts. *Molecular Cell,* 6**,** 839-849.

KUMARI, G., ULRICH, T. & GAUBATZ, S. 2013. A role for p38 in transcriptional elongation of p21 (CIP1) in response to Aurora B inhibition. *Cell Cycle,* 12**,** 2051-60.

KUNITOKU, N., SASAYAMA, T., MARUMOTO, T., ZHANG, D., HONDA, S., KOBAYASHI, O., HATAKEYAMA, K., USHIO, Y., SAYA, H. & HIROTA, T. 2003. CENP-A Phosphorylation by Aurora-A in Prophase Is Required for Enrichment of Aurora-B at Inner Centromeres and for Kinetochore Function. *Developmental Cell,* 5**,** 853-864.

LAKKANIGA, N. R., WANG, Z., XIAO, Y., KHARBANDA, A., LAN, L. & LI, H.-Y. 2024. Revisiting Aurora Kinase B: A promising therapeutic target for cancer therapy. *Medicinal Research Reviews,* 44**,** 686-706.

LAMPERT, F., HORNUNG, P. & WESTERMANN, S. 2010. The Dam1 complex confers microtubule plus end–tracking activity to the Ndc80 kinetochore complex. *Journal of Cell Biology,* 189**,** 641-649.

LAMPSON, M. A. & GRISHCHUK, E. L. 2017. Mechanisms to Avoid and Correct Erroneous Kinetochore-Microtubule Attachments. *Biology (Basel),* 6.

LAN, W., ZHANG, X., KLINE-SMITH, S. L., ROSASCO, S. E., BARRETT-WILT, G. A., SHABANOWITZ, J., HUNT, D. F., WALCZAK, C. E. & STUKENBERG, P. T. 2004. Aurora B phosphorylates centromeric MCAK and regulates its localization and microtubule depolymerization activity. *Current Biology,* 14**,** 273-286.

LAVIN, M. F., KOZLOV, S., GATEI, M. & KIJAS, A. W. 2015. ATM-Dependent Phosphorylation of All Three Members of the MRN Complex: From Sensor to Adaptor. *Biomolecules,* 5**,** 2877-2902.

LEE, C.-Y., ANDERSEN, R. O., CABERNARD, C., MANNING, L., TRAN, K. D., LANSKEY, M. J., BASHIRULLAH, A. & DOE, C. Q. 2006. Drosophila Aurora-

A kinase inhibits neuroblast self-renewal by regulating aPKC/Numb cortical polarity and spindle orientation. *Genes & development,* 20**,** 3464-3474.

LEE, D. H., ACHARYA, S. S., KWON, M., DRANE, P., GUAN, Y., ADELMANT, G., KALEV, P., SHAH, J., PELLMAN, D., MARTO, J. A. & CHOWDHURY, D. 2014. Dephosphorylation Enables the Recruitment of 53BP1 to Double-Strand DNA Breaks. *Molecular Cell,* 54**,** 512-525.

LEE, J. H. & PAULL, T. T. 2004. Direct activation of the ATM protein kinase by the Mre11/Rad50/Nbs1 complex. *Science,* 304**,** 93-6.

LEIMBACHER, P. A., JONES, S. E., SHORROCKS, A. M. K., DE MARCO ZOMPIT, M., DAY, M., BLAAUWENDRAAD, J., BUNDSCHUH, D., BONHAM, S., FISCHER, R., FINK, D., KESSLER, B. M., OLIVER, A. W., PEARL, L. H., BLACKFORD, A. N. & STUCKI, M. 2019. MDC1 Interacts with TOPBP1 to Maintain Chromosomal Stability during Mitosis. *Molecular Cell,* 74**,** 571-583.e8.

LENS, S. M. A., WOLTHUIS, R. M. F., KLOMPMAKER, R., KAUW, J., AGAMI, R., BRUMMELKAMP, T., KOPS, G. & MEDEMA, R. H. 2003. Survivin is required for a sustained spindle checkpoint arrest in response to lack of tension. *The EMBO Journal,* 22**,** 2934-2947.

LI, M., LIU, H., ZHAO, Q., HAN, S., ZHOU, L., LIU, W., LI, W. & GAO, F. 2021. Targeting Aurora B kinase with Tanshinone IIA suppresses tumor growth and overcomes radioresistance. *Cell Death and Disease,* 12.

LI, P., NIJHAWAN, D., BUDIHARDJO, I., SRINIVASULA, S. M., AHMAD, M., ALNEMRI, E. S. & WANG, X. 1997. Cytochrome c and dATP-Dependent Formation of Apaf-1/Caspase-9 Complex Initiates an Apoptotic Protease Cascade. *Cell,* 91**,** 479-489.

LI, Z., GAO, X., PENG, X., CHEN, M. J. M., LI, Z., WEI, B., WEN, X., WEI, B., DONG, Y., BU, Z., WU, A., WU, Q., TANG, L., LI, Z., LIU, Y., ZHANG, L., JIA, S., ZHANG, L., SHAN, F., ZHANG, J., WU, X., JI, X., JI, K., WU, X., SHI, J., XING, X., WU, J., LV, G., SHEN, L., JI, X., LIANG, H. & JI, J. 2020. Multi-omics characterization of molecular features of gastric cancer correlated with response to neoadjuvant chemotherapy. *Science Advances,* 6.

LIM, Y., DE BELLIS, D., SANDOW, J. J., CAPALBO, L., D'AVINO, P. P., MURPHY, J. M., WEBB, A. I., DORSTYN, L. & KUMAR, S. 2021. Phosphorylation by Aurora B kinase regulates caspase-2 activity and function. *Cell Death and Differentiation,* 28**,** 349-366.

LIN, J., LIU, B., ZHANG, Y., LV, L., CHENG, D., ZHANG, W., SHI, Y., JIANG, X., TANG, L., YUAN, Y., ZHAI, H., SHEN, Q., XIONG, Q., JIN, Z., CHEN, Y. & YANG, C. 2022. Gemin6 promotes c-Myc stabilisation and non-small cell lung cancer progression via accelerating AURKB mRNA maturation. *Clin Transl Med,* 12**,** e811.

LINDON, C., GRANT, R. & MIN, M. 2016. Ubiquitin-mediated degradation of Aurora kinases. *Frontiers in Oncology,* 5.

LISCHETTI, T. & NILSSON, J. 2015. Regulation of mitotic progression by the spindle assembly checkpoint. *Molecular & Cellular Oncology,* 2**,** e970484.

LIU, D., VADER, G., VROMANS, M. J. M., LAMPSON, M. A. & LENS, S. M. A. 2009. Sensing Chromosome Bi-Orientation by Spatial Separation of Aurora B Kinase from Kinetochore Substrates. *Science,* 323**,** 1350-1353.

LIU, N., WANG, Y. A., SUN, Y., ECSEDY, J., SUN, J., LI, X. & WANG, P. 2019. Inhibition of Aurora A enhances radiosensitivity in selected lung cancer cell lines. *Respiratory Research,* 20.

LIU, Q., KANEKO, S., YANG, L., FELDMAN, R. I., NICOSIA, S. V., CHEN, J. & CHENG, J. Q. 2004. Aurora-A Abrogation of p53 DNA Binding and Transactivation Activity by Phosphorylation of Serine 215*. *Journal of Biological Chemistry,* 279**,** 52175-52182.

LIU, X., FIELDS, R., SCHWEPPE, D. K. & PAULO, J. A. 2021. Strategies for mass spectrometry-based phosphoproteomics using isobaric tagging. *Expert Rev Proteomics,* 18**,** 795-807.

LONATI, L., BARBIERI, S., GUARDAMAGNA, I., OTTOLENGHI, A. & BAIOCCO, G. 2021. Radiation-induced cell cycle perturbations: a computational tool validated with flow-cytometry data. *Scientific Reports,* 11**,** 925.

LOSADA, A., HIRANO, M. & HIRANO, T. 2002. Cohesin release is required for sister chromatid resolution, but not for condensin-mediated compaction, at the onset of mitosis. *Genes & Development,* 16**,** 3004-3016.

LÖWENBERG, B., MUUS, P., OSSENKOPPELE, G., ROUSSELOT, P., CAHN, J.-Y., IFRAH, N., MARTINELLI, G., AMADORI, S., BERMAN, E., SONNEVELD, P., JONGEN-LAVRENCIC, M., RIGAUDEAU, S., STOCKMAN, P., GOUDIE, A., FADERL, S., JABBOUR, E. & KANTARJIAN, H. 2011. Phase 1/2 study to assess the safety, efficacy, and pharmacokinetics of barasertib (AZD1152) in patients with advanced acute myeloid leukemia. *Blood,* 118**,** 6030-6036.

LUCA, M. D., LAVIA, P. & GUARGUAGLINI, G. 2006. A Functional Interplay Between Aurora-A, Plk1 and TPX2 at Spindle Poles: Plk1 Controls Centrosomal Localization of Aurora-A and TPX2 Spindle Association. *Cell Cycle,* 5**,** 296-303.

LÜDERS, J., PATEL, U. K. & STEARNS, T. 2006. GCP-WD is a γ-tubulin targeting factor required for centrosomal and chromatin-mediated microtubule nucleation. *Nature Cell Biology,* 8**,** 137-147.

LUEDEMAN, M. E., STROIK, S., FENG, W., LUTHMAN, A. J., GUPTA, G. P. & RAMSDEN, D. A. 2022. Poly(ADP) ribose polymerase promotes DNA polymerase theta-mediated end joining by activation of end resection. *Nature Communications,* 13**,** 4547.

LUKASIEWICZ, K. B. & LINGLE, W. L. 2009. Aurora A, centrosome structure, and the centrosome cycle. *Environmental and Molecular Mutagenesis,* 50**,** 602-619.

LUO, A., HAO, R., ZHOU, X., JIA, Y., TANG, H., LUO, A., HAO, R., ZHOU, X., JIA, Y. & TANG, H. 2022. Integrative Proteomic and Phosphoproteomic Analyses of Hypoxia-Treated Pulmonary Artery Smooth Muscle Cells. *Proteomes 2022, Vol. 10, Page 23,* 10.

LUO, X., BUDIHARDJO, I., ZOU, H., SLAUGHTER, C. & WANG, X. 1998. Bid, a Bcl2 interacting protein, mediates cytochrome c release from mitochondria in response to activation of cell surface death receptors. *Cell,* 94**,** 481-90.

LUSTBERG, M. B. 2012. Management of neutropenia in cancer patients. *Clin Adv Hematol Oncol,* 10**,** 825-6.

MA, H. T. & POON, R. Y. C. 2020. Aurora kinases and DNA damage response. *Mutation Research/Fundamental and Molecular Mechanisms of Mutagenesis,* 821**,** 111716.

MA, N., MATSUNAGA, S., MORIMOTO, A., SAKASHITA, G., URANO, T., UCHIYAMA, S. & FUKUI, K. 2011. The nuclear scaffold protein SAF-A is required for kinetochore–microtubule attachment and contributes to the targeting of Aurora-A to mitotic spindles. *Journal of Cell Science,* 124**,** 394.

MA, P., HAO, Y., WANG, W., ZHANG, Y. F., YU, K. H. & WANG, W. X. 2023. AURKB activates EMT through PI3K/AKT signaling axis to promote ICC progression. *Discov Oncol,* 14**,** 102.

MACŮREK, L., LINDQVIST, A., LIM, D., LAMPSON, M. A., KLOMPMAKER, R., FREIRE, R., CLOUIN, C., TAYLOR, S. S., YAFFE, M. B. & MEDEMA, R. H. 2008. Polo-like kinase-1 is activated by aurora A to promote checkpoint recovery. *Nature,* 455**,** 119-123.

MAGNAGHI-JAULIN, L., EOT-HOULLIER, G., GALLAUD, E. & GIET, R. 2019. Aurora a protein kinase: To the centrosome and beyond. *Biomolecules,* 9.

MAILAND, N., BEKKER-JENSEN, S., BARTEK, J. & LUKAS, J. 2006. Destruction of Claspin by SCFβTrCP Restrains Chk1 Activation and Facilitates Recovery from Genotoxic Stress. *Molecular Cell,* 23**,** 307-318.

MALLM, J. P. & RIPPE, K. 2015. Aurora Kinase B Regulates Telomerase Activity via a Centromeric RNA in Stem Cells. *Cell Reports,* 11**,** 1667-1678.

MARÉCHAL, A. & ZOU, L. 2013. DNA Damage Sensing by the ATM and ATR Kinases. *Cold Spring Harbor Perspectives in Biology,* 5.

MAREI, H. E., ALTHANI, A., AFIFI, N., HASAN, A., CACECI, T., POZZOLI, G., MORRIONE, A., GIORDANO, A. & CENCIARELLI, C. 2021. p53 signaling in cancer progression and therapy. *Cancer Cell Int,* 21**,** 703.

MARKOVÁ, E., SCHULTZ, N. & BELYAEV, I. Y. 2007. Kinetics and dose-response of residual 53BP1/γ-H2AX foci: Co-localization, relationship with DSB repair and clonogenic survival. *International Journal of Radiation Biology,* 83**,** 319-329.

MARTINEZ-PASTOR, B., SILVEIRA, G. G., CLARKE, T. L., CHUNG, D., GU, Y., COSENTINO, C., DAVIDOW, L. S., MATA, G., HASSANIEH, S., SALSMAN, J., CICCIA, A., BAE, N., BEDFORD, M. T., MEGIAS, D., RUBIN, L. L., EFEYAN, A., DELLAIRE, G. & MOSTOSLAVSKY, R. 2021. Assessing kinetics and recruitment of DNA repair factors using high content screens. *Cell Reports,* 37**,** 110176.

MARUMOTO, T., HONDA, S., HARA, T., NITTA, M., HIROTA, T., KOHMURA, E. & SAYA, H. 2003. Aurora-A Kinase Maintains the Fidelity of Early and Late Mitotic Events in HeLa Cells. *Journal of Biological Chemistry,* 278**,** 51786-51795.

MARUMOTO, T., ZHANG, D. & SAYA, H. 2005. Aurora-A — A guardian of poles. *Nature Reviews Cancer,* 5**,** 42-50.

MASANI, S., HAN, L., MEEK, K. & YU, K. 2016. Redundant function of DNA ligase 1 and 3 in alternative end-joining during immunoglobulin class switch recombination. *Proceedings of the National Academy of Sciences,* 113**,** 1261-1266.

MASON, P. J. & BESSLER, M. 2011. Cytokinesis failure and attenuation: new findings in Fanconi anemia. *J Clin Invest,* 121**,** 27-30.

MATTHEWS, H. K., BERTOLI, C. & DE BRUIN, R. A. M. 2022. Cell cycle control in cancer. *Nature Reviews Molecular Cell Biology,* 23**,** 74-88.

MATTIROLI, F., VISSERS, J. H. A., VAN DIJK, W. J., IKPA, P., CITTERIO, E., VERMEULEN, W., MARTEIJN, J. A. & SIXMA, T. K. 2012. RNF168 ubiquitinates K13-15 on H2A/H2AX to drive DNA damage signaling. *Cell,* 150**,** 1182-1195.

MC GEE, M. M. 2015. Targeting the Mitotic Catastrophe Signaling Pathway in Cancer. *Mediators Inflamm,* 2015**,** 146282.

MCBRIDE, W. H. & SCHAUE, D. 2020. Radiation-induced tissue damage and response. *The Journal of Pathology,* 250**,** 647-655.

MCMILLAN, E. A., RYU, M.-J., DIEP, C. H., MENDIRATTA, S., CLEMENCEAU, J. R., VADEN, R. M., KIM, J.-H., MOTOYAJI, T., COVINGTON, K. R., PEYTON, M., HUFFMAN, K., WU, X., GIRARD, L., SUNG, Y., CHEN, P.-H., MALLIPEDDI, P. L., LEE, J. Y., HANSON, J., VORUGANTI, S., YU, Y., PARK, S., SUDDERTH, J., DESEVO, C., MUZNY, D. M., DODDAPANENI, H., GAZDAR, A., GIBBS, R. A., HWANG, T.-H., HEYMACH, J. V., WISTUBA, I., COOMBES, K. R., WILLIAMS, N. S., WHEELER, D. A., MACMILLAN, J. B., DEBERARDINIS, R. J., ROTH, M. G., POSNER, B. A., MINNA, J. D., KIM,

H. S. & WHITE, M. A. 2018. Chemistry-First Approach for Nomination of Personalized Treatment in Lung Cancer. *Cell,* 173**,** 864-878.e29.

MELICHAR, B., ADENIS, A., LOCKHART, A. C., BENNOUNA, J., DEES, E. C., KAYALEH, O., OBERMANNOVA, R., DEMICHELE, A., ZATLOUKAL, P., ZHANG, B., ULLMANN, C. D. & SCHUSTERBAUER, C. 2015. Safety and activity of alisertib, an investigational aurora kinase A inhibitor, in patients with breast cancer, small-cell lung cancer, non-small-cell lung cancer, head and neck squamous-cell carcinoma, and gastro-oesophageal adenocarcinoma: a five-arm phase 2 study. *The Lancet Oncology,* 16**,** 395-405.

MERALDI, P., HONDA, R. & NIGG, E. A. 2002. Aurora-A overexpression reveals tetraploidization as a major route to centrosome amplification in p53-/- cells. *EMBO Journal,* 21**,** 483-492.

MINOSHIMA, Y., KAWASHIMA, T., HIROSE, K., TONOZUKA, Y., KAWAJIRI, A., BAO, Y. C., DENG, X., TATSUKA, M., NARUMIYA, S., MAY, W. S., NOSAKA, T., SEMBA, K., INOUE, T., SATOH, T., INAGAKI, M. & KITAMURA, T. 2003. Phosphorylation by Aurora B Converts MgcRacGAP to a RhoGAP during Cytokinesis. *Developmental Cell,* 4**,** 549-560.

MO, F., ZHUANG, X., LIU, X., YAO, P. Y., QIN, B., SU, Z., ZANG, J., WANG, Z., ZHANG, J., DOU, Z., TIAN, C., TENG, M., NIU, L., HILL, D. L., FANG, G., DING, X., FU, C. & YAO, X. 2016. Acetylation of Aurora B by TIP60 ensures accurate chromosomal segregation. *Nature Chemical Biology,* 12**,** 226-232.

MOHIUDDIN, I. S. & KANG, M. H. 2019. DNA-PK as an Emerging Therapeutic Target in Cancer. *Frontiers in Oncology,* 9.

MONACO, L., KOLTHUR-SEETHARAM, U., LOURY, R., MURCIA, J. M.-D., DE MURCIA, G. & SASSONE-CORSI, P. 2005. Inhibition of Aurora-B kinase activity by poly(ADP-ribosyl)ation in response to DNA damage. *Proceedings of the National Academy of Sciences of the United States of America,* 102**,** 14244.

MOORE, D. C. 2016. Drug-Induced Neutropenia: A Focus on Rituximab-Induced Late-Onset Neutropenia. *P t,* 41**,** 765-768.

MORA-BERMÚDEZ, F., GERLICH, D. & ELLENBERG, J. 2007. Maximal chromosome compaction occurs by axial shortening in anaphase and depends on Aurora kinase. *Nature Cell Biology,* 9**,** 822-831.

MORI, D., YANO, Y., TOYO-OKA, K., YOSHIDA, N., YAMADA, M., MURAMATSU, M., ZHANG, D., SAYA, H., TOYOSHIMA, Y. Y., KINOSHITA, K., WYNSHAW-BORIS, A. & HIROTSUNE, S. 2007. NDEL1 Phosphorylation by Aurora-A Kinase Is Essential for Centrosomal Maturation, Separation, and TACC3 Recruitment. *Molecular and Cellular Biology,* 27**,** 352.

MORI, N., ISHIKAWA, C., SENBA, M., KIMURA, M. & OKANO, Y. 2011. Effects of AZD1152, a selective Aurora B kinase inhibitor, on Burkitt's and Hodgkin's lymphomas. *Biochem Pharmacol,* 81**,** 1106-15.

MORTLOCK, A. A., FOOTE, K. M., HERON, N. M., JUNG, F. H., PASQUET, G., LOHMANN, J.-J. M., WARIN, N., RENAUD, F., DE SAVI, C., ROBERTS, N. J., JOHNSON, T., DOUSSON, C. B., HILL, G. B., PERKINS, D., HATTER, G., WILKINSON, R. W., WEDGE, S. R., HEATON, S. P., ODEDRA, R., KEEN, N. J., CRAFTER, C., BROWN, E., THOMPSON, K., BRIGHTWELL, S., KHATRI, L., BRADY, M. C., KEARNEY, S., MCKILLOP, D., RHEAD, S., PARRY, T. & GREEN, S. 2007. Discovery, Synthesis, and in Vivo Activity of a New Class of Pyrazoloquinazolines as Selective Inhibitors of Aurora B Kinase. *Journal of Medicinal Chemistry,* 50**,** 2213-2224.

MOTYCKA, T. A., BESSHO, T., POST, S. M., SUNG, P. & TOMKINSON, A. E. 2004. Physical and functional interaction between the XPF/ERCC1 endonuclease and hRad52. *J Biol Chem,* 279**,** 13634-9.

MOUMEN, A., MASTERSON, P., O'CONNOR, M. J. & JACKSON, S. P. 2005. hnRNP K: An HDM2 Target and Transcriptional Coactivator of p53 in Response to DNA Damage. *Cell,* 123**,** 1065-1078.

MUKHERJEE, B., KESSINGER, C., KOBAYASHI, J., CHEN, B. P. C., CHEN, D. J., CHATTERJEE, A. & BURMA, S. 2006. DNA-PK phosphorylates histone H2AX during apoptotic DNA fragmentation in mammalian cells. *DNA Repair,* 5**,** 575-590.

MUNDT, A. J., ROESKE, J. C. & CHUNG, T. D. 2003. Biologic Basis of Radiation Therapy. *In:* KUFE, D., POLLOCK, R. & WEICHSELBAUM, R. (eds.) *Holland-Frei Cancer Medicine.* 6 ed. Hamilton (ON): BC Decker.

MURATA-HORI, M. & WANG, Y. L. 2002. Both midzone and astral microtubules are involved in the delivery of cytokinesis signals: Insights from the mobility of aurora B. *Journal of Cell Biology,* 159**,** 45-53.

MUSACCHIO, A. & SALMON, E. D. 2007. The spindle-assembly checkpoint in space and time. *Nature Reviews Molecular Cell Biology,* 8**,** 379-393.

NAKAMURA, A. J., RAO, V. A., POMMIER, Y. & BONNER, W. M. 2010. The complexity of phosphorylated H2AX foci formation and DNA repair assembly at DNA double-strand breaks. *Cell Cycle,* 9**,** 389-397.

NAVANI, N., BALDWIN, D. R., EDWARDS, J. G., EVISON, M., MCDONALD, F., NICHOLSON, A. G., FENEMORE, J., SAGE, E. K. & POPAT, S. 2022. Lung Cancer in the United Kingdom. *Journal of Thoracic Oncology,* 17**,** 186-193.

NCLA 2022. National Lung Cancer Audit annual report. Royal College of Physicians.

NDRS. 2024. *Treatment Breakdown, 2013-2020* [Online]. National Disease Registration Service. Available: Treatment Breakdown, 2013-2020 [Accessed 22-03-2024 2024].

NEAL, J. A., DUNGER, K., GEITH, K. & MEEK, K. 2020. Deciphering the role of distinct DNA-PK phosphorylations at collapsed replication forks. *DNA Repair,* 94**,** 102925.

NELSON, G., BUHMANN, M. & VON ZGLINICKI, T. 2009. DNA damage foci in mitosis are devoid of 53BP1. *Cell Cycle,* 8**,** 3379-3383.

NGUYEN, H. G., MAKITALO, M., YANG, D., CHINNAPPAN, D., ST. HILAIRE, C. & RAVID, K. 2009. Deregulated Aurora-B induced tetraploidy promotes tumorigenesis. *FASEB Journal,* 23**,** 2741-2748.

NICKLAS, R. B. 1997. How Cells Get the Right Chromosomes. *Science,* 275**,** 632-637.

NIE, M., WANG, Y., YU, Z., LI, X., DENG, Y., WANG, Y., YANG, D., LI, Q., ZENG, X., JU, J., LIU, M. & ZHAO, Q. 2020. AURKB promotes gastric cancer progression via activation of CCND1 expression. *Aging,* 12**,** 1304-1321.

NIERMANN, K. J., MORETTI, L., GIACALONE, N. J., SUN, Y., SCHLEICHER, S. M., KOPSOMBUT, P., MITCHELL, L. R., KIM, K. W. & LU, B. 2011. Enhanced radiosensitivity of androgen-resistant prostate cancer: AZD1152-mediated Aurora kinase B inhibition. *Radiat Res,* 175**,** 444-51.

NIKONOVA, A. S., ASTSATUROV, I., SEREBRIISKII, I. G., DUNBRACK, R. L., JR. & GOLEMIS, E. A. 2013. Aurora A kinase (AURKA) in normal and pathological cell division. *Cellular and molecular life sciences : CMLS,* 70**,** 661-687.

NIKULENKOV, F., SPINNLER, C., LI, H., TONELLI, C., SHI, Y., TURUNEN, M., KIVIOJA, T., IGNATIEV, I., KEL, A., TAIPALE, J. & SELIVANOVA, G. 2012. Insights into p53 transcriptional function via genome-wide chromatin occupancy and gene expression analysis. *Cell Death & Differentiation,* 19**,** 1992-2002.

NISHIBUCHI, G., MACHIDA, S., NAKAGAWA, R., YOSHIMURA, Y., HIRAGAMI-HAMADA, K., ABE, Y., KURUMIZAKA, H., TAGAMI, H. & NAKAYAMA, J. I. 2019. Mitotic phosphorylation of HP1a regulates its cell cycle-dependent chromatin binding. *Journal of Biochemistry,* 165**,** 433-446.

NURAINI, R. & WIDITA, R. 2019. Tumor Control Probability (TCP) and Normal Tissue Complication Probability (NTCP) with Consideration of Cell Biological Effect. *Journal of Physics: Conference Series,* 1245**,** 012092.

OCHS, F., SOMYAJIT, K., ALTMEYER, M., RASK, M. B., LUKAS, J. & LUKAS, C. 2016. 53BP1 fosters fidelity of homology-directed DNA repair. *Nature Structural and Molecular Biology,* 23**,** 714-721.

OKE, A., PEARCE, D., WILKINSON, R. W., CRAFTER, C., ODEDRA, R., CAVENAGH, J., FITZGIBBON, J., LISTER, A. T., JOEL, S. & BONNET, D. 2009. AZD1152 Rapidly and Negatively Affects the Growth and Survival of Human Acute Myeloid Leukemia Cells In vitro and In vivo. *Cancer Research,* 69**,** 4150-4158.

ORSBURN, B. C. 2021. Proteome Discoverer-A Community Enhanced Data Processing Suite for Protein Informatics. *Proteomes,* 9.

ORTHWEIN, A., FRADET-TURCOTTE, A., NOORDERMEER, S. M., CANNY, M. D., BRUN, C. M., STRECKER, J., ESCRIBANO-DIAZ, C. & DUROCHER, D. 2014. Mitosis inhibits DNA double-strand break repair to guard against telomere fusions. *Science,* 344**,** 189-193.

PACHIS, S. T. & KOPS, G. J. P. L. 2018. Leader of the SAC: molecular mechanisms of Mps1/TTK regulation in mitosis. *Open Biology,* 8**,** 180109.

PANNONE, G., HINDI, S. A. H., SANTORO, A., SANGUEDOLCE, F., RUBINI, C., CINCIONE, R. I., DE MARIA, S., TORTORELLA, S., ROCCHETTI, R., CAGIANO, S., PEDICILLO, C., SERPICO, R., LO MUZIO, L. & BUFO, P. 2011. Aurora B expression as a prognostic indicator and possibile therapeutic target in oral squamous cell carcinoma. *International Journal of Immunopathology and Pharmacology,* 24**,** 79-88.

PANNUNZIO, N. R., WATANABE, G. & LIEBER, M. R. 2018. Nonhomologous DNA end-joining for repair of DNA double-strand breaks. *The Journal of biological chemistry,* 293**,** 10512-10523.

PARSONS, J. L., DIANOVA, I. I., ALLINSON, S. L. & DIANOV, G. L. 2005. DNA Polymerase β Promotes Recruitment of DNA Ligase IIIα−XRCC1 to Sites of Base Excision Repair. *Biochemistry,* 44**,** 10613-10619.

PAULL, T. T. & GELLERT, M. 1999. Nbs1 potentiates ATP-driven DNA unwinding and endonuclease cleavage by the Mre11/Rad50 complex. *Genes & Development,* 13**,** 1276-1288.

PAWLIK, T. M. & KEYOMARSI, K. 2004. Role of cell cycle in mediating sensitivity to radiotherapy. *International Journal of Radiation Oncology*Biology*Physics,* 59**,** 928-942.

PESCHIAROLI, A., DORRELLO, N. V., GUARDAVACCARO, D., VENERE, M., HALAZONETIS, T., SHERMAN, N. E. & PAGANO, M. 2006. SCFβTrCP-Mediated Degradation of Claspin Regulates Recovery from the DNA Replication Checkpoint Response. *Molecular Cell,* 23**,** 319-329.

PETSALAKI, E., AKOUMIANAKI, T., BLACK, E. J., GILLESPIE, D. A. F. & ZACHOS, G. 2011. Phosphorylation at serine 331 is required for Aurora B activation. *Journal of Cell Biology,* 195**,** 449-466.

PETSALAKI, E. & ZACHOS, G. 2016. Clks 1, 2 and 4 prevent chromatin breakage by regulating the Aurora B-dependent abscission checkpoint. *Nat Commun,* 7**,** 11451.

PETSALAKI, E. & ZACHOS, G. 2020. DNA damage response proteins regulating mitotic cell division: double agents preserving genome stability. *The FEBS Journal,* 287**,** 1700-1721.

PETSALAKI, E. & ZACHOS, G. 2021a. The Abscission Checkpoint: A Guardian of Chromosomal Stability. *Cells,* 10.

PETSALAKI, E. & ZACHOS, G. 2021b. An ATM–Chk2–INCENP pathway activates the abscission checkpoint. *Journal of Cell Biology,* 220.

PHOSPHOSITE. 2023. *Phosphosite:MTOR s2448* [Online]. Available: https://www.phosphosite.org/siteAction.action?id=2199) [Accessed 25-01-2024].

PHOSPHOSITE. 2024. *Myc proto-oncogene protein* [Online]. Available: https://www.phosphosite.org/proteinAction.action?id=947&showAllSites=true [Accessed 9/12/2024].

PIEKNY, A., WERNER, M. & GLOTZER, M. 2005. Cytokinesis: Welcome to the Rho zone. *Trends in Cell Biology,* 15**,** 651-658.

PODHORECKA, M., SKLADANOWSKI, A. & BOZKO, P. 2010. H2AX Phosphorylation: Its Role in DNA Damage Response and Cancer Therapy. *Journal of nucleic acids,* 2010**,** 920161.

POHL, A., AZUMA, M., ZHANG, W., YANG, D., NING, Y., WINDER, T., DANENBERG, K. & LENZ, H. J. 2011. Pharmacogenetic profiling of Aurora kinase B is associated with overall survival in metastatic colorectal cancer. *Pharmacogenomics Journal,* 11**,** 93-99.

POON, R. Y. C. 2016. Cell Cycle Control: A System of Interlinking Oscillators. *In:* COUTTS, A. S. & WESTON, L. (eds.) *Cell Cycle Oscillators: Methods and Protocols.* New York, NY: Springer New York.

POPP, H. D., MEYER, M., BRENDEL, S., PRINZHORN, W., NAUMANN, N., WEISS, C., SEIFARTH, W., SCHOENBERG, S. O., HOFMANN, W.-K., HENZLER, T. & FABARIUS, A. 2016. Leukocyte DNA damage after reduced and conventional absorbed radiation doses using 3rd generation dual-source CT technology. *European Journal of Radiology Open,* 3**,** 134-137.

POWELL, S. & MCMILLAN, T. J. 1990. DNA damage and repair following treatment with ionizing radiation. *Radiotherapy and Oncology,* 19**,** 95-108.

PRASAD, R., SINGHAL, R. K., SRIVASTAVA, D. K., MOLINA, J. T., TOMKINSON, A. E. & WILSON, S. H. 1996. Specific Interaction of DNA Polymerase β and DNA Ligase I in a Multiprotein Base Excision Repair Complex from Bovine Testis*. *Journal of Biological Chemistry,* 271**,** 16000-16007.

PUGACHEVA, E. N. & GOLEMIS, E. A. 2005. The focal adhesion scaffolding protein HEF1 regulates activation of the Aurora-A and Nek2 kinases at the centrosome. *Nature Cell Biology,* 7**,** 937-946.

QI, G., OGAWA, I., KUDO, Y., MIYAUCHI, M., SIRIWARDENA, B. S. M. S., SHIMAMOTO, F., TATSUKA, M. & TAKATA, T. 2007. Aurora-B expression and its correlation with cell proliferation and metastasis in oral cancer. *Virchows Archiv,* 450**,** 297-302.

QIAN, Y.-W., ERIKSON, E., TAIEB, F. E. & MALLER, J. L. 2001. The Polo-like Kinase Plx1 Is Required for Activation of the Phosphatase Cdc25C and Cyclin B-Cdc2 in Xenopus Oocytes. *Molecular Biology of the Cell,* 12**,** 1791-1799.

QIN, B., GAO, B., YU, J., YUAN, J. & LOU, Z. 2013. Ataxia telangiectasia-mutated- and Rad3-related protein regulates the DNA damage-induced G2/M checkpoint through the Aurora A cofactor Bora protein. *Journal of Biological Chemistry,* 288**,** 16139-16144.

RAY CHAUDHURI, A. & NUSSENZWEIG, A. 2017. The multifaceted roles of PARP1 in DNA repair and chromatin remodelling. *Nat Rev Mol Cell Biol,* 18**,** 610-621.

REBOUTIER, D., TROADEC, M.-B., CREMET, J.-Y., FUKASAWA, K. & PRIGENT, C. 2012. Nucleophosmin/B23 activates Aurora A at the centrosome through phosphorylation of serine 89. *Journal of Cell Biology,* 197**,** 19-26.

REDA, M., BAGLEY, A. F., ZAIDAN, H. Y. & YANTASEE, W. 2020. Augmenting the therapeutic window of radiotherapy: A perspective on molecularly targeted therapies and nanomaterials. *Radiother Oncol,* 150**,** 225-235.

REITSEMA, T., KLOKOV, D., BANÁTH, J. P. & OLIVE, P. L. 2005. DNA-PK is responsible for enhanced phosphorylation of histone H2AX under hypertonic conditions. *DNA Repair,* 4**,** 1172-1181.

RHEINGOLD, S. N., AI; MEADOWS, AT 2003. Therapy-Related Secondary Cancers. *In:* KUFE, D. P., RE; WEICHSELBAUM, RR (ed.) *Holland-Frei Cancer Medicine.* 6th edition ed. Hamilton (ON).

RICKMAN, K. & SMOGORZEWSKA, A. 2019. Advances in understanding DNA processing and protection at stalled replication forks. *Journal of Cell Biology,* 218**,** 1096-1107.

RIEDER, C. L., COLE, R. W., KHODJAKOV, A. & SLUDER, G. 1995. The checkpoint delaying anaphase in response to chromosome monoorientation is mediated by an inhibitory signal produced by unattached kinetochores. *J Cell Biol,* 130**,** 941-8.

RIEDL, S. J. & SHI, Y. 2004. Molecular mechanisms of caspase regulation during apoptosis. *Nature Reviews Molecular Cell Biology,* 5**,** 897-907.

RODGERS, K. & MCVEY, M. 2016. Error-Prone Repair of DNA Double-Strand Breaks. *Journal of cellular physiology,* 231**,** 15-24.

ROGAKOU, E. P., BOON, C., REDON, C. & BONNER, W. M. 1999. Megabase chromatin domains involved in DNA double-strand breaks in vivo. *Journal of Cell Biology,* 146**,** 905-915.

ROMÉ, P., MONTEMBAULT, E., FRANCK, N., PASCAL, A., GLOVER, D. M. & GIET, R. 2010. Aurora A contributes to p150glued phosphorylation and function during mitosis. *Journal of Cell Biology,* 189**,** 651-659.

ROSNER, M., SIEGEL, N., VALLI, A., FUCHS, C. & HENGSTSCHLÄGER, M. 2010. mTOR phosphorylated at S2448 binds to raptor and rictor. *Amino Acids,* 38**,** 223-8.

ROTHENBERG, E., GRIMME, J. M., SPIES, M. & HA, T. 2008. Human Rad52-mediated homology search and annealing occurs by continuous interactions between overlapping nucleoprotein complexes. *Proceedings of the National Academy of Sciences,* 105**,** 20274-20279.

ROUILLARD, A. G., GW; FERNANDEZ, NF; WANG, Z; MONTEIRO, CD; MCDERMOTT, MG; MA'AYAN, A 2016. The harmonizome: a collection of processed datasets gathered to serve and mine knowledge about genes and proteins. *Database (Oxford)*.

ROY, A., VEROLI, M. V., PRASAD, S. & WANG, Q. J. 2018. Protein Kinase D2 Modulates Cell Cycle By Stabilizing Aurora A Kinase at Centrosomes. *Molecular Cancer Research,* 16**,** 1785.

ROYOU, A., GAGOU, M. E., KARESS, R. & SULLIVAN, W. 2010. BubR1- and Polo-Coated DNA Tethers Facilitate Poleward Segregation of Acentric Chromatids. *Cell,* 140**,** 235-245.

RYSER, S., DIZIN, E., JEFFORD, C. E., DELAVAL, B., GAGOS, S., CHRISTODOULIDOU, A., KRAUSE, K.-H., BIRNBAUM, D. & IRMINGER-FINGER, I. 2009. Distinct Roles of BARD1 Isoforms in Mitosis: Full-Length BARD1 Mediates Aurora B Degradation, Cancer-Associated BARD1β Scaffolds Aurora B and BRCA2. *Cancer Research,* 69**,** 1125.

SABBATTINI, P., CANZONETTA, C., SJOBERG, M., NIKIC, S., GEORGIOU, A., KEMBALL-COOK, G., AUNER, H. W. & DILLON, N. 2007. A novel role for the Aurora B kinase in epigenetic marking of silent chromatin in differentiated postmitotic cells. *The EMBO Journal,* 26**,** 4657-4669.

SADAIE, M., DILLON, C., NARITA, M., YOUNG, A. R., CAIRNEY, C. J., GODWIN, L. S., TORRANCE, C. J., BENNETT, D. C., KEITH, W. N. & NARITA, M. 2015. Cell-based screen for altered nuclear phenotypes reveals senescence progression in polyploid cells after Aurora kinase B inhibition. *Mol Biol Cell,* 26**,** 2971-85.

SAGULENKO, E., SAVELYEVA, L., EHEMANN, V., SAGULENKO, V., HOFMANN, W., ARNOLD, K., CLAAS, A., SCHERNECK, S. & SCHWAB, M. 2007. Suppression of polyploidy by the BRCA2 protein. *Cancer Letters,* 257**,** 65-72.

SAID, M., BARRA, V., BALZANO, E., TALHAOUI, I., PELLICCIA, F., GIUNTA, S. & NAIM, V. 2022. FANCD2 promotes mitotic rescue from transcription-mediated replication stress in SETX-deficient cancer cells. *Communications Biology,* 5**,** 1395.

SAIPRASAD, G., CHITRA, P., MANIKANDAN, R. & SUDHANDIRAN, G. 2014. Hesperidin induces apoptosis and triggers autophagic markers through inhibition of Aurora-A mediated phosphoinositide-3-kinase/Akt/mammalian

target of rapamycin and glycogen synthase kinase-3 beta signalling cascades in experimental colon carcinogenesis. *Eur J Cancer,* 50**,** 2489-507.

SAK, A., STUSCHKE, M., GRONEBERG, M., KUBLER, D., POTTGEN, C. & EBERHARDT, W. E. 2012. Inhibiting the aurora B kinase potently suppresses repopulation during fractionated irradiation of human lung cancer cell lines. *Int J Radiat Oncol Biol Phys,* 84**,** 492-9.

SALEH, T., TYUTYUNYK-MASSEY, L., MURRAY, G. F., ALOTAIBI, M. R., KAWALE, A. S., ELSAYED, Z., HENDERSON, S. C., YAKOVLEV, V., ELMORE, L. W., TOOR, A., HARADA, H., REED, J., LANDRY, J. W. & GEWIRTZ, D. A. 2019. Tumor cell escape from therapy-induced senescence. *Biochemical Pharmacology,* 162**,** 202-212.

SÁNCHEZ, R., PANTOJA-UCEDA, D., PRIETO, J., DIERCKS, T., MARCAIDA, M. J., MONTOYA, G., CAMPOS-OLIVAS, R. & BLANCO, F. J. 2010. Solution Structure of Human Growth Arrest and DNA Damage 45α (Gadd45α) and Its Interactions with Proliferating Cell Nuclear Antigen (PCNA) and Aurora A Kinase*. *Journal of Biological Chemistry,* 285**,** 22196-22201.

SAURIN, A. T., VAN DER WAAL, M. S., MEDEMA, R. H., LENS, S. M. A. & KOPS, G. J. P. L. 2011. Aurora B potentiates Mps1 activation to ensure rapid checkpoint establishment at the onset of mitosis. *Nature Communications,* 2**,** 316.

SAZONOVA, E. V., PETRICHUK, S. V., KOPEINA, G. S. & ZHIVOTOVSKY, B. 2021. A link between mitotic defects and mitotic catastrophe: detection and cell fate. *Biol Direct,* 16**,** 25.

SCHMITT, C. A., WANG, B. & DEMARIA, M. 2022. Senescence and cancer — role and therapeutic opportunities. *Nature Reviews Clinical Oncology,* 19**,** 619-636.

SCHWARTZ, G. K., CARVAJAL, R. D., MIDGLEY, R., RODIG, S. J., STOCKMAN, P. K., ATAMAN, O., WILSON, D., DAS, S. & SHAPIRO, G. I. 2013. Phase I study of barasertib (AZD1152), a selective inhibitor of Aurora B kinase, in patients with advanced solid tumors. *Invest New Drugs,* 31**,** 370-80.

SCOTT, S. L., EARLE, J. D. & GUMERLOCK, P. H. 2003. Functional p53 Increases Prostate Cancer Cell Survival After Exposure to Fractionated Doses of Ionizing Radiation1. *Cancer Research,* 63**,** 7190-7196.

SCULLY, R., PANDAY, A., ELANGO, R. & WILLIS, N. A. 2019. DNA double-strand break repair-pathway choice in somatic mammalian cells. *Nature Reviews Molecular Cell Biology,* 20**,** 698-714.

SEHDEV, V., KATSHA, A., ARRAS, J., PENG, D., SOUTTO, M., ECSEDY, J., ZAIKA, A., BELKHIRI, A. & EL-RIFAI, W. 2014. HDM2 regulation by AURKA promotes cell survival in gastric cancer. *Clinical Cancer Research,* 20**,** 76-86.

SEKI, A., COPPINGER, J. A., JANG, C.-Y., YATES, J. R. & FANG, G. 2008. Bora and the Kinase Aurora A Cooperatively Activate the Kinase Plk1 and Control Mitotic Entry. *Science,* 320**,** 1655.

SENGLE, G., TSUTSUI, K., KEENE, D. R., TUFA, S. F., CARLSON, E. J., CHARBONNEAU, N. L., ONO, R. N., SASAKI, T., WIRTZ, M. K., SAMPLES, J. R., FESSLER, L. I., FESSLER, J. H., SEKIGUCHI, K., HAYFLICK, S. J. & SAKAI, L. Y. 2012. Microenvironmental regulation by fibrillin-1. *PLoS Genetics,* 8.

SESSA, F., MAPELLI, M., CIFERRI, C., TARRICONE, C., ARECES, L. B., SCHNEIDER, T. R., STUKENBERG, P. T. & MUSACCHIO, A. 2005. Mechanism of Aurora B activation by INCENP and inhibition by hesperadin. *Mol Cell,* 18**,** 379-91.

SESSA, F. & VILLA, F. 2014. Structure of Aurora B-INCENP in complex with barasertib reveals a potential transinhibitory mechanism. *Acta Crystallogr F Struct Biol Commun,* 70**,** 294-8.

SEVERSON, A. F., HAMILL, D. R., CARTER, J. C., SCHUMACHER, J. & BOWERMAN, B. 2000. The Aurora-related kinase AIR-2 recruits ZEN-4/CeMKLP1 to the mitotic spindle at metaphase and is required for cytokinesis. *Current Biology,* 10**,** 1162-1171.

SFEIR, A. & SYMINGTON, L. S. 2015. Microhomology-Mediated End Joining: A Back-up Survival Mechanism or Dedicated Pathway? *Trends in Biochemical Sciences,* 40**,** 701-714.

SHAO, S., WANG, Y., JIN, S., SONG, Y., WANG, X., FAN, W., ZHAO, Z., FU, M., TONG, T., DONG, L., FAN, F., XU, N. & ZHAN, Q. 2006. Gadd45a Interacts with Aurora-A and Inhibits Its Kinase Activity*. *Journal of Biological Chemistry,* 281**,** 28943-28950.

SHERMAN, B. T., HAO, M., QIU, J., JIAO, X., BASELER, M. W., LANE, H. C., IMAMICHI, T. & CHANG, W. 2022. DAVID: a web server for functional enrichment analysis and functional annotation of gene lists (2021 update). *Nucleic Acids Res,* 50**,** W216-w221.

SHILOH, Y. & ZIV, Y. 2013. The ATM protein kinase: regulating the cellular response to genotoxic stress, and more. *Nature Reviews Molecular Cell Biology,* 14**,** 197-210.

SIA, J., SZMYD, R., HAU, E. & GEE, H. E. 2020. Molecular Mechanisms of Radiation-Induced Cancer Cell Death: A Primer. *Frontiers in Cell and Developmental Biology,* 8**,** 41.

SINCLAIR, W. K. & MORTON, R. A. 1965. X-Ray and Ultraviolet Sensitivity of Synchronized Chinese Hamster Cells at Various Stages of the Cell Cycle. *Biophysical Journal,* 5**,** 1-25.

SINGLETON, B. K., TORRES-ARZAYUS, M. I., ROTTINGHAUS, S. T., TACCIOLI, G. E. & JEGGO, P. A. 1999. The C terminus of Ku80 activates the DNA-dependent protein kinase catalytic subunit. *Molecular and Cellular Biology,* 19**,** 3267-3277.

SMIRNOVA, E., TOUEILLE, M., MARKKANEN, E. & HÜBSCHER, U. 2005. The human checkpoint sensor and alternative DNA clamp Rad9-Rad1-Hus1 modulates the activity of DNA ligase I, a component of the long-patch base excision repair machinery. *Biochemical Journal,* 389**,** 13-17.

SMITH, S. L., BOWERS, N. L., BETTICHER, D. Ç., GAUTSCHI, O., RATSCHILLER, D., HOBAN, P. R., BOOTON, R., SANTIBÁEZ-KOREF, M. F. & HEIGHWAY, J. 2005. Overexpression of aurora B kinase (AURKB) in primary non-small cell lung carcinoma is frequent, generally driven from one allele, and correlates with the level of genetic instability. *British Journal of Cancer,* 93**,** 719-729.

SMITS, V. A. J., KLOMPMAKER, R., VALLENIUS, T., RIJKSEN, G., MÄKELÄ, T. P. & MEDEMA, R. H. 2000. p21 Inhibits Thr¹⁶¹ Phosphorylation of Cdc2 to Enforce the G₂ DNA Damage Checkpoint *. *Journal of Biological Chemistry,* 275**,** 30638-30643.

SO, S., DAVIS, A. J. & CHEN, D. J. 2009. Autophosphorylation at serine 1981 stabilizes ATM at DNA damage sites. *Journal of Cell Biology,* 187.

SOURISSEAU, T., MANIOTIS, D., MCCARTHY, A., TANG, C., LORD, C. J., ASHWORTH, A. & LINARDOPOULOS, S. 2010. Aurora-A expressing tumour cells are deficient for homology-directed DNA double strand-break repair and sensitive to PARP inhibition. *EMBO Molecular Medicine,* 2**,** 130-142.

STARK, G. R. & TAYLOR, W. R. 2006. Control of the G2/M transition. *Molecular Biotechnology,* 32**,** 227-248.

STEIGEMANN, P., WURZENBERGER, C., SCHMITZ, M. H. A., HELD, M., GUIZETTI, J., MAAR, S. & GERLICH, D. W. 2009. Aurora B-Mediated Abscission Checkpoint Protects against Tetraploidization. *Cell,* 136**,** 473-484.

STIRLING, D. R., SWAIN-BOWDEN, M. J., LUCAS, A. M., CARPENTER, A. E., CIMINI, B. A. & GOODMAN, A. 2021. CellProfiler 4: improvements in speed, utility and usability. *BMC Bioinformatics,* 22**,** 433.

STUCKI, M., CLAPPERTON, J. A., MOHAMMAD, D., YAFFE, M. B., SMERDON, S. J. & JACKSON, S. P. 2005. MDC1 Directly Binds Phosphorylated Histone H2AX to Regulate Cellular Responses to DNA Double-Strand Breaks. *Cell,* 123**,** 1213-1226.

STURGEON, C. & ROBERGE, M. 2007. G2 Checkpoint Kinase Inhibitors Exert Their Radiosensitizing Effects Prior to the G2/M Transition. *Cell Cycle,* 6.

SUBHAN, M. A., YALAMARTY, S. S., FILIPCZAK, N., PARVEEN, F. & TORCHILIN, V. P. 2021. Recent Advances in Tumor Targeting via EPR Effect for Cancer Treatment. *Journal of Personalized Medicine* [Online], 11.

SUMARA, I., VORLAUFER, E., STUKENBERG, P. T., KELM, O., REDEMANN, N., NIGG, E. A. & PETERS, J.-M. 2002. The Dissociation of Cohesin from Chromosomes in Prophase Is Regulated by Polo-like Kinase. *Molecular Cell,* 9**,** 515-525.

SUN, H., WANG, Y., WANG, Z., MENG, J., QI, Z. & YANG, G. 2014a. Aurora-A controls cancer cell radio- and chemoresistance via ATM/Chk2-mediated DNA repair networks. *Biochimica et Biophysica Acta (BBA) - Molecular Cell Research,* 1843**,** 934-944.

SUN, J., KNICKELBEIN, K., HE, K., CHEN, D., DUDGEON, C., SHU, Y., YU, J. & ZHANG, L. 2014b. Aurora Kinase Inhibition Induces PUMA via NF-κB to Kill Colon Cancer Cells. *Molecular Cancer Therapeutics,* 13**,** 1298.

SYED, A. & TAINER, J. A. 2018. The MRE11–RAD50–NBS1 Complex Conducts the Orchestration of Damage Signaling and Outcomes to Stress in DNA Replication and Repair. *Annual Review of Biochemistry,* 87**,** 263-294.

TAI, Q., ZHANG, L. & HU, X. 2020. Clinical characteristics and treatments of large cell lung carcinoma: a retrospective study using SEER data. *Transl Cancer Res,* 9**,** 1455-1464.

TANG, A., GAO, K., CHU, L., ZHANG, R., YANG, J. & ZHENG, J. 2017. Aurora kinases: novel therapy targets in cancers. *Oncotarget,* 8**,** 23937-23954.

TAO, Y., LETEUR, C., CALDERARO, J., GIRDLER, F., ZHANG, P., FRASCOGNA, V., VARNA, M., OPOLON, P., CASTEDO, M., BOURHIS, J., KROEMER, G. & DEUTSCH, E. 2009. The aurora B kinase inhibitor AZD1152 sensitizes cancer cells to fractionated irradiation and induces mitotic catastrophe. *Cell Cycle,* 8**,** 3172-81.

TAO, Y., ZHANG, P., GIRDLER, F., FRASCOGNA, V., CASTEDO, M., BOURHIS, J., KROEMER, G. & DEUTSCH, E. 2008. Enhancement of radiation response in p53-deficient cancer cells by the Aurora-B kinase inhibitor AZD1152. *Oncogene,* 27**,** 3244-55.

TATSUKA, M., SATO, S., KANDA, A., MIKI, T., KAMATA, N., KITAJIMA, S., KUDO, Y. & TAKATA, T. 2009. Oncogenic role of nuclear accumulated Aurora-A. *Molecular Carcinogenesis,* 48**,** 810-820.

TAYLOR, R. C., CULLEN, S. P. & MARTIN, S. J. 2008. Apoptosis: controlled demolition at the cellular level. *Nature Reviews Molecular Cell Biology,* 9**,** 231-241.

TENG, C.-L., HSIEH, Y.-C., PHAN, L., SHIN, J., GULLY, C., VELAZQUEZ-TORRES, G., SKERL, S., YEUNG, S.-C. J., HSU, S.-L. & LEE, M.-H. 2012. FBXW7 is involved in Aurora B degradation. *Cell Cycle,* 11**,** 4059-4068.

TERADA, Y. 2006. Aurora-B/AIM-1 Regulates the Dynamic Behavior of HP1α at the G2–M Transition. *Molecular Biology of the Cell,* 17**,** 3232-3241.

TERASIMA, T. & TOLMACH, L. J. 1963. Variations in Several Responses of HeLa Cells to X-Irradiation during the Division Cycle. *Biophysical Journal,* 3**,** 11-33.

TERRANO, D. T., UPRETI, M. & CHAMBERS, T. C. 2010. Cyclin-Dependent Kinase 1-Mediated Bcl-xL/Bcl-2 Phosphorylation Acts as a Functional Link Coupling Mitotic Arrest and Apoptosis. *Molecular and Cellular Biology,* 30**,** 640-656.

THINGHOLM, T. E. & LARSEN, M. R. 2016. The Use of Titanium Dioxide for Selective Enrichment of Phosphorylated Peptides. *Methods Mol Biol,* 1355**,** 135-46.

THOMAS, Y., CIRILLO, L., PANBIANCO, C., MARTINO, L., TAVERNIER, N., SCHWAGER, F., VAN HOVE, L., JOLY, N., SANTAMARIA, A., PINTARD, L. & GOTTA, M. 2016. Cdk1 Phosphorylates SPAT-1/Bora to Promote Plk1 Activation in C. elegans and Human Cells. *Cell Reports,* 15**,** 510-518.

THORESEN, S. B., CAMPSTEIJN, C., VIETRI, M., SCHINK, K. O., LIESTØL, K., ANDERSEN, J. S., RAIBORG, C. & STENMARK, H. 2014. ANCHR mediates Aurora-B-dependent abscission checkpoint control through retention of VPS4. *Nature Cell Biology,* 16**,** 547-557.

THORSLUND, T., RIPPLINGER, A., HOFFMANN, S., WILD, T., UCKELMANN, M., VILLUMSEN, B., NARITA, T., SIXMA, T. K., CHOUDHARY, C., BEKKER-JENSEN, S. & MAILAND, N. 2015. Histone H1 couples initiation and amplification of ubiquitin signalling after DNA damage. *Nature,* 527**,** 389-393.

TIEN, J. F., UMBREIT, N. T., GESTAUT, D. R., FRANCK, A. D., COOPER, J., WORDEMAN, L., GONEN, T., ASBURY, C. L. & DAVIS, T. N. 2010. Cooperation of the Dam1 and Ndc80 kinetochore complexes enhances microtubule coupling and is regulated by aurora B. *Journal of Cell Biology,* 189**,** 713-723.

TOMITA, M. & MORI, N. 2010. Aurora A selective inhibitor MLN8237 suppresses the growth and survival of HTLV-1-infected T-cells in vitro. *Cancer Science,* 101**,** 1204-1211.

TOYOSHIMA-MORIMOTO, F., TANIGUCHI, E. & NISHIDA, E. 2002. Plk1 promotes nuclear translocation of human Cdc25C during prophase. *EMBO Rep,* 3**,** 341-8.

TOYOSHIMA-MORIMOTO, F., TANIGUCHI, E., SHINYA, N., IWAMATSU, A. & NISHIDA, E. 2001. Polo-like kinase 1 phosphorylates cyclin B1 and targets it to the nucleus during prophase. *Nature,* 410**,** 215-220.

TRAKALA, M., FERNÁNDEZ-MIRANDA, G., DE CASTRO, I. P., HEESCHEN, C. & MALUMBRES, M. 2013. Aurora B prevents delayed DNA replication and premature mitotic exit by repressing p21Cip1. *Cell Cycle,* 12**,** 1030-1041.

TRIESELMANN, N., ARMSTRONG, S., RAUW, J. & WILDE, A. 2003. Ran modulates spindle assembly by regulating a subset of TPX2 and Kid activities including Aurora A activation. *Journal of Cell Science,* 116**,** 4791-4798.

TSAI, C. Y., NGO, B., TAPADIA, A., HSU, P.-H., WU, G. & LEE, W.-H. 2011. Aurora-A Phosphorylates Augmin Complex Component Hice1 Protein at an N-terminal Serine/Threonine Cluster to Modulate Its Microtubule Binding Activity during Spindle Assembly. *Journal of Biological Chemistry,* 286**,** 30097-30106.

TSUDA, Y., IIMORI, M., NAKASHIMA, Y., NAKANISHI, R., ANDO, K., OHGAKI, K., KITAO, H., SAEKI, H., OKI, E. & MAEHARA, Y. 2017. Mitotic slippage and the subsequent cell fates after inhibition of Aurora B during tubulin-binding agent-induced mitotic arrest. *Sci Rep,* 7**,** 16762.

TURINETTO, V. & GIACHINO, C. 2015. Multiple facets of histone variant H2AX: a DNA double-strand-break marker with several biological functions. *Nucleic acids research,* 43**,** 2489-2498.

UMBREIT, N. T., GESTAUT, D. R., TIEN, J. F., VOLLMAR, B. S., GONEN, T., ASBURY, C. L. & DAVIS, T. N. 2012. The Ndc80 kinetochore complex directly modulates microtubule dynamics. *Proceedings of the National Academy of Sciences,* 109**,** 16113-16118.

UPRETI, M., GALITOVSKAYA, E. N., CHU, R., TACKETT, A. J., TERRANO, D. T., GRANELL, S. & CHAMBERS, T. C. 2008. Identification of the Major Phosphorylation Site in Bcl-xL Induced by Microtubule Inhibitors and Analysis of Its Functional Significance*. *Journal of Biological Chemistry,* 283**,** 35517-35525.

UZIEL, T., LERENTHAL, Y., MOYAL, L., ANDEGEKO, Y., MITTELMAN, L. & SHILOH, Y. 2003. Requirement of the MRN complex for ATM activation by DNA damage. *The EMBO journal,* 22**,** 5612-5621.

VADER, G., KAUW, J. J. W., MEDEMA, R. H. & LENS, S. M. A. 2006. Survivin mediates targeting of the chromosomal passenger complex to the centromere and midbody. *EMBO Reports,* 7**,** 85-92.

VAN DER WAAL, M. S., HENGEVELD, R. C. C., VAN DER HORST, A. & LENS, S. M. A. 2012. Cell division control by the Chromosomal Passenger Complex. *Experimental Cell Research,* 318**,** 1407-1420.

VAN VUGT, M. A. T. M., GARDINO, A. K., LINDING, R., OSTHEIMER, G. J., REINHARDT, H. C., ONG, S. E., TAN, C. S., MIAO, H., KEEZER, S. M., LI, J., PAWSON, T., LEWIS, T. A., CARR, S. A., SMERDON, S. J., BRUMMELKAMP, T. R., YAFFE, M. B. & LICHTEN, M. 2010. A mitotic phosphorylation feedback network connects Cdk1, Plk1, 53BP1, and Chk2 to inactivate the G2/M DNA damage checkpoint. *PLoS Biology,* 8.

VENOUX, M., BASBOUS, J., BERTHENET, C., PRIGENT, C., FERNANDEZ, A., LAMB, N. J. & ROUQUIER, S. 2008. ASAP is a novel substrate of the

oncogenic mitotic kinase Aurora-A: phosphorylation on Ser625 is essential to spindle formation and mitosis. *Human Molecular Genetics,* 17**,** 215-224.

VIGNERON, S., SUNDERMANN, L., LABBÉ, J. C., PINTARD, L., RADULESCU, O., CASTRO, A. & LORCA, T. 2018. Cyclin A-cdk1-Dependent Phosphorylation of Bora Is the Triggering Factor Promoting Mitotic Entry. *Developmental Cell,* 45**,** 637-650.e7.

VISCHIONI, B., OUDEJANS, J. J., VOS, W., RODRIGUEZ, J. A. & GIACCONE, G. 2006. Frequent overexpression of aurora B kinase, a novel drug target, in non–small cell lung carcinoma patients. *Molecular Cancer Therapeutics,* 5**,** 2905-2913.

VITALE, I., GALLUZZI, L., CASTEDO, M. & KROEMER, G. 2011. Mitotic catastrophe: a mechanism for avoiding genomic instability. *Nature Reviews Molecular Cell Biology,* 12**,** 385-392.

WAN, X.-B., LONG, Z.-J., YAN, M., XU, J., XIA, L.-P., LIU, L., ZHAO, Y., HUANG, X.-F., WANG, X.-R., ZHU, X.-F., HONG, M.-H. & LIU, Q. 2008. Inhibition of Aurora-A suppresses epithelial–mesenchymal transition and invasion by downregulating MAPK in nasopharyngeal carcinoma cells. *Carcinogenesis,* 29**,** 1930-1937.

WANG, E., BALLISTER, E. R. & LAMPSON, M. A. 2011a. Aurora B dynamics at centromeres create a diffusion-based phosphorylation gradient. *Journal of Cell Biology,* 194**,** 539-549.

WANG, F., DAI, J., DAUM, J. R., NIEDZIALKOWSKA, E., BANERJEE, B., STUKENBERG, P. T., GORBSKY, G. J. & HIGGINS, J. M. G. 2010. Histone H3 Thr-3 Phosphorylation by Haspin Positions Aurora B at Centromeres in Mitosis. *Science,* 330**,** 231-235.

WANG, F., ULYANOVA, NATALIA P., VAN DER WAAL, MAIKE S., PATNAIK, D., LENS, SUSANNE M. A. & HIGGINS, JONATHAN M. G. 2011b. A Positive Feedback Loop Involving Haspin and Aurora B Promotes CPC Accumulation at Centromeres in Mitosis. *Current Biology,* 21**,** 1061-1069.

WANG, H., PAN, H. & HUANG, X. 2023. AURKB Enhances Chromosomal Remodeling of Telomeric Genes and Accelerates Tumorigenesis of Uveal Melanoma. *Invest Ophthalmol Vis Sci,* 64**,** 23.

WANG, H., PENG, B., PANDITA, R. K., ENGLER, D. A., MATSUNAMI, R. K., XU, X., HEGDE, P. M., BUTLER, B. E., PANDITA, T. K., MITRA, S., XU, B. & HEGDE, M. L. 2017. Aurora kinase B dependent phosphorylation of 53BP1 is required for resolving merotelic kinetochore-microtubule attachment errors during mitosis. *Oncotarget,* 8**,** 48671-48687.

WANG, H., SOMERS, G. W., BASHIRULLAH, A., HEBERLEIN, U., YU, F. & CHIA, W. 2006. Aurora-A acts as a tumor suppressor and regulates self-renewal of Drosophila neuroblasts. *Genes & Development,* 20**,** 3453-3463.

WANG, J., HU, T., WANG, Q., CHEN, R., XIE, Y., CHANG, H. & CHENG, J. 2021. Repression of the AURKA-CXCL5 axis induces autophagic cell death and promotes radiosensitivity in non-small-cell lung cancer. *Cancer Letters,* 509**,** 89-104.

WANG, L., LYNCH, C., PITRODA, S. P., PIFFKÓ, A., YANG, K., HUSER, A. K., LIANG, H. L. & WEICHSELBAUM, R. R. 2024. Radiotherapy and immunology. *Journal of Experimental Medicine,* 221**,** e20232101.

WANG, W., ZHANG, N., WANG, J., BU, X.-M. & ZHAE, C.-H. 2011c. Inhibition of Proliferation, Viability, Migration and Invasion of Gastric Cancer Cells by Aurora-A Deletion. *Asian Pacific Journal of Cancer Prevention,* 12**,** 2717-2720.

WANG, X., LU, N., NIU, B., CHEN, X., XIE, J. & CHENG, N. 2012. Overexpression of Aurora-A enhances invasion and matrix metalloproteinase-2 expression in esophageal squamous cell carcinoma cells. *Molecular Cancer Research,* 10**,** 588-596.

WANG, Y., WANG, Z., QI, Z., YIN, S., ZHANG, N., LIU, Y., LIU, M., MENG, J., ZANG, R., ZHANG, Z. & YANG, G. 2014. The negative interplay between Aurora A/B and BRCA1/2 controls cancer cell growth and tumorigenesis via distinct regulation of cell cycle progression, cytokinesis, and tetraploidy. *Molecular Cancer,* 13.

WARD, I. M. & CHEN, J. 2001. Histone H2AX Is Phosphorylated in an ATR-dependent Manner in Response to Replicational Stress *. *Journal of Biological Chemistry,* 276**,** 47759-47762.

WARD, I. M., MINN, K. & CHEN, J. 2004. UV-induced Ataxia-telangiectasia-mutated and Rad3-related (ATR) Activation Requires Replication Stress*. *Journal of Biological Chemistry,* 279**,** 9677-9680.

WARD, J. F. 1988. DNA Damage Produced by Ionizing Radiation in Mammalian Cells: Identities, Mechanisms of Formation, and Reparability. *In:* COHN, W. E. & MOLDAVE, K. (eds.) *Progress in Nucleic Acid Research and Molecular Biology.* Academic Press.

WATANABE, N., ARAI, H., NISHIHARA, Y., TANIGUCHI, M., WATANABE, N., HUNTER, T. & OSADA, H. 2004a. M-phase kinases induce phospho-dependent ubiquitination of somatic Wee1 by SCF<sup>β-TrCP</sup&gt. *Proceedings of the National Academy of Sciences of the United States of America,* 101**,** 4419.

WATANABE, N., ARAI, H., NISHIHARA, Y., TANIGUCHI, M., WATANABE, N., HUNTER, T. & OSADA, H. 2004b. M-phase kinases induce phospho-dependent ubiquitination of somatic Wee1 by SCF^{β-TrCP}. *Proceedings of the National Academy of Sciences of the United States of America,* 101**,** 4419.

WELBURN, J. P. I., GRISHCHUK, E. L., BACKER, C. B., WILSON-KUBALEK, E. M., YATES, J. R. & CHEESEMAN, I. M. 2009. The Human Kinetochore Ska1 Complex Facilitates Microtubule Depolymerization-Coupled Motility. *Developmental Cell,* 16**,** 374-385.

WELBURN, J. P. I., VLEUGEL, M., LIU, D., YATES III, J. R., LAMPSON, M. A., FUKAGAWA, T. & CHEESEMAN, I. M. 2010. Aurora B Phosphorylates Spatially Distinct Targets to Differentially Regulate the Kinetochore-Microtubule Interface. *Molecular Cell,* 38**,** 383-392.

WESTBROOK, J. A., NOIREL, J., BROWN, J. E., WRIGHT, P. C. & EVANS, C. A. 2015. Quantitation with chemical tagging reagents in biomarker studies. *Proteomics Clin Appl,* 9**,** 295-300.

WETERINGS, E. & VAN GENT, D. C. 2004. The mechanism of non-homologous end-joining: a synopsis of synapsis. *DNA Repair,* 3**,** 1425-1435.

WHITAKER, R. H. & COOK, J. G. 2021. Stress Relief Techniques: p38 MAPK Determines the Balance of Cell Cycle and Apoptosis Pathways. *Biomolecules,* 11.

WHITEHOUSE, C. J., TAYLOR, R. M., THISTLETHWAITE, A., ZHANG, H., KARIMI-BUSHERI, F., LASKO, D. D., WEINFELD, M. & CALDECOTT, K. W. 2001. XRCC1 Stimulates Human Polynucleotide Kinase Activity at Damaged DNA Termini and Accelerates DNA Single-Strand Break Repair. *Cell,* 104**,** 107-117.

WIEDERHOLD, L., LEPPARD, J. B., KEDAR, P., KARIMI-BUSHERI, F., RASOULI-NIA, A., WEINFELD, M., TOMKINSON, A. E., IZUMI, T., PRASAD, R., WILSON, S. H., MITRA, S. & HAZRA, T. K. 2004. AP Endonuclease-Independent DNA Base Excision Repair in Human Cells. *Molecular Cell,* 15**,** 209-220.

WILKINSON, R. W., ODEDRA, R., HEATON, S. P., WEDGE, S. R., KEEN, N. J., CRAFTER, C., FOSTER, J. R., BRADY, M. C., BIGLEY, A., BROWN, E., BYTH, K. F., BARRASS, N. C., MUNDT, K. E., FOOTE, K. M., HERON, N. M., JUNG, F. H., MORTLOCK, A. A., BOYLE, F. T. & GREEN, S. 2007. AZD1152, a Selective Inhibitor of Aurora B Kinase, Inhibits Human Tumor Xenograft Growth by Inducing Apoptosis. *Clinical Cancer Research,* 13**,** 3682.

WINTERS, T. A., RUSSELL, P. S., KOHLI, M., DAR, M. E., NEUMANN, R. D. & JORGENSEN, T. J. 1999. Determination of human DNA polymerase utilization for the repair of a model ionizing radiation-induced DNA strand break lesion in a defined vector substrate. *Nucleic Acids Research,* 27**,** 2423-2433.

WORDEMAN, L. & MITCHISON, T. J. 1995. Identification and partial characterization of mitotic centromere-associated kinesin, a kinesin-related protein that associates with centromeres during mitosis. *Journal of Cell Biology,* 128**,** 95-104.

WRIGHT, W. D., SHAH, S. S. & HEYER, W.-D. 2018. Homologous recombination and the repair of DNA double-strand breaks. *Journal of Biological Chemistry,* 293**,** 10524-10535.

WU, L., MA, C. A. & JAIN, A. 2011a. When Aurora B met p53: newly revealed regulatory phosphorylation in an old protein. *Cell Cycle,* 10**,** 171-2.

WU, L., MA, C. A., ZHAO, Y. & JAIN, A. 2011b. Aurora B interacts with NIR-p53, leading to p53 phosphorylation in its DNA-binding domain and subsequent functional suppression. *Journal of Biological Chemistry,* 286**,** 2236-2244.

WU, Q., LI, B., LIU, L., SUN, S. & SUN, S. 2020. Centrosome dysfunction: a link between senescence and tumor immunity. *Signal Transduct Target Ther,* 5**,** 107.

WYATT, DAVID W., FENG, W., CONLIN, MICHAEL P., YOUSEFZADEH, MATTHEW J., ROBERTS, STEVEN A., MIECZKOWSKI, P., WOOD, RICHARD D., GUPTA, GAORAV P. & RAMSDEN, DALE A. 2016. Essential Roles for Polymerase θ-Mediated End Joining in the Repair of Chromosome Breaks. *Molecular Cell,* 63**,** 662-673.

XIA, Y., SHEN, S. & VERMA, I. M. 2014. NF-κB, an active player in human cancers. *Cancer immunology research,* 2**,** 823-830.

XIAO, M., ZHANG, S., LIU, Z., MO, Y., WANG, H., ZHAO, X., YANG, X., BOOHAKER, R. J., CHEN, Y., HAN, Y., LIU, H. & XU, B. 2022. Dual-functional significance of ATM-mediated phosphorylation of spindle assembly checkpoint component Bub3 in mitosis and the DNA damage response. *Journal of Biological Chemistry,* 298**,** 101632.

XIAO, S., QIN, D., HOU, X., TIAN, L., YU, Y., ZHANG, R., LYU, H., GUO, D., CHEN, X. Z., ZHOU, C. & TANG, J. 2023. Cellular senescence: a double-edged sword in cancer therapy. *Front Oncol,* 13**,** 1189015.

XU, D. R., HUANG, S., LONG, Z. J., CHEN, J. J., ZOU, Z. Z., LI, J., LIN, D. J. & LIU, Q. 2011. Inhibition of mitotic kinase Aurora suppresses Akt-1 activation and induces apoptotic cell death in all-trans retinoid acid-resistant acute promyelocytic leukemia cells. *J Transl Med,* 9**,** 74.

YAMAGISHI, Y., HONDA, T., TANNO, Y. & WATANABE, Y. 2010. Two Histone Marks Establish the Inner Centromere and Chromosome Bi-Orientation. *Science,* 330**,** 239-243.

YAMAUCHI, T., UZUI, K., SHIGEMI, H., NEGORO, E., YOSHIDA, A. & UEDA, T. 2013. Aurora B inhibitor barasertib and cytarabine exert a greater-than-additive cytotoxicity in acute myeloid leukemia cells. *Cancer Sci,* 104**,** 926-33.

YAN, M., WANG, C., HE, B., YANG, M., TONG, M., LONG, Z., LIU, B., PENG, F., XU, L., ZHANG, Y., LIANG, D., LEI, H., SUBRATA, S., KELLEY, K. W., LAM, E. W. F., JIN, B. & LIU, Q. 2016. Aurora-A Kinase: A Potent Oncogene and Target for Cancer Therapy. *Medicinal Research Reviews,* 36**,** 1036-1079.

YANG, C., TANG, X., GUO, X., NIIKURA, Y., KITAGAWA, K., CUI, K., WONG, STEPHEN T. C., FU, L. & XU, B. 2011a. Aurora-B Mediated ATM Serine 1403 Phosphorylation Is Required for Mitotic ATM Activation and the Spindle Checkpoint. *Molecular Cell,* 44**,** 597-608.

YANG, F., GUO, X., YANG, G., ROSEN, D. G. & LIU, J. 2011b. AURKA and BRCA2 expression highly correlate with prognosis of endometrioid ovarian carcinoma. *Modern pathology : an official journal of the United States and Canadian Academy of Pathology, Inc,* 24**,** 836-845.

YANG, G., CHANG, B., YANG, F., GUO, X., CAI, K. Q., XIAO, X., WANG, H., SEN, S., HUNG, M.-C., MILLS, G. B., CHANG, S., MULTANI, A. S., MERCADO-URIBE, I. & LIU, J. 2010a. Aurora Kinase A Promotes Ovarian Tumorigenesis through Dysregulation of the Cell Cycle and Suppression of BRCA2. *Clinical Cancer Research,* 16**,** 3171.

YANG, H., HE, L., KRUK, P., NICOSIA, S. V. & CHENG, J. Q. 2006. Aurora-A induces cell survival and chemoresistance by activation of Akt through a p53-dependent manner in ovarian cancer cells. *Int J Cancer,* 119**,** 2304-12.

YANG, J., IKEZOE, T., NISHIOKA, C., NOBUMOTO, A., UDAKA, K. & YOKOYAMA, A. 2013. CD34+/CD38- acute myelogenous leukemia cells aberrantly express Aurora kinase A. *International Journal of Cancer,* 133**,** 2706-2719.

YANG, K. T., LI, S. K., CHANG, C. C., TANG, C. J. C., LIN, Y. N., LEE, S. C. & TANG, T. K. 2010b. Aurora-C kinase deficiency causes cytokinesis failure in meiosis I and production of large polyploid oocytes in mice. *Molecular Biology of the Cell,* 21**,** 2371-2383.

YAO, J. E., YAN, M., GUAN, Z., PAN, C. B., XIA, L. P., LI, C. X., WANG, L. H., LONG, Z. J., ZHAO, Y., LI, M. W., ZHENG, F. M., XU, J., LIN, D. J. & LIU, Q. 2009. Aurora-A down-regulates IkappaBalpha via Akt activation and interacts with insulin-like growth factor-1 induced phosphatidylinositol 3-kinase pathway for cancer cell survival. *Mol Cancer,* 8**,** 95.

YASUI, Y., URANO, T., KAWAJIRI, A., NAGATA, K., TATSUKA, M., SAYA, H., FURUKAWA, K., TAKAHASHI, T., IZAWA, I. & INAGAKI, M. 2004. Autophosphorylation of a newly identified site of Aurora-B is indispensable for cytokinesis. *J Biol Chem,* 279**,** 12997-3003.

YU, J., ZHOU, J., XU, F., BAI, W. & ZHANG, W. 2018. High expression of Aurora-B is correlated with poor prognosis and drug resistance in non-small cell lung cancer. *Int J Biol Markers,* 33**,** 215-221.

YU, T. W., MOCHIDA, G. H., TISCHFIELD, D. J., SGAIER, S. K., FLORES-SARNAT, L., SERGI, C. M., TOPÇU, M., MCDONALD, M. T., BARRY, B. J., FELIE, J. M., SUNU, C., DOBYNS, W. B., FOLKERTH, R. D., BARKOVICH, A. J. & WALSH, C. A. 2010. Mutations in WDR62, encoding a centrosome-associated protein, cause microcephaly with simplified gyri and abnormal cortical architecture. *Nature Genetics,* 42**,** 1015-1020.

YU, X., MINTER-DYKHOUSE, K., MALUREANU, L., ZHAO, W.-M., ZHANG, D., MERKLE, C. J., WARD, I. M., SAYA, H., FANG, G., VAN DEURSEN, J. & CHEN, J. 2005. Chfr is required for tumor suppression and Aurora A regulation. *Nature Genetics,* 37**,** 401-406.

ZANNINI, L., DELIA, D. & BUSCEMI, G. 2014. CHK2 kinase in the DNA damage response and beyond. *J Mol Cell Biol,* 6**,** 442-57.

ZAYTSEV, A. V., MICK, J. E., MASLENNIKOV, E., NIKASHIN, B., DELUCA, J. G. & GRISHCHUK, E. L. 2015. Multisite phosphorylation of the NDC80 complex gradually tunes its microtubule-binding affinity. *Molecular Biology of the Cell,* 26**,** 1829-1844.

ZEITLIN, S. G., SHELBY, R. D. & SULLIVAN, K. F. 2001. CENP-A is phosphorylated by Aurora B kinase and plays an unexpected role in completion of cytokinesis. *Journal of Cell Biology,* 155**,** 1147-1158.

ZENG, W. F., NAVARATNE, K., PRAYSON, R. A. & WEIL, R. J. 2007. Aurora B expression correlates with aggressive behaviour in glioblastoma multiforme. *Journal of Clinical Pathology,* 60**,** 218-221.

ZHANG, D., HIROTA, T., MARUMOTO, T., SHIMIZU, M., KUNITOKU, N., SASAYAMA, T., ARIMA, Y., FENG, L., SUZUKI, M., TAKEYA, M. & SAYA, H. 2004. Cre-loxP-controlled periodic Aurora-A overexpression induces mitotic abnormalities and hyperplasia in mammary glands of mouse models. *Oncogene,* 23**,** 8720-8730.

ZHANG, J., LIN, X., WU, L., HUANG, J.-J., JIANG, W.-Q., KIPPS, T. J. & ZHANG, S. 2020. Aurora B induces epithelial–mesenchymal transition by stabilizing Snail1 to promote basal-like breast cancer metastasis. *Oncogene,* 39**,** 2550-2567.

ZHANG, X., LAN, W., EMS-MCCLUNG, S. C., STUKENBERG, P. T. & WALCZAK, C. E. 2007. Aurora B Phosphorylates Multiple Sites on Mitotic Centromere-associated Kinesin to Spatially and Temporally Regulate Its Function. *Molecular Biology of the Cell,* 18**,** 3264-3276.

ZHANG, Y., CHEN, X., FENG, J., SHEN, Y. & HUANG, Y. 2023. The Proteome and Phosphoproteome Uncovers Candidate Proteins Associated With Vacuolar Phosphate Signal Multipled by Vacuolar Phosphate Transporter 1 (VPT1) in Arabidopsis. *Molecular & Cellular Proteomics,* 22.

ZHANG, Y., JIANG, C., LI, H., LV, F., LI, X., QIAN, X., FU, L., XU, B. & GUO, X. 2015. Elevated Aurora B expression contributes to chemoresistance and poor prognosis in breast cancer. *Int J Clin Exp Pathol,* 8**,** 751-7.

ZHAO, W., STEINFELD, J. B., LIANG, F., CHEN, X., MARANON, D. G., JIAN MA, C., KWON, Y., RAO, T., WANG, W., SHENG, C., SONG, X., DENG, Y., JIMENEZ-SAINZ, J., LU, L., JENSEN, R. B., XIONG, Y., KUPFER, G. M., WIESE, C., GREENE, E. C. & SUNG, P. 2017. BRCA1-BARD1 promotes RAD51-mediated homologous DNA pairing. *Nature,* 550.

ZHAO, Z.-S., LIM, J. P., NG, Y.-W., LIM, L. & MANSER, E. 2005. The GIT-Associated Kinase PAK Targets to the Centrosome and Regulates Aurora-A. *Molecular Cell,* 20**,** 237-249.

ZHOU, Y., ZHOU, B., PACHE, L., CHANG, M., KHODABAKHSHI, A. H., TANASEICHUK, O., BENNER, C., CHANDA, S. K., ZHOU, Y., ZHOU, B., PACHE, L., CHANG, M., KHODABAKHSHI, A. H., TANASEICHUK, O., BENNER, C. & CHANDA, S. K. 2019. Metascape provides a biologist-oriented resource for the analysis of systems-level datasets. *Nature Communications 2019 10:1,* 10.

ZOU, L. & ELLEDGE, S. J. 2003. Sensing DNA damage through ATRIP recognition of RPA-ssDNA complexes. *Science,* 300**,** 1542-1548.

ZOU, Z., TAO, T., LI, H. & ZHU, X. 2020. mTOR signaling pathway and mTOR inhibitors in cancer: progress and challenges. *Cell & Bioscience,* 10**,** 31.

ZOU, Z., YUAN, Z., ZHANG, Q., LONG, Z., CHEN, J., TANG, Z., ZHU, Y., CHEN, S., XU, J., YAN, M., WANG, J. & LIU, Q. 2012. Aurora kinase A inhibition-induced autophagy triggers drug resistance in breast cancer cells. *Autophagy,* 8**,** 1798-1810.

ZUAZUA-VILLAR, P., RODRIGUEZ, R., GAGOU, M. E., EYERS, P. A. & MEUTH, M. 2014. DNA replication stress in CHK1-depleted tumour cells triggers premature (S-phase) mitosis through inappropriate activation of Aurora kinase B. *Cell Death Dis,* 5**,** e1253.